CRANFIELD UNIVERSITY

E K ALIMIN

DISSIPATION AND DISCRETIZATION IN TIME MARCHING CFD CALCULATION

SCHOOL OF MECHANICAL ENGINEERING

PhD THESIS

CRANFIELD UNIVERSITY

SCHOOL OF MECHANICAL ENGINEERING

PhD THESIS

Academic Year 1992-95

E K ALIMIN

Dissipation and Discretization In Time Marching CFD Calculation

Academic Supervisor: R. L. Elder
Industrial Supervisors: P. Stow (Rolls-Royce plc)
Y. K. Ho

July 1995

This thesis is submitted in partial fulfilment
of the requirements for the degree of Doctor of Philosophy

ABSTRACT

This thesis concentrates on accuracy improvements for an existing software package that solves the three dimensional Reynolds Averaged Navier-Stokes equations in rotating coordinates. It is a cell centred explicit time marching code. Two topics are considered: improvement to the discretization scheme, and reduction of the artificial dissipation.

The first topic is the analysis of the straight averaging process which demonstrates that the process can result in inconsistency with a skewed grid. An alternative consistent scheme is proposed which is based upon quadratic interpolation. Improved accuracy can also be obtained by modifying the grid or adopting a cell vertex scheme. The stability of the iterative process is also shown to depend on the time step.

The reduction of artificial dissipation (second topic) first considers the role of the so called aspect ratio and velocity functions. These are found to be limited in influence and a new function is proposed based upon the local flow gradient. Both two and three dimensional turbomachinery cases are tested and improvements demonstrated. In the second part of the analysis, the eigenvalues of the stability matrix are used to reduce the dissipation in overdamped regions. Again this method is applied to various test cases and improvements demonstrated.

The management part of this Total Technology PhD

Program discusses topics concerned with collaboration and technology development in the aero engine industry with particular emphasis on the role of an " emerging " partner.

ACKNOWLEDGEMENTS

I would like to thank Professor R.L. Elder, Dr P. Stow and Dr Y.K. Ho for their supervision and constant encouragement throughout the course of this study and also to my employer, IPTN for providing the opportunity to pursue advance study in engineering. On the management part of the study, I would like to thank Mr M. Clarke for his guidance. Also, I have learned a great deal about turbomachinery aerodynamics during my three years attachment in the Aerothermal Methods Group in Rolls-Royce. I would like to thank Rolls-Royce for the opportunity to carry out most of my work in the company.

Finally , I would like to thank my wife for her support and patience during my study.

CONTENTS

List of Figures

List of Tables

NOTATION

A = area

A^* = throat area

C = speed of sound

D = dissipation

e = total energy/mass

f_e = external forces

F_f = friction force

F_p = pressure force

H = rothalpy

$\hat{i},\hat{j},\hat{k}$ = unit vectors in cartesian coordinate

k = thermal conductivity

K_2 = coefficient of second order dissipation

K_4 = coefficient of fourth order dissipation

M_L = local Mach number

M_{max} = maximum Mach number

p = static pressure

P_{mean} = mean total pressure at the intake

P_r = Prandtl number

P_{60} = lowest value of mean total pressure over a 60^o at the fan face

q = heat flux

SE = entropy

S = scaling factor

ΔS_x = area of cell face with normal in x direction

ΔS_y = area of cell face with normal in y direction

t = time

T = static temperature

u,v,w = velocity in x, y, and z cartesian coordinate.

V_L = local velocity

V_{inf} = boundary layer edge velocity

V_{ref} = reference velocity

Vol = cell volume

x,y,z = cartesian coordinate

δ^* = boundary layer thickness

γ = specific heat ratio = 1.4

θ_i = incident angle

λ = eigenvalues

μ = fluid flow viscosity

μ_e = effective viscosity

μ_l = laminar viscosity

μ_T = turbulent viscosity

ν = scalar viscosity constant

ρ = density

τ = viscous shear stress

w = vorticity

Ω = rotational speed

1.0 INTRODUCTION

1.1 Background

In the competitive worldwide aerospace market, the capability to design and manufacture aero engines with good performance, within budget and to time is crucial for survival. In order to achieve these goals, an aero engine company has to take into consideration aspects of fuel prices, regulatory requirements in safety and the environment, passenger comfort and other matters (Ford, 1992, and Jewell, 1994). The matter is further complicated by potential changes in all related matters at the same time in the future.

Fuel prices and usage have a direct effect on engine competitiveness through engine efficiency (specific fuel consumption). So much so that a decrease in the specific fuel consumption of 1.1 % and 0.4 % for the V2500 and RB211 turbofan engines respectively can be translated to a cost change to the aircraft operator per year of US $12,000 and $33,500. This change in specific fuel consumption could typically be caused by a reduction in compressor efficiency of 1 % (Robinson, 1991).

On the other hand, the efficiency depends upon the level of the technology involved in the design. This is confirmed by the historical development from the turbojet to the early high bypass turbofan engines, figure-1.1 (Flax, 1974). Recent developments have resulted in further reduction of fuel consumption and predictions for the 21st century suggest that the trend will continue, figure-1.2

(Stryker, 1994). The many aspects of material process, manufacturing and aerodynamic technology contribute significantly to the improved performance of aero-engines (Hall, 1994)). The present work, however, concentrates on the aerodynamic aspect of turbomachinery design and development alone.

Nowadays, aerodynamic technology has reached such a level of sophistication that details of the airflow through the engine components can be predicted with reasonable accuracy. In the past, such information depended largely upon experiments and engine testing work, with designs relying heavily on empirically based methods. Advances in computer has provided high speed computing tolls for solving approximations to the Navier Stokes equations. This has been achieved through developments in algorithms and physical modelling of the governing equations of the air flow which has facilitated techniques now capable of numerical simulation of the flow through engine components.

This has resulted in the emergence of the new technology Computational Fluid Dynamics (CFD) as a complementary tool to earlier design methods. This technology now enables engine designers to carry out a large numbers of computations in a shorter time scale providing more optmized designs. In the past, the design verification required extensive testing of model hardware. With the CFD technology almost all the testing can be performed numerically. Thus, the costly and time

consuming exercise of building and testing the hardware can largely be avoided (Douglass and Ramshaw, 1994). Currently complex computer models are now beginning to be used in many engine components (such as cooling systems of the turbine) which has not been possible before (Hill and Langdell, 1993).

The airflow through the complex geometry of engine components is characterized by shocks, flow separation, vortices, unsteadiness and various viscous and secondary flow phenomena. The physical processes are embodied in the Navier Stokes equations which require discretization and simplification before even a time averaged solution can be obtained.

These processes introduce errors although the solution can still be used to qualitatively select a better design. For instance, based upon computational results, a designer can distinguish aerodynamically well designed blades from aerodynamically less well designed blades (Hah, 1989). Currently, even with the availability of the Navier Stokes solvers, design calculations of the flow within engine components still require tests to simulate other aspect of flow which as yet can not be modelled. However, the contribution of CFD technology is to reduce the testing required to produce competitive engines and to permit engine components to be designed "right first time" leading to significantly reduced development time and cost (Hill and Langdell, 1993).

It is significant to also note that if an engine

efficiency is less than predicted to the customer (who has purchased on the basis of these predictions) then it is often the case that the engine manufacturers will have to finance any loss in the productivity under fuel burn guarantees. The discrepancies generated by prediction methods (experiment and computationally) therefore carry significant cost consequences to manufacturers, (Robinson, 1991). Part of the problem is due to inaccurate CFD modelling of the airflow through engine components

1.2 Objective of the Thesis

Accuracy of CFD prediction becomes a problem because of the simplified mathematical nature of the equations solved inevitably incorporate terms which generate false physics. Therefore, the model suffers inaccuracy whereas industry requires an accurate and reliable design tool in order to have competitive design capabilities. In the light of this goal, the present research work concentrates on improving the accuracy of an available CFD program which solves the Reynolds Averaged Navier Stokes equations. This software has been produced for the solution of internal flow-problems within engine components such as compressor and turbine blades, as well as engine intake nacelles and nozzles (Ho, 1992).

In this thesis, the investigation concentrates on the discretization scheme used by the code (in an arbitrary grid arrangement which is covered in chapter 4) and the reduction of artificial dissipation (covered in chapters 5 and 6).

The discretization analysis studies both standard and modified schemes and in order to provide better accuracy, especially with skewed grids, an improved discretization scheme is also proposed. In addition as an alternative to adopting an improved scheme, grid modification is investigated to improve the accuracy. As an alternative to the cell centred scheme used in the standard software, a cell vertex scheme is considered. In addition to the spatial discretization analyzed in the above, time discretization is carried out to provide stability constraints.

Dissipation reduction is investigated by analyzing various dissipation models (chapter 5) and exploiting an eigenvalues analysis (chapter 6).

The errors generated by the standard dissipation are firstly analyzed and various correction functions proposed by other researchers examined. An improved correction function is then proposed which can reduce dissipation in critical regions of flows. Various test cases are considered including Ni's Bump, and two and three dimensional blading configurations.

The eigenvalues for a given level of dissipation are calculated from a stability matrix (derived from the governing equations). Based on the relationship between eigenvalues and dissipation, two ideas are proposed which try to obtain a balance between accuracy and robustness. The first method attempts to set the eigenvalues (or rate of convergence) and calculate the dissipation, and the

second method, to reduce the dissipation in the ov: damped regions where the eigenvalues are unnecessarily large and negative.

Collaboration within the aero-engine industry is a feature of modern programmes and is also considered as part of this thesis. Collaboration is undertaken to reduce risk and get market share where there are currently too many products and the market share for each company is likely to reduce. Aero-engine companies are ,therefore, collaborating to both finance the investment and capture market share.

A feature of the discussion is to establish the importance of technology to each partner in such a collaboration together with the project management techniques required for the development of technology with an inexperienced partner.

2. COLLABORATION AND TECHNOLOGY IN THE AERO ENGINE INDUSTRY

2.1 Introduction

Collaboration within the Aero Engine industry is being increasingly accepted as a logical means for companies to survive in difficult conditions, and to expand into new markets. Because of the high levels of investment required for engine developments, a large market share is essential for Aero Engine companies to make a satisfactory return. According to Aviation Week and Space Technology (28 February 1994), an engine must now capture at least fifty percent of its market share in order for it to be profitable.

However, when there are too many companies launching their products into the same market, the potential share of each company within that market will be limited. Those companies which succeed in securing only a small share of their market, will, therefore, need to rationalize if they are to remain in business (Regional Air, August 1993).

Thus, it is logical that companies which are already in the market should seek partners in order to share costs and combine their respective market shares. Where international partnerships are formed, such collaborations will also facilitate expansion into new markets.

Many governments now demand that, for engines purchased by national airlines and other state

organisations, a proportion of the engine components must be produced locally. This arrangement provides a means by which local industry can enter into the aero engine business. However, such new entrants face strong competition and do not usually have the capability to fully establish an indigenous industry (Hemmings, 1992). In such circumstances a collaboration with well established companies can provide the opportunity for local companies to gain access to invaluable expertise in technology, marketing, or other associated areas. This chapter tries to analyze what new entrants need, in terms of technological capability, when they decide to enter into such collaboration with an established partner.

If the new entrant plans to enter into the collaboration by taking responsibility for the development, design, and manufacture of the engine components, it will need to acquire the necessary expertise so that it will be able to undertake the design using advanced technology. The acquisition of this capability, which is crucial to competitiveness, will be scrutinized by the more established partners, or their sponsoring governments, to safeguard proprietary information.

Protection of intellectual property is a very important issue to be discussed during negotiation for any collaboration. In order to be considered as a partner in a collaboration, the new entrant must have a minimum technological capability, in addition to having

other assets such as investment capital, or access to foreign markets. A strategic plan to build such technological capability is elaborated through project management in this paper.

2.2 Historical Background

The world's Aerospace industries have been established through high investment ventures. Such industries always manufacture products according to market demand; however, they are characterised by the high levels of technology they need to remain competitive, and some stringent requirements in terms of safety and the environment.

Aerospace industries are normally established either to exploit the market commercially, or to lead technological developments. Most civil aerospace industries are established to exploit the market commercially, and, historically, this has been done as a result of spin offs from developments in military hardware. The market, though, has often proved insufficient to support such industries for long. After the first world war, for example, in 1921, all United Kingdom airline companies went out of business (Fearon, 1969). Such difficulties were caused by the high operating costs of the early airliners due to uneconomic fuel consumption, and inadequate equipment (Todd and Simpson, 1986). As the industry matured, however, and the market grew, the aerospace industry in the United Stated (US) and other countries successfully worked at

exploiting the market commercially.

It is stated by Hayward (1986) that the industry in the US would not be able to exploit the market profitably without state support. Such support can be in the form of government subsidy, state ownership, or large contracts for military aircraft.

Current free market policy tends to lead to the formation of private companies for many business ventures, and such companies invariably seek to capture market share. However, the products of newly formed aerospace companies cannot easily penetrate markets when they are competing with established products. Furthermore, difficulties are encountered due to: the need to fulfill quality standards; trade barriers; and the need for high investment. Such difficulties mean that newly formed private aerospace companies are unlikely to be profitable within a reasonable time span.

In developing countries, or newly industrialised countries, there are normally insufficient resources for large capital projects. Additionally, industrial skills are often limited to the manufacture of simple products. Therefore, it is difficult to build high technology industries, such as aero engine industries, without the backing of government policy and funding.

The government policy is often laid out to support various goals in the national development of sectors such as technology and agriculture, and could be set according to the goal of acquiring high technology through

establishment of the aero engine industry. Such policy, of course, varies from country to country but the purpose is to provide a means for agents of the development to facilitate the achievement of the goal. In almost all countries that have an aircraft industry, the government sets industrial policy to support that industry.

2.3. Collaboration as a Global Trend

2.3.1 Initiation of Collaboration

The aero engine market and the aero engine industry have gone through a transformation. Before 1960, an airline would buy a transport plane as a complete unit of airframe and engine. In the current market, engines and airframes are treated as separate products, and aero engine companies have to compete in the market place whenever airlines purchase an aircraft from an airframe manufacturer (Hayward, 1986). The role of aero engine companies has, therefore, changed, from that of supplier to airframe manufacturers, to that of supplier to airlines. In consequence they now directly interact with the users of their products.

In general, it may be considered that an industry, including the aero engine industry, sells either existing or new products to existing or new markets. Market expansion is considered to take place when either new products are sold, or existing products are sold into new markets. This is illustrated in figure-2.1.

If the existing products are sold into new markets which are located in another country, a collaboration may

be proposed. Since new engine development requires very high levels of investment, it is often difficult to guarantee the necessary return of investment from existing markets. In order to obtain such a return, new products often need to be sold in both existing and new markets. If the new market is located in another country, a collaboration may be proposed which may include research, development and design.

If the airframe products do not have sufficiently large markets, it will not be possible for sales to support the development of new engines. In such circumstances the airframe manufacturer will have to design its products around the engines available in the market place.

If, on the other hand, the market for the airframe products is sufficiently large, it may be possible for airframe sales to support the development of new engines, and for several companies to compete in the same market for these. Because of the fiercely competitive engine market, and the high cost of new engine development and production, the industries may wish to enter into collaborations to expand their market, share the risk, and share the cost.

A collaboration may involve research and development, design, testing, manufacturing, or sales. In manufacturing, the collaboration will often involve only production under license or co-production.

Other forms of collaboration are based on

subcontracting parts of the engines either for research and development, or design. In research, for example, high technology collaboration is currently being conducted for next generation supersonic transport engines and Rolls-Royce, SNECMA, MTU, and FIAT are all developing such engines through collaborative ventures (Aviation Week, 11 April 1994).

The collaboration arrangement may involve established partners only, or established partners and a new entrant. A collaboration may be initiated when an established company, which has experience in technology, marketing, and sales, is short of financial resources, or is uncertain about the financial return of investment due to pressures from competition.

In this situation, the new entrant, which may have strong financial resources and potential access to new markets, could plan to enter into the aero engine industry. Thus, gains in market share and capital infusion, may be traded for technology transfer and experience in the aero engine industry.

For the established industry, the purpose of the collaboration may be to maintain the present market and expand into new markets. For the new entrant, collaboration is usually the only way of getting into the industry.

On other occasions, collaboration may be part of an offset arrangement where an aero engine company sells its products to a foreign customer. In such circumstances,

the purchasing state may set conditions for purchase so that parts of the products need to be manufactured locally in that state.

The method of sale may differ between private and state supported companies (Cornell, 1981). Private companies usually compete in the open market, whereas state companies can rely on more protected markets.

In a protected civil aerospace market, for instance, the government may set conditions where the national airlines have to purchase the domestic products. In the open market, the manufacturers have to compete aggressively to sell their products, and this may involve financing the purchase, particularly with exports. The government may also provide a means of supporting the sales campaign. However, where the market is protected, the state ensures the availability of customers to support the industry.

2.3.2 Reasons for Collaboration

Technological advances in engine products are dependent upon advances in other fields of technology such as materials or electronics (Hayward, 1986). Aerospace products are becoming increasingly complex due to such advancement, and this is creating specialization whereby many other supporting companies build and service specific parts of the engines such as pumps or measuring instruments.

In an aero engine project, the aero engine company usually acts as the prime contractor, and the supporting

companies usually act as subcontractors that supply the specialized equipment. Nowadays, there are a few prime contractors and numerous subcontractors (Bracher, 1981). The complexity of the specialized technology, and the division of responsibility in product development among contractors, tends to lead to the need for high levels of investment.

Aircraft manufacturers need to continually improve productivity and competitiveness wherever high technology in aircraft engines has an important role. In this context, productivity is a measure of efficiency of aircraft production (James, 1982). Among the factors that influence the airlines to choose engines are: fuel consumption; reliability; noise; emission levels; price; cost of overhaul; the financial package; and political considerations (Cedar, 1986).

The fuel consumption, reliability, noise and emission levels of engines may all be improved through technological advancement. Therefore, highly competitive engines tend to require high levels of technology, which tend to require high levels of investment. However, aircraft manufacturers are not willing to invest in new equipment which does not give a satisfactory return, even though it may be technologically superior.

Where an aero engine company needs to invest heavily in high technology, it may, therefore, seek collaboration in order to improve the return on investment or reduce the risk.

In order to satisfy market demand for planes of 50 to 400 passengers, aero-engine companies have to make products that cover a wide range of engine types. Developing new engines, and producing a wide range of engines, requires large capital investments, and, in collaborations, this large investment is likely to be shared among partners.

A company which has a world wide market needs to enter into a global manufacturing policy in order to maintain the overall level of business in an increasingly competitive market. This policy leads to the establishment of manufacturing facilities for different markets in different countries. With this strategy, the products tend to be manufactured in one part of the world and shipped to another part for assembly (Gopal, 1992). The nature of global manufacturing involves different technologies in different plants. The technology level ranges from sub-assembly, through to assembly and manufacturing.

The levels of technology employed in different countries is closely associated with the overall levels of technology possessed by the countries where the facilities are located.

Facilities may still be opened in countries with low levels of technology if there is cheap labour as an incentive. In fact, one of the goals of a global manufacturing policy is to gain access to such cheap labour. With different products coming from different

manufacturing plants, the performance criteria of each plant is important, and it depends on the technology and objectives of the plant.

Such a global strategy tends to be based on production at several plants, sourcing from multiple locations, and the implementation of monitoring systems for major processes ranging from the supply of raw materials to the final assembly of products (Gopal, 1992). Through effective integration with such a global manufacturing policy, a broad international collaboration can be successfully formed.

The aerospace industry needs high levels of investment coupled with the use of high technology. In order to get a satisfactory return on investment, it, therefore, has to be able to achieve high levels of product sales, and these need to be supported by the economies inherent from large scale production capacity and a large market size. A collaboration between partners from different countries is one means of achieving these goals.

A collaboration arrangement can pull together the resources from several partners to create a large critical mass which can match some strong competition. The Airbus consortium, in the airframe sector, is one such example. Airbus is a consortium of a number of European civil aerospace companies which have been able to consolidate their resources and successfully match the strong competition faced from the United States civil

aerospace sector.

Other factors that are putting financial pressure on the aero engine industry are the depressed state of airline finances, price competition among airframe manufacturers, and a reduction in the returns obtained from investment by airframe manufacturers (Hayward, 1986).

Price competition among airframe manufactuers has an effect on aero engine manufacturers since engines can only be sold when airframes are sold. It has been estimated that 80% of engines are sold directly to airframe manufacturers (Hemmings, 1992), and it is only by adjusting the price of engines that airframes can be profitably sold.

2.4 Technology in the Aero Engine Industry

The well being and development of the aerospace industry is dependent upon technological progress. This can be pushed by research laboratories or pulled by the market or industry. It varies from being basic to commercially oriented.

2.4.1 The Role and Requirement of Technology

Since basic research does not have an immediate return on investment, it is often supported by a government agency. The research that can have immediate impact on the industry is affected by conditions in the market such as operating costs. The level of technology depends on: the technical requirement; the governing authority; and the market demand. Several items that can

be affected by the technological development are: engine efficiency; noise; emissions; and ease of operation (Ford, 1992).

The market can drive the acquisition of the technology. For instance, a research project to develop an efficient engine may either be cancelled or delayed when fuel is cheap and there is little demand from the market for an engine with low specific fuel consumption. When fuel is expensive, however, it is likely to be worth funding such research since the demand for engines with low specific fuel consumption is likely to be high. In such circumstances a satisfactory return on investment is quite possible.

With technological push, the laboratory can provide an increased level of technology. If the market cannot support the technology on that level, the technology will never find any application in industry. Propfan technology failed to reach the market because the propfan engines could not compete with other jet engines. Therefore, the Boeing 7J7 project was cancelled (Aviation Week, 14 March 1988). Learning through experience is essential to maintain the technology. The experience of a customer about the use of a product is important information required to improve the technology of the future product. British Airways' experience with the Boeing 747 was incorporated into the new Boeing 777 design features (Sunday Times, 19 June 1994). In order to achieve early Extended Twin Operation (ETOP) over

water clearance, Boeing researched what caused in-flight shut down, and addressed the problem (Aviation Week, 19[illegible] April 1993). Based upon this knowledge, an ETOP airplane was designed, manufactured and tested.

Low technology design is characterized by making many assumptions about a large number of parameters, which are not universally valid. High technology design is characterized by the ability to take account of, and calculate, a large number of different parameters. Such high technology design, in the field of aerodynamics, is expensive because it needs more computing power, and sophisticated measuring devices. For instance, the application of such high technology requires the calculation of more parameters because it takes into account of a wider range of physical processes that can affect the design. This leads to the requirement for new knowledge about the behaviour of certain physical processes which, in turn, need to be researched.

Such research inevitably requires further applications of high technology. Due to a limited budget and time, the resulting parameters that could have been obtained from that research are assumed to fulfil certain conditions, which are not always universally valid. The new instrumentation such as laser anemometer measurement, ensemble averaged hot wire data, and a better numerical method for flow prediction in three dimensions, show that air flow inside aircraft engines is extremely complicated (Denton, 1993). Other parameters have to be calculated

to understand this complicated flow. However, this effort very often cannot be afforded. Therefore, some parameters are assumed to fulfil certain conditions. The uncertainty is due to discrepancies that are introduced where the assumptions are invalid.

In fact, the above argument applies also to low technology. The difference from high technology is that the low technology limits areas of exploration which, in consequence, limits the resulting design capability. In other words, the design is not able to fulfil wide areas of operational conditions such as high level of performance efficiency. Thus, all levels of the technology make assumptions, but the higher technology has a wider area of application. For example, the area of exploration of viscous flow is wider than that of the inviscid flow.

In order to reduce the uncertainty and gain confidence in the results, a large number of tests have to be carried out. Since the increase in efficiency of a gas turbine engine or aircraft engine is influenced by the increase in turbine entry temperature, Rolls Royce actively develops high temperature turbine technology. 10,000 cycle tests have been completed in temperatures above 1800 K (Rolls-Royce Private Communication).

Such large numbers of tests will inevitably incur a high cost and also will increase lead time. Thus, uncertainty can contribute to high development costs. In another example, new technology makes the engines more

cost effective by reducing their size and weight, and increasing their simplicity and ruggedness (Wennerstroom, 1989). In engine components such as compressors, the development cost is affected by the need for ever higher efficiency, demand for lower manufacturing cost, and by reduction in size and weight. This will push the mechanism of the compressor into higher aerodynamic loading which will require better prediction methods (Fottner, 1989).

Inability of low technology to predict aerodynamic losses because of the many assumptions it makes, may result in high losses, for instance, in an engine. These high losses result in high specific fuel consumption. It is then not possible to fulfil stringent requirements such as low specific fuel consumption, low emissions, or others, with low technology.

Increased engine efficiency will not only make the engine more competitive and cost effective, but it will fulfil requirements for the environment. However, it must not make the engines difficult to maintain and less durable (Matson, 1993). A success in improving the efficiency and reduction in maintenance cost is a good selling point. CFM International introduced a new design of CFM 56-3XS which had 15 % lower maintenance cost and 5 % lower specific fuel consumption than the other model CFM 56-3C (Flight International, 9 June 1993).

The demands of the travelling public, such as shorter flying time, higher levels of comfort, less noise

in the cabin, lower fares, etc; and those of regulatory authorities, such as reduction in noise, have created new markets for certain types of aircraft and engines (Ford, June 1992). The market determines the choice of engines for the airliners. These factors are translated into the requirement for certain types of technology.

For instance, high reliability tends to be due to better prediction of component behaviour in the harsh engine environment, such as inside the combustion chamber ; or lower fuel consumption tends to be due to better prediction of losses. The technology of prediction methods needs investment in research and development. One thing that new technology has to avoid is, ultimately, to increase product costs to such an extent that they are no longer competitive. However, new technology, such as CFD technology, can reduce development costs for a given level of requirement. The goal is to produce engines at competitive prices, for a given requirement. The requirement can be fulfilled by the application of high technology. The acquisition of such technology needs investment that will tend to drive up the development cost.

2.4.2 Cost Effective Technology

The way in which technology will affect the development cost, and fulfil the engine design requirement, can be illustrated by a three dimensional chart of technology, development cost and design requirement (figure-2.2). There are many aspects of

engine requirement. In this chapter, one of the most important requirements is low specific fuel consumption which will be considered as a parameter along the axis of the requirement. A new requirement of low specific fuel consumption has to be fulfilled by higher levels of technology, and it is represented as point B on the technology axis. If the location of B is not correctly estimated, there will either be insufficient or surplus technology, as is illustrated in the two dimensional chart of requirement and technology (figure-2.3).

In the field of aerodynamics, increased levels of technology mean more sophisticated analytical methods, and fewer experimental tests. In the two dimensional chart of cost and level of technology (figure-2.4), the analytical solution covers potential methods to direct simulation methods of turbulent flow. The experimental tests with a wind tunnel are required to verify the analytical predictions. As the analytical methods become more sophisticated, they become capable of replacing more wind tunnel tests. This is possible because the analytical method is able to simulate the aerodynamic flows that were previously predicted by wind tunnel tests. There will be a decreasing overall cost of tests, due to a decreasing number of tests, but the cost of each particular test increases as the technology advances.

The potential solutions contain only pressure and velocity distributions. Other essential parameters, such as drag or losses, are obtained by experimental tests.

The cost of potential methods decrease, and the cost of wind tunnel tests increase, with time. It is much cheaper to use potential methods now, in the 1990's, than it was in the 1960's. The advancement of computer technology reduces the computing cost. CFD methods which were prohibitively expensive in the 1960's, can now be afforded.

Due to the requirement for more accurate results through the application of new technology, wind tunnel costs per unit time increase. If the number of hours of wind tunnel tests remains the same, wind tunnel costs will, therefore, increase. This relationship can be seen in figure-2.5. The target of acquiring the technology to fulfil the requirement and control the cost is to choose the level of technology that will result in minimum cost. This is illustrated in the chart of cost and technology (figure-2.4).

The higher level of technology is capable of simulating more complicated flow such that it needs less wind tunnel test time. The cost of CFD rises with increasing levels of technology, even though the cost of wind tunnel testing decreases, because fewer tests are required. This results in a higher overall, cost, which is shown by point C on the chart. The case with an insufficient level of technology will be similar. Even though the cost of computing is low due to the simple method of solution, this will result in a need for a large number of wind tunnel tests, which will cause costs

to rise. This is shown by point A on the chart.

An important slice of the three dimensional chart describes the relationship between design requirement and cost (figure-2.6). The development cost required to fulfil the design requirement, as it is related to the level of technology, has to be carefully justified. The use of insufficient or surplus technology for certain design requirements results in unnecessarily high development costs.

2.4.3 Technology Acquisition

The new entrant, that is sponsored by government, has to consider management of technological innovation and this can follow two broad approaches. The first is a gradual evolution of the existing technology; and the second is a sudden high risk strategy to exploit new technology (Hayward, 1986). Technology is part of the industrial asset that needs investment by either the sponsoring government or a private venture (Draper, 1987). In other words, the new entrant can participate in a collaborative project in research and development which will involve several companies. The mastering of the technology is accomplished through research and development. In order to overcome difficulties with sharing high technology in Europe, there should be an umbrella organization formed in order to promote research cooperation. For instance, the EC commissioned a study of major European airframe companies which was used to form the basis of the European Research Programme

(Hayward, 1991).

This type of collaboration is aimed at producing major financial savings through sharing of costs at the development stage. The new entrant has to consider taking responsibility for one engine component from development to manufacturing since it will motivate its employees to achieve targets for the project because their work has a direct impact on sales.

If the objective of the collaboration project is to develop a new aeroengine, the technology is likely to be the most important aspect of the project. In this case, each partner is likely to use similar design procedures for the aero engine. The established partners can lead the design process since they will have a comprehensive data base and much design experience. The new entrants can learn through involvement in the project. The reason for participating in the design of the new engine will be to learn about the technology by drawing from the experience of the established partners. The skills acquisition will concentrate on base technology for minimum capability, and advanced technology for competitive advantage.

Base Technology

An aero engine industry product clearly has to meet the customer requirements. These requirements are driven by market conditions. In order to achieve that goal, the technology and cost requirements have to be satisfied. The engine requirement leads to its specification. After

studying the market conditions and producing the engine specification, the cost and technology that are required will be clear, and collaboration can be considered in terms of risk and benefit.

The new engine specification is a basic description of what the engine has to be capable of. The next step is a preliminary study where the technical subject starts to be addressed. From a preliminary study, engine cycle and layout are obtained. Engine sizing follows where component design begins. Before the components that go into the design start to be manufactured, they will need to be tested. If the test result is not satisfactory, the components will need to be redesigned or modified. Once, the engine passes its certification, the delivery of the engine will commence.

Even though each partner in the collaboration does not need to have the same level of technology, each partner needs to have a base level of technology. This base level of technology is the minimum technology from which any partner can gradually build up to the competitive level that is being pursued in the collaboration project.

Advanced Technology

High technology has a crucial role to play in producing improved and competitive engines. The decision on the level of technology to employ is based on the target so that the project has to be completed within time and budget. One of the high technologies that is

essential to competitiveness is Computational Fluid Dynamics (CFD), which is used to design engine components such as compressors, turbine blades, etc. This technology is capable of modelling the airflow accurately and providing a better understanding of physical processes (Rolls-Royce Private Communication).

This capability will reduce design lead times and will result in greater levels of efficiency, that will help to guarantee the delivery of products within time and budget. The CFD technology is embodied in software, hardware, people and methods. Without proper understanding, the technology is treated as a black box and users only concern themselves with input and output. In such circumstances the danger is that the users or designers may have great difficulty in producing an acceptable design for all range of conditions. This is because a thorough understanding of the CFD method is required for the users to have an adequate understanding of its capability.

In the early days, compressor and turbine blades were designed by empirical methods and experimental tests. The rising cost of these tests, and the advancement of computing technology and methods have brought CFD technology into the design environment. One criteria that the airline takes into consideration when it chooses aircraft engines is efficiency, which is a measure of the losses in the real system. The losses are generated as the available energy in fuel is converted

into useful propulsive power. Low losses, or high efficiency, can be achieved through an understanding of the physical loss mechanisms, and investigating ways to reduce the losses. CFD technology provides the tools for that purpose, such that the engine components can be correctly designed, according to their requirements, on the first attempt. In this case, there will be no need for repeated tests in order to obtain the correct component specification. There will only need to be a single test. Therefore, the design costs will be reduced.

2.5 Plan to Develop Technology Capability

2.5.1 Introduction

It is quite clear from the above section that technological capability is an important requirement for any new entrant to enter into a collaborative project in the aero-engine industry. In order to support a new entrant as it embarks upon a collaborative project, a strategic plan to develop technological capability from a basic level to an advanced level is needed. Such a plan is developed below.

Project management techniques are proposed as a suitable method for efficiently managing such a plan. As a first step towards entering into the industry, the goal of having design, development and manufacturing capability, of certain parts of an engine, will be established, through this strategy.

2.5.2 Plan

The strategic plan consists of three parts. These

are: manufacturing; licensed production or co-production; design and development. Establishing an aero engine company capable of undertaking all parts requires a huge investment. In order to obtain sufficient capital, a new entrant can follow one of two policies which are either based upon the free market or state planning.

Each part of this strategy requires an increasing level of technological capability. However, each part also has technology which is specific to that part.

Manufacturing

In the first instance, the manufacturing technology has to be capable of manufacturing engine parts which have already been designed by the lead company. The sale of company products where the company has only manufacturing responsibility will depend on the sale of the complete engines. The dependence on the lead company puts the manufacturing company at risk. Its market size and output are controlled by the lead company. Manufacturing products are shipped to other companies for engine assembly.

As long as the engines have a world wide market, the manufactured product will have a world wide market as well. In this situation, the company aims at a global market but it may not have the goal of indigenous engine production. Its success depends on the success of a global manufacturing policy to support a large manufacturing project (Gopal, 1992). This part is usually pursued by the new entrant before entering into a

collaboration.

Licensed Production

Technology of manufacturing, assembling and producing engines can be acquired when the new entrant enters into licensed production arrangements with another company. This arrangement provides a first opportunity for the new entrant to learn the technology to produce and market complete engines. The development and design of the engines will remain the responsibility of the lead company. In contrast with the manufacturing company, the licensed production company has more control over the markerting of its products because it sells directly to the engine customer.

The licensed production project can start with assembling of a complete engine, with no parts being manufactured, and can move progressively to manufacturing parts. The technological skills acquired, gradually progress from those of simple assembly to manufacturing of simple and sophisticated parts. Manufacturing of sophisticated parts, such as turbine or compressor blades requires high levels of investment. Furthermore, the technology for manufacturing those parts is very closely guarded.

Design and Development

As the new entrant masters the technology through licensed production and manufacturing projects, it moves into a position where it is able to enter into an indigenous design project with partners.

2.5.3 Technological Capability of Design and Development

Planning the development of the technological capability at each stage, can be achieved through adopting project management techniques (Cleland and Kocaoglu, 1981).

Project Management

This part of the chapter concentrates on development of the technological capability for design and development. In project management several areas may be considered simultaneously, such as human resources, technology, hardware, cost, etc. The purpose of the project management technique is to minimize the time and resource required to achieve a single goal. The goal in this instance is technological capability to support design and development of aero engines.

Organization

The project is organized into four groups which are: finance; forecast and technology definition; technology development; and implementation (figure-2.7). This is a project based organization where the four functional groups will provide the overall resources necessary for the accomplishment of the project (Lecture Notes of School of Management, 1993).

Work Breakdown Structure

The project itself is broken down into several parts. They are: human resources; technology; cost control; and hardware (figure-2.8). The work breakdown defines the scope of the project. In each part, several functional groups work to achieve the project goal. For

instance, in the human resource part, the forecast and technology, development and implementation groups, all work together to forecast available human resources, develop these to have the capabilities needed to achieve the project goals, and implement their capability. These three functional groups are to achieve the project goal in human resources. The goal here is to provide the man power that is capable of carrying out design and development in aero engine projects.

Execution Logic

This leads to matrix responsibility, which is division of responsibility for each functional group into parts of the project (table-2.1). The execution logic of the project explains how the project is going to be undertaken (figure-2.9). For instance, after one part of the project is complete, deciding which parts should follow. These parts are taken from the breakdown of the project. It starts with forecast and financial resources. The financial resources will not be elaborated further, but will determine the choice of hardware, etc.

Phases

The project is carried out in phases which are: feasibility study; definition; execution and implementation. The feasibility study will gather information on what to expect, how much it is expected to cost and what resources are available. The definition will define the technology based upon the available resources, and the requirement for the technological

capability. The execution phase will actually build up the capability by recruiting personnel, modifying, adopting, creating the technology, and hardware acquisition. The implementation will be possible when all elements of the technological capability bave been achieved. In order to limit the scope of the study, it is the Computational Fluid Dynamic technology that will be discussed.

2.6 Project Management for Development of Computational Fluid Dynamic Technology

2.6.1 Introduction

The application of the project management technique for the development of the Computational Fluid Dynamic (CFD) technology is elaborated in this part of the chapter. As the technique is used to manage several disciplines simultaneously, the execution of the project is done in phases such as feasibility study, definition, execution, and implementation.

The feasibility study may find that accurate prediction methods are expected to come from the application of CFD technology. This method may also incur less cost than the application of empirical and experimental methods. However, the technological capability would depend upon available human resources. The goal of the capability must be achievable within time and budget. As the technology is defined in the next phase, the required capability is set according to the capability in the current aero engine industry such as

Computer Aided Engineering (CAE). The development of the technological capability in personnel, technology and hardware is in the execution phase. A core team is formed and the capability is actually developed in stages from recruitment of inexperienced personnel, to establishing a fully capable team. The technology can be obtained from open literature, it can be developed from basic information, or it can be created. The practical application aspect will facilitate the technological development. The implementation phase is reached when the team has all elements of the technological capability, and is ready to take an assignment in design and development.

2.6.2 Feasibility Study

Past Design Method

The past design practice based its approach on empirical prediction or cook book and experimental methods (Fottner, 1989). It allowed only limited variation of design features. This method was formulated from experimental data that had been compiled and verified. The results of the calculations by this method need to be verified by experiment. New design features that lie outside the known range of validity have to be verified by extensive experiment. An empirical method is fast because the calculation can be done using general purpose computers, or even by hand. Since it is fast, it is generally cheap. However, experimental testing is becoming more expensive. The design technology based

upon iteration of the empirical correlation and experimental testing is, therefore, becoming more expensive.

Such an approach also is unlikely to eventually result in competitive engine performance, because of the limitations of the methods employed. The engine will not be competitive in the market because it is likely to have a low efficiency. The engine efficiency is one the most important criteria that is assessed by airlines (Cedar, 1986). The engine is likely to be inefficient because it generates high losses. The loss is the amount of energy or thrust that is lost due to design imperfections, physical limitations, etc. The losses, in turn, can be represented as extra cost of the operation of the aero engine. The engine that is designed by the cook book method may well be able to fulfil the basic requirement, but will entail higher operational costs. For instance, in order to achieve the design goal, the less efficient engine consumes more fuel than the efficient one. The extra fuel consumption is necessary to generate extra energy to compensate for the high losses.

As an example, blading design will be elaborated. A blade has a function to increase pressure and consume power, or decrease pressure and produce power. It functions by turning the air flow. In the cook book approach, there are a series of blades that are available to choose from. The air flow through these types of blades have many undesirable features that generate high

losses. Those features can be minimized by design iteration of the empirical calculation and experimental verification. There are two disadvantages with this technological approach. The first is the growing cost of the experimental verification. The second is that the method does not provide blade geometry that guarantees low losses.

Computational Fluid Dynamics

The source of the limitation above is the inability of the empirical method to predict accurately the aerodynamic parameters such as pressure, velocity, etc. The accuracy of the prediction depends upon the ability to solve the aerodynamic equations. In figure-2.10, the internal flow pattern of an aero engine is shown to be very complex (Rolls-Royce Private Communication). Although all the flow phenomena can be simulated experimentally, it will be at very high cost. The aerodynamic physical nature in general is divided into viscous or inviscid flow, and high or low speed flow. The empirical method has sets of rules that are usually valid only in each of the flow regimes. The better way to obtain accurate solutions is to solve the aerodynamic equations.

The Computational Fluid Dynamics (CFD) technology provides methods to predict airflow characteristics by solving the aerodynamic equations. Some degree of approximation is still imposed because complete solution of the equations is still beyond the capability of

present day technology (Hussaini, 1988). In the early days, CFD was demonstrated by hand calculation. It is the advancement of computer technology, in terms of the memory size and computational speed that makes CFD technology attractive to the designers as a more advanced method. Use of this technology is a fast and cost effective way to obtain superior design.

The current development of CFD technology has reached a stage where the governing equations of the aerodynamics or Navier Stokes equations can be solved for practical applications in an industrial environment. Therefore, it is worthwhile to look back twenty years of development in CFD technology. There are four stages which are: linearized inviscid; nonlinear inviscid (Euler); Reynolds Average Navier Stokes; and full Navier Stokes (Hessemus, 1992). The linearized inviscid has been extensively used in an industrial environment for over two decades.

A limitation with this method is that it is acceptable only for low speed flow. If the flow speed is close to the speed of sound, the flow becomes more complex, and the validity of the linearized method is severely limited. The nonlinear inviscid method was developed to handle high speed flows. This method has already been used by the industry. For flow through very complex geometries such as turbine blade tips, the linear and nonlinear inviscid methods can not capture critical physical phenomena such as flow separation, etc.

The Reynolds Averaged Navier Stokes method is valid for either high or low speeds and is capable of computing flow through complex geometries. A very important phenomena in the flow which is turbulence, is not directly computed but is modelled. The accuracy of this method very much depends on the accuracy of the turbulence model. The accuracy of this model is restricted in range, and hence the accuracy of the Reynolds Averaged Navier Stokes methods is also restricted.

The full Navier Stokes method is, in principle, valid universally since the limitation due to the turbulence modelling is eliminated by directly computing the turbulence. This last method is still in the research stage because it demands high computational power. All of the methods from the linear inviscid through to the full Navier Stokes methods, represent degrees of approximation. According to Hessemus (1992), the numerical algorithms for the first three stages have already reached their full efficiency. The computer speed is the only limiting factor in order to reduce their CPU time.

The next generation of computer systems are based on parallel computing (Skerret, 1992). In such systems many small processors are arranged in parallel. This type of computer is capable of calculating vast amounts of data at high speed. The performance is achieved by distributing the computation among the many processors,

and carrying them out simultaneously.

Flow phenomena such as flow separation, that cannot be simulated by the inviscid methods, has to be complemented by the experimental methods. Since the more sophisticated methods, such as the Reynold Averaged Navier Stokes method, can simulate that kind of flow phenomena, the experimental methods are being replaced by CFD methods. As computers become more powerful, and the prediction methods become more reliable, the role of the CFD and experimental methods will gradually change with time. The time when the CFD method is considered as the main solver for the flow simulation, and the experimental method is considered as the verification means for the simulation result, is likely to be in the near future (figure-2.11).

Human Resource

Human resource capability is an essential part of technological capability and in general consists of users, or designers, code developers and system developers. The human resource capability is initiated by forming a core team. Its initial capability depends upon the educational background, training, and experience of the team members. If the team members have adequate educational background, but they do not have any experience, they will carry out the task of developing technology by using available methods. Those methods can be obtained from internal or external resources. The latter is third party software.

It is important that the team will try to define a task that can make a contribution to any existing project in the company. This will give them an opportunity to learn through practical problems. Since the objective of the project is to develop technology, the development task is initiated as soon as the required man power becomes available. The hardware will certainly be purchased from outside, but its maximum utilization needs time to build up through application. This part of the technological capability is the responsibility of the system developer.

The capability can be described by comparison between different teams. Team A, that has already achieved a certain level of capability, needs n time to accomplish an assignment. Team B, which has achieved a different level of capability, needs m time to accomplish the same assignment. If the m time is much longer than the n time, other issues will arise. The team B may have difficulty in achieving the objectives. The investment in man hours and other resources may exceed the savings and benefits that can be incurred when the team finally completes the project and provides the technology. If that is the case, the project objectives have to be adjusted.

2.6.3 Definition

Level of Current Aero Engine Technology

In the definition phase, technology base is defined according to the level of technology that is possessed by

a current aero engine company. The goal of design and development actually requires application of a Computer Aided Engineering (CAE) system in the aerothermodynamic design and analysis of all major aero engine components (Rolls-Royce Private Communication).

Computer Aided Engineering (CAE)

In the core of the CAE system is aerothermodynamic design and CFD methods. These methods cover basic aerothermodynamic design through CFD methods at the cutting edge of the technology. The technology base resulting from this project has to fulfil the requirement of the CAE. An example of an application is a compressor. It is an engine component that compresses incoming air to high pressure. The objective of the compressor blade design is to obtain a blade profile that turns the flow, and results in high pressure in the most efficient way, and does not suffer from any vibration and structural problems.

Methods

The basic method, or simple performance prediction method, is computationally cheap and provides a good result of a compressor system over a whole range of operating speed. The next level of sophistication is to use analytical methods based upon a quasi three dimensional method. This method is still cheap because it runs routinely on a general purpose computer. Due to the requirement for reduced cost, reduced design time, and higher performance, CFD methods to solve the Navier

Stokes equations are necessary. These cover steady and unsteady solutions, in two or three dimensions.

Software to facilitate interaction between the user and computational results are part of the technological capability. They consist of preprocessors and postprocessors. The preprocessor processes data from the geometry of the compressor to be compatible with the input of the CFD methods. The postprocessor processes data from the computational result, to be presented to users in a very easily interpreted form such as colour graphics. For other engine components, or other areas of application, the aerothermodynamic design and CFD method are similar.

2.6.4 Execution

In the execution phase, the building of the technology capability is carried out.

Core Team

The core personnel have already been recruited or are available. This phase is divided into five stages.

Stages

The stage where this phase can start depends upon the background education and experience of the personnel (see appendix - 2.1). At this phase, the number of people involved is higher than the number of people in earlier phases.

Practical Application

The activity in this phase is solving practical problems, modifying, adapting and creating technology.

If the necessary hardware is not available, it will have to be purchased in this phase. The practical problem is part of an existing project in the company which is relevant to the aero engine design. For instance, if the team is going to work in an aircraft design environment, the practical problem can be design, installation, etc. It is important to get involved in practical problems in order to keep pace with existing project demands, and make a real contribution to the company. During the project of developing the capability, the application to practical problems can be considered as an early financial return on investment.

Technology

A method of solution, or technology can often be obtained from published literature, but cannot usually be applied directly. Some of the information about the methods may be omitted because it is proprietary. Therefore, this type of method must be developed and modified based upon a large number of publications. Another type of technology such as the three dimensional Navier Stokes solver has to be created because little information about this technology is available in published literature.

2.6.5 Implementation

By the time this phase is reached, the team is fully capable and ready to take assignments from any aero engine projects in design and development. The project of developing technological capability is complete.

2.7 Conclusion

Collaboration in the aero engine industry is a strategy to overcome increasing costs and shrinking markets. In this situation well established companies may seek partners to share costs and expand into foreign markets. Such collaboration can provide an opportunity for local industry to gain access to technological expertise, and other skills, as the more established partners are able to acquire the necessary capital infusion to compete in the market.

Technology has an important role to play in collaborations since it may be that product requirements can only be fulfilled through the use of high technology. However, application of the technology will only be cost effective if a product, designed or produced using that technology, is able to fulfil its requirement at a reduced cost compared to conventional means.

Attempts to introduce high technology too early in the design process may not be successful since designers tend to prefer established methods. However, the failure to promptly introduce such technology may lead to uncompetitive products since, even if a product fulfils its end requirements, it may be uncompetitive due to excessive cost of design or production.

The opportunity to acquire technological skills may provide the new entrant in a collaboration with a resource of base technology or minimum technology and advanced technology. The technological skills can be

acquired through technological innovation, and participation in design, development, and research.

Therefore, the new entrant has to develop the technological capability from a minimum level at which it can be accepted as a partner. The development of technological skills may be accomplished through a strategic plan which will eventually provide capability at an advanced level acceptable to the competitive nature of a collaboration project.

The objectives of such a plan may be to acquire the design, development, and manufacturing capability for a certain proportion of an engine.

Since the process of developing technological capability is multidisciplinary, the project management technique, which manages those diciplines simultaneously, will save time in achieving the objective of developing Computational Fluid Dynamics Technology.

3.0 BACKGROUND

3.1 Introduction

The approach to solve the Navier-Stokes equation depends upon the numerical treatment of the time and spatial derivative in the equations. Since in this thesis, we are concerned only with the steady state solution, the time derivative can be set to zero or used to estimate the rate of convergence to the steady state solution. In these solutions, the spatial derivatives, which consist of convection and diffusion terms, are discretized by finite difference, finite element or finite volume methods.

The finite difference method is the oldest method first developed by Euler in 1768 (Hirsch, 1989). Its concept is based upon Taylor series expansion and the flow variables are approximated by values at grid points. The derivatives terms are replaced by differences over a small finite interval (Smith, 1978). Kuntz and Lashkminarayana (1992) used such finite difference method to compute two and three dimensional flows in turbomachinery cases.

With the finite element method, the flow region is divided into elements and a flow variable is prescibed within an element in terms of its nodal values. Numerical procedures such as the variational and weighted residual methods can then be used to compute the nodal values so that they satisfy the differential equations. This method was used by Whitehead (1972) to compute two dimensional cases, and later developed by Cedar (1985) to compute three dimensional cases. The choice of this method was

rather arbitrary, however, the element can be of irregular shape.

The finite volume method is based on the integration of the convection and diffusion terms over a cell which can have any arbitrary shape (in a complicated geometry). It preserves the properties of conservation (Peyret and Taylor, 1984). The flow variables can be stored at cell centres as proposed by Jameson et al (1981) or at cell vertices as proposed by Ni (1982). In cartesian coordinate systems, the finite volume approach will reduce to the finite difference method. This method also can be considered as a special case of the method of weighted residuals of finite element (Hirsch, 1989).

The resulting discretized equations can be solved by either pressure correction or time marching methods. The pressure correction method originates from an effort to solve the incompressible Navier-Stokes equations where the main dependent variables are pressure and velocity. (density cannot be used as the main dependent variable in an incompressible computation). Alternatively the pressure can be computed from the equation of state as in the case of the time marching method. At low speeds, however, the change of density becomes very small and therefore the density-pressure coupling becomes very weak.

Almost all of the pressure correction methods have their origins from SIMPLE (Simple Implicit Method for Pressure Linked Equations) scheme by Patankar and Spalding

(1972) and detail procedures can be found in the book by Patankar (1980). This scheme is based upon the steady state equation. However, Hirsch (1989) devised an unsteady development using explicit time integration. Alternative method proposed by McGuirk and Page (1990) implemented the unsteady equation but using (backward Euler) implicit time integration. This technique of integration will be explained later.

The basis of the pressure correction method involves an iterative procedure to solve for velocity and enthalpy for a given pressure from the linearized momentum and energy equations (Stow, 1989). In this method, the initial velocity derived does not satisfy the continuity equation, and thus has to be corrected. This correction is a function of the pressure field (hence pressure correction). This procedure is briefly described by Stow (1989), and Hirsch (1989) and the detail are elaborated by Connel (1983), Moore and Moore (1985), and Demirdzic et al (1993). Even though this method was originally developed for solutions of the incompressible flow, compressible flow extention have been developed by Karki and Patankar (1988), McGuirk and Page (1990), Demirdzic et al (1993), and Kobayashi and Pereira (1992). Its application to turbomachinery cases has been developed by Hah (1983) and Rhie (1986).

The alternative time marching method integrates the unsteady equations in time as well as space. The aim being to use natural transient process to obtain a steady

state solution. This solution is required as quickly as possible as integration does not have to be time accurate. The integration technique consists of either explicit or implicit methods.

The explicit method suffers from small time step in order to maintain stability during the iteration. It therefore needs large numbers of iterations to achieve convergence. However, it is easier to program and more amenable for parallel computation than the implicit method (Pierce, 1994). This last characteristic is important with the availability of parallel machines. Denton (1974) used such a method for blade-to-blade flows.

The implicit method can have larger time step therefore it needs fewer iterations to achieve convergence. However, the computational cost per time step is more expensive. In general, it is more difficult to program an implicit time marching procedure. This method was used by Beam and Warming (1976) and McDonnald and Briley (1975).

This thesis is concerned with the development of a particular code to better simulate internal flows. A much fuller description of this code is given by Ho (1992) and its application area includes flow through blades, intakes and nozzles as described by Stow (1989) and Hill and Langdell (1993). The code represents a compressible three dimensional implementation of the governing equations of fluid flow.

In this code, the unsteady Navier Stokes equations

are solved by an explicit time marching algorithm and use the cell centred finite volume discretization scheme of Jameson et al (1981). Evaluation of fluxes at cell face centres is approximated by straight averaging values at cell centres located on either side of the faces. In an arbitrary grid, the numerical solution suffers an accuracy problem because the approximated fluxes are not exactly located at the cell face centres. The spatial discretization used in this flow solver is central difference which has the disadvantage of admiting oscillations in the solutions. In order to damp out the oscillations, artificial dissipation is added to the equations but it can result in inaccuracy as shown by Pulliam (1986), Hirsch (1989, vol-I) and Swanson and Turkel (1992).

From the conservative form of the governing equation, the flux terms can be written as products of Jacobian matrices and state variables. The spatial discretization of the flux terms results in the discretization of the Jacobian matrices which results in a stability matrix. Real positive eigenvalues of this matrix indicate instabilities as explained by Eriksson (1985), Hirsch (1989,vol-I) and Santos (1993,1994) and in order to obtain stability, artificial dissipation has to be added to shift the eigenvalues to negative. Therefore, the eigenvalues act as a sensor to determine the dissipation required to maintain stability.

3.2 Governing Equations

The unsteady Navier-Stokes equations in three dimensions consist of the mass conservation equation, three momentum equations and an energy equation. In a relative frame of reference which is rotating about the x-axis with blade speed Ω, they are

$$\frac{\partial W}{\partial t} + \frac{\partial (F_i + F_v)}{\partial x} + \frac{\partial (G_i + G_v)}{\partial y} + \frac{\partial (K_i + K_v)}{\partial z} = S \qquad (3.2.1)$$

$$W = \begin{pmatrix} \rho \\ \rho u \\ \rho v \\ \rho w \\ \rho e \end{pmatrix} \quad F_i = \begin{pmatrix} \rho u \\ \rho u^2 + p \\ \rho uv \\ \rho uw \\ \rho uH \end{pmatrix} \quad F_v = \begin{pmatrix} 0 \\ -\tau_{xx} \\ -\tau_{xy} \\ -\tau_{xz} \\ -u\tau_{xx} - v\tau_{xy} - w\tau_{xz} + q_x \end{pmatrix}$$

$$G_i = \begin{pmatrix} \rho v \\ \rho uv \\ \rho v^2 + p \\ \rho vw \\ \rho vH \end{pmatrix} \quad G_v = \begin{pmatrix} 0 \\ -\tau_{yx} \\ -\tau_{yy} \\ -\tau_{yz} \\ -u\tau_{yx} - v\tau_{yy} - w\tau_{yz} + q_y \end{pmatrix} \quad K_i = \begin{pmatrix} \rho w \\ \rho wu \\ \rho wv \\ \rho w^2 + p \\ \rho wH \end{pmatrix}$$

$$K_v = \begin{pmatrix} 0 \\ -\tau_{zx} \\ -\tau_{zy} \\ -\tau_{zz} \\ -u\tau_{zx} - v\tau_{zy} - w\tau_{zz} + q_z \end{pmatrix} \quad S = \begin{pmatrix} 0 \\ 0 \\ \Omega^2 y + 2\Omega w \\ \Omega^2 z - 2\Omega v \\ 0 \end{pmatrix}$$

Description of the coordinate system is in figure-3.1

and

$$e = \frac{1}{1-\gamma}\frac{p}{\rho} + \frac{1}{2}(u^2 + v^2 + w^2) - \frac{1}{2}(\Omega^2 r^2)$$

$$H = \frac{\gamma}{1-\gamma}\frac{p}{\rho} + \frac{1}{2}(u^2 + v^2 + w^2) - \frac{1}{2}(\Omega^2 r^2)$$

The viscous stress, τ is a function of the flow effective viscosity and velocity derivatives. For laminar flow, the effective viscosity is calculated from Sutherland's law which relates the viscosity to absolute temperature (White, 1974). For turbulent flow, the

effective viscosity consists of both the laminar and turbulent (eddy's) viscosities which can be expressed as

$$\mu_e = \mu_L + \mu_T$$

The turbulent viscosity depends upon detail unsteady structures of the flow. Thus, fully turbulent flow can be calculated by solving the unsteady three dimensional Navier-Stokes equations. However, the time and length scales required vary very considerably. The length scales range from the size of the smallest eddies to the largest ones. The time step depends upon the size of these eddies and the kolmogorov velocity (Giles, 1992). In order to capture these fully, very fine mesh and very small time step are needed. In the current situation, it is only practical to compute the turbulence directly for very simple geometry such as a flat plate.

Therefore, almost all calculations resort to turbulence modelling by considering time averaged properties of the flow. Turbulence models can be classified according to the number of additional transport equation required for the turbulent parameter. The simplest model is the algebraic model first proposed by Cebeci and Smith (1974). It is based upon a two layer formula where the viscosity is calculated in the inner and outer layers. The viscosity in the inner layer involves the calculation of mixing length. The outer formulation requires the search for δ^*, the viscous layer thickness and U_e the velocity at the edge of the viscous layer.

Problems in determining δ^* and U_e led Baldwin and Lomax to develop an alternative algebraic model based on that of Cebeci Smith, but avoids the need to search for the edge of the boundary layer. Since the algebraic model does not need additional transport equation, it is often refered to as the zero equation model. It gives good result in attached flow but not in separated flow and in regions of boundary layer and shock interaction.

In k-l model, the mixing length is calculated from an algebraic expression and the local turbulent kinetic energy, k is computed from a transport equation. Since there is only one transport equation, this model is called one- equation model. The implementation of this model leads to improved flow prediction (Coupland, 1993). In k-ϵ model, the turbulent kinetic energy, k and the dissipation energy ϵ are computed from the corresponding transport equations. Since there are two tranport equations, this model is called two-equation model. This model can predict separation and improve three dimensional flow calculation (Hirsch, 1989).

The turbulence modelling used in this investigation is the mixing length model by Moore and Moore (1988) which is a modification of the Baldwin and Lomax model. Due to the grid spacing that can be afforded for a typical three dimensional case, the wall function is used (Birch, 1987 and Ho, 1992).

3.3 Discretization

The governing equations are discretized by a cell

centred finite volume scheme in which the system of equations is expressed as

$$\frac{\partial W}{\partial t}+\frac{\partial F}{\partial x}+\frac{\partial G}{\partial y}+\frac{\partial K}{\partial z}=S \qquad (3.3.1)$$

In integral form, equation (3.3.1) becomes

$$\frac{\partial}{\partial t}\int^{v} W dV+\int^{s}\overline{H}.\overline{n}dS=\int^{v} S dV \qquad (3.3.2)$$

where ,on the left hand side, the first integration is over a control volume V and second integration is over a control surface S, and n is unit outward normal to this surface, and

$$\overline{H}=(F_i+F_v)\hat{i}+(G_i+G_v)\hat{j}+(K_i+K_v)\hat{k} \qquad (3.3.3)$$

The second integral in equation (3.3.2) can be approximated as

$$\int^{s}\overline{H}.\overline{n}dS\simeq\sum_{p}\overline{H}_p.\overline{N}_p\Delta S_p \qquad (3.3.4)$$

Expanding the right hand side (figure-3.2)

$$\sum_{p}\overline{H}_p.\overline{N}_p\Delta S_p=\overline{H}_{i+\frac{1}{2},j,k}.\overline{N}_{i+\frac{1}{2},j,k}\Delta S_{i+\frac{1}{2},j,k}+\overline{H}_{i-\frac{1}{2},j,k}.\overline{N}_{i-\frac{1}{2},j,k}\Delta S_{i-\frac{1}{2},j,k}+$$

$$\overline{H}_{i,j+\frac{1}{2},k}.\overline{N}_{i,j+\frac{1}{2},k}\Delta S_{i,j+\frac{1}{2},k}+\overline{H}_{i,j-\frac{1}{2},k}.\overline{N}_{i,j-\frac{1}{2},k}\Delta S_{i,j-\frac{1}{2},k}+$$

$$\overline{H}_{i,j,k+\frac{1}{2}}.\overline{N}_{i,j,k+\frac{1}{2}}\Delta S_{i,j,k+\frac{1}{2}}+\overline{H}_{i,j,k-\frac{1}{2}}.\overline{N}_{i,j,k-\frac{1}{2}}\Delta S_{i,j,k-\frac{1}{2}} \qquad (3.3.4a)$$

where

$$\overline{N}_{i+\frac{1}{2},j,k}\Delta S_{i+\frac{1}{2},j,k}=\left(\Delta S_{i+\frac{1}{2},j,k}\right)_x\hat{i}+\left(\Delta S_{i+\frac{1}{2},j,k}\right)_y\hat{j}+\left(\Delta S_{i+\frac{1}{2},j,k}\right)_z\hat{k} \qquad (3.3.4b)$$

$$\overline{H}_{i+\frac{1}{2},j,k}=(F_i+F_v)_{i+\frac{1}{2},j,k}\hat{i}+(G_i+G_v)_{i+\frac{1}{2},j,k}\hat{j}+(K_i+K_v)_{i+\frac{1}{2},j,k}\hat{k} \qquad (3.3.4c)$$

All the variables and their first derivatives are stored at the cell centres. The viscous and heat fluxes in F_v ,G_v and K_v are evaluated at the face centres of each cell.

In the present code, the face centred values are evaluated from values of the neigbouring cell centres that are separated by that surface by straight averaging. For instance at face (i+1/2,j,k), flux H is approximated as

$$H_{i+\frac{1}{2},j,k} = \frac{H_{i+1,j,k} + H_{i,j,k}}{2} \qquad (3.3.4d)$$

From this formulation, the flux $H_{i+1/2,j}$ is geometrically located at the mid point between cell centre (i,j) and (i+1,j). In a non-uniform grid such as stretched and skewed grids, the mid point (i+1/2,j) is not necessarily located at the cell face centre (figure-3.3). This discrepancy generates inaccuracy.

In order to improve the accuracy, the fluxes should be evaluated at the cell face centre. Several proposals lead to different types of averaging which try to model the cell face values from the cell centre values and are described by Turkel (1986), Turkel, Yaniv, and Landau (1986) and Alimin (1994). These are analyzed in Chapter 4. It is essential that the scheme be formulated as compactly as possible in order not to incorporate unnecessary surrounding cells. Thus, spurious modes generated by the compact scheme can be kept to a minimum level. Also, any improved scheme proposed must not greatly increase the computational time.

3.4 Artificial Dissipation

Application of central differencing in the finite volume scheme above leads to oscillation in solutions which can occur near shocks because of the discontinuity

and in smooth regions because of odd-even decoupling. The last effect can be shown by the scheme in a one dimensional equation,

$$\frac{\partial u}{\partial t} + a\frac{\partial u}{\partial x} = 0 \qquad (3.4.1)$$

Integration of the above equation results in semi discretized equation

$$\frac{du}{dt} + a\frac{\left(u_{i+\frac{1}{2}} - u_{i-\frac{1}{2}}\right)}{\mathcal{L}} = 0 \qquad (3.4.2)$$

Applying straight averaging approximation in uniform grid it becomes

$$\frac{du}{dt} + a\frac{(u_{i+1} - u_{i-1})}{2\triangle x} = 0 \qquad (3.4.3)$$

Location of the discrete u is as follows

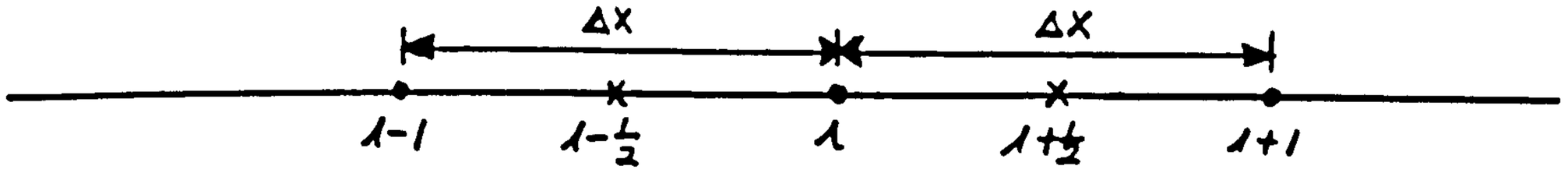

Since the flux is independent of the u_i, the variation of u does not depend on u_i itself. Then chequerboard solutions which in fact describes odd-even decoupling effects illustrated by the following figures satisfy the semi discretized equation obtained from the central difference implementation

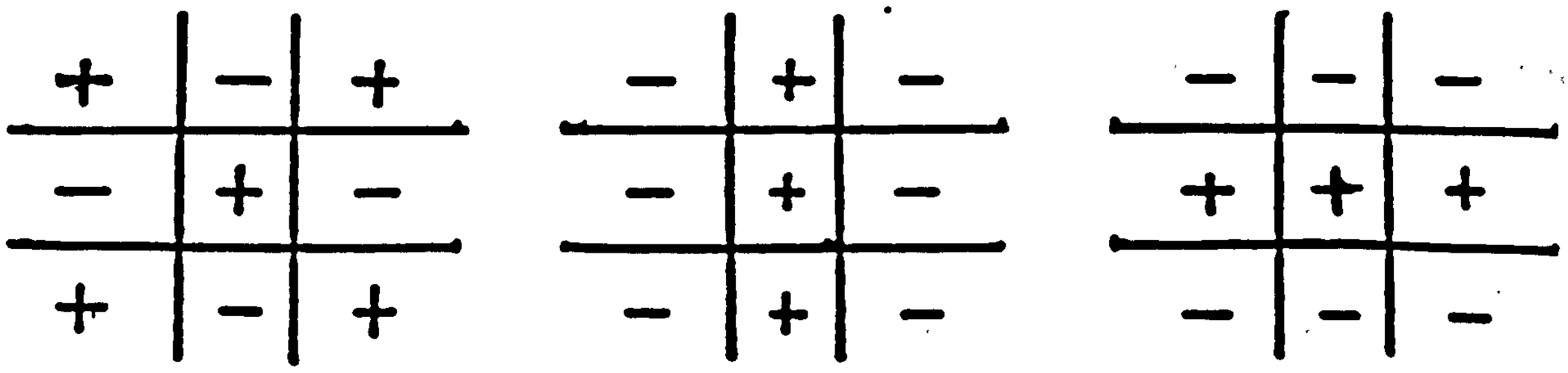

These solutions can be superimposed on a uniform flow and

each of them is a solution to the steady discrete equation as described by Giles (1992). The viscous discretization adopted does not provide sufficient coupling to damp the oscillations and in order to achieve this, artificial dissipation (which has to simulate physical viscosity) must be added, see Hirch (1989,vol-II) and Fletcher (1991,vol-I). In the Navier Stokes equation, the viscous terms actually generate diffusive effects which smooth out gradients of the flow properties as explained by Vemuri (1981). Since these terms contain second order derivatives, the artificial dissipation is formulated based upon even order derivatives, see Anderson (1984) and Fletcher (1991,vol-II). The dissipation model adopted is based on Jameson's scheme (1981) which consists of a blend of second and fourth order differences. This is also applied by others such as Swanson (1987) and Caughey (1988) where,

- A second order difference is nonzero near a shock and zero in any other regions.
- A fourth order difference is required in regions away from the shock and is zero near a shock (its use is motivated by dissipative character of the mathematical formulation).

The discretized equations with dissipation flux can be represented as

$$\frac{\partial W_{i,j,k}}{\partial t} + Q_{i,j,k} + V_{i,j,k} - D_{i,j,k} = 0 \qquad (3.4.4)$$

$Q_{i,j,k}$= inviscid flux

$V_{i,j,k}$= viscous flux

$D_{i,j,k}$= dissipation flux

where $D_{i,j,k} = D_\xi + D_\eta + D_\zeta$

and $D_\xi = d_{i+1/2,j,k} - d_{i-1/2,j,k}$ is the dissipation flux in the ξ - direction. The dissipation component in the ξ - direction is

$$d_{i+\frac{1}{2},j,k} = \left(\frac{Volume}{\Delta t}\right)_{i+\frac{1}{2},j,k} \{\epsilon^2_{i+\frac{1}{2},j,k}\left(W_{i+1,j,k} - W_{i,j,k}\right)$$

$$-\epsilon^4_{i+\frac{1}{2},j,k}\left(W_{i+2,j,k} - 3W_{i+1,j,k} + 3W_{i,j,k} - W_{i-1,j,k}\right)\} \qquad (3.4.5)$$

where

$$\epsilon^2_{i+\frac{1}{2},j,k} = K_2\{max\left(\delta_{i+1,j,k}, \delta_{i,j,k}\right)\}fm \qquad (3.4.5a)$$

$$\epsilon^4_{i+\frac{1}{2},j,k} = max\{0, fac_\xi K_4 - \epsilon^2_{i+\frac{1}{2},j,k}\} \qquad (3.4.5b)$$

$$\delta_{i,j,k} = \frac{|p_{i+1,j,k} - 2p_{i,j,k} + p_{i-1,j,k}|}{|p_{i+1,j,k} + 2p_{i,j,k} + p_{i-1,j,k}|} \qquad (3.4.5c)$$

$$fm = max\left(0, min\left(1, (Mach - 0.9)\,5\right)\right) \qquad (3.4.5d)$$

where Mach is Mach Number

$\delta_{i,j,k}$ is a pressure sensor

K_2 & K_4 are user specified constants

fac_ξ is anisotropic factor in ξ - direction,

$0 < fac_\xi < 1$

f_m is a local Mach number function

The dissipation components in the η and ζ directions are similarly defined. By using the Taylor expansion, the difference terms in equation (3.4.5) is written as

$$d_{i+\frac{1}{2},j,k} = \left(\frac{vol}{\Delta t}\right)_{i+\frac{1}{2},j,k} \{\epsilon^2_{i+\frac{1}{2},j,k} \Delta\xi \left(\frac{\partial W}{\partial \xi}\right)_{i+\frac{1}{2},j,k}$$

$$- \epsilon^4_{i+\frac{1}{2},j,k} 6 (\Delta\xi)^3 \left(\frac{\partial^3 W}{\partial \xi^3}\right)_{i+\frac{1}{2},j,k} \} \quad (3.4.6)$$

The expression for Δ t will be given later.

Therefore the terms which affect the dissipation are

1) Grid size $\Delta\xi$ (and $\Delta\eta$, $\Delta\zeta$)

   The size is determined by computational grid (figure-3.2) which varies across the region of the flow but it does not vary during the iteration.

2) Second order dissipation function (ϵ^2)

   This function determines the magnitude of second order dissipation which is required to capture a shock wave. It depends upon a constant K_2 and a pressure sensor parameter. In order to avoid switching on second order dissipation in regions of high accelerating flow for example around leading edge of turbine blade, the $\delta_{i,j,k}$ is multiplied by a local Mach number function (f_m)

3) Fourth order dissipation function (ϵ^4)

   This function determines the magnitude of fourth order dissipation which is required to damp out oscillations in regions of nearly uniform flow. It depends upon a constant K_4 and since the fourth order dissipation introduces overshoots near the shock, it has to be set to zero in that region.

4) Anisotropic Factors, fac_ξ (and fac_η , fac_ζ)

   This factor varies from zero to one which reduces the

fourth order dissipation in ξ - direction. Other similar factor such as fac_η and fac_ζ reduce the dissipation in the corresponding directions.

5) Scaling factor (vol/Δ t)

In three dimensions

$$\frac{vol}{\Delta t} = \frac{vol}{\Delta t_\xi} + \frac{vol}{\Delta t_\eta} + \frac{vol}{\Delta t_\zeta} \qquad (3.4.7)$$

where

$$\frac{vol}{\Delta t_\xi} = |uS_{\xi x}| + |vS_{\xi y}| + |wS_{\xi z}| + c\sqrt{S_{\xi x}^2 + S_{\xi y}^2 + S_{\xi z}^2} + \frac{2\mu}{\rho vol}(S_{\xi x}^2 + S_{\xi y}^2 + S_{\xi z}^2) \qquad (3.4.7a)$$

and $S_{\xi x}$ is the x-component of the surface area which has it. normal along the ξ - direction (figure-3.2). Other surface areas are defined accordingly. C is the speed of sound and vol is the volume of a cell. Along each direction, for instance, the ξ - direction the scaling factor (vol/Δ t_ξ) consist of a convective and a diffusive components.

The viscous component is given by

$$\left(\frac{vol}{\Delta t_\xi}\right)_v = \frac{2\mu}{\rho vol}(S_{\xi x}^2 + S_{\xi y}^2 + S_{\xi z}^2) \qquad (3.4.8)$$

and the convection component is given by

$$\left(\frac{vol}{\Delta t_\xi}\right) = |uS_{\xi u}| + |vS_{\xi y} + |wS_{\xi z}| + c\sqrt{S_{\xi x}^2 + S_{\xi y}^2 + S_{\xi z}^2} \qquad (3.4.9)$$

It can easily be shown in a cartesian coordinate system where ξ , η and ζ coincide with x,y and z respectively that the scaling factor in ξ - direction is

$$\frac{vol}{\Delta t_\xi} = |u\Delta\eta\Delta\zeta| + c\Delta\eta\Delta\zeta + \frac{2\mu}{\rho vol}(\Delta\eta\Delta\zeta)^2 \qquad (3.4.10)$$

It will be noted that (vol/Δ t) depends upon cell aspect ratio $\frac{\Delta\xi}{\Delta\eta}, \frac{\Delta\xi}{\Delta\zeta}, \frac{\Delta\eta}{\Delta\zeta}$ and it follows from equation (3.4.7a) that Δt_ξ can be interpreted as the maximum time required for physical information to propagate with physical speed across the grid in the ξ - direction and similarly in other directions.

6) Derivatives, $\frac{\partial^2 w}{\partial \xi^2}$ and $\frac{\partial^4 w}{\partial \xi^4}$ (and other directions)

The flow parameter derivatives depend on the magnitude of the flow parameter variation in each direction.

It will be clear from the foregoing analysis that each term in the expression of equation (3.4.5) makes a different contribution to the total dissipation. Three dimensional internal flow generally has grid sizes, cell aspect ratios and flow gradients which vary in all three directions. By appropriately formulating the dissipation terms, improved accuracy can be obtained in critical regions such as near walls, the blade leading edge, trailing edge and exit flows. Results of such treatment are discussed in chapter 5.

3.5 Eigenvalue Analysis

The time evolution of the semi discretized equation can be analyzed by computing the eigenvalues of the matrices derived from the spatial discretization. The influence of the dissipation on these eigenvalues will be studied for the purpose of dissipation reduction.

The analysis is applied to the governing equations of

the fluid flow. The Navier Stokes equation in two dimensions can be written as

$$\frac{\partial q}{\partial t} + \frac{\partial F}{\partial x} + \frac{\partial G}{\partial y} = 0 \qquad (3.5.1)$$

where q, F and G terms are two dimensional version of the terms given in section 3.2

In finite volume formulation, the semi-discretized equation (3.5.1)

becomes

$$A\frac{\partial q_{i,j}}{\partial t} + \sum_{p=1}^{4} \overline{H}_p . \overline{N}_p \Delta S_p = 0 \qquad (3.5.2)$$

where A is the cell area and $q_{i,j}$ is the state variable at cell centre (i,j) and the summation term is the two dimensional version of equation (3.3.4a)

At cell face (i+1/2.j)

$$\overline{H}_{i+\frac{1}{2},j} . \overline{N}_{i+\frac{1}{2},j} \Delta S_{i+\frac{1}{2},j} = \left(F_{i+\frac{1}{2},j} \Delta S_{i+\frac{1}{2},j}\right)_x + \left(G_{i+\frac{1}{2},j} \Delta S_{i+\frac{1}{2},j}\right)_y \qquad (3.5.3)$$

and the flux F consists of

$$F = F_I + F_V$$

F_I and F_V stand for inviscid and viscous parts of the vector F respectively. Vector G is similarly defined.

With Jacobian matrices, the inviscid vector F_I and G_I can be written as

$$F_I = A\ q \qquad \text{and} \qquad G_I = B\ q \qquad (3.5.4a)$$

and the viscous vector F_V and G_V can be written as

$$F_V = C\ q \qquad \text{and} \qquad G_V = D\ q \qquad (3.5.4b)$$

Matrices A, B, C and D are defined in appendix-3.1 and the derivation presented above wil be further elaborated in chapter 6. Substituting equation (3.5.4a) and (3.5.4b)

into equation (3.5.3) and applying straight averaging $q_{i+1/2,j} = (q_{i+1,j} + q_{i,j})/2$ provides

$$\overline{H}_{i+\frac{1}{2},j}.\overline{N}_{i+\frac{1}{2},j}\Delta S_{i+\frac{1}{2},j} = (A+C)_{i+\frac{1}{2},j}\, q_{i+\frac{1}{2},j}\,(\Delta S_x)_{i+\frac{1}{2},j}$$

$$+(B+D)_{i+\frac{1}{2},j}\, q_{i+\frac{1}{2},j}\,(\Delta S_y)_{i+\frac{1}{2},j} \qquad (3.5.5)$$

Similar expression can be derived for the other faces and the fluxes at cell faces can be substituted back into equation (3.5.2). Then, the semi-discretized equation (3.5.2) can be written as

$$\frac{dq_{i,j}}{dt} = - M_G\, q_{i,j} + R_G \qquad (3.5.6)$$

where M_G is a matrix which governs the stability of equation (3.5.1) at semi-discretized level and R_G contains nonhomogenous terms. This matrix has the size 16 x n x n where n is the number of grid points and evaluating its eigenvalues can consume considerable computational time. By using an approximate explicit formulation which does not take into account the effect of the neighbouring grid points (i+1,j) ,(i-1,j), (i,j+1), and (i,j-1) the stability of the semi descritized equation (3.5.2) can be analyzed locally using 4 x 4 matrix as Santos (1993, 1994) had shown. The resulting equation is written as

$$A\frac{dq_{i,j}}{dt} = -M_J q_{i,j} + R_J \qquad (3.5.7)$$

where $M_J = \sum_{p=1}^{4}(A_p + B_p)\Delta S_{xp} + (B_p + D_p)\Delta S_{yp}$ 3.5.7a)

p is at cell face

R_J contains terms that belongs to neighbouring

cells and nonhomogenous terms.

S_{xp} and S_{yp} are x and y components of face area at p

The eigenvalues of matrix M_j are, in general, complex. Positive real eigenvalues indicate that $q_{i,j}$ grows without bound so that the semi discretized equation (3.5.2) is unstable. In order to achieve a stable solution, artificial dissipation has to be added so that all eigenvalues will be negative on convergence. Then equation (3.5.1) becomes

$$\frac{\partial q}{\partial t} + \frac{\partial F}{\partial x} + \frac{\partial G}{\partial y} + \frac{\partial D}{\partial x} + \frac{\partial D}{\partial y} = 0 \qquad (3.5.8)$$

where D is the dissipation vector. This formulation is discussed in section 3.4. The dissipation is the summation of the second and fourth order difference of the state variable which contain $q_{i,j}$ and its neighbours such as $q_{i+1,j}$, $q_{i-1,j}$, $q_{i,j+1}$ and $q_{i,j-1}$. Using the approximate formulation the dissipation effect is locally analyzed and can be formulated as

$$D = M_D\, q_{i,j} + R_D \qquad (3.5.9)$$

where M_D = matrix coefficient

R_D = term with neighbouring cells

The addition of matrix coefficient M_D to the Jacobian matrix contributes to the diagonal element only. The stability matrix then becomes,

$$M_T = M_J + M_D \qquad (3.5.10)$$

and

$$M_D = \{(-2\epsilon_\xi^2 + 6\epsilon_\xi^4) + (-2\epsilon_\eta^2 + 6\epsilon_\eta^4\} I \qquad (3.5.10a)$$

where $$\epsilon_{\xi}^{2} = \left(\frac{vol}{\Delta t}\right)_{i+\frac{1}{2},j} \epsilon_{i+\frac{1}{2},j}^{2} - \left(\frac{vol}{\Delta t}\right)_{i-\frac{1}{2},j} \epsilon_{i-\frac{1}{2},j}^{2} \qquad (3.5.10b)$$

I = Identity Matrix

and where ϵ_{ξ}^{4}, ϵ_{η}^{2} and ϵ_{η}^{4} are similarly defined and are two dimensional versions of equation (3.4.5a) and (3.4.5b)

Since the eigenvalues provide information about the stability of the system, the effect of artificial dissipation can be examined. The plan is to selectively reduce the dissipation at each grid point during iterations without violating the stability condition. This condition is fulfilled by ensuring the eigenvalues remain negative on convergence. This will be discussed in chapter 6.

3.6 Summary

A numerical method to solve and analyze the unsteady Navier Stokes equations has been briefly described. The governing equations in three dimensions in a rotating coordinate system is elaborated. The space discretization is a cell centred finite volume scheme. The required cell face centre value is approximated by straight averaging the cell centre values which are located on either sides of that face. Inaccuracy is generated in arbitrary grids because the resulting value from straight averaging is not necessarily located at the cell face centres. Improved schemes which approximate the values directly at the cell face centre and are as compact as possible with reasonable computational time will be discussed in chapter 4.

Since the central difference scheme admits an oscillatory solution, artificial dissipation is applied to suppress oscillations near shocks due to discontinuity and in smooth regions due to odd-even decoupling. The dissipation model proposed is a blend of second and fourth order differences. The magnitude of the dissipation throughout the flow region depends upon variations of flow parameters, grid size and cell aspect ratio. A proposed improved model developed in chapter 5 will take advantage of these variations in order to reduce the dissipation.

The eigenvalue analysis of the Jacobian matrix extracted from the spatial discretization provides information about the stability limit of the semi discretized equations. Since the eigenvalues depend upon the magnitude of the artificial dissipation, they can be used to check the effect of the dissipation on the stability. The aim is to selectively reduce the artificial dissipation at each grid point during the iteration in order to improve accuracy whilst maintaining stability.

4.0 DISCRETIZATION

4.1 Introduction

The numerical solution of the partial differential equations of fluid flow such as the Navier-Stokes equations at grid points within the flow domain requires spatial discretization of the terms. The current investigation of the spatial discretization concentrates on accuracy improvement of the explicit time marching method based on the cell centre finite volume method of Jameson et al (1981) and discussed in chapter 3.

In the finite volume scheme, the partial differential equations are converted into ordinary differential equations by integrating the flux terms, which are the spatial derivatives, over the cell surfaces. The flux contributions are obtained by the evaluation of those terms on the surfaces. In the cell centred scheme, the values on the surfaces are calculated by an approximation formulae involving cell centre values. With the current procedure these values are found by averaging the values at the cell centres located on either side of the surfaces.

With a uniform grid, this approximation produces the fluxes at the centre of the cell faces. In general, however, the grid will be distributed nonuniformly throughout the flow field because of the geometric complexity of the body over which the flow is computed. The nonuniformity in general can be described by stretching, skewing and shearing of the grid lines. With

general grids, the straight averaging approximation generates errors since the resulting values are not located at the centre of the cell faces. The errors can affect the stability and accuracy of the computed solution.

This phenomena is elaborated in a study of discretization errors by Rossow, Kroll, Radespiel and Scherr (62nd AGARD), Turkel, Yaniev and Landau (1986), and Turkel (1986). Rossow (62nd AGARD) investigated the accuracy of the cell centre and cell vertex methods. He showed that with the cell centre scheme, grid refinement can reduce the error from grid stretching but it does not reduce those from grid skewness. In contrast, with the cell vertex scheme, since the flow variables are evaluated at the cell vertices, the effect of the skewness can be incorporated into the scheme with no additional errors.

Turkel, Yaniev and Landau (1986) used the cell centre scheme and implemented a more accurate formula than the straight averaging one to evaluate the flux terms on the cell faces. The improvement introduced was to use linear interpolation taking into account the distance between cell centres and the cell faces. Turkel (1986) produced an extensive analysis of the effects of various schemes for arbitrary grids in one dimension. He arrived at formulations based upon linear interpolation that related grid stretching to stability by using the Von Neumann method. Skewness was not incorporated in this analysis because it is essentially a two or three dimensional

effect. Steger (1981) investigated a straight averaging approximation in finite difference scheme. He concluded that the resulting accuracy is sensitive to grid skewing and strecthing.

On the application side, various discretization schemes have been used by Martinelli (1987), Holmes and Tongs (1985), Arnone and Swanson (1993), Kuntz and Lakshminarayana (1992) , and Cheng (1992) in two and three dimensional flow. Martinelli (1987) proposed a discretization for the cell centre scheme based upon Gauss's theorem. In two dimensions, the discretization requires nine neighbouring points for the viscous flux evaluation. Since the formulation of the discretization incorporates values at grid points, it takes into account the grid skewness. The scheme of Holmes and Tongs (1985) did not take the nonuniformity of the grid into account. The discretization in the cell centred scheme by Arnone and Swanson(1993) used straight averaging for the inviscid terms and followed Martinelli's discretization scheme for the viscous terms. Kuntz and Lakshminarayana (1992) used the finite difference method and evaluated the fluxes by straight averaging. For the viscous flux evaluation, Cheng(1992) formulated the discretization in the cell centre scheme using four neighbouring cells in two dimensions and six neighbouring cells in three dimensions. It is the most compact scheme, however, the grid skewness was not taken into account.

The main emphasis of the present work is in the discretization of the viscous terms. It starts by reviewing the discretization schemes of Martinelli (1987) and Cheng (1992) which have been elaborated above. The straight averaging approximation used in the current scheme will be analyzed. In addition, the linear interpolation approximation will also be analyzed to understand the improvements that this offers. An improved discretization scheme that takes into account the grid stretching, skewing and shearing will be formulated and analyzed

Based upon the truncation error expressions, the impact of the flow gradient, grid expansion and grid size on the error from the grid will be studied. This provides the means to reduce the error by modifying the grid. Therefore, grid modification is an alternative to adopting an improved scheme. The investigation continues with a stability analysis that includes time step discretization which concentrates on a discussion of mesh Reynolds number. In order to broaden the research into spatial discretization, the cell vertex scheme based upon the work of other researchers is reviewed. Besides reviewing the work of Matinelli and Cheng, details of each topic of the investigation are elaborated in the following sections.

4.2 Other Schemes

Other available spatial discretization methods for the cell centre scheme that are discussed in this chapter are those proposed by Martinelli (1987) and Cheng (1992).

This section will concentrate on the discretization of the viscous flux only.

4.2.1 Martinelli's Scheme

In two dimensions, by using Gauss theorem, the derivative can be obtained from

$$\int^{s} \frac{\partial f}{\partial x} ds = \oint^{os} f(x,y)\, ds \qquad (4.2.1)$$

where S is the area and S is the boundary or contour

In discrete form, it is

$$\left(\frac{\partial f}{\partial x}\right)_{i,j} S_{i,j} = \frac{1}{2}\{\sum_{k=1}^{4} (f_{k+1} + f_k)(y_{k+1} - y_k)\} \qquad (4.2.2)$$

The given values are f_k where k is the index of cell face.

In the implementation of this theorem, Martinelli proposed two methods where the integration is performed over two different types of control volumes. In the first method, the control volume is bounded by two cell vertices and two cell centres and f_k are values at those locations (figure-4.1a). The integration path is along the boundary of that control volume with the resulting derivatives directly approximated at the cell face centres. This method requires averaging cell centre values to obtained the f_k at the two cell vertices.

In the second method, the derivatives at the face centres are calculated from the average of the derivatives at the edges of the face located at the cell vertices (figure-4.1b). The derivatives at the cell vertices in turn are calculated by the Gauss theorem around two

control volumes. These are formed by lines joining the cell centres that surround each of the those two cell vertices (figure-4.1.b).

Since in this scheme the cell vertex variables are included in the calculation of the derivatives, this scheme is more accurate for skewed grids than the straight averaging scheme. It is a nine point scheme in two dimensions.

4.2.2 Cheng Scheme

This scheme calculates the flow derivatives at the cell faces directly from the values at the neighbouring cell centers and stores the results at cell corners. The flow derivatives, for instance, is

$$\left(\frac{\partial u}{\partial x}\right)_{i+\frac{1}{2},j,k} = \frac{u_{i+1,j,k} - u_{i,j,k}}{\Delta x} \qquad (4.2.3)$$

In an arbitrary grid, this scheme suffers inaccuracy because the derivatives at cell faces are obtained from straight averaging of the stored values at cell corners. It is five point scheme in two dimensions and seven point scheme in three dimensions, therefore it is a more compact scheme than Martinelli's scheme.

4.3 Analysis of the Discretization Scheme

Analysis of the standard discretization scheme for a nonuniform grid is carried out in two dimensions using a scalar convection equation, which is, as follows,

$$\frac{\partial u}{\partial t} + a\frac{\partial u}{\partial x} + b\frac{\partial u}{\partial y} = 0 \qquad (4.3.1)$$

where u is a parameter and a and b are convective velocity

components. In the integral formulation

$$\frac{d}{dt}\int^{S} udA + \int^{AB} + \int^{BC} + \int^{CD} + \int^{DA} (audy - budx) = 0 \qquad (4.3.2)$$

(figure-4.2) where A is cell area

Evaluating the surface integral by the midpoint rule

$$\int^{AB} + \int^{BC} + \int^{CD} + \int^{DA} (audy - budx) = \qquad (4.3.3)$$

$$\left(u_{i+\frac{1}{2},j} - u_{i-\frac{1}{2},j}\right)(ay_{AB} - bx_{AB}) + \left(u_{i+\frac{1}{2},j} - u_{i-\frac{1}{2},j}\right)(-ay_{BC} + bx_{BC})$$

where the grid lines are sheared but locally parallel (figure-4.2).

Thus, the semi discretized equation is

$$A\frac{du_{i,j}}{dt} + \left(u_{i+\frac{1}{2},j} - u_{i-\frac{1}{2},j}\right)(ay_{AB} - bx_{AB}) + \left(u_{i,j+\frac{1}{2}} - u_{i,j-\frac{1}{2}}\right)(-ay_{BC} + bx_{BC}) = 0 \qquad (4.3.4)$$

For a nonsheared grid the semi discretized equation is

$$\frac{du_{i,j}}{dt} + a\frac{\left(u_{i+\frac{1}{2},j} - u_{i-\frac{1}{2},j}\right)}{h_i} + b\frac{\left(u_{i,j+\frac{1}{2}} - u_{i,j-\frac{1}{2}}\right)}{l_j} = 0 \qquad (4.3.5)$$

where $A=h_i l_j$, $Y_{AB}=l_j$, $x_{AB}=0$, $Y_{BC}=0$, $x_{BC}=h_i$

The following analysis uses the von Neumann and Equivalent Partial Differential Equation (EPDE) methods to investigate the effects of the truncation error for different types of grid non-uniformity, including stretching and skewing.

Von Neumann Method

The Von Neumann method is an available tool to estimate the accuracy and stability of a linear scalar equation. This method represents a solution $u_{i,j}$ as a Fourier series

$$u^n_{i,j} = \sum_{x_x, x_y} V^n e^{Ix_x x_{i,j}} e^{Ix_y y_{i,j}} \qquad (4.3.6)$$

where $I = \sqrt{-1}$

$x_{i,j}$ and $y_{i,j}$ are grid points

χ_x and χ_y are wave numbers in the x and y directions

v^n is the time dependent amplitude

n is time step level

Since the analysis is at semi discretized level, the time index n is dropped and the amplitude is normalized to one. The real and imaginary parts represent the dissipative and oscillatory parts of $u_{i,j}$ respectively.

Considering each term in the series separately, the parameter $u_{i,j}$ becomes

$$u_{i,j} = e^{I(\chi_x x_{i,j} + \chi_y y_{i,j})} \qquad (4.3.7a)$$

In trigonometric terms this becomes

$$u_{i,j} = cos(\chi_x x_{i,j} + \chi_y y_{i,j}) + I sin(\chi_x x_{i,j} + \chi_y y_{i,j}) \qquad (4.3.7b)$$

This method will be applied in the following sections.

<u>Equivalent Partial Differential Equation Method (EPDE)</u>

The Von Neumann method does not directly provide the order of the truncation error. In order to obtain the order of the error, the trigonometric functions in equation (4.3.7b) have to be expanded and high order terms neglected. On the other hand, the EPDE method will directly provide the order of the truncation error.

This method uses Taylor expansions of the various terms in the neighbourhood of the grid (i,j), see Hirsch (1989). From this, the truncation error can be expressed

as a summation of derivative terms which in general can be written as

$$TRUNCATION\quad ERROR=\sum_{i=1}^{\infty}\left(c_i\frac{\partial^i u}{\partial\xi^i}+d_i\frac{\partial^i u}{\partial\eta^i}+e_i\frac{\partial^i u}{\partial\zeta^i}\right) \qquad (4.3.8)$$

where c_i,d_i and e_i depends upon parameters of the grid nonuniformity such as grid size, skewed angles, etc. and which represent the order of the accuracy.

4.3.1 Straight Averaging

Refering to equation (3.3.4d) section 3.3, the cell face value in the current version is approximated as

$$u_{i+\frac{1}{2},j}=\frac{u_{i+1,j}+u_{i,j}}{2} \qquad (4.3.9)$$

In an arbitrary grid, $u_{i+1/2,j}$ is not necessarily located at the cell faces. Since the finite volume scheme approximates flux derivatives by taking the differences of the fluxes on the cell faces, this discrepancy will introduce an error.

4.3.1.1 Von Neumann Method

The application of the Von Neumann method to the straight averaging approximation results in the following expression for $u_{i+1/2,j}$

$$u_{i+\frac{1}{2},j}=\frac{u_{i,j}}{2}\{1+cos\chi_x\,(x_{i+1,j}-x_{i,j})+Isin\chi_y\,(y_{i+1,j}-y_{i,j})\} \qquad (4.3.10)$$

and $u_{i-1/2,j}$,$u_{i,j+1/2}$ and $u_{i,j-1/2}$ are similarly evaluated.

Uniform Cartesian Grid

For uniform cartesian grid, $u_{i+1/2,j}$, $u_{i-1/2,j}$,

$u_{i,j+1/2}$ and $u_{i,j-1/2}$ are exactly located at cell faces (figure-4.3). Substituting the expression for $u_{i+1/2,j}$ from equation (4.3.10) and others into equation (4.3.5), it becomes

$$\frac{du_{i,j}}{dt} + Iu_{i,j}[a\frac{sin\chi_x h_i}{h_i} + b\frac{sin\chi_y l_j}{l_j}] = 0 \qquad (4.3.11)$$

The solution is

$$u_{i,j} = constant \quad e^{I\omega_i t} \qquad (4.3.11a)$$

where

$$\omega_i = a\frac{sin\chi_x h_i}{h_i} + b\frac{sin\chi_y l_j}{l_j} \qquad (4.3.11b)$$

This generates a dispersive error which results in oscillatory solutions in the x and y directions. This error is due to odd even decoupling found with the central difference scheme.

<u>Straight Stretched Grid</u>

Since the grid will not in general be equally spaced, we write

$$x_{i+1,j} - x_{i,j} = \frac{h_{i+1} + h_i}{2} \qquad (4.3.12)$$

The other directions are defined simlilarly (figure-4.4) This will be substituted to equation (4.3.10). Let us define flux in x direction as

$$F_i = \frac{u_{i+\frac{1}{2},j} - u_{i-\frac{1}{2},j}}{h_i} \qquad (4.3.13)$$

where $u_{i+1/2,j}$ is calculated based upon equation (4.3.9) and $u_{i-1/2,j}$ is similarly derived. Substituting $u_{i+1/2,j}$ and $u_{i-1/2,j}$ into equation (4.3.13) and after

simplification, the flux becomes

$$F_i = -\frac{au_{i.j}}{h_i}[sin(\chi_x h_i)\left(cos\chi_x\left(\frac{h_{i+1}-2h_i+h_{i-1}}{4}\right)\right)sin(\chi_x)\left(\frac{h_{i+1}-h_{i-1}}{4}\right)+$$

$$cos(\chi_x h_i)\left(sin\chi_x\left(\frac{h_{i+1}-2h_i+h_{i-1}}{4}\right)\right)sin\chi_x\left(\frac{h_{i+1}-h_{i-1}}{4}\right)]$$

$$I\frac{au_{i.j}}{h_i}[sin(\chi_x h_i)\left(cos\chi_x\left(\frac{h_{i+1}-2h_i+h_{i-1}}{4}\right)\right)cos\chi_x\left(\frac{h_{i+1}-h_{i-1}}{4}\right)+$$

$$cos(\chi_x h_i)\left(sin\chi_x\left(\frac{h_{i+1}-2h_i+h_{i-1}}{4}\right)\right)cos\chi_x\left(\frac{h_{i+1}-h_{i-1}}{4}\right)] \qquad (4.3.14)$$

In order to interpret equation (4.3.14), a Taylor expansion about cell i is applied to the terms in the bracket. The flux F_i then becomes

$$F_i = Iau_{i,j}\{\chi_x + \chi_x\left(\frac{h_{i+1}-2h_i+h_{i-1}}{4h_i}\right)+O(h)\} \qquad (4.3.15)$$

A similar derivation can be carried out for flux in y direction.

In a quasi uniform grid where the grid ratio is

$$\frac{h_{i+1}}{h_i} = 1+O(h) \qquad (4.3.16)$$

the term

$$\frac{h_{i+1}-2h_i+h_{i-1}}{h_i} = O(h) \qquad (4.3.17)$$

and total flux term reduces to

$$F = Iu_{i,j}(a\chi_x + b\chi_y) \qquad (4.3.18)$$

as grid size reduces to zero.

Thus, for a quasi uniform grid, straight averaging results in a consistent discretization scheme.

In exponential grid where grid ratio is

$$\left(\frac{h_{i+1}}{h_i}\right)\Big/\left(\frac{h_i}{h_{i-1}}\right) = 1 + O(h) \qquad (4.3.19)$$

the term

$$\frac{h_{i+1} - 2h_i + h_{i-1}}{h_i} \neq O(h) \qquad (4.3.20)$$

and is not reduced to zero as the grid size reduces to zero. Thus, for an exponential grid, the fluxes in the x and y directions contain additional terms showing that the straight averaging approximation is inconsistent. Substituting these fluxes into the semi discretized equation, the additional terms generate oscillations because they represent imaginary parts of the Fourier series terms.

<u>Skewed Stretched Grid</u>

With this type of grid, the analysis using the Von Neumann method is not attempted because the geometric variables that represent the grid skewness such as skew angle, etc are not easily incorporated into the flux expressions. However, a study will be carried out using the EPDE method in the next section.

<u>4.3.1.2 Equivalent Partial Differential Equations</u>

With this method, $u_{i+1,j}$ is expanded as a Taylor series about (i,j) which is, as follows,

$$u_{i+1,j} = u_{i,j} + (x_{i+1,j} - x_{i,j}) \left(\frac{\partial u}{\partial x}\right)_{i,j} + \frac{(x_{i+1,j} - x_{i,j})^2}{2} \left(\frac{\partial^2 u}{\partial x^2}\right)_{i,j} + O(h^3) \quad (4.3.21)$$

$u_{i+1/2,j}$ is evaluated by substituting $u_{i+1,j}$ into equation (4.3.9) which leads to

$$u_{i+\frac{1}{2},j} = u_{i,j} + \left(\frac{x_{i+1,j} - x_{i,j}}{2}\right) \left(\frac{\partial u}{\partial x}\right)_{i,j} + \frac{(x_{i+1,j} - x_{i,j})^2}{4} \left(\frac{\partial^2 u}{\partial x^2}\right)_{i,j} + O(h^3) \quad (4.3.22)$$

and $u_{i-1/2,j}$, $u_{i,j+1/2}$ and $u_{i,j-1/2}$ are similarly evaluated.

<u>Uniform Cartesian Grid</u>

Since the grid is equally spaced

$$x_{i+1,j} - x_{i,j} = h_i \quad (4.3.23)$$

Subsituting this into equation (4.3.22) and using a similar derivation for $u_{i-1/2,j}$, the flux in the x - direction will be

$$\frac{u_{i+\frac{1}{2},j} - u_{i-\frac{1}{2},j}}{h_i} = \left(\frac{\partial u}{\partial x}\right)_{i,j} + \frac{h_i^2}{3} \left(\frac{\partial^3 u}{\partial x^3}\right)_{i,j} + O(h^4) \quad (4.3.24)$$

The flux in y direction is similarly derived. Substituting the fluxes in x and y directions into equation (4.3.5), the equivalent partial differential equation becomes

$$\frac{\partial u_{i,j}}{\partial t} + a\left(\frac{\partial u}{\partial x}\right)_{i,j} + b\left(\frac{\partial u}{\partial y}\right)_{i,j} = -a\frac{h_i^2}{3} \left(\frac{\partial^3 u}{\partial x^3}\right)_{i,j} - b\frac{l_j^2}{3} \left(\frac{\partial^3 u}{\partial y^3}\right)_{i,j} + O(h^4, l^4) \quad (4.3.25)$$

The lowest order term of the truncation error has odd

derivatives of $u_{i,j}$ and is second order in h_i. This generates a dispersive error which results in an oscillatory solution. It reaches the same conclusion as the analysis with Von Neumann method but in addition the order of the error can be estimated.

Straight Stretched Grid

The grid spacing is the same as that given ealier which is

$$x_{i+1,j} - x_{i,j} = \frac{h_{i+1} + h_i}{2} \tag{4.3.26}$$

By following a similar derivation as in the case with the cartesian grid, the flux in the x - direction will be

$$\frac{u_{i+\frac{1}{2},j} - u_{i-\frac{1}{2},j}}{h_i} = \left(\frac{\partial u}{\partial x}\right)_{i,j} + \left(\frac{h_{i+1} - 2h_i + h_{i-1}}{4h_i}\right)\left(\frac{\partial u}{\partial x}\right)_{i,j} + \left(\frac{h_{i+1} - 2h_i + h_{i-1}}{8h_i}\right)\left(\frac{h_{i+1} - h_{i-1}}{2}\right)\left(\frac{\partial^2 u}{\partial x^2}\right)_{i,j} + O\left(h^3\right) \tag{4.3.27}$$

A similar derivation can be carried out for the flux in the y - direction. The lowest order term in the equivalent partial differential equation now contains a coefficient

$$\left(\frac{h_{i+1} - 2h_i + h_{i-1}}{4h_i}\right) \tag{4.3.28}$$

This is the same as that found in the analysis by the Von Neumann method. Thus, the EPDE method gives the same result as the Von Neumann method where the truncation error generates oscillations.

Skewed Stretched Grid

Figure-4.5 illustrate the grid being considered. From equation (4.3.9), the value $u'_{i+1/2,j}$ is expanded as

a Taylor series about (i,j) to give

$$u'_{i+\frac{1}{2},j} = u_{i,j} + \left(\frac{h'_{i+1} + h'_i}{2}\right)\left(\frac{\partial u}{\partial \xi}\right)_{i,j} + \frac{\left(h'_{i+1} + h'_i\right)^2}{4}\left(\frac{\partial^2 u}{\partial \xi^2}\right)_{i,j} + O\left(h^3\right) \quad (4.3.29)$$

but this value is not the one that goes into the flux evaluation in equation (4.3.5). In order to obtain $u_{i+1/2,j}$ from $u'_{i+1/2,j}$, $u_{i+1/2,j}$ is expanded about (i+1/2,j)' which is

$$u_{i+\frac{1}{2},j} = u'_{i+\frac{1}{2},j} - \left(\frac{h'_{i+1} + h'_i}{4}\right) sin\alpha \left(\frac{\partial u}{\partial \xi}\right)'_{i+\frac{1}{2},j} + O\left(h^2\right) \quad (4.3.30)$$

Subsituting equation (4.3.29) into equation (4.3.30), the result of a Taylor series expansion of $u_{i+1/2,j}$ about (i,j) is as follows,

$$u_{i+\frac{1}{2},j} = u_{i,j} + \left(\frac{h'_{i+1} + h'_i}{4}\right)\left(\frac{\partial u}{\partial \xi}\right)_{i,j} - \left(\frac{h'_{i+1} + h'_i}{4}\right) sin\alpha \left(\frac{\partial u}{\partial \eta}\right)_{i,j}$$

$$- \frac{\left(h'_{i+1} + h'_i\right)^2}{8} sin\alpha \left(\frac{\partial^2 u}{\partial \xi \partial \eta}\right)_{i,j} + O\left(h^2\right) \quad (4.3.31)$$

The flux of $u_{i-1/2,j}$ is derived accordingly.

The total flux in the ξ - direction is

$$\frac{u_{i+\frac{1}{2},j} - u_{i-\frac{1}{2},j}}{h_i} = \left(\frac{\partial u}{\partial \xi}\right)_{i,j} + \left\{\left(\frac{h'_{i+1} - 2h_i + h_{i-1}}{4h_i}\right) + \left(\frac{h'_i + h_i}{4h_i}\right)\right\}\left(\frac{\partial u}{\partial \xi}\right)_{i,j}$$

$$- \left(\frac{h'_{i+1} + h'_i}{4h_i}\right) sin\alpha \left(\frac{\partial u}{\partial \eta}\right)_{i,j} \quad (4.3.32)$$

and total flux in the η - direction is derived accordingly. Substituting the total fluxes in the ξ - and η - directions into the discretized equation (4.3.5) and after simplification, the equivalent partial differential

equation is

$$\frac{\partial u_{i,j}}{\partial t} + a\left(\frac{\partial u}{\partial x}\right)_{i,j} + b\left(\frac{\partial u}{\partial y}\right)_{i,j} = a[\{\underbrace{\left(\frac{h'_{i+1} - 2h_i + h_{i-1}}{4h_i}\right)}_{\text{I}} + \underbrace{\left(\frac{h'_i - h_i}{4h_i}\right)}_{\text{II}}\}\left(\frac{\partial u}{\partial \xi}\right)_{i,j}$$

$$+ \underbrace{\left(\frac{h'_{i+1} + h_i}{4h_i}\right)}_{\text{III}} sin\alpha \left(\frac{\partial u}{\partial \eta}\right)_{i,j}] - b\underbrace{\left(\frac{l_{j+1} - 2l_j + l_{j-1}}{4l_j}\right)}_{\text{IV}}\left(\frac{\partial u}{\partial \eta}\right)_{i,j}$$

(4.3.33)

Case a: Algebraic or quasi uniform grid (see equation (4.3.16))

As the grid sizes h and l reduce to zero then the term I and term IV reduce to zero. However terms II and III do not go zero. Therefore, the application of straight averaging for a skewed grid results in an inconsistency in a cell where the skewing occurs. Since the truncation error contains an odd order derivative, it is dispersive and generates oscillations.

Case b: Exponential grid (see equation(4.3.19))

The terms I and IV will not now reduce to zero eventhough the grid size h and l reduce to zero. In addition, the terms II and III also do not reduce to zero. Therefore, the scheme is inconsistent with a dispersive error that generates oscillations. The application of the straight averaging technique for a skewed stretched grid for the test case of flow over a circular arc resulted in an oscillatory solution as shown by Rossow, Kroll, Radespiel and Scherr (62nd AGARD).

4.3.2 Linear Interpolation

The inaccuracy of the straight averaging scheme stems from the fact that it is assumed that the cell face lies mid way between the cell centres. For a non-uniform grid this can be improved by taking into account the distances between the face and the cell centres (figure-4.6).

Assuming a linear variation

$$u_{i+1/2,j} = \frac{h_i\, u_{i+1,j} + h_{i+1}\, u_{i,j}}{h_i + h_{i+1}} \qquad (4.3.34)$$

where the known values are $u_{i+1,j}$ and $u_{i,j}$. This interpolation was proposed by Turkel (1986). The interpolated values are $u_{i+1/2,j}$ and located at cell face (i+1/2,j). The accuracy of this interpolation is analyzed by the Von Neumann and EPDE methods.

4.3.2.1 Von Neumann

The application of the Von Neumann method to the linear interpolation approximation results in the expression for $u_{i+1/2,j}$ which is as follows

$$u_{i+\frac{1}{2},j} = \frac{u_{i,j}[h_i\{cos\chi_x\,(x_{i+1,j} - x_{i,j}) + Isin\chi_x\,(x_{i+1,j} - x_{i,j})\} + h_{i+1}]}{h_i + h_{i+1}} \qquad (4.3.35)$$

and $u_{i-1/2,j}$, $u_{i,j+1/2}$ and $u_{i,j-1/2}$ are similarly defined

Straight Stretched Grid

As previously defined, the distance between cell centres in the x-direction is

$$x_{i+1,j} - x_{i,j} = \frac{h_{i+1} + h_i}{2} \qquad (4.3.36)$$

and other distance are similarly defined (figure-4.4).

Substituting equation (4.3.36) into equation (4.3.35)

leads to

$$u_{i+\frac{1}{2},j} = \frac{u_{i,j}[h_i\{cos\chi_x\left(\frac{h_{i+1}+h_i}{2}\right) + Isin\chi_x\left(\frac{h_{i+1}+h_i}{2}\right)\} + h_{i+1}]}{h_i + h_{i+1}} \tag{4.3.37}$$

Case a: Quasi uniform or algebraic grid

The ratio of the grid sizes is

$$\frac{h_{i+1}}{h_i} = 1 + O(h) \qquad and \qquad \frac{h_i}{h_{i-1}} = 1 + O(h) \tag{4.3.38}$$

for O(h) << 1

$$\frac{h_{i-1}}{h_i} \simeq 1 - O(h) \tag{4.3.39}$$

The distance between cell centres (i+1,j) and (i,j)

becomes

$$\frac{h_{i+1} + h_i}{2} \simeq h_i + \frac{1}{2}h_i O(h) \tag{4.3.40}$$

Substituting this approximation into equation (4.3.37)

leads to

$$u_{i+\frac{1}{2},j} \simeq \frac{u_{i,j}[h_i\{cos\chi_x h_i + Isin\chi_x h_i\} + h_{i+1}]}{h_i + h_{i+1}} \tag{4.3.41}$$

$u_{i-1/2,j}$, $u_{i,j+1/2}$ and $u_{i,j-1/2}$ can be similarly defined.

Substituting $u_{i+1/2,j}$, $u_{i-1/2,j}$, $u_{i,j+1/2}$ and $u_{i,j-1/2}$ into the semi discretized equation (4.3.5) and after simplification this equation becomes

$$\frac{du_{i.j}}{dt} + \frac{au_{i,j}}{h_i}[\frac{h_i\,(h_{i+1} - h_{i-1})}{(h_{i+1} + h_i)\,(h_{i-1} + h_i)}\,(1 - cos\chi_x h_i) +$$

$$I\left(1 + \frac{h_i^2 - h_{i+1}h_{i-1}}{(h_{i+1} + h_i)\,(h_{i-1} + h_i)}\right) sin\chi_x h_i] + \frac{bu_{i.j}}{l_j}[\frac{l_j\,(l_{j+1} - l_{j-1})}{(l_{j+1} + l_j)\,(l_{j-1} + l_j)}$$

$$(1 - cos\chi_y l_j) + I\left(1 + \frac{l_j^2 - l_{j+1}l_{j-1}}{(l_{j+1} + l_j)\,(l_{j-1} + l_j)}\right) sin\chi_y l_j] = 0 \qquad (4.3.42)$$

where l_j is grid size in y-direction.

The solution of the equation (4.3.42) can be expressed as

$$u_{i,j} = constant \quad e^{(\omega_r + I\omega_i)t} \qquad (4.3.43)$$

where ω_r is real part and ω_i is imaginary part.

The real part give rise to dissipation or amplification effects and the imaginary part to oscillatory effects. Dissipation is possible if

$$(h_{i+1} - h_{i-1}) > 0 \qquad or \qquad (l_{j+1} - l_{j-1}) > 0 \qquad (4.3.44)$$

which depends upon the grid expansion or contraction. Since the Von Neuman method decomposes the $u_{i,j}$ into its wave components, the result of the analysis describes the effect of the wave propagation in arbitrary grid. If the wave propagates in the direction of expansion, it will be dissipated. If the wave propagates in the direction of contraction, it will be amplified. The direction of the

propagation is in the direction of the convective velocity which is a vector summation of convective velocities a and b along the x- and y-directions. The influence of the grid expansion and contraction in x- and y- directions are decoupled because the linear averaging formulation is used along each direction separately.

Order of accuracy can not be determined directly without expanding the trigonometric terms in equation (4.3.42). The EPDE method will be able to determine the accuracy and will be discussed in the next section.

Stretched Skewed Grid

In addition to the error due to the stretching, the application of the linear interpolation technique to a stretched, skewed grid will generate additional errors. Inclusion of the skewing effect can be incorporated through the expression,

$$u_{i+1/2,j} = \frac{h'_i\, u_{i+1,j} + h'_{i+1}\, u_{i,j}}{h'_i + h'_{i+1}} + (\Delta u)_{skew} \qquad (4.3.45)$$

in two dimensions and with one skewness direction (figure-4.6), where now the lengths h'_i and h'_{i+1} are different from the case of streching only and are shown in figure-4.6. The magnitude of $(\Delta u)_{skew}$ depends on the variation of $u_{i,j}$ in the η - direction. This dependence can be expressed as

$$(\Delta u)_{skew} = m\, t \qquad (4.3.46)$$

where m is the derivative of $u_{i,j}$ in the η - direction and given as follows,

$$m = \text{function}(u_{i,j}, u_{i,j+1}, u_{i,j-1}, l_j, l_{j+1}, l_{j-1})$$

The slope m can be estimated as

$$m = \frac{u_{i+\frac{1}{2},j} + u_{i-\frac{1}{2},j}}{l_j} \qquad (4.3.47)$$

where $u_{i,j+1/2}$ is defined as

$$u_{i,j+1/2} = \frac{l_j\, u_{i,j+1} + l_{j+1}\, u_{i,j}}{l_j + l_{j+1}}$$

$u_{i,j-1/2}$ follows similarly.

t is an offset distance due to skewness along cell boundary (i+1/2,j). After substituting $u_{i,j+1/2}$ and $u_{i,j-1/2}$, the result of the manipulation is

$$(\Delta u)_{skew} = -u_{i,j}\left[\frac{(l_{j+1} - l_j)(1 - cos\chi_y \Delta y) + I\,(l_{j-1} + 2l_j + l_{j+1})\, sin\chi_y \Delta y}{(h_{i+1} + h_i)(h_{i-1} + h_i)}\right]t \qquad (4.3.48)$$

Due to the skewness effect,

$$h'_i \neq h_i$$
$$h'_{i+1} \neq h_{i+1} \qquad (4.3.49)$$

In geometrical terms the effect can produce an increment in length segment such that,

$$h'_i = h_i + \Delta h_i$$
$$h'_{i+1} = h_{i+1} + \Delta h_{i+1} \qquad (4.3.50)$$

The expressions for h_i and h_{i+1} are substituted into equation (4.3.45) together with $(\Delta u)_{skew}$ and after some manipulation, the following equation is obtained,

$$\frac{du_{i,j}}{dt} + \frac{au_{i,j}}{h_i}\{[\frac{h_i(h_{i+1}-h_{i-1})-(l_{j+1}-l_{j-1})t}{(h_{i+1}+h_i)(h_{i-1}+h_i)}$$

$$+ \frac{h_i h_{i+1}}{(h_i+h_{i+1})^2}\left(\frac{\Delta h_{i+1}}{h_{i+1}} - \frac{\Delta h_i}{h_i}\right)](1-cos\chi_x h_i)$$

$$+ I[1 + \frac{h_i^2 - h_{i+1}h_{i-1} - (l_{j-1}+2l_j+l_{j+1})t}{(h_{i+1}+h_i)(h_{i-1}+h_i)} -$$

$$\frac{h_i h_{i+1}}{(h_i+h_{i+1})^2}\left(\frac{\Delta h_{i+1}}{h_i} - \frac{\Delta h_i}{h_i}\right)]sin\chi_x h_i\} + \frac{bu_{i,j}}{l_j}\{\left(\frac{l_j(l_{j+1}-l_{j-1})}{(l_{j+1}+l_j)(l_{j-1}+l_j)}\right)$$

$$(1-cos\chi_y l_j) + I\left(1 + \frac{l_j^2 - l_{j+1}l_{j-1}}{(l_{j+1}+l_j)(l_{j-1}+l_j)}\right)sin\chi_y l_j\} = 0 \qquad (4.3.51)$$

This equation will be dissipative if

$$[\frac{h_i(h_{i+1}-h_{i-1})-(l_{j+1}-l_{j-1})t}{(h_{i+1}+h_i)(h_{i-1}+h_i)} - \frac{h_i h_{i+1}}{(h_i+h_{i+1})^2}\left(\frac{\Delta h_{i+1}}{h_{i+1}} - \frac{\Delta h_i}{h_i}\right)] > 0 \qquad (4.3.52a)$$

$$\frac{l_j(l_{j+1}-l_{j-1})}{(l_{j+1}+l_j)(l_{j-1}+l_j)} > 0 \qquad (4.3.52b)$$

The first term of the inequality (4.3.52a) and the inequality (4.3.52b) represent stretching effect. The second and third terms of the inequality (4.3.52a) represent a skewing effect. The second term generates an amplification effect in a grid expanding in the positive direction ,ie where $l_{j+1} > l_j$. The third term, which depends upon the relative magnitude of $\Delta h_{i+1}/h$ and $\Delta h_i/h_i$,is always positive and generates an amplification effect, too. This is based upon observations from figure-4.6 and a derivation in appendix-4.1. The skewing effect in geometry is represented by the offset distance t

which depends on the skew angle and cell length. Therefore, the effect of the skewed grid will be destablizing if the grid expands towards the skewed direction. In this particular case, the skewed direction is in the positive coordinate direction. The additional term due to the skewing effect is imaginary and is given by

$$\frac{(l_{j-1}+2l_j+l_{j+1})t}{(h_{i+1}+h_i)(h_{i-1}+h_i)} - \frac{h_i h_{i+1}}{(h_i+h_{i+1})^2}\left(\frac{\Delta h_{i+1}}{h_{i+1}} - \frac{\Delta h_i}{h_i}\right) \qquad (4.3.53)$$

This term contributes to the dispersive effect whether it is positive or negative.

The solution of equation (4.3.51) can be represented as

$$u_{i,j} = constant \quad e^{(\omega_r' + I\omega_i')t} \qquad (4.3.54)$$

The additional error due to skewing affect both in and ω_i' compared with the ones from equation (4.3.43).

4.3.2.2 Equivalent Partial Differential Equation Method

By following the previous analysis of the Equivalent Partial Differential Equation (EPDE) method in subsection 4.3.1.2, the Taylor expansion of $u_{i+1/2,j}$ about $u_{i,j}$ is substituted into equation (4.3.34) and after simplification $u_{i+1/2,j}$ is expressed as

$$u_{i+\frac{1}{2},j} = u_{i,j} + \left(\frac{h_i}{2}\right)\left(\frac{\partial u}{\partial x}\right)_{i,j} + \frac{h_i}{8}(h_{i+1}+h_i)\left(\frac{\partial^2 u}{\partial x^2}\right)_{i,j} + O(h^3) \qquad (4.3.55)$$

Even though $u_{i+1/2,j}$ is located at the cell face (i+1/2,j) in a skewed grid, it is not located at the centre of that

face.

Straight Stretched Grid

By substituting the grid spacings from equation (4.3.26) and other similar expressions, the flux in the x -direction is

$$\frac{u_{i+\frac{1}{2},j} - u_{i-\frac{1}{2},j}}{h_i} = \left(\frac{\partial u}{\partial x}\right)_{i,j} + (h_{i+1} - h_{i-1})\left(\frac{\partial^2 u}{\partial x^2}\right)_{i,j} + \frac{1}{48}[(h_i + h_{i+1})^2 + (h_{i+1} + h_{i-1})^2]\left(\frac{\partial^3 u}{\partial x^3}\right)_{i,j} + O(h^3) \qquad (4.3.56)$$

and the flux in the y - direction is similarly defined. Substituting these fluxes into equation (4.3.5), the equivalent partial differential equation is

$$\frac{\partial u_{i,j}}{\partial t} + a\left(\frac{\partial u}{\partial x}\right)_{i,j} + b\left(\frac{\partial u}{\partial y}\right)_{i,j} = -a(h_{i+1} - h_{i-1})\left(\frac{\partial^2 u}{\partial x^2}\right)_{i,j} - b(l_{j+1} - l_{j-1})\left(\frac{\partial^2 u}{\partial y^2}\right)_{i,j} + O(h^2, l^2) \qquad (4.3.57)$$

The lowest order terms of the truncation error have an even order derivative of $u_{i,j}$ and are first order in h and l. These can generate dissipation or amplification effects. They will be dissipative if

$$a(h_{i+1} - h_{i-1}) > 0 \qquad (4.3.58a)$$

and

$$b(l_{j+1} - l_{j-1}) > 0 \qquad (4.3.58b)$$

The terms in the bracket are due to the grid expansion. By reversing the inequality signs in the above, the terms will induce amplification. This is the same conclusion as the Von Neumann analysis for this type of the grid.

Skewed Stretched Grid

The linear interpolation of equation (4.3.34) is

written as

$$u'_{i+1/2,j} = \frac{h'_i\, u_{i+1,j} + h'_{i+1}\, u_{i,j}}{h'_i + h'_{i+1}} \qquad (4.3.59)$$

where $h'_{i+1,j}$ and $h'_{i,j}$ are defined in figure-4.6. Note that since the $u'_{i+1/2,j}$ is not located at the centre of the cell face, it is not used in the flux calculation. In order to obtain the Taylor expansion of the $u_{i+1/2,j}$ about $u_{i,j}$, the following steps are carried out,

1) Obtain a Taylor expansion for $u'_{i+1/2,j}$ about $u_{i,j}$ by using the above interpolation function.

2) Taylor expand $u_{i+1/2,j}$ about $u'_{i+1/2,j}$ which gives

$$u_{i+\frac{1}{2},j} = u'_{i+\frac{1}{2},j} - \frac{h'_i}{2} sin\alpha \left(\frac{\partial u}{\partial \eta}\right)'_{i+\frac{1}{2},j} + \frac{1}{2}\left(\frac{h'_i}{2} sin\alpha\right)^2 \left(\frac{\partial^2 u}{\partial \eta^2}\right)'_{i+\frac{1}{2},j} + O(h^3) \qquad (4.3.60)$$

Since is skewed angle this expression describes the effect of the grid skewness.

3) Substitute the $u'_{i+1/2,j}$, $(\frac{\partial u}{\partial \eta})'_{i+1/2,j}$ and $(\frac{\partial^2 u}{\partial \eta^2})'_{i+1/2,j}$ from results of the step-1 into the $u_{i+1/2,j}$ expresssion of step-2

Thus, $u_{i+1/2,j}$ is

$$u_{i+\frac{1}{2},j} = u_{i,j} + \frac{h'_i}{2}\left(\frac{\partial u}{\partial \xi}\right)_{i,j} - \frac{h'_i}{2} sin\alpha \left(\frac{\partial u}{\partial \eta}\right)_{i,j} + O(h^2) \qquad (4.3.61)$$

Flux $u_{i-1/2,j}$ has similar expression but with skew angle =0 since the grid is not skewed between (i-1,j) and (i,j). This is also the case for the η - direction. Substituting the fluxes in the ξ - and η - directions, the equivalent partial differential equation can be written as

$$\frac{\partial u_{i,j}}{\partial t} + a\left(\frac{\partial u}{\partial \xi}\right)_{i,j} + b\left(\frac{\partial u}{\partial \eta}\right)_{i,j} = -\frac{1}{2}\left(\frac{1}{cos\alpha} - 1\right)\left(\frac{\partial u}{\partial \xi}\right)_{i,j} + \frac{1}{2}tan\alpha\left(\frac{\partial u}{\partial \eta}\right)_{i,j} + O(h^2) \qquad 4.3.62)$$

The lowest order term of the truncation error has an odd order derivative of $u_{i,j}$ and zeroth order in the grid size. This will generate oscillations and its magnitude is independent of the grid size. Therefore, the linear interpolation approximation generates inconsistent errors which depend on the skew angle.

4.3.3 Improved Scheme

An accurate scheme is one that takes into account the skewing and streching effects. The grid compactness is also an important consideration. The more points a discretization scheme incorporates the more spurious modes it can suffer. The most compact scheme in three dimensions is a seven point scheme and this will be investigated. It consists of the cell center with six neighbouring cell centers (figure-4.7a). The discretization scheme provides information about the variation in the value of the variables in the seven point configuration. Since this investigation concentrates on the viscous discretization, the derivative of the flow variables derived from that scheme is the main consideration. Any new scheme has to fulfil certain criteria in order to provide better accuracy. They are,

1) The scheme must be symmetric and it must not depend on the choice of any coordinate system used.
2) The first derivative of the variable must not be

constant otherwise the second derivative will be zero

3) An isoparametric transformation must exist in order to keep computational time low

The following analysis explains the reasons for the requirements.

4.3.3.1 Interpolation Function

In view of the above conditions, a new interpolation function is proposed. The local variation is calculated by this interpolation function. By considering a local Taylor series expansion about a cell centre for the interpolation function in cartesian coordinates, the improved interpolation function in three dimensions is defined as,

$$u(x,y,z)= A_1 +A_2x +A_3y +A_4z +A_5x^2 +A_6y^2 +A_7z^2 \qquad (4.3.63)$$

where u(x,y,z) can be a velocity variable.

4.3.3.2 Isoparametric function

The constant A_1 through A_7 can be calculated from values of u at seven points. In general, the application of this scheme in the whole field requires the calculation of a 7X7 matrix inversion for every cell centre. This can be avoided if an isoparametric transformation of this scheme can be found as Turkel, Yaniv and Landau (1986) has done in two dimensions. The general seven point configuration is transformed to a diamond configuration (figure-4.7b). The mapping functions are

$$x(\xi,\eta,\zeta) = B_1 + B_2\xi + B_3\eta + B_4\zeta + B_5\xi^2 + B_6\eta^2 + B_7\zeta^2 \qquad (4.3.64a)$$

$$y(\xi,\eta,\zeta) = C_1 + C_2\xi + C_3\eta + C_4\zeta + C_5\xi^2 + C_6\eta^2 + C_7\zeta^2 \qquad (4.3.64b)$$

$$z(\xi,\eta,\zeta) = D_1 + D_2\xi + D_3\eta + D_4\zeta + D_5\xi^2 + D_6\eta^2 + D_7\zeta^2 \qquad (4.3.64c)$$

where ξ , η and ζ are coordinates in the transformed space. B_i, C_i and D_i of the equation (4.3.64a,b,c) are evaluated by substituting the locations of the cell centres in ξ, η and ζ of the transformed space and the corresponding values of x, y, z of the physical space. With given values of those constants, and the x, y and z coordinates of the face centres, the values of ξ, η and ζ corresponding to the value of the centre faces can be calculated by solving the system of three nonlinear equations (4.3.64a,b,c) with three unknown ξ, η, and ζ .

The evaluation of the viscous derivatives which are at the centres of the cell faces are calculated from the equation (A.4.2.12) (see appendix-4.2),

$$\frac{\partial u}{\partial x} = \sum_{i=1}^{7} u_i \frac{\partial N_i}{\partial x} \qquad (4.3.65a)$$

$$\frac{\partial u}{\partial y} = \sum_{i=1}^{7} u_i \frac{\partial N_i}{\partial y} \qquad (4.3.65b)$$

$$\frac{\partial u}{\partial z} = \sum_{i=1}^{7} u_i \frac{\partial N_i}{\partial z} \qquad (4.3.65c)$$

where u_i are the values of the variable at the cell centres and where the derivatives of the cell functions $\partial N_i/\partial x$, $\partial N_i/\partial y$, $\partial N_i/\partial z$ depend on the values of ξ, η, and ζ corresponding to the location of face centres. Their formulation is derived in appendix-4.2.

Because of the form of the interpolation function of the equation (4.3.63), the variable derivatives vary only in one coordinate direction namely

$$\frac{\partial u}{\partial x} = A_2 + 2A_5 x \tag{4.3.66a}$$

$$\frac{\partial u}{\partial y} = A_3 + 2A_6 y \tag{4.3.66b}$$

$$\frac{\partial u}{\partial z} = A_4 + 2A_7 z \tag{4.3.66c}$$

4.3.3.3 Scheme

The seven point scheme provides variables and derivatives which depend on the magnitude and location of the variables at those seven points. Those points are actually located at the cell centres. Since the grid nonuniformity will be taken into account, it will be more accurate than a discretization scheme that uses straight averaging. The improved scheme is basically a quadratic interpolation. Because of the utilization of an interpolation function, this scheme requires more computational time than a straight averaging scheme.

4.3.3.4 Truncation Error Analysis

The truncation error analysis for the improved scheme using either a coupled or decoupled formulation is calculated using the EPDE method. The analysis is carried out in two dimensions (but can be extended to three dimensions) and for skewed stretched grids only. The reason is that the improved scheme is purposely formulated to take into account the effect of the grid skewness.

Decoupled Formulation

The decoupled formulation is merely an extension of linear interpolation which provides quadratic variation in each coordinate direction. The evaluation of the cell face values along the ξ - direction is based upon the

expression

$$u(\xi) = A_1 + A_2'\xi + A_5'\xi^2 \qquad (4.3.67)$$

It is the two dimensional version of the improved scheme where variation in one coordinate direction is considered at a time. Since this is a quadratic equation, it needs three given values at known locations in order to obtain expressions for A_1 ,A_2' and A_5' . In this improved scheme, the values are at cell centres located at (i-1,j),(i,j) and (i+1,j). These three cell centres are connected by two segments of straight lines which meet at a skewed angle (figure-4.6). Thus, u varies quadratically along these two segments.

By looking at the geometry of the grid, the resulting u, which is located at (i+1/2,j)', not at the face centre , is

$$u'_{i+\frac{1}{2},j} = A_1 + A_2'\left(\frac{h_i'}{2}\right) + A_5'\left(\frac{h_i'}{2}\right)^2 \qquad (4.3.68)$$

Coefficient A_1 ,A'_2 and A'_5 are functions of the cell centre values $u_{i,j}$,$u_{i+1,j}$ and $u_{i-1,j}$, grid sizes h_i, h_{i-1} and weighted length h_i', h_{i+1}' (see appendix-4.3). This weighted length is the same weighted length as in the linear interpolation in the subsection 4.3.2.2.

The Taylor expansion of $u'_{i+1/2,j}$ about $u_{i+1/2,j}$ will provide the relationship $u'_{i+1/2,j}$ in terms of $u_{i+1/2,j}$ and skewed angle which is equation (4.3.60). $u'_{i+1/2,j}$ and its derivatives are obtained from equation (4.3.68).

Substituting these expressions back into equation (4.3.60)

and after simplication, the values of u at face centre (i+1/2,j) is

$$u_{i+\frac{1}{2},j} = u_{i,j} + \frac{h_i'}{2}\left(\frac{\partial u}{\partial \xi}\right)_{i,j} - \frac{h_i'}{2} sin\alpha \left(\frac{\partial u}{\partial \eta}\right)_{i,j} + O\left(h^2\right) \qquad (4.3.69)$$

Since the grid is not skewed in (i,j) to (i-1,j) direction u at the face centre i-1/2,j is

$$u_{i-\frac{1}{2},j} = u_{i,j} + \frac{h_i}{2}\left(\frac{\partial u}{\partial \xi}\right)_{i,j} + O\left(h^2\right) \qquad (4.3.70)$$

The values of u along the η - direction at the face centre (i,j+1/2) and (i,j-1/2) have similar expressions to the one at (i-1/2,j) where the cell length in ξ - direction h_i and the derivatives with respect to ξ are replaced by the cell length in the η - direction, l_j and the derivatives with respect to η . By substituting the fluxes at the face centres (i+1/2,j),(i-1/2,j),(i,j+1/2) and (i,j-1/2) into the semi discretized equation (4.3.5) and after simplification, the equivalent partial differential equation is

$$\frac{\partial u_{i,j}}{\partial t} + a\left(\frac{\partial u}{\partial \xi}\right)_{i,j} + b\left(\frac{\partial u}{\partial \eta}\right)_{i,j} = -\frac{1}{2}\left(\frac{1}{cos\alpha} - 1\right)\left(\frac{\partial u}{\partial \xi}\right)_{i,j} + \frac{1}{2} tan\alpha \left(\frac{\partial u}{\partial \eta}\right)_{i,j}$$

(4.3.71)

The truncation error, which is the right hand side, is zeroth order and dispersive which generates oscillations and depends upon the skew angle α but it does not depend upon the grid size. Therefore, the decoupled quadratic interpolation scheme is inconsistent for a skewed stretched grid because the error terms do not go to zero as the grid size reduces to zero. The truncation error

generated in the skewed stretched grid is not reduced by going from linear interpolation to quadratic interpolation. This arises from the error generated by the imbalance of the fluxes along the ξ- direction created by skewing the grid along the same direction. The quadratic interpolation does not model the flux imbalance more accurately than the linear interpolation.

Coupled Formulation

In coupled formulation, the evaluation of the cell face value is based upon a two dimensional interpolation in cartesian coordinates x and y which is given by

$$u(x,y)= A_1 + A_2x + A_5x^2 + A_3y + A_6y^2 \qquad (4.3.72)$$

describing variation of u in a five point scheme. In this formulation, the general curvilinear coordinate can be replaced by the cartesian coordinate x and y. Constants A_1 ,A_2 A_5, A_3 and A_6 are calculated from the known values of u at five cell centres (i,j), (i+1,j), (i-1,j), (i,j+1) and (i,j-1). It follows that the total flux in the x - direction is

$$\frac{u_{i+\frac{1}{2},j} - u_{i-\frac{1}{2},j}}{h_i} = A_2 \qquad (4.3.73a)$$

and the total flux in the y - direction is

$$\frac{u_{i,j+\frac{1}{2}} - u_{i,j-\frac{1}{2}}}{l_j} = A_3 \qquad (4.3.73b)$$

where A_2 = function($u_{i+1,j}$,$u_{i,j}$,$u_{i-1,j}$,$u_{i,j+1}$,$u_{i,j-1}$,h_{i+1}, h_i, h_{i-1}, l_{j+1} ,l_j ,l_{j-1}, $\propto$)

A_3 = function($u_{i+1,j}$,$u_{i,j}$,$u_{i-1,j}$,l_{j+1} ,lj ,l_{j-1})

(see appendix-4.3)

Expressing $u_{i+1,j}$, $u_{i-1,j}$, $u_{i,j+1}$ and $u_{i,j-1}$ as Taylor series about $u_{i,j}$ then for $u_{i+1,j}$,

$$u_{i+1,j} = u_{i,j} + \frac{1}{2}(h_i + h_{i+1}cos\alpha)\left(\frac{\partial u}{\partial x}\right)_{i,j} + \frac{1}{2}h_{i+1}sin\alpha\left(\frac{\partial u}{\partial y}\right)_{i,j}$$

$$+\frac{1}{2}\left(\frac{h_i + h_{i+1}cos\alpha}{2}\right)^2\left(\frac{\partial^2 u}{\partial x^2}\right)_{i,j} + \left(\frac{h_{i+1}}{2}sin\alpha\right)\left(\frac{h_i + h_{i+1}cos\alpha}{2}\right)\left(\frac{\partial^2 u}{\partial y \partial x}\right)_{i,j}$$

$$+\frac{1}{2}\left(\frac{h_{i+1}}{2}sin\alpha\right)^2\left(\frac{\partial^2 u}{\partial y^2}\right)_{i,j} \qquad (4.3.74)$$

This particular expression contains the skew angle because the cell centre (i+1,j) is skewed relative to the cartesian coordinates x-y (figure-4.8). Other expressions for $u_{i-1,j}$, $u_{i,j+1}$, $u_{i,j-1}$ do not have terms with the skew angle. Substituting back the Taylor series for $u_{i+1,j}$, $u_{i-1,j}$, $u_{i,j+1}$ and $u_{i,j-1}$ into the total flux expression of equation (4.3.73a) and (4.3.73b), then the flux in the x - direction is

$$\frac{u_{i+\frac{1}{2},j} - u_{i-\frac{1}{2},j}}{h_i} = \left(\frac{\partial u}{\partial x}\right)_{i,j} + \frac{1}{24}(h_i + h_{i-1})(h_i + h_{i+1}cos\alpha)\left(\frac{\partial^3 u}{\partial x^3}\right)_{i,j}$$

$$\frac{1}{48}(h_{i-1} + h_i)h_{i+1}sin\alpha \quad function(h_{i+1}, h_i, h_{i-1}, l_{j+1}, l_j, l_{j-1}, \alpha)\left(\frac{\partial^3 u}{\partial y^3}\right)_{i,j}$$

$$+O(h^3, l^3) \qquad (4.3.75)$$

As it was mentioned in the above, the flux contains the skew angle. The flux in the y - direction is

$$\frac{u_{i,j+\frac{1}{2}} - u_{i,j-\frac{1}{2}}}{l_j} = \left(\frac{\partial u}{\partial y}\right)_{i,j} + \frac{1}{24}(l_j + l_{j-1})(l_j + l_{j+1})\left(\frac{\partial^3 u}{\partial y^3}\right)_{i,j} + O(l^3)$$

(4.3.76)

This flux does not contain the skew angle because the grid line is not skewed in the y - direction.

Substituting the fluxes in the x and y directions into the discretzed equation (4.3.5) then the equivalent partial differential equation is

$$\frac{\partial u_{i,j}}{\partial t} + a\left(\frac{\partial u}{\partial x}\right)_{i,j} + b\left(\frac{\partial u}{\partial y}\right)_{i,j} = O\left(h^2, \alpha\right)\left(\frac{\partial^3 u}{\partial x^3}\right)_{i,j}$$

$$+O\left(h^2, l^2\right) sin\alpha\left(\frac{\partial^3 u}{\partial y^3}\right)_{i,j} + O\left(h^3, l^3\right) \qquad (4.3.77)$$

The truncation error is second order and dispersive giving rise to oscillations. The coupled formulation of the improved scheme is consistent because as the grid sizes h and l are reduced to zero, the truncation error reduces to zero. The dominant effect of the skewness is in the second term of the right hand side that contains odd order derivatives in y and is second order in the grid size h and l. Thus, it generates oscillations in the y direction that depend on the grid size h and l. If the skewness diminishes, this term will go to zero.

After understanding the advantage of the couple formulation of the improved scheme, the effect of the shearness of the grid is investigated. However, the grid lines in each coordinate direction are assumed to be parallel.

4.3.3.5 Analysis of Sheared Grid

This analysis is carried out for the coup formulation of the improved discretization sche.... n a sheared skewed stretched grid by using the EPDE method. In addition to skew angle α, shear angle β describes the

angle of intersection between two coordinate directions (figure-4.2). The two dimensional interpolation in the general coordinates ξ and η is

$$u(\xi,\eta) = A_1 + A_2\xi + A_5\xi^2 + A_3\eta + A_6\eta^2 \qquad (4.3.78)$$

As it is similar to the previous case where the grid is not sheared, the total flux in ξ and η - direction has the same expression as in equation (4.3.73a) and (4.3.73b). However, the A_2 is also a function of shear angle β which is as follows,

$$A_2 = \text{function}(u_{i+1,j}, u_{i,j}, u_{i-1,j}, u_{i,j+1}, u_{i,j-1}, h_{i+1}, h_i, h_{i-1}, l_{j+1}, l_j, l_{j-1}, \alpha, \beta)$$

By expressing $u_{i+1,j}$, $u_{i-1,j}$, $u_{i,j+1}$ and $u_{i,j-1}$ in Taylor series about $u_{i,j}$ then for $u_{i+1,j}$

$$u_{i+1,j} = u_{i,j} + \frac{1}{2}\left[h_i + h_{i+1}\frac{\sin(\beta-\alpha)}{\sin\beta}\right]\left(\frac{\partial u}{\partial \xi}\right)_{i,j} + \frac{h_{i+1}}{2}\frac{\sin\alpha}{\sin\beta}\left(\frac{\partial u}{\partial \eta}\right)_{i,j} + O(h^2) \qquad (4.3.79)$$

This equation is reduced to equation (4.3.74) as β approaches 90 degree or the shearness diminishes. Other expressions for $u_{i-1,j}$, $u_{i,j+1}$, $u_{i,j-1}$ are similar to the ones for a nonsheared grid. Substituting the Taylor series for $u_{i+1,j}$, $u_{i-1,j}$, $u_{i,j+1}$ and $u_{i,j-1}$ into the total flux expression, then the flux in the ξ - direction is

$$\frac{u_{i+\frac{1}{2},j} - u_{i-\frac{1}{2},j}}{h_i} = \left(\frac{\partial u}{\partial \xi}\right)_{i,j} + \frac{1}{24}(h_i + h_{i-1})\left(h_i + h_{i+1}\frac{sin(\beta-\alpha)}{sin\beta}\right)\left(\frac{\partial^3 u}{\partial \xi^3}\right)_{i,j} +$$

$$\frac{1}{48}(h_{i-1} + h_i)\,h_{i+1} \quad function(h_{i+1}, h_i, h_{i-1}, l_{j+1}, l_j, l_{j-1}, \alpha, \beta)\left(\frac{\partial^3 u}{\partial \eta^3}\right)_{i,j} \tag{4.3.80}$$

and the flux in the η - direction is the same as in the nonsheared grid. Substituting fluxes in the ξ - and η - directions into the semi descritized equation (4.3.4), the equivalent partial differential equations is

$$\frac{\partial u_{i,j}}{\partial t} + \frac{(ay_{AB} - bx_{AB})}{A}\left(\frac{\partial u}{\partial \xi}\right)_{i,j} + \frac{(-ay_{BC} + bx_{BC})}{A}\left(\frac{\partial u}{\partial \eta}\right)_{i,j} =$$

$$\{\frac{1}{24}(h_i + h_{i-1})\left(h_i + h_{i+1}\frac{sin(\beta-\alpha)}{sin\beta}\right)\}\frac{(ay_{AB} - bx_{AB})}{A}\left(\frac{\partial^3 u}{\partial \xi^3}\right)_{i,j} +$$

$$\{\frac{1}{48}(h_{i-1} + h_i)\,h_{i+1}\frac{sin\alpha}{sin\beta} \quad function(h_{i+1}, h_i, h_{i-1}, l_{j+1}, l_j, l_{j-1}, \alpha, \beta)\}$$

$$\frac{(-ay_{BC} + bx_{BC})}{A}\left(\frac{\partial^3 u}{\partial \eta^3}\right)_{i,j} + O(h^3, l^3) \tag{4.3.81}$$

As the skew angle α increases, the coefficients of $(\frac{\partial^3 u}{\partial \xi^3})_{i,j}$ and $(\frac{\partial^3 u}{\partial \eta^3})_{i,j}$ on the right hand side increase and oscillations will tend to increase. As the shear angle decreases, those coefficients also increase. Therefore, in a sheared skewed stretched grid the effects of shear are to increase oscillations in the solution.

4.3.3.6 Convection Diffusion Equation

The foregoing analysis which uses a scalar convection equation as a test model concentrated on the accuracy of the convection terms. In order to investigate the accuracy of the scheme for the diffusion terms, a scalar

convection-diffusion equation is analysed. This analysis is also carried out for the coupled formulation of the improved discretization for skewed stretched grid by using the EPDE method. The equation is, as follows,

$$\frac{\partial u}{\partial t} + a\frac{\partial u}{\partial x} + b\frac{\partial u}{\partial y} = \mu_1 \frac{\partial^2 u}{\partial x^2} + \mu_2 \frac{\partial^2 u}{\partial y^2} \tag{4.3.82}$$

After discretizing the equation with the finite volume method, the equation becomes,

$$\frac{du_{i,j}}{dt} + a\frac{\left(u_{i+\frac{1}{2},j} - u_{i-\frac{1}{2},j}\right)}{h_i} + b\frac{\left(u_{i,j+\frac{1}{2}} - u_{i,j-\frac{1}{2}}\right)}{l_j} =$$

$$\mu_1 \frac{\left(\frac{\partial u}{\partial x}\right)_{i+\frac{1}{2},j} - \left(\frac{\partial u}{\partial x}\right)_{i-\frac{1}{2},j}}{h_i} + \mu_2 \frac{\left(\frac{\partial u}{\partial y}\right)_{i,j+\frac{1}{2}} - \left(\frac{\partial u}{\partial y}\right)_{i,j-\frac{1}{2}}}{l_j} \tag{4.3.83}$$

The first term on the right hand side which represents viscous effect in the x-direction is

$$\mu_1 \frac{\frac{\partial}{\partial x}(u_{i+\frac{1}{2},j} - u_{i-\frac{1}{2},j})}{h_i} = \mu_1 \frac{\partial}{\partial x}(Flux \quad in \quad x-direction) \tag{4.3.84}$$

Since this analysis is carried out for the coupled formulation in a skewed grid, the flux in the x-direction can be taken from equation (4.3.73a), then the above

$$\mu_1 \frac{\partial}{\partial x}\frac{(u_{i+\frac{1}{2},j} - u_{i-\frac{1}{2},j})}{h_i} = \mu_1 \left(\frac{\partial^2 u}{\partial x^2}\right)_{i,j} + \frac{\mu_1}{24}(h_i + h_{i-1})(h_i + h_{i+1}cos\alpha)\left(\frac{\partial^4 u}{\partial x^4}\right)_{i,j}$$

$$\frac{\mu_1}{48}(h_{i-1} + h_i)h_{i+1}sin\alpha \quad function(h_{i+1}, h_i, h_{i-1}, l_{j+1}, l_j, l_{j-1}, \alpha)\left(\frac{\partial^4 u}{\partial x \partial y^3}\right)_{i,j}$$

$$+O(h^3, l^3) \tag{4.3.85}$$

The second term on the right hand side of equation (4.3.83) which represents the flux in the y - direction is expressed similarly but does not depend on the skew angle.

Substituting the fluxes in the x and y direction, the equivalent partial differential equation becomes

$$\frac{\partial u_{i,j}}{\partial t} + a\left(\frac{\partial u}{\partial x}\right)_{i,j} + b\left(\frac{\partial u}{\partial y}\right)_{i,j} = \mu_1\left(\frac{\partial^2 u}{\partial x^2}\right)_{i,j} + \mu_1\left(\frac{\partial^2 u}{\partial y^2}\right)_{i,j}$$

$$O(h^2,\alpha)\{-a\left(\frac{\partial^3 u}{\partial x^3}\right)_{i,j} + \mu_1\left(\frac{\partial^4 u}{\partial y^4}\right)_{i,j}\} + O(l^2)\{-b\left(\frac{\partial^3 u}{\partial y^3}\right)_{i,j} + \mu_2\left(\frac{\partial^4 u}{\partial y^4}\right)_{i,j}\} +$$

$$O(h^2,\alpha)\{-a\left(\frac{\partial^3 u}{\partial y^3}\right)_{i,j} + \mu_1\left(\frac{\partial^4 u}{\partial x \partial y^3}\right)_{i,j}\} + O(h^3,l^3) \quad (4.3.86)$$

The diffusive truncation error is

$$O(h^2,\alpha)\left(\mu_1\frac{\partial^4 u}{\partial x^4}\right) + O(l^2)\left(\mu_2\frac{\partial^4 u}{\partial y^4}\right) \quad (4.3.86a)$$

which is second order in h and depends on the skew angle and contains even order derivatives. In the convection diffusion equation, the improved scheme of the coupled formulation generates an additional higher order dissipative error which is second order in the grid size.

4.4 Alternative Grid Modification

From the analysis of the truncation error of the straight averaging approximation in an arbitrary grid discussed in section 4.3.1, it is seen that the error depends upon the grid expansion, the grid size and flow variable gradients. Instead of adopting an improved discretization scheme, the grid used could be modified to reduce the truncation error by taking into account that dependency. As a test example, the investigation in this section is based upon the analysis of a straight stretched grid. The flux in the x - direction can be expressed as

$$\frac{u_{i+\frac{1}{2},j} - u_{i-\frac{1}{2},j}}{h_i} = \left(\frac{\partial u}{\partial x}\right)_{i,j} + C_1\left(\frac{\partial u}{\partial x}\right)_{i,j} + C_2\left(\frac{\partial^2 u}{\partial x^2}\right)_{i,j}$$

$$+ High\ \ Order\ \ Terms \qquad (4.4.1)$$

this equation is taken from equation (4.3.27) where C_1, and C_2 are

$$C_1 = \frac{h_{i+1} - 2h_i + h_{i-1}}{4h_i} \qquad (4.4.2a)$$

$$C_2 = \frac{(h_{i+1} + 2h_i + h_{i-1})(h_{i+1} - h_{i-1})}{16h_i} \qquad (4.4.2b)$$

Writting the grid size ratio as

$$\frac{h_{i+1}}{h_i} = 1 + E_{i+1} \qquad (4.4.3a)$$

$$\frac{h_i}{h_{i-1}} = 1 + E_{i-1} \qquad (4.4.3b)$$

where E_{i+1} and E_{i-1} are parameters of the grid expansion and $E_{i+1}<<1$ and $E_{i-1}<<1$, then we obtain

$$C_1 \simeq E_{i+1} - E_{i-1} \qquad (4.4.4a)$$

$$C_2 \simeq \frac{h_i}{2}(E_{i+1} + E_{i-1})\left(2 + \frac{E_{i+1} - E_{i-1}}{2}\right) \qquad (4.4.4b)$$

By reducing the grid expansion ratio, the grid size or the derivative terms in equation (4.4.1), the truncation error of the discretized flux can be reduced.

In an area of high gradient region near a wall, then the grid size must be small enough to resolve that gradient. However, using this grid resolution everywhere would require high computational time and such resolution is not necessary in low gradient regions away from the

wall such as the free stream region. For economy it is sensible to expand the grid from the high gradient to the low gradient regions.

The truncation error of the straight averaging approximation in the straight stretched grid generates an inconsistency such as the term $C_1(\frac{\partial u}{\partial x})_{i,j}$. It depends upon the grid expansion and the first derivatives. Thus, for example using a high grid expansion for instance near a wall to resolve the boundary layer, where there are high gradients, can generate inconsistency.

By ensuring low grid expansion in the high gradient regions the C_1 can be kept small but the requirement of the small grid size to resolve the high flow gradients results in high computational cost. This can be avoided by increasing the grid size. However, this can generate dissipatives error from C_2 $(\frac{\partial^2 u}{\partial x^2})_{i,j}$ since C_2 depends on grid size h_i. Thus, it is important that the generation of low grid expansion in high gradient regions must not increase other errors in those regions. There must be a balance between reduction of the grid expansion and increase in the grid size. The first one will be able to reduce zero order inconsistency errors and the second one will increase first order dissipative errors.

4.5 Mesh Reynold Number

In this section, a stability analysis that includes time discretization is carried out for a scalar convection diffusion equation. The purpose of the investigation is to derive additional stability constraints generated by the

time discretization. The scheme used is explicit in time and central difference in space or Forward Time and Central Space (FTCS) and is applied to the equation. The fully discretized equation is

$$\frac{u_{i,j}^{n+1}-u_{i,j}^{n}}{\Delta t}+a\frac{u_{i+1,j}^{n}-u_{i-1,j}^{n}}{2h_i}+b\frac{u_{i,j+1}^{n}-u_{i,j-1}^{n}}{2l_j}=$$

$$\mu_1\frac{u_{i-1,j}^{n}-2u_{i,j}^{n}+u_{i+1,j}^{n}}{2h_i}+\mu_2\frac{u_{i,j-1}^{n}-2u_{i,j}^{n}+u_{i,j+1}^{n}}{2l_j} \qquad (4.5.1)$$

By using the Von Neumann stability method, the amplification factor is defined as

$$G=\frac{ER^{n+1}}{ER^{n}} \qquad (4.5.2)$$

where ER^n is the error at n time level. It is derived as

$$G=1+I\left(\frac{a\Delta t}{h_i}sin\chi_x h_i+\frac{b\Delta t}{l_j}sin\chi_y l_j\right)-4\left(\frac{\mu_1\Delta t}{h_i^2}sin^2\frac{\chi_x h_i}{2}+\frac{\mu_2\Delta t}{l_j^2}sin^2\frac{\chi_y l_j}{2}\right) \qquad (4.5.3)$$

The scheme will be stable, if |G| < 1, thus

$$|G|=\sqrt{[1-4\left(\frac{\mu_1\Delta t}{h_i^2}sin^2\frac{\chi_x h_i}{2}+\frac{\mu_2\Delta t}{l_j^2}sin^2\frac{\chi_y l_j}{2}\right)]^2+[\frac{a\Delta t}{h_i}sin\chi_x h_i+\frac{b\Delta t}{l_j}sin\chi_y l_j]^2}<1 \qquad (4.5.3a)$$

The analysis of this inequality for two extreme conditions of high and low frequencies Fouries series components leads to stability conditions as shown by Hirsch (1989),

$$0 < \frac{\mu_1 \Delta t}{h_i^2} + \frac{\mu_2 \Delta t}{l_j^2} \leq \frac{1}{2} \qquad \text{for high frequency} \qquad (4.5.4a)$$

$$0 < \frac{a^2 \Delta t}{\mu_1} + \frac{b^2 \Delta t}{\mu_2} \leq 2 \qquad \text{for low frequency} \qquad (4.5.4b)$$

We assume that the diffusion coefficients μ_1 and μ_2 in x - and - y directions respectively are the same namely

$$\mu = \mu_1 = \mu_2 \qquad (4.5.5)$$

The high frequency wave corresponds to the smallest wave length resolvable in the grid space h_i or l_j. As the grid size decreases, the length of the smallest wave decreases or the frequency increases such that the first stability condition can be violated. In order to satisfy this stability condition, the time step has to be decreased. However, as the diffusion factor μ reduces to zero or the equation becomes pure convective the time constraint from the high frequency condition is not violated. Thus, the high frequency wave is still stable. Also the smallest wave will not grow unbounded in FTCS scheme for a pure convection equation. However, the high frequency waves can grow in a diffusive flow if the grid size is too small or if the frequency is too high for a given time step. Let us define mesh Reynold numbers parameters as

$$R_x = \frac{ah_i}{\mu} \quad and \quad R_y = \frac{bl_j}{\mu} \qquad (4.5.6)$$

With these parameters, the second stability condition for the low frequency harmonic can be written as

$$\sigma_x R_x + \sigma_y R_y \leq 2 \qquad (4.5.7a)$$

where

$$\sigma_x = \frac{a\triangle t}{h_i} \quad and \quad \sigma_y = \frac{b\triangle t}{l_j} \tag{4.5.7b}$$

are CFL numbers in the x - and y - directions respectively. Therefore, the stability condition for the low frequency components depends on the product of CFL and mesh Reynold numbers and is governed by the time step and diffusion factor. It can be violated easily as the diffusion factor decreases. Since the solution consist of waves from low to high frequencies, the diffusion stability condition is always required to obtained a stable solution.

4.6 Cell Vertex Scheme

An alternative to the finite volume cell centred scheme is the cell vertex scheme. Instead of locating the discretized values at the cell centres, this scheme locates those values at the nodal points or cell vertices. Accuracy of the cell vertex scheme will be investigated for inviscid and viscous flux evaluation. Where possible, comparisons of the cell centred and cell vertex schemes will be drawn.

4.6.1 Inviscid Flux Evaluation

Even though this chapter concentrates on viscous discretization, it is beneficial to start with the inviscid flux discretization since many of the features from the inviscid discretization are applicable to the viscous discretization. The inviscid flux used to update a cell vertex value is calculated from values that belong to

the cells that surround that vertex. Those cells form a super-cell and in three dimensions it consists of eight cells and in two dimensions it consist of four cells (figure-4.9). In each cell, the fluxes are evaluated by taking a line integral or trapezoidal rule around the cell boundary. The integration directly takes values at the cell vertices. This integration technique is equivalent to taking the flux differences on opposite cell faces.

In an arbitrary two dimensional grid, the fluxes at the cell faces, obtained from straight averaging of the cell vertex values, are exactly located at the cell centre faces. However, in the cell centred scheme, the straight averaging of the cell centre values will not result in the flux that is located at the cell face centre for an arbitrary grid. This is a source of error which is eliminated with the cell vertex scheme.

In three dimensions, if the cell faces are not rectangular, Rossow, Kroll, Radespiel and Scherr (62nd AGARD) show how to evaluate the fluxes at those faces by using bilinear interpolation. In the case where the cell faces may not be planes, the variation of the normal must be taken into account in the integration of the fluxes. By dividing the curved cell faces into triangles as was done by the above authors, constant normals over the triangular faces can be obtained and used in the flux evaluations.

The fluxes at the cell vertices are calculated from the fluxes of the cell components of the super-cell. In this calculation, Radespiel, Rossow and Swanson (1989),

Radespiel and Rossow (1989), and Martinelli (1987) used an averaging technique and Mackenzie (1989), Andrew(1993), Crumpton, Macknezie and Morton (1993) used distribution functions. Both calculation methods will be discussed in the following section.

4.6.1.1 Averaging of Fluxes

The averaging that takes into account the geometry of the cell component of the super-cell is more accurate than the averaging that does not. This statement can be validated by analyzing a test function ψ_i in one dimension. The first derivative $(\psi_x)_i$ is calculated from the derivatives at segment line i-1/2 and i+1/2 (figure-4.10). Two cases are disscused

Case a: Straight Averaging

This analysis follows that of Radespiel and Swanson(1989) and Martinelli (1987).

Thus, the value $(\frac{\partial \psi}{\partial x})$ at i is

$$\left(\frac{\partial \psi}{\partial x}\right)_i^N = \frac{1}{2}\left[\left(\frac{\partial \psi}{\partial x}\right)_{i-\frac{1}{2}} + \left(\frac{\partial \psi}{\partial x}\right)_{i+\frac{1}{2}}\right] \qquad (4.6.1)$$

where

$$\left(\frac{\partial \psi}{\partial x}\right)_{i+\frac{1}{2}} = \frac{\psi_{i+1} - \psi_i}{\Delta x_+} \quad \text{and} \quad \left(\frac{\partial \psi}{\partial x}\right)_{i-\frac{1}{2}} = \frac{\psi_i - \psi_{i-1}}{\Delta x_-}$$

A Taylor expansion of ψ_{i+1} about i gives

$$\psi_{i+1} = \psi_i + \Delta x_+ \left(\frac{\partial \psi}{\partial x}\right)_i + \frac{(\Delta x_+)^2}{2}\left(\frac{\partial^2 \psi}{\partial x^2}\right)_i + O\left(\Delta x_+^3\right) \qquad (4.6.2)$$

and similarly for ψ_{i-1}. Substituting back into the expression for $(\frac{\partial \psi}{\partial x})_{i+1/2}$ and $(\frac{\partial \psi}{\partial x})_{i-1/2}$ gives the result

$$\left(\frac{\partial \psi}{\partial x}\right)_i^N = \left(\frac{\partial \psi}{\partial x}\right)_i + \frac{1}{2}(\Delta x_+ - \Delta x_-)\left(\frac{\partial \psi}{\partial x}\right)_i + O\left(\Delta x_\pm^2\right) \qquad (4.6.3)$$

Therefore, the truncation error is first order and dissipative for an arbitrary grid. It should be noted that the application of the straight averaging scheme in the cell centre scheme resulted in an inconsistency for arbitrary grid as shown in section 4.3.1. For a quasi uniform or algebraic grid where

$$\Delta x_- = \Delta x_+ (1 + O(\Delta x_+)) \qquad (4.6.4)$$

then the above derivative becomes

$$\left(\frac{\partial \psi}{\partial x}\right)^N_i = \left(\frac{\partial \psi}{\partial x}\right)_i + \frac{1}{2} O(\Delta x_\pm^2) \left(\frac{\partial^2 \psi}{\partial x^2}\right)_i + High \quad Order \quad Terms \qquad (4.6.5)$$

Thus the truncation error becomes second order and dissipative. As was also shown in section 4.3.1, for the cell centre scheme, the straight averaging in a quasi uniform grid resulted in consistency and a first order dispersive error.

In a two dimensional case, Martinelli (1987), Ni (1982) and Turkel (1986) took the average of the cell component residuals in order to obtain the residual at the cell vertices using the trapezoidal integration rule around the supercells. The residual is ,in fact, the total flux differences for all cell faces. This can be expressed as

$$R_{i,j} = \frac{R_A + R_B + R_C + R_D}{4} \qquad (4.6.6)$$

This, in fact, is equivalent to straight averaging of the residuals of the cell components of the super-cell because the relative size of those cell components and the

geometrical location of the cell vertex in the super-cell are not taken into account. For an arbitrary grid, this averaging gives poor convergence and can even lead to divergence as shown by Usab (1983).

Case b: Weighted averaging

Hall (1986), Rossow, Kroll, Radespiel and Scherr (62nd AGARD) and Mackenzie (1989) calculate the residual for the cell vertex from the residuals of the cell components by weighting each cell residual by its cell area in two dimension or volume in three dimensions. Thus, in two dimensions, the residual for the cell vertex (i,j) is

$$R_{i,j} = \frac{S_A R_A + S_B R_B + S_C R_C + S_D R_D}{S_A + S_B + S_C + S_D} \qquad (4.6.7)$$

This averaging give a more robust scheme than the straight averaging. It takes information about relative areas but it does not take the information about the distance between the centres of the cell components and the cell vertex. If the areas in the cell components are kept the same but the shape of the cells are changed the distances between each centre of the cell components and cell vertex will change. Thus, this type of averaging is not strictly equivalent to linear interpolation. It can be derived from a Taylor Galerkin formulation explained by Morton (1988).

4.6.1.2 Distribution Function

The distribution function mentioned in the above will

transfer residuals that are computed in the cell components into one for the cell vertex. The transfer is carried out by

$$R^N_{i,j,k} = \frac{\sum_{m=1}^{M} Vol_m D_m R_m}{\sum_{m=1}^{M} Vol_m} \qquad (4.6.8)$$

where $R_{i,j,k}$ is cell vertex residual at (i,j,k). M is the number of cell components in the super-cell which is eight in three dimensions. Vol_m is volume of the each cell component. D_m is the distribution matrix that relates cells and cell vertices. R_m is the residual of each cell component. This is explained by Crumpton, Mackenzie and Morton (1993).

4.6.2 Viscous Flux Evaluation

The viscous flux is also calculated from values that belong to the cells that surround a common vertex that also form a super-cell. Within that super-cell, an auxillary cell is constructed by connecting the cell centres of the cell components (figure-4.9).

For viscous flux evaluation, a technique using Gauss's theorem was proposed by Martinelli (1987) for a two dimensional case. The viscous residual, which contains second order derivatives is calculated by using a Gauss's theorem for an auxillary cell boundary. The integration involves first derivatives at the cell vertices of the auxillary cell. Since these cell vertices are cell centres of the cell components, the derivatives

are calculated by taking another integration around the cell components. This integration involves values at the cell vertices of the cell components.

Radespiel, Rossow and Swanson (1989) and Radespiel and Swanson (1989) proposed a method to obtain the viscous residual by taking flux differences of the cell faces. This is, in fact, equivalent to the above mentioned integration. Instead of averaging the fluxes of all cell components of the super-cell in order to obtain the cell vertex flux as in the case of the inviscid flux, the averaging is only performed for one auxillary cell face at a time. For instance, average value at cell face AB (figure-4.9) is

$$u_{i+\frac{1}{2},j} = \frac{u_A + u_B}{2} \qquad (4.6.9)$$

This averaging will ensure that the result is located at the centre of the face, for instance AB. The viscous flux which is located at the cell vertex (i,j) is the difference of the flux at the faces of the auxillary cell ABCD (figure-4.9).

Mackenzie (1989) proposed two methods for the viscous flux evaluation in which derivatives are calculated. In the first method, an auxillary cell is constructed by connecting four cell vertices and the first derivative is calculated by taking trapezoidal integration around this cell (figure-4.11). In the second method, the first derivatives in the cell components are calculated by taking trapezoidal integration around these cells. The

derivatives at the cell vertex surrounded by those cells are obtained by taking an area average of the cell component derivarives. For two dimensional case, this can be expressed ,as

$$\left(\frac{\partial \psi}{\partial x}\right)_{i,j} = \frac{S_A\left(\frac{\partial \psi}{\partial x}\right)_C + S_B\left(\frac{\partial \psi}{\partial x}\right)_D + S_C\left(\frac{\partial \psi}{\partial x}\right)_A + S_D\left(\frac{\partial \psi}{\partial x}\right)_C}{S_A + S_B + S_C + S_D} \qquad (4.6.10)$$

This type of averaging is approximately the same as bilinear interpolation.

4.7 Conclusion

The requirement to evaluate fluxes at cell faces in the finite volume discretization leads to approximation formulae involving the stored flow variables as known values. In the cell centre scheme, the known values are located at the cell centres. The straight averaging approximation, which is a standard technique adopted, results in an inaccurate solution in a nonuniform grid because the approximated values are not located at the cell faces. The effects of the grid nonuniformity described by stretching, skewing and shearing of the grid lines can be analyzed by the Von Neumann and the Equivalent Partial Differential Equation (EPDE) methods.

The truncation error of the straight averaging is second order in a uniform grid and first order dispersive in an algebraic or quasi uniform grid. In an exponential stretched grid and stretched skewed grid, it results in an inconsistent scheme. A linear interpolation scheme can be used to improve matters, however, in a straight stretched

grid, the truncation error will be first order dissipative if the convection is in the direction of the grid expansion. On the other hand the error will be amplified if the convection is in the direction of the grid contraction. In a skewed stretched grid, this approximation results in an inconsistent discretization scheme. The Von Neumann method shows the destabilizing effect of grid skewness ; the EPDE method shows that this effect is at higher order level than that causing the inconsistency.

An improved scheme is proposed which is basically quadratic interpolation and is analyzed in coupled and decoupled formulations for skewed stretched grid. The implementation of the decoupled formulation has the same overall error as the linear interpolation scheme. The reason is that this formulation can not take into account the flux imbalance generated by the grid skewness. The implementation of the coupled formulation results in a second order dispersive error. In a sheared grid, the coupled formulation generates an additional dispersive error. For a convection diffusion equation, this formulation also generates second order dispersive and dissipative errors. The dissipative error being generated by the discretization of the diffusion terms.

An alternative approach to reduce truncation errors by careful choice of the grid has been investigated. Analysis indicates that the truncation error can be reduced by constructing a grid with a low grid expansion

ratio in high gradient regions and using a high grid expansion ratio in low gradient regions. However, the grid size in high gradient regions should not be too small in order to avoid high computational cost.

A stability analysis of a fully discretized convection diffusion equation for an explicit central difference scheme shows that the time step is the determining factor. The mesh Reynold number enters the stability constraints, being multiplied by the CFL number.

As an alternative to the cell centre scheme, the cell vertex scheme based on published work is reviewed in order to understand any accuracy improvement with this scheme compared with the cell centre scheme. Straight averaging in a two dimensional arbitrary grid results in accurate face centre values. However, it will not always be the case in three dimensions if the cell surfaces are not rectangular. Updating of the cell vertex values is obtained from the values of the cell components that meet at that vertex and form a super-cell. This is carried out by an averaging techniques.

An analysis of straight averaging in one dimension shows that the cell vertex scheme is more accurate than the cell centre scheme. However, the implementation of this averaging to an arbitrary multidimensional grid can result in poor convergence and even lead to divergence. In order to produce an accurate and robust scheme, an averaging technique has been proposed that takes into account the geometry of the cell components.

5.0 ARTIFICIAL DISSIPATION

5.1 Introduction

The spatial discretization used in solving the three dimensional Navier-Stokes equations is central differencing. This has the disadvantage of admitting oscillations in the solution. In order to control the oscillation, artificial dissipation is explicitly added to the governing equations. This can result in errors in the solution. These errors are characterized by inaccuracies in predicting total pressure losses, boundary layer growth and shock sharpness in transonic flow calculations.

The dissipation model adopted in this code is based on Jameson's scheme (Jameson, Turkel and Schmith, 1981) which consists of a blend of second and fourth order dissipations. The accuracy of the scheme depends on the grid size, dissipative scaling factors, the second and fourth order controlling coefficients and the second and fourth order differences of the flow parameters. The scaling factors depend upon the cell aspect ratio, the controlling coefficients are user input constants and the differencing depends upon flow gradients and grid sizes.

In general three dimensional computation, the grid sizes, cell aspect ratios and flow gradients vary throughout the whole domain especially in critical areas such as the near wall region, leading and trailing edges and flow exit region. These parameters will be incorporated in the formulation of the improved dissipation model so that the dissipation in these regions

can be controlled more effectively. Therefore, the improved model has the capability to sense the important parameters that affect the dissipation in those critical regions.

In this chapter first, the source of the inaccuracy with the standard dissipation model and the improvement offered by the alternative models proposed by various researchers will be assesed. The test cases are inviscid Ni's bump (Ni(1982)), a flat plate and a viscous transonic two dimensional high pressure turbine blade. Then, the above mentioned improved model is proposed. In addition to the above test cases, the improved model is also tested in three dimensional cases : a subsonic high pressure turbine blade, a transonic generic fan blade and a engine intake nacelle.

5.2 Alternative Dissipation Models

This section summarizes the different approaches proposed by various reseachers.

5.2.1 Models Based on Modifications to the Original Scaling Factors

The standard model of Jameson's dissipation is shown in equation (3.4.5) and is reproduced below

$$d_{i+\frac{1}{2},j,k} = \left(\frac{Volume}{\Delta t}\right)_{i+\frac{1}{2},j,k} \{\epsilon^2_{i+\frac{1}{2},j,k}\left(W_{i+1,j,k} - W_{i,j,k}\right) \qquad (3.4.5)$$

$$-\epsilon^4_{i+\frac{1}{2},j,k}(W_{i+2,j,k} - 3W_{i+1,j,k} + 3W_{i,j,k} - W_{i-1,j,k})\}$$

which contains a scaling factor. In three dimensions, this factor actually represents the volume rate ,(Vol/Δ t) of the dissipation flux.

5.2.1.1 Standard Scaling Factor

This scaling factor was originally proposed by Jameson, Schmidt and Turkel (1981). In cartesian coordinate, this type of scaling factor can be analyzed, as follows,

$$\text{Total dissipation} = d_{total} = d_x + d_y + d_z \qquad (5.2.1)$$

d_x represents the dissipation fluxes on the cell faces in the x - direction, similarly for d_y and d_z. Thus, d_{total} is basically the summation of the differences in the three coordinate directions multiplied by a scaling factor. By using equation (3.4.10) and neglecting the viscous term, the scaling factor

in x-direction is

$$S_x = vol\left(\frac{u + c}{\Delta x}\right) \qquad (5.2.2a)$$

in y-direction is

$$S_y = vol\left(\frac{v + c}{\Delta Y}\right) \qquad (5.2.2b)$$

in z-direction is

$$S_z = vol\left(\frac{w + c}{\Delta z}\right) \qquad (5.2.2c)$$

For large aspect ratio cells such as those at the near wall where $\Delta x >> \Delta y$ and $\Delta x >> \Delta z$, thus $S_x << S_y$ and $S_x << S_z$. Since the difference in x-direction is multiplied by the total scaling factor which is

$$S = S_x + S_y + S_z \qquad (5.2.3)$$

the dissipation in the x-direction can become excessive.

d_x from the decomposition of the standard dissipation is

$$d_x = S(\epsilon^2 \delta_x^2 W - \epsilon^4 \delta_x^4 W) \qquad (5.2.4)$$

whilst d_x with S_x is

$$d_x = S_x(\epsilon^2\delta_x^2 W - \epsilon^4\delta_x^4 W) \qquad (5.2.5)$$

Excessive dissipation component will be generated because $S >> S_x$. This leads to exessive total dissipation. Therefore, the standard dissipation is acceptable only where the aspect ratio is not much greater than one.

5.2.1.2 Decompositions of the Scaling Factor

The standard scaling factor is decomposed into x, y and z directions, see Martinelli (1987) and Swanson and Turkel (1987). For instance the second order dissipation in the x-direction is

$$d_x^2 = S_x \epsilon^2 (W_{i+1,j,k} - 2W_{i,j,k} + W_{i-1,j,k}) \qquad (5.2.6)$$

where S_x is from equation (5.2.2a) and W is the state variable. By using a Taylor expansion, equation (5.2.6) can be expressed as

$$d_x^2 = S_x \epsilon^2 \Delta x^2 \frac{\partial^2 W}{\partial x^2} \qquad (5.2.7)$$

The analysis for the fourth order dissipation follows the same derivation as in the above. For a high aspect ratio cell, the dissipation in the x - direction can be very small as it is compared with the standard scaling factor which is

$$d_x^2 = S\epsilon^2 \Delta x^2 \frac{\partial^2 W}{\partial x^2} \qquad (5.2.8)$$

since $S_x << S$

Thus, the total dissipation of equation (5.2.1) is severely reduced. According to Martinelli (1987), the use of the decomposed scaling factor is acceptable for aspect ratios of up to 10.

5.2.1.3 Redistribution of Scaling Factor

In order to redistribute the scaling factor to each coordinate direction, a function which depends upon the cell aspect ratio was proposed by Martinelli (1987) and Kuntz and Lakshminarayana (1992). This idea is based on the techniques of flux splitting (Van Leer(1977) and Stager and Warming(1981)). In the ξ- direction of the curvilinear coordinate system, the scaling factor becomes

$$s_\xi = \phi_\xi(r_\eta, r_\zeta)\left(\frac{Vol}{\Delta t_\xi}\right) \qquad (5.2.9)$$

where $r_\eta = \frac{\Delta t_\xi}{\Delta t_\eta}$, $r_\zeta = \frac{\Delta t_\zeta}{\Delta t_\eta}$ and $\frac{Vol}{\Delta t_\xi}$ is defined in equation (3.4.7a). In two dimensions, Martinelli (1987) defined the scaling factor as

$$\phi_\xi(r_\eta) = 1 + r_\eta^{\alpha} \qquad (5.2.10)$$

$\phi_\eta(r_\xi)$ are defined accordingly.

Kuntz and Lakshminarayana (1992) defined the scaling factor in three dimensions as

$$\phi_\xi(r_\eta, r_\zeta) = (1 + r_\eta + r_\zeta)^{\alpha} \qquad (5.2.11)$$

where $0 < \alpha < 1$ for equation (5.2.10) and (5.2.11).

Cheng (1992) proposed a slight variation to the Martinelli scaling factor in three dimensions, as follows,

$$\phi_\xi(r_\eta, r_\zeta) = 1 + \max(r_\eta^\alpha, r_\zeta^\alpha) \qquad (5.2.12)$$

In two dimensions, Cheng's modification reduces to that of Martinelli.

An alternative to Kuntz's aspect ratio function is a modified form of the function originated from Cheng's aspect ratio function of equation (5.2.11),

$$\phi_\xi(r_\eta, r_\zeta) = [1 + \max(r_\eta, r_\zeta)]^\alpha \qquad (5.2.13)$$

Refering to equation (5.2.11) and (5.2.13), the modified formula is different from that of Kuntz in the use of the maximum function. The value of ϕ_ξ from equation (5.2.11) is always more than that from equation (5.2.13) because this maximum function eliminates the smallest contribution between r_η and r_ζ

Following the analysis in sections 5.2.1.2, the effect of the distribution function $\phi(r)$ in cartesian coordinate in two dimensions can be shown as follows. The second order dissipation in x-direction

$$d_x^{(2)} = \phi_x \frac{Vol}{\Delta t_x} \epsilon^2 \quad (W_{i+1,j} - 2W_{i,j} + W_{i-1,j}) \qquad (5.2.14a)$$

and in y direction

$$d_y^{(2)} = \phi_y \frac{Vol}{\Delta t_y} \epsilon^2 \quad (W_{i,j+1} - 2W_{i,j} + W_{i,j-1}) \qquad (5.2.14b)$$

Using Martinelli model which can be expressed as

$$\phi_x = 1 + \left(\frac{S_y}{S_x}\right)^{\alpha} \qquad (5.2.15)$$

where $S_y/S_x = \Delta t_x / \Delta t_y$ represents the cell aspect ratio effect, ϕ_y is expressed accordingly. Using a Taylor series expansion and substituting ϕ_x and ϕ_y into equation (5.2.14a) and (5.2.14b) respectively the total second order dissipation which is the summation of equations (5.2.14a) and (5.2.14b) is

$$d^2 = \epsilon^2 \left\{ \phi_x \frac{Vol}{\Delta t_x} \Delta x^2 \frac{\partial^2 W}{\partial x^2} - \phi_y \frac{Vol}{\Delta t_y} \Delta y^2 \frac{\partial^2 W}{\partial y^2} \right\} \qquad (5.2.16)$$

The effect of cell aspect ratio on the scaling factors is distributed by the function ϕ_x and ϕ_y which depend on the ratio S_y/S_x. The analysis for the fourth order dissipation follows the same derivation as above. According to Martinelli, the use of the distributed scaling factor is acceptable for aspect ratio of up to 500.

The Martinelli and Kuntz models have different effects on the dissipation and it will be elaborated in the following sections.

A) Martinelli's Model

The effect of the Martinelli's aspect ratio function on the dissipation for a two dimensional case can be illustrated in figure-5.1a. For high aspect ratio cells, it can be shown that the dissipation component along the length of the cells is reduced and that along the width of the cells increased relative to the original (standard model). Thus this may result in an increase of the

dissipation in some regions. In three dimensions, Cheng modified the function by eliminating the smallest aspect ratio terms.

B) Kuntz's Model

The effect of Kuntz's aspect ratio function on the dissipation for a two dimensional case can be illustrated in figure-5.1b. For a high aspect ratio cell, it can be shown that the dissipation component along both directions is reduced. The magnitude of the reduction is proportional to the length of the cell in each direction. The largest reduction is along the length of the high aspect ratio cell and its implementation always results in the reduction of the total dissipation.

5.2.2 Model Based on Velocity Scaling Factor

Dissipation has to be reduced in high viscous regions in order to obtain physically meaningful results. This can be achieved by multiplying the dissipation with a velocity scaling function as in Swanson and Turkel (1987), and Kuntz and Lakshminarayana (1992). This is

$$f\left(\frac{V_i}{V_{ref}}\right)=\left(\frac{V_i}{V_{ref}}\right) \qquad (5.2.17)$$

In low velocity regions, this function can also reduce dissipation by a suitable choice of the reference velocity. Instead of velocity, this function can also be defined based on Mach Number.

5.2.3 Model based on Vorticity Scaling Factor

In order to reduce the dissipation in high viscous regions Hall (1994) uses vorticity as a sensor as follows

$$f(w) = \frac{1}{1 + F_w} \qquad (5.2.18)$$

where $F_w \propto \mu_T$ AND $w = |\nabla \times V|$

In two dimensions $\nabla \times V = \left(\frac{\partial v}{\partial x} - \frac{\partial u}{\partial y}\right)\hat{k}$ AND $V = \hat{i}u + \hat{j}v$

This function is multiplied by the dissipation flux of equation (3.4.5). The resulting dissipation fluxes are much smaller than the viscous fluxes in the high viscous region near to the wall.

5.2.4 Modification of Scaling Factor based on Characteristic Dissipation

The time dependent Euler equations can be expressed in characteritic form which describes the propagation of characteristic waves. In one dimension, the Euler equation is

$$\frac{\partial W}{\partial t} + \frac{\partial F}{\partial x} = 0 \qquad (5.2.19)$$

where F is flux vector in the x - direction expressed in equation (3.2.1). With Jacobian matrix, it becomes

$$\frac{\partial W}{\partial t} + A_1 \frac{\partial W}{\partial x} = 0 \qquad (5.2.19a)$$

The matrix A_1 is the one dimensional version of matrix A in appendix-3.1. Diagonalizing matrix A_1 and writting the equation in decoupled form

$$\frac{\partial Q}{\partial t} + \Lambda_Q \frac{\partial Q}{\partial x} = 0 \qquad (5.2.20)$$

where $Q = T^{-1} W$ and T is a matrix of eigenvectors and Λ_Q is the diagonal matrix where the elements are the eigenvalues of matrix A_1 :

$$\Lambda_Q = \begin{bmatrix} u & 0 & 0 \\ 0 & u+c & 0 \\ 0 & 0 & u-c \end{bmatrix} \qquad (5.2.21)$$

Thus equation (5.2.20) describes the characteristic wave field, the propagating speeds of which are the diagonal elements of Λ_Q.

In explicit time marching methods, the convergence of the iterative process can be improved upon if each characteritic field is marched forward by its characteristic time step, which is a function of the propagating speed of the characteristic. The speed of propagation of the characteristic governs the size of the time step. In the standard model, the same scaling factor is used for all the characteristic fields. As such the slow characterics can get an excessive amount of dissipation. With characteristic based dissipation, the scaling factor is dependent on the characteric speed which will not generate excessive dissipation for the slow characteristics, see Pierce (1994).

5.2.5 Models that aimed at Improving the shock resolutions by modifying the Second Order Dissipation

The second order dissipation is turned on wherever a shock exists. The accuracy of the shock in terms of its location and strength is strongly influenced by the second order dissipation. The following sections present several improved versions based on modification to the sensor for second order dissipation, the capturing capability of the shock and the shock strength.

5.2.5.1 Model that modify the Sensor for the Second Order Dissipation

The standard sensor δ_{ijk} of equation (3.4.5c) does not distinguish between expansion and compression waves. In order to eliminate the possibility of the dissipation being switched on by expansion waves, Jameson and Liu (1988) replaced the pressure switch by an entropy or a divergence of velocity switch.

In the ξ - direction for the two dimensional case, the sensor with the entropy switch becomes

$$\delta_{i,j} = | SE_{i+1/2,j} - SE_{i-1/2,j} | \qquad (5.2.22)$$

and the sensor with the divergence velocity switch becomes

$$\delta_{i,j} = \begin{cases} -\nabla.V_L & \text{if} \quad \nabla.V_L < 0 \\ 0 & \text{if} \quad \nabla.V_L > 0 \end{cases} \qquad (5.2.23)$$

where $\nabla.V_L$ is the divergence of the local velocity.

5.2.5.2 Model that Improve on the Shock Capturing Capability

At or near to the shock front, the sensor

$$\delta_{i,j} = \frac{|p_{i+1,j} - 2p_{i,j} + p_{i-1,j}|}{|p_{i+1,j} + 2p_{i,j} + p_{i-1,j}|} \qquad (3.4.5c)$$

will detect a change in static pressure which will be strong enough to turn on the second order dissipation. In the standard model,

$$\epsilon^2 = K^2 \max(\delta_{i,j}, \delta_{i+1,j}) \qquad (5.2.24)$$

This sensor is calculated on cell (i,j) and (i+1,j). By calculating the sensors over more grid points, the sensors are more likely to capture the shock over wider region. In this case ,Kuntz and Lakshminarayana (1992) proposed

$$\epsilon^2 = K^2 \max(\delta_{i-1,j}, \delta_{i,j}, \delta_{i+1,j}) \qquad (5.2.25b)$$

and Turkel (1988) proposed

$$\epsilon^2 = K^2 \max(\delta_{i-1,j}, \delta_{i,j}, \delta_{i+1,j}, \delta_{i+2,j}) \qquad (5.2.25c)$$

Thus, the shock capturing capability is increased because the shock can be captured over a wider region.

5.2.5.3 Improvement on the Shock Strength

The resulting shock wave from the standard model tends to be smeared over several grid points. Three improvements are available but they may require more computational time.

A) Matrix Dissipation

The standard scaling factor is the summation of the maximum eigenvalue of the Jacobian matrices expressed in equation (5.2.3). The Jacobian matrices are

$$A = \frac{\partial F}{\partial W} \quad \text{in the x - direction} \qquad (5.2.26a)$$

$$B = \frac{\partial G}{\partial W} \quad \text{in the y - direction} \qquad (5.2.26b)$$

where F, G and W are from equation (3.2.1)
In cartesian coordinates, the maximum eigenvalue in the x - direction is S_x of equation (5.2.3) and the ones in the other directions are defined accordingly.

In order to improve the shock sharpness, the maximum eigenvalues are replaced by the absolute values of the

matrices. This idea comes from the upwind scheme discussed by Turkel (1988), Swanson and Turkel (1992), and Turkel and Vatsa (1994). Thus the scaling factors become,

$$S_x = | A | \qquad \text{and } S_y = | B | \tag{5.2.27}$$

The calculation of the absolute values of these matrices is quite complicated and is discussed by Turkel and Vatsa (1994).

B) Total Variant Diminishing (TVD)

Pre-shock overshoot and post-shock undershoot can be limited by ensuring TVD property in the solution (Causon, 1988). The total variation of a variable , for instance u, is

$$TV(u) = \int_{-\infty}^{+\infty} \left| \frac{du}{dx} \right| dx \tag{5.2.28}$$

where TV = Total Variant

The TVD property will be fulfilled if

$$TV(u(x,t_2)) < TV(u(x,t_1)) \text{ for } t_2 > t_1 \tag{5.2.29}$$

where t is time (see, Pierce(1994)).

From equation (5.2.29) a function ψ^2 can be defined as

$$\psi^2_{i+1,j} = \frac{|p_{i+1,j} - 2p_{i,j} + p_{i-1,j}|}{(1-\omega)(|p_{i+1,j} - p_{i,j}| + |p_{i,j} - p_{i-1,j}|) + \omega(p_{i+1,j} + 2p_{i,j} + p_{i-1,j})} \tag{5.2.30}$$

where ω = a user input constant

Thus, any overshoot and undershot can be minimized by replacing second order coefficient ϵ^2 with the function ψ^2 because the second order dissipation with ψ^2 is larger than that with ϵ^2. Implementation of the TVD

function and matrix dissipation will produce low dissipation in smooth regions of the flow as well as damp out overshoots near shocks (Swanson and Turkel, 1992) .

5.2.6 Shock Resolution Improvement by Grid Refinement

By refining the grid, a sharp shock can be obtained but the computational time will increase.

5.2.7 Controlling the generation of dispersive error

The formulation of the fourth order dissipation as in equation (3.4.5) generates dissipation as well as dispersion which can create wiggles in the solution. In order to generate dissipation only, the fourth order dissipation is changed to

$$d^4_{i+\frac{1}{2},j,k} = \epsilon^4_{i+\frac{1}{2},j,k}[(\frac{Vol}{\Delta t})_{i+1,j,k}(W_{i+2,j,k} - 2W_{i+1,j,k} + W_{i,j,k}) - (\frac{Vol}{\Delta t})_{i-1,j,k}(W_{i+1,j,k} - 2W_{i,j,k} + W_{i-1,j,k})] \qquad (5.2.31)$$

as presented by Caughey (1988), Turkel (1988), and Swason and Turkel (1987).

However, Caughey found that the solution with the fourth order dissipation of equation (5.2.31) is almost identical to the solution of equation (3.4.5). The dispersive error is actually introduced by the second order dissipation.

5.3 Proposed Flow Gradient Dissipation Function

One of the important factors in the formulation of artificial dissipation is the differencing such as second order differencing,

$$\delta_i^2 W = W_{i+1,j,k} - 2W_{i,j,k} + W_{i-1,j,k} \qquad (5.3.1)$$

It depends on the grid size and flow derivatives. For a given arbitrary function such as the one that describes the variation in the flow variables, the derivatives of that function will have a contribution to the magnitude of the dissipation. The level of its contribution depends upon the order of the derivatives in question. Higher order derivatives make greater contribution than lower order derivatives. The standard dissipation model which contains fourth order derivatives is large in regions of large flow gradient such as the leading and trailing edges and near wall region.

A flow gradient correction function is proposed in order to reduce the dissipation where the flow gradient is high. There is a built-in sensor for detecting the variations of flow properties and it is based on Mach number difference. In the ξ - direction, the function is as follows,

$$(f(\nabla)_\xi)_{i+\frac{1}{2},j,k} = \frac{1}{1+(\delta_\xi M)_{i+\frac{1}{2},j,k}} \tag{5.3.2}$$

where $$(\delta_\xi M)_{i+\frac{1}{2},j,k} = \frac{|M_{i+1,j,k} - M_{i,j,k}|}{M_{inlet}}$$

In order to avoid divergence during the iterative process due to insufficient dissipation, the magnitude of the gradient function can be controlled either by a factor B or by defining a cut off value f_D, as elaborated below.

A) Controlling Factor B

The magnitude of the sensor δM is reduced by a factor B

$$f(\nabla)_\xi = \frac{1}{1 + B\delta_\xi M} \qquad (5.3.3)$$

where B < 1

B) Cut off values

By setting B = 1, a cut off value can be defined as the lower limit of the function along each of the coordinate direction. For instance, along the ξ - direction

$$f_{D_\xi} < f(\nabla)_\xi < 1 \qquad (5.3.4)$$

and $$0 < f_{D_\xi} < 1$$

If f_{D_ξ} is set to zero , the values of the $f(\nabla)_\xi$ will cover the entire range of the Mach number variation.

5.4 Implementation of Various Models

The cell aspect ratio functions of equation (5.2.10), through equation (5.2.13) are implemented to study the effect of the cell aspect ratio on the accuracy of the solution. The ability of the velocity or Mach number correction function (5.2.17) to reduce dissipations in the near wall region will be verified with the inviscid and viscous test cases. As a comparison results with the anisotropic factors approach in equation (3.4.5b) will also be included in this study.

The proposed gradient correction function of equation (5.3.2) will be implemented to investigate its effect on the high viscous region. The result of the dissipation modification is represented in all the figures by the total dissipation flux of the x - momentum. Note that the dissipative and viscous fluxes are plotted along grid points.

5.4.1 Test Cases

An inviscid test case will provide the understanding about the geometric effect of the dissipation modification since the inaccuracy due to turbulence modelling is eliminated. On the other hand, laminar and turbulent cases of the flat plate case will provide understanding of the effect of the dissipation on the viscous flow without any geometric complexity.

5.4.1.1 Inviscid Test Case

This test case is computed for flow over a Ni's bump (Ni(1982)) with inlet Mach numbers of 0.5 and 0.675. For the first case the flow remains subsonic throughout. For the second case the flow becomes transonic and a shock wave appears. The second and fourth order dissipation coefficient K_2 and K_4 used are shown in table-5.1 to table-5.4. The grid has 78 X 15 points (figure-5.2). The cell aspect ratios near to the wall are high with their lengths in the flow direction. In the inviscid flow, there is no large velocity gradient near to the wall in the normal direction. However, a change in the flow direction near to the leading and trailing edges of the bump will create a large variation of flow properties which in time generates a large gradient in that direction. Since the dissipation is a function of the flow gradient, it will be dominant along the length of the high aspect ratio cells.

Thus, the total dissipation in the two dimensional case is

$$D_{i,j} = D_{\xi} + D_{\eta} \qquad (5.4.1)$$

where the flow direction is along ξ - direction

Near to the leading and trailing edges

$$D_{\xi} > D_{\eta} \qquad (5.4.2)$$

where η is normal to the wall.

A) Results with the Aspect Ratio Function

Two aspect ratio functions are implemented. These are Kuntz's aspect ratio function of equation (5.2.11) and the modified aspect ratio function of equation (5.2.13). The modified function gives more reduction in the dissipation than Kuntz's function but the resulting dissipation may be too low to obtain a converged solution. Thus, the Kuntz's formula is implemented first with the results shown in table-5.1. It shows a reduction of the mass mean losses for both the subsonic and transonic cases relative to the results with the standard model. However, the total pressure generation at the inlet region has increased in the transonic case (figure-5.3 and -5.4).

The magnitude of the scaling factor is a function of the cell geometry and propagation speed of the characteristics (equation (5.2.2)). This speed is derived from the eigenvalue of the jacobian of the convective term in the governing equations of the flow. It is found that the influence of the cell geometry on the scaling factor in high Mach number flow regions is small because the speed of the characteristic is high. In order to obtain significant improvement with the aspect ratio function, the constant α in equation (5.2.11) has to be reduced as

the flow speed increases. Therefore, the constant α in the aspect ratio function used for the transonic case is 0.4 and the one for the subsonic case is 0.6666. The detailed explaination is in Appendix-5.1.

In the subsonic case, the isentropic Mach number plots on the bump and the upper boundary for both the standard and the modified dissipations are approximately the same. The error in the mass flow rate of the standard case is slightly lower than that from the modified case. In the transonic case, the use of the aspect ratio correction function results in a slight improvement in the shock sharpness (figure-5.5). The error in the mass flow rate is slightly increased.

In the near wall region, the dominant dissipation D_ξ is significantly reduced in the leading and trailing edge regions for subsonic and transonic cases since it is along the length of the high aspect ratio cell (figure-5.6 & 5.7). The plots in these figures are along one grid line next to the bump. Near the upper boundary in the area where the cell aspect ratio is close to one, the effect of the aspect ratio is not significant. However, the implementation of the aspect ratio function for subsonic and transonic cases still results in the reduction of the dissipation in that region (figure-5.8a and b). Even though the cell aspect ratio is close to one in the inlet and exit regions near to the upper boundary, the investigation finds that the scaling factor due to the aspect ratio function is less than the standard scaling

factor because the value of α is less than one. This will be shown in the following paragraph.

In two dimensions, the scaling factor with Kuntz model is,

$$S_\xi = \left(\frac{Vol}{\Delta t_\xi}\right)\left[1 + \left(\frac{\Delta t_\xi}{\Delta t_\eta}\right)\right]^\alpha \qquad (5.4.4)$$

The isotropic scaling factor of the standard version is,

$$S = \left(\frac{Vol}{\Delta t_\xi}\right)\left[1 + \left(\frac{\Delta t_\xi}{\Delta t_\eta}\right)\right] \qquad (5.4.5)$$

as the aspect ratio ($\Delta t_\xi / \Delta t_\eta$) approaches one, S_ξ is still less than S since α is less than one.

In regions away from the bump, the length of the cell is along the η - direction. The aspect ratio function reduces the dissipation component along the η- direction more than it reduces the dissipation component along the ξ- direction.

For the subsonic case, the modified aspect ratio function (equation(5.2.13)) generates lower total pressure loss than the Kuntz's aspect ratio function (table-5.3 and figure-5.9). For the transonic case, the modified function does not introduce any significant reduction in the total pressure loss.

Since this test case is actually quasi three dimensional with one cell thickness in the ζ - direction, the r_ζ is not zero. In its implementation, the Kuntz's aspect ratio function is in the form of equation (5.2.11). The modified aspect ratio function (equation (5.2.13)) eliminates either r_η or r_ζ terms. The result is that the

scaling factor of the modified function is less than the scaling factor of the Kuntz function. Because of the lower α value for the transonic case compared with the value for the subsonic case, that elimination has little effect on the modification of the scaling factor.

B) Results with Mach Number Function

In this test case, the Mach number function is defined as

$$f(M) = M_L/M_{max} \qquad (5.4.6)$$

The ratio of M_L/M_{max} is always less than one since M_{max} is the maximum Mach number in the region. Mutiplying the dissipation flux by this ratio evaluated at the cell faces results in a reduction of the dissipation. Since the Mach number varies, this reduction also varies in the region. The Mach number correction function is implemented in combination with the aspect ratio function due to Kuntz. In order to obtain a converged solution the value of the fourth order constant K_4 has to be increased from the standard value for both the subsonic and transonic cases. During the iteration, M_L can be very low so that the resulting dissipation with standard K_4 is too low to achieve convergence. The results of the implementation of the combination of the aspect ratio and Mach number function are shown in table-5.3.

For the subsonic case, the total pressure loss with Mach number function is higher than the total pressure loss without Mach number function. This is partly due to the fact that a higher value of fourth order constant

is needed to obtain a converged solution. Thus, the implementation of the Mach number function does not result in a more accurate solution. The magnitude of the Mach number function is not low enough to compensate for the increase in the fourth order dissipation due to the increase in the value of the fourth order coefficient, K_4.

For the transonic case, the total pressure loss with the Mach number function is lower than the total pressure loss without the Mach number function (figure-5.10). The Mach number function is low enough to reduce the increase of the fourth order dissipation due to the increase of the K_4. Almost all of the reduction of the dissipation due to Mach number function is in the regions of leading and trailing edges of the bump because of the low Mach number in those regions. However, the resulting total pressure generation increases.

C) Results of Grid Refinement

A sharper shock can be obtained by refining the grid around the shock. The fine grid system is 90 X 24 (figure-5.11). The fine grid solution has a sharper shock, lower total pressure loss and slightly better conservation of mass (table-5.4, figure-5.12 & -5.13). However, the fine grid computation requires more CPU time. This result is computed with the standard dissipation.

5.4.1.2 Flat Plate Test Case

In order to eliminate geometric complexity and investigate the effect of the dissipation on viscous flow, flat plate flow is computed for laminar and turbulent

cases. The computation is done with the standard condition of zero static pressure gradient along the flat plate. The inlet Mach number is equal to 0.5. Two grid systems are used with sizes 78 X 61 and 76 X 31 (figure 5.14).

The laminar flow is computed on both grids whereas the turbulent flow is computed only on the second grid system because the first grid is not fine enough to resolve the boundary layer. The results of the computations of the laminar and turbulent flows are compared with the Blasius and 1/7th power law solutions respectively (White (1974) and Schlichting (1979)).

A) Results with Standard Model

The flow is first computed with the standard dissipation. In the first grid system, the laminar computation can converge without dissipation, but the displacement thickness and velocity profile are inaccurate in relation to the analytical solution. In the second grid system, a small amount of dissipation is required for both laminar and turbulent computations. K_4 is set to be 0.0005 for this test case whereas K_4 for other test cases is 0.008.

Because the dissipation is only a small amount, the viscous fluxes is larger than the dissipation in the high viscous region. The laminar cases are computed at Reynolds Numbers of $2X10^5$, $3X10^5$ and $7X10^5$ with the second grid but still show discrepancies in the boundary layer velocity profiles. However, the results are still more accurate than those with the first grid system

(figure-5.15). Therefore, the investigation will continue with the second grid only. The turbulent computation also shows discrepancies in the skin friction and velocity profile at Reynolds Number = 1.221×10^6 (figure-5.16).

The dissipation is a function of the grid size and flow gradient which in the normal y - direction can be expressed as

$$D_y = S\{\epsilon_y^2 \delta_y^2 W - \epsilon_y^4 \delta_y^4 W\} \qquad (5.4.7)$$

(see equation (3.4.3))

where the fourth order difference can be expressed as

$$\delta_y^4 W = (\Delta y)^2 \frac{\partial^4 W}{\partial y^4} \qquad (5.4.8)$$

The second order difference is eliminated because this is a subsonic case. With the 78 X 61 grid, Δ y near to the wall is not small enough to reduce the effect of the high flow gradient normal to the wall $(\frac{\partial^4 W}{\partial y^4})$ so that the near wall differencing is larger than the differencing near to the boundary layer edge. Since the dissipation in the normal direction is the dominating one , the near wall dissipation is larger than that at the boundary layer edge.

With the 78 X 31 grid, the near the wall Δ y is so small that the differencing near to the wall is smaller than the differencing near to the boundary layer edge. Thus, the near wall dissipation is smaller than the dissipation near to the boundary layer edge.

B) Results with the Aspect Ratio Function

In this computation, the aspect ratio function used

is that due to Kuntz with α set to 0.6666 and 0.0 for the laminar case ,and 0.6666 for the turbulent flow.

Analysis in the leading edge regions of the laminar and turbulent cases shows that the flow gradient along the length of the high aspect ratio cell is higher than that along the width of the cell. As a consequence, the component of the dissipation along to the length of the cell is dominating. Thus, the aspect ratio function is very effective in reducing the total dissipation in the leading edge region. The reduction of the dissipation in the laminar case with α = 0.0 is more than that with α = 0.6666 because the aspect ratio function with the first value severely reduces the dominant component along the length of the high aspect ratio cell.

For the case with α = 0.0, the scaling factor is redistributed anisotropically. The differences in each direction are multiplied by a scaling factor in that direction. Since the dissipation component in the direction of the length of the high aspect ratio cell is reduced significantly which results in significant reduction of the total dissipation, the computational results show large oscillation in the flow solutions. This large oscillation generates high error. Thus, the total pressure loss with α = 0.0 is higher than that with α = 0.6666. The loss is also higher than that without the aspect ratio function (figure-5.17).

In regions away from the leading edge but still close to the solid surface, the flow gradient across the

boundary layer results in the dominant dissipation component being normal to the wall. The flow gradient parallel to the wall is zero because of zero pressure gradient. The aspect ratio function will not be effective in the boundary layer since the dominant component is along the width of the high aspect ratio cell.

For laminar flow with both values of α , the aspect ratio function has very little effect in reducing the discrepancies in the boundary layer velocity profile in this region. For the case with α =0.6666, the computational results show reduction in total pressure loss.

For the turbulent flow, the aspect ratio function also has very little effect in reducing the above mentioned discrepancies in the same region.

C) Results with the Anisotropic Factor

By setting the anisotropic factor in the normal direction to 0.025, the dissipation in laminar and turbulent cases is effectively reduced (figure-5.18). However, discrepancies in the boundary layer velocity profile still exist. For the laminar flow, the total pressure loss is reduced (figure-5.19).

D) Results with the Velocity Function

The velocity function of equation (5.2.17) with V_{ref} = V_{inf} is implemented together with the aspect ratio function. This reduces the dissipation in the boundary layer. Because the viscous fluxes are larger than the dissipation, the reduction of the dissipation in that

region does not have any significant effect on the accuracy.

Also, the implementation of the velocity function with quadratic formulation such as

$$f\left(\frac{V_L}{V_{inf}}\right) = \left(\frac{V_L}{V_{inf}}\right)^2 \qquad (5.4.9)$$

severely reduces dissipation in the near wall.

E) Results with the Gradient Function

The gradient function with controlling factor B (equation (5.3.3)) is implemented in combination with Kuntz's aspect ratio function. Since the K_4 value of 0.0005 will result in small dissipation relative to other cases with higher K_4, the reduction of the dissipation due to the gradient function is small.

5.4.2 Two Dimensional Test Case

5.4.2.1 Computational Result with Standard Dissipation Model

The flow over a two dimensional high pressure (HP) turbine blade has been computed for turbulent flow. Flow at the inlet is subsonic with supersonic outlet. The sheared H-type grid used has grid size 134 X 41 (figure-5.20). The inlet flow conditions are

P_t = 159.519 kPa

T_t = 298.15 ^{o} K

θ_i = 56.75

Exit static pressure, P_{outlet}= 65.722 kPa

The dissipation coefficients are K_2 = 0.008 and K_4 = 0.008

The mass flow is approximately conserved within 1.57 %.

The computed total pressure loss at the exit is 11 % whereas the experimental data is about 9 %.

A contour of flow density clearly shows shocks on the suction and pressure sides of the blade (figure-5.21). The pressure side trailing edge shock is weak. Velocity vectors show that the boundary layer on the suction side stays attached.

Analysis of the computational results shows that the dissipation is higher than the viscous fluxes in the highly viscous region by factors of 2 to 10. A contour of the viscous fluxes of the energy equation indicates that the high viscous regions are located near the surface of the blade, in the wake region and near leading edge. The value of the second order dissipation is high at the suction side shock but is zero at the pressure side shock because the pressure side shock is too weak to turn on the second order dissipation.

A) Analysis of the Computational Result

By comparing with the experimental result (Xu, 1986), the computational result is inaccurate because the boundary layer on the suction surface is not separated, the pressure surface shock is too weak and the loss is high.

A.1) Contributing Factors to the Inaccuracy

A.1.1) Effect of Cell Aspect Ratio

The clustering of grid lines near to the solid wall results in cells of high aspect ratio. The scaling factor will be high for the dissipation component along the cell

length direction in high aspect ratio cells. This phenomena is explained in section 5.2.1.1. Since the dissipation in each direction is also dependent on other factors such as the flow gradient, grid size, etc., the high scaling factor may not result in excessive dissipation in that direction.

A.1.2) Effect of Grid Refinement

The grid refinement in the η - direction can reduce the dissipation. However, the computational results do not show this effect because the grid size is not small enough to reduce the effect of the flow gradient. The detail of the explanation is in the analysis section 5.4.1.2.

A.1.3) Effect of Difference

In this case, the differencing of the flow parameters has a dominant effect. This can be explained by following the analysis of the section 5.4.1.2. The fourth difference in the approximate normal direction is

$$\delta_\eta^4 W = (\Delta\eta)^4 \frac{\partial^4 W}{\partial \eta^4} \qquad (5.4.10)$$

where $\Delta\eta$ is the grid size.

In the highly viscous region with the coarse grid used in this case, the dominant effect is from the large variation of the flow parameters approximately normal to the wall. It is approximately normal because the differencing in equation (5.4.10) is along the blade to blade direction which is not quite normal to the blade surface because of the sheared grid.

A.2) Inaccuracy in Flow Phenomena

A.2.1) Nonseparated Boundary Layer due to Excessive Dissipation

Since the numerical dissipation is higher than the viscous fluxes, the high dissipation energizes the boundary layer so that it is stronger and can overcome tne adverse pressure gradient on the suction surface of the blade. Therefore, the boundary layer is more difficult to separate. However, other factors such as turbulent modelling or viscous discretization can also contribute to the inaccuracy of the nonseparated boundary layer.

A.2.2) Computational Shock Wave

A.2.2.1) Shock Strength

The computed shock on the pressure surface near to the trailing edge is rather weak (figure-5.21). The experimental result has a much stronger shock which extends all the way to the suction surface of the adjacent blade and causes the boundary layer to separate (figure-5.22). Factors which affect the shock strength include the second order dissipation coefficient and grid size.

A.2.2.2) Overshoot due to the Domination of Fourth Order Dissipation over Second Order Dissipation

The total dissipation for a cell centre at (i,j,k) location is decomposed into the second and fourth order dissipations for comparison. On a face located at i+1/2,j,k, the dissipation is expressed in equation (3.4.5). The second and fourth order dissipations at cell faces actually depend on the first and third order

differences.

If there is a discontinuity along the flow direction at face (i+1/2,j), the second order coefficient $\epsilon^2_{i+1/2,j} \neq 0$ and the fourth order coefficient $\epsilon^4_{i+1/2,j} \cong 0$.

At face (i-1/2,j),

$$\epsilon^2_{i-1/2,j} = K^2 \{\max(\delta_{i,j}, \delta_{i-1,j})\} \qquad (5.4.11)$$

which is equivalent to equation (3.4.5a) where

$$\delta_{i-1,j} = \frac{|p_{i,j}-2p_{i-1,j}+p_{i-2,j}|}{|p_{i,j}+2p_{i-1,j}+p_{i-2,j}|} \qquad (5.4.11a)$$

and $\delta_{i,j}$ is from equation (3.4.5c)

If the variation in p along the flow direction at face (i-1/2,j) is so small that the value of the sensor $\delta_{i,j}$ and $\delta_{i-1,j}$ are negligible then the second order coefficient $\epsilon^2_{i-1/2,j}$ =0 and fourth order coefficient $\epsilon^4_{i-1/2,j} \neq 0$. If there is no discontinuity in the blade to blade direction $\epsilon^2_{i,j+1/2}$ =0 and $\epsilon^4_{i,j-1/2} \neq 0$.

Thus, the fourth order dissipation is not turned off at the faces of (i-1/2,j), (i,j+1/2), and (i,j-1/2). The total dissipation at the cell centre is the summation of the second and fourth order dissipation at all cell faces. Unless $\epsilon^2 \neq 0$ and $\epsilon^4 = 0$ at all cell faces, the fourth order dissipation still exists on some of the faces. Since in this case the fourth derivative is larger than the second derivative, the fourth order dissipation is still dominating even in the presence of shocks. According to Jameson (1981), the fourth order dissipation

near the shock introduces overshoots.

5.4.2.2 Improved Models

A) Results with Aspect Ratio Function

With Kuntz's function, the computation cannot achieve convergence since the reduced dissipation is not enough to damp out the oscillation in the solution. Thus, the subsequent computations are done with Cheng's function setting α = 0.8333.

On the suction surface, the dissipation component in the blade to blade direction is higher than the dissipation component in the streamwise direction because the gradient in the former is higher than the latter. This high gradient is generated by the boundary layer effect. Since the length of the high aspect ratio cell on the suction surface is along the flow direction, Cheng's aspect ratio function will increase the high dissipation and decrease the low dissipation components. Thus, the total dissipation increases.

In the exit region, the dissipation component in the streamwise direction is higher than the dissipation component in the blade to blade direction because of the high aspect ratio cell in the flow direction. The aspect ratio function reduces the dissipation because the dominant component is reduced.

At the leading and trailing edge regions away from the blade surfaces, the dominant dissipation generated by the high flow gradient is along the length of the high aspect ratio cells which is in the blade to blade

direction. Thus, the aspect ratio function reduces the dissipation which makes a significant contribution to the overall reduction of total pressure loss (figure-5.23).

B) Results with the Mach Number Function

In order to reduce the dissipation in the boundary layer region such as the near wall region, a Mach number function is implemented. However, this function does not sufficiently reduce the dissipation because the grid lines in that region cannot resolve the boundary layer accurately. The computation with the velocity function also gives the same results. Kuntz and Lakshminarayana (1992) successfully reduced the dissipation in the boundary layer by using the velocity function with grid of 129 X 100 whereas the current computation is with grid of 134 X 41. Their grid system had a grid line distribution fine enough to resolve the boundary layer.

C) Result with the Anisotropic Factor

The anisotropic factors in the ξ - and η - directions used for the three test cases of different outlet Mach numbers 0.9, 1.0, and 1.2 are fac_{ξ} =0.5 and fac_{η} =0.05. The reduced dissipation modifies the solution. Because the solution is modified, the viscous fluxes is also reduced. The ratio of the dissipation with respect to the viscous fluxes for the standard solution is almost the same as that with the improved model. However, the summation of the dissipation and viscous fluxes of the improved model is less than that of the standard model. Since the accuracy depends upon that summation, the

application of the anisotropic factors resulted in the reduction of the total pressure loss (figure-5.24) and slight improvement in the prediction of the isentropic Mach number on the suction side (figure-5.25a and b).

D) Result with the Gradient Function

The proposed gradient function of equation (5.3.2) is implemented to reduce the dissipation in high flow gradient regions. The function with controlling factor B of equation (5.3.3) is implemented first. This results in an increase in dissipation in the near wall region because the flow gradient changes but the total pressure loss are reduced. The reason is that the effectiveness of the sensor $\delta_\xi M$ is reduced severely because B has to be equal to 0.01 in order to achieve convergence. The flow gradient function with cut off values of equation (5.3.2) is implemented. These cut off values are,

$$f_{D_\xi} = 1 \qquad (5.4.12a)$$

$$0.75 < f_{D_\eta} < 1 \qquad (5.4.12b)$$

The result shows that the dissipation is slighly reduced and the total pressure loss is also reduced (figure-5.26).

5.4.3 Three Dimensional Test Cases

Three test cases are computed. These are flows over a high pressure turbine blade, a transonic fan blade and an engine intake nacelle. The purpose of implementing the gradient and aspect ratio function is to reduce the dissipation in critical regions where cell aspect ratio and flow gradient are high.

5.4.3.1 High Pressure Turbine Test Case

The flow over three dimensional high pressure turbine blade has been computed for turbulence flow. The grid used is 97 X 37 X 33 and is of the sheared H typed (figure-5.27). Inlet boundary condition are total pressure, P_t = 179.86kPa, total temperature, T_t = 287^{o}K with inlet flow angle θ_i varying from hub to casing. On the outlet plane, a constant static pressure distribution is specified. The computation converges with K_2 = 0.0 and K_4 = 0.008. The mass flow is approximately conserved to within 1.2 %. The computational result of the mass mean total pressure at a distance of approximately 7 mm downstream of the trailing edge is 174.7 kPa whereas the experimental result is 176 kPa (Jefferson, 1990). There is total pressure generation in the blade passage (figure-5.28). The plots of isentropic Mach number at a mid height section on the suction and pressure side show relatively accurate results (figure-5.29).

A) Analysis of the Computational Result

Input parameters used for the Kuntz aspect ratio function of equation (5.2.11) and gradient function of equation (5.3.2) are in table-5.5. In the implementation of both functions, the α value used is the smallest below which the computation starts to diverge. In fact, the f_{D_f} cannot be reduced below one. The implementation of the aspect ratio function reduces the total pressure loss at the exit but it does not eliminate the total pressure generation. Whereas the implementation of the flow

gradient function results in the increase of the total pressure loss at the exit and the elimination of the total pressure generation (figure-5.30).

A.1) Relationship of Total Pressure Generation, Dissipation and Flow Acceleration

Analysis reveals the existence of positive dissipation in regions of flow acceleration which appears to result in the total pressure generation. Analysis will be carried out for a quasi one dimensional flow through a diverging nozzle (Shapiro,(1953)) (figure-5.31) to explain this,

The momentum equation

$$p_x A_x + m V_x = p_y A_y + m V_y + F_f + F_p + D \qquad (5.4.13)$$

The continuity equation

$$\dot{m} = \rho_x V_x A_x = \rho_y V_y A_y \qquad (5.4.14)$$

Substituting equation (5.4.14) into equation (5.4.13) and using the ideal gas law the result gives

$$p_x(1+ M^2_x)A_x = p_y(1+ M^2_y)A_y + F_f + F_p + D \qquad (5.4.15)$$

Normalization with P_t and A^* and expressing the ratio P/P_t and A/A^* as a function of Mach number, the result is

$$P_{tx} f(M_x) A_x = P_{ty} f(M_y) A_y + F_f + F_p + D \qquad (5.4.16)$$

where $$f(M_x) = \frac{1+\gamma M_x^2}{(1+\frac{\gamma-1}{2}M_x^2)^{\frac{\gamma}{1-\gamma}}} \qquad (5.4.16a)$$

and $f(M_y)$ is defined accordingly.

Assuming the total pressure difference as

$$P_{ty} = P_{tx} + \Delta P_t \qquad (5.4.17)$$

$$\text{then } \Delta P_t = \frac{P_{tx}(f(M_x)A_x - f(M_y)A_y) - F_f - F_p - D}{f(M_y)A_y} \quad (5.4.17a)$$

Without dissipation and friction force, F_f, $\Delta P_t = 0$, since the rate of change of momentum balances the pressure force, F_p.

The acceleration effect comes through the momentum flux difference which is

$$f(M_x)\ A_x - f(M_y)\ A_y > 0 \quad (5.4.18)$$

With the dissipation present, this value will decrease because in the presence of the viscous effect the acceleration is slowed down. Thus, the imbalance between the momentum flux and the forces is created. The addition of the positive dissipation will try to rebalance these quantities but its magnitude is so large that it also generates total pressure. The result of the two dimensional turbine blade of section 5.4.2 does not show total pressure generation because the dissipation is mostly negative.

A.2) Analysis of the Computational Result in Various Region of the Flow

The effects of the improved dissipation function is elaborated at each of the local region depicted in figure-5.32. Except for the endwall regions, the analysis will be concentrating on the midspan region where the dissipation component along the radial direction is smaller than the ones along the streamwise and blade to blade directions.

A.2.1) Leading Edge

In a region away from the blade leading edge, designated region A in figure-5.33, the length of the high aspect ratio cells is in the blade to blade direction. This results in the dominant dissipation component along the length of the cells.

In region B in figure-5.33, the dominant effect of the flow deceleration on the flow gradient is along the flow direction because of the stagnation point. The dominant dissipation is along that direction which is along the width of the high aspect ratio cells. Therefore, the aspect ratio function is more effective in reducing the dissipation in region A than in B. The reason is that the direction of the dominant dissipation is changing from that along the length to that along the width of the high aspect ratio cells. Whereas the gradient function is more effective in reducing the dissipation in region B than that in A because of the high gradient in B (figure-5.34).

A.2.2) Suction Surface

Here the dissipation component in the blade to blade direction is dominant near the wall because of the high flow gradient in the boundary layer. The dissipation component in the flow direction is dominant in the leading and trailing edge regions because of the high flow gradient in that direction. This component is also dominant in the wake because of the high scaling factor in the flow direction (figure-5.35).

A plot of the dissipation component along the span shows that the dominant component in the blade to blade direction reaches its maximum near to the midspan blade passage. The reason is that the boundary layer is thinner near midspan than near to the endwalls. However, the dissipation component in the radial direction is dominant near to the endwalls because of the gradient in the endwall boundary layer (figure-5.36). The dissipative fluxes are higher than the viscous fluxes in the front part but the two become comparable in the rear part of the blade (figure-5.37). The reason is that in the front part the boundary layer is thin and in the rear part the boundary layer is thick. The boundary layer becomes thick because of the the diffusion in the flow

Except for the regions near to the leading and trailing edges, the gradient function reduces the dominant component more than it does the nondominant component because the former component has higher gradients than the latter. The Kuntz's aspect ratio function reduces the nondominant component more than the dominant component because the first component is along the length of the high aspect ratio cell. Therefore, the gradient function is more effective in reducing the dissipation than the aspect ratio function (figure-5.38). The combination of the gradient function and aspect ratio function reduces the dissipation even more than the gradient function alone (figure-5.39). The plot along the span shows that the dissipation reduction due to the gradient function is

larger than the one due to the aspect ratio function. This plot also shows the effect of the flow gradient function where the maximum reduction is achieved in the midspan region (figure-5.40). The reduced dissipation is still higher than the viscous fluxes because the viscous fluxes are also affected by the modification function (figure-5.37).

A.2.3) Pressure Surface

The effects of flow gradient, aspect ratio, etc. on the dissipation near to the pressure surface are the same as the ones on the suction surface where the dominant dissipation is generated by the large flow gradient. This is especially so near to the leading and trailing edges where the dissipation is large. However, the dissipation level is lower than the one on the suction surface. The gradient function is more effective in reducing the large dissipation near to the trailing edge than the aspect ratio function (figure-5.41).

A.2.4) Trailing Edge

The dissipation is generated by the high flow gradient because of the change of flow direction near to the trailing edge. However, as one goes from the trailing edge to the exit, the flow gradient diminishes because the influence of the trailing edge diminishes. Therefore, the reduction of the dissipation due to the gradient function diminishes (figure-5.42). The aspect ratio function does not reduce the dissipation because the dominant component is along the width of the high aspect ratio cell.

A.2.5) Exit Region

The dominant component is in the flow direction because of the high aspect ratio cell along that direction. In this region, the aspect ratio function is more effective in reducing the dissipation than the gradient function because the flow gradient is not large enough to cause significant dissipation reduction through the gradient function (figure-5.43).

A.2.6) Endwalls

The effects of the flow gradient, cell aspect ratio etc, on the dissipation in the hub and casing are the same. The effect due to the blade surfaces in the corner region between the endwalls and the blade surfaces is the same as that in midspan. The additional effect of the endwalls is to increase the dissipation component along the radial direction so that it becomes dominant because of the high flow gradient generated by the endwall boundary layer. In the corner region where the cell aspect ratio is high, the width and height of the cells which are along the blade to blade and radial direction respectively are much smaller than the length.

The aspect ratio function reduces the dominant component along the width and height of the cell less than it reduces the nondominant component along the length of the cells. The gradient function reduces the dominant component (along the high gradient direction) more than it does the nondominant component (along the low gradient direction). Therefore, the gradient function is more

effective in reducing the dissipation than the aspect ratio function (figure-5.44).

In regions away from the blade surfaces, the effect of the blade surfaces diminishes so that the blade to blade direction is no longer dominant. The remaining dominant component is that along the height of the cell or in the radial direction which is still smaller than the width and the length of the cells. Thus, the aspect ratio function reduces the dominant components less than it does the nondominant ones. The gradient function also reduces the dominant component more than it reduces the nondominant one. This is especially the case downstream of the trailing edge as illustrated in figure-5.45.

Therefore, the gradient function is more effective in reducing the dissipation than the aspect ratio function, whereas the combination of the gradient and aspect ratio function is even more effective in reducing the dissipation than the gradient function alone.

Plots of velocity vectors on a meridional plane in the middle of the blade passage show the hub boundary layer separating in the diffusion region as a result of the implementation of the combined aspect ratio and gradient function (figure-5.46 a and b). This phenomena has already been explained for the two dimensional case in section 5.4.2.1.

The dissipation is comparable to the viscous fluxes near to the corner of the hub and suction surface but it is larger than the viscous fluxes near to the corner of

the hub and pressure surface. As the dissipation is reduced by the flow gradient function, the viscous fluxes are shifted towards positive values. However, the reduced dissipation is still dominanting compared with the modified viscous fluxes (figure-5.47).

A.3) Secondary Flow of the Computational Result

The investigation will concentrates on the flow phenomena near to the hub on different axial planes (figure-5.48). The horseshoe vortices are captured by the plot of the secondary velocity at a location downstream of the leading edge (figure-5.49a). The suction surface vortex stays at the corner of the hub and suction surface whereas the pressure side vortex moves away from the pressure side toward the suction side as one traces the vortices in the blade passage (figure-5.49 b & c). The boundary layer migration is observed to occur in the blade passage from pressure side towards the suction surface (figure-5.50). This induces a blade to blade flow which turns radially upward from the hub to the suction surface (Niehuis, Lucking and Stubert, 1990, and Horton, 1990) (figure-5.51). This flow finally wraps around to become a passage vortex (figure-5.52). At about this location, the suction side horseshoe vortex is dissipated by the passage vortex since it rotates in the opposite direction to the passage vortex. As the horseshoe vortex from the pressure surface moves towards the suction surface, it finally merges with the passage vortex since these two vortices rotate in the same direction.

The development of the above horseshoe and passage vortices confirms the flow model decribed by Sieverding and Van den Bosch (1983). They describes the synchronous evolution of the horseshoe and passage vortices obtained by experimental methods which are also discussed by Sieverding (1984 and 1985) and Denton (1993).

At about half way through the blade passage, a small vortex at the corner of the hub and suction side begins to develop which rotates in the opposite direction to the blade passage vortex (figure-5.54).

The effect of the dissipation reduction is clearly seen near to the trailing edge which increases the vorticity at the corner. This can be explained by the following analysis.

Momentum equation

$$\rho\frac{\partial\overline{V}}{\partial t}+\rho(\overline{V}.\nabla)\overline{V}=-\nabla p+\nabla.\overline{\overline{\tau}}+\rho\overline{f}_e \qquad (5.4.19)$$

Vortex identity

$$(\overline{V}.\nabla)\overline{V}=\nabla(\frac{V^2}{2})-\overline{V}X\overline{\omega} \qquad (5.4.20)$$

where $\overline{\omega}=\nabla X\overline{V}$

Substituting equation (5.4.20) to equation (5.4.19) and analyzing for steady state without external forces, the result is

$$\nabla p+\rho\nabla(\frac{V^2}{2})=\rho(\overline{V}X\overline{\omega})+\nabla.\overline{\overline{\tau}} \qquad (5.4.21)$$

where the viscous term $\nabla.\overline{\overline{\tau}}$ includes the artificial dissipation.

For a given pressure gradient ∇p and velocity gradient $\nabla(\frac{V^2}{2})$, the reduction in dissipation will increase

the vorticity, ω. Thus, the dissipation will quicken the decay of the vortices. As disccused above, the gradient function is more effective in reducing the dissipation near to the endwalls than the aspect ratio function . Thus, the gradient function has greater effect on the vortex development than the aspect ratio function. The combined aspect ratio and gradient functions will generate even higher vortex development than the gradient function alone.

The resulting effect is the growth of the strength of the corner vortex with the consequence of decreasing of the strength of the passage vortex (figure-5.54). This is a consequence of the friction between the corner vortex and passage vortex that rotate in the opposite directions.

The generation of the secondary flow near to the casing is similar to the one near to the hub. However, there is a radially inward flow towards the hub so that the passage vortex near to the casing is being pulled towards the hub (Zaccaria and Lakshminarayana (1995)). Therefore, the vortex does not rotate the fluid close enough to the corner of the suction surface and casing to generate the corner vortex.

At the exit, the reduction of the dissipation by the combined aspect ratio and gradient function generate an increase in the radial flow. With less viscosity, the flow is likely to become more three dimensional (figure-5.55).

A.4) Comparison of Computational Wake and Experimental Data

Contour plots of the total pressure show that the wake from the computational result is thicker than that from the test (Jefferson, 1990) (figure-5.56a & 5.56b). The implementation of the aspect ratio function and gradient functions or the combination of both functions do not lead to a reduction of the wake thickness. Most of the wake thickness originates from the suction surface where the total pressure loss starts to grow significantly from the leading edge. Improvement of the grid resolution in the leading edge region may be able to reduce the wake thickness.

A.5) Effect of Dissipation Reduction to Exit Whirl Angle

A plot of the whirl angle in the radial direction at the exit plane indicates flow underturning and overturning toward the casing and hub respectively. The effect of the cell aspect ratio and flow gradient functions in the wake is to increase the underturning and overturning. However, the effect of these functions near to the endwalls is to decrease the underturning and overturning. This phenomena is induced by an increase in the vorticity of the secondary flow (figure-5.57). The vertical axis in this plot is in millimeters. Thus, the reduction of the dissipation due to the aspect ratio and gradient functions changes the whirl angle.

5.4.3.2 Three Dimensional Transonic Fan

A three dimensional generic fan blade has been

computed. The grid used is 99 X 33 X 33 and of the sheared H-type (figure-5.58). Total pressure, total temperature and whirl velocity are specified on the inlet plane. The total temperature is set constant at 287^{o}K but the total pressure and whirl velocity vary radially on the inlet plane. At the exit plane, a static pressure distribution is speficied. The computation converges with K_2 = 0.01 and K_4 = 0.008. The mass flow is approximately conserved to within 1.1 %. The computated total pressure loss at the exit is 5.0 % (figure-5.59). An oblique shock appears on the leading edge pressure side and merges with the normal shock in the blade passage the suction surface (figure-5.60).

A) Analysis of the Computational Result

Both the gradient function and the aspect ratio function of Martinelli are applied here. The implementation of Kuntz's aspect ratio function of equation (5.2.11) does not achieve convergence because the dissipation is reduced in the entire region. On the other hand, the three dimensional version of the Martinelli's function of equation (5.2.10) increases the dissipation in the region where the dominant component is along the width of the high aspect ratio cells.

The cut off value of the gradient function is set to be 0.75 for the blade to blade and radial directions, but there is no dissipation reduction in the flow direction. The constant α for the aspect ratio function is 0.75. The loss shows very little change after implementing the

gradient and the combined gradient and aspect ratio functions. Since the computation with reduced K_4, which is equal to 0.004, fails to converge, the computational result with standard dissipation, where K_4 is equal to 0.008, does not have a large amount of excessive dissipation that can be reduced by the modification function. The analysis of the result with modified dissipation is elaborated as follows:

A.1) Analysis of the Dissipation near Suction Surface

At the front part where the boundary layer is thin, the dissipation is higher than the viscous fluxes and in the rear part where the boundary layer is thick the dissipation is lower than the viscous fluxes (figure-5.61). As the flow enters the diffusion region, the boundary layer is thickened. The component along the blade to blade direction is dominant and the one along the radial direction becomes dominant in the rear part of the blade. A plot of the dissipation in the spanwise direction shows that the dissipation component along the blade to blade direction reaches its maximum at mid span where the boundary layer is thin and it decreases towards the endwalls where the boundary layer is thick. In the near wall region, the thin boundary layer generates steeper gradients than the thick boundary layer. The dissipation along the radial direction is also large around mid span (figure-5.62).

The implementation of the gradient function reduces the dissipation because it reduces the component with

large gradient which is the dominant one (figure-5.63). The results show that the dissipation is larger than the viscous fluxes in the front part of the blade. They also show that the dissipation is smaller than the viscous fluxes in the rear part of the blade (figure-5.64).

The implementation of the combined aspect ratio and gradient functions show less dissipation reduction than the implementation of the gradient function alone (figure-5.63). This indicates that the magnitude of the reduction due to the gradient function is larger than the magnitude of the increment due to the aspect ratio function. Thus, the aspect ratio correction to the scaling factor has less effect than the gradient correction.

A.2) Analysis of the Dissipation near Pressure Surface

The dissipation reaches its maximum value near to the leading edge because of large flow gradient, and it is larger than the dissipation on the suction surface (figure-5.65). This can be clearly seen from the plot of the dissipation along the blade to blade direction close to the leading edge. The dissipation is large towards the pressure surface where the shock stands (figure-5.66). The effect of the gradient function on the pressure surface is smaller than on the suction surface.

5.4.3.3 Three Dimensional Engine Intake Nacelle

The flow through a three dimensional intake nacelle has been computed for a turbulence case. The grid used is 97 X 18 X 35 and is of C-type (figure-5.67a and b). The

flow conditions at the inlet are

P_t = 101.325 kPa

T_t = 288°K

angle of incidence θ_i = 21

and it converges with K_2 = 0.0 and K_4 = 0.008

Exit static pressure p_{fan} = 80kPa and the free stream Mach number, $M_{free\ stream}$ = 0.35. The computed mass flow is 2 % higher than the experimental data.

A) Solution with Standard Dissipation

For a given incidence, the flow is distorted in the radial as well as the circumferential direction. The flow distortion can be measured by the distortion coefficient DC_{60} which is defined as follows

$$DC_{60} = \frac{P_{60} - P_{mean}}{(1/2)\rho V^2} \qquad (5.4.21)$$

This is a measure of the worst mean total pressure loss over a 60° sector at the fan face (Seddon and Goldsmith, 1985). The experimental DC_{60} is -0.10 and the computed DC_{60} is -0.0917.

Plots of streamwise surface isentropic Mach number at different circumferential locations indicate inaccuracy in the lip region in the inner wall (figure-5.68).

B) Solution with Modified Dissipation

The combined gradient and aspect ratio function is used because this provided the largest dissipation reduction in the earlier high pressure turbine case. The cut off values of the gradient function, and the constant

α of the aspect ratio function used are the same as the ones in the turbine case. The resulting DC_{60} is -0.0982.

The dissipation component along the radial direction is dominant because of the flow gradient in that direction generated by the boundary layer. The component parallel to the wall is large in the inner wall towards the fan face and towards the outer exit region. The component along the circumferential direction is negligible because the flow gradient is negligible (figure-5.69).

The combined function is effective in reducing the dissipation at the different circumferential positions. It also smooths out the kink in the dissipation due to the geometric changes in the inner wall (figure-5.70a, b). The gradient function significantly reduces the dominant component because it is generated by the high gradient. The aspect ratio function signicantly reduces the nondominant component along the wall because it is along the length of the high aspect ratio cells

In the near wall region at the circumferential position where the angle of incidence is almost zero, the viscous fluxes are larger than the dissipation from the inner lip through to the outer wall. The viscous fluxes are also comparable with the dissipation in some parts of the inner wall. However, the dissipation is larger than the viscous fluxes near to the inner wall downstream of the lip up to a location where the dissipation plot has a kink (figure-5.71a).

In the near wall region at the circumferential

position where the angle of incidence is maximum, the viscous fluxes are larger than the dissipation near to the inner wall because of the thick boundary layer (figure-5.71b). At this position, the flow has to overcome the adverse pressure gradient downstream of the shock (figure-5.72). This eventually results in the formation of a separation bubble. The boundary layer on the outer wall is thinner than the one on the inner wall, therefore the viscous fluxes are smaller than the dissipation on the outer wall (figure-5.71b). However, the viscous fluxes are also comparable with the dissipation close to the highlight region. The effect of the dissipation reduction is to reduce the viscous fluxes so that the dissipation is still higher than the viscous fluxes.

The flow with reduced dissipation has higher distortion coefficient than the one with standard dissipation which indicates that the flow has higher losses. However, the distortion coefficient of the reduced dissipation is approaching the experimental values. The higher losses are generated by a larger separation bubble. In the presence of the adverse pressure gradient, the boundary layer with reduced dissipation is more likely to produce a larger separation bubble. This is shown by a larger extent of reversed flow in the velocity profile plot dowmstream of the shock (figure-5.73a, b and c)

5.5 Conclusion

The artificial dissipation is shown to be dependent on the scaling factors, second and fourth order coefficients, flow parameter gradients and the grid spacing. With the present test cases, the standard version results in discrepancies in losses, shock sharpness, nonseparated boundary layer growth, and total pressure generation. The test cases for this investigation are Ni's bump, flat plate, two and three dimensional high pressure turbine blades, a three dimensional fan blade and a three dimensional intake nacelle.

The inviscid Ni's bump flow is computed to investigate the effect of the aspect ratio function, Mach number function and the grid refinements. In the absence of large flow gradient normal to the wall, the dominant component of the dissipation is along the length of the high aspect ratio cell around the leading and trailing edges of the bump. The Kuntz's aspect ratio function is very effective in reducing the dominant component of the dissipation. Thus, the reduction of the total dissipation leads to the reduction of the total pressure losses for subsonic and transonic cases and also results in slight improvement in shock sharpness for the transonic case.

The total pressure loss with the combined aspect ratio and Mach number function is higher for the subsonic case and lower for the transonic case than the one due to the aspect ratio function only. The reason is that the

fourth order coefficient has to be increased in order to achieve convergence. The implementation of the modified aspect ratio function originating from Cheng results in a further reduction of the total pressure loss relative to that of Kuntz. Refinement of the grid around the shock results in a sharper shock, lower total pressure loss and lower mass flow error but it requires more CPU time.

The flat plate is a simple test case for investigating the effect of the dissipation on the viscous flow in both fine and coarse grids. With the fine grid, the grid spacing near to the wall is so small that it reduces the effect of the flow gradient to the dissipation. The computation of both the laminar and turbulent flow cases can converge with a small amount of dissipation. Therefore, the reduction of dissipation has little effect in reducing the difference in the boundary layer velocity profile compared to the analytical solutions.

In the near wall region away from the leading edge, the dissipation is dominated by the normal component. The anisotropic factor reduces the dissipation in the boundary layer. The velocity function severely reduces the dissipation but the combined gradient and Kuntz's aspect ratio function only reduces a small amount of the dissipation. For laminar flow, the total pressure loss is reduced by the aspect ratio function. In the leading edge region, the dissipation component parallel to the wall along the length of the high aspect ratio cells is

dominanting. Thus the aspect ratio function reduces the total dissipation in this region.

The computational results of the two dimensional high pressure turbine blade with the standard dissipation shows inaccuracy in the solution. A comparison with the experimental data indicates that the computed shock is smeared, suction surface boundary layer separation is not predicted and the loss is too high. Analysis of the results shows that the dissipation contributes to the inaccuracy.

In the boundary layer region, the dissipation is higher than the viscous fluxes. The high gradient and coarse grid size near to the wall in the blade to blade direction result in large differences which generate dominant dissipation component in that direction. Since this component is actually in the width of the high aspect ratio cells, the Cheng's aspect ratio increases the dissipation near to the wall. However, this function reduces the dissipation near to the leading edge, trailing edge and exit region because the dominant component is in the length of the high aspect ratio cell. Thus, it results in the reduction of losses. The implementation of the Kuntz's aspect ratio function does not lead to a converged solution because the dissipation is reduced in the entire region. The anisotropic factors reduce the dissipation in all regions and results in the highest reduction of the losses. However, the reduced dissipation is still higher than the viscous fluxes.

The gradient function with the controlling factor and cut off values reduces the losses. Since the case with the cut off values provide slight dissipation reduction in high viscous region and does not reduce the effectiveness of the gradient sensor, it is implemented in three dimensional cases.

The computed results of the three dimensional high pressure turbine blade with the standard dissipation for subsonic turbulent case produces high losses and total pressure generation. The gradient function eliminates total pressure generation but it results in an increase in losses at the exit region. However, the Kuntz's aspect ratio function cannot eliminate the total pressure generation but it slightly reduces the losses at the exit region.

The gradient function is more effective in reducing the dissipation than the Kuntz's aspect ratio function in the near wall region, leading and trailing edge regions because the dominant component is along the direction of high flow gradient. The aspect ratio function is more effective in reducing the dissipation than the gradient function near the exit because the effect of the scaling factor is large in the dominant component of the dissipation. The combined gradient and aspect ratio function is more effective in reducing the dissipation than the gradient function alone.

The secondary flow described by the horseshoe, passage and corner vortices are captured successfully and

they agree with the experimental observation. The effect of the combined gradient and aspect ratio function is an increase in the corner vortex strength which results in an increased rate of mixing. At the exit plane, this effect is described by the increase in radial flow and the change of the whirl angle. The accuracy of the wake very much depends on the resolution of the boundary layer in the leading edge region.

A three dimensional generic fan is computed to investigate the effect of the dissipation reduction in transonic flow. However, this particular case does not have excessive dissipation that can be reduced by the modification function. Instead of the Kuntz's aspect ratio function, the Martinelli's aspect ratio function is implemented because the computation with Kuntz's function cannot achieve convergence. Near to the wall, the gradient function is more effective in reducing the dissipation than the combined gradient and aspect ratio function because the effect of the gradient is larger than the effect of the scaling factor.

An intake flow at high incidence is computed to investigate the effect of the combined gradient and aspect ratio function. The loss generated by the flow distortion is measured by a distortion coefficient. The predicted coefficient is slightly less than the test data. The reduction in dissipation due to the combined function at the near wall provides better prediction because here the flow is more lossy. This is because of

lower viscosity where the flow is less capable of overcoming an adverse pressure gradient generated by the shock. This results in a wider region of separation and hence higher losses.

From all of the computational cases several common features of the effect of the modification function can be summarized in the following paragraph.

The excessive dissipation component normal to the wall is due to the large differences of the flow parameters in the boundary layers. The excessive dissipation component along the length of the high aspect ratio cell is due to the large scaling factor in that direction. The solutions are also inaccurate because the dissipation is larger than the viscous fluxes.

The anisotropic factors have already been implemented in the standard version and it effectively reduces the excessive total dissipation. The aspect ratio function effectively reduces the excessive dissipation component along the direction of the cell length through the reduction of the scaling factor. The Mach number or the velocity function reduces the dissipation in the boundary layer as well as low speed region. The grid refinement to the near shock leads to increase in the shock sharpness. The proposed gradient function effectively reduces the excessive dissipation component along the high flow gradient region.

6.0 EIGENVALUES ANALYSIS

6.1 Introduction

A consequence of using the central difference scheme in the spatial discretization is that oscillations in the solution that grow to cause divergence (Hirsch, 1989). To overcome the problem, artificial dissipation is added to damp out these oscillations but this generates inaccuracy (usually manifest as excessive diffusion and losses). By reducing the dissipation, the damping of the oscillation becomes less and the convergence of the computation becomes slower but the solution becomes more accurate (so long as convergence can still be achieved). The intention is to balance accuracy and robustness and the method proposed here involves selectively reducing the dissipation at each grid point, (especially in the overdamped region) based on an " eigenvalue" criteria. The intention here, therefore, is to develop a robust method that will provide a more accurate solution.

The method involves the use of a matrix technique to calculate the eigenvalues for each grid point. These values contain information about the stability of the scheme (Hirsch, 1989). The addition of the dissipation results in reducing the numerical values of the eigenvalue spectrum. In general, sufficient dissipation must added to make all real parts of eigenvalues negative. Reduction of the dissipation increases the numerical values of the eigenvalues and eventually some of them may be positive so destablizing the scheme. In this way, eigenvalues can be

used as a "sensor" to determine how much the dissipation can be reduced without causing the computation to diverge. In other words, the local eigenvalues can be used as a means of tailoring the dissipation whilst maintaining stability.

A full implementation of the matrix method to assess the eigenvalues of the two dimensional Navier-Stokes equations involves spatial discretization of the flux terms providing a semi-discretized equation with both transient and steady terms. The transient terms are decomposed into a stability matrix (which is actually the discretized Jacobian matrix) and a vector which represents the discretized state variables. The resulting stability matrix, however, is 16 x n x n (where n is total number of grid points) and evaluation of the eigenvalues of this matrix is currently prohibitively expensive.

The objective of utilizing the eigenvalues as sensors requires the computation of the eigenvalues at every grid point per iteration within affordable time. Erickson and Rizzi (1985), and Mahajan, Dowel and Bliss (1989, 1991) discussed methods of calculating eigenvalues but the size of the stability matrix was still 16 x n x n. To overcome this problem assumptions are adopted which involve taking advantage of the explicit formulation where an approximate matrix analysis does not include the influence of the neighbouring cells (Santos 1993, 1994). This results in n 4 x 4 matrices which can be evaluated relatively quickly. It should be appreciated, however, that the eigenvalues of

the reduced matrix (resulting from the above assumption) contain only an approximation of the odd-even decoupling, viscous dissipation and nonlinearity influences.

As already explained, after implementing the approximate matrix analysis, the stability matrix is reduced to n 4 x 4 matrices (four eigenvalues per point). Each state variable such as ρ, ρu, ρv and ρe is decomposed into four eigenmodes where they depend on all four eigenvalues in a manner defined by the eigenvectors. Instability then occurs if any of the eigenmodes grow without bound and the computation of the Navier-Stokes equations requires the addition of artificial dissipation to obtain a converged solution where all the real parts of the eigenvalues are negative.

Having assesed the eigenvalues of the system, two methods of controlling dissipation are discussed. The first method is direct and involves establishing rates of convergence (which depends upon eigenvalues) and then calculating the necessary dissipation to maintain that rate. The method is based upon a system of non-linear equations and the method of Inverse Eigenvalue Problem (IEP). In order to implement this method, further study is required on well posedness of the non-linear equation set. In addition, further extension of the IEP is required to solve the non-symmetric matrices which characterize the stability problem. The second method is indirect and based much more simply on reducing dissipation in regions of large negative eigenvalues (i.e. overdamped region).

This method is implemented for the inviscid flow over Ni's bump (Ni, 1985) and the viscous flow over a two dimensional high pressure turbine blade.

6.2 Analysis

6.2.1 Spatial Discretization

The implementation of the matrix method to the Navier Stokes equations requires spatial discretization of the flux terms. By following the derivation in section 3.5, a system of linear equations for the entire flow field is obtained which is expressed in equation (3.5.6), as follows

$$A \frac{dq_{i,j}}{dt} = -M_G \, q_{i,j} + R_G \qquad (3.5.6)$$

where

$$q_{i,j} = \begin{bmatrix} q_{11} \\ q_{21} \\ \cdot \\ \cdot \\ q_{N1} \\ q_{12} \\ q_{22} \\ \cdot \\ \cdot \\ q_{N2} \\ \cdot \\ \cdot \\ \cdot \\ q_{1M} \\ q_{2M} \\ \cdot \\ \cdot \\ q_{NM} \end{bmatrix}$$

where N and M are the maximum index of i and j , respectively and the derivation of matrix M_G will be elaborated in the following paragraph.

In the two dimensional case, the flux at face (i+1/2,j) (represented by equation (3.5.5)) is

$$\text{Flux}_{i+1/2,j} = \{(A+C)\,\Delta S_x - (B+D)\,\Delta S_y\}(q_{i+1/2},j)/2$$

Similar expressions are substituted into equation (3.5.2) which is

$$A\frac{dq_{i,j}}{dt} + \sum_{p=1}^{4} \overline{H}_p . \overline{N}_p \Delta S_p = 0$$

$M_G\, q_{i,j}$ can then be expanded as

$$M_G q_{i,j} =$$

$$\{-(A+C)\Delta S_x - (B+D)\Delta S_y\}_{i,j-\frac{1}{2}} q_{i,j-1} + \{-(A+C)\Delta S_x + (B+D)\Delta S_y\}_{i-\frac{1}{2},j} q_{i-1,j}$$

$$+[\{(A+C)\Delta S_x - (B+D)\Delta S_y\}_{i+\frac{1}{2},j} + \{-(A+C)\Delta S_x + (B+D)\Delta S_y\}_{i-\frac{1}{2},j} +$$

$$\{(A+C)\Delta S_x + (B+D)\Delta S_y\}_{i,j+\frac{1}{2}} + \{-(A+C)\Delta S_x - (B+D)\Delta S_y\}_{i,j-\frac{1}{2}}]q_{i,j} +$$

$$\{(A+C)\Delta S_x - (B+D)\Delta S_y\}_{i+\frac{1}{2},j} q_{i+1,j} + \{(A+C)\Delta S_x + (B+D)\Delta S_y\}_{i,j+\frac{1}{2}} q_{i,j+1}$$

(6.2.1)

Since the viscous Jacobian matrices C and D (in equation 6.2.1) contain derivative operators, the terms belonging to neighbouring cells $q_{i+1,j}$, $q_{i-1,j}$, $q_{i,j+1}$ and $q_{i,j-1}$ are expanded to cover other neighbouring cells (figure-6.1) (this is a consequence of the viscous discretization scheme adopted). After decomposing $M_G\, q_{i,j}$ into matrix (M_G) and vector ($q_{i,j}$) format, the matrix M_G becomes

$M_G = \{m_{i+2,j}, m_{i+1,j}, m_{i,j}, m_{i-1,j}, m_{i-2,j}, m_{i+1,j+1},$
$m_{i,j+1}, m_{i-1,j+1}, m_{i+1,j-1}, m_{i,j-1}, m_{i-1,j-1}, m_{i,j+2},$
$m_{i,j-2}\}$ (6.2.2)

The size is 16 x n x n where n is the total number of grid points. The elements depend upon the inviscid and viscous Jacobian matrices.

The major effects described by the eigenvalues of the

matrix M_G are i) the odd-even decoupling from the convection term, ii) viscous dissipation from the diffusion term, and, iii) nonlinearity of the Navier-Stokes equations. A detailed analysis of these effects will be elaborated by using a test model of a scalar equation.

6.2.1.1 Odd-Even Decoupling

The background to odd-even decoupling was explained in section 3.4, and the semi discretized equation (3.4.3) which is

$$\frac{du}{dt} + a\frac{(u_{i+1} - u_{i-1})}{2\Delta x} = 0$$

can be expressed in matrix form as

$$\frac{dU}{dt} + M_o U = R_o \qquad (6.2.3)$$

where

$$M_o = \frac{a}{2\Delta x}\begin{bmatrix} 0 & 1 & & & & & \\ -1 & 0 & 1 & & & & \\ & -1 & 0 & 1 & & & \\ & & \cdots & \cdots & & & \\ & & & \cdots & \cdots & & \\ & & & & -1 & 0 & 1 \\ & & & & & -1 & 0 \end{bmatrix} \quad \text{and} \quad U = \begin{bmatrix} u_1 \\ u_2 \\ u_3 \\ \cdot \\ \cdot \\ \cdot \\ u_{n-1} \\ u_n \end{bmatrix}$$

Thus, U is a vector of the one dimensional variable u_i; matrix M_o is an n x n tridiagonal matrix of the form $M_o(l,c,r)$ where the diagonal element c is zero (n is number of grid points) and R_o contains the nonhomogenous terms. By incorporating periodic boundary conditions, the eigenvalues can be calculated with the following formula (Hirsch, 1989)

$$\lambda_j = c + (l+r)cos\frac{2\pi j}{n} - IN(l-r)sin\frac{2\pi j}{n} \qquad (6.2.4)$$

and R_o is zero.

In this case, c=0, l=-a/(2Δx), r=a/(2Δx), and IN = $\sqrt{-1}$ then the eigenvalues are

$$\lambda_j = -\frac{a}{2\Delta x}(IN)sin\frac{2\pi j}{n} \qquad (6.2.5)$$

where j=1,...,n

Since all eigenvalues are imaginary, the solution is oscillatory. This is, in fact, due to the odd-even decoupling because the matrix M_o does not depend on the values at the cell i itself. Since all real eigenvalues are zero, the matrix method indicates that the time evolution of the variable u_i in the semi discretized equation (6.2.3) is neutrally stable.

6.2.1.2 Viscous Dissipation

The diffusion terms generate dissipation which, in the Navier Stokes equations, are represented by the viscous terms. In order to investigate the viscous dissipation, a linear scalar convection-diffusion equation is used as a test. This equation has the following form

$$\frac{\partial u}{\partial t} + a\frac{\partial u}{\partial x} = \nu\frac{\partial^2 u}{\partial x^2} \qquad (6.2.6)$$

With the finite volume method, this equation is integrated and the resulting semi discretized equation is

$$\frac{du}{dt} + a\frac{u_{i+\frac{1}{2}} - u_{i-\frac{1}{2}}}{\Delta x} = \nu\left\{\left(\frac{\partial u}{\partial x}\right)_{i+\frac{1}{2}} - \left(\frac{\partial u}{\partial x}\right)_{i-\frac{1}{2}}\right\}\frac{1}{\Delta x} \qquad (6.2.7)$$

(The values at the faces (i+1/2) and (i-1/2) are

approximated by straight averaging). The convection term becomes similar to the one in equation (3.4.2) whereas the derivatives $\left(\frac{\partial u}{\partial x}\right)$ of the diffusion term is evaluated in a similar manner to the convection terms. Substituting the result into equation (6.2.7), for a uniform grid, this equation becomes

$$\frac{dU}{dt} + a\,\frac{U_{i+1} - U_{i-1}}{2\Delta x} = \nu\,\left(\frac{U_{i+2} - U_i + U_{i-2}}{\Delta x^2}\right) \qquad (6.2.8)$$

By writing the above equation in matrix form, it simplifies to

$$A\,\frac{dU}{dt} = M_s U + R_s \qquad (6.2.9)$$

where the formulation of matrix M_s is

$$M_s = \left\{ \frac{\nu}{\Delta x^2}, -\frac{a}{2\Delta x}, \frac{2\nu}{\Delta x^2}, \frac{a}{2\Delta x}, -\frac{\nu}{\Delta x^2} \right\} \qquad (6.2.10)$$

and its size is n x n (n being the number of grid points) and again R_s contains the nonhomogenous terms. This matrix is no longer tridiagonal. Because the matrix M_s contains a diffusion constant ν ,its eigenvalues contain information about the viscous effect. Since the diagonal elements of matrix M_s are not zero, the time evolution of u_i depends upon u_i and its neighbours which provide coupling among the values at cell i and its neighbours.

6.2.1.3 Nonlinearity

Nonlinear effects are investigated by using a non-linear scalar convection equation as a test model which is

$$\frac{\partial u}{\partial t} + \frac{\partial a(u)u(x)}{\partial x} = 0 \qquad (6.2.11)$$

where a(u) is a function u

In the finite volume method, this equation is integrated and the resulting semi-discretized equation is

$$\frac{du}{dt} - \frac{a_{i+\frac{1}{2}}u_{i+\frac{1}{2}} - a_{i-\frac{1}{2}}u_{i-\frac{1}{2}}}{\Delta x} = 0 \qquad (6.2.12)$$

where $a_{i+1/2} = a(u_i + u_{i+1})/2$

As in the previous section, $u_{i+1/2}$ is evaluated by a straight averaging approximation and in a uniform grid the above equation can be written as

$$\frac{du_i}{dt} - \frac{a_{i-\frac{1}{2}}}{2\Delta x}u_{i-1} + \frac{a_{i+\frac{1}{2}} - a_{i-\frac{1}{2}}}{2\Delta x}u_i + \frac{a_{i+\frac{1}{2}}}{2\Delta x}u_{i+1} = 0 \qquad (6.2.13)$$

By writing the above equation in matrix form then

$$\frac{dU}{dt} + M_L U = R_L \qquad (6.2.14)$$

For a linear case, variable a does not depend on variable u so $a_{i+1/2} - a_{i+1/2} = 0$ and the above equation then becomes the same as equation (3.4.3). In the non-linear case, the matrix M_L is n x n tridiagonal with the form of

$$M_L = \left\{ -\frac{a_{i-\frac{1}{2}}}{2\Delta x}, \frac{a_{i+\frac{1}{2}} - a_{i-\frac{1}{2}}}{2\Delta x}, \frac{a_{i+\frac{1}{2}}}{2\Delta x} \right\} \qquad (6.2.15)$$

and R_L contains the nonhomogenous terms

Its eigenvalues contain information about nonlinear effects which come from the diagonal elements. Because those elements are not zero, the time evolution of u_i depends upon u_i and its neighbours. Thus nonlinear effects provide coupling between u_i and its neighbours.

6.2.1.4 Approximate Formula

The computation of the eigenvalues of matrix M_G of equation (3.5.6) with the size 16 x n x n would consume considerable computing time and memory. As a first step towards reducing this, an approximate method is studied. This method discards the dependence of the time evolution of u_i on its neighbours and was first proposed by Santos, (1993 and 1994).

It should be clear from the above analysis that the coefficient of the terms belonging to neighbouring cells determine the effect of the odd-even decoupling as well as viscous dissipation. If the terms belonging to the neighbouring cell are not included in the calculation of the eigenvalues, the resulting eigenvalues will not contain the effect of the odd-even decoupling and will not represent the full effect of the viscous dissipation. Thus, they represent a reduced effect of the viscous dissipation and nonlinearity which will be analyzed in the following paragraphs.

The combination of the viscous dissipation and nonlinearity effect can be expressed by combining equation (6.2.8) and (6.2.13). Then, the combined equation in semi discretized form will be

$$\frac{dU_i}{dt} - \left(\frac{2\nu}{\Delta x^2} - \frac{a_{i+\frac{1}{2}} - a_{i-\frac{1}{2}}}{2\Delta x}\right) U_i = r_A \qquad (6.2.16)$$

which in matrix form is

$$\frac{dU}{dt} + M_A U = R_A \qquad (6.2.17)$$

where the size of the matrix is still n x n. R_A contains

terms belonging to the neighbouring cells and nonhomogenous terms. Thus, the elements of the diagonal matrix M_A is

$$m_1 = -\left(\frac{2\nu}{\Delta x^2} - \frac{a_{1+\frac{1}{2}} - a_{1-\frac{1}{2}}}{2\Delta x}\right) \qquad (6.2.18)$$

In this analysis, the variables U and R_A can be expressed as a summation of the eigenvectors of the matrix M_A (Tropper, 1969 and Ayres, 1974), which will be

$$U(t) = \sum_{j=1}^{n} U_j(t) V^{(j)} \,, \; R_A = \sum_{j=1}^{n} R_{Aj} V^{(j)} \qquad (6.2.19)$$

where $U_j(t)$ is the time dependent coefficient of U(t), R_{Aj} are coefficients of R_A, and $V^{(j)}$ are the eigenvectors.

Following the derivation by Hirsch (1989), the solution for U(t) can be expressed as

$$U(t) = \sum_{j=1}^{n} [(U_{0j} + \frac{R_{Aj}}{\lambda_j}) e^{\lambda_j t} - \frac{R_{Aj}}{\lambda_j}] V^{(j)} \qquad (6.2.20)$$

where U_{oj} is the coefficient of the expansion of u(t)at t=0. Thus, the solution of equation (6.2.20) is the summation of n eigenmodes and in order to achieve a converged solution none of the modes should grow without bound during the iteration. Since the eigenvalues of the diagonal matrix M_A are the diagonal elements, then

$$\lambda_j = -\left(\frac{2\nu}{\Delta x^2} - \frac{a_{1+\frac{1}{2}} - a_{1-\frac{1}{2}}}{2\Delta x}\right) \qquad (6.2.21)$$

At convergence, the eigenvalues must be negative then

$$-\left|\frac{2\nu}{\Delta x^2} - \frac{a_{i+\frac{1}{2}} - a_{i-\frac{1}{2}}}{2\Delta x}\right) < 0 \qquad (6.2.22)$$

The contribution of the dissipation - $(\frac{2\nu}{\Delta x^2})$ is always stabilizing. The destabilizing effect come from the nonlinearity which depends on $\frac{a_{i+\frac{1}{2}} - a_{i-\frac{1}{2}}}{2\Delta x}$.

The value of the variable a(u) of equation (6.2.11) at any location contributes to one eigenvalue controling time evolution of one eigenmode at every u_i. It should be noted that each element (u_i) of vector U depends upon the entire eigenvalue spectrum.

6.3 Navier Stokes Equations

In the implementation of the above mentioned approximate formula to the two dimensional Navier Stokes equations, each diagonal element of the matrix M_A in equation (6.2.17) becomes a 4 x 4 matrix. By multiplying the matrix M_A with a state variable vector the result is a system of semi-discretized equations such as

$$\frac{d}{dt}\begin{bmatrix} q_{11} \\ q_{21} \\ . \\ . \\ q_{MN} \end{bmatrix} = \begin{bmatrix} (M_J)_{11}\ q_{11} \\ (M_J)_{21}\ q_{21} \\ . \\ . \\ (M_J)_{MN}\ q_{MN} \end{bmatrix} + \begin{bmatrix} (R_J)_{11} \\ (R_J)_{21} \\ . \\ . \\ (R_J)_{MN} \end{bmatrix} \qquad (6.3.1)$$

where M and N are maximum indices of i and j.

This system of equations is decoupled because the time evolution of the variable $q_{i,j}$ depends only on the corresponding values of $q_{i,j}$. Thus, further simplification is possible and the system can be expressed

as a series of simple equations of the form

$$\frac{dq_{i,j}}{dt} = M_J\, q_{i,j} + R_J \qquad (3.5.7)$$

which is, in fact equation (3.5.7) derived in section 3.5. Thus, the computation of the eigenvalues has been greatly reduced because they are computed from a series of n 4 x 4 matrices.

6.3.1 Viscous Jacobian Matrix

The matrix M_J of the above equation consists of contributions from convection and diffusion terms of the Navier Stokes equations. From equation (3.2.1) vectors of the diffusion terms F_v and G_v can be written as matrix operators multiplied by vectors of primitive variables. For instance,

$$F_v = M_c\, P \qquad (6.3.2)$$

where

$$M_c = \begin{pmatrix} 0 & 0 & 0 & 0 \\ 0 & \frac{4}{3}\mu\frac{\partial}{\partial x} & -\frac{2}{3}\mu\frac{\partial}{\partial x} & 0 \\ 0 & \mu\frac{\partial}{\partial y} & \mu\frac{\partial}{\partial x} & 0 \\ a_1 & a_2 & a_3 & a_4 \end{pmatrix}, \quad P = \begin{pmatrix} \delta\rho \\ \delta u \\ \delta y \\ \delta e \end{pmatrix} \qquad (6.3.2a)$$

$$a_1 = -\frac{T}{\rho}k\frac{\partial}{\partial x}$$

$$a_2 = (\tau_{xx} + \frac{4}{3}\mu u\frac{\partial}{\partial x} + \mu v\frac{\partial}{\partial y}) \qquad \tau_{xx} = \mu(\frac{4}{3}\frac{\partial u}{\partial x} - \frac{2}{3}\frac{\partial v}{\partial y})$$

$$a_3 = (\tau_{xy} - \frac{2}{3}\mu u\frac{\partial}{\partial y} + \mu v\frac{\partial}{\partial x}) \qquad \tau_{xy} = \mu(\frac{\partial u}{\partial y} + \frac{\partial v}{\partial x})$$

$$a_4 = \frac{T}{p}k\frac{\partial}{\partial x}$$

In order to extract the Jacobian matrices from the vectors F_v and G_v (so that they can be expressed as equation (3.5.4b)),

$$F_v = C\,q \quad ; \quad G_v = D\,q$$

the vector of the primitives variables is decomposed into the form

$$P = M_{pq}\,q_D \tag{6.3.3}$$

where M_{pq} is a conversion matrix from vector q_D to vector P which is

$$M_{pq} = \begin{pmatrix} 1 & 0 & 0 & 0 \\ -\frac{u}{\rho} & \frac{1}{\rho} & 0 & 0 \\ -\frac{u}{\rho} & 0 & \frac{1}{\rho} & 0 \\ \frac{\gamma-1}{2}(u^2+v^2) & (1-\gamma)u & (1-\gamma)v & \gamma-1 \end{pmatrix} \quad and \quad q_D = \begin{pmatrix} \delta\rho \\ \delta(\rho u) \\ \delta(\rho v) \\ \delta(\rho e) \end{pmatrix}$$

(6.3.4)

Substituting P of equation (6.3.3) into equation (6.3.2) results in

$$F_v = M_c\,M_{pq}\,q_D \tag{6.3.5}$$

Equation (6.3.2a) shows that the matrix operator M_c must be applied to matrix M_{pq} and vector q_D in order to represent the full effects of the diffusion terms. Also, as M_c is a matrix operator, then

$F_v = M_c$ operates on M_{pq} while q_D is constant + M_c operates on q_D while M_{pq} is constant.

then

$$F_v = M_{cpq}\,q_D + M_c\,(M_{pq}\,q_D) \tag{6.3.6}$$

where M_{cpq} is the result of the first operation and in the second term M_c does not operate on M_{pq}. After some

manipulation, the vector F_v become

$$F_v = (M_{cpq} + M'_{cpq}) \, q = C \, q \qquad (6.3.7)$$

where M'_{cpq} is a matrix which is extracted from the second term of equation (6.3.6). The contribution of M_{cpq} and M'_{cpq} can be clearly shown by inspecting an element of the matrix C, for instance (see appendix-3.1)

$$c_{22} = \mu\{\frac{4}{3}\frac{\partial(\frac{1}{\rho})}{\partial x} + \frac{4}{3}\frac{\partial}{\partial x}\} \qquad (6.3.8)$$

where the first term is an element of M_{cpq} and the second term is an element of matrix M'_{cpq}.

The matrix M'_{cpq} expresses derivatives on the cell faces which simulate viscous dissipation. This can be shown, for instance, by evaluating the contributions of an element of matrix C at face i+1/2,j. By using the same element as in the above, the viscous flux will be

$$\text{Flux} = \frac{\partial}{\partial x}(C_{22} \, q_2) \qquad (6.3.9)$$

where q_2 is equal to ρu. Subtituting c_{22} and q_2 into equation (6.3.9), then

$$\text{Flux} = \frac{\partial}{\partial x}\mu\{\frac{4}{3}\frac{\partial(\frac{1}{\rho})}{\partial x} + \frac{4}{3}\frac{\partial}{\partial x}\}\rho u \qquad (6.3.10)$$

In this case, the second term of equation (6.3.10) is

$$\text{Second term} = \frac{4}{3}\mu\frac{\partial}{\partial x}\{\frac{1}{\rho}\frac{\partial \rho u}{\partial x}\} \qquad (6.3.11)$$

For simplicity assume $\rho \simeq$ constant (valid for low subsonic Mach numbers), then

$$\text{Second term} = \frac{4}{3}\mu\frac{\partial^2 u}{\partial x^2} \qquad (6.3.12)$$

This term simulates dissipation originating from the viscous terms.

Since the second matrix M'_{cpq} is diagonally dominant, the eigenvalues of that matrix are strongly influenced by those diagonal elements. These eigenvalues determine the stability of the computation, therefore these diagonal elements contain information about the contribution of the viscous dissipation to stability. Thus, comparison of these diagonal elements and the element of the matrix M_D (representing artificial dissipation, equation (3.5.10a)) indicates the influence of the viscous terms and artificial dissipation on the stability.

If the diagonal elements of the matrix M'_{cpq} are less than the elements of the matrix M_D in highly viscous regions then the viscous term will not be sufficient to damp out the oscillations (i.e. the computation will be unstable). This phenomena has been observed in the two dimensional high pressure turbine blade case discussed in chapter 5. If these diagonal elements are more than the elements of the matrix M_D, then the viscous dissipation will dominate convergence. This phenomena has been observed in the flat plate case in chapter 5.

Thus, the ability of the viscous fluxes to damp out the oscillation can be estimated by comparing the diagonal elements of matrix M'_{cpq} with elements of matrix M_D. This compares the viscous fluxes with the artificial dissipation which is further discussed in chapter 5.

6.3.2 Matrix Method

In the implementation of the matrix method, each element of vector $q_{i,j}$ of equation (3.5.7) can be expressed as a summation of four eigenmodes. For instance, the expression for element ρ at cell (i,j) is

$$\rho(t) = \sum_{j=1}^{4}[(\rho_{0j} + \frac{R_j}{\lambda_j})e^{\lambda_j t} - \frac{R_j}{\lambda_j}]v_1^{(j)} \tag{6.3.13}$$

This follows from equation (6.2.20) where ρ_{oj} and R_j are the coefficient of the vector $\rho(t)$ at time t=0 and vector R_J, respectively. $v_1^{(j)}$ is the first element of eigenvector V^j. The other elements such as ρu, ρv and ρe can also be expressed as summations of the eigenvectors and written in a similar manner.

These eigenvalues are subject to similar constraints to the scalar equations. Therefore, the eigenvalues of matrix M_j of equation (3.5.7) contain the influence of non-linearity but a reduced effect of the viscous dissipation. In general, convergence cannot be achieved in the standard Navier-Stokes code without additional dissipation being added.

6.3.3 Dissipation

With the addition of artificial dissipation, converged solutions can be obtained where eigenvalues are all negative. The dissipation model adopted expressed in equation (3.4.5) can be expanded for the ξ - direction, and in two dimensions it is as follows (Jameson, Schmith, and Turkel, 1981),

$$d_\xi = (\frac{Vol}{\Delta t})_{i+\frac{1}{2},j,k}\epsilon^2_{i+\frac{1}{2},j}(q_{i+1,j} - q_{i,j}) - (\frac{Vol}{\Delta t})_{i-\frac{1}{2},j,k}\epsilon^2_{i-\frac{1}{2},j}(q_{i,j} - q_{i-1,j}) -$$

$$(\frac{Vol}{\Delta t})_{i+\frac{1}{2},j,k}\epsilon^4_{i+\frac{1}{2},j}(q_{i+2,j} - 3q_{i+1,j} + 3q_{i,j} - q_{i-1,j}) +$$

$$(\frac{Vol}{\Delta t})_{i-\frac{1}{2},j,k}\epsilon^4_{i-\frac{1}{2},j}(q_{i+1,j} - 3q_{i,j} + 3q_{i-1,j} - q_{i-2,j})$$

(6.3.14)

By expanding the dissipation in the η - direction as in equation (6.3.14), the total dissipation will be

$$d_{total} = d_\xi + d_\eta$$

which depends upon variable $q_{i,j}$ at 12 locations corresponding to the computational molecule required for the viscous flux evaluation (figure-6.1). In matrix form, it will be similar to matrix M_G of equation (6.2.2). The addition of the dissipation to the semi-discretized equation (3.5.6) contributes to the corresponding elements of matrix M_G so that the eigenvalues at convergence are all negative.

After implementing the approximation formula, the semi-discretized equation with the artificial dissipation becomes

$$A\frac{dq_{i,j}}{dt} = -M_T q_{i,j} + R_{i,j} \qquad (6.3.15)$$

where M_T is expressed in equation (3.5.10)

6.4 Dissipation Control

Large negative eigenvalues result in a high rate of convergence and low level of residual but the computation requires large amounts of artificial dissipation so that the accuracy of the solution suffers. Such eigenvalues

indicate overdamped regions which are the result of excessive dissipation that may not be necessary to achieve convergence. Methods of dissipation reduction which guarantee enough dissipation to achieve convergence will now be investigated.

6.4.1 Characteristic Equation

The eigenvalues of a matrix are the roots of a characteristic equation which is obtained by setting a determinant of the matrix equal to zero. The determinant of a matrix, M is defined as

$$\text{Determinant} = | M - \lambda I | \qquad (6.4.1)$$

where I is an identity matrix and λ are eigenvalues. When the determinant is expanded, it is equivalent to the characteristic equation. For a 4 x 4 matrix, this equation is a fourth order polynomial. Then

$$\text{Determinant} = \lambda^4 + l_3 \lambda^3 + l_2 \lambda^2 + l_1 \lambda + l_0 \qquad (6.4.2)$$

By setting the determinant = 0, the four roots of this equation are the eigenvalues of the matrix M.

In this investigation, the matrix M is equal to matrix M_T of equation (3.5.10). With the objective of modifying the dissipation, the diagonal elements of the matrix M_T are considered to be the unknowns since the dissipation is only from the diagonal elements. Other elements are given. Based upon the calculation of the determinant of the matrix M_T (Spencer, 1978), the resulting coefficient l_o, l_1, l_2, and l_3 are non-linear functions of the unknown diagonal elements. Since the matrix M_T is of the form

$$M_T = \begin{bmatrix} m_{11} & 0 & 0 & 0 \\ m_{21} & m_{22} & m_{23} & 0 \\ m_{31} & m_{32} & m_{33} & 0 \\ m_{41} & m_{42} & m_{43} & m_{44} \end{bmatrix} \qquad (6.4.3)$$

then the non-linear function is

$$l_3 = m_{11} + m_{22} + m_{33} + m_{44} \qquad (6.4.4a)$$

$$l_2 = m_{11}m_{22}+m_{33}m_{44}+(m_{11}+m_{22})(m_{33}+m_{44})-m_{32}m_{23} \qquad (6.4.4b)$$

$$l_1 = m_{11}m_{22}(m_{33}+m_{44})-m_{33}m_{44}(m_{11}+m_{22})$$

$$+m_{32}m_{23}(m_{11}+m_{44}) \qquad (6.4.4c)$$

$$l_0 = m_{11}m_{22}m_{33}m_{44}+(m_{32}m_{23})m_{11}m_{44} \qquad (6.4.4d)$$

and since the eigenvalues are the roots of the characteristic equation, equation (6.4.2) is equal to

$$\lambda^4 + l_3\lambda^3 + l_2\lambda^2 + l_1\lambda + l_0 = (\lambda-\lambda_1)(\lambda-\lambda_2)(\lambda-\lambda_3)(\lambda-\lambda_4) \qquad (6.4.5)$$

By expanding the right hand side, then

$$\lambda^4 + l_3\lambda^3 + l_2\lambda^2 + l_1\lambda + l_0 = \lambda^4 + r_3\lambda^3 + r_2\lambda^2 + r_1\lambda + r_0 \qquad (6.4.6)$$

Coefficients (r_o, r_1, r_2, r_3) are constant which depend upon the given eigenvalues. The equality sign of the above equation will be correct if the coefficients of the left hand side are equal to the corresponding coefficients of the right hand side. Then, the system of non-linear equations of the diagonal elements for the given eigenvalues is

$$m_{11} + m_{22} + m_{33} + m_{44} = \lambda_1 + \lambda_2 + \lambda_3 + \lambda_4 \qquad (6.4.7a)$$

$$m_{11}m_{22}+m_{33}m_{44}+(m_{11}+m_{22})(m_{33}+m_{44})-m_{32}m_{23} =$$

$$\lambda_1\lambda_2+\lambda_3\lambda_4+(\lambda_1+\lambda_2)(\lambda_3+\lambda_4) \qquad (6.4.7b)$$

$$m_{11}m_{22}(m_{33}+m_{44})-m_{33}m_{44}(m_{11}+m_{22})$$
$$+m_{32}m_{23}(m_{11}+m_{44}) =$$
$$\lambda_1\lambda_2(\lambda_3+\lambda_4)-\lambda_3\lambda_4(\lambda_1+\lambda_2) \qquad (6.4.7c)$$

$$m_{11}m_{22}m_{33}m_{44}+(m_{32}m_{23})m_{11}m_{44} = \lambda_1\lambda_2\lambda_3\lambda_4 \qquad (6.4.7d)$$

The unknowns are the diagonal elements m_{11}, m_{22}, m_{33}, and m_{44} and the eigenvalues are $\lambda_1, \lambda_2, \lambda_3$, and λ_4

The objective of setting the rate of convergence and computing the required dissipation to sustain that rate is elaborated in the following section. It is based upon the solution of the system of non-linear equations.

6.4.1.1 Non-linear Solution

In accordance with the above objective, the system of non-linear equations is solved iteratively by Newton's method which is elaborated in appendix 6.1 (Ralston, 1965).

However, methods of finding solutions of system of non-linear equations (including the Newton method) do not always converge. One difficulty of the iterative Newton method is to find initial guess values at the begining of the iteration which will lead to convergence. In general, there has not been any methods that always results in a converged solution (Ralston, 1965).

If a method can be defined, then solutions of diagonal elements of matrix M_T, equation (6.4.7), can be obtained for given eigenvalues. From these elements, a parameter d_1 can be calculated as

$$m_{11} - m_{j11} = d_1 \qquad (6.4.8)$$

The parameter d_1 corresponds to an element of matrix M_D of equation (3.5.10a) and m_{j11} is an element of matrix M_J of equation(3.5.7a) and other diagonal elements follow accordingly.

Since, in general, the diagonal elements of matrix M_T are

$$m_{11} \neq m_{22} \neq m_{33} \neq m_{44} \qquad (6.4.9)$$

and the diagonal element of matrix M_J of equation (3.5.7a) are

$$m_{j11} \neq m_{j22} \neq m_{j33} \neq m_{j44} \qquad (6.4.10)$$

the element of matrix M_D are

$$d_{11} \neq d_{22} \neq d_{33} \neq d_{44} \qquad (6.4.11)$$

Also, from equation (3.5.9) $M_D\, q_{i,j}$ can be expanded as

$$M_D q_{1.1} = \begin{bmatrix} d_1 & 0 & 0 & 0 \\ 0 & d_2 & 0 & 0 \\ 0 & 0 & d_3 & 0 \\ 0 & 0 & 0 & d_4 \end{bmatrix} \begin{bmatrix} \rho \\ \rho u \\ \rho v \\ \rho e \end{bmatrix}_{1.1} \qquad (6.4.12)$$

Thus d_1 belongs to the continuity equation and the others belong to the other conservation equations. With the calculated d_1, a factor for dissipation reduction is defined as

$$f_{d1} = d_1/d_s \qquad (6.4.13)$$

where d_s is an element of matrix M_D expressed in equation (3.5.10a). Since these factor are different, the dissipation reduction is different for the continuity, momentum and energy equations. By applying these factors

to the second and fourth order dissipation constants which are K_2 and K_4 of equation (3.4.5a) and (3.4.5b), the reduced dissipations for the continuity, momentum and energy equations are computed to achieve given rates of convergence. This is only a realistic approach, however, if a general solution to the non-linear equation can be formulated.

6.4.1.2 Linearized Solution

Difficulties with the non-linear solution technique can often be overcome by linearizing the system of non-linear equations (6.4.7a, b ,c and d). In which case the eigenvalues are calculated for a given dissipation. Perturbations of the eigenvalues are introduced,

$$\lambda_j = \lambda_{cj} + \Delta\lambda_j \qquad (6.4.14)$$

to observe any reduction in dissipation. The reduction is extracted from the perturbation of the diagonal elements of matrix M_T which is

$$m_{jj} = m_{cjj} + \Delta m_{jj} \qquad (6.4.15)$$

m_{cjj} and λ_{cj} are the diagonal elements of matrix M_T and eigenvalues calculated for a given dissipation, respectively. Δm_{jj} and $\Delta\lambda_j$ are the perturbations of the coressponding parameters where it is assumed that

$$\frac{\Delta m_{jj}}{m_{cjj}} << 1 \quad and \quad \frac{\Delta\lambda_j}{\lambda_{cj}} << 1 \qquad (6.4.16)$$

Substituting λ_j and m_{jj} into equation (6.4.7) and neglecting high order terms, a system of linear equation is obtained and in matrix form is

$$M_m \Delta m = M_\lambda \Delta\lambda + constant \qquad (6.4.17)$$

where M_m and M_λ are functions of m_{cjj} and λ_{cj} respectively. If the perturbation of the eigenvalues results in large Δm_{jj} or

$$\frac{\Delta m_{jj}}{m_{cjj}} \geq 1 \qquad (6.4.18)$$

the linear equations which are represented by equation (6.4.17) are ill posed.

In the computation of the flow, the dissipation can be varied continuously from zero to the amount necessary to obtain a converged solution, and at each level of dissipation the eigenvalues can be computed. The ill posed condition means that for small changes of dissipation, which in this case is represented by small changes of the diagonal elements of matrix M_T, results in large changes in the eigenvalues (or convergence characteristic). This also means that small changes in convergence characteristic require large changes in dissipation. In general well posed conditions cannot always be guaranteed. In order to use the linearized system of equations further study is necessary to investigate the well posedness of the above problem (Vemuri and Karplus, 1981).

6.4.2 Inverse Eigenvalues Problem

This method has the same objective as in section 6.4.1 which is to set the rate of convergence or eigenvalues and to compute the required dissipation to maintain that rate. In this method, M_I is defined to be a square matrix (n x n) where its elements, $(m_{i,j})_I$ are functions of parameters d_i:

$$(m_{i,j})_I = \text{function}(d_i)$$

These parameters will be calculated for given eigenvalues of matrix M_I. In the implementation to the semi-discretized equation (6.3.15), matrix M_I is equal to matrix M_T (with the size of 4 x 4) and the parameters are elements of matrix M_D, equation (3.5.10a). The diagonal elements of matrix M_T are functions of these parameters such that

$$M_T = \begin{bmatrix} m_{11}(d_1) & 0 & 0 & 0 \\ m_{21} & m_{22}(d_2) & m_{23} & 0 \\ m_{31} & m_{32} & m_{33}(d_3) & 0 \\ m_{41} & m_{42} & m_{43} & m_{44}(d_4) \end{bmatrix} \qquad (6.4.19)$$

where the parameters are d_1, d_2, d_3, and d_4.

Wilkinson (1988) presented an iterative method of solution to calculate d_i for given eigenvalues of the matrix M_T for a symmetric matrix but the matrix M_T is not symmetric. Application of this method to non-symmetric matrices lead to difficulties in convergence. Further study is required to modify this method so that it is applicable to a case with a non-symmetric matrix.

6.4.3 Eigenvalues Control

Since the dissipation is directly related to the eigenvalues, it is proposed to selectively reduce the dissipation at each grid point per iteration by using the eigenvalues as sensors. The proposed method will reduce dissipation in overdamp regions indicated by large negative eigenvalues. This is carried out by implementing

the following function,

$$K_r = 1 - f_r\, e^{-m\lambda} \qquad \lambda \geq 0$$

$$K_r = 1 - f_r(2 - e^{-m\lambda}) \qquad \lambda < 0 \qquad (6.4.20)$$

which is plotted in figure-6.2

Factor f_r determines how low the artificial dissipation can be reduced as the eigenvalues go to large negative values. If the majority of eigenvalues are close to zero, m will have to be high enough so that the K_r still gives variation of the dissipation reduction. Otherwise,

$$K_r = 1 - f_r$$

which leads to constant dissipation reduction throughout the region.

Since at every grid point at every iteration there are four eigenvalues, the input to the reduction function equation (6.4.20) is the maximum of the four eigenvalues. Thus eigenmodes with maximum eigenvalues are sufficiently damped whereas the other modes are still overdamped.

The eigenvalues are evaluated at the cell centre (i,j). Thus, the reduction factor K_r belongs to that cell centre. However, the dissipation reduction is applied at cell faces such that the reduced dissipation is

$$d'_{i+1/2,j} = K_{r(i+1/2,j)}\, d_{i+1/2,j} \qquad (6.4.21)$$

where $d_{i+1/2,j}$ is the two dimensional version of equation (3.4.5) and K_r at the cell face can be approximated by

$$K_{r(i+\frac{1}{2},j)} = \frac{K_{r(i+1,j)} + K_{r(i,j)}}{2} \qquad (6.4.22)$$

This method of dissipation reduction is tested on inviscid

and viscous flows as follows.

6.5 Results and Discussion

6.5.1 Inviscid Test Case - Ni's Bump

The inviscid Ni's bump case had been discussed is section 5.4.1.1. For subsonic and transonic cases at 26000 and 13000 iterations respectively, the logarithmic root mean square of the residuals of ρ, ρu, ρv and ρe reach sufficiently low levels that the solution is converged. All of the real eigenvalues for both cases are negative at convergence (figure-6.3 & -6.4). This supports the validity of the approximation technique introducted in section 6.2.1.4.

6.5.1.1 Subsonic Case

This is the first test case for dissipation reduction using eigenvalues as a sensor. Through numerical experimentation, it was found that suitable factors m and f_r of equation (6.4.20) are 0.0001 and 0.375 respectively. These values will provide the best combination of robustness and accuracy. From figure-6.2, the reduction factor $K_{ri,j}$ of equation (6.4.20) reduces to 0.25 as the eigenvalues become large and negative, and it goes to one as the eigenvalues approach large positive values.

In this computation, even though the level of residual is higher than that for standard dissipation, it is low enough that the computation is considered to be converged (figure-6.5 & -6.6). The mass mean total pressure loss reduces from about 0.5 % to 0.3 % at the

exit (figure-6.7). Thus, the reduction in the total pressure loss is 40 % at the exit. As dissipation reduces the oscillations start to appear upstream of the leading and trailing edges. Downstream of the trailing edge, there are also an increase in oscillation in of the total pressure. These originate from the less well damped oscillations due to the effect of the odd-even decoupling of the central difference scheme. The increase in oscillation which is concentrated near the leading and trailing edges, is partly due to the discretization error which is large in these regions. A plot along a grid line near to the bump (from inlet to exit) shows that the reduction in dissipation occurs especially around the leading and trailing edges (figure-6.8)

The spectrum of the negative eigenvalues move towards the positive side which indicates that the eigenvalue control successfully reduces the level of the overdamping (figure-6.9).

6.4.1.2 Transonic Case

In order to evaluate a standardised function of the dissipation reduction in equation (6.4.20) the factors m and f_r are kept the same as in the subsonic case. Thus, the variation for the reduction factor, K_r with respect to the eigenvalues is still the same. The convergence rate is flatened out at 6000 iterations. However, the computation continues to 13000 iterations because the computation with the standard dissipation requires 13000 iterations to converge.

The level of residual is relatively high compared with the level of residual obtained by using the standard dissipation (figure-6.10 & -6.11). The solution is actually in a pseudo unsteady state. Let us consider the fluxes and time rate of change of the state variables which are related by

$$\frac{dU}{dt} = I + V - D$$

in a converged solution $I + V - D \simeq 0$,

with a high residual $I + V - D \neq 0$

where U is the state variable vector, I is the inviscid flux vector , V is the viscous flux vector and D is the dissipative flux vector. Thus, in the case with high residual, the state varibles in U is still changing with respect to time. As a consequence, there are positive eigenvalues which are indicated by the plot of four eigenvalues near the bump from inlet to exit (figure-6.12). The positive eigenvalues located in the shock region (where large variation of flow properties exists) are not sufficiently damped by the reduced dissipation. Even though the solution is still in a pseudo-unsteady state, the reduction of the total pressure loss is almost the same as that due to the implementation of the combined aspect ratio and Mach number function in chapter 5. The total pressure loss at the exit is reduced from about 1.64 % (with the standard dissipation) to about 1.58 % (with the reduced dissipation) (figure(6.13).

In order to study the effect of the dissipation reduction on the losses without taking into account the shock loss, the shock loss is substracted from the total pressure loss downstream of the shock. Since the shock loss is about 1.34 %, the loss associated with the standard dissipation without shock loss is 0.3 % and the one with the reduced dissipation is 0.24 %. The reduction of loss excluding shock losses, is therefore 20 %.

Upstream of the leading edge, however, the reduction of dissipation increases the oscillation. On the other hand, the oscillation in the leading edge region is reduced. In front of the shock, the oscillation increases again. A plot along a grid line near the bump from inlet to exit shows that the reduced dissipation occurs especially around the leading and trailing edges and shock regions (figure-6.14)

The spectrum of the negative eigenvalues moves towards the positive side so that some of the eigenvalues become positive. The eigenvalue control reduces the dissipation so that the computation does not have sufficient dissipation to shift the eigenvalues to the negative side (figure-6.15).

6.5.2 Viscous Test Case

The eigenvalues of the converged two dimensional flow over a high pressure turbine blade with the standard dissipation have been computed and the real parts of these eigenvalues are all negative (figure-6.16). Result with

eigenvalue control is discussed next.

6.5.2.1 Case a (f_r=0.5 and m=0.0001 - equation (6.4.20))

With factor f_r = 0.5, the artificial dissipation reduces to zero when eigenvalues have large negative values. The convergence history shows that after 8000 iterations no further significant reduction is achieved (whereas the standard results take 12000 iterations to achieve this). However, the level of residual is relatively high compared with the level of residual obtained by using the standard dissipation (figure-6.17 & -6.18). It is also apparent that the solution is in a pseudo-unsteady state with some eigenvalues becoming positive at least in some iterations.

However, there is a reduction of the computed total pressure loss in the blade passage and wake region. The net effect is that the losses reduce from about 11.4 % (for the standard dissipation) to about 10.6 % (for the reduced dissipation) (figure-6-19). A plot of the dissipation along a grid line near the suction surface from inlet to exit shows that the reduced dissipation is much smaller (figure-6.20) in this region which no doubt leads to the slower convergence. Along the same grid line, the result with the reduced dissipation shows that the viscous dissipation is larger than the artificial dissipation (figure-6.21). In this case, the viscous dissipation controls the physics of the flow in the near wall region (the addition of artificial dissipation being unnecessary).

The spectrum of the eigenvalues shows the same phenomena as in the inviscid transonic case where the existence of positive eigenvalues indicates a pseudo unsteady state (figure-6.22)

6.5.2.1 Case b (f_r=0.375 and m=0.0001 - equation (6.4.20))

With f_r = 0.375, the reduction factor $K_{ri,j}$ of equation (6.4.20) reduces to 0.25 as the eigenvalues approach large negative values. The factor m is the same as in the Case (a). The residual again asymptotes at 8000 iterations (figure-6.23). The level of residual is still relatively high compared with the standard dissipation and the solution is still pseudo unsteady.

However, a reduction of the total pressure loss is apparent in the blade passage and wake region. At the exit, the loss reduces from about 11.4 % (with standard dissipation) to about 10.5 % (with reduced dissipation) (figure-6.19). A plot along a grid line near the suction side from inlet to exit shows dissipation reduction upstream of the leading edge, in the blade passage and in the wake region close to exit. There is a region downstream of the trailing edge where the dissipation actually increases (figure-6.20).

The spectrum of the eigenvalues still shows positive eigenvalues which confirms the pseudo-unsteady state but the magnitude of the maximum positive eigenvalues is less than that in Case (a) (figure-6.24). Since the lower limit of the dissipation in the overdamped region is higher than for Case (a), the dissipation in that region

of Case (b) is more than for Case (a). This explains the reduction of the magnitude of the maximum positive eigenvalue because there is more dissipation in Case (b) to shift the eigenvalues to negative side than there is in Case (a).

The computation of Case (b) is continued up to 20000 iterations in order to approach a steady state. This can be seen from the change of the total pressure loss which diminishes as the iteration number approaches 20000 (figure-6.25). The residuals do not change as the computation is continued further.

6.5.2.3 Comparison of Case (a) and Case (b)

The total pressure loss of Case (b) is lower than the total pressure loss of Case (a) although the dissipation reduction of Case (b) is limited to one quater of the standard dissipation whereas the one for Case (a) can go to zero. This can be explained by the higher level of unsteadiness of Case (a) and its higher residual. In comparing the results of the computation it is important to take into account the level of the residuals.

The rates of convergence depends upon the amount of dissipation available to damp out the oscillations. The less dissipation available, the slower the computation converges. A comparison of the dissipation near the suction surface confirms that Case (a) which has virtually zero dissipation, has the slowest rate of convergence, (figure-6.20). Improvement in the convergence rate is obtained by increasing the dissipation but larger computed

losses are incurred.

6.6 Conclusion

The reduction of artificial dissipation , especially in the overdamped regions, have to be balanced between the need for accuracy and robustness.

The implementation of the method presented here to the Navier-Stokes equations results in a semi discretized equation from which a stability matrix can be extracted. This matrix is actually the discretized Jacobian matrix the eigenvalues of which contain information about stability since they determine the rate of convergence. The addition of the artificial dissipation which is necessary to stabilize the Navier-Stokes computation will shift the eigenvalues to the negative side and at convergence all the eigenvalues are negative. Since the computation of the eigenvalues of the stability matrix is prohibitively expensive, an approximate analysis is adopted to reduce the size of the matrix leading to reduce computational time. The eigenvalues of the reduced matrix contain information about the reduced effect of the viscous dissipation and the effects of the nonlinearity of the Navier-Stokes equations.

From the calculation of the determinant of the stability matrix, a system of non-linear equations relating eigenvalues to the dissipation is derived. The first idea proposed is to set the rate of convergence or eigenvalues and calculate the necessary dissipation to maintain that rate. This requires solution of the

non-linear equations involved which has so far proved impractical. Further investigation is necessary to formulate a method that can always solve a system of non-linear equations.

In order to overcome the difficulty with the non-linear solution, the system of non-linear equation is linearized which leads to perturbation equations of dissipation. However, the validity of the linearization process will not be valid when small changes in dissipation lead to large changes in eigenvalues (i.e when the problem is not well posed). Further investigation about the well posedness of the above problem is required before using the system of linearized equations.

Another approach to implement the first idea is to use the Inverse Eigenvalue Problem which can solve the dissipation for given eigenvalues of the stability matrix. However, the Wilkinson iterative method adopted in this investigation is devised for symmetric matrix only. Since the stability matrix is non-symmetric further study is again required to pursue this method.

The implemented eigenvalue control is based on another idea which reduces the dissipation in overdamped regions using eigenvalues as a sensor. A function of reduced artificial dissipation is devised which can be implemented to reduce the dissipation as the eigenvalues go to negative values and is demonstrated.

The test cases involved are the inviscid flow over Ni's bump and the two dimensional viscous flow over

a high pressure turbine blade. For the standard converged solution all the real parts of the eigenvalues computed are negative which in part confirms the validity of the approximate method used to obtain the eigenvalues.

In the implementation of the eigenvalue control to the inviscid case, the dissipation is reduced to one quarter of the standard dissipation as the eigenvalues go to large negative values (in overdamped regions). In the subsonic case, the level of residual is acceptably low and the solution is largely converged which is confirmed by the spectrum of eigenvalues where all real part are negative. The reduction of the total pressure loss achieved is 40 %. As the artificial dissipation reduces, the damping of the odd-even decoupling and discretization errors become less, leading to an increase in the oscillation of the total pressure, especially around the leading and trailing edges.

In the transonic case, a high level of residual manifests itself as a pseudo unsteady state where the state variables still change with time. An analysis indicates the presence of positive eigenvalues, for instance, around the location of shocks apparently because the reduced dissipation is insufficient to damp out the oscillation. Excluding the shock loss, the reduction of the total pressure loss is significant at 20 % of outlet dynamic head. The major reduction of the dissipation occurs in the regions of the leading and trailing edges, and shock.

In the implementation of the eigenvalue control to the viscous two dimensional flow over the high pressure turbine blade, two cases are considered. In the first case, the artificial dissipation is reduced to zero as the eigenvalues go to large negative values. In the second case, instead of reducing to zero, the dissipation is reduced to one quater of the standard dissipation.

In both cases, a high level of residuals results in a pseudo-unsteady state as for the transonic case. However, as the computation in the second case is continued, the results approach a steady state and total pressure losses reach a converged value. A reduction of the total pressure loss occurs in these cases for both the blade passage and wake regions. In the first case, the dissipation near the wall is negligibly small so that the physical viscous effects control the flow physics. In the second case, the dissipation in the same region is less than the standard dissipation. However, the viscous flux is less than the artificial dissipation and the viscous effect does not control the flow physics.

Since the results of the first and second cases are obtained at different convergence level they should not be compared directly. However, the total pressure loss of the first case is higher than the total pressure loss of the second case (which is probabaly a result of non-convergence as the dissipation of the first case is the smaller).

7.0 CONCLUSION

Collaboration is now becoming attractive in the aero - engine industry as markets are shrinking and the costs escalate. One of the most important factors escalating costs is technology, but this has to be scrutinized to ensure that it will reduce development time and/or cost. A collaborative project can most easily be initiated where established partners (known to each other) can contribute equally with expertise and workshare. New entrants, on the other hand, need to offer alternative benefits such as capital and markets.

In order to be considered as a partner, however, the new entrant has to develop a minimum level of technology to participate. In addition, the new entrant will eventually have to develop advanced technology so that it will be able to more fully share in the benefits of competitive engine production (which implies a more technically developed base). Computational Fluid Dynamics (CFD) represents such an advanced technology and is likely to be adopted by any new entrant interested in a future design role. Chapter 2 discusses the background to such an argument.

The major contribution of this thesis involves the analysis and improvement of a numerical method capable of solving the unsteady Navier Stokes equations. The method is briefly described in chapter 3 where the governing equations (in a three dimensional rotating coordinate system) are elaborated. The method involves a cell

centred finite volume scheme. The requirement of evaluating the cell face value leads to the formulation of an interpolation function which better approximates these face values from the cell centre values.

The straight averaging interpolation currently in many codes and adopted in the original program generates errors for a non-uniform grid system because the resulting face values are not located at cell face centres. The spatial discretization analysis undertaken uses a Von Neumann and Equivalent Partial Differential Equation method and the results show that the truncation error of the straight averaging is second order dispersive for cartesian grids, and first order dispersive for algebraic or quasi uniform grids. This interpolation is also inconsistent with exponentially straight stretched grids and skewed stretched grids. It is inconsistent because the resulting truncation errors do not reduce to zero as the grid size reduces to zero.

Another approximation generally available is based upon linear interpolation. Its implementation in straight stretched grids results in a consistent scheme. It is first order dissipative if the convection is in the direction of the grid expansion and is first order non-dissipative if the convection is in the direction of the grid contraction. If the scheme is non-dissipative, the truncation error will grow. An analysis of this interpolation in skewed grids shows that the dominant effect of the inaccuracy comes from an inconsistency of

the scheme.

A quadratic interpolation scheme is proposed which improves the accuracy with skewed grids. This scheme is analyzed in coupled and decoupled formulations. In the first formulation, the interpolation is carried out separately in each coordinate direction whereas in the second formulation the interpolation is carried out in all coordinate directions simultaneously. Even though the decoupled formulation improves accuracy for the straight stretched grid, it has the same order of error as linear interpolation for a skewed grid. The coupled formulation eliminates the inconsistency in a skewed grid and results in a second order dispersive error.

Alternatively, it is shown that instead of using an improved discretization scheme, improved accuracy can be obtained by constructing low grid expansion in high gradient areas and high grid expansion in low gradient area.

In addition to the spatial discretization analyzed in the above, time discretization is carried out on the convection diffusion equations providing information relating diffusion, grid size and time step. Stability constraints can be extracted from this and shown to be determined by the time step and not to involve the cell based Reynolds number as popularly believed.

As an alternative to the cell centred scheme, the cell vertex scheme based on other work has been reviewed. In the cell vertex scheme, the straight averaging of the

cell vertex values in arbitrary grids results in accurate face centred values in two dimensions but errors arise in three dimensions. Updated values at a cell vertex are calculated from values of the surrounding cells (sharing the same cell vertex). The straight averaging used in this calculation shows that in one dimension the cell vertex scheme is more accurate than the cell centre scheme. However, this averaging may lead to divergence in multidimensional cases.

In the study of artificial dissipation reduction, several test cases have been examined including Ni's bump, flow over a flat plate, two and three dimensional turbine blades, a three dimensional fan blade, and a three dimensional engine intake nacelle.

Since the second order dissipation is very much less than the fourth order dissipation, the total dissipation does not depend on the second order coefficient which determines the level of second order dissipation. In all the test cases (except for the flat plate) the fourth order coefficient which determines the fourth order dissipation is the same. Thus, with the same value of the fourth order coefficient, the total dissipation may be sufficient for some cases but excessive for other cases (leading to unrealistic dissipation and losses). It is fairly obvious to note that the fourth order coefficient will generate sufficient dissipation if the computation diverges when that coefficient is reduced, whereas the fourth order coefficient will generate excessive

dissipation if the computation still converges when that coefficient is reduced. Changing this coefficient can therefore be used to examine the role of dissipation in the computation of the selected test cases.

If the results with the standard dissipation formulation have excessive dissipation, the correction functions developed in the chapter 5 can be very effective, for example in the case of three dimensional high pressure turbine blade. If the results with the standard dissipation formulation have sufficient dissipation, the correction functions developed in that chapter is not very effective, for example for the three dimensional fan case.

The flat plate case has a low value of fourth order coefficient and can converge with a small amount of dissipation. Thus, the reduction of the dissipation by using the proposed method does not improve computational accuracy as gauged by the comparison of computational boundary layer velocity profile with the analytical one.

The dissipation component along the length of a high aspect ratio cell is large and an attempt to correct this by introducing the cell aspect ratio into the dissipation formulation has been undertaken, as discussed in chapter 5. Several aspect ratio functions attempting to accommodate this have been proposed by Martinelli, Kuntz and used by Cheng. It should be noted, however, that total dissipation is the sum of all dissipation components and that the implementation of the aspect ratio function may

not necessarily result in the reduction of total dissipation.

In the two dimensional high pressure turbine blade example, the use of Cheng's aspect ratio function increases the dissipation near to the wall (because this function reduces the non-dominant component, which has an excessive scaling factor, and increases the dominant component). It is therefore concluded that this function cannot improve accuracy in the near wall regions.

Since Martinelli's aspect ratio function is similar to Cheng's aspect ratio function, Martinelli's function suffers similarly and for a two dimensional case, Cheng's function reduces to the Martinelli's function.

Furthermore, although Kuntz's aspect ratio function reduces all dissipation components, its effectiveness depends upon details of the computational case. In all test cases, there are regions where the dominant component is along the length of the high aspect ratio cell, for instance in the leading and trailing edges and exit regions. In the leading and trailing edges, the dissipation is magnified by changes in the flow direction and in the near exit region by the change of velocity. It is concluded, however, that as long as the length of the high aspect ratio cell is aligned with the flow direction then Kuntz's aspect ratio function is effective in reducing the dissipation in those region.

A modified aspect ratio function have been proposed which is similar to Kuntz's aspect ratio function, but

modifies all dissipation components and reduces that already reduced by Kuntz's function. This is confirmed by its implementation to the Ni's bump case.

A velocity or Mach number correction function is formulated to reduce dissipation in the boundary layer and low velocity regions.

The implementation of the combined Mach number and Kuntz's aspect ratio functions in the Ni's bump case requires an increase in the fourth order dissipation coefficient to achieve convergence. The results show that for the transonic case, the total pressure loss with the combined function is less than that with the aspect ratio function alone. However, for the subsonic case, the total pressure loss with the combined function is more than that with the aspect ratio function alone. The Mach number function introduces a larger reduction of dissipation in the transonic case than in the subsonic case because there is larger variation of Mach number.

With very fine grids such as that used for the flat plate case, the velocity function can severely reduce the dissipation in the near wall region. The application of this function in the cases with coarse grids which do not resolve the boundary layers (such as the two dimensional high pressure turbine blade) does not result in significant dissipation reduction.

The formulation of the dissipation terms contains second and fourth order differences which depends upon grid size and the derivatives of state variables. If the

grid size, for instance near to the wall is not small enough to reduce the effect of the high derivatives, the dissipation will be large. The required size of the grid to reduce this effect can only be computationally afforded for the flat plate case. Thus in general, the dissipation in critical regions such as near to the wall and around leading and trailing edges is large because of large flow gradients. Thus, a new correction function has been proposed which takes into account the flow gradient. The sensor for this function is Mach number difference.

This function was first tested for the flat plate and the two dimensional high pressure turbine cases. The total pressure loss in the second case is reduced whereas that for the flat plate is not changed. The implementation of the combined gradient and aspect ratio functions in the three dimensional turbomachinery cases leads to a reduction of the dissipation near to the wall and leading and trailing edges. The total pressure generation in the three dimensional high pressure turbine blade is eliminated by this combined function. In the three dimensional engine intake case, this function reduces the dissipation in the near wall region which result in stronger flow reversal (because the flow has less energy to overcome the adverse pressure gradient). This results in higher losses which agree better with the experimental values.

It is shown that by using anisotropic functions, the dissipation along each coordinate direction can be

selectively reduced. These factors can be very effective if they reduce the dominant dissipation component such as that occuring in the flat plate and the two dimensional high pressure turbine blade cases. In addition, the total pressure loss in the second case is reduced.

Since the reduction of the dissipation often leads to divergence, the following stability investigation has been carried out to find a means to balance accuracy and robustness.

The implementation of a matrix analysis of the Navier-Stokes equations results in a stability matrix from which eigenvalues can be calculated. These eigenvalues relate the dissipation which determines the accuracy and the rate of convergence which determines the robustness. Thus, the eigenvalues can be used as sensors to selectively reduce the dissipation in the overdamped regions (where the local rate of convergence is unnecessarily high).

Since the idea is to detect the overdamped regions and reduce the dissipation during the iteration, the eigenvalues are calculated at every time step. In order to avoid prohibitively expensive computation, an approximate method to simplify the stability matrix was adopted. The resulting approximate matrix describes the effect of viscous terms and the nonlinearity of the Navier-Stokes equations.

A system of nonlinear equations relating the eigenvalues to the dissipation is derived from the

calculation of the determinant of the approximate matrix. Thus, these equations can be solved for dissipation for given eigenvalues. However, the available solution method is not robust enough and a solution cannot always be found. The development of a robust solution method for systems of nonlinear equations should be pursued. On the other hand, an attempt to linearized this system of equations and reformulate it as perturbation equations encountered problems of well posedness. The reason is that perturbations in eigenvalues induce large changes in dissipation. Thus, investigation of the well poseness of this problem should also be pursued. Another method that can solve dissipation for given eigenvalues is the Inverse Eigenvalue Problem but this is currently only available for a symmetric matrix. Since the approximate matrix is not symmetric, further extension of this method is required for the non-symmetric matrix.

In order to use eigenvalues directly as sensors, a correction function is proposed which reduces dissipation where the eigenvalues are negative. This function is implemented for the inviscid Ni's bump and the two dimensional high pressure turbine blade cases. The computation with the standard dissipation confirms that all real eigenvalues are negatives at convergence.

For the Ni's bump case, the dissipation is reduced to one quarter of the standard value as the eigenvalues become large and negative. In the subsonic flow, the computation converges and all real eigenvalues are

negative. The total pressure loss is reduced by 40 % but the total pressure oscillations increase because of the dissipation reduction. In the transonic flow, the computation results in pseudo-unsteady oscillations and some real eigenvalue are positive. The total pressure loss (excluding the shock loss) is reduced by 25 % but the total pressure oscillations increase especially in front of the leading edge and in the region of shock.

In the turbine blade case, the flow is computed with two different levels of dissipation reduction. In the first case, the dissipation is reduced all the way to zero as the eigenvalues become large and negative. The second case is the same as in the Ni's bump case. In both cases, the computation results in a pseudo unsteady state and some real eigenvalues are positive. However, the level of the residuals in the first case are higher than in the second case (the reduction of the dissipation slows down the rate of convergence).

In the first case, near to the wall, the dissipation is negligible and less than the viscous fluxes. In the second case, the dissipation near to the wall is reduced. The total pressure losses in both cases are reduced and depend on the level of the residuals. It appears to the author that when comparing computational solutions, the level of residuals has to be taken into consideration.

Overall it is felt that a number of significant and current CFD problems have been identified and at least partial solutions defined, listed and analyzed. Although

this has been undertaken with the scope of a particular code, it is felt that the conclusions can be readily generalized.

REFERENCES

Anderson, D.A., Tannehil, J.C. and Pletcher, R.H.,'Computational Fluid Dynamics and Heat Transfer,' McGraw-Hill Book Company, New York, 1984.

Andrews, J.G.,'Spurious Entropy Generation as a Mesh Quality Indicator,' Report No. 93/12, Oxford University Computing Laboratory, Oxford, December 1993.

Alimin, E.K.,'Analysis and Improvement of Discretization Scheme,' Rolls-Royce, Derby, 1994.

Arnone, A., and Swanson, R.C.,' A Navier-Stokes Solver for Turbomachinery Applications,' Journal of Turbomachinery, Vol. 115, April 1993, pp 305-313.

Aviation Week and Space Technology,'BR715 to power MD-95 Transport,' 28 February, 1994, p 22-24.

Aviation Week and Space Technology,'European Firms Team on Supersonic Studies,' 11 April 1994, p 20.

Aviation Week and Space Technology,'US Airframer Firms Foresee Prosperous World Market,' 14 March 1988, pp 179-181.

Aviation Week & Space Technology,'GE 90 Program Moves into High Gear, 19 April 1993.

Ayres, Jr. F.,'Theory and Problem of Matrices,' Schaum's Outline McGraw-Hill Company, New York, 1974.

Baldwin, B.,and Lomax, H.,'Thin layer approximation and algebraic model for separated turbulent flow,' AIAA 78-0257, AIAA 16th Aerospace Sciences Meeting, 1978.

Beam, R.M., and Warming, R.F.,'An Implicit Factored Scheme for the Compressible Navier-Stokes Equation,' AIAA Journal Vol. 36, p 393.

Birch, N.T.,'Turbulence and Transition Modelling in Turbomachinery Flows,'PhD Thesis, Cranfield Institute of Technology, 1987.

Bracher, T., Boeing Commercial Aircraft Corporation, Feb. 1981, p 10.

Caughey, D.A. and Turkel, E.,'Effects of Numerical Dissipation on Finite Volume Solutions of Compressible Flow Problems,' AIAA-88-0621, 1988.

Causon, D.M.,'A Total Variation Diminishing Scheme for Computational Aerodynamics,' IN: Numerical Methods for Fluid Dynamics III; Proceedings of the Conference, Oxford, England, March 21-24 1988.

Cebeci, T.,and Smith,'Analysis of Turbulent Boundary Layers, New York, Academic Press, 1974.

Cedar, R., 'The Development of A Finite Element Methods for the Analysis of Steady and unsteady Turbomachinery Blade Flows,' PhD Thesis, Cranfield University, July, 1986, p 26.

Cheng, C.P., 'The Modelling of Three-dimensional Transonic Flow in Turbomachinery Using Time-marching Technique,' PhD Thesis, Cranfield Institute of Technology, 1992.

Cleland, D.I. and Kocaoglu, D.F.,'Engineering Management', McGraw-Hill, 1981.

Connel, S.D.,'Numerical Solution of the Equations of Viscous Flow,' PhD Thesis, University of Nottingham, May 1983.

Cornell, A. ,'International Collaboration in Weapon and Equipment Development and Production by the NATO Allies :Ten years and Beyond,' Martinis Nijhoff, 1981, London, p 80.

Coupland, J.,'Turbulent Modelling for Turbomachinery,' Rolls-Royce, Derby,1993.

Crumpton, P.I., Mackenzie, J.A., and Morton, K.W.,'Cell Vertex Algorithms for the Compressible Navier-stokes Equations,'Journal of Computational Physics, 109, pp 1-15, 1993.

Demirdzic, I., Lilek, Z., and Peric, M.,'A Collocated Finite Volume Method for Predicting at all Speeds,' International Journal for Numerical Methods in Fluid, Vol. 16, p 1029-1050, 1993.

Denton, J.D.,'A Time Marching Method for Two- and Three-Dimensional Blade to Blade Flows,' A.R.C. R. & M. No. 3775, 1974.

Denton, J.D.,'Loss Mechanism in Turbomachines,'presented at the International Gas Turbine and Aeroengine Conggres and Exposition Cicinnati, Ohio, 24-27 May, 1993, ASME-93-GT-435.

Douglass, R.W. and Ramshaw, J.D.,'Perspective: Future Research Direction in Computational Fluid Dynamics,' Journal of Fluid Engineering, Vol. 116, June 1994, p 212-215

Draper, A.G., 'European Defence Equipment Collaboration - British Involvement,' 1957-87, p 8.

Eriksson, L.E. and Rizzi, A.,'Computer-Aided Analysis of Convergence to Steady State of Discrete Approximations to the Euler Equations,'Journal of Computational Physics 57,p 90-128, 1985.

Fearon,P., 'The Formative Years of the British Aircraft Industry, 1913-1924,' Business History Review, Vol. 43 (1969), pp 476-495.

Flax, A.H.,'Aeronautics-a Study in Technological and Economic Growth and Form,' Aeronautics Journal, December 1974, p537-552.

Fletcher, C.A.J.,'Computational Technique Fluid Dynamics,'Vol-I and Vol-II, Spring-Verlag, 2nd edition, 1991.

Flight International,'Powering Up', 9-15 June 1993, p 21.

Ford,T.,'Aero Engine Design,'Aircraft Engineering, June 1992, p 2-5.

Fottner, L., 'Review on Turbomachinery blading Design Problem,' AGARD-LS-167, May 1989.

Giles,M.,'A Finite Volume Methods for Euler Equation,' Short Course Notes, 27-31 July 1992, Rolls-Royce, Derby.

Gopal, C., 'Manufacturing Logistics System for A Competitive Global Strategy,' Logistics - The Strategic Issues, Chapman & Hall, London, 1992,p 130-139.

Hah, C.'A Navier-Stokes Analysis of Three-dimensional Turbulent Flows Inside Turbine Blade Rows at Design and off-design Condition. ASME Paper No. 83-GT-40, 1983.

Hah, C.,'Generation and Decay of Secondary Flows and Their Impact on Aerodynamics Performance of Modern Turbomachinery Components,' AGARD-CP-469, 1989.

Hall, M.,' On the Reduction of Artificial Dissipation in Viscous Flow Solutions,' presented at a special meeting in celebration of Jameson's 60th birthday, November 1994.

Hall, M.G.,'Cell Vertex Scheme for Solution of the Euler Equations,' Proceeding Conference on Numerical Method for Fluid Dynamic, University of Reading , U.K., 1986 (ed Morton, K.W. and Baines, J.) Oxford University Press pp-303-345.

Hall, U.,'Future Trends in Gas Turbine Technology,' Engine Design International'94, Sterling Publication Limited, London, 1994, p 35-38.

Hayward, K., 'International Collaboration in Civil Aerospace,' London, 1986, p 157.

Hayward, K., 'European Aerospace Collaboration in Transition', Royal United Services Institute for Defence Studies, 1991, p 61.

Hemmings, S, 'A study of Civil Engine Business', MSc Thesis, Cranfield University, October 1992.

Hessemus, K. A. and Richardson, P. F., 'NASA and Computational Fluid Dynamic:Making Investment for the Future', Aerospace America, January 1992.

Hill, R.J. and Langdell P.V.,'Achieving Faster and More Ecomonic Engine Design and Development,' The Rolls-Royce Magazine, Number 56, March 1993, p 8-13.

Hirsch, C.,'Numerical Computation of Internal and External Flows,' Vol-I and Vol-II, John Wiley and Sons, Chichester, 1989.

Ho, Y.K.,'CFDS-ANSE: An Explicit Time Marching Navier-Stokes Solver,' Roll-Royce, Derby, 1992.

Holmes, D.G., and Tong, S.S.,' A Three-Dimensional Euler Solver for Turbomachinery Blade Rows,' Transaction of the ASME, Vol. 107, April 1985.

Horton, G.C.,'Secondary Flow Prediction for A Transonic Nozzle Guide,'AGARD-CP-469, 1990.

Hussaini, M.Y.,'Computational Fluid Dynamics-A Personal View,' 11th International Conference on Numerical Methods in Fluid Dynamics, Williamburg, 27 June-1 July 1988, p 3-17.

James, G.W., 'Airline Economics', Lexington Books, Lexington, 1982, p 16-17.

Jameson, A. and Liu, F.,'Multigrid Calculation for Cascade,' 11th International Conference on Numerical Methods in Fluid Dynamics, 1988, p 318-325.

Jameson, A., Schmith, W., and Turkel, E,.'Numerical Solutions of the Euler Equations by Finite Volume Methods Using Runge-Kutta Time Stepping Scheme,' AIAA-81-1259, June 1981,

Jefferson, A.,'Three Dimensional Transonic Code Capability Evaluation Part I: RT60HP NGV,'Rolls-Royce, Derby, 1990.

Jewell, J.,'Jet Engines - Less NO_xise,' Engine Design International'94, Sterling Publication Limited, London, 1994, p 43-45.

Karki, K.C., and Patankar, S.V.,'A Pressure Based Calculation Procedure for Viscous Flows at all Speeds in Arbitrary Configuration,' AIAA-88-0058, 1988.

Kobayashi, M.H., and Pereira, J.C.F.,'Prediction of Compressible Viscous Flows at all Mach Number Using Pressure Correction, Collocated Primitive Variable and Non-Orthogonal Meshes,' AIAA-92-0426, 1992.

Korkegi, R. H., 'Impact of Computational Fluid Dynamic on Development Test Facilities,' National Research Council, Washington, D.C., Journal of Aircraft, Vol. 22, No. 3, pp 182-187.

Kuntz, R.F. and Lakshminarayana, B., 'Explicit Navier-Stokes Computation of Cascade Flows Using the k-ϵ Turbulent Model', AIAA Journal, Vol. 30, No. 1, January 1992, pp 13-22.

Kuntz, R.F. and Lakshminarayana, B., 'Three dimensional Navier-Stokes Computation of Turbomachinery Flows Using an Explicit Numerical Procedure and a Coupled k-ϵ Turbulence Model', Journal of Turbomachinery, Vol. 114, July 1992, pp 627-642.

Lecture Notes, 'Management for Technology,' School of Mechanical Engineering, Cranfield University, 4-18 January 1993.

Lomax, H.,'Recent Progress in Numerical Techniques for Flow Simulation,' AIAA Journal, Vol. 14 No. 4, p 512-518, 1976.

Mackenzie, J.,'The Cell Vertex Method for Viscous Transport Problems,' Report No. 89/4, Oxford University Computing Laboratory, March 1989.

Mackenzie, J.,'An Improved Artificial Dissipation Model for The Cell-Vertex Finite Volume Method,' Report No.93/13, Oxford University Computing Laboratory, October 1993.

Mahajan, A.J., Dowell, E.H., and Bliss, D.B.,'On the Role of Artificial Viscosity in Navier-Stokes Solvers,' AIAA-89-1947-CP ,1989.

Mahajan, A.J., Dowell, E.H., and Bliss, D.B.,'Eigenvalues Calculation Procedure for an Euler/Navier-Stokes Solver with Application to Flow over Airfoils,' Journal of Computational Physics 97, p 398-413, 1991.

Martinelli, L., 'Calculation of Viscous Flow with Multigrid Method', PhD Thesis, Department of Aerospace & Mechanical Engineering, Princeton University, October 1987.

Matson, R., 'Cost Effective Engine Design for Commercial Aircraft,' AIAA 93-1059.

McDonald, H., and Briley, W.R.,'Three-Dimensional Supersonic Flow of a Viscous or Inviscid Gas,' Journal of Computational Physics, Vol. 19, p 150, 1975.

McGuirk, J.J., and Page, G.P.,'Shock Capturing Using a Pressure-Correction Method,'Journal AIAA, Vol. 28, No. 10, October, 1990. p 1975-1857.

Moore, J., and Moore, J.G,'Performance Evaluation of a Linear Turbine Cascade Using a 3D Viscous Calculation. Transaction ASME, Journal of Engineering for Gas Turbines and Power, Vol. 107, p 969-975, 1975.

Moore, J., and Moore, J.G,'A vorticity based serach procedure for boundary and shear layers,' VPI & SU Report no. JM/88-6, 1988.

Morton, K.W., Childs, P.N., and Rudgyard, M.A,'The Cell Vertex Method for Steady Compressible Flow,' Report No.88/5, Oxford University Computing Laboratory, Oxford, 1988.

Ni, R.H.,'A Multiple-Grid Scheme for Solving the Euler Equation,' AIAA 81-1025R, November, 1982.

Niehuis, R., Lucking, P., and Stubert, B.,'Experimental and Numerical Study on Basic Phenomena of Secondary Flows in Turbine,' AGARD-CP-469, 1990.

Patankar, S.V., and Spalding, D.B.,'A Calculation Procedure for Heat, Mass, adn Moemntum Transfer in Three-Dimensional Parabolic Flows,' International Journal Heat and Mass Transfer, Vol. 15, 1972, p 1787.

Patankar, S.V.,'Numerical Heat Transfer and Fluid Flow, McGraw-Hill, Washington, D.C., 1980.

Peyret, R., and Taylor, T.D.,'Computational Methods for Fluid Flow,'Spring-Verlag, New York, 1984.

Pierce, N.A.,'Characteristic-Based Dissipative Schemes and Characteristic Time Stepping for the Euler Equations,'PhD transfer report, Oxford University Computing Laboratory, Numerical Analysis Group, 1994.

Pulliam,T.H.,'Artificial Dissipation Models for the Euler Equations,' AIAA Journal, Vol.24, No.12, December, 1986.

Radespiel, R., Rossow, C., and Swanson, R.C.,'An Efficient Cell-Vertex Multigrid Scheme for the Three-Dimensional Navier-Stokes Equations,'AIAA-89-1953, June 1989, Buffalo.

Radespiel, R., Swanson, R.C.,'An Investigation of Cell Centred and Cell Vertex Multigrid Schemes for the Navier-Stokes Equations,'AIAA-89-0548, 1989.

Ralston, A.,'A First Course in Numerical Analyisis,' McGraw-Hill Book Company, Tokyo, p 348-350, 1965.

Regional Air International,'Manufacturers are Forging Alliance for Future Growth,' August 1993, p 22-24.

Rhie, C.M.,'A pressure based Navier-Stokes Solver using the Multigrid method,' AIAA-86-0207, 1986.

Robinson, C.J.,'End-Wall Flows and Blading Design For Axial Flow Compressors,' PhD Thesis, School of Mechanical Engineering, Cranfield Institute of Technology, 1991.

Rossow, C., Kroll, N., Radespiel, R., and Scherr, S., 'Investigation of the Accuracy of Finite Volume Methods for 2- and 3-Dimensional Flows,' 62nd AGARD-Meeting on Validation of Computational Fluid Dymanics.

Santos, L.,'Local Stability Analysis of Explicit Schemes,' Technical Report, Rolls-Royce, Atlanta, August 1993.

Santos, L.,'Conceptual Ideas for Eigensystem Acceleration of a Finite Volume Scheme for The Navier Stokes Equations,' Rolls-Royce, Atlanta, 1994.

Schlichting, H.,'Boundary-Layer Theory,'McGraw-Hill Book Company, New York, 1979.

Seddon, J., and Goldsmith, E.L.,'Intake Aerodynamic,' Collins, London, 1985.

Shapiro, A.H.,'The Dynamics and Thermodynamics of Compressible Flows,' Vol. I, Ronald Press, New York, 1953.

Sieverding, C.H.,'Recent Progress in the Understanding of Basic Aspect of Secondary Flows in Turbine Blade Passage,'ASME 84-GT-78, 1984.

Sieverding, C.H.,'Secondary Flows in Straight and Annular Turbine Cascade,' Thermodynamics and Fluid Mechanics of Turbomachinery, Vol. II, NATO ASI Series, Series E: Applied Science - No. 97B, 1985, p 621-664.

Sieverding, C.H., and Van den Bosch, P.,'The use of Coloured Smoke to Visualize Secondary Flows in a Turbine-Blade Cascade,' Journal of Fluid Mechanics, Vol. 134, September 1983, p 85-89.

Skerret, P.J., 'The Teraflops,' Popular Science, March 1992.

Smith, G.D.,'Numerical Solution of Partial Differential Equations: Finite Difference Methods,' Claredon Press, Oxford, 1978.

Spencer, A.J.M.,'Engineering Mathematics,' Vol-I, Van Nostrand Reinhold Company, Ltd., London, p 320-325, 1978.

Stager, J.L. and Warming, R.F.,'Flux Vector Splitting of the Inviscid Gas Dynamics Equations with Applications to Finite Difference Methods,' Journal of Computational Physics, Vol.40, 1981, p 263-293.

Steger, J.L.,'On Application of Body Conforming Curvilinear Grids for Finite Difference Solution of External Flow,' Numerical Grid Generation, April 1981.

Stow, P.,'Navier Stokes method Applied to Turbomachinery Blade Design,' Rolls-Royce, Derby, 1989.

Stryker, H.,'Twenty-First Century Commercial Transport Engines,' Engine Design International'94, Sterling Publication Limited, London, 1994, p 39-42.

Sunday Times,'Boeing's New Jumbo join Airliner Dogfight', 19 June, 1994.

Swanson, R.C. and Turkel, E,'Artificial Dissipation and Central Difference Schemes for the Euler and Navier-Stokes Equation,' ASME, 87-1107, 1987.

Swanson, R.C. and Turkel, E.,'On Central Difference and Upwind Scheme,' Journal of Computational Physics, 101, 1992, p 292-306

Thompson, H.D., Webb, B.W., and Hoffman, J.D.,'The Cell Reynolds Number Myth,' International Journal for Numerical Methods in Fluids, Vol. 5, 1985, pp 305-310.

Todd, D. and Simpson, J., 'The World Aircraft Industry,' Croom Helm, London, 1986, p 29.

Tropper, A.M.,'Linear Algebra,' Thomas Nelson and Sons, Ltd., London, 1969.

Turkel, E.,'Accuracy of Schemes with Nonuniform Meshes for Compressible Fluid Flow,' Applied Numerical Mathematics 2, 1986, North-Holland, pp 529-550.

Turkel, E., Yaniv, S., and Landau, U.,'Accuracy of Schemes for the Euler Equations with Non-Uniform meshes,' AIAA-88-0341, June 1986, Reno.

Turkel, E.,'Improving the Accuracy of Central Difference Schemes,' 11th International Conference on Numerical Methods in Fluid Dynamics, 1988 p 586-591.

Turkel, E. and Vatsa V.N.,'Effect of Artificial Viscosity on Three Dimensional Flow Solutions,' Journal of AIAA, Vol. 32, No. 1, January 1994, p 39-45.

Usab ,W.J.,'Embedded Mesh Solutions of the Euler Equations Using a Multiple-Grid Method,' Ph. D. Thesis, MIT, Cambridge, 1983. Van Leer, B,'Toward the Ultimate Conservative Difference Scheme IV: A New Approach to Numerical Convection,' Journal of Computational Physics, Vol. 23, 1977, p 276-299.

Vemuri,V, and Karplus, W.J.,'Digital Computer Treatment of Partial Differential Equation,' Prentice-Hall, Inc., 1981.

Wennerstroom, A.J.,'Highly Loaded Axial Flow Compressors: History and Current Development', ISABE 89-7002, 1989.

White, F.M.,'Viscous Fluid Flow,' McGraw-Hill Book Company, New York, 1974.

Whitehead, D.S.,'Proceedings of a workshop on Aeroelasticity in Turbomachinery, Edited by S. Fleeter, Detroid Diesel Allison, 1972.

Wilkinson, J.H.,'The Algebraic Eigenvalues Problem,' Monographs on Numerical Analysis, Clarendon Press, UK , 1988

Xu, L.,'The base pressure and Trailing Edge Loss of Transonic Turbine Blades PhD Dissertation, Cambrige University, 1986.

Zaccaria, M., and Lakshminarayana, B.,'Investigation of Three-Dimensional Flowfield at the Exit of a Turbine Nozzle,' Journal of Propulsion and Power, Vol. 11, No. 1 January-February 1995,p 55-63.

APPENDIX-2.1 Stages of Human Resource Development

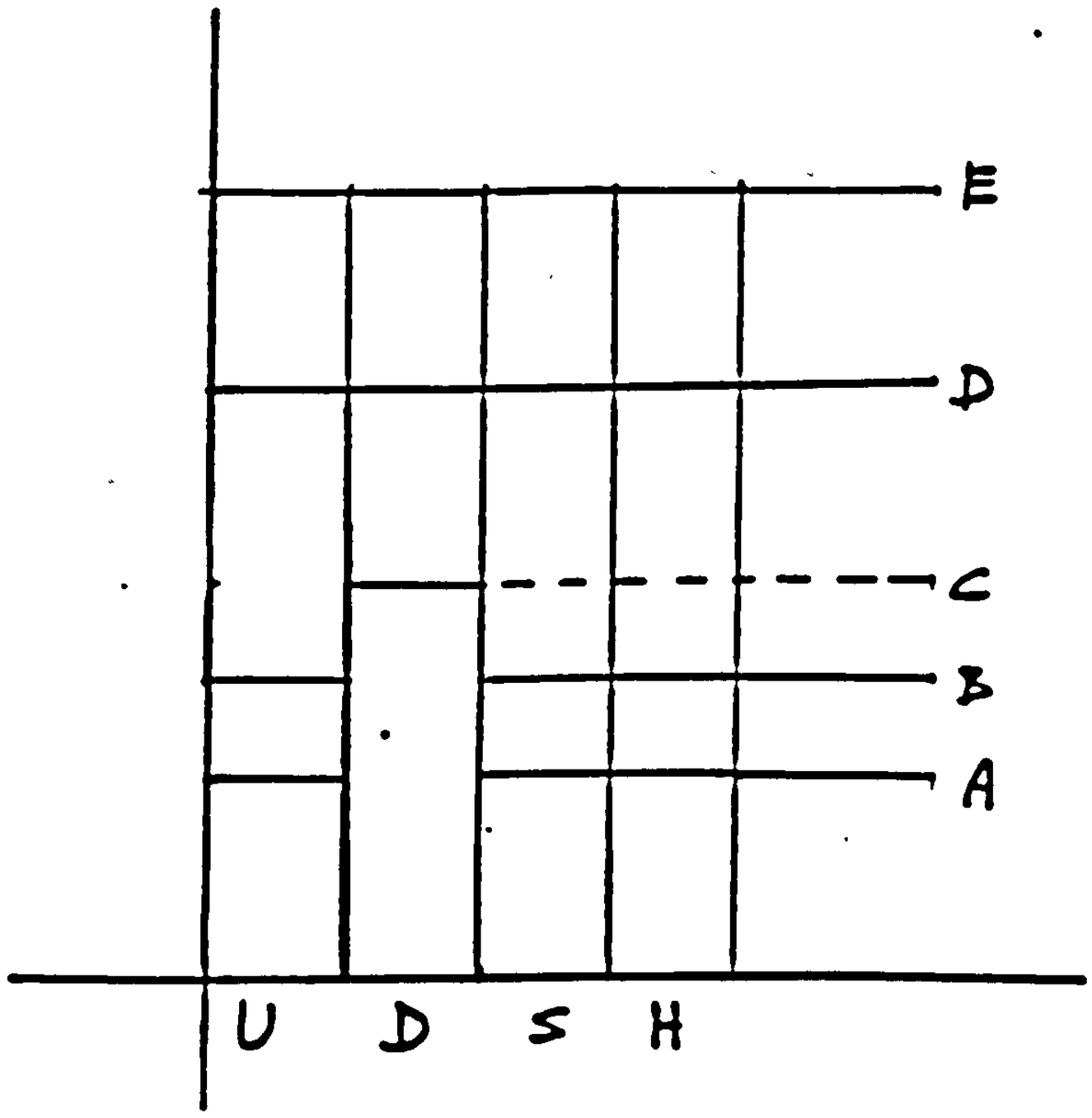

U=user

D=Developer

S=Software

H=Hardware

Stage - A

-Users have been recruited but they do not have any experience. Even though the necessary hardware is available, the team will not take any assignment from existing design projects. They study basic material that quickly makes them capable of doing that assignment.

Stage - B

-The team is capable of solving practical problem from the design project. The technology is still acquired from other sources. There is no technology development.

Stage - C

-Developers have just been recruited. The team continues with the practical problem but the development work that eventually provides the tehnology is started.

Stage - D

-All elements of the development of the technological capability is according to plan. At this level, the team is capable of taking a development and design project but it will take longer than the fully capable team.

Stage - E

-At this stage, the team is fully capable and is ready to take any projects of development and design, to be completed within time and budget.

APPENDIX-3.1: Jacobian Matrices

Inviscid Jacobian matrices

$$A = \begin{pmatrix} 0 & 1 & 0 & 0 \\ \frac{\gamma-3}{2}u^2 + \frac{\gamma-1}{2}v^2 & (3-\gamma)u & (1-\gamma)v & (1-\gamma) \\ uv & v & u & 0 \\ -\gamma eu + (\gamma-1)u(u^2+v^2) & \gamma e + \frac{1-\gamma}{2}(3u^2+v^2) & (1-\gamma)uv & \gamma u \end{pmatrix}$$

$$B = \begin{pmatrix} 0 & 0 & 1 & 0 \\ -uv & v & u & 0 \\ \frac{\gamma-3}{2}u^2 + \frac{\gamma-1}{2}v^2 & (1-\gamma)v & (3-\gamma)u & (1-\gamma) \\ -\gamma eu + (\gamma-1)v(u^2+v^2) & (1-\gamma)uv & \gamma e + \frac{1-\gamma}{2}(3u^2+v^2) & \gamma v \end{pmatrix}$$

and viscous Jacobian matrices

$$C = \begin{pmatrix} 0 & 0 & 0 & 0 \\ c_{21} & c_{22} & c_{23} & 0 \\ c_{31} & c_{32} & c_{33} & 0 \\ c_{41} & c_{42} & c_{43} & c_{44} \end{pmatrix}$$

$$D = \begin{pmatrix} 0 & 0 & 0 & 0 \\ d_{21} & d_{22} & d_{23} & 0 \\ d_{31} & d_{32} & d_{33} & 0 \\ d_{41} & d_{42} & d_{43} & d_{44} \end{pmatrix}$$

Element of matrix C

$$c_{21} = -\mu\{\frac{4}{3}\frac{\partial(\frac{u}{\rho})}{\partial x} - \frac{2}{3}\frac{\partial(\frac{v}{\rho})}{\partial y} + \frac{4}{3}\frac{u}{\rho}\frac{\partial}{\partial x} - \frac{2}{3}\frac{v}{\rho}\frac{\partial}{\partial y}\}$$

$$c_{22} = \mu\{\frac{4}{3}\frac{\partial(\frac{1}{\rho})}{\partial x} + \frac{4}{3}\frac{1}{\rho}\frac{\partial}{\partial x}\}$$

$$c_{23} = -\mu\{\frac{2}{3}\frac{\partial(\frac{1}{\rho})}{\partial y} + \frac{2}{3}\frac{1}{\rho}\frac{\partial}{\partial y}\}$$

$$c_{31} = \mu\{\frac{\partial(\frac{u}{\rho})}{\partial y} + \frac{\partial(\frac{v}{\rho})}{\partial x} + \frac{u}{\rho}\frac{\partial}{\partial y} + \frac{v}{\rho}\frac{\partial}{\partial x}\}$$

$$c_{32} = \mu\{\frac{\partial(\frac{1}{\rho})}{\partial y} + \frac{1}{\rho}\frac{\partial}{\partial y}\}$$

$$c_{33} = \mu\{\frac{\partial(\frac{1}{\rho})}{\partial x} + \frac{1}{\rho}\frac{\partial}{\partial x}\}$$

$$c_{41} = \mu\{-(\frac{4}{3} - \frac{\gamma}{P_r})\frac{\partial(\frac{u^2}{\rho})}{\partial x} - (1 - \frac{\gamma}{P_r})\frac{\partial(\frac{v^2}{\rho})}{\partial x} - \frac{\gamma}{P_r}\frac{\partial(\frac{e}{\rho})}{\partial x} - v\frac{\partial(\frac{u}{\rho})}{\partial y} + \frac{2}{3}u\frac{\partial(\frac{v}{\rho})}{\partial y}$$

$$-\frac{v}{\rho}\frac{\partial u}{\partial y} + \frac{2}{3}\frac{u}{\rho}\frac{\partial v}{\partial y} - (\frac{4}{3} - \frac{\gamma}{P_r})\frac{u^2}{\rho}\frac{\partial}{\partial x} - (1 - \frac{\gamma}{P_r})\frac{v^2}{\rho}\frac{\partial}{\partial x} - \frac{\gamma}{P_r}\frac{e}{\rho}\frac{\partial}{\partial x} + \frac{1}{3}\frac{uv}{\rho}\frac{\partial}{\partial y}\}$$

$$c_{42} = \mu\{\frac{4}{3}\frac{\partial(\frac{u}{\rho})}{\partial x} - \frac{\gamma}{P_r}\frac{\partial(\frac{u}{\rho})}{\partial x} + v\frac{\partial(\frac{1}{\rho})}{\partial y} - \frac{2}{3}\frac{1}{\rho}\frac{\partial v}{\partial y} + \frac{4}{3}\frac{u}{\rho}\frac{\partial}{\partial x} - \frac{\gamma}{P_r}\frac{u}{\rho}\frac{\partial}{\partial x} + \frac{v}{\rho}\frac{\partial}{\partial y}\}$$

$$c_{43} = \mu\{\frac{\partial(\frac{v}{\rho})}{\partial x} - \frac{\gamma}{P_r}\frac{\partial(\frac{v}{\rho})}{\partial x} - \frac{2}{3}u\frac{\partial(\frac{1}{\rho})}{\partial y} + \frac{1}{\rho}\frac{\partial u}{\partial y} - \frac{2}{3}\frac{u}{\rho}\frac{\partial}{\partial y} - \frac{\gamma}{P_r}\frac{v}{\rho}\frac{\partial}{\partial x} + \frac{v}{\rho}\frac{\partial}{\partial x}\}$$

$$c_{44} = \mu\{\frac{\gamma}{P_r}\frac{\partial(\frac{1}{\rho})}{\partial x} + \frac{\gamma}{P_r}\frac{1}{\rho}\frac{\partial}{\partial x}\}$$

Element of matrix D

$$d_{21} = -\mu\{\frac{\partial(\frac{v}{\rho})}{\partial x} + \frac{\partial(\frac{u}{\rho})}{\partial y} + \frac{u}{\rho}\frac{\partial}{\partial y} + \frac{v}{\rho}\frac{\partial}{\partial x}\}$$

$$d_{22} = \mu\{\frac{\partial(\frac{1}{\rho})}{\partial y} + \frac{1}{\rho}\frac{\partial}{\partial y}\}$$

$$d_{23} = \mu\{\frac{\partial(\frac{1}{\rho})}{\partial x} + \frac{1}{\rho}\frac{\partial}{\partial x}\}$$

$$d_{31} = -\mu\{\frac{4}{3}\frac{\partial(\frac{v}{\rho})}{\partial y} - \frac{2}{3}\frac{\partial(\frac{u}{\rho})}{\partial x} + \frac{1}{3}\frac{v}{\rho}\frac{\partial}{\partial y} - \frac{2}{3}\frac{u}{\rho}\frac{\partial}{\partial x}\}$$

$$d_{32} = -\mu\{\frac{2}{3}\frac{\partial(\frac{1}{\rho})}{\partial x} + \frac{2}{3}\frac{1}{\rho}\frac{\partial}{\partial x}\}$$

$$d_{33} = \mu\{\frac{4}{3}\frac{\partial(\frac{1}{\rho})}{\partial y} + \frac{4}{3}\frac{1}{\rho}\frac{\partial}{\partial x}\}$$

$$d_{41} = \mu\{-(\frac{4}{3} - \frac{\gamma}{P_r})\frac{\partial(\frac{v^2}{\rho})}{\partial y} - (1 - \frac{\gamma}{P_r})\frac{\partial(\frac{u^2}{\rho})}{\partial y} - \frac{\gamma}{P_r}\frac{\partial(\frac{e}{\rho})}{\partial x} - u\frac{\partial(\frac{v}{\rho})}{\partial x} + \frac{2}{3}v\frac{\partial(\frac{u}{\rho})}{\partial x}$$

$$-\frac{u}{\rho}\frac{\partial v}{\partial x}+\frac{2}{3}\frac{v}{\rho}\frac{\partial u}{\partial x}-(\frac{4}{3}-\frac{\gamma}{P_r})\frac{v^2}{\rho}\frac{\partial}{\partial y}-(1-\frac{\gamma}{P_r})\frac{u^2}{\rho}\frac{\partial}{\partial y}-\frac{\gamma}{P_r}\frac{e}{\rho}\frac{\partial}{\partial y}+\frac{2}{3}\frac{uv}{\rho}\frac{\partial}{\partial x}\}$$

$$d_{42}=\mu\{\frac{\partial(\frac{u}{\rho})}{\partial y}-\frac{\gamma}{P_r}\frac{\partial(\frac{u}{\rho})}{\partial y}-\frac{2}{3}v\frac{\partial(\frac{1}{\rho})}{\partial x}+\frac{1}{\rho}\frac{\partial v}{\partial x}-\frac{2}{3}\frac{v}{\rho}\frac{\partial}{\partial x}-\frac{\gamma}{P_r}\frac{u}{\rho}\frac{\partial}{\partial y}+\frac{u}{\rho}\frac{\partial}{\partial y}\}$$

$$d_{43}=\mu\{\frac{4}{3}\frac{\partial(\frac{v}{\rho})}{\partial x}-\frac{\gamma}{P_r}\frac{\partial(\frac{v}{\rho})}{\partial y}+u\frac{\partial(\frac{1}{\rho})}{\partial x}-\frac{2}{3}\frac{1}{\rho}\frac{\partial u}{\partial x}+\frac{4}{3}\frac{v}{\rho}\frac{\partial}{\partial y}-\frac{\gamma}{P_r}\frac{v}{\rho}\frac{\partial}{\partial y}+\frac{u}{\rho}\frac{\partial}{\partial x}\}$$

$$d_{44}=\mu\{\frac{\gamma}{P_r}\frac{\partial(\frac{1}{\rho})}{\partial y}+\frac{\gamma}{P_r}\frac{1}{\rho}\frac{\partial}{\partial y}\}$$

APPENDIX 4.1 Skewed Grid

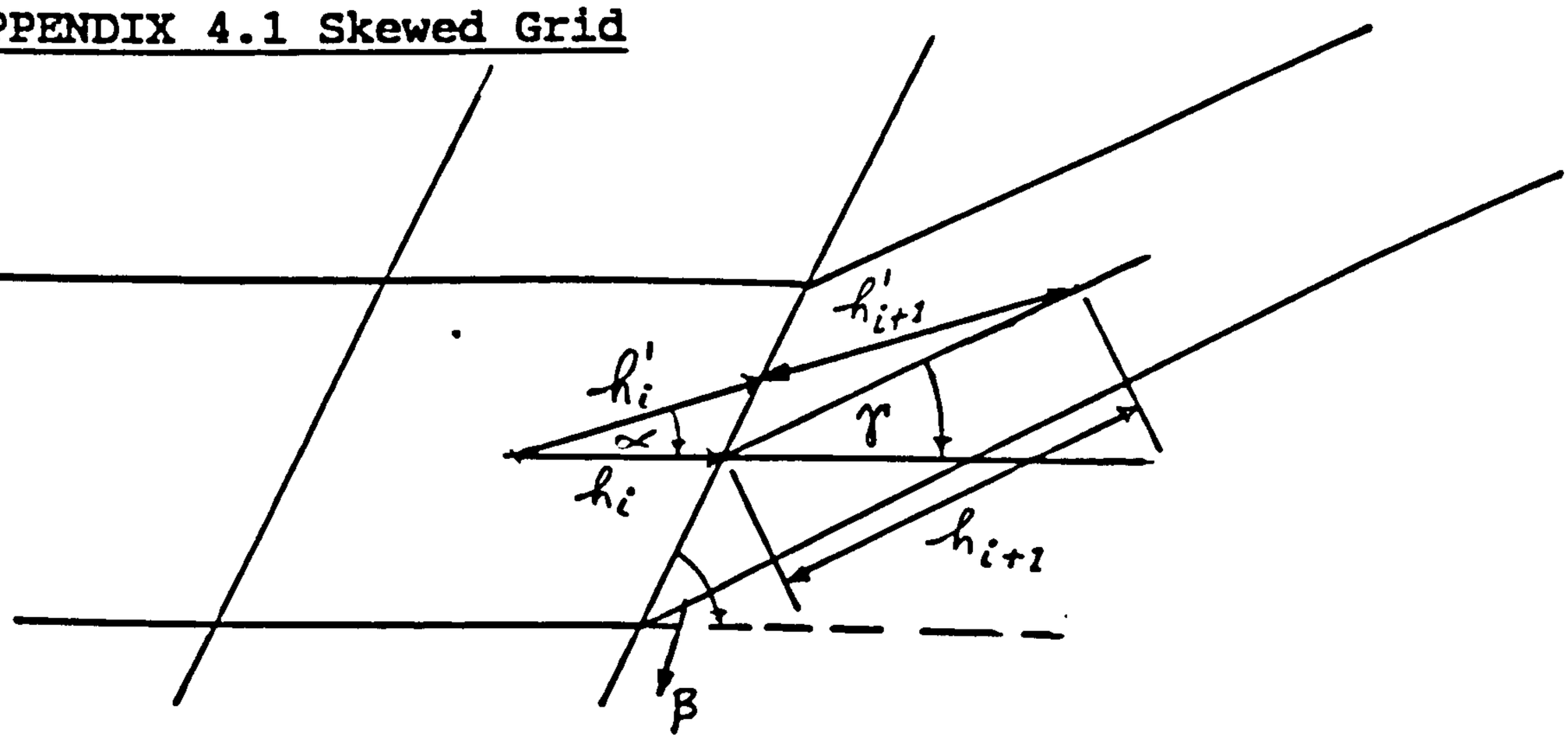

$$\frac{h'_i + h'_{i+1}}{sin(\pi - \gamma)} = \frac{h_{i+1}}{sin\alpha}$$

$$\frac{h'_i}{sin(\pi - \gamma)} = \frac{h_i}{sin(\beta - \alpha)}$$

$$\frac{h'_{i+1}}{sin(\beta - \gamma)} = \frac{h_{i+1}}{sin(\pi - (\beta - \alpha))}$$

$$h'_i = \frac{sin\beta}{sin(\beta - \alpha)} h_i, \qquad h'_{i+1} = \frac{sin(\beta - \gamma)}{sin(\beta - \alpha)} h_{i+1}$$

$$\Delta h_i = h'_i - h_i = \left(\frac{sin\beta - sin(\beta - \alpha)}{sin(\beta - \alpha)} \right) h_i$$

$$\Delta h_{i+1} = h'_{i+1} - h_{i+1} = \left(\frac{sin(\beta - \gamma) - sin(\beta - \alpha)}{sin(\beta - \alpha)} \right) h_{i+1}$$

Since $\beta > \gamma > \alpha$

$$\frac{\Delta h_{i+1}}{h_{i+1}} < \frac{\Delta h_i}{h_i}$$

Appendix-4.2 : Shape Function

Consider u as a variable in three dimensional space.

Locally over an element, we approximate the variation as

$$u(\xi,\eta,\zeta) = A_1 + A_2\xi + A_3\eta + A_4\zeta + A_5\xi^2 + A_6\eta^2 + A_7\zeta^2 \quad (A.4.2.1)$$

The value of u at point 1 (figure-4.7a)

$$u_1 = A_1 + A_2\xi_1 + A_3\eta_1 + A_4\zeta_1 + A_5\xi_1^2 + A_6\eta_1^2 + A_7\zeta_1^2 \quad (A.4.2.2)$$

and other points refer to an element.

After substituting the coordinates in the transformed space, we can write

$$[u_1,u_2,u_3,u_4,u_5,u_6,u_7]=[A_1,A_2,A_3,A_4,A_5,A_6,A_7][S] \quad (A.4.2.3)$$

where [S] is 7X7 matrix of coordinates of the seven points

$$S = \begin{pmatrix} 1 & 1 & 1 & 1 & 1 & 1 & 1 \\ \xi_1 & \xi_2 & \xi_3 & \xi_4 & \xi_5 & \xi_6 & \xi_7 \\ \eta_1 & \eta_2 & \eta_3 & \eta_4 & \eta_5 & \eta_6 & \eta_7 \\ \zeta_1 & \zeta_2 & \zeta_3 & \zeta_4 & \zeta_5 & \zeta_6 & \zeta_7 \\ (\xi_1)^2 & (\xi_2)^2 & (\xi_3)^2 & (\xi_4)^2 & (\xi_5)^2 & (\xi_6)^2 & (\xi_7)^2 \\ (\eta_1)^2 & (\eta_2)^2 & (\eta_3)^2 & (\eta_4)^2 & (\eta_5)^2 & (\eta_6)^2 & (\eta_7)^2 \\ (\zeta_1)^2 & (\zeta_2)^2 & (\zeta_3)^2 & (\zeta_4)^2 & (\zeta_5)^2 & (\zeta_6)^2 & (\zeta_7)^2 \end{pmatrix} \quad (A.4.2.4)$$

By inverting the 7X7 matrix on the right hand side, the constants $A_1,A_2,A_3,A_4,A_5,A_6,A_7$ can be expressed as

$$[A_1,A_2,A_3,A_4,A_5,A_6,A_7]=[u_1,u_2,u_3,u_4,u_5,u_6,u_7][S]^{-1} \quad (A.4.2.5)$$

$u(\xi,\eta,\zeta)$ can then be expressed as

$$u(\xi,\eta,\zeta) = [A_1,A_2,A_3,A_4,A_5,A_6,A_7]\begin{pmatrix}1\\ \xi\\ \eta\\ \zeta\\ \xi^2\\ \eta^2\\ \zeta^2\end{pmatrix} \qquad (A.4.2.6)$$

Substitung matrix [A] from equation (A.4.2.5) into equation (A.4.2.6)

Thus

$$u(\xi,\eta,\zeta)=[u_1,u_2,u_3,u_4,u_5,u_6,u_7][S]^{-1}\begin{pmatrix}1\\ \xi\\ \eta\\ \zeta\\ \xi^2\\ \eta^2\\ \zeta^2\end{pmatrix} \qquad (A.4.2.7)$$

The matrix S is obtained by substituting the value of ξ,η ,and ζ of the seven points which gives

$$[S] = \begin{bmatrix}1 & 1 & 1 & 1 & 1 & 1 & 1\\ 1 & 0 & 0 & -1 & 0 & 0 & 0\\ 0 & 1 & 0 & 0 & -1 & 0 & 0\\ 0 & 0 & 1 & 0 & 0 & -1 & 0\\ 1 & 0 & 0 & 1 & 0 & 0 & 0\\ 0 & 1 & 0 & 0 & 1 & 0 & 0\\ 0 & 0 & 1 & 0 & 0 & 1 & 0\end{bmatrix} \qquad (A.4.2.8)$$

The inverse of [S] is

$$[S]^{-1} = \begin{bmatrix} 0 & 0.5 & 0 & 0 & 0.5 & 0 & 0 \\ 0 & 0 & 0.5 & 0 & 0 & 0.5 & 0 \\ 0 & 0 & 0 & 0.5 & 0 & 0 & 0.5 \\ 0 & -0.5 & 0 & 0 & 0.5 & 0 & 0 \\ 0 & 0 & -0.5 & 0 & 0 & 0.5 & 0 \\ 0 & 0 & 0 & -0.5 & 0 & 0 & 0.5 \\ 1 & 0 & 0 & 0 & 1 & 1 & 1 \end{bmatrix} \quad \text{(A.4.2.9)}$$

Substituting the equation (A.4.2.9) into equation (A.4.2.7) and multiply the matrices,

$$u(\xi,\eta,\zeta) = \frac{u_1}{2}(\xi+\xi^2) + \frac{u_2}{2}(\eta+\eta^2) + \frac{u_3}{2}(\zeta+\zeta^2) + \frac{u_4}{2}(-\xi+\xi^2)$$
$$+\frac{u_5}{2}(-\eta+\eta^2) + \frac{u_6}{2}(-\zeta+\zeta^2) + \frac{u_7}{2}(1-\xi^2-\eta^2-\zeta^2) \quad \text{(A.4.2.10)}$$

By expressing $u(\xi,\eta,\zeta) = \sum_{i=1}^{7} u_i N_i$, the shape functions N_i are given by $N_1 = \frac{1}{2}(\xi+\xi^2)$, $N_2 = \frac{1}{2}(\eta+\eta^2)$, $N_3 = \frac{1}{2}(\zeta+\zeta^2)$

$$N_4 = \frac{1}{2}(-\xi+\xi^2), \quad N_5 = \frac{1}{2}(-\eta+\eta^2), \quad N_6 = \frac{1}{2}(-\zeta+\zeta^2) \quad \text{(A.4.2.11)}$$
$$N_7 = 1-\xi^2-\eta^2-\zeta^2$$

The derivatives of u with respect to x,y and z are

$$\frac{\partial u}{\partial x} = \sum_{i=1}^{7} u_i \frac{\partial N_i}{\partial x}$$

$$\frac{\partial u}{\partial y} = \sum_{i=1}^{7} u_i \frac{\partial N_i}{\partial y} \quad \text{(A.4.2.12)}$$

$$\frac{\partial u}{\partial z} = \sum_{i=1}^{7} u_i \frac{\partial N_i}{\partial z}$$

The evaluation of $\frac{\partial N_i}{\partial x}$, $\frac{\partial N_i}{\partial y}$, and $\frac{\partial N_i}{\partial z}$ require some manipulation because the shape function N_i are function of ξ, η, and ζ

Write

$$\frac{\partial N}{\partial \xi} = \frac{\partial x}{\partial \xi}\frac{\partial N}{\partial x} + \frac{\partial y}{\partial \xi}\frac{\partial N}{\partial y} + \frac{\partial z}{\partial \xi}\frac{\partial N}{\partial z}$$

$$\frac{\partial N}{\partial \eta} = \frac{\partial x}{\partial \eta}\frac{\partial N}{\partial x} + \frac{\partial y}{\partial \eta}\frac{\partial N}{\partial y} + \frac{\partial z}{\partial \eta}\frac{\partial N}{\partial z}$$

$$\frac{\partial N}{\partial \zeta} = \frac{\partial x}{\partial \zeta}\frac{\partial N}{\partial x} + \frac{\partial y}{\partial \zeta}\frac{\partial N}{\partial y} + \frac{\partial z}{\partial \zeta}\frac{\partial N}{\partial z} \qquad \text{(A.4.2.13)}$$

Thus, for instance, at point 1

$$\begin{pmatrix} N_x \\ N_y \\ N_z \end{pmatrix} = \begin{pmatrix} x_\xi & y_\xi & z_\xi \\ x_\eta & y_\eta & z_\eta \\ x_\zeta & y_\zeta & z_\zeta \end{pmatrix}^{-1} \begin{pmatrix} N_\xi \\ N_\eta \\ N_\zeta \end{pmatrix} \qquad \text{(A.4.2.14)}$$

Since the coordinates x, y, and z can also be expressed in terms of the same shape function, their derivatives with respect to ξ, η, and ζ can be expressed as

$$\frac{\partial x}{\partial \xi} = x_1\frac{\partial N_1}{\partial \xi} + x_4\frac{\partial N_4}{\partial \xi} + x_7\frac{\partial N_7}{\partial \xi}$$

$$\frac{\partial x}{\partial \eta} = x_2\frac{\partial N_2}{\partial \eta} + x_5\frac{\partial N_5}{\partial \eta} + x_7\frac{\partial N_7}{\partial \eta} \qquad \text{(A.4.2.15)}$$

$$\frac{\partial x}{\partial \zeta} = x_3\frac{\partial N_3}{\partial \zeta} + x_6\frac{\partial N_6}{\partial \zeta} + x_7\frac{\partial N_7}{\partial \zeta}$$

and Y_ξ, Y_η, Y_ζ, z_ξ, z_η and z_ζ follow similarly.

The derivatives of the shape functions N_i with respect to ξ, η, and ζ are calculated from equation (A.4.2.11). The

values that correspond to each location are evaluated the appropriate ξ , η ,and ζ coordinates (figure-4.7a).

APPENDIX-4.3 : Formulation of Improved Scheme

Decoupled Formulation

In two dimensions, the interpolation function is

$$u(\xi, \eta) = A_1 + A_2'\xi + A_5'\xi^2 + A_3'\eta + A_6'\eta^2$$

Flux along the ξ - direction at face (i+1/2,j)' is

$$u_{i+1/2,j} = A_1 + A_2'(h_i'/2) + A_5'(h_i'/2)^2$$

where

$$A_2' = 2\frac{(h_i + h_{i-1})^2(u_{i+1} - u_i) - (h_i' + h_{i+1}')^2(u_{i-1} - u_i)}{(h_i' + h_{i+1}')(h_i + h_{i-1})(h_{i+1}' + h_i' + h_i + h_{i-1})}$$

$$A_5' = 4\frac{(h_i + h_{i-1})(u_{i+1} - u_i) + (h_i' + h_{i+1}')(u_{i-1} - u_i)}{(h_i' + h_{i+1}')(h_i + h_{i-1})(h_{i+1}' + h_i' + h_i + h_{i-1})}$$

Coupled Formulation

Coefficients A_2' and A_5' are replaced by A_2 and A_5 and coordinates ξ and η are replaced by x and y, then

$$A_2 = [(u_{i+1,j} - u_{i,j})(h_i + h_{i+1})^2 - (u_{i-1,j} - u_{i,j})(h_i + h_{i+1}cos\alpha)^2$$

$$-\frac{1}{2}A_3 h_{i+1}(h_i + h_{i+1})^2 sin\alpha - \frac{1}{4}A_6 h_{i+1}^2(h_i + h_{i+1})^2 sin^2\alpha]/$$

$$[(h_i + h_{i-1})(h_i + h_{i+1}cos\alpha)(h_{i-1} + 2h_i + h_{i+1}cos\alpha)]$$

$$A_3 = \frac{2[(l_j + lj - 1)^2(u_{i,j+1} - u_{i,j}) - (l_j + l_{j+1})^2(u_{i,j-1} - u_{i,j})}{(l_j + l_{j-1})(l_j + l_{j+1})(l_{j-1} + 2l_j \quad + l_{j+1})]}$$

APPENDIX - 5.1 High Speed Flow Aspect Ratio Function

For a given high aspect ratio cell, high Mach number can reduce the influence of the cell geometry on the aspect ratio correction function. For instance, two dimensoinal Kuntz's aspect ratio function in

ξ- direction is

$$\phi_r(r) = \left(1 + \frac{\Delta t_\xi}{\Delta t_\eta}\right)^\alpha \qquad \text{(A.5.1.1)}$$

The scaling factor is,

$$\xi - \text{DIRECTION}: \left(\frac{A}{\Delta t_\xi}\right) = (|u| + c)\Delta\eta$$

$$\eta - \text{DIRECTION}: \left(\frac{A}{\Delta t_\eta}\right) = (|v| + c)\Delta\xi \qquad \text{(A.5.1.2)}$$

Assume | v | << | u | then the ratio $\left(\frac{\Delta t_\xi}{\Delta t_\eta}\right)$ that goes into the equation of the aspect ratio correction function is

$$\frac{\Delta t_\xi}{\Delta t_\eta} = m\left(\frac{\Delta\xi}{\Delta\eta}\right) \qquad \text{(A.5.1.3)}$$

where $m = \frac{1}{1+M}$ and $M = \frac{|u|}{c}$

Thus for a given cell aspect ratio $\left(\frac{\Delta\xi}{\Delta\eta}\right)$

$$\left(\frac{\Delta t_\xi}{\Delta t_\eta}\right)_{M\simeq 1} < \left(\frac{\Delta t_\xi}{\Delta t_\eta}\right)_{M<1} \qquad \text{(A.5.1.4)}$$

For dissipation in ξ - direction

$$d_\xi = s\ (\epsilon^2 \delta_\xi^2 w - \epsilon^4 \delta_\xi^4 w) \qquad \text{(A.5.1.5)}$$

where $s = \left(\frac{A}{\Delta t_\xi}\right)\left(1 + \frac{\Delta t_\xi}{\Delta t_\eta}\right)^\alpha$ (A.5.1.5a)

In the standard dissipation model $\alpha = 1$. The effect of the dissipation reduction due to the aspect ratio function is determined by the ratio of the modified scaling factor with respect to standard scaling factor, or

$$R_r = (1 + r)^{\alpha - 1} \qquad \text{(A.5.1.6)}$$

where $r = \frac{\Delta t_\xi}{\Delta t_\eta}$

For a given α and $\left(\frac{\Delta\xi}{\Delta\eta}\right)$

$$R_r)_{M\simeq 1} > R_r)_{M<1} \qquad \text{(A.5.1.7)}$$

where $r_{M\simeq 1} < r_{M<1}$

From equation (A.5.1.4), $r_{M\simeq 1}$ when the flow is transonic, and $r_{M<1}$ when the flow is subsonic flow. Therefore, for a given $\frac{\Delta\xi}{\Delta\eta}$, the effect of the dissipation reduction in the transonic flow is less than the one in subsonic flow. In order to obtain the same effect of the dissipation reduction in both flow conditions α has to be reduced.

Appendix - 6.1 Newton Method

The system of non-linear equations is solved by Newton's iterative method, For instance, the system is

$$m_{11} + m_{22} + m_{33} + m_{44} = \lambda_1 + \lambda_2 + \lambda_3 + \lambda_4 \qquad \text{(A.6.1a)}$$

$$m_{11}m_{22} + m_{33}m_{44} + (m_{11} + m_{22})(m_{33} + m_{44}) - m_{23}m_{32} = \lambda_1\lambda_2 + \lambda_3\lambda_4 + (\lambda_1 + \lambda_2)(\lambda_3 + \lambda_4) \qquad \text{(A.6.1b)}$$

$$m_{11}m_{22}(m_{33} + m_{44}) + m_{33}m_{44}(m_{11} + m_{22}) + m_{32}m_{23}(m_{11} + m_{44}) = \lambda_1\lambda_2(\lambda_3 + \lambda_4) + \lambda_3\lambda_4(\lambda_1 + \lambda_2) \qquad \text{(A.6.1c)}$$

$$m_{11}\, m_{22}\, m_{33}\, m_{44} = \lambda_1\, \lambda_2\, \lambda_3\, \lambda_4 \qquad \text{(A.6.1b)}$$

which can be written as

$$p(m_{11}, m_{22}, m_{33}, m_{44}) = 0$$
$$q(m_{11}, m_{22}, m_{33}, m_{44}) = 0$$
$$r(m_{11}, m_{22}, m_{33}, m_{44}) = 0$$
$$s(m_{11}, m_{22}, m_{33}, m_{44}) = 0$$

where m_{23}, m_{32} and eigenvalues λ_i are constant.

In this method, values of the unknown m_{11}, m_{22}, m_{33}, and m_{44} at iteration n are

$$m_{11}^{\,n} = m_{11}^{\,n-1} + h^{n-1}$$
$$m_{22}^{\,n} = m_{22}^{\,n-1} + k^{n-1}$$
$$m_{33}^{\,n} = m_{33}^{\,n-1} + l^{n-1}$$
$$m_{44}^{\,n} = m_{44}^{\,n-1} + j^{n-1} \qquad \text{(A.6.2)}$$

where h,k,l, and j have to satisfy

$$p_{m11}{}^{n-1}h^{n-1} + p_{m22}{}^{n-1}k^{n-1} + p_{m11}{}^{n-1}l^{n-1} + p_{m22}{}^{n-1}j^{n-1} = -p^{n-1} \qquad \text{(A.6.3.a)}$$

$$q_{m11}{}^{n-1}h^{n-1} + q_{m22}{}^{n-1}k^{n-1} + q_{m33}{}^{n-1}l^{n-1} + q_{m44}{}^{n-1}j^{n-1} = -q^{n-1} \qquad \text{(A.6.3.b)}$$

$$r_{m11}{}^{n-1}h^{n-1} + r_{m22}{}^{n-1}k^{n-1} + r_{m33}{}^{n-1}l^{n-1} + r_{m44}{}^{n-1}j^{n-1} = -r^{n-1} \qquad \text{(A.6.3.c)}$$

$$s_{m11}{}^{n-1}h^{n-1} + s_{m22}{}^{n-1}k^{n-1} + s_{m33}{}^{n-1}l^{n-1} + s_{m44}{}^{n-1}j^{n-1} = -s^{n-1} \qquad \text{(A.6.3.d)}$$

which can be written in matrix form as

$$M\ D = R \qquad \text{(A.6.4)}$$

where

$$M = \begin{bmatrix} p_{m11} & p_{m12} & p_{m33} & p_{m44} \\ q_{m11} & q_{m12} & q_{m33} & q_{m44} \\ r_{m11} & r_{m12} & r_{m33} & r_{m44} \\ s_{m11} & s_{m12} & s_{m33} & r_{m44} \end{bmatrix}^{n-1}, \quad D = \begin{bmatrix} h \\ k \\ l \\ j \end{bmatrix}^{n-1} \text{ and } R = -\begin{bmatrix} p \\ q \\ r \\ s \end{bmatrix}^{n-1}$$

and $p_{m11} = \frac{\partial p}{\partial m_{11}}$. Others follow accordingly.

Procedure to calculate m_{11}, m_{22}, m_{33}, and m_{44} are

step 1. Guess initial values of m_{11}, m_{22}, m_{33}, and m_{44}

step 2. Calculate matrix M with initial guess values

step 3. Solve for h, k, l and j by using equation (A.6.4)

step 4. Update m_{11}, m_{22}, m_{33}, and m_{44} by using equation (A.6.2)

step 5. Repeat step 1, 2, 3, and 4 until h, k, l, and j diminish

step 6. Solution are m_{11}, m_{22}, m_{33}, and m_{44} of equation (A.6.2)

Table-2.1 Matrix of Responsibility

	Finance	Planning & Definition	Development	Implementation
Human Resource	X	X	X	X
Technology	X	X	X	X
Cost	X			
Hardware	X	X		X

Table-5.1 Results of the application of Kuntz Aspect Ratio Function to the inviscid Ni's bump test case

M	K_2	K_4	α	P_t Losses	$\Delta \dot{m}$
0.5 0.5	0 0	0.008 0.008	1. 0.6666	0.5 % 0.37 %	0.42 % 0.414 %
0.675 0.675	0.25 0.25	0.01 0.01	1. 0.4	1.64 % 1.61 %	0.93 % 1.1 %

Table-5.2 Results of the application of Modified Aspect Ratio Function to the inviscid Ni's bump test case

M	K_2	K_4	α	P_t Losses	f(AR)
0.5 0.5	0 0	0.008 0.008	0.6666 0.6666	0.37 % 0.33 %	Kuntz Modified

Table-5.3 Results of the application of Kuntz Aspect Ratio and Mach Number Function to the inviscid Ni's bump test case

M	K_2	K_4	α	P_t Losses	$f(M_L/M_{max})$
0.5 0.5	0 0	0.008 0.008	0.6666 0.6666	0.373 % 0.39 %	No Yes
0.675 0.675	0.25 0.25	0.01 0.02	0.4 0.4	1.61 % 1.58 %	No Yes

Table-5.4 Result of the application of Grid Refinement to the inviscid Ni's bump test case

M	K_2	K_4	GRID	P_t Losses	$\Delta \dot{m}$
0.675 0.675	0.25 0.25	0.01 0.01	78X15 90X24	1.64 % 1.49 %	0.93 % 0.89 %

Table-5.5 Constant of Modification Function for Three Dimensional High Pressure Turbine case

No	α	f_{D_ξ}	f_{D_η}	f_{D_ζ}	Comments
1	1.0	1.0	1.0	1.0	No Modification
2	0.75	1.0	1.0	1.0	Aspect Ratio Function
3	1.0	0.25	0.0	0.0	Gradient Function
4	0.75	1.0	0.0	0.0	Aspect and Gradient Function

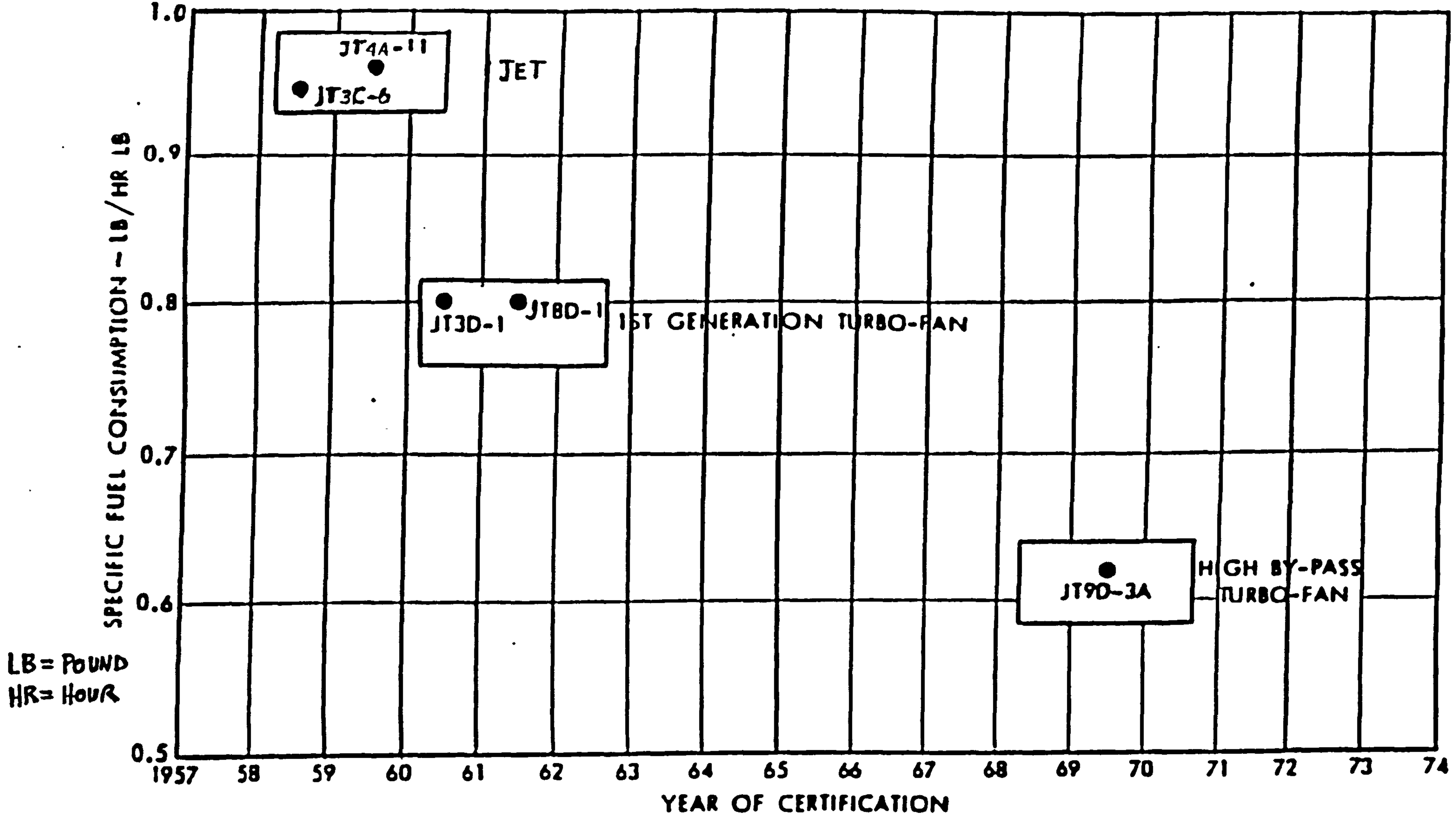

Figure-1.1 History of Specific Fuel Consumption

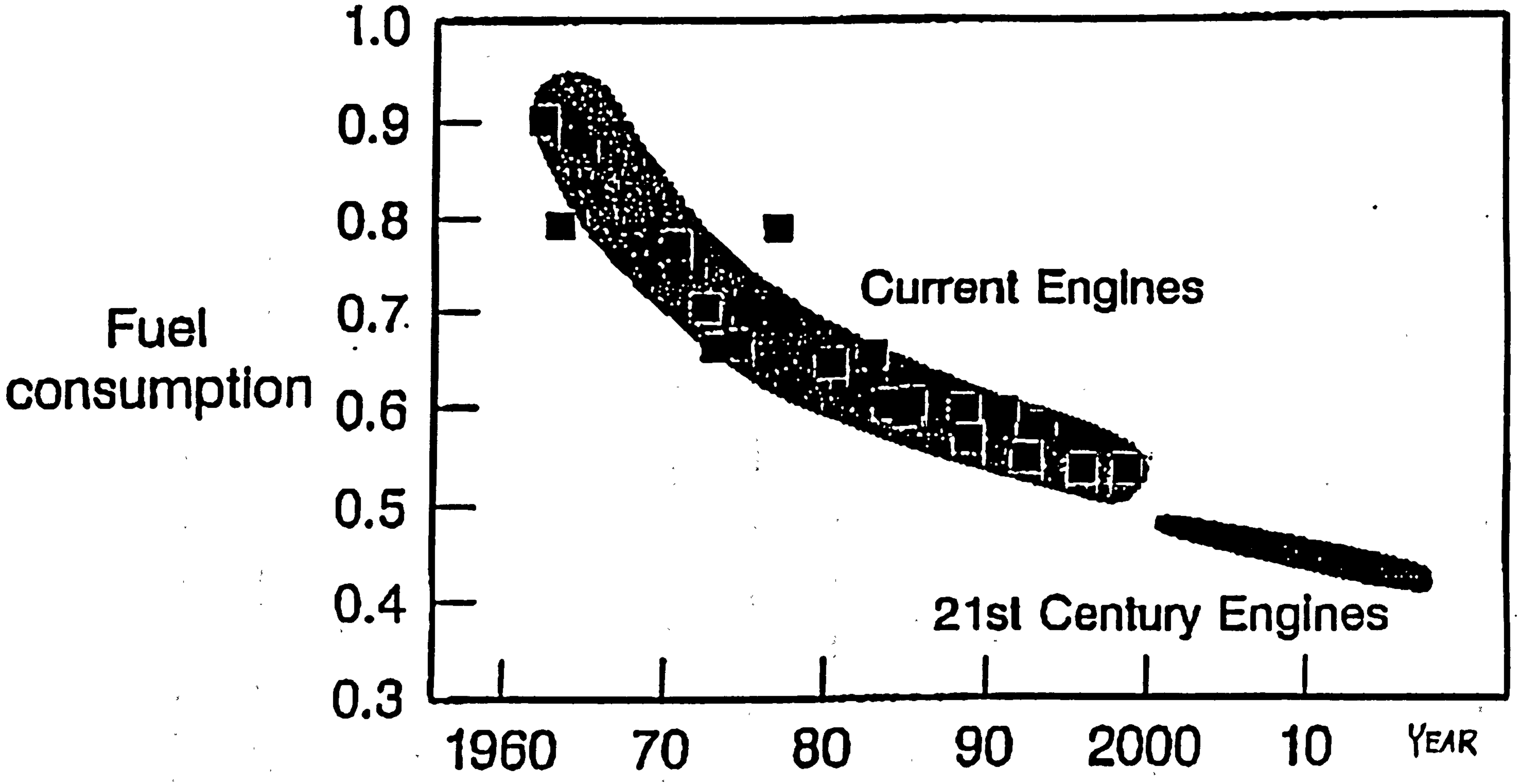

Figure-1.2 Specific Fuel Consumption

No Market Expansion

- Modernisation
- No need for collaboration

Existing Product	New Product Product
Existing Market	New Market

Market Expansion

- Collaboration helps to gain Access to new markets

Existing Product	New Product Product
Existing Market	New Market

Market Expansion

- Collaboration helps both in developing new products and accessing new markets.

Existing Product	New Product Product
Existing Market	New Market

Figure-2.1 Market

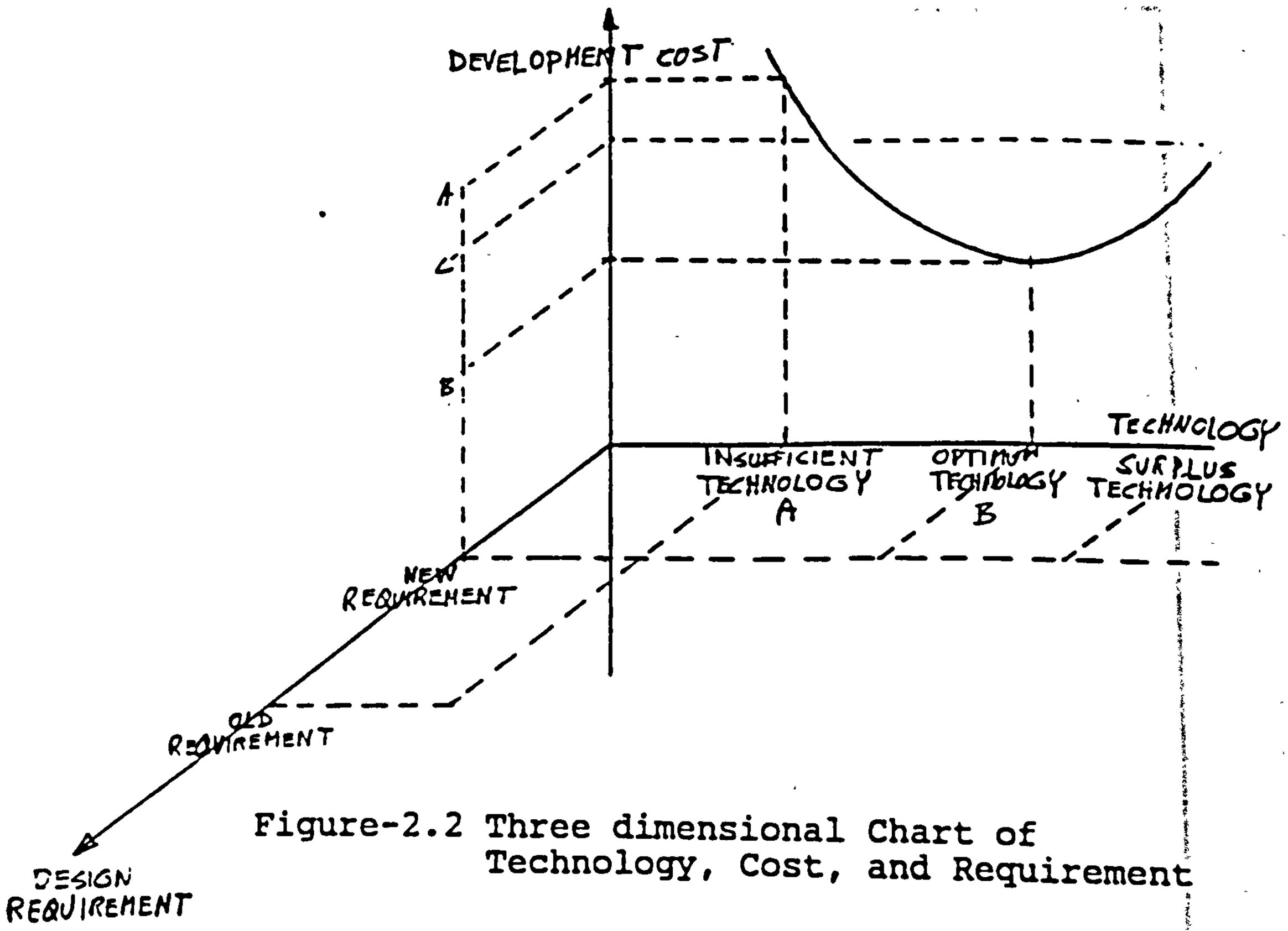

Figure-2.2 Three dimensional Chart of Technology, Cost, and Requirement

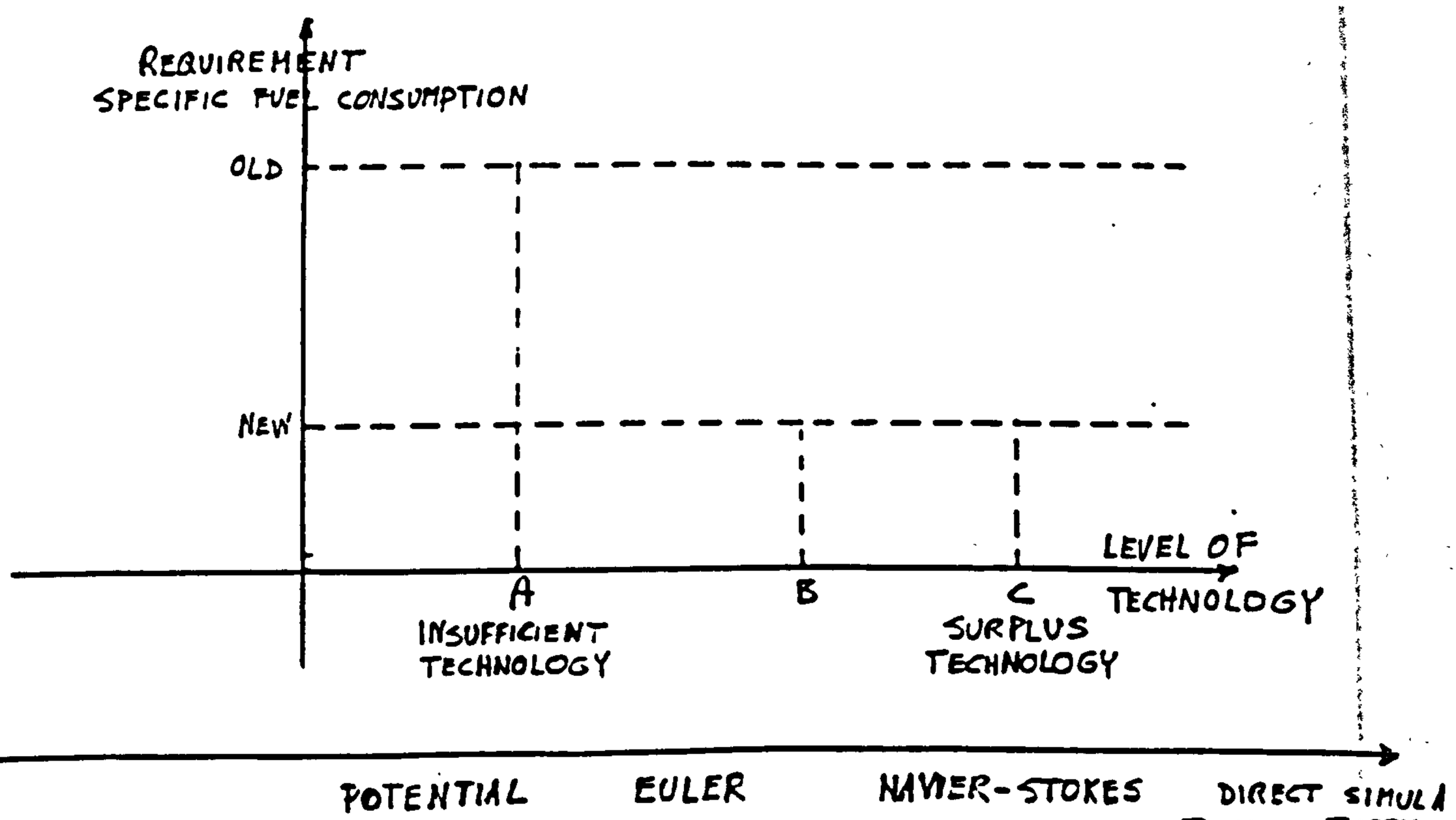

Figure-2.3 Requirement Versus Technology

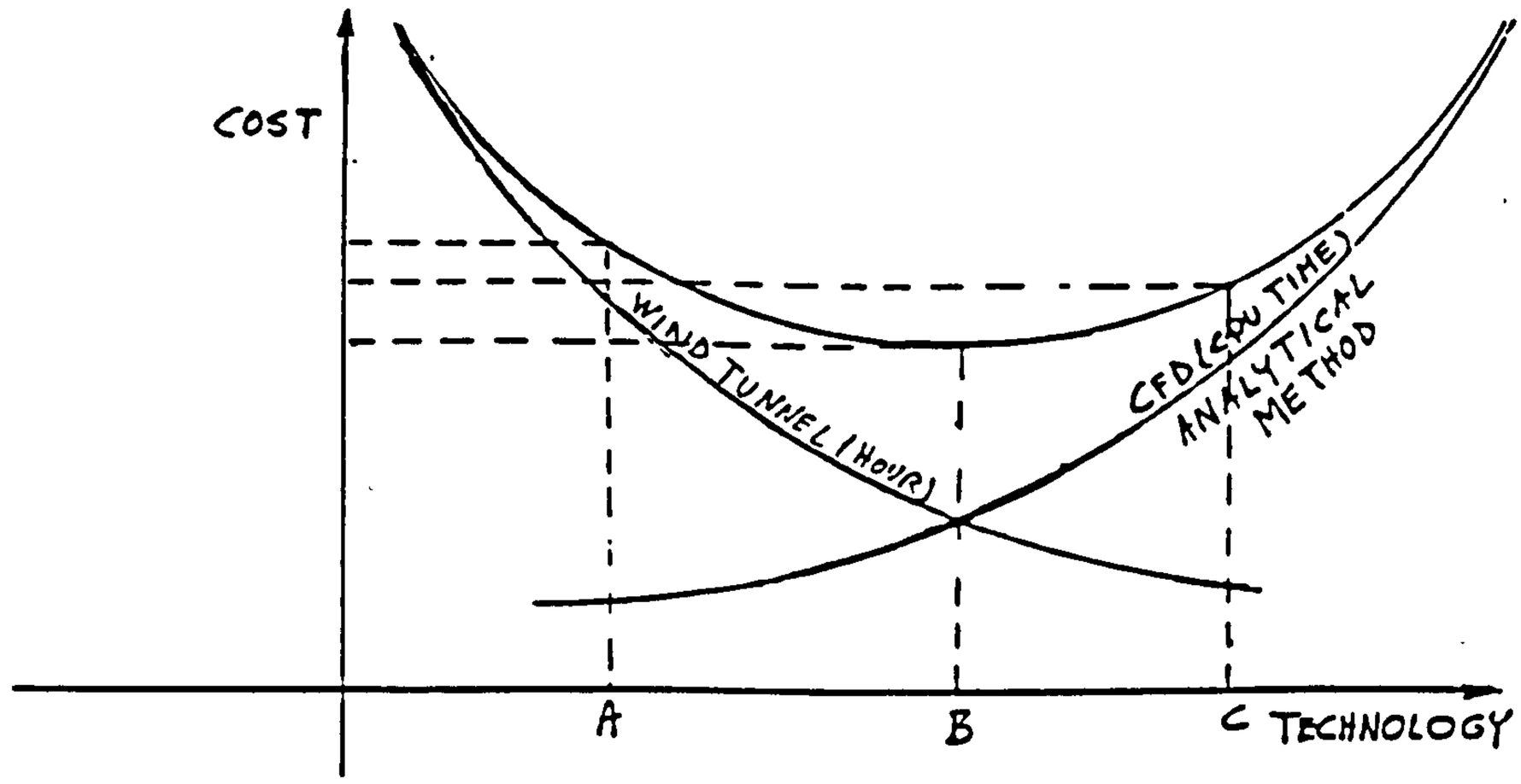

Figure-2.4 Cost Versus Technology

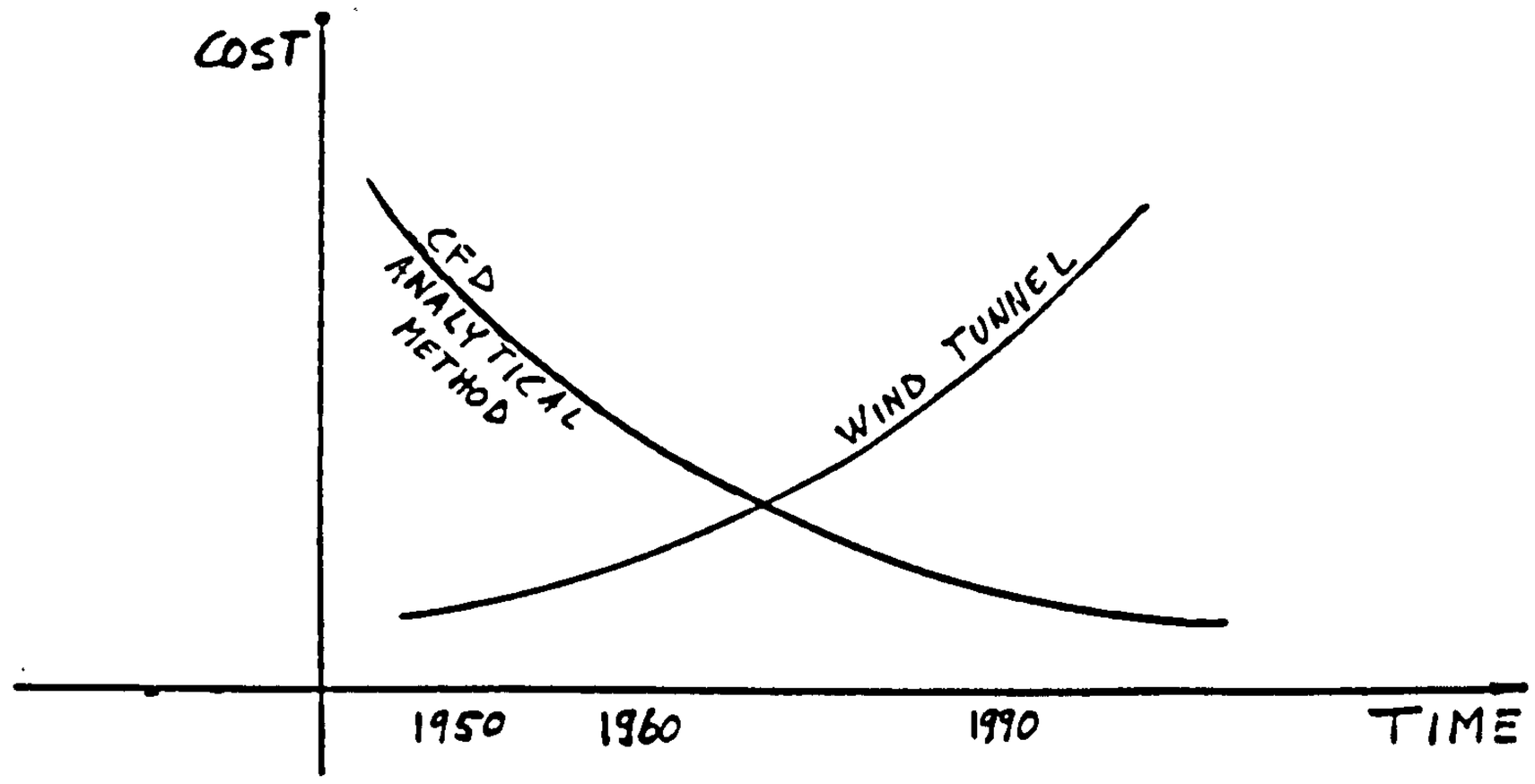

Figure-2.5 Cost of CFD and Wind Tunnel Versus Time

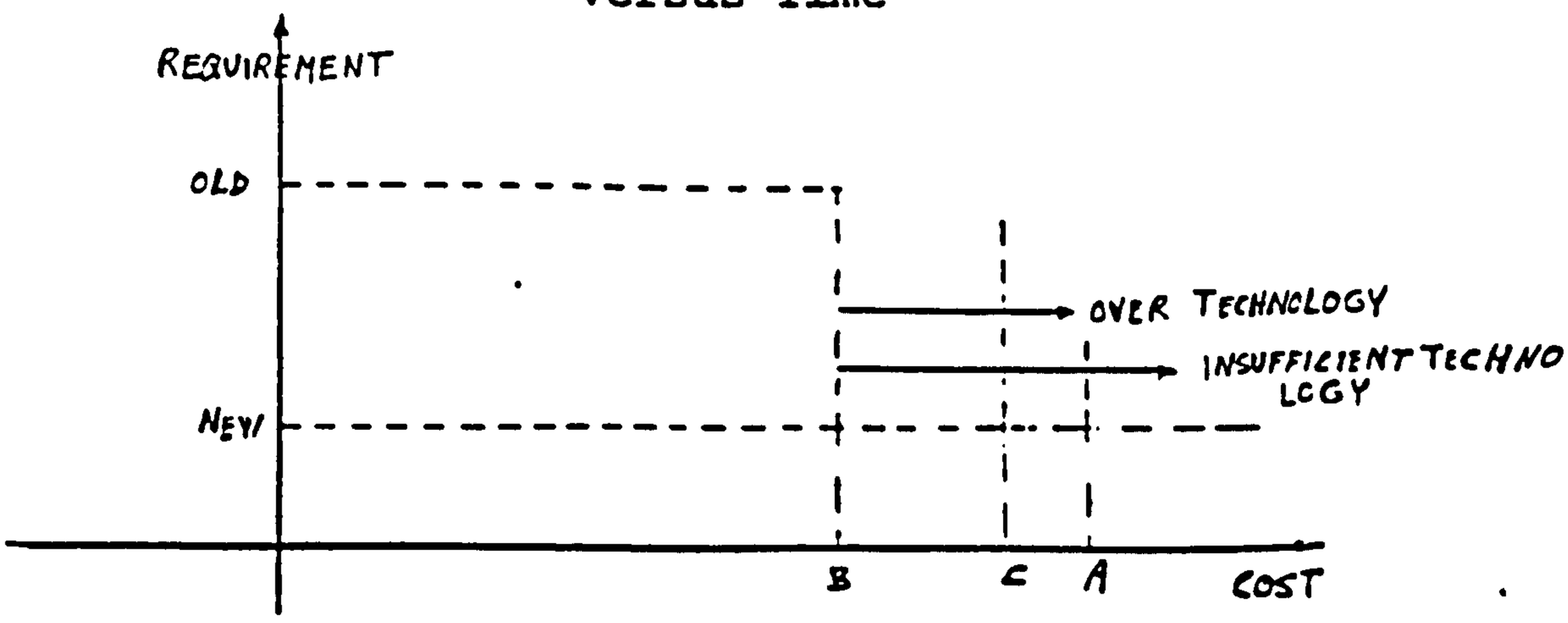

Figure-2.6 Requirement Versus Cost

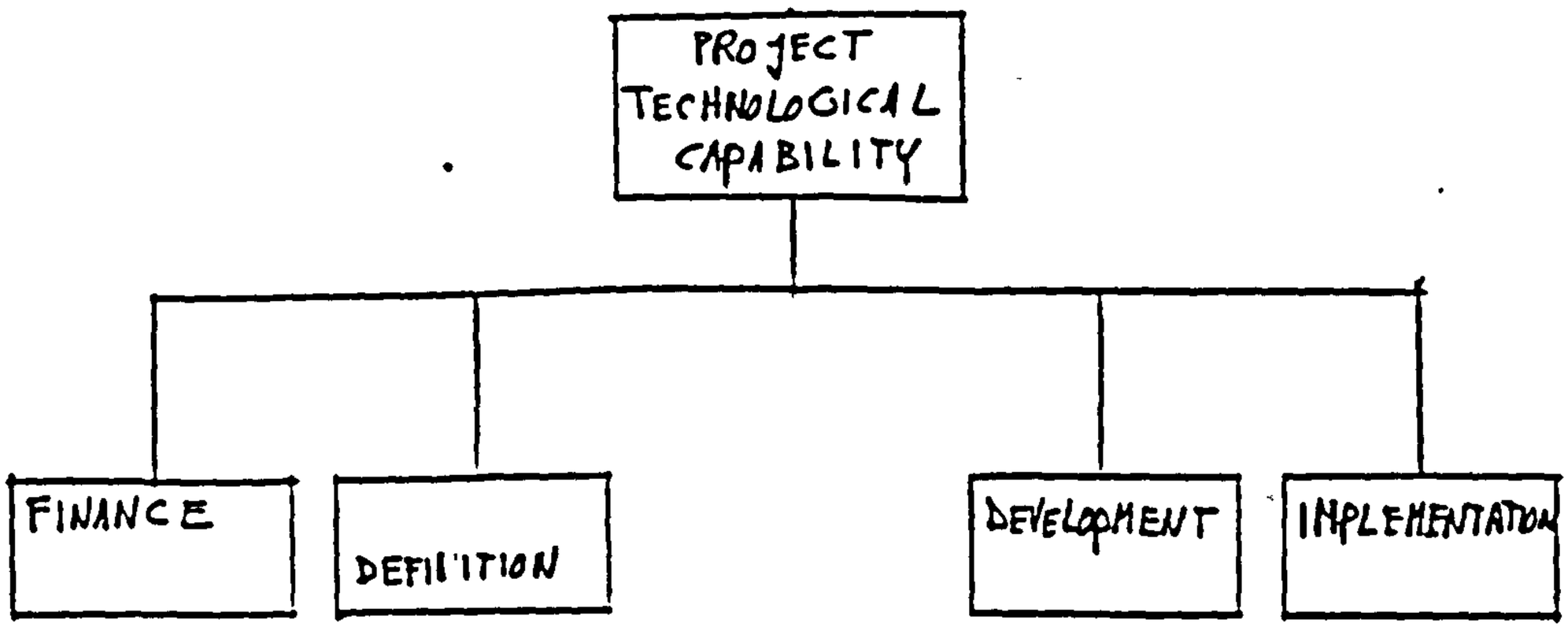

Figure-2.7 Organization

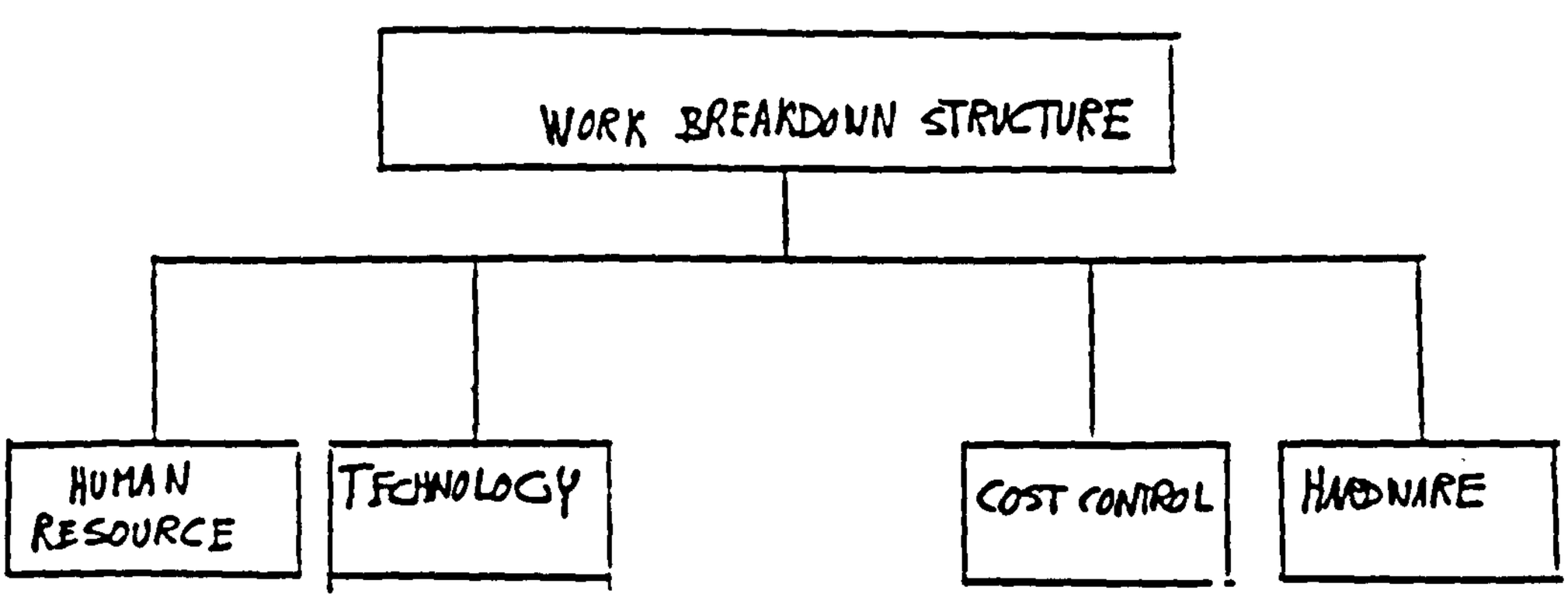

Figure-2.8 Work Breakdown Structure

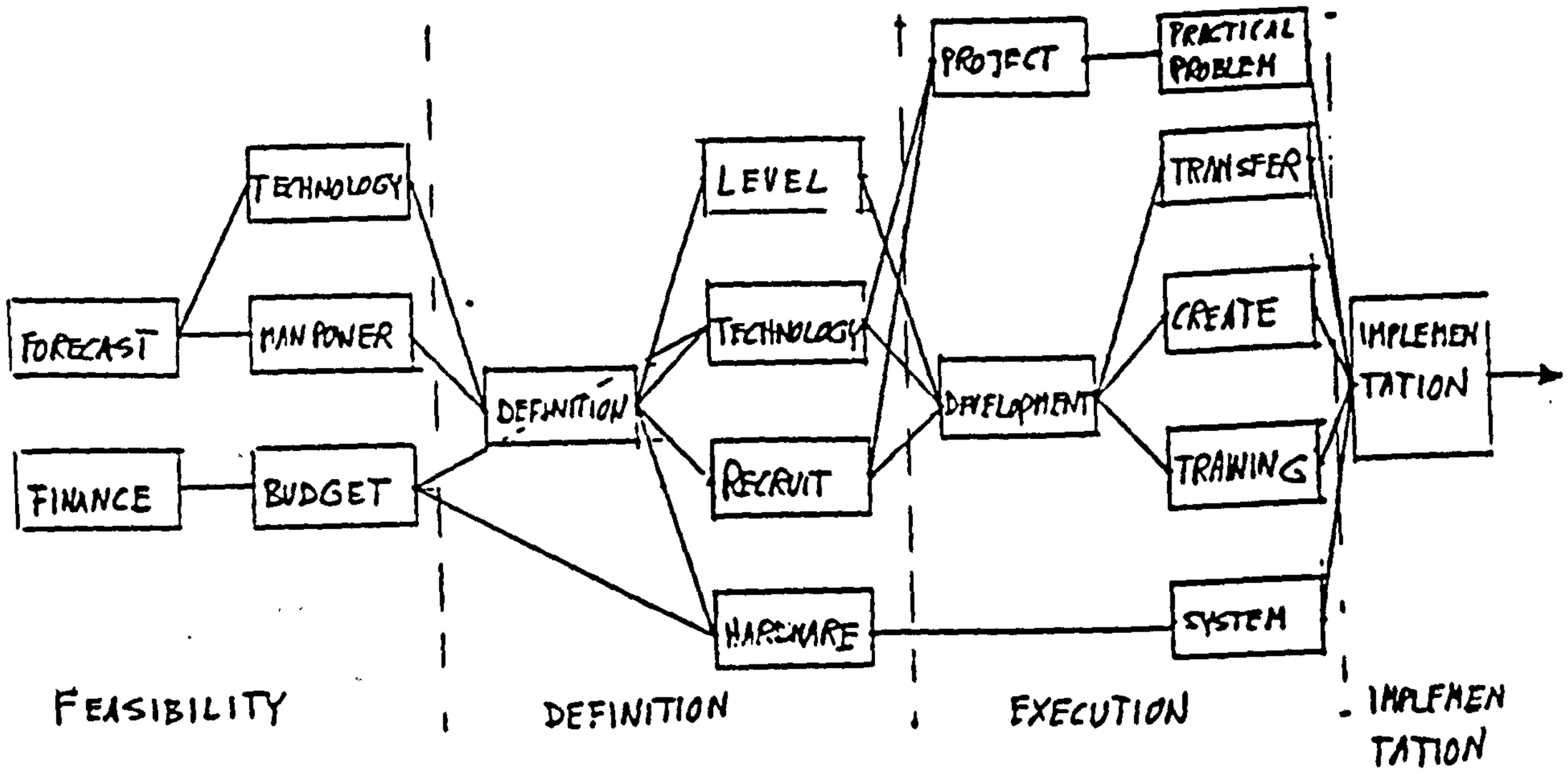

Figure-2.9 Execution Logic

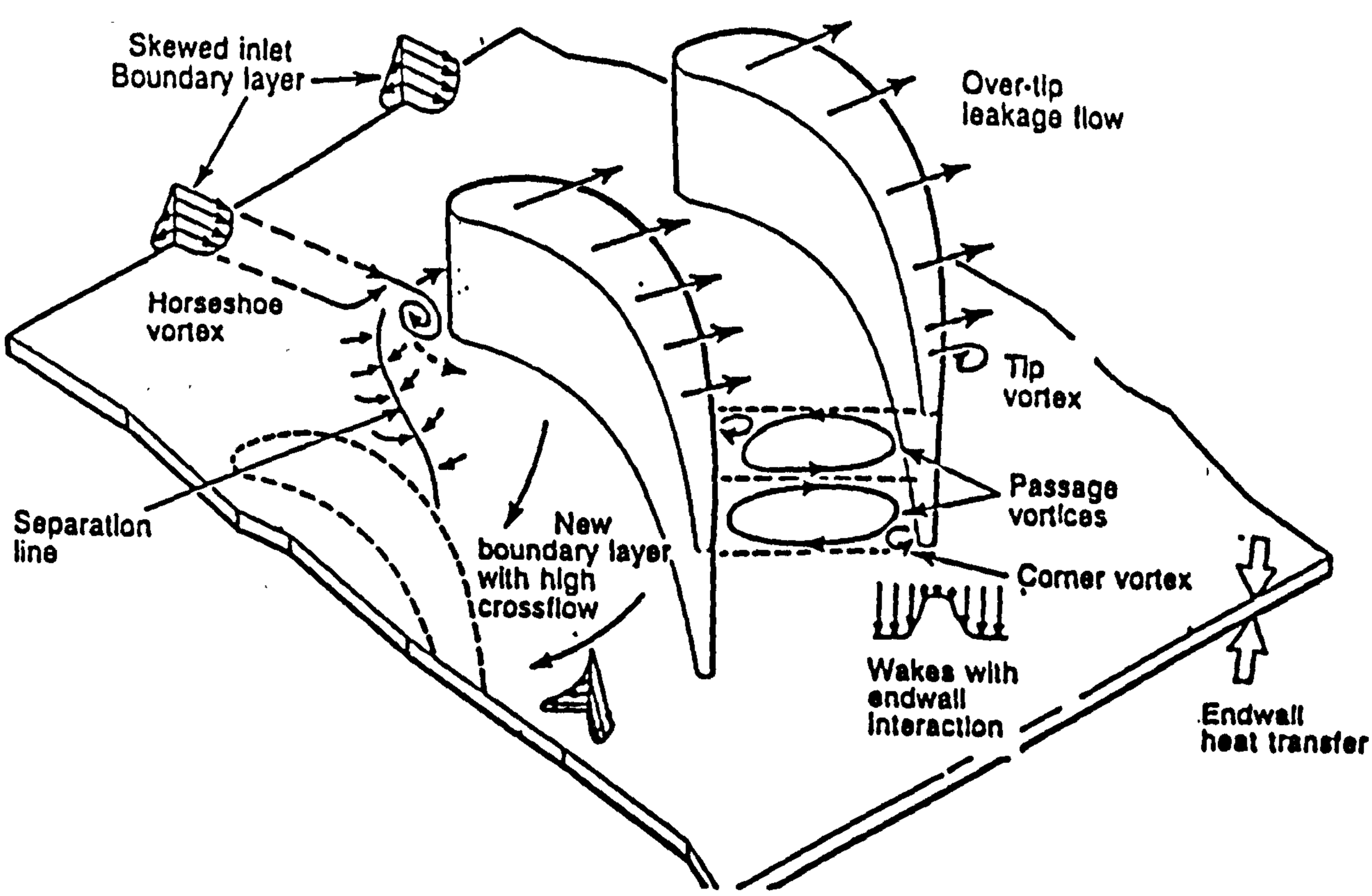

Figure-2.10 Internal Flow of an Aero Engine

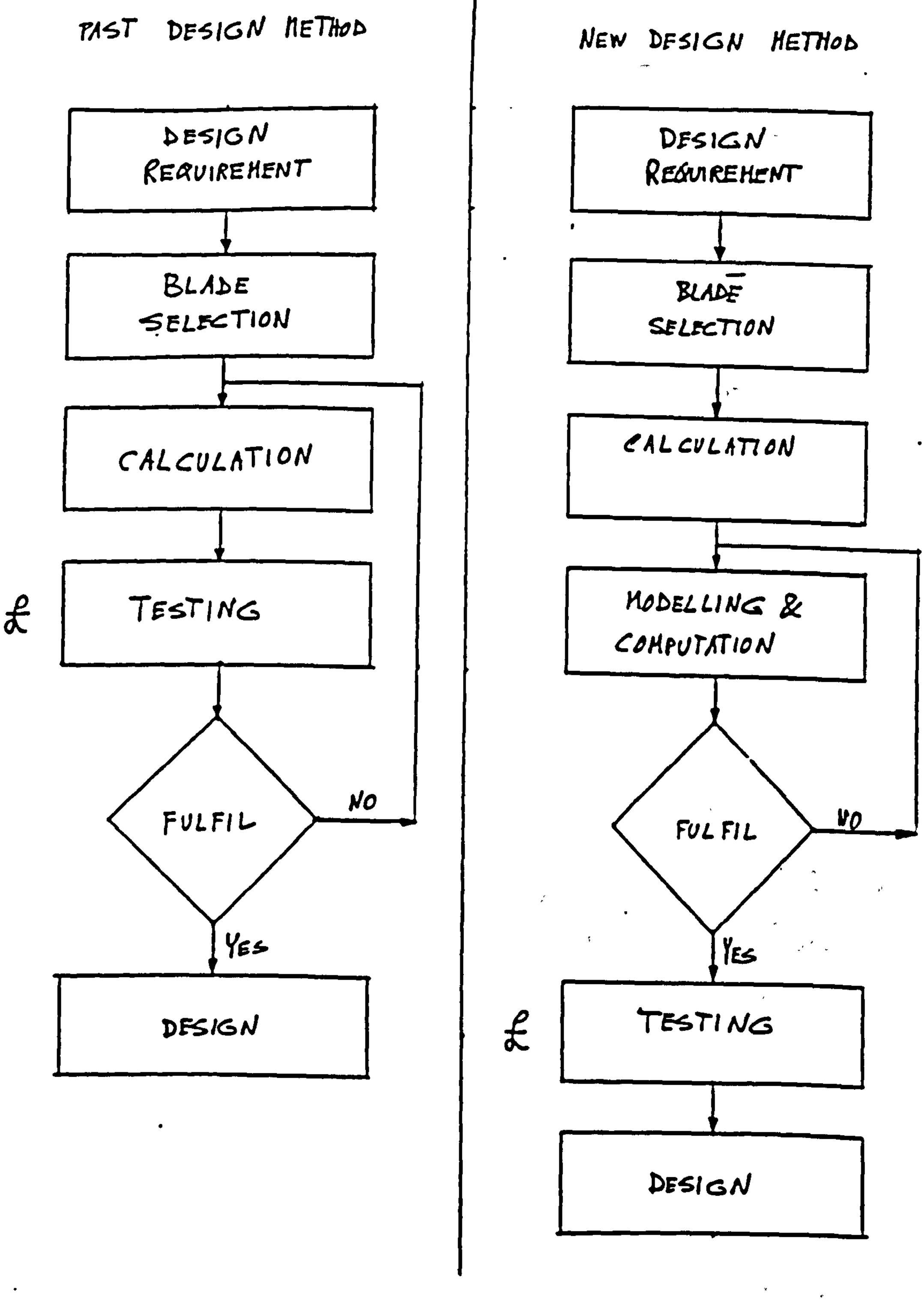

Figure-2.1! Design Methods

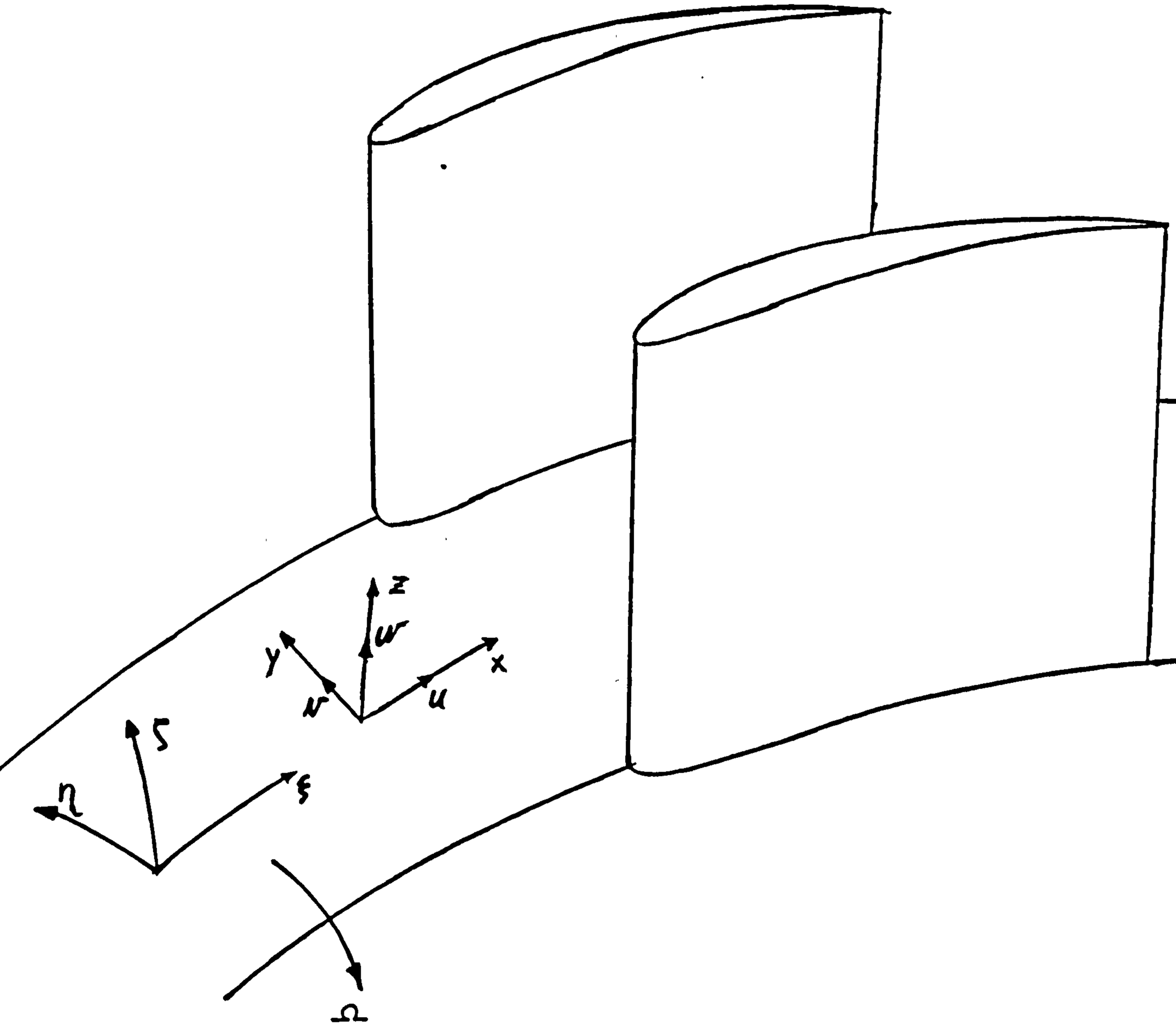

Figure-3.1 Coordinate Systems

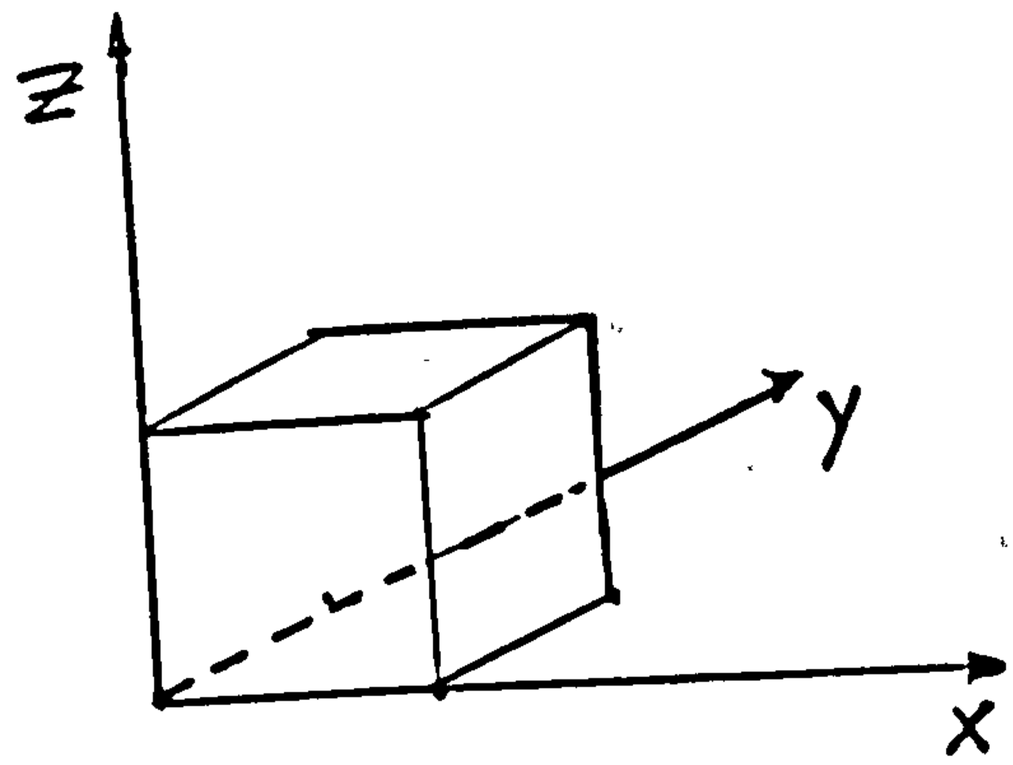

Figure-3.2a Cartesian Grid

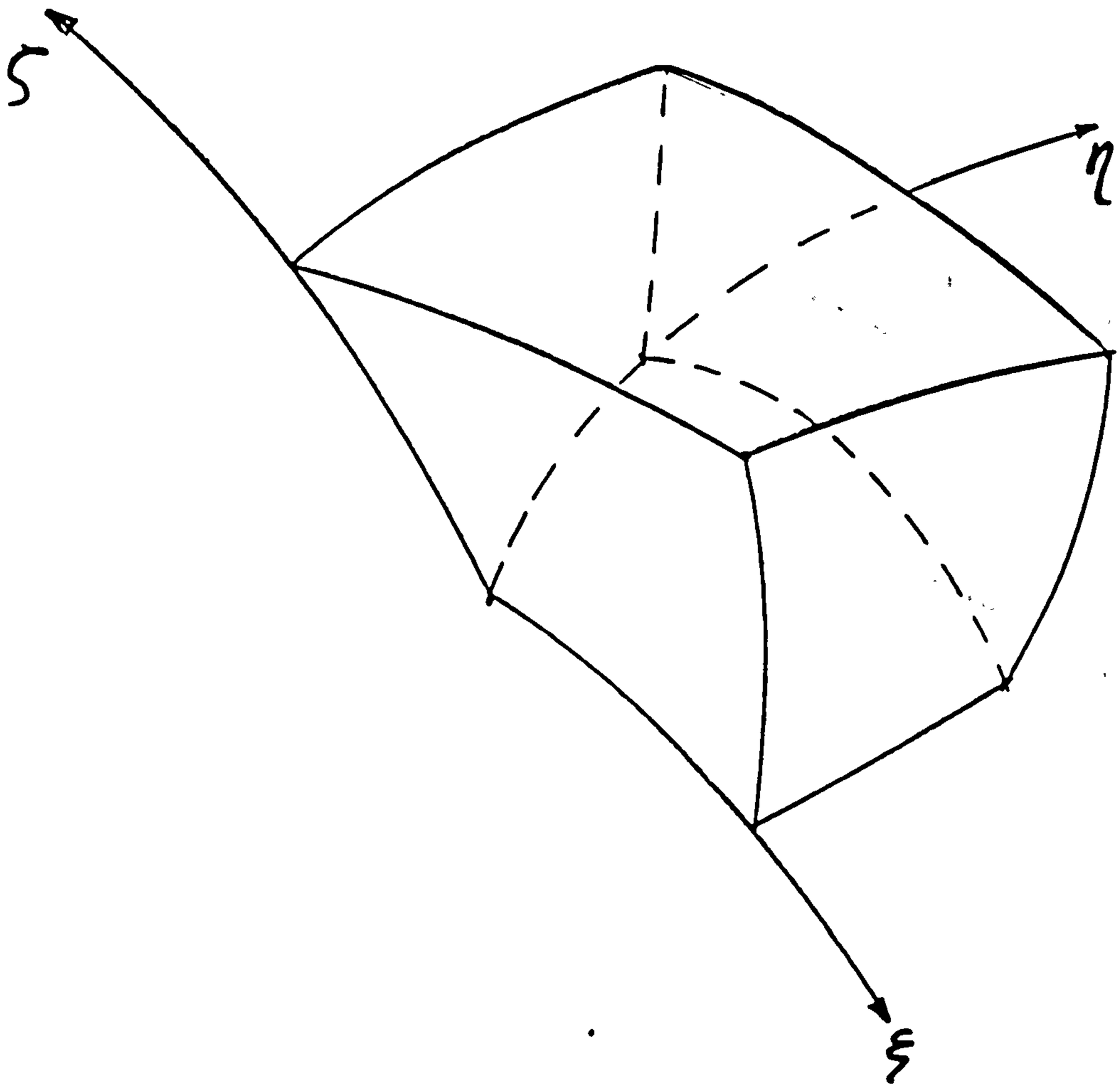

Figure-3.2b Sheared Grid

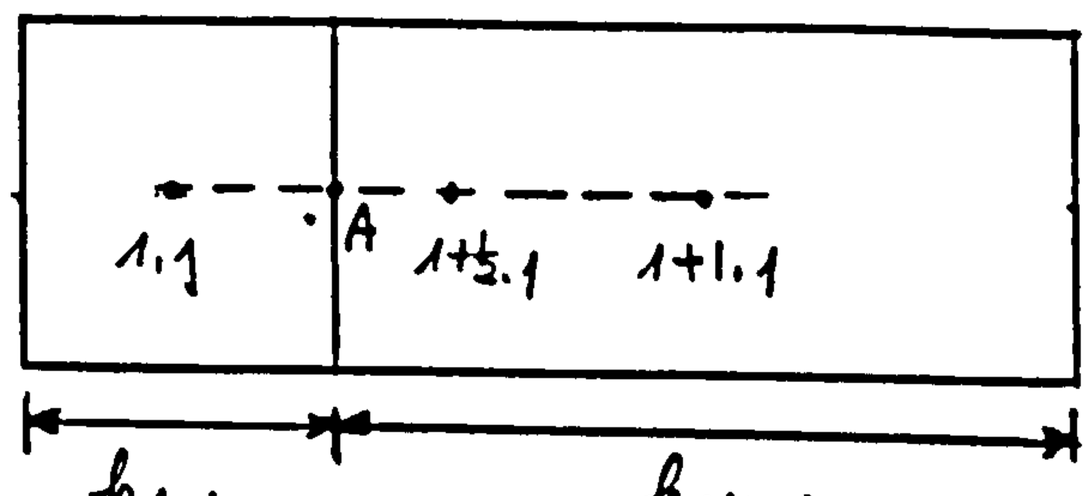

Figure-3.3a Straight Grid

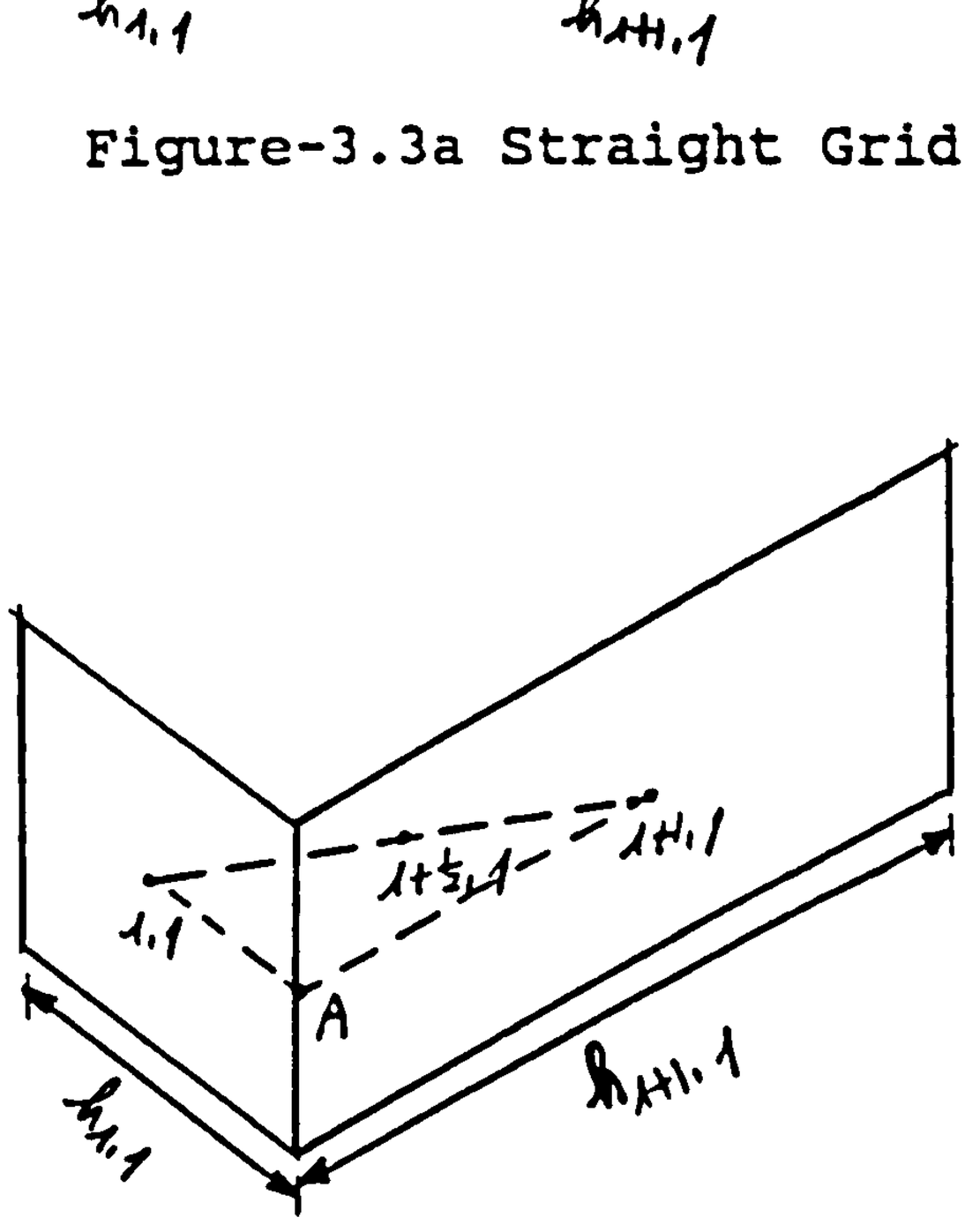

Figure-3.3b Skewed Grid

i+1/2,j is at mid point between (i+1,j) and (i,j)
A is at cell face centre

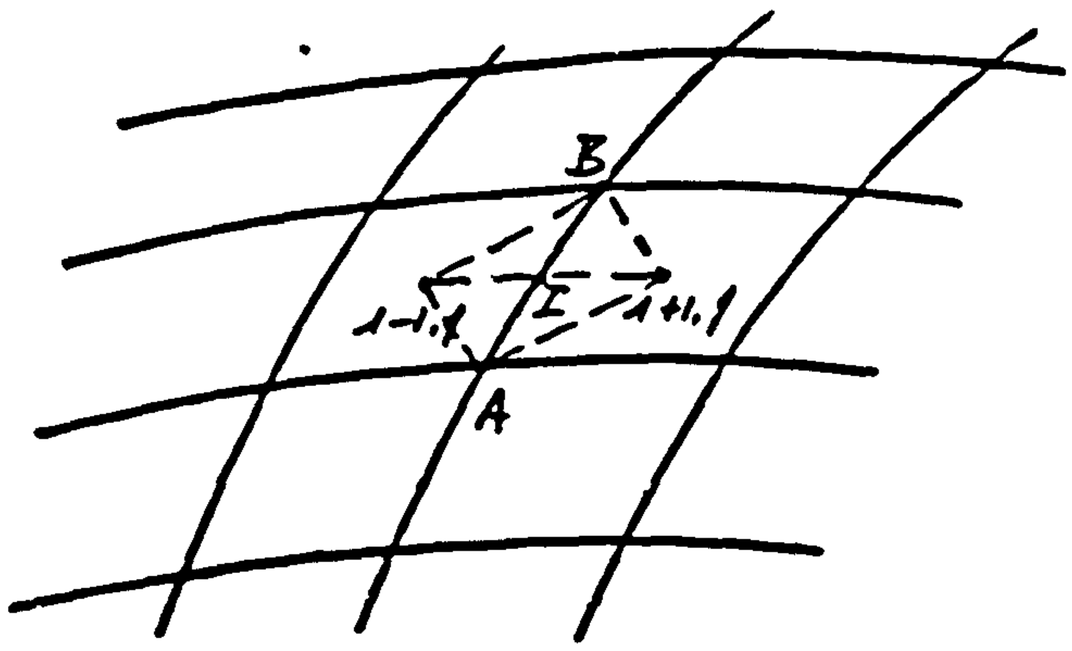

Figure-4.1a Martinelli Scheme with First Method

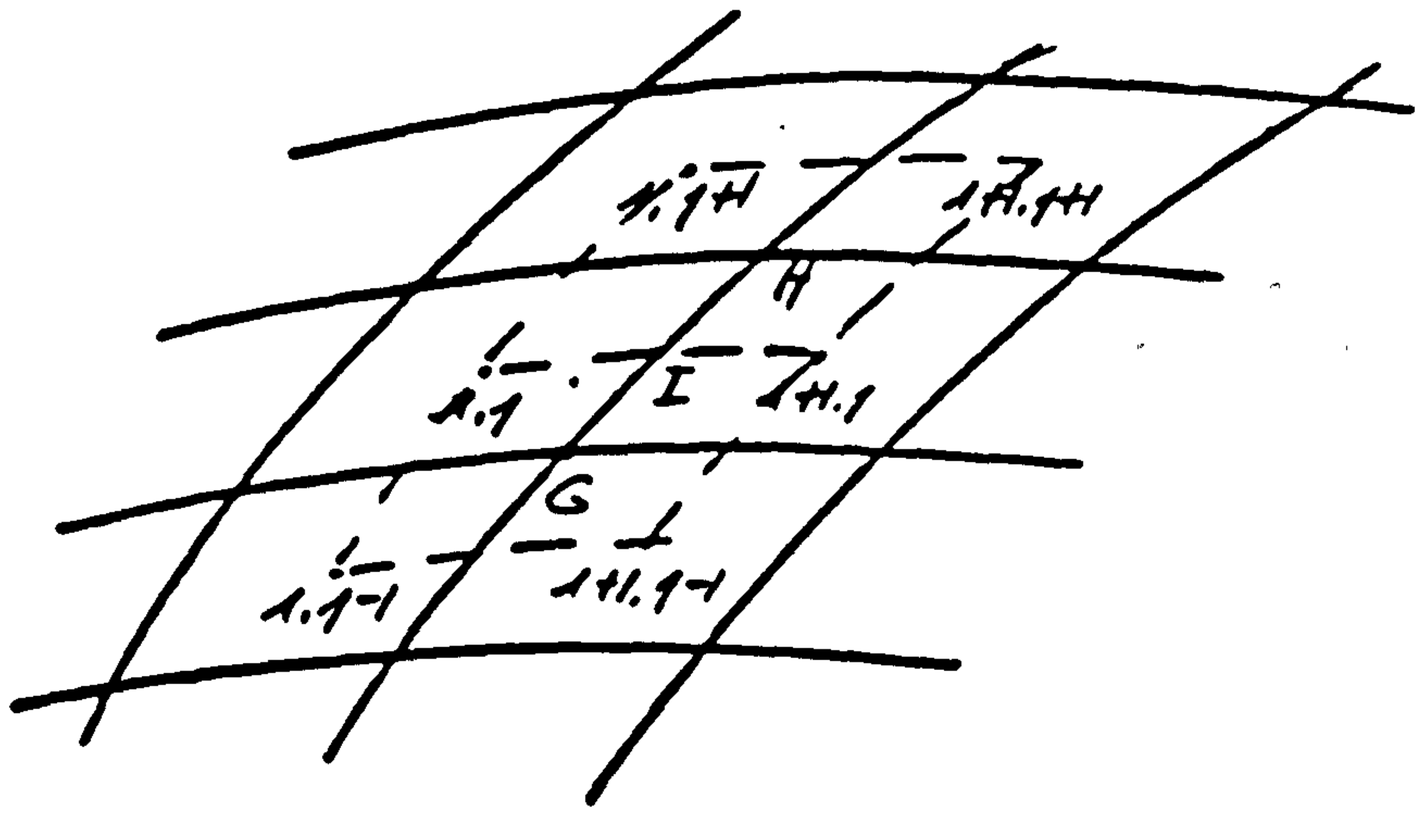

Figure-4.1b Martinelli Scheme with Second Method

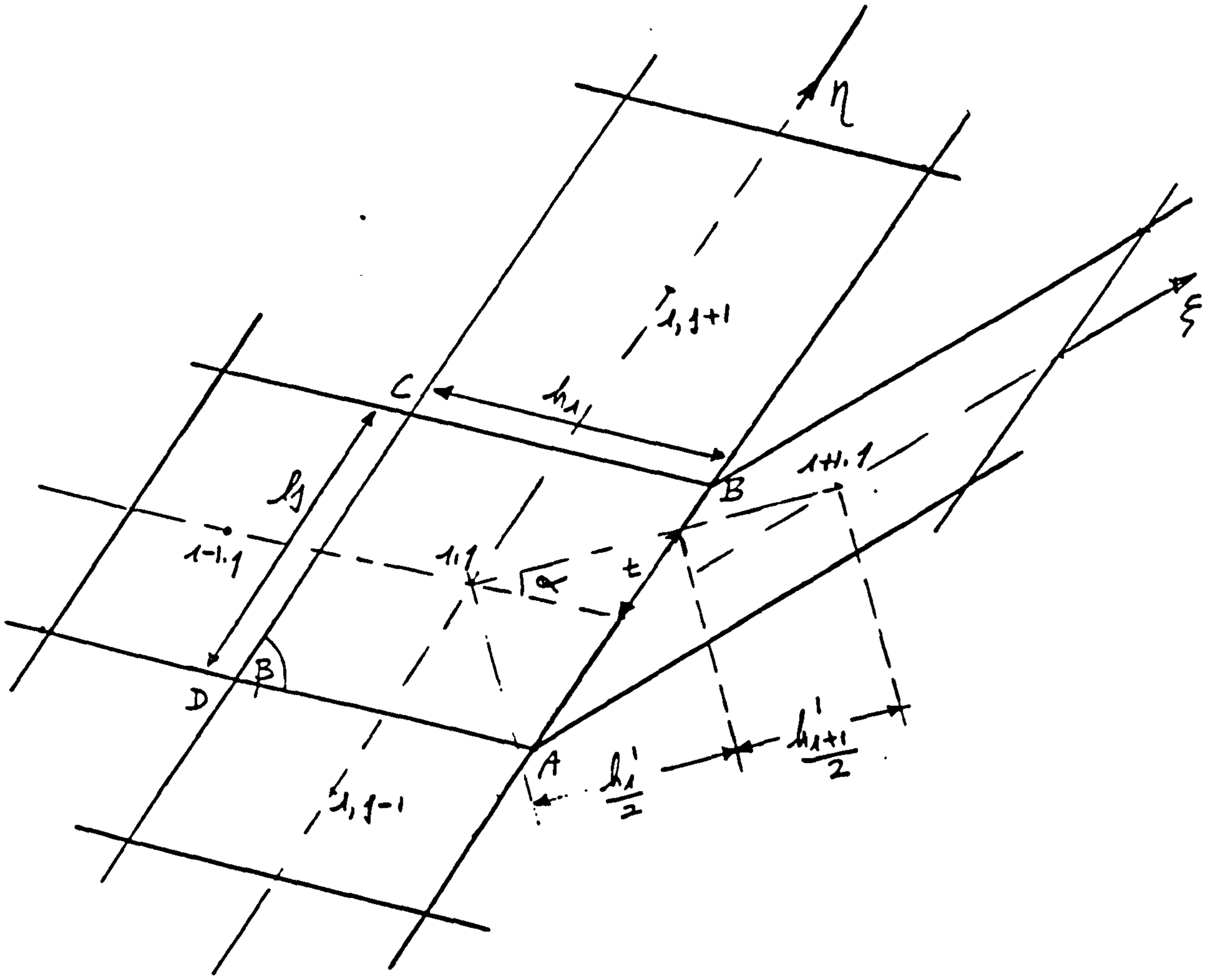

Figure-4.2 Sheared Skewed Stretched Grid

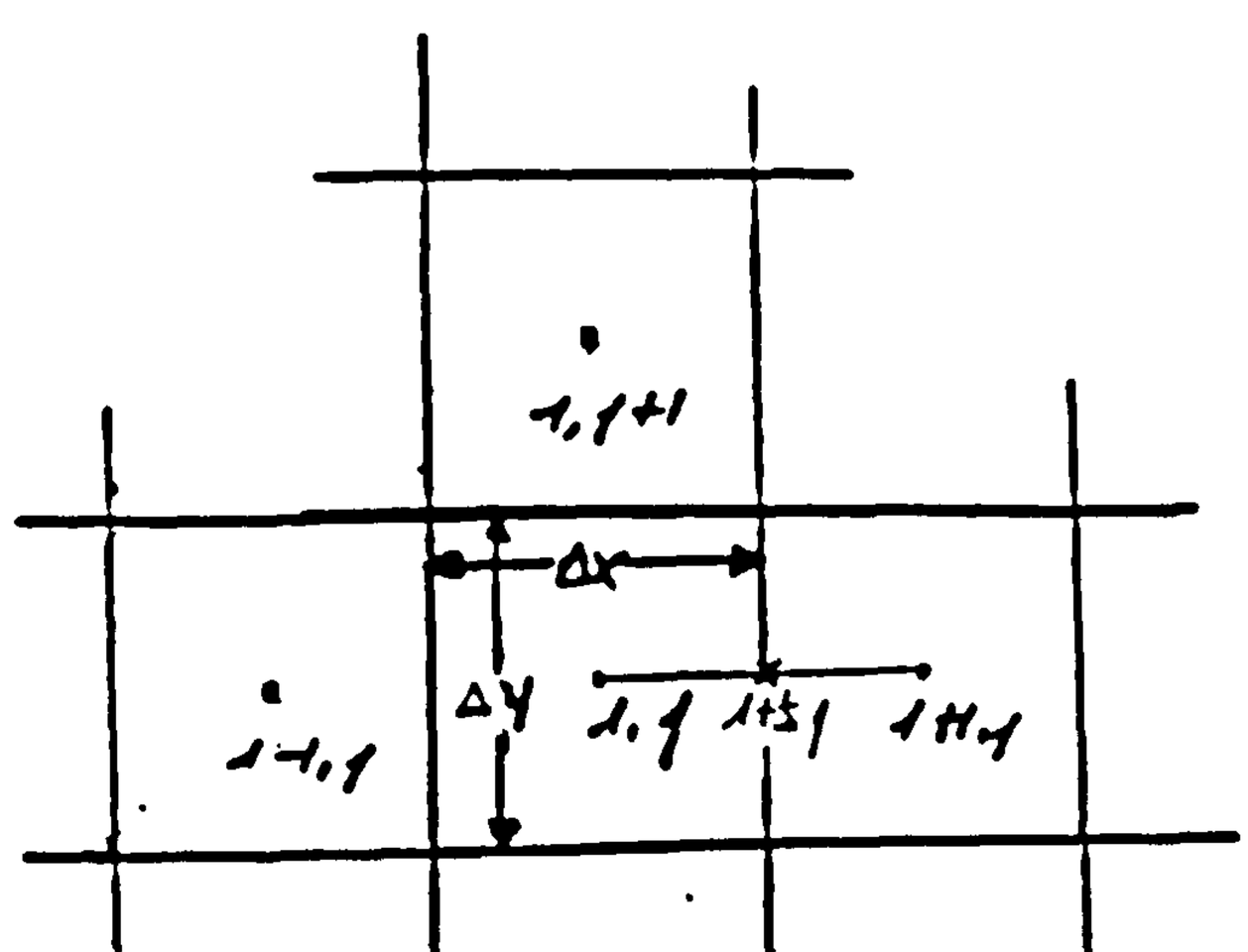

$\Delta x = \Delta y$

Figure-4.3 Cartesian Grid

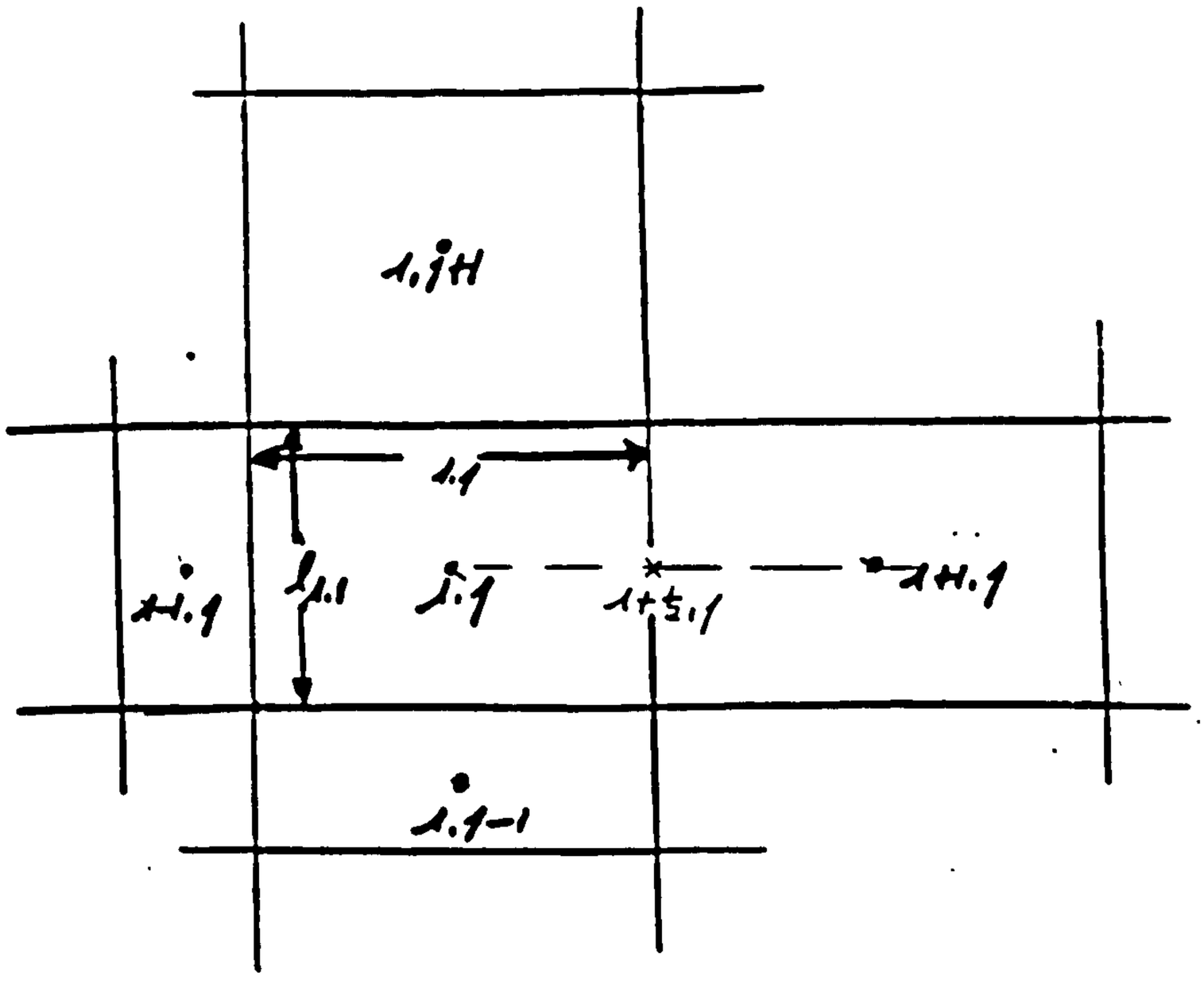

Figure-4.4 Straight Stretched Grid

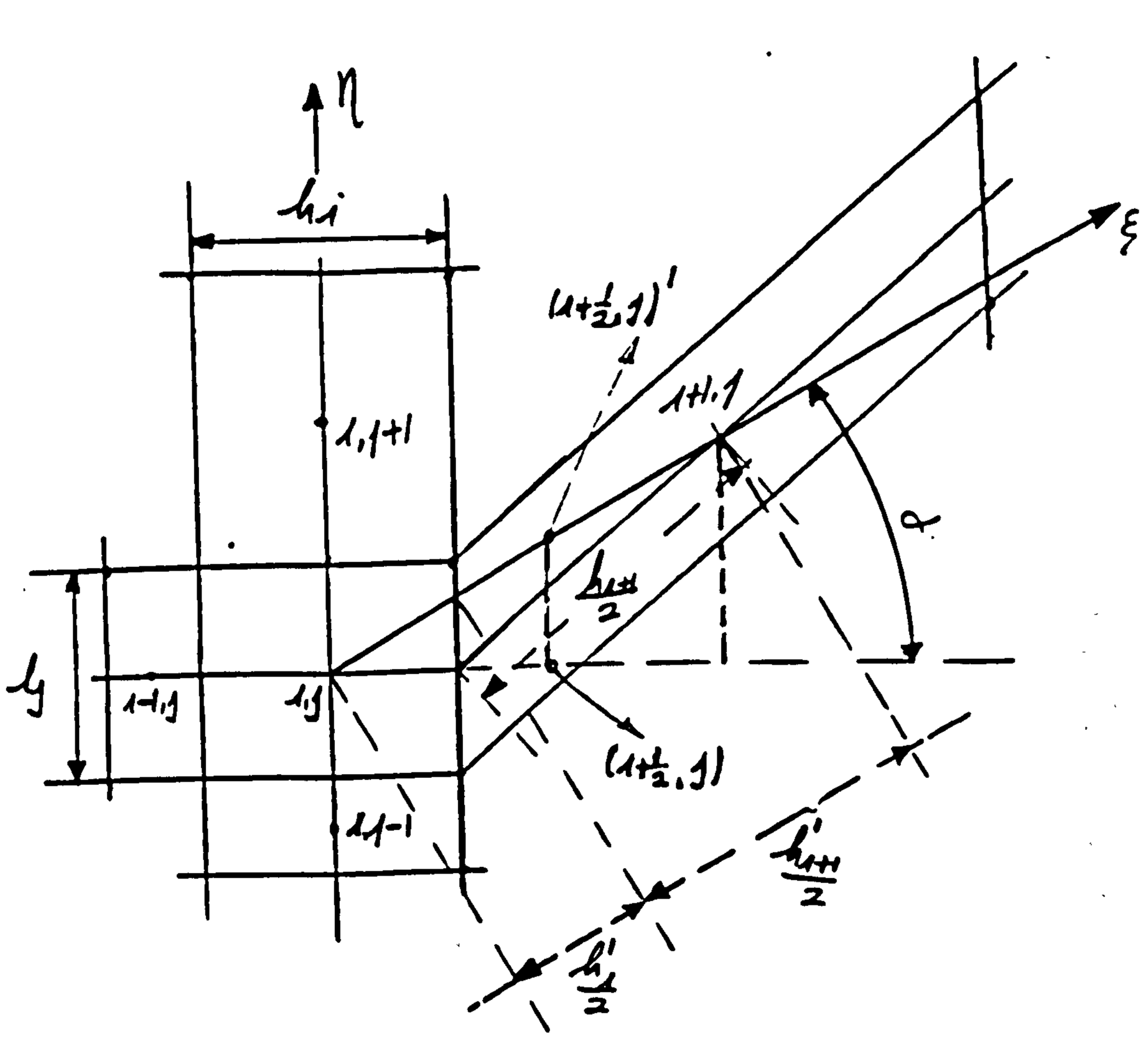

Figure-4.5 Straight Averaging

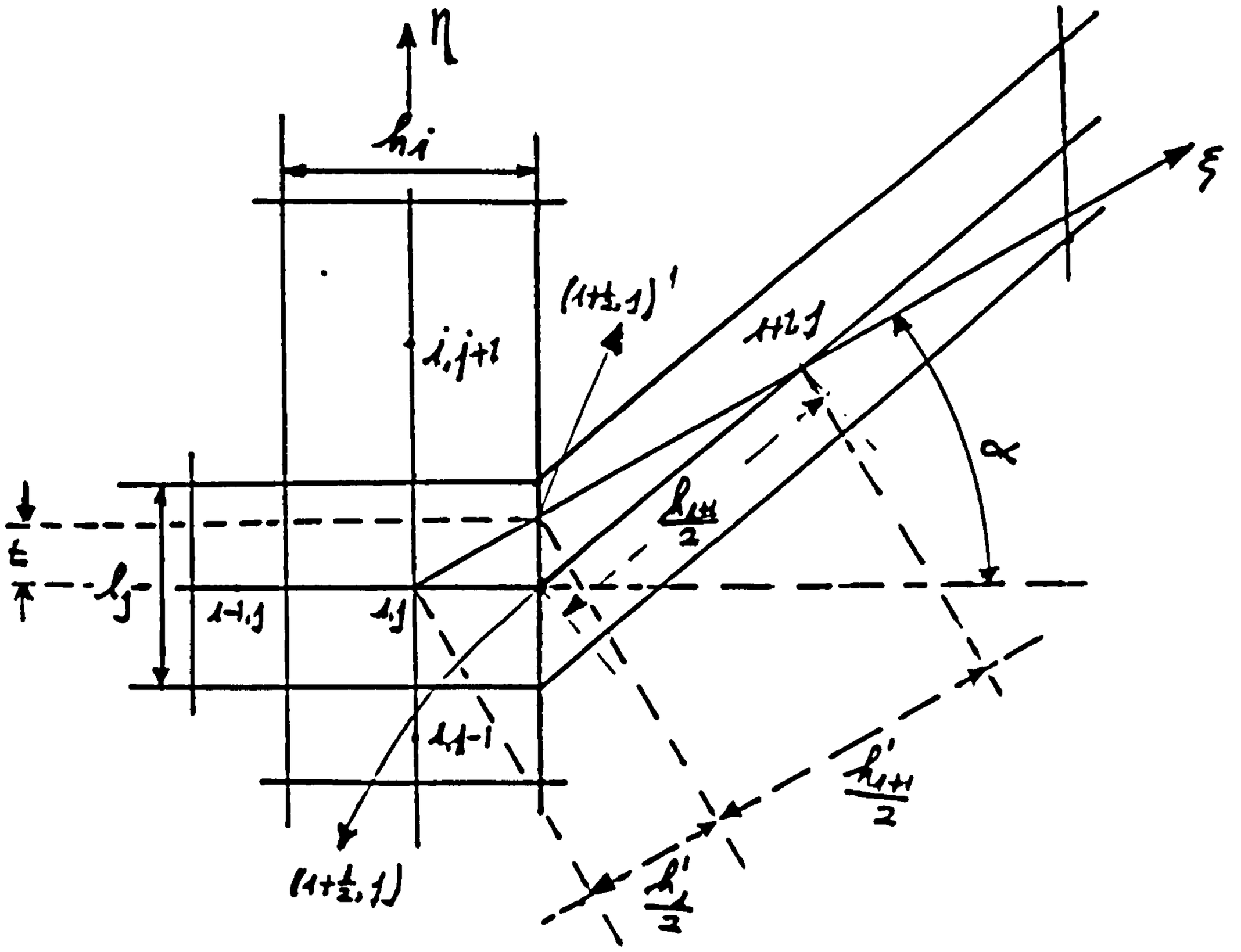

Figure-4.6 Linear Interpolation

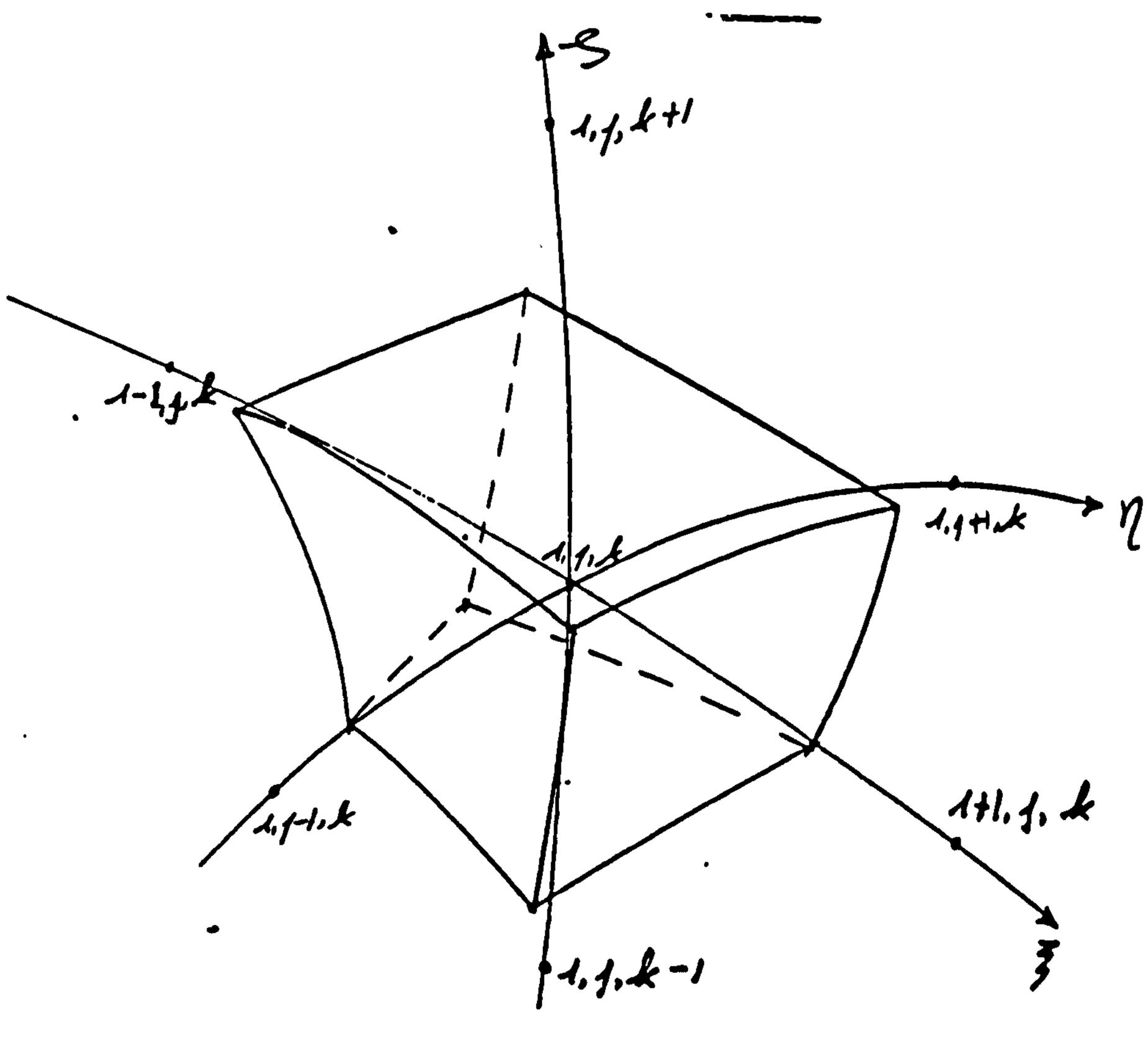

Figure-4.7a Quadratic Interpolation

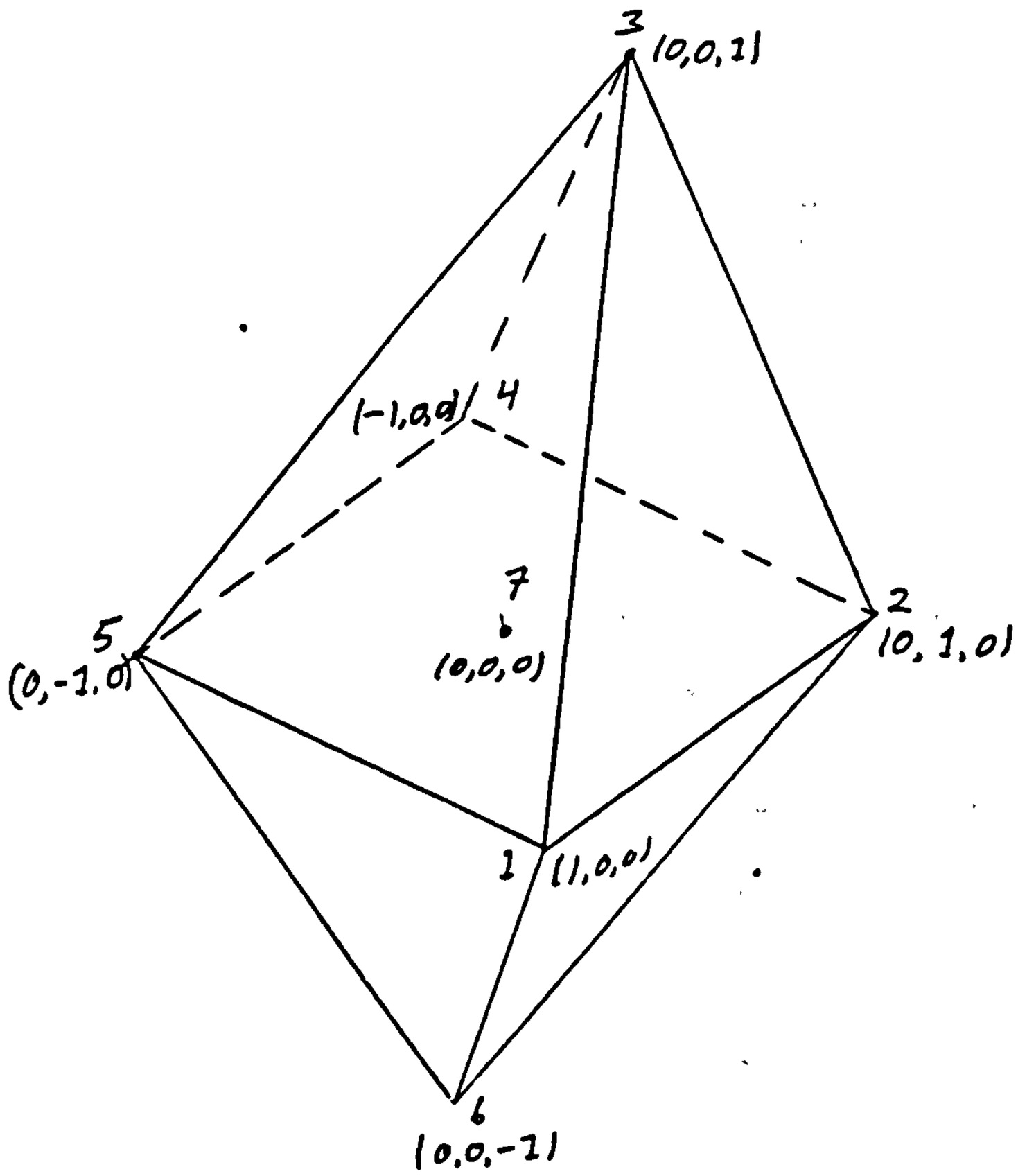

Figure-4.7b Diamond Configuration

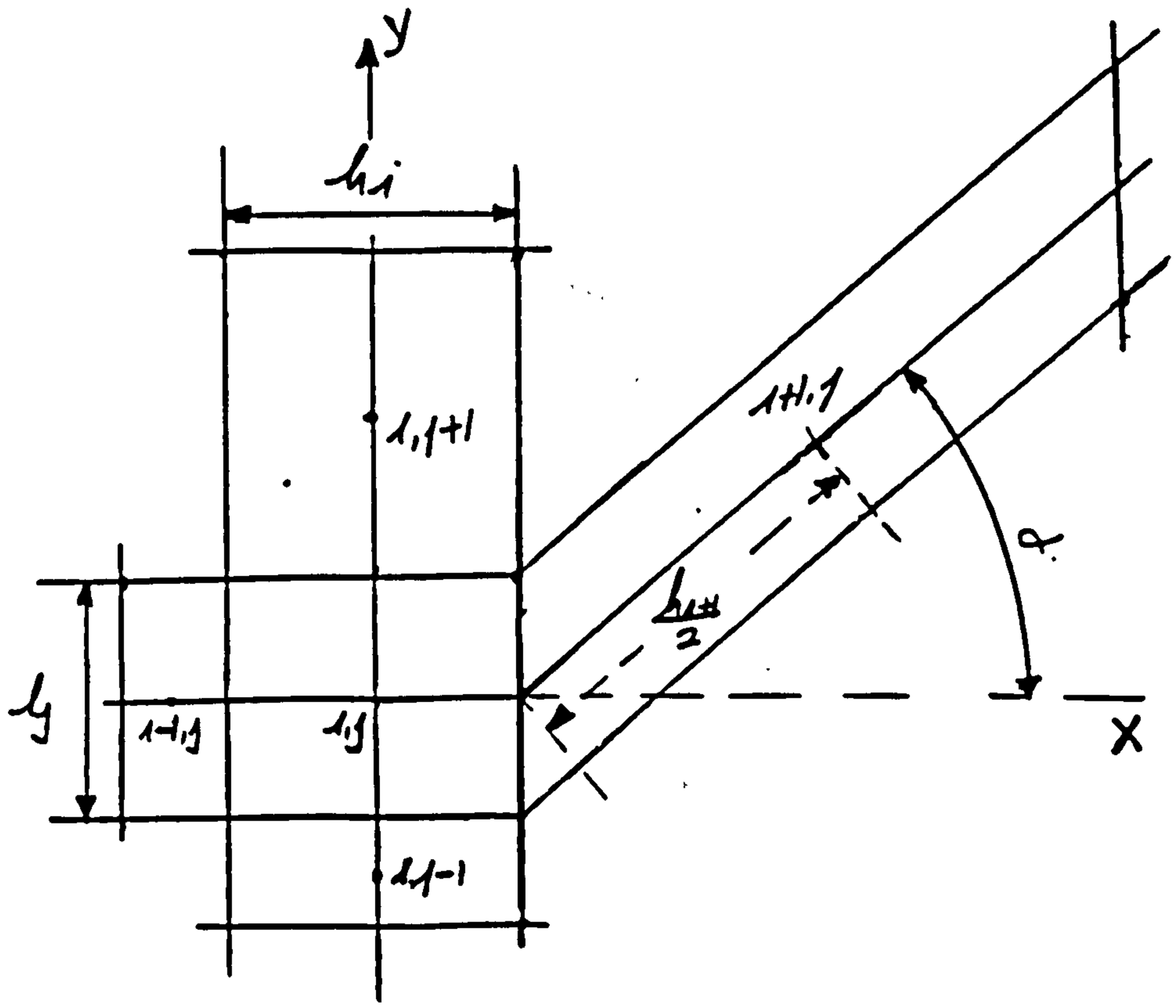

Figure-4.8 Coupled Quadratic Interpolation

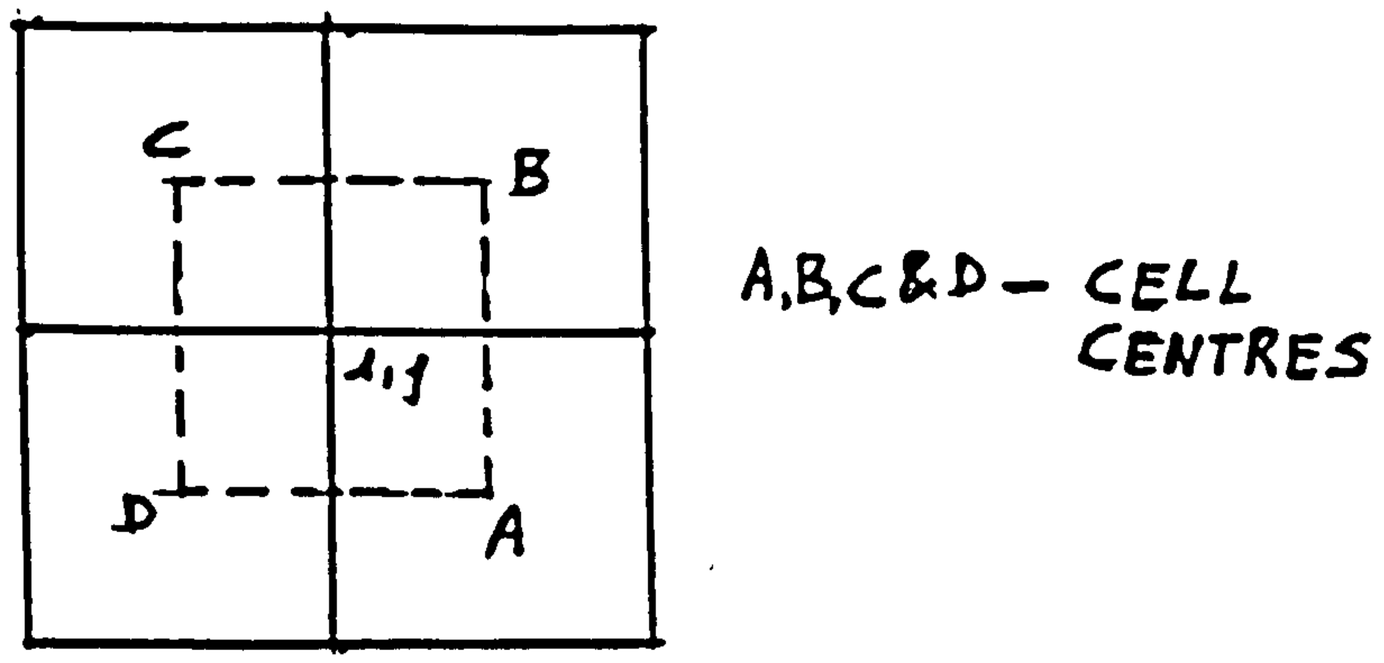

Figure-4.9 Two Dimensional Supercell

Figure-4.10 One Dimensional Cell Vertex

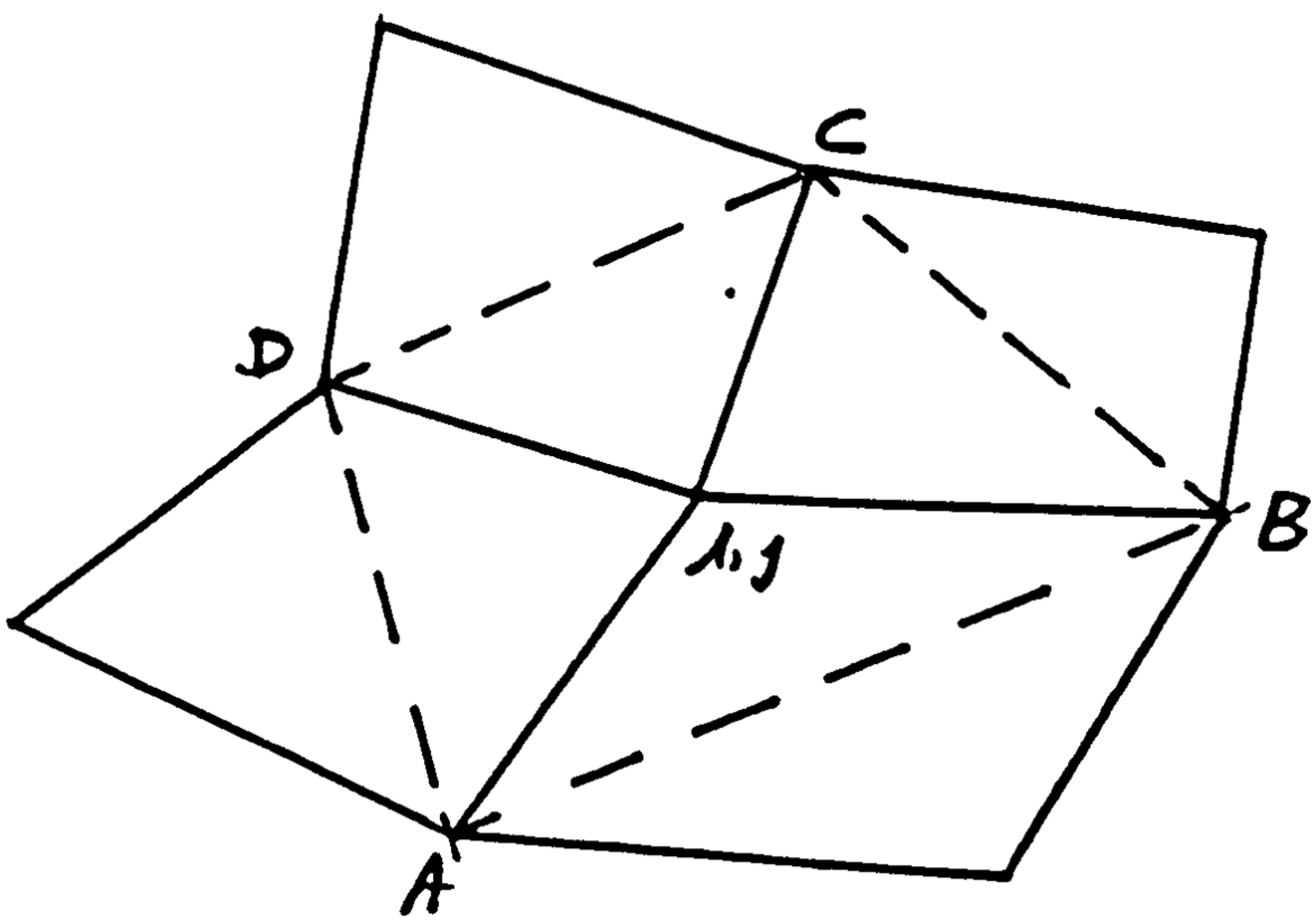

Figure-4.11 Two Dimensional Cell Vertex

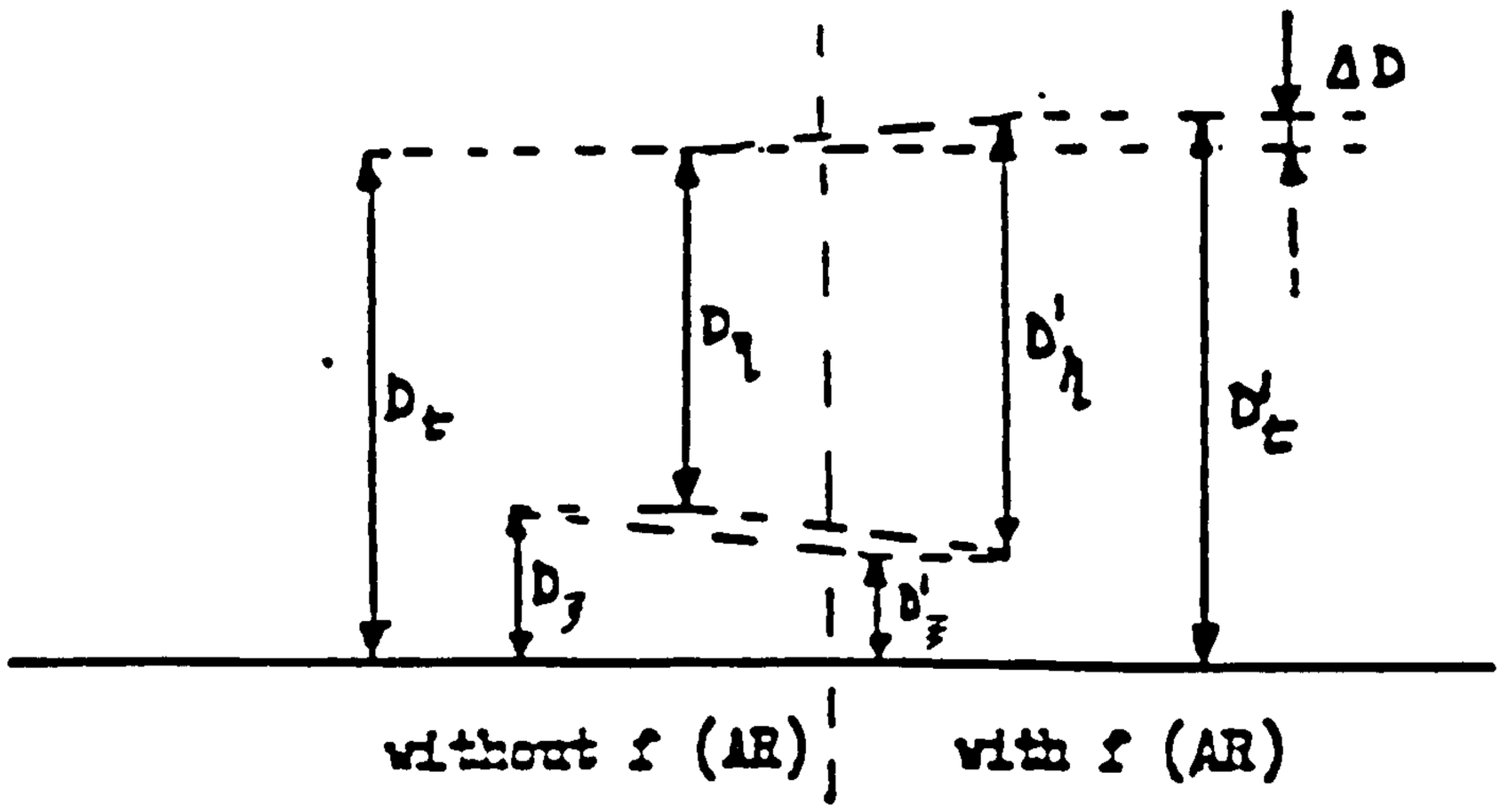

Figure-5.1a Graphical representation of the effect of Martinelli Aspect Ratio Function to the total dissipation relative to that from the standard model for a high aspect ratio cell.
f(AR) is Martinelli aspect ratio function (equation (5.2.10))

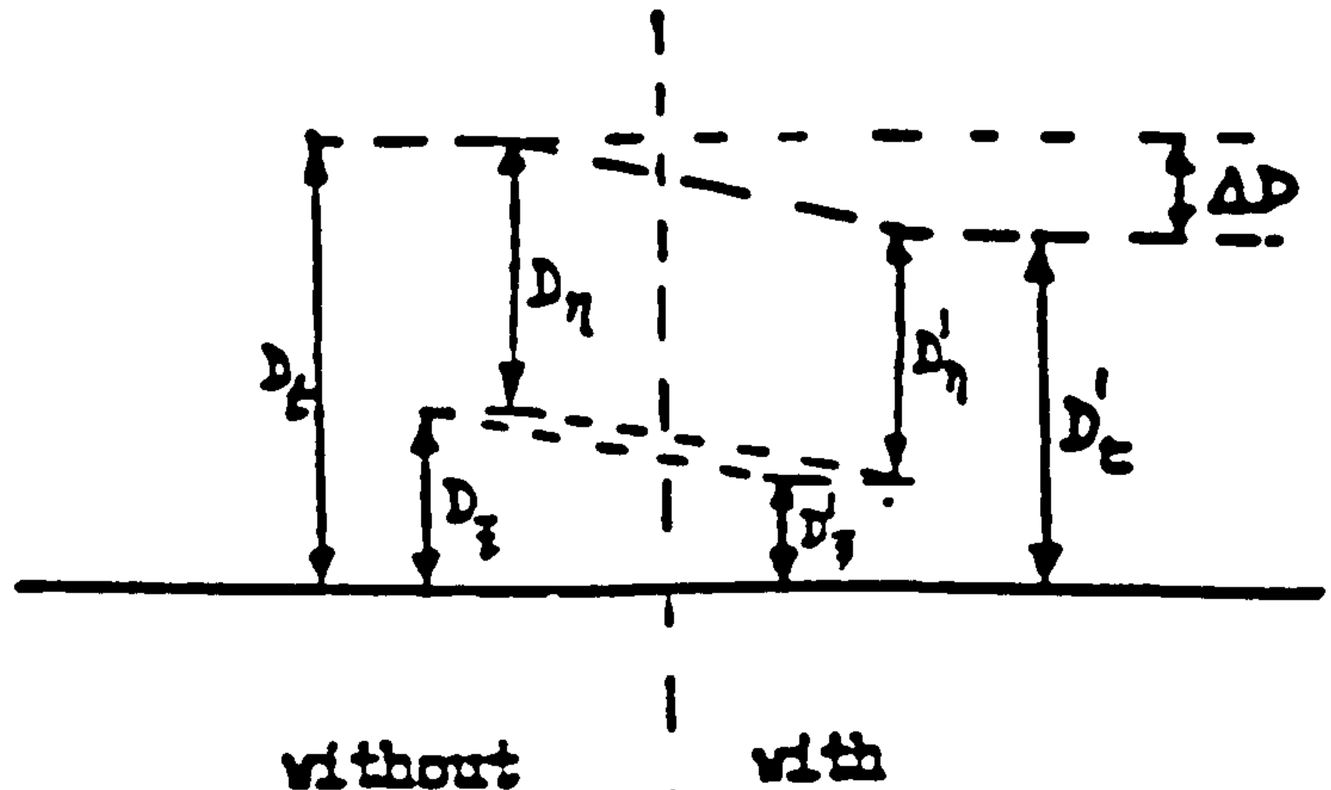

Figure-5.1b Graphical representation of the effect of Kuntz Aspect Ratio Function to the total dissipation relative to that from the standard model for a high aspect ratio cell.
f(AR) is Kuntz aspect ratio function (equation(5.2.11)

Symbols for figure-5.1a and -5.1b
D_t = total standard dissipation
D_ξ^t = ξ - direction standard dissipation (length)
D'_η = η - direction standard dissipation (width)
D'_t = total modified dissipation
D'^t_ξ = ξ - direction modified dissipation
D'_η = η - direction modified dissipation
ΔD = change in dissipation

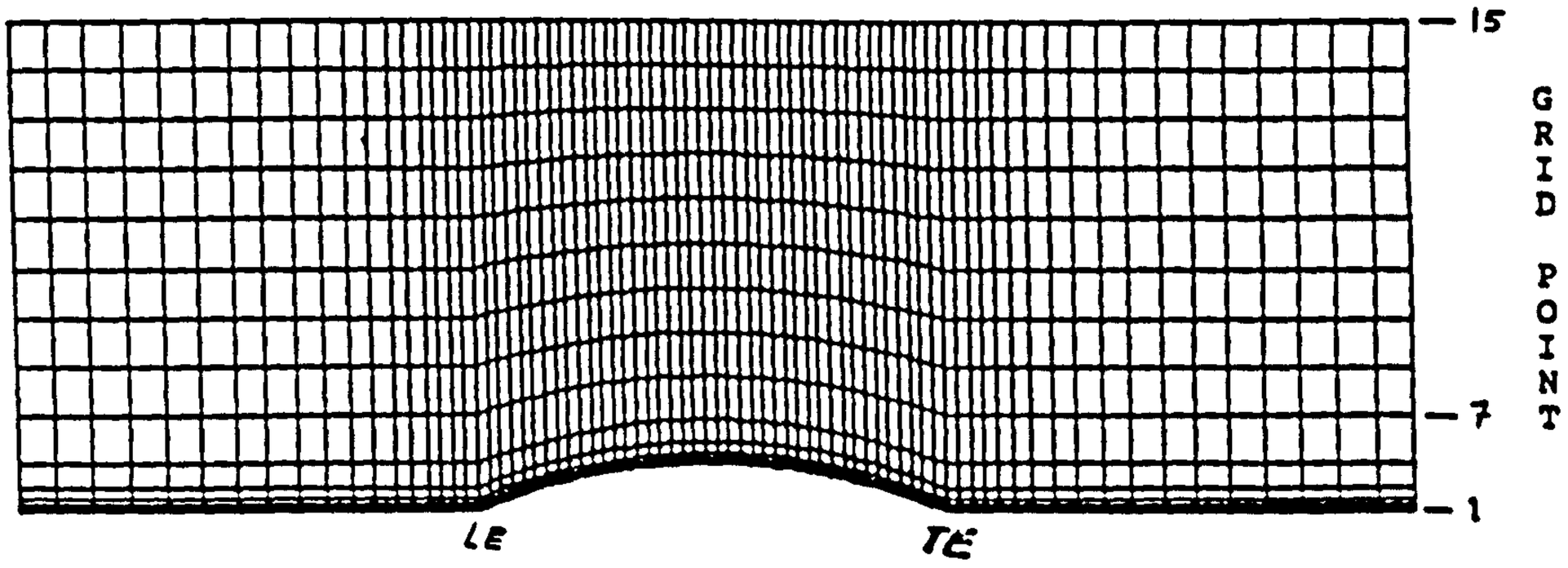

Figure-5.2 Ni's Bump Grid

LE = Leading Edge
TE = Trailing Edge

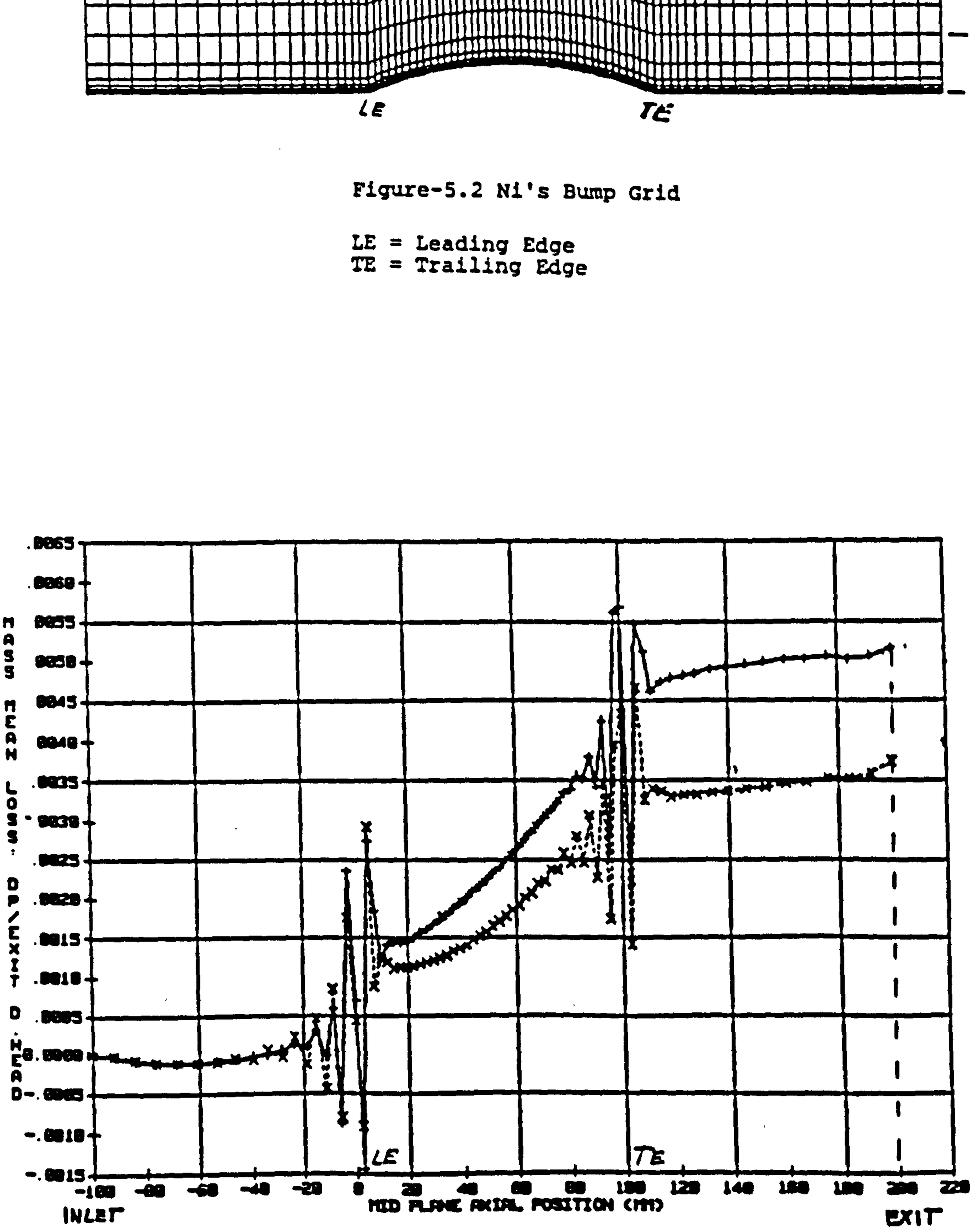

Figure-5.3 Total Pressure loss
Subsonic case

-+--+- No modification
-x--x- Aspect ratio function

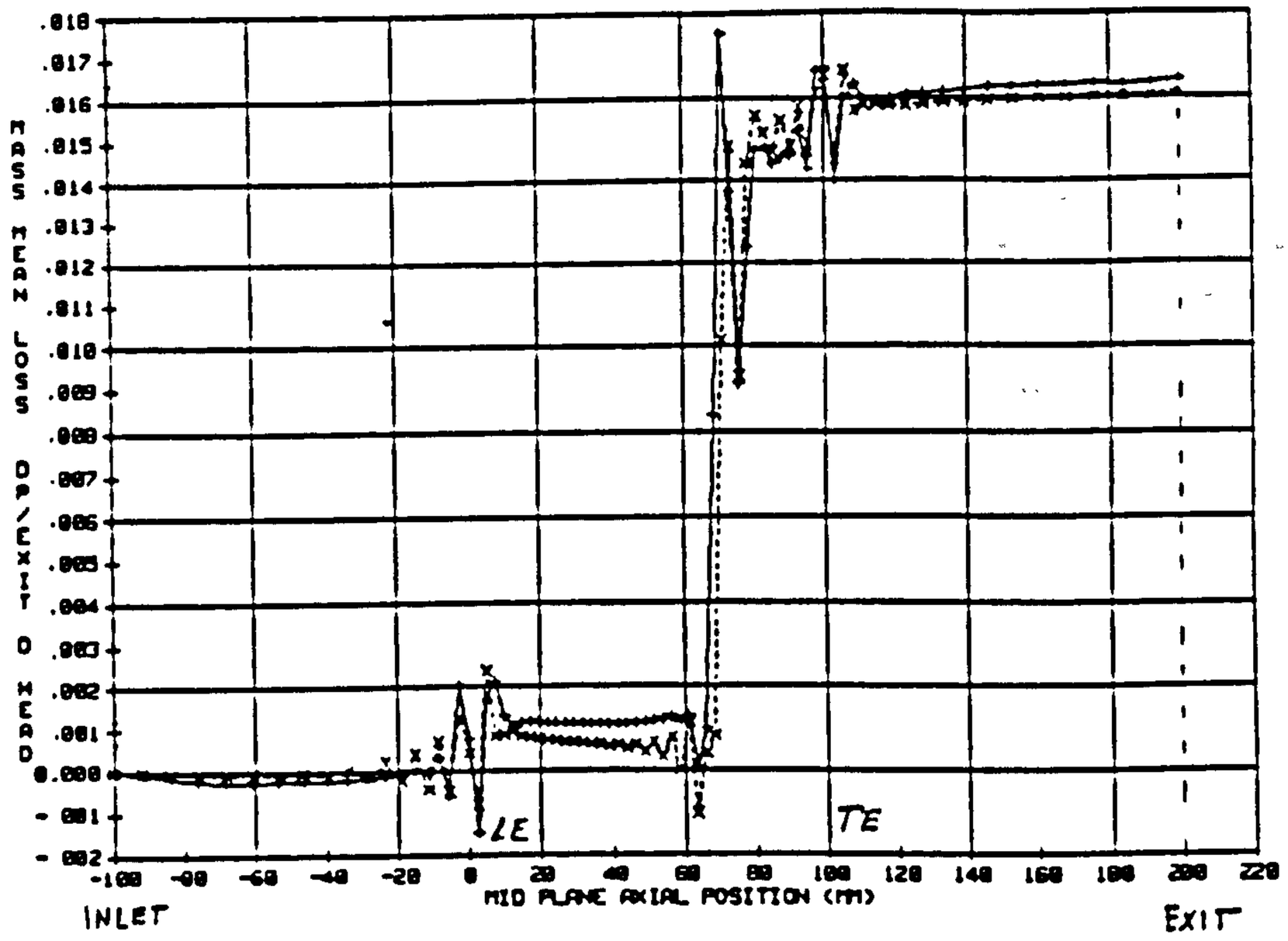

Figure-5.4 Total Pressure loss
Transonic case

-+--+- No modification
-x--x- Aspect ratio function

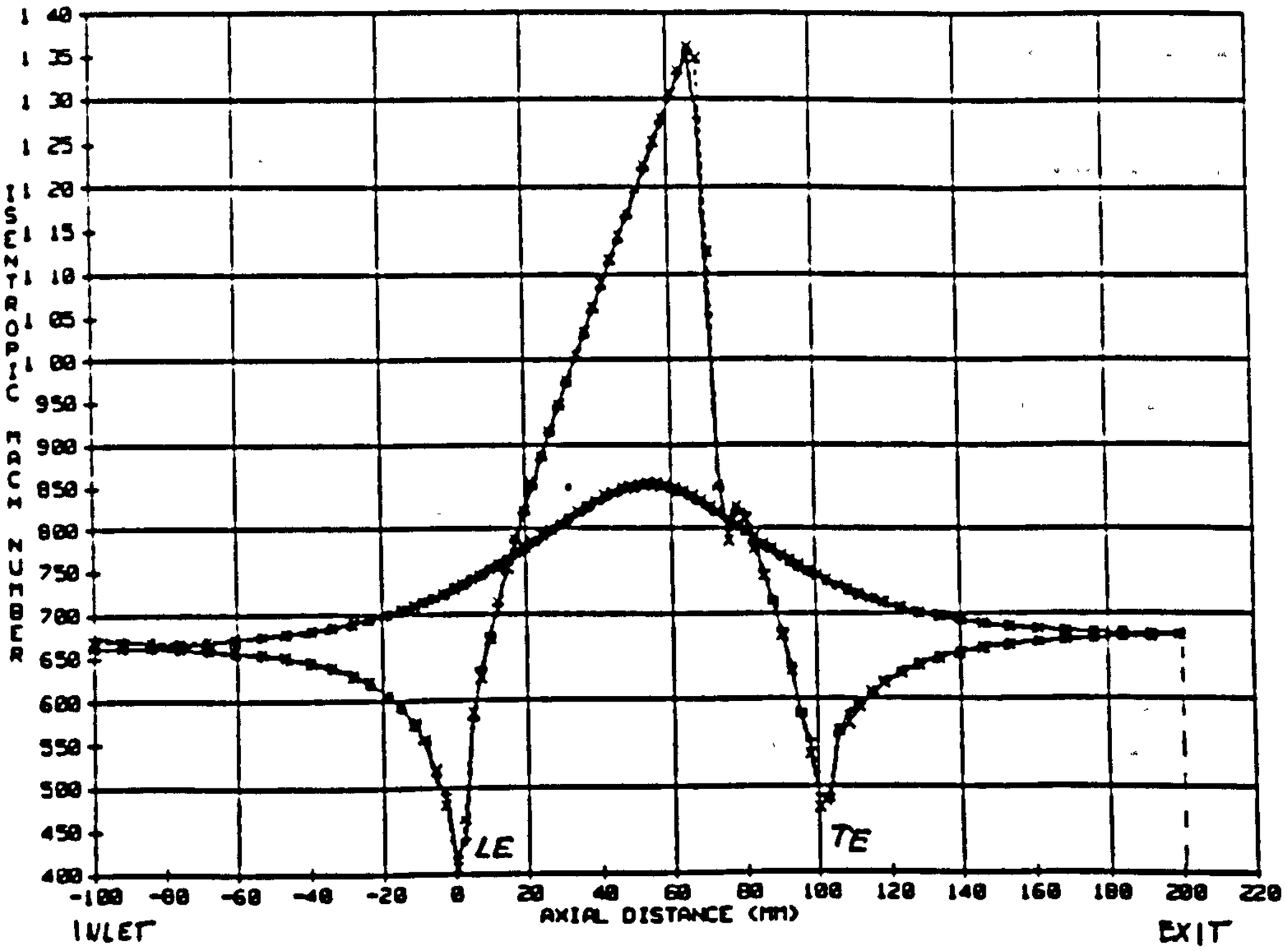

Figure-5.5 Isentropic Mach Number
for Transonic Case

-+--+- No modification
-x--x- Aspect ratio function

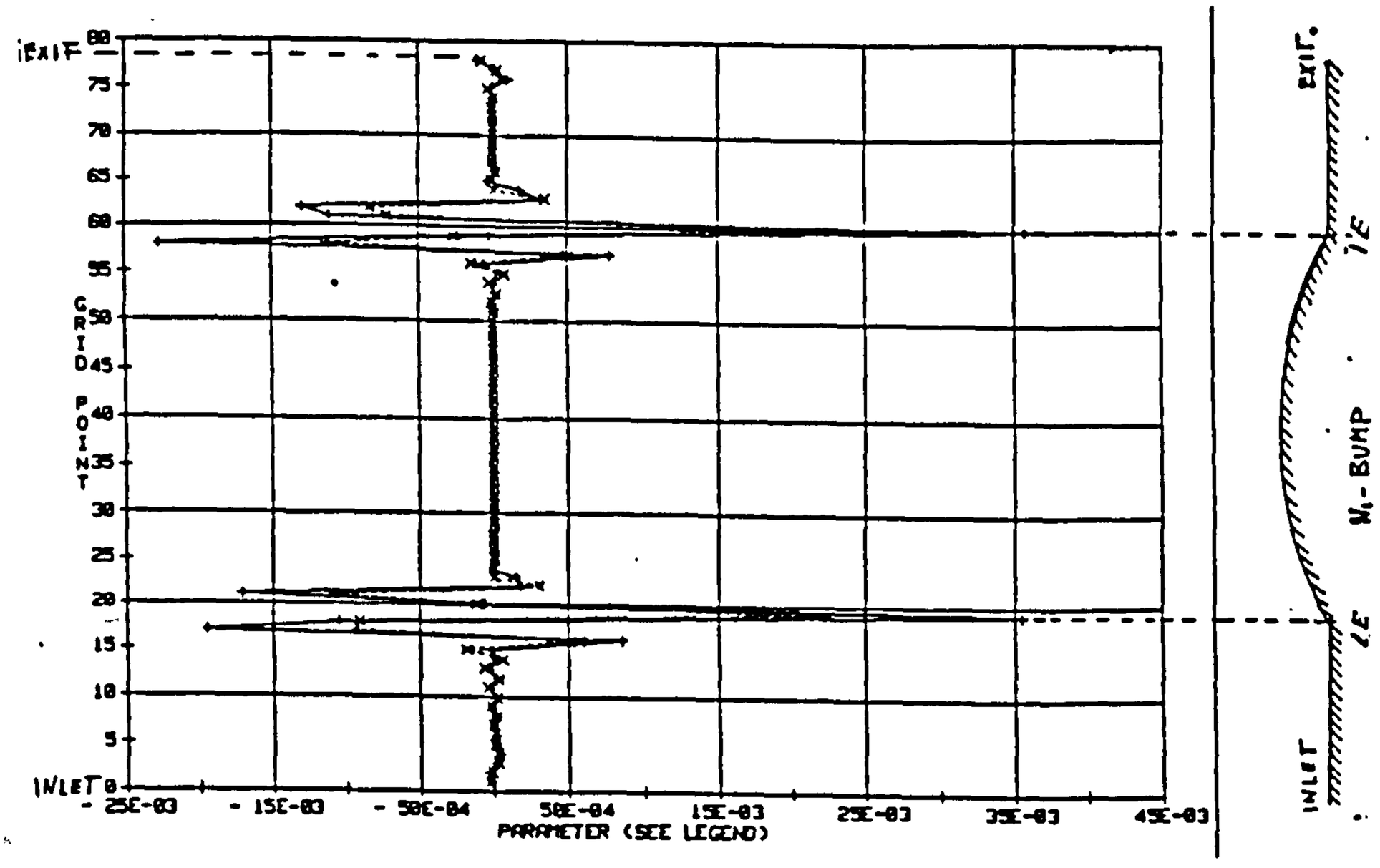

Figure-5.6 Dissipation of ρu near Bump of Ni's Bump Subsonic Case
ξ — Component

-+--+- No modification
-x--x- Aspect ratio function

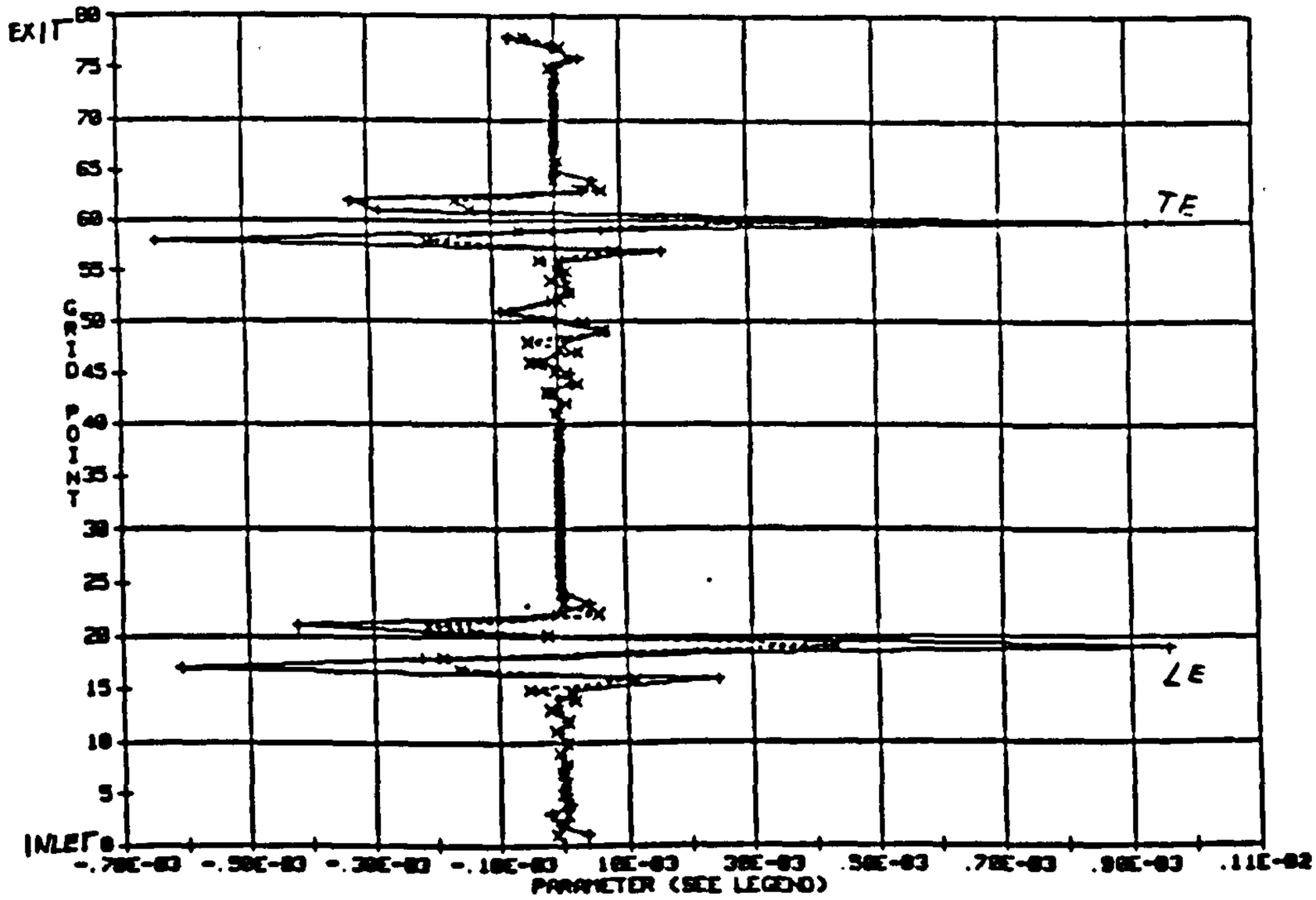

Figure-5.7 Dissipation of ρu near Bump of Ni's Bump Transonic Case
ξ - Component

-+--+- No modification
-x--x- Aspect ratio function

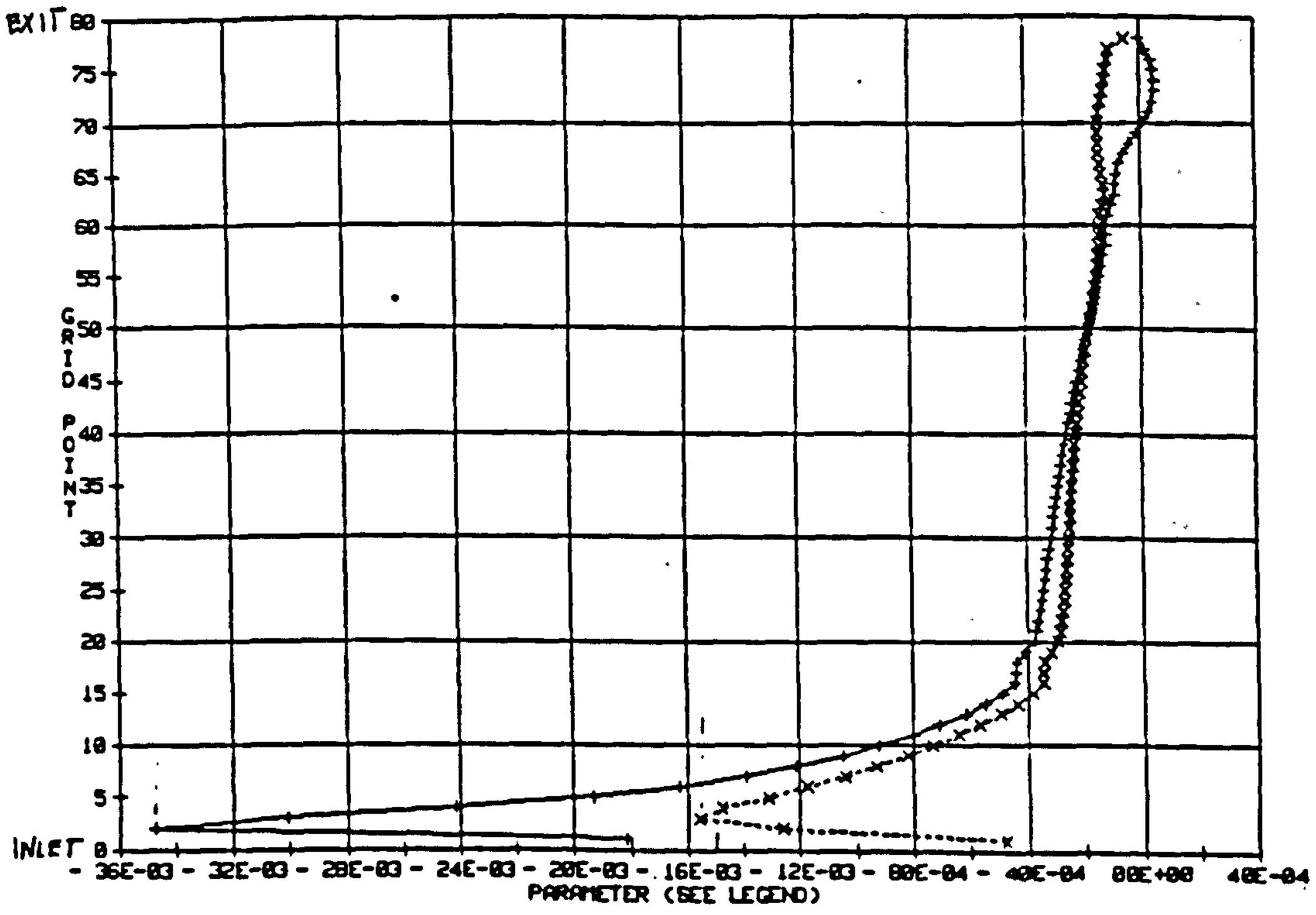

Figure-5.8a Dissipation of ρu near Upper Wall
of Ni's Bump Subsonic Case
η- Component

-+--+- No modification
-x--x- Aspect ratio function

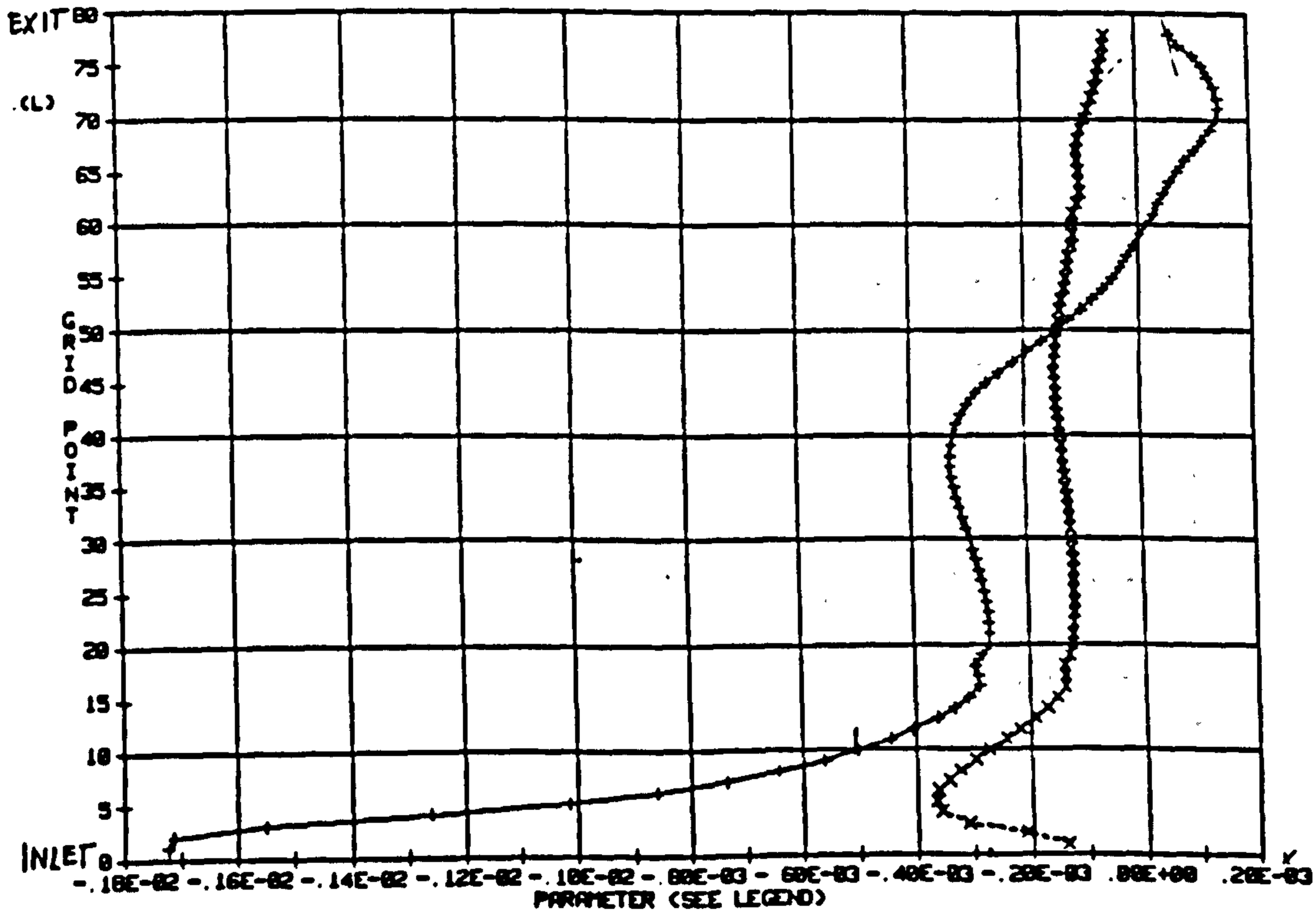

Figure-5.8b Dissipation of ρu near Upper Wall
of Ni's Bump Transonic Case
η-Component

-+--+- No modification
-x--x- Aspect ratio function

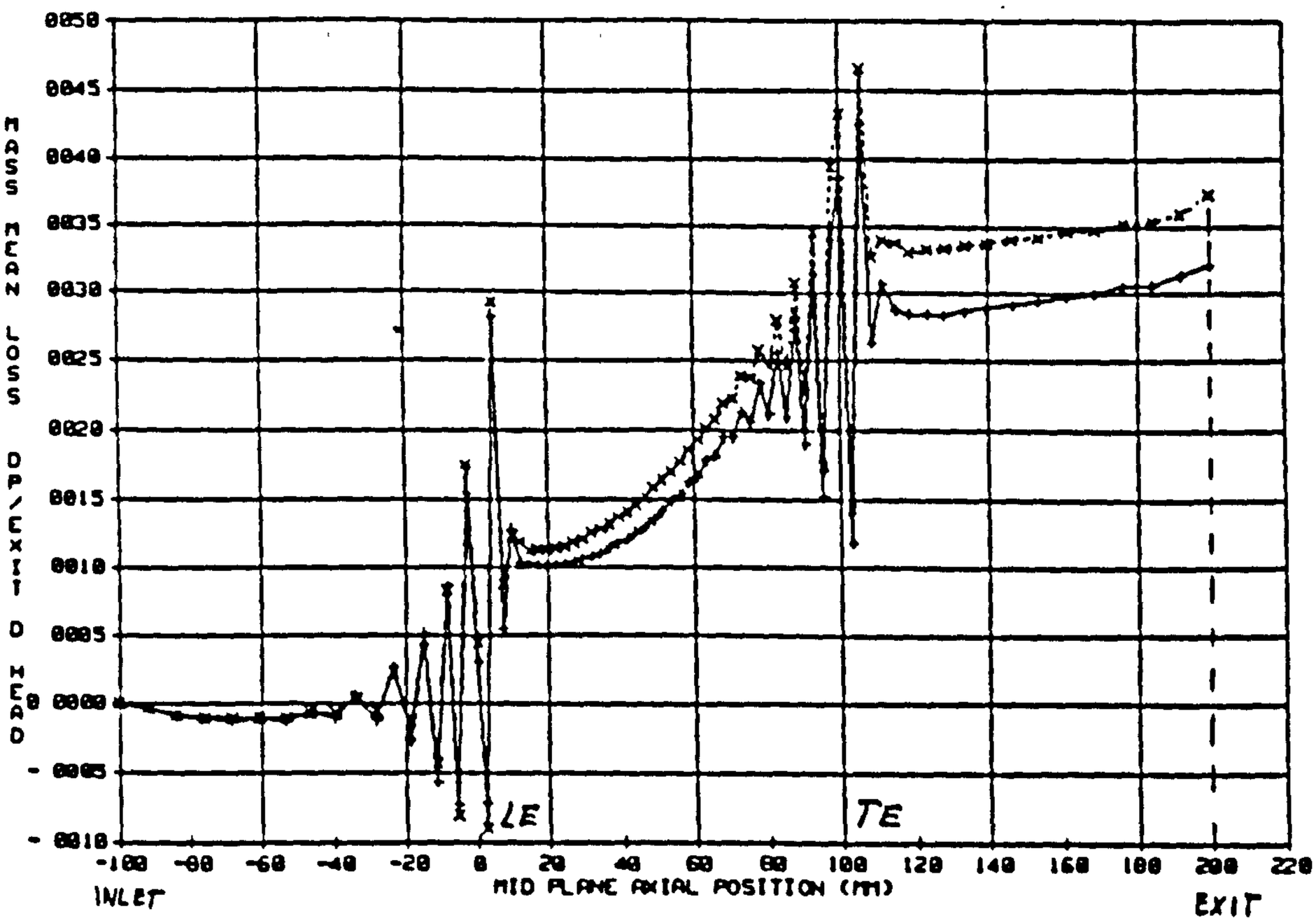

Figure-5.9 Total Pressure loss
Subsonic Case

-+--+- Modified aspect ratio function
-x--x- Kuntz aspect ratio function

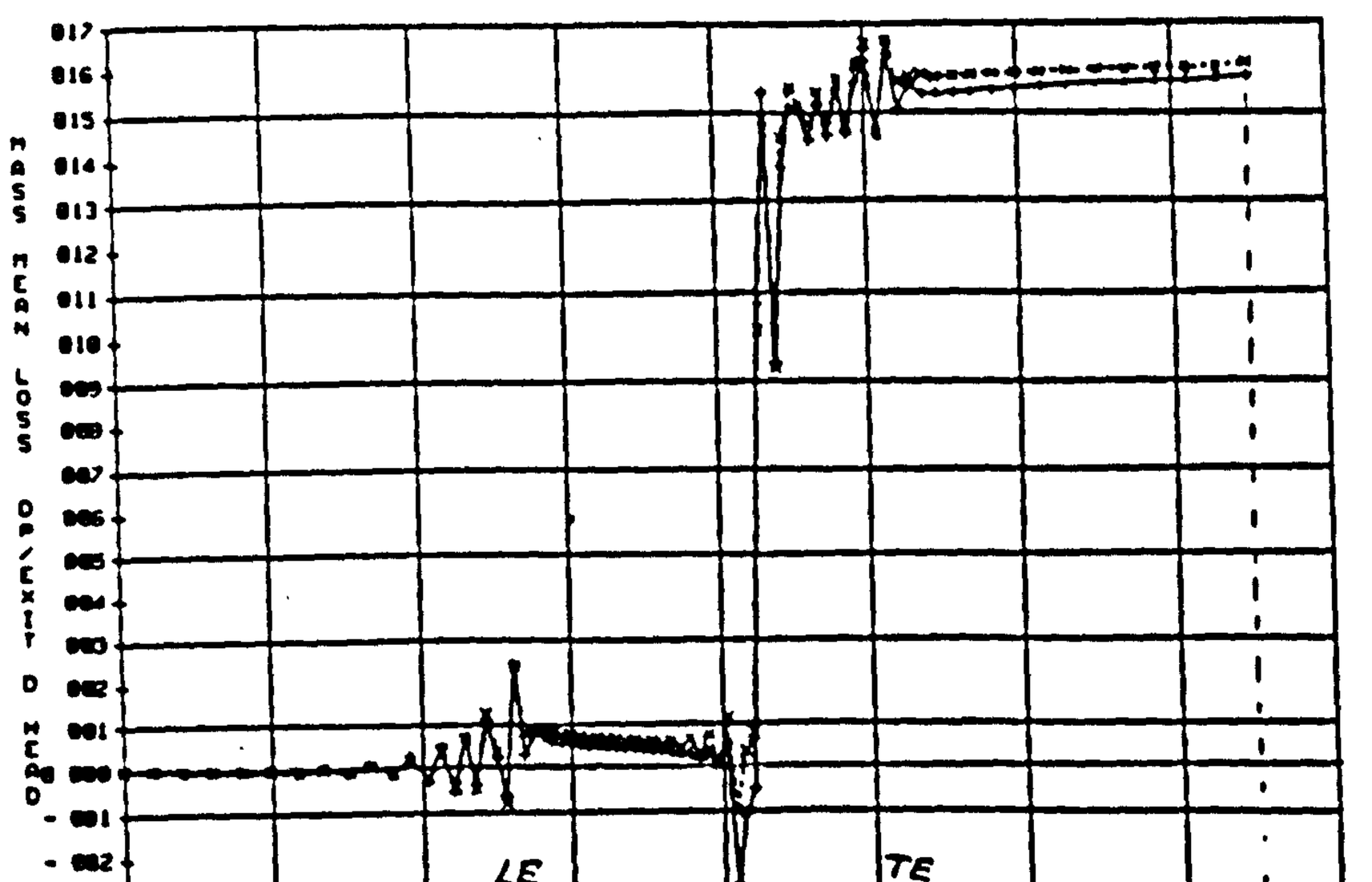

Figure-5.10 Total Pressure loss
Transonic Case

-+--+- Aspect ratio and Mach Number Function
-x--x- Aspect ratio function

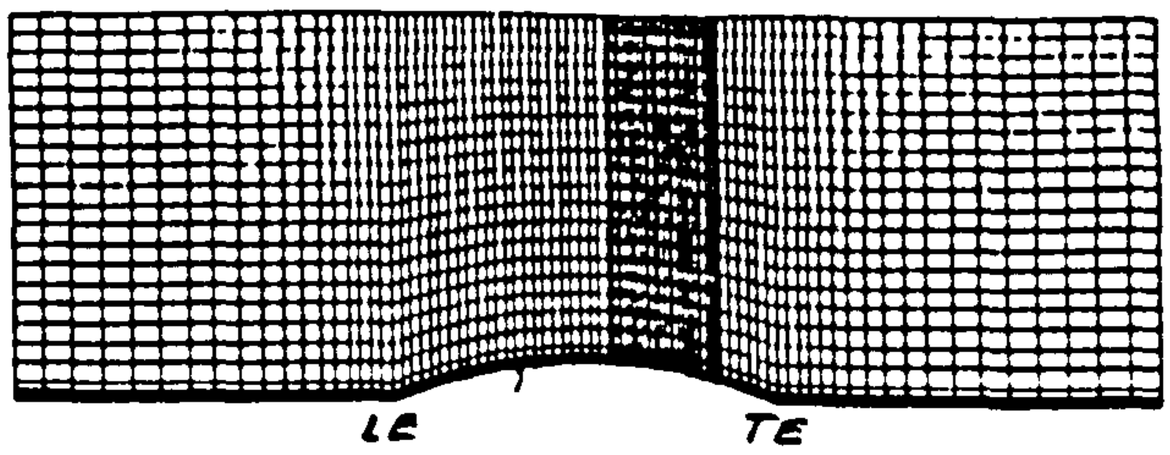

Figure-5.11 Refined Grid for
Transonic Flow

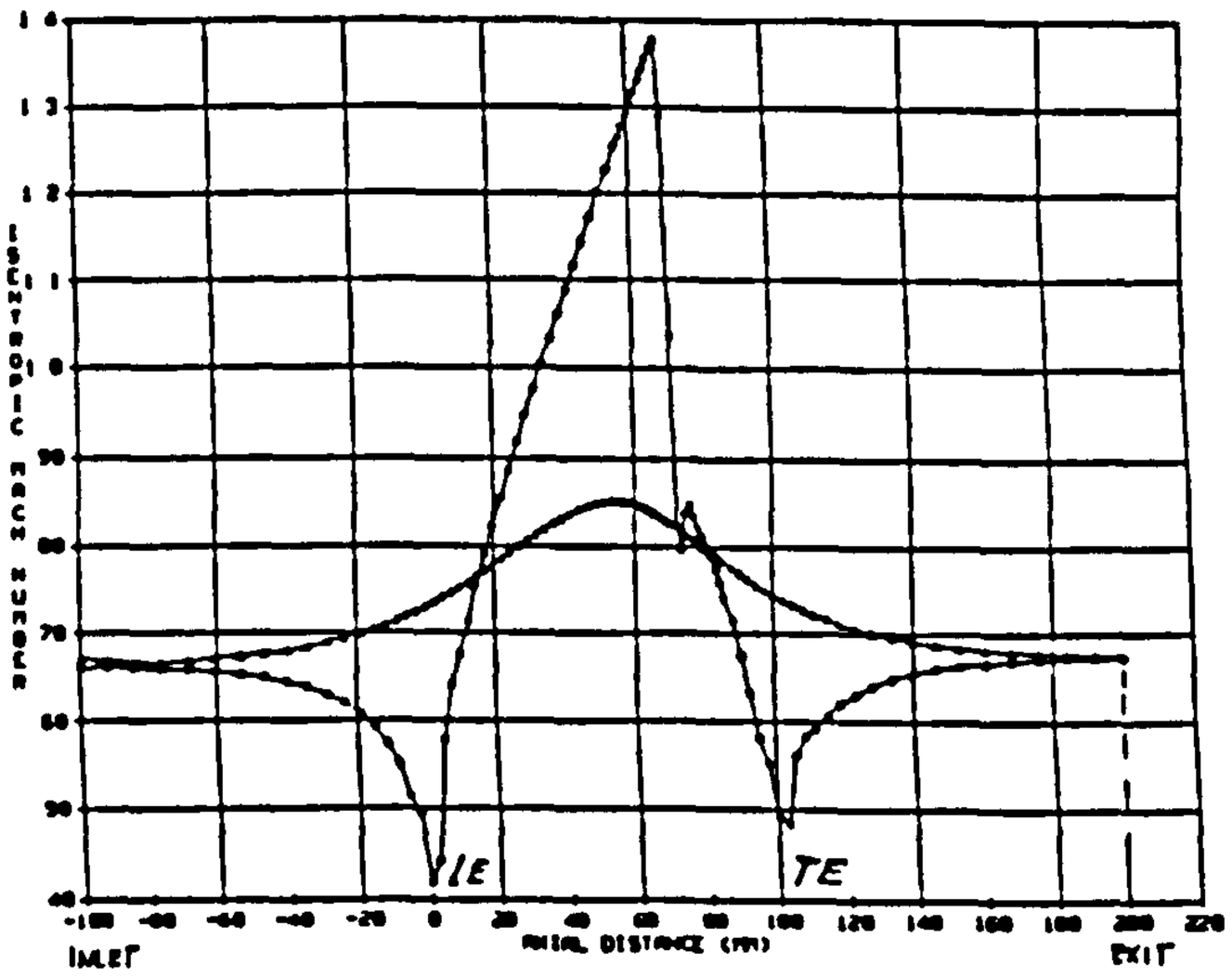

Figure-5.12 Isentropic Mach Number
with the Refined Grid

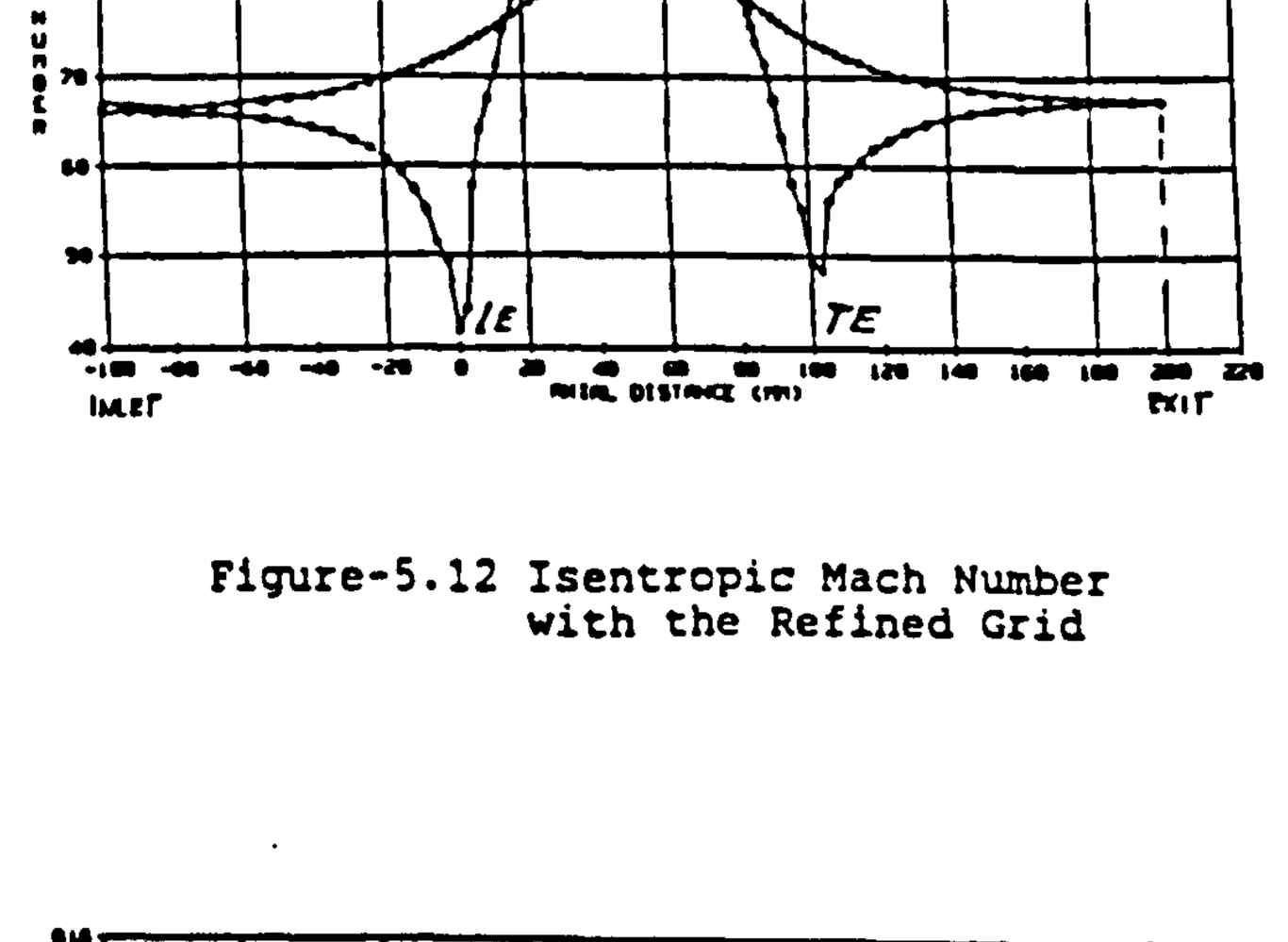

Figure-5.13 Total Pressure loss Transonic
Case with Refined Grid

First grid system

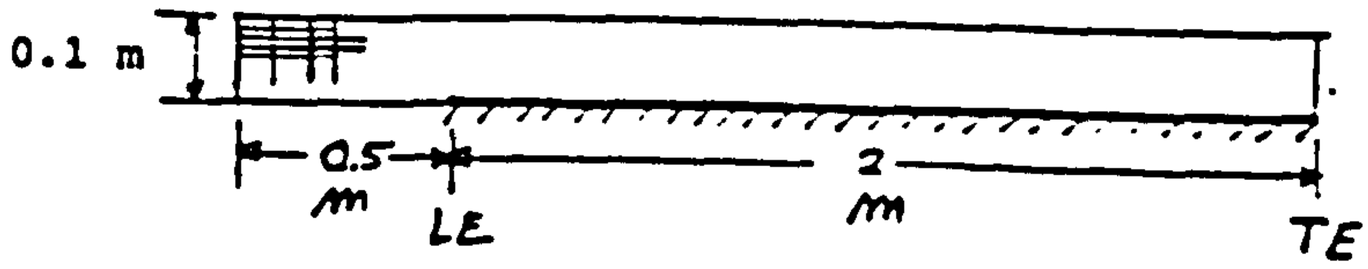

Grid Size 78 X 61

LE=Leading Edge
TE=Trailing Edge

Second grid syster

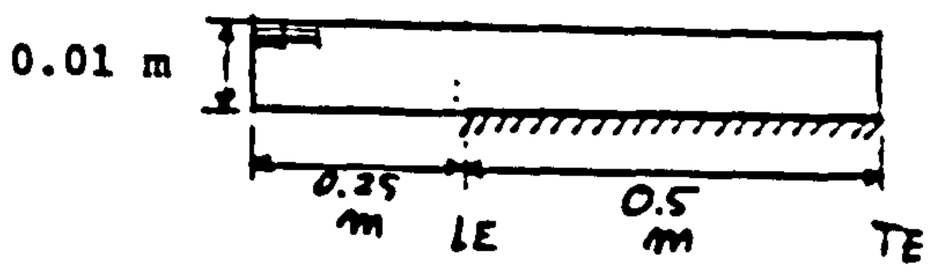

Grid Size 76 X 31

Figure-5.14 Grid System of Flat Plate

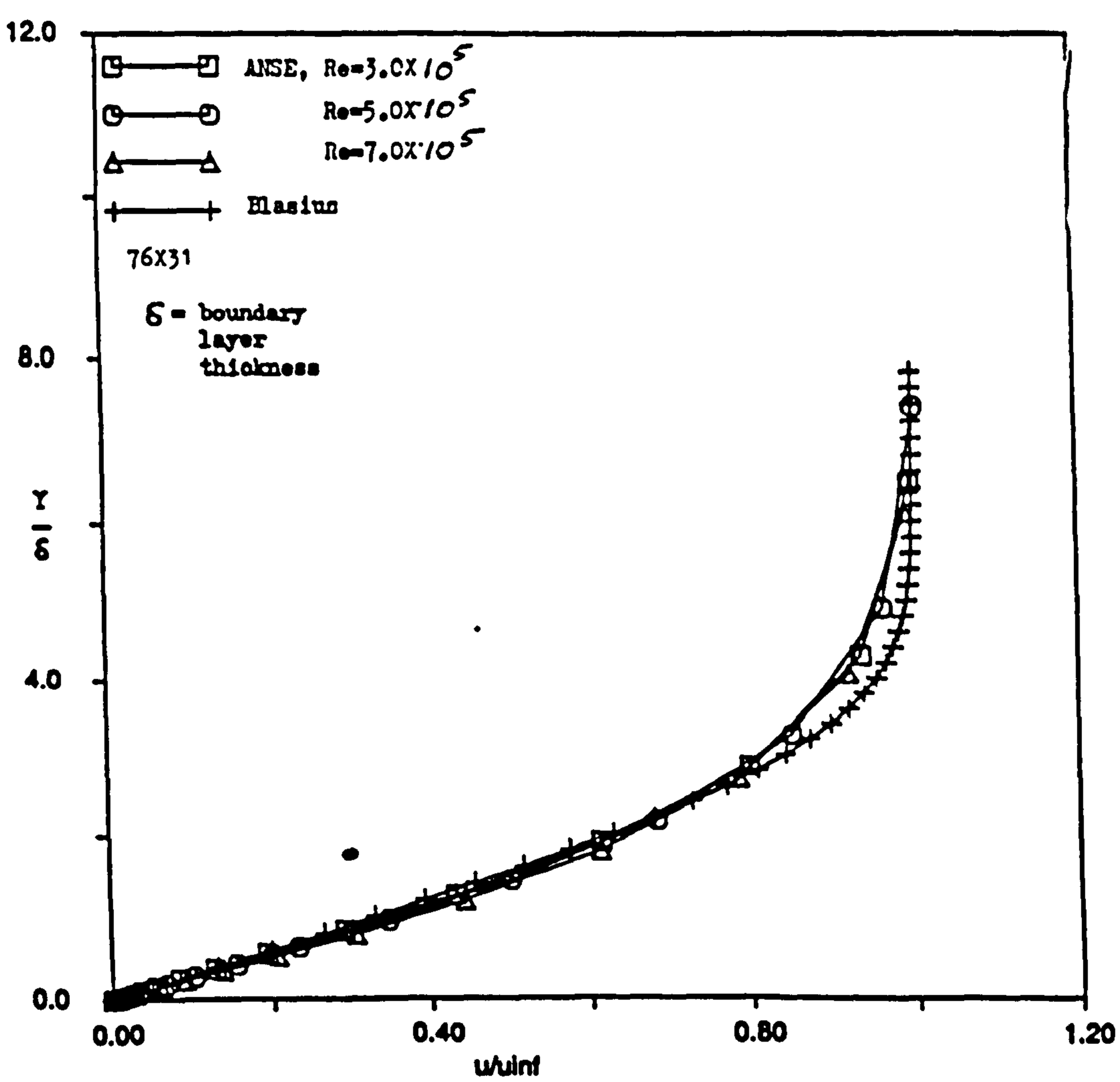

Figure-5.15 Laminar Velocity Profile

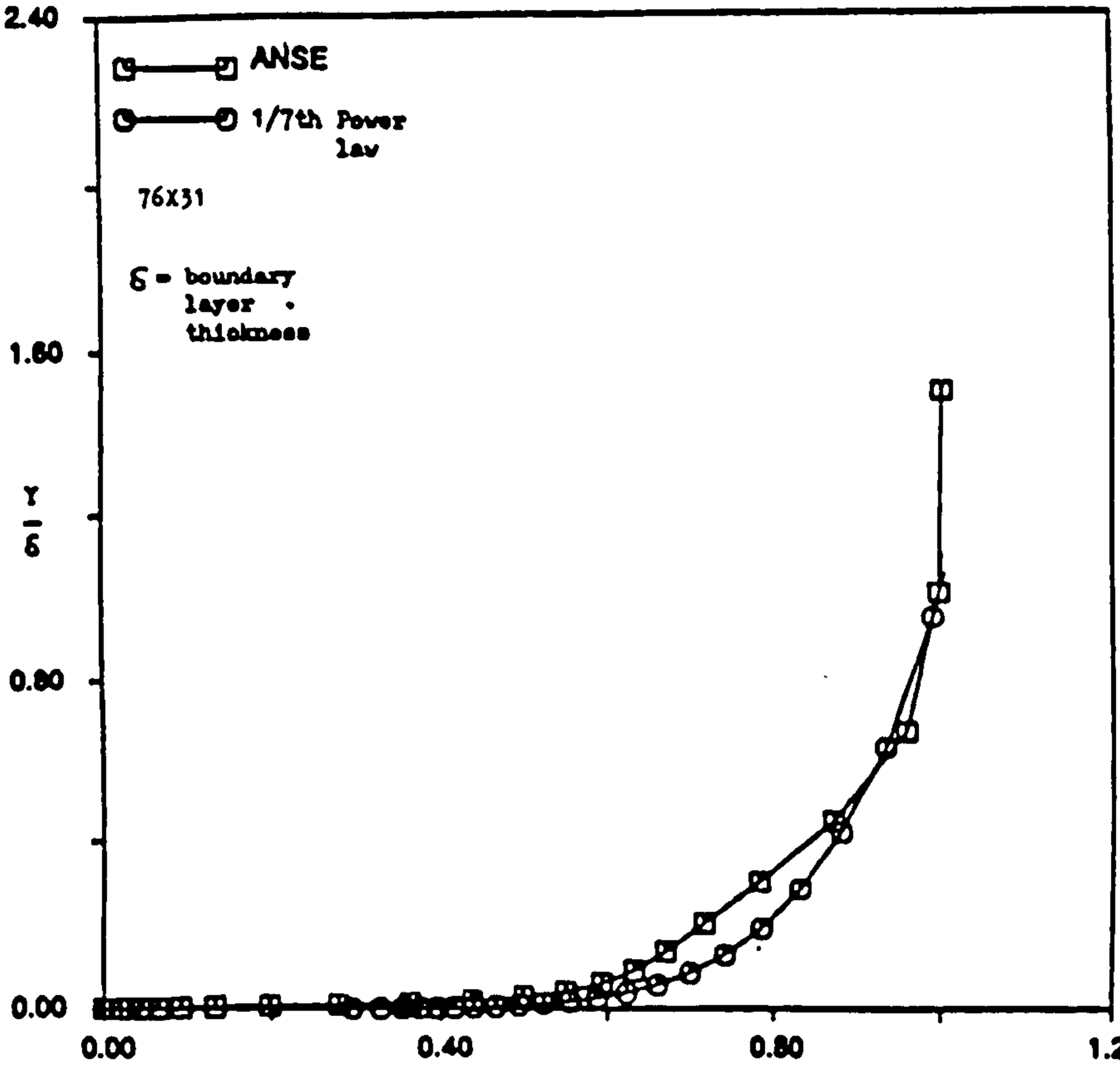

Figure-5.16 Turbulent Velocity Profile
At Reynolds Number = 1.221×10^6

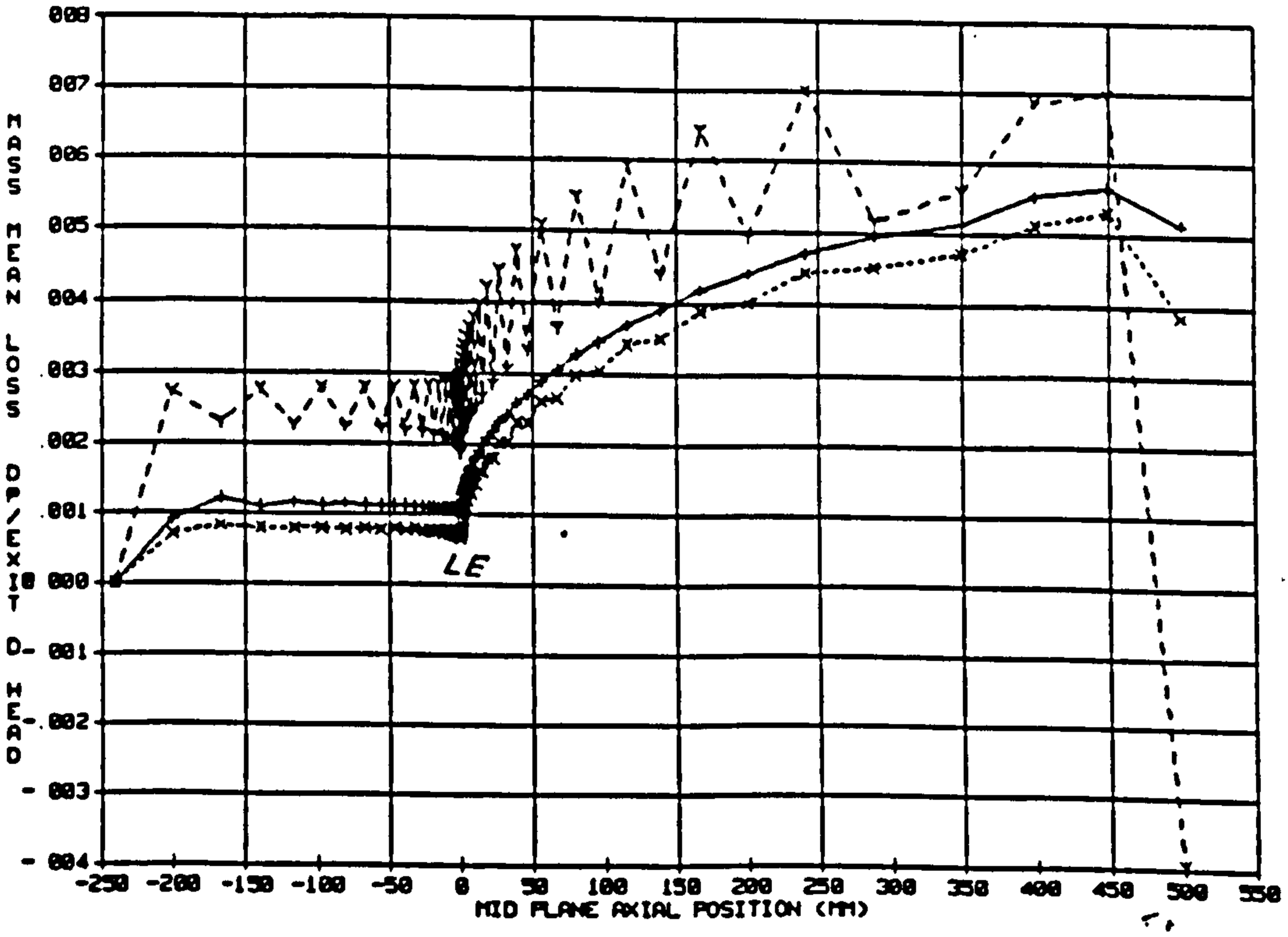

Figure-5.17 Total Pressure loss of Laminar Flat Plate

-+--+- No modification
-x--x- Aspect Ratio Function, α =0.6666
-Y--Y- Aspect Ratio Function, α =0.0

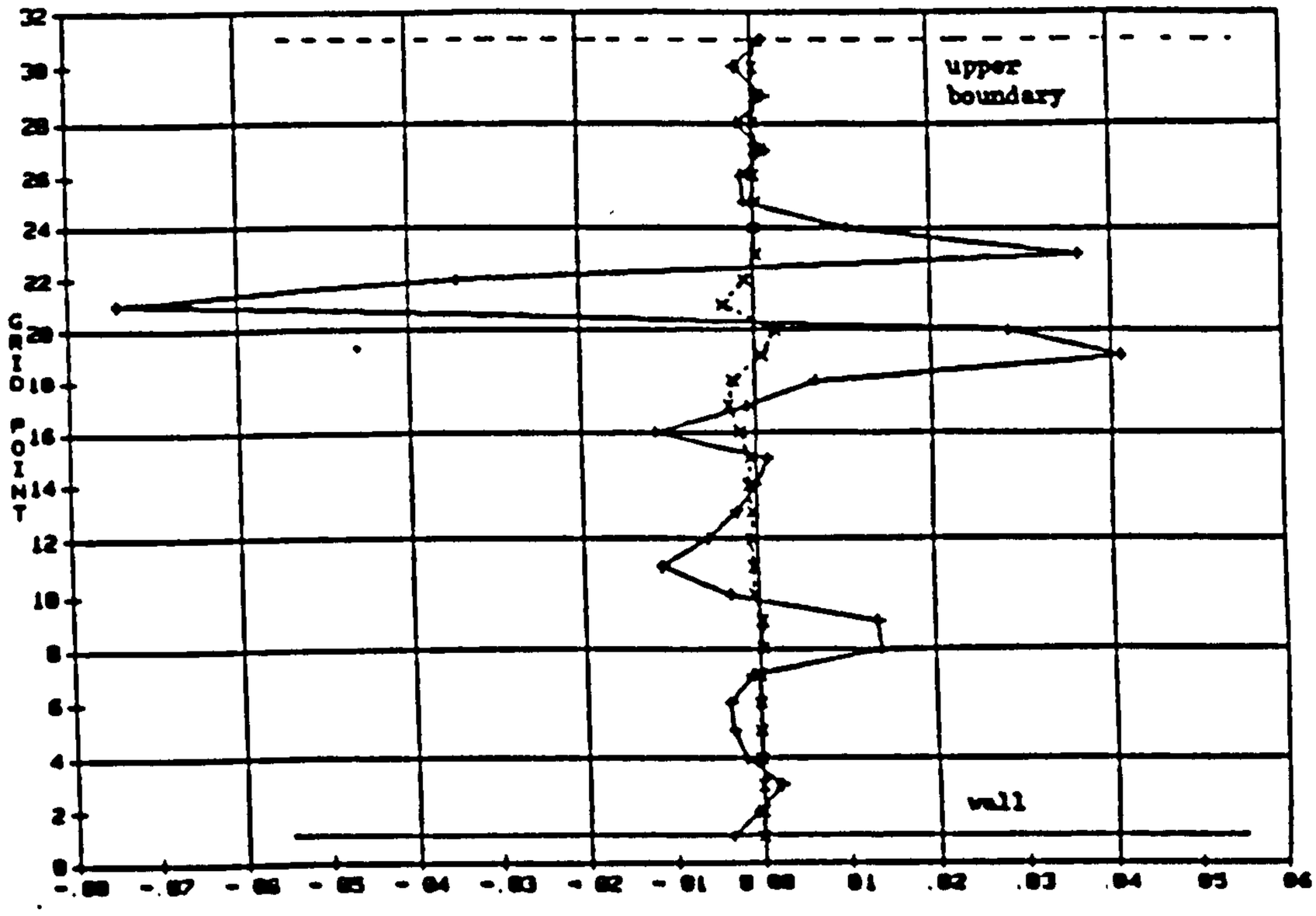

Figure-5.18 Dissipation of ρu on Turbulent Flat Plate At Reynold Number=$1.221X10^6$

-+--+- No modification
-x--x- Anisotropic Factor, f_η =0.025

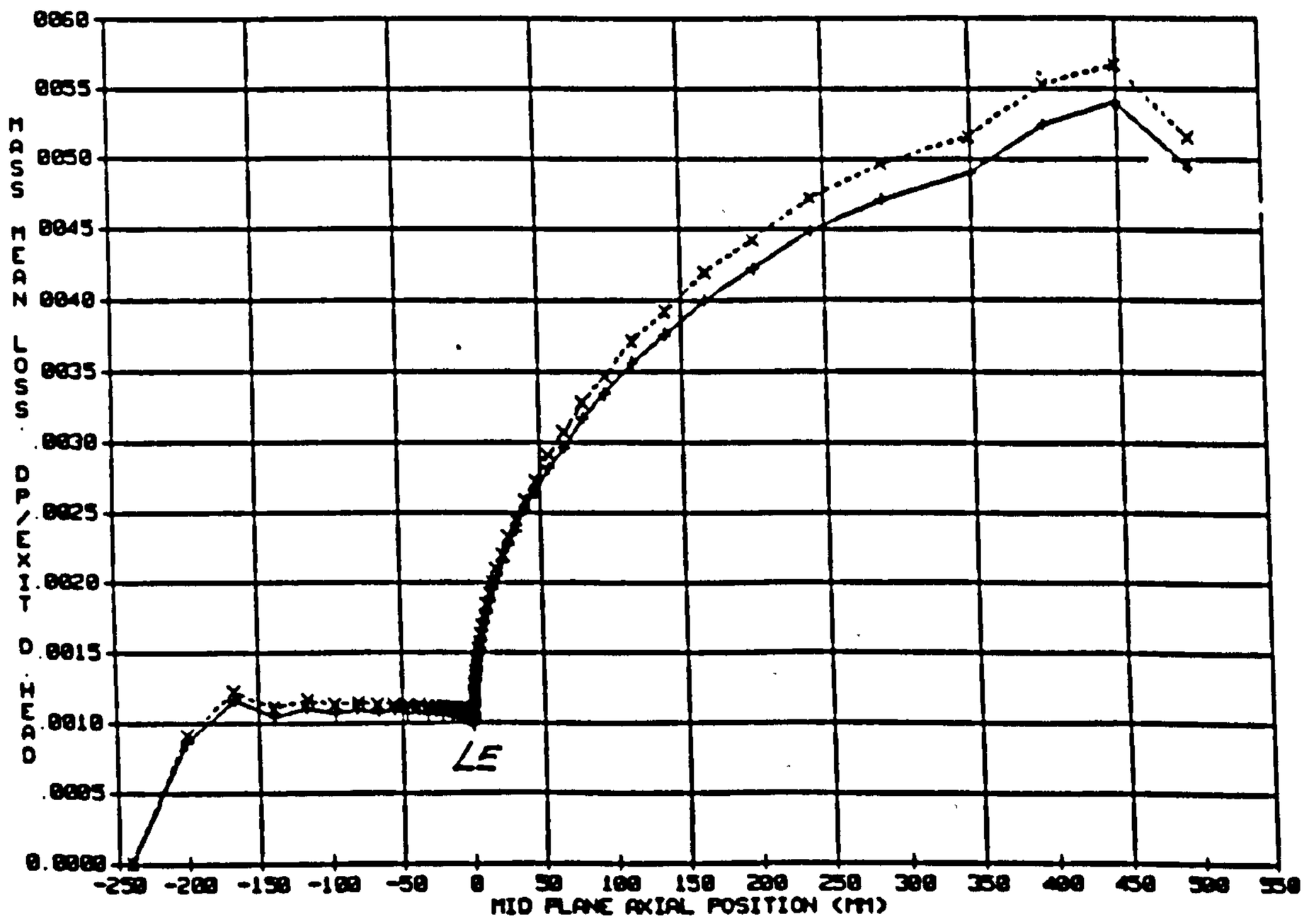

Figure-5.19 Total Pressure loss of Laminar Flat Plate

-x--x- No modification
-+--+- Anisotropic Factor, f_η =0.025

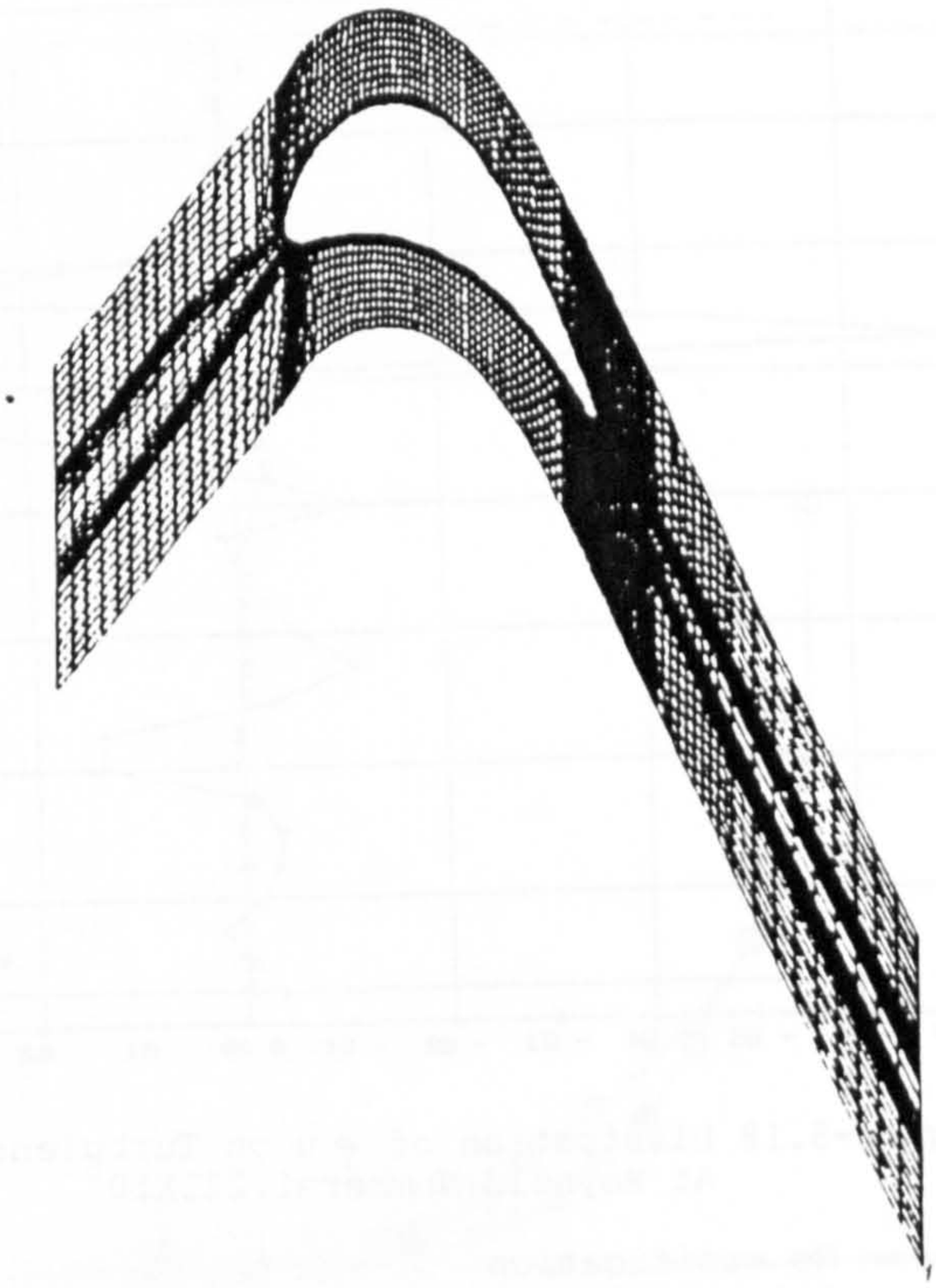

Figure-5.20 Grid of Two Dimensional
High Pressure Turbine Blade

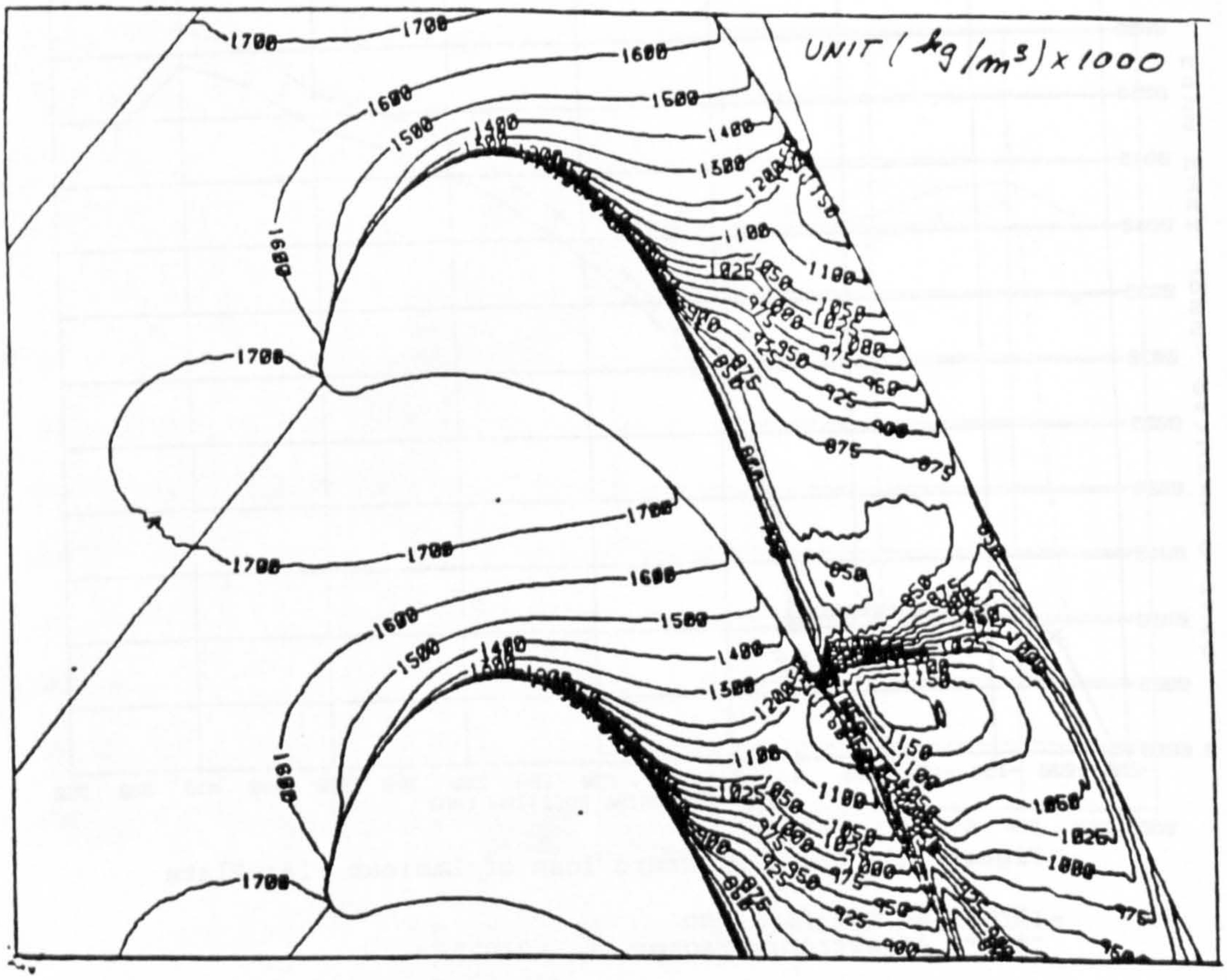

Figure-5.21 Density Countor of Two Dimensional
High Pressure Turbine Blade

Figure-5.22 Measured Density Contour of the
Two Dimensional High Pressure Turbine
(Xu, 1986)

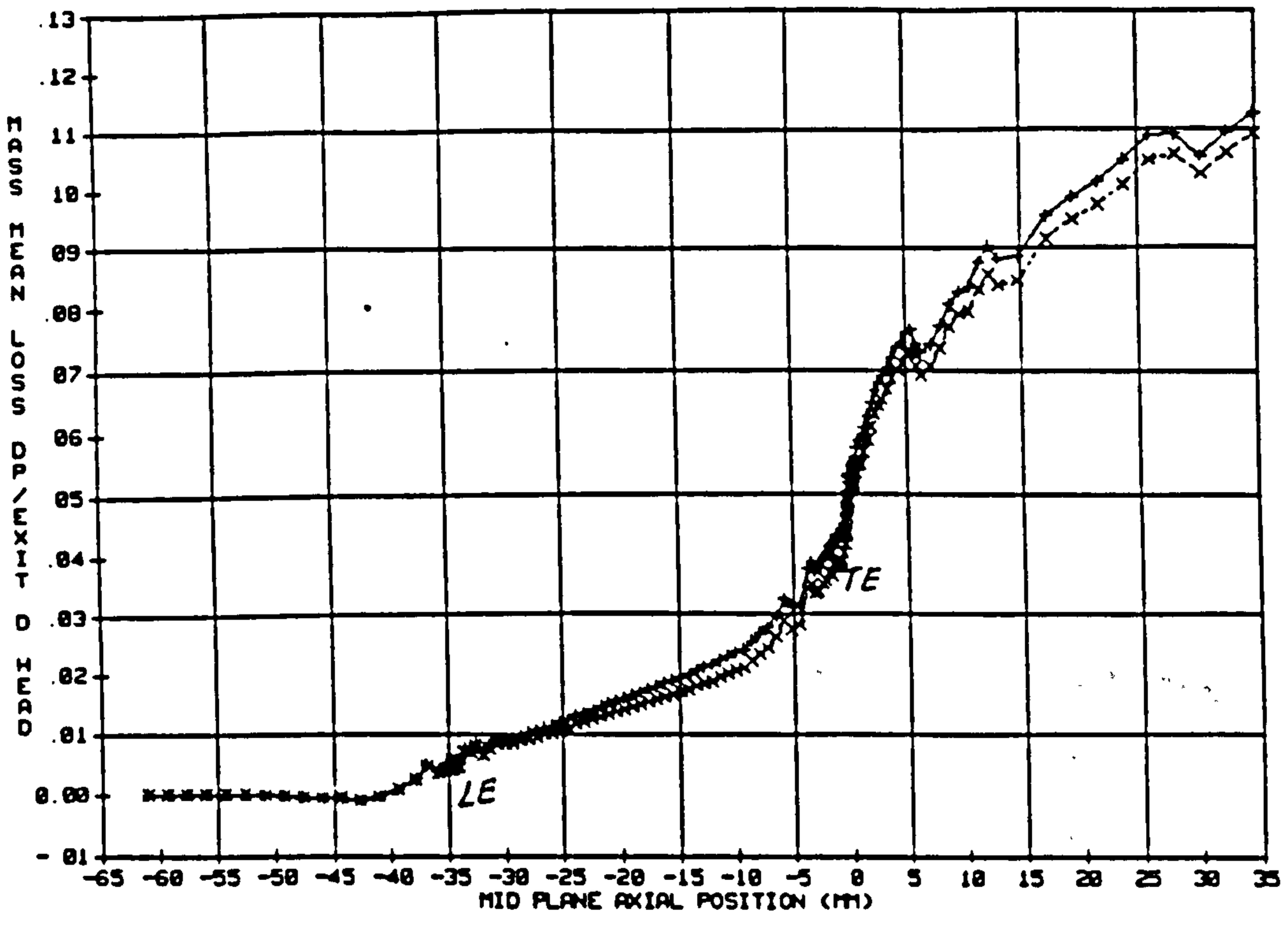

Figure-5.23 Total Pressure loss: Two Dimensional
High Pressure Turbine Blade

-+--+- No modification
-x--x- Aspect ratio function, α = 0.8333

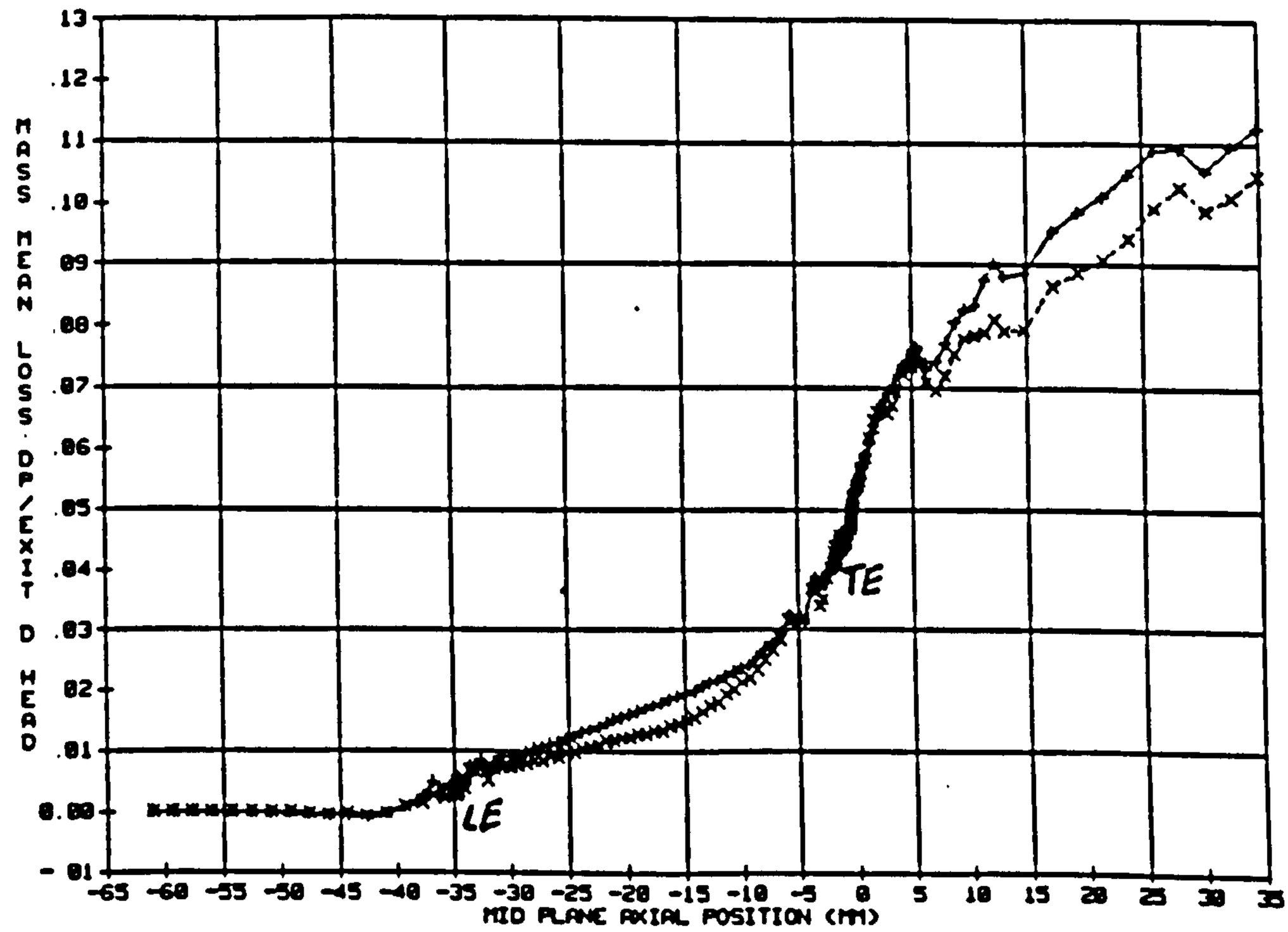

Figure-5.24 Total Pressure loss: Two Dimensional
High Pressure Turbine Blade

-+--+- No modification
-x--x- Anisotropic Factors, f_s=0.5, f_n=0.05
LE=Leading Edge
TE= Trailing Edge

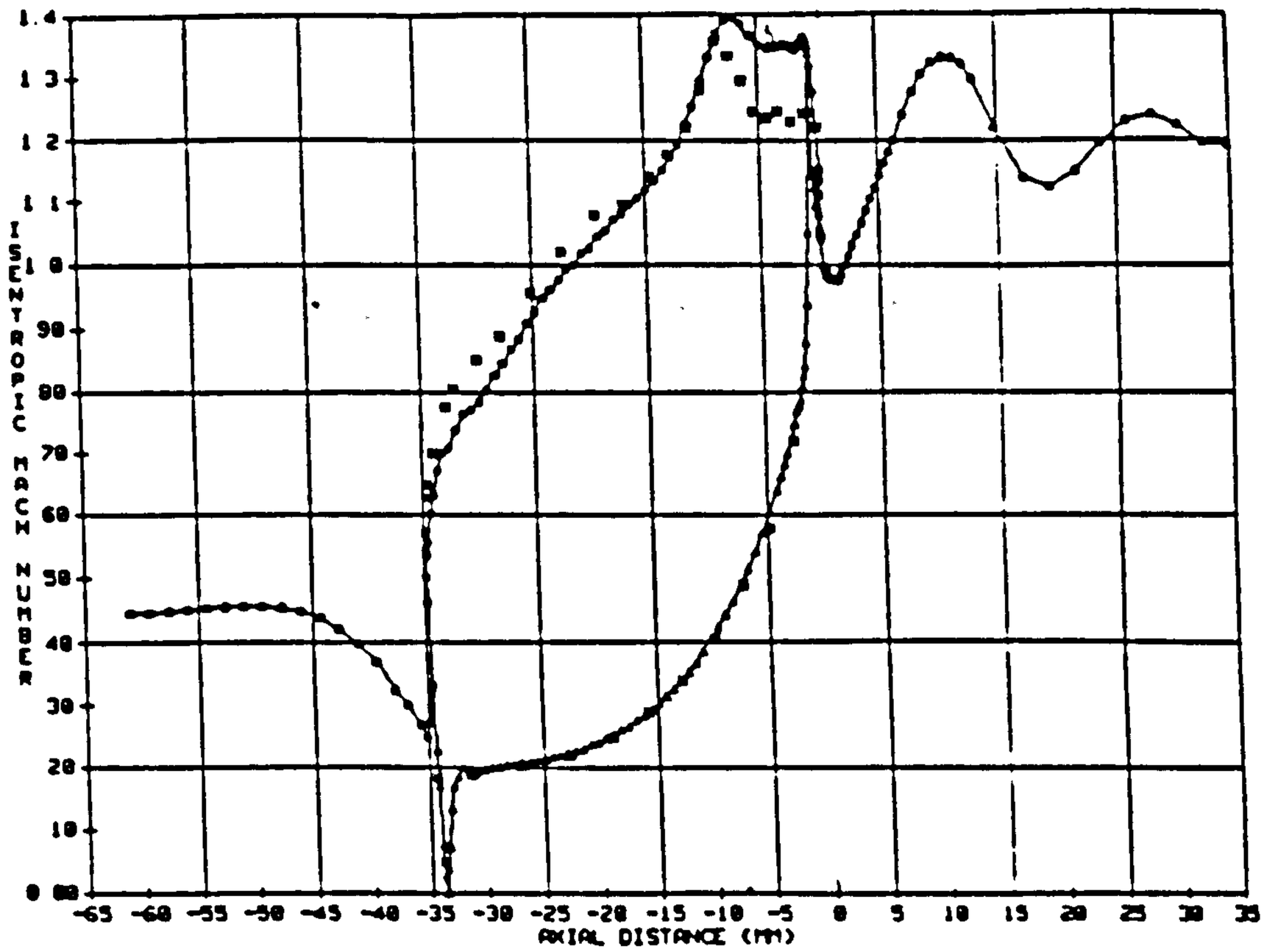

Figure-5.25a Isentropic Mach Number
Distribution with Standard Model
* Experimental Result

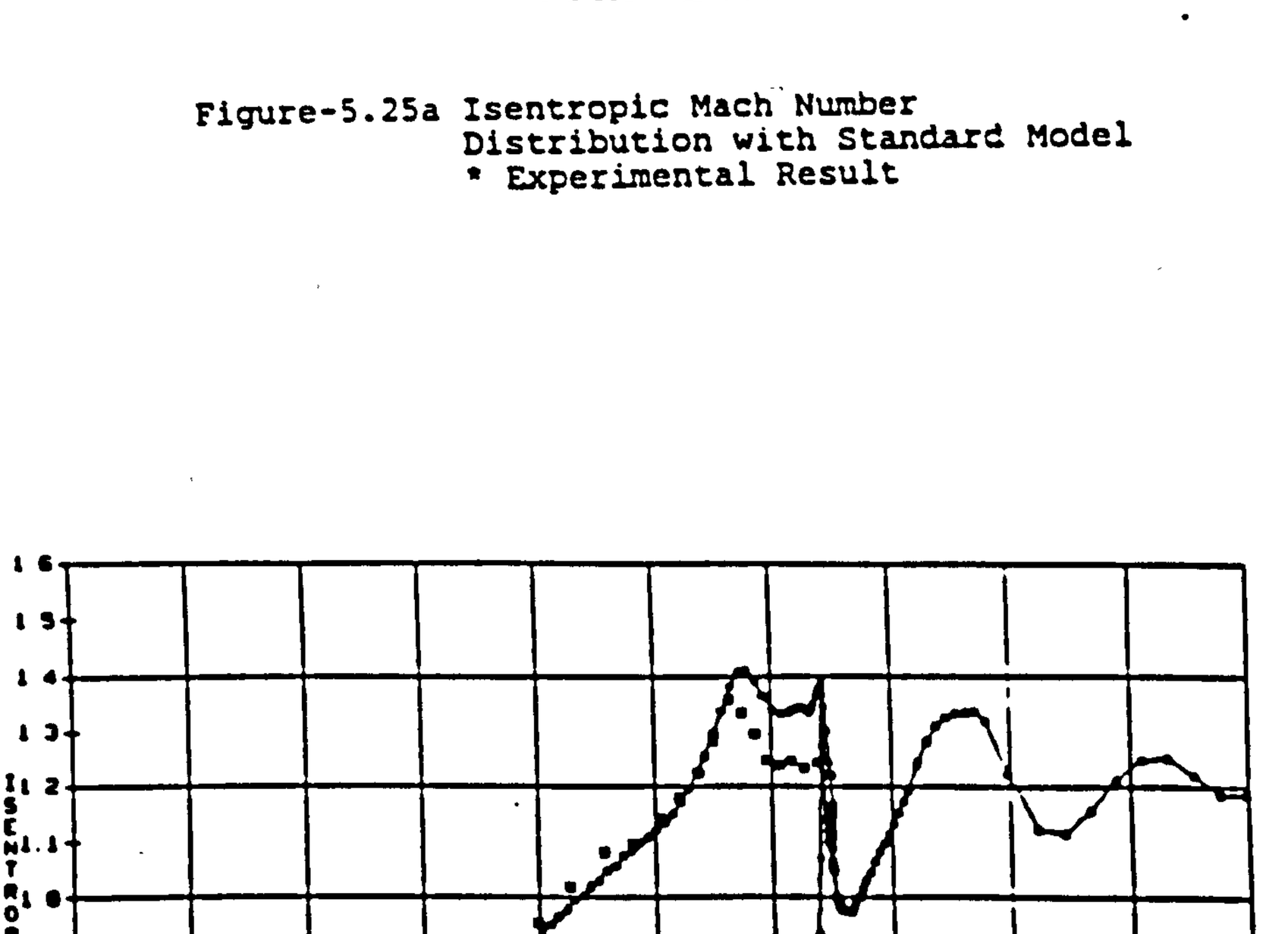

Figure-5.25b Isentropic Mach Number Distribution
with Anisotropic Factors
f_ξ =0.5 and f_η =0.05

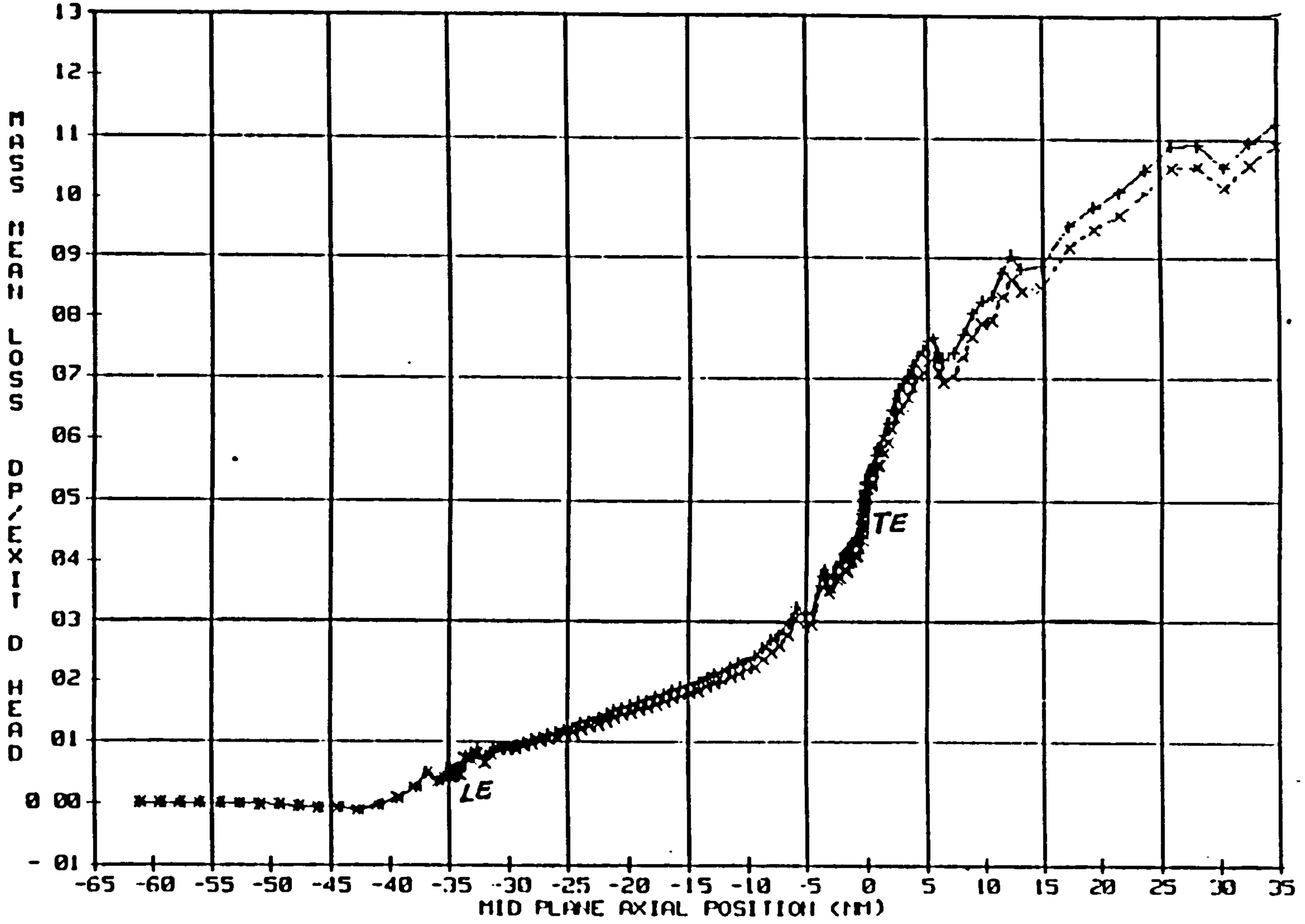

Figure-5.26 Total Pressure loss Two Dimensional
High Pressure Turbine Blade

-+--+- No modification
-x--x- Gradient function

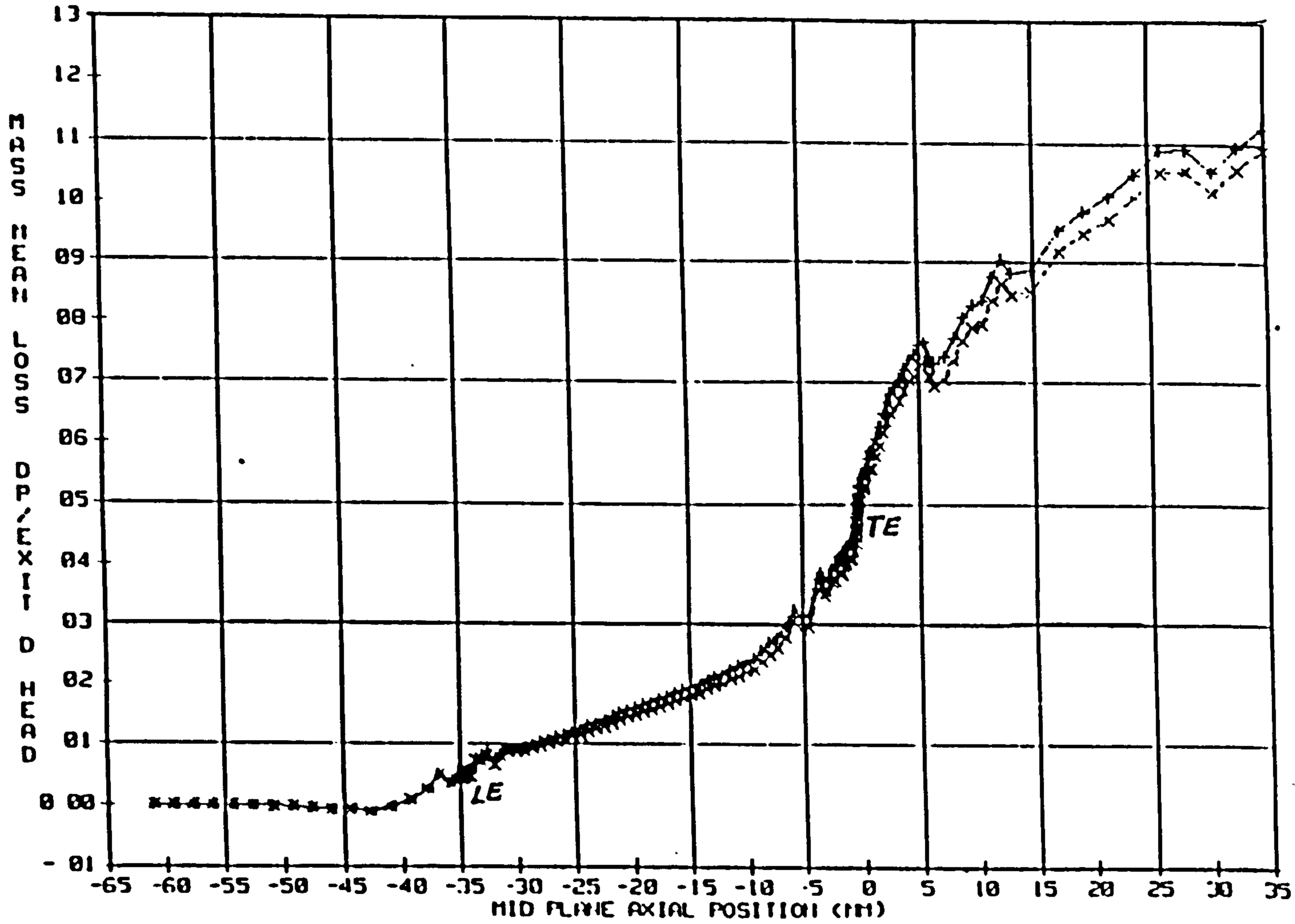

Figure-5.26 Total Pressure loss Two Dimensional
High Pressure Turbine Blade

-+--+- No modification
-x--x- Gradient function

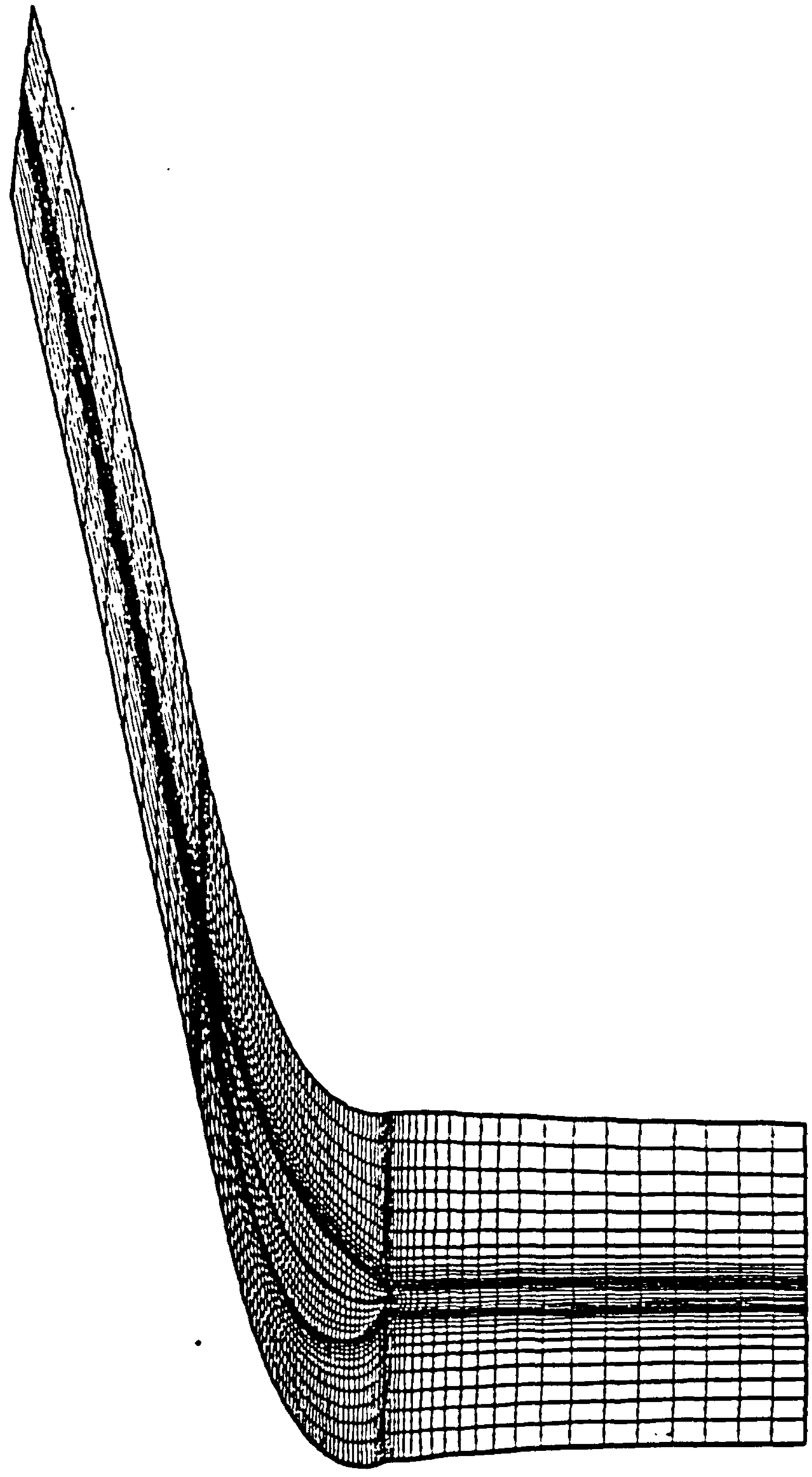

Figure-5.27a Grid of Three Dimensional
High Pressure Turbine Blade
Blade-to-Blade Plane at Mid Height

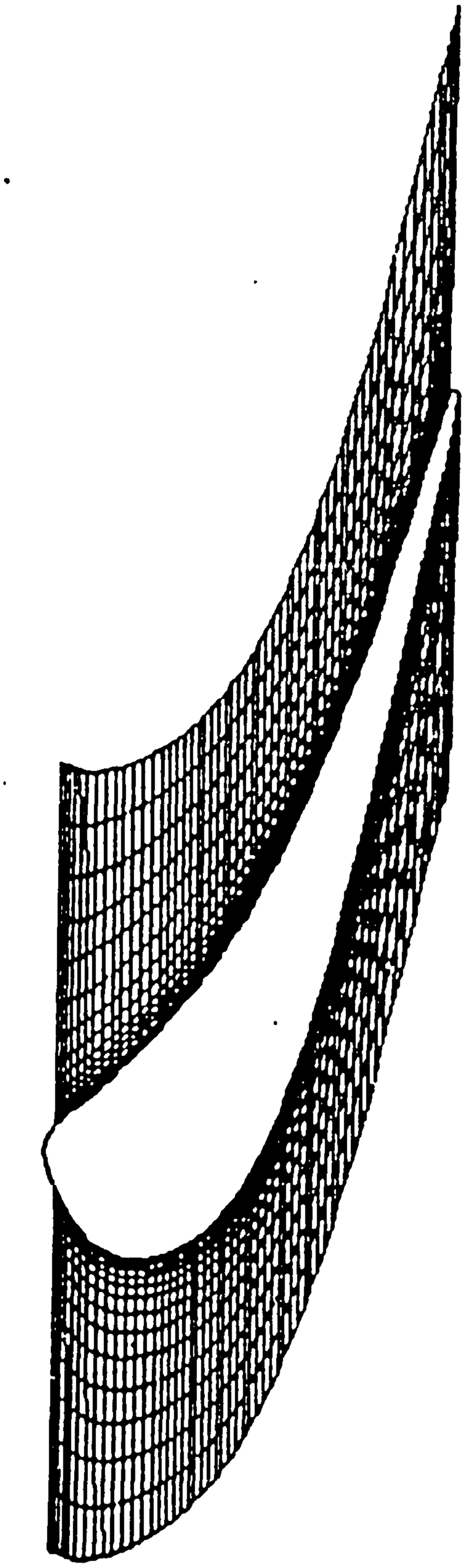

Figure-5.27b Grid of Three Dimensional
High Pressure Turbine Blade
Grid within the Blade Passage

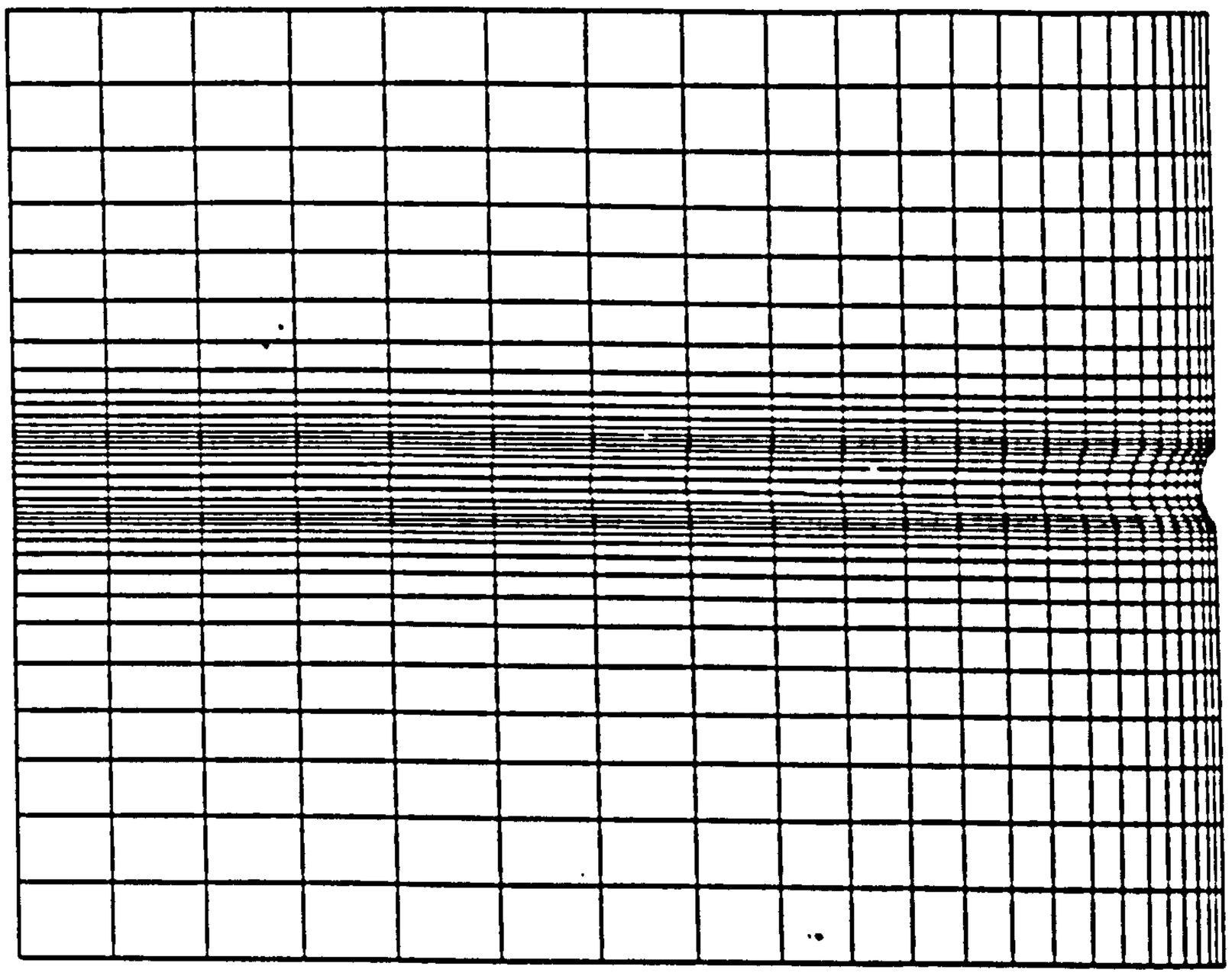

Figure-5.27c Grid of Three Dimensional
High Pressure Turbine Blade:
Blade-to-Blade Plane Upstream
of the Leading Edge Region

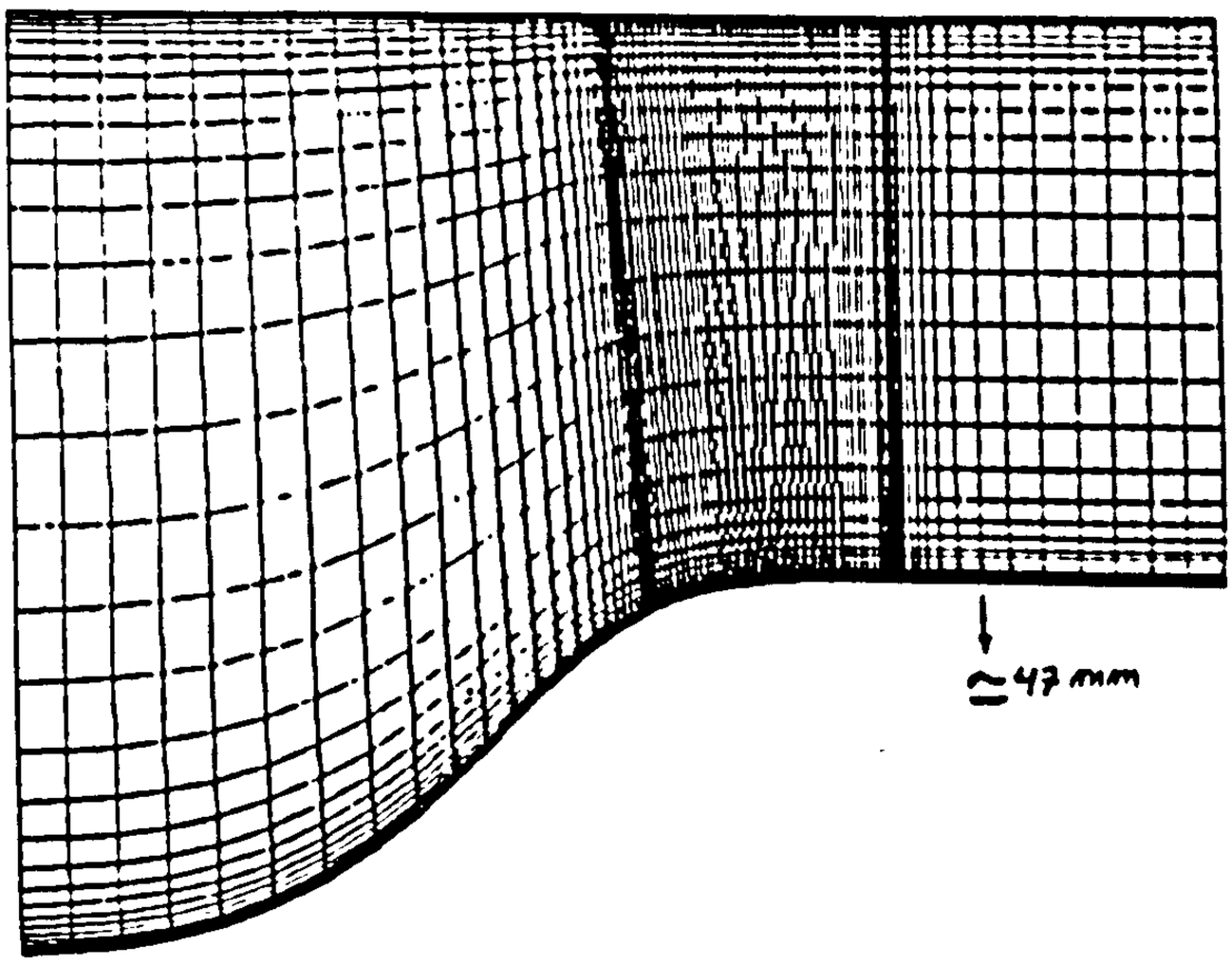

Figure-5.27d Grid of Three Dimensional
High Pressure Turbine Blade:
Meridional Plane

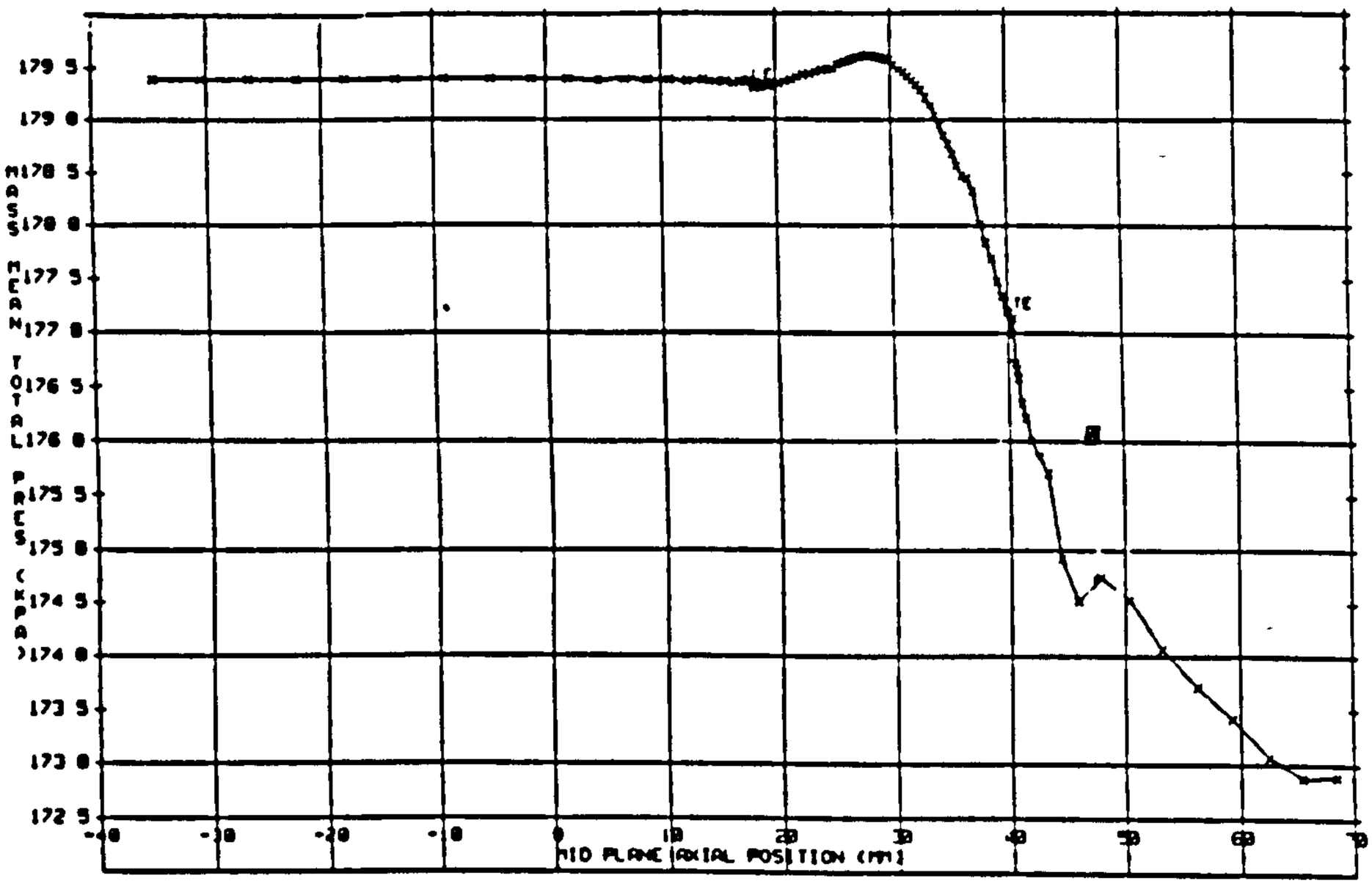

Figure-5.28 Total Pressure loss the three Dimensional High Pressure Turbine

LE = Leading Edge
TE = Trailing Edge
● Experimental data

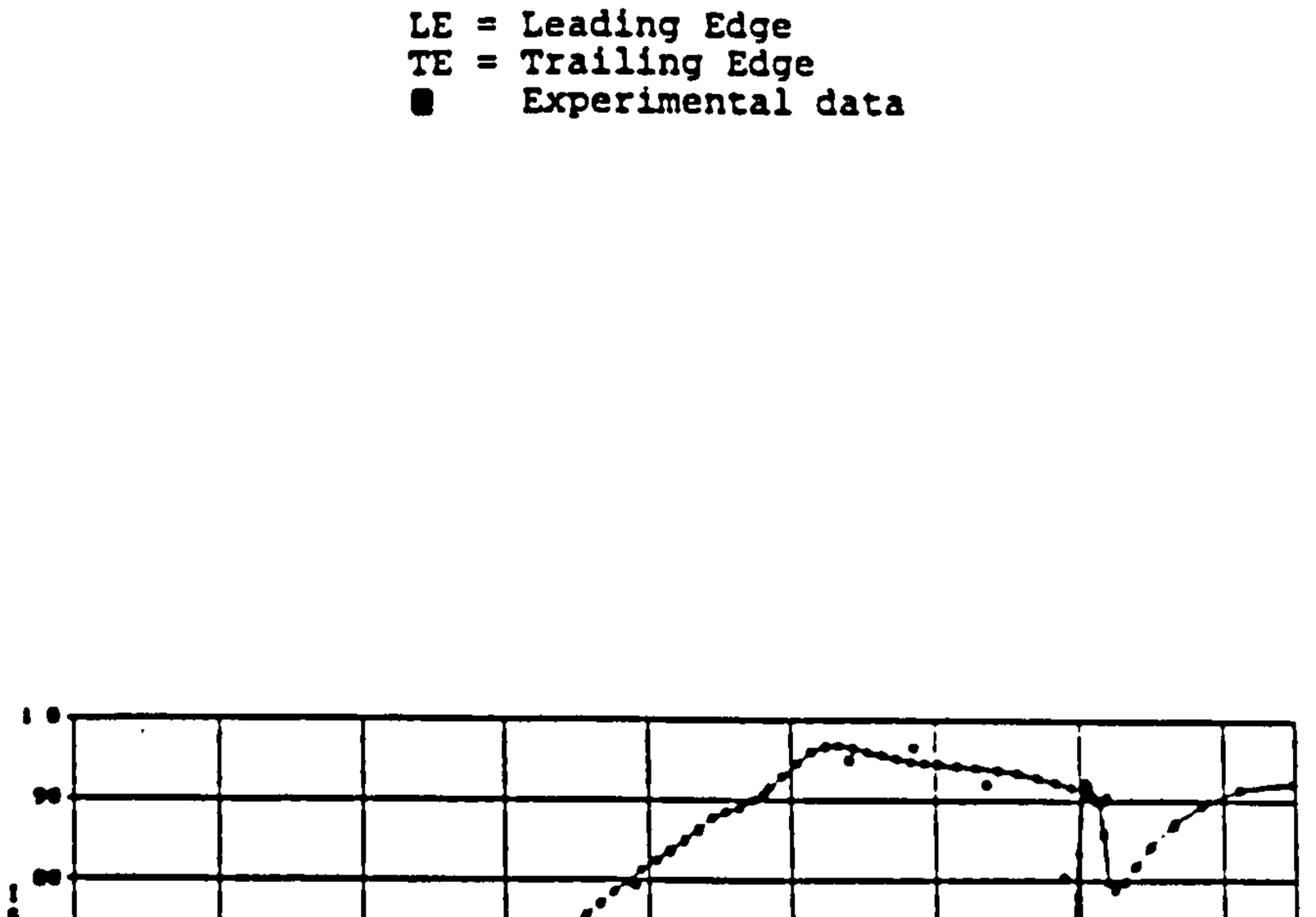

Figure-5.29 Isentropic Mach Number Distribution of Three Dimensional High Pressure Turbine Blade
* Experimental data

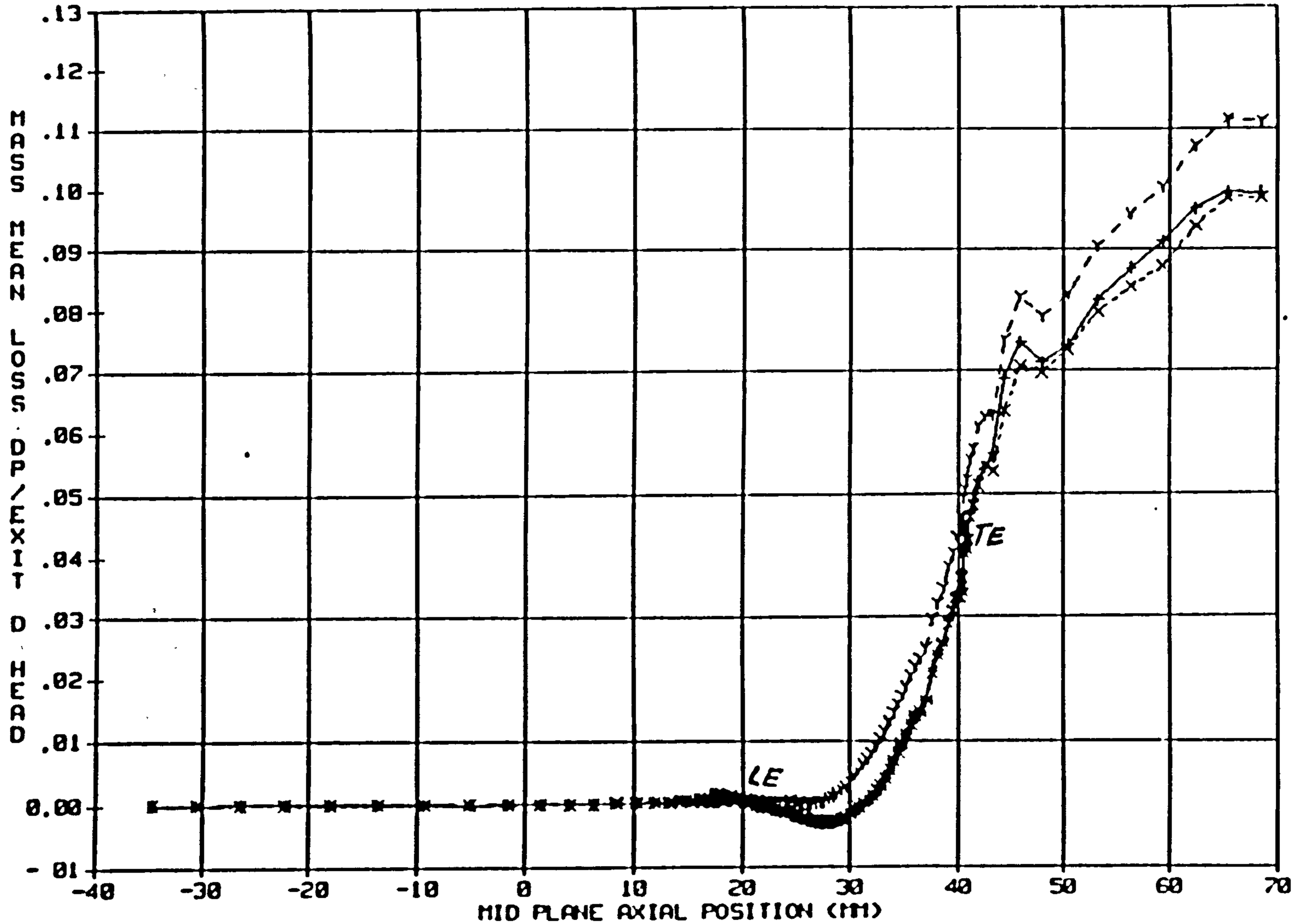

Figure-5.30 Total Pressure loss of
Three Dimensional High Pressure Turbine

-+--+- No modification .
-x--x- Aspect ratio function(Kuntz)
-Y--Y- Gradient Function

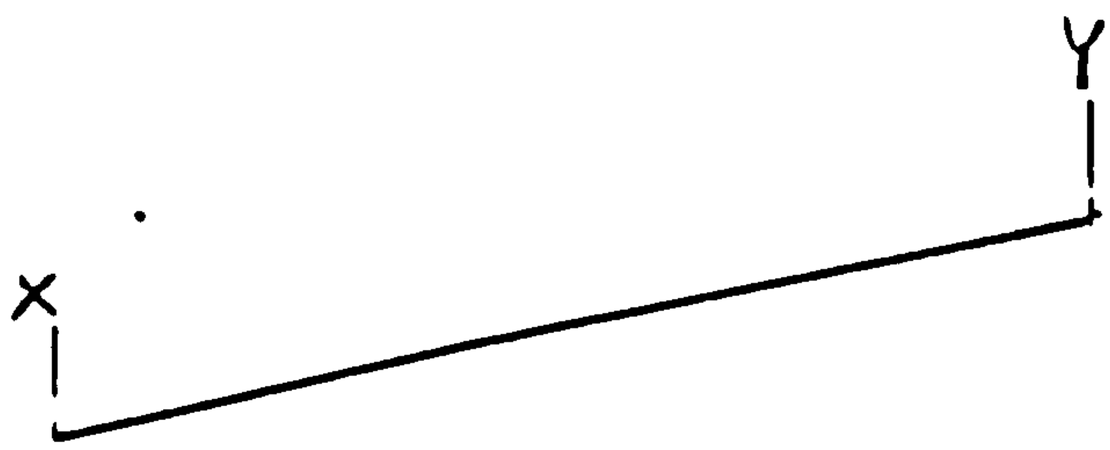

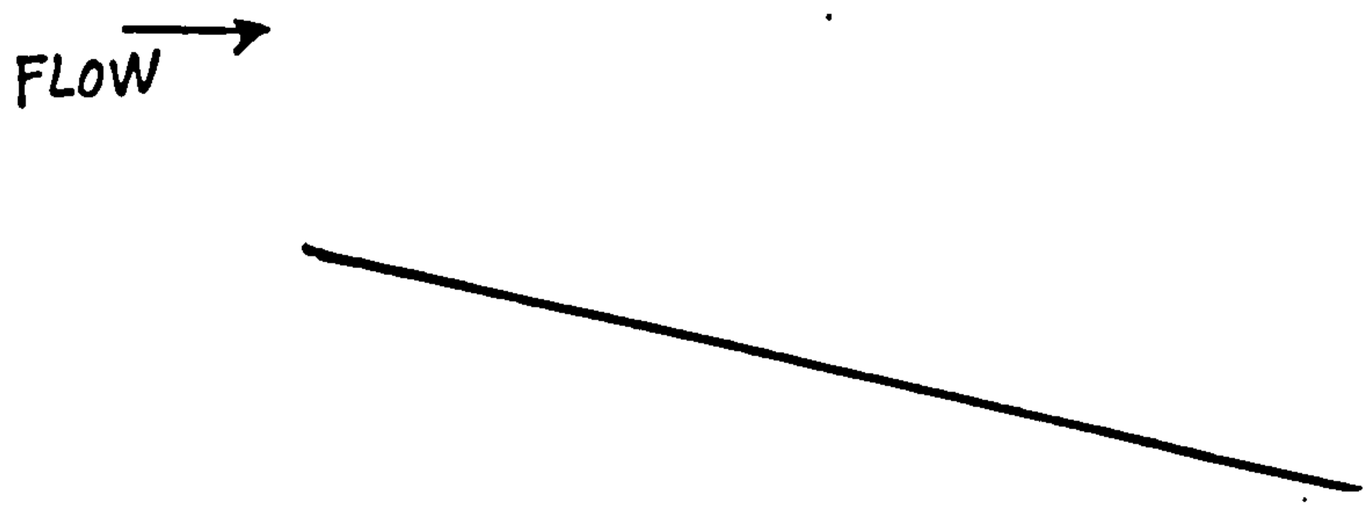

Figure-5.31 Quasi-One Dimensional Nozzle

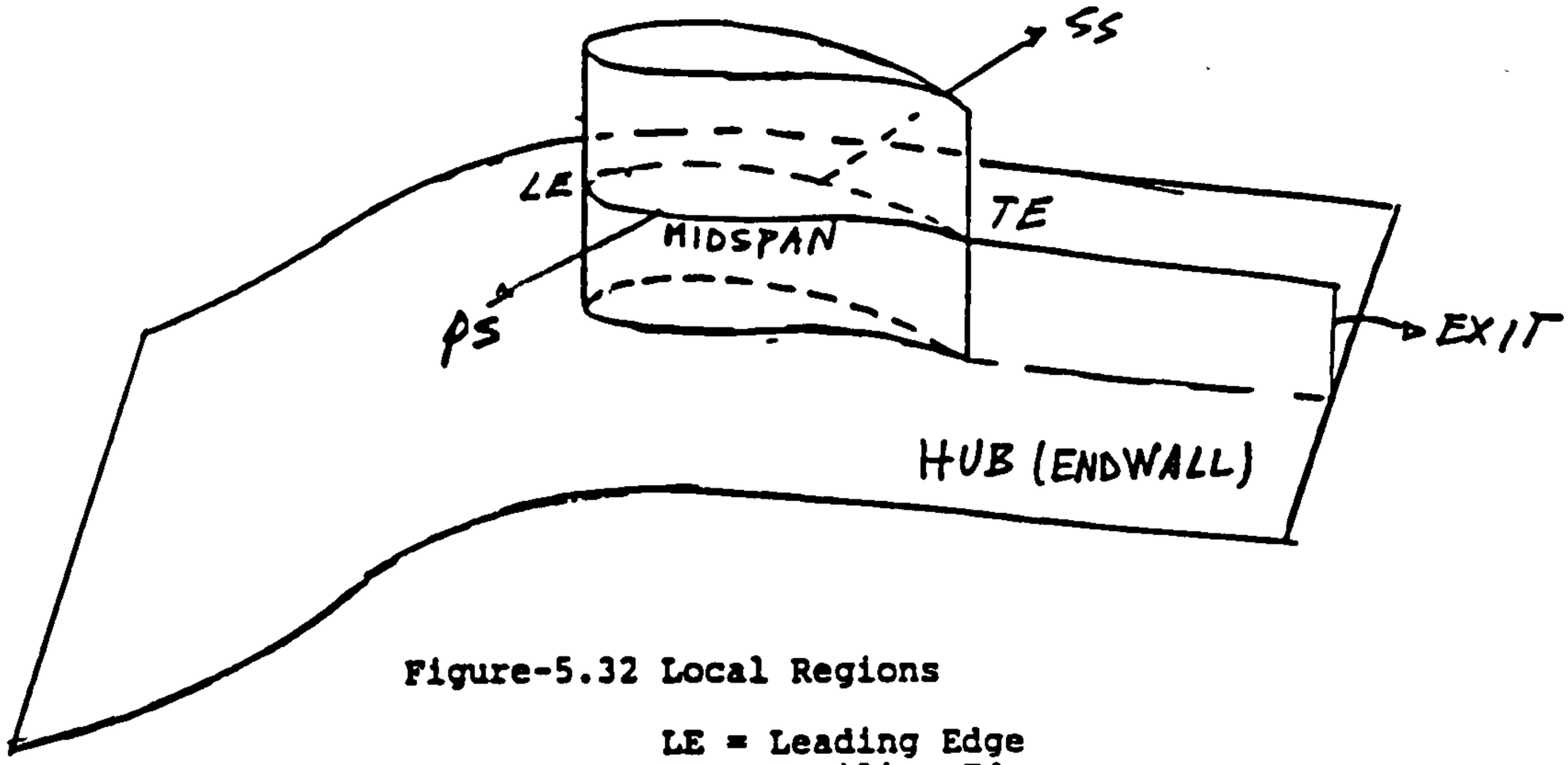

Figure-5.32 Local Regions

LE = Leading Edge
TE = Trailing Edge
SS = Suction Surface
PS = Pressure Surface

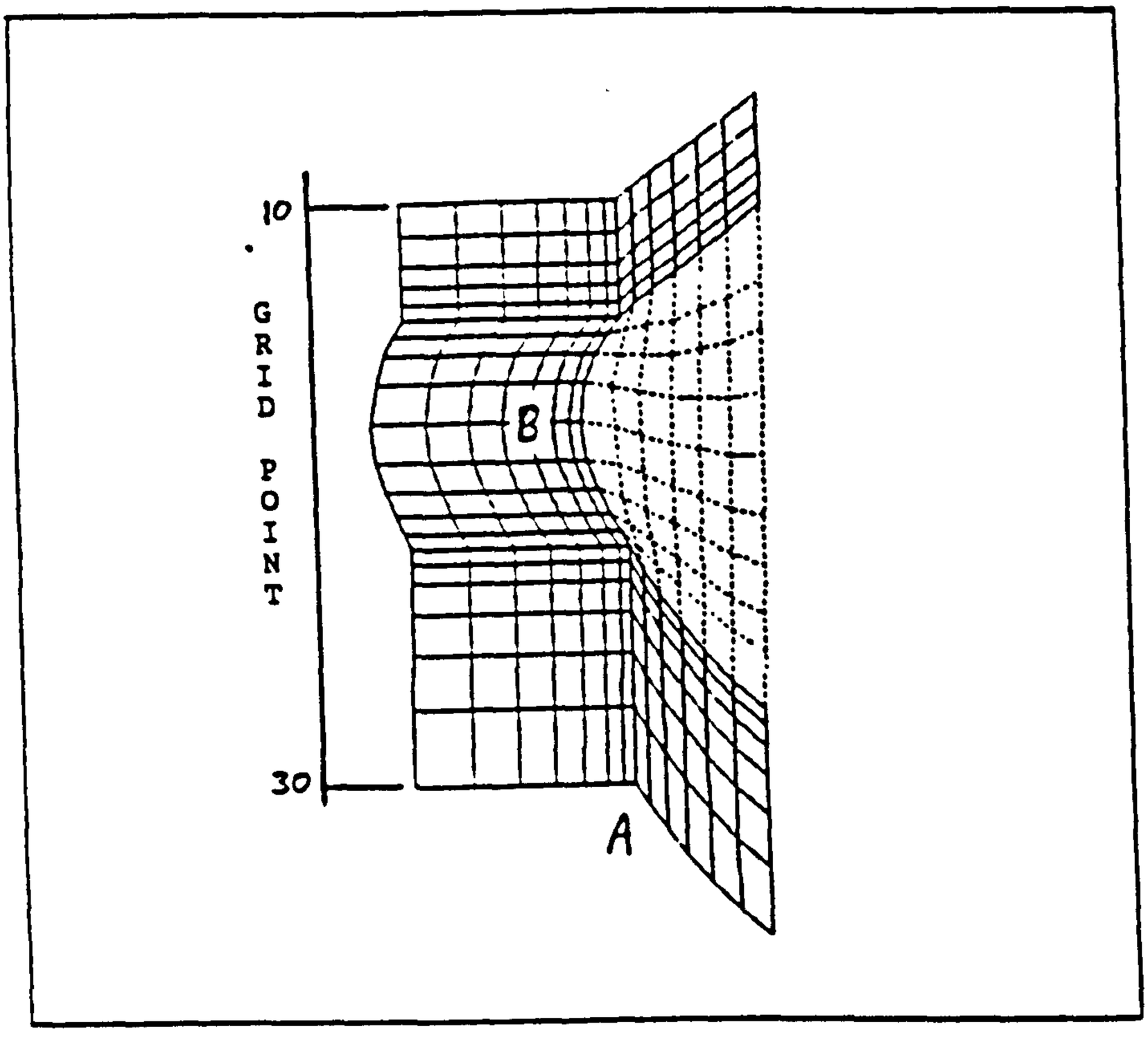

Figure-5.33 Leading Edge Region

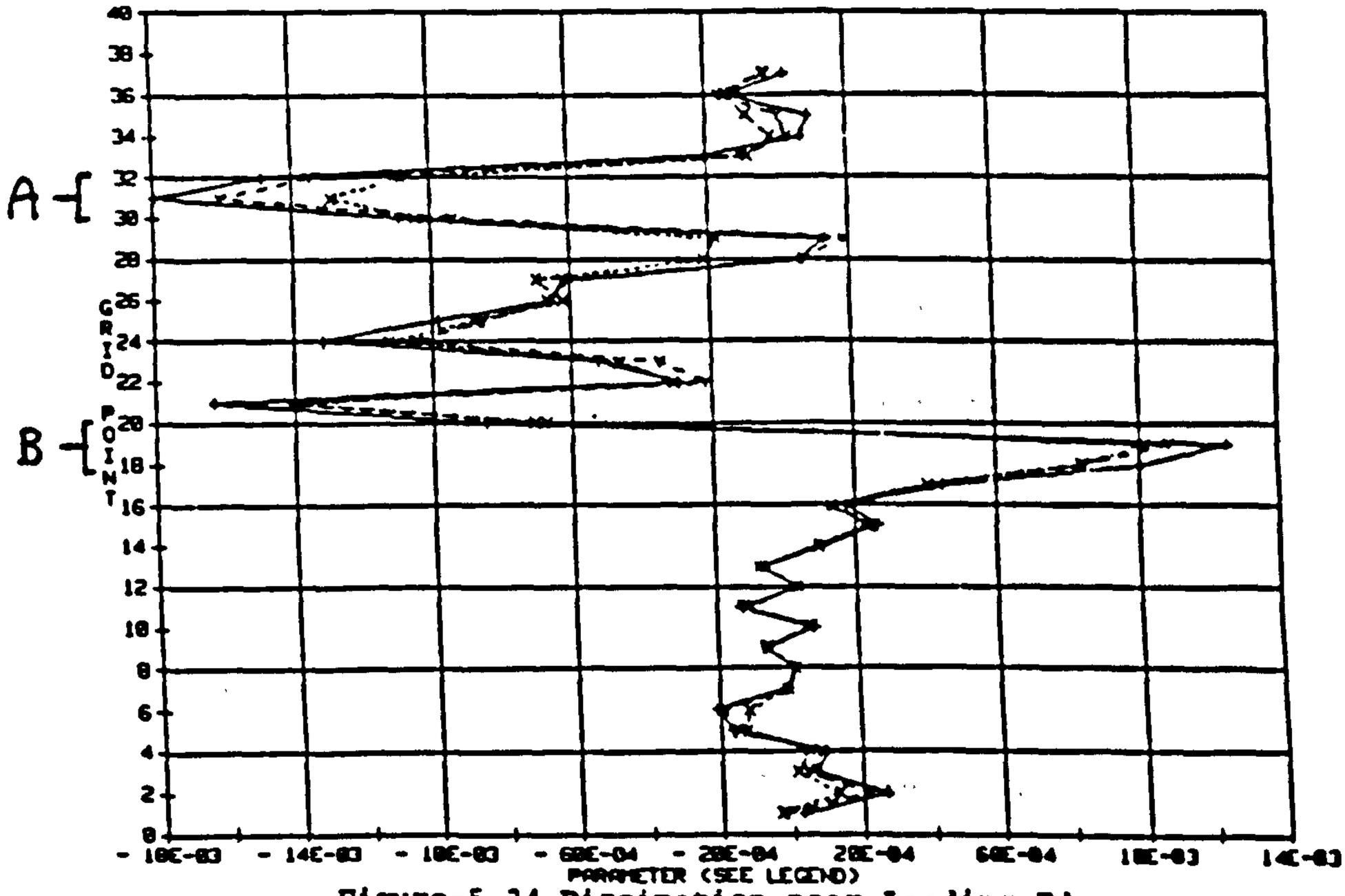

Figure-5.34 Dissipation near Leading Edge
in Blade-to-Blade Direction

-+--+- No modification.
-x--x- Aspect ratio function
-Y--Y- Gradient Function

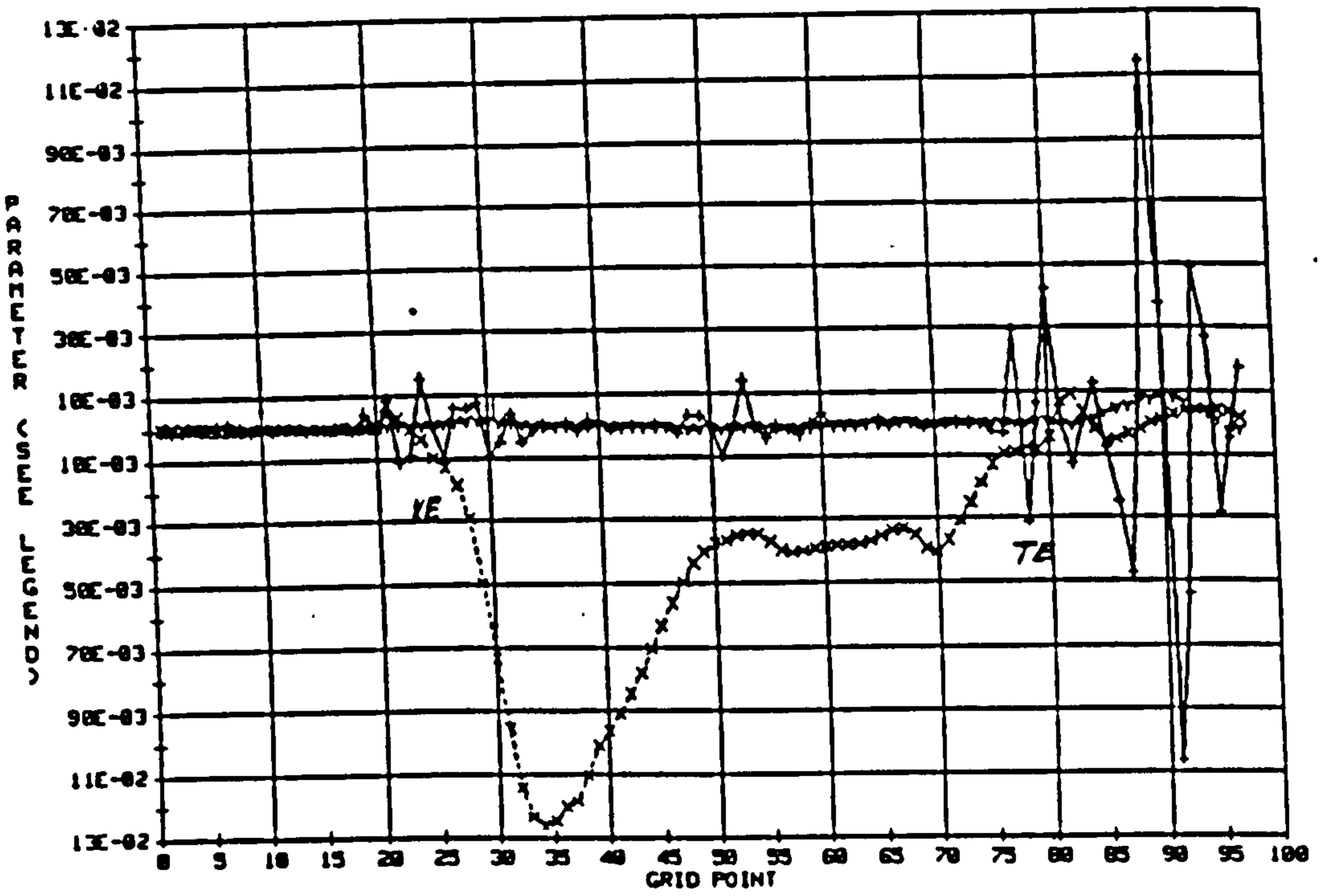

Figure-5.35 Dissipation near Suction Surface
from Inlet to Exit

-+--+- Flow Direction
-x--x- Blade to blade direction
-Y--Y- Radial direction

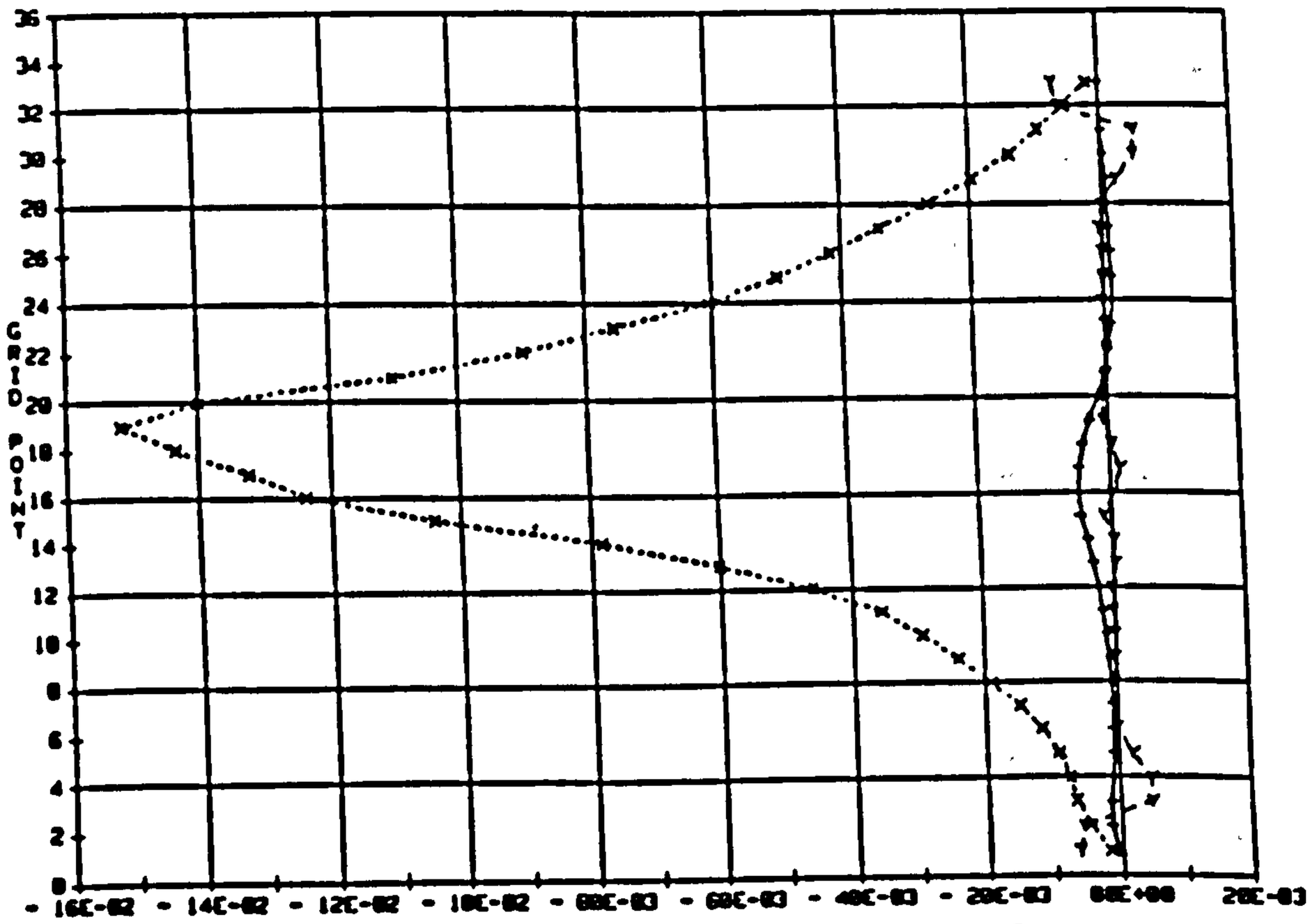

Figure-5.36 Dissipation near Suction Surface
along the Span

-+--+- Flow Direction
-x--x- Blade to blade direction
-Y--Y- Radial direction

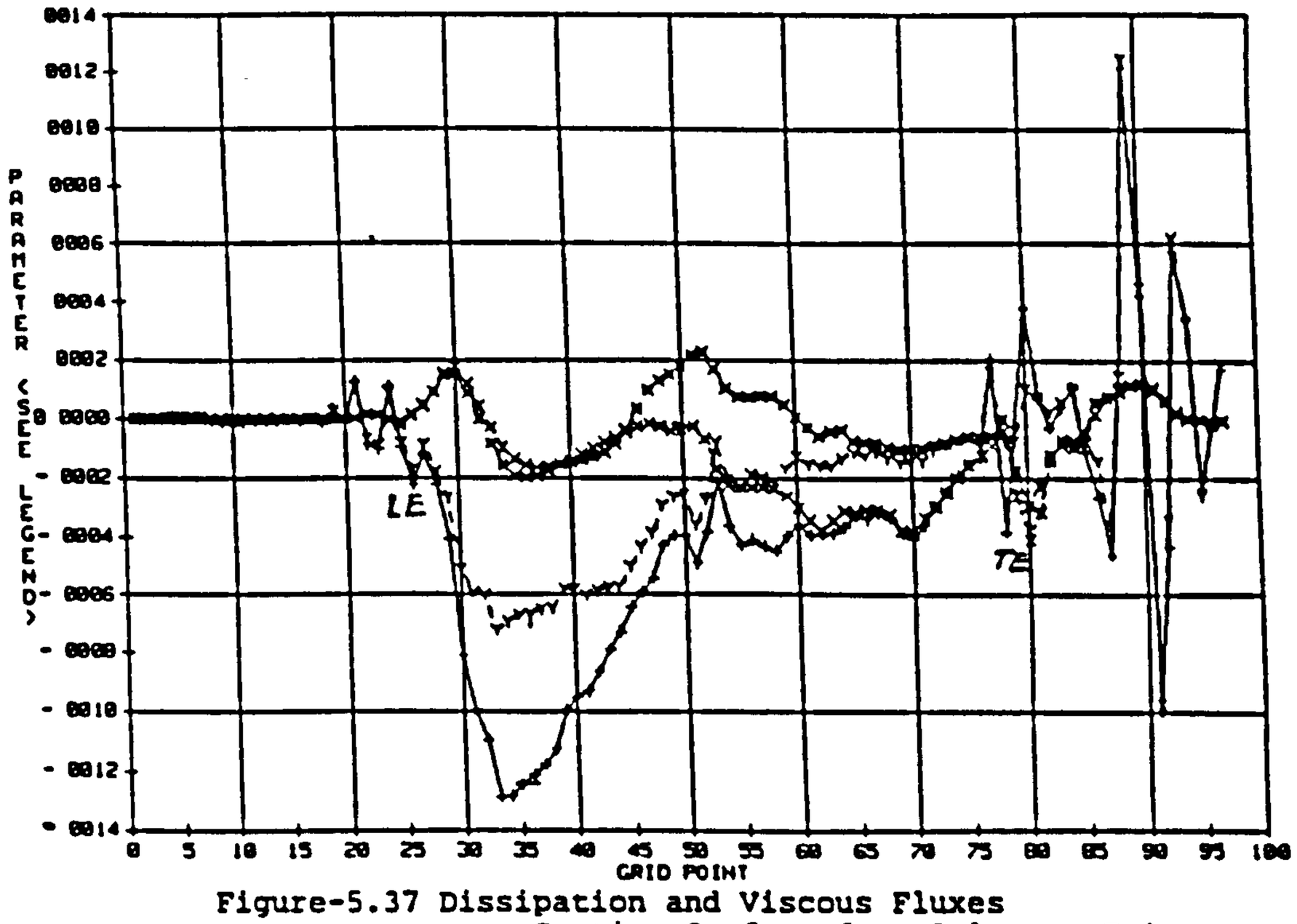

Figure-5.37 Dissipation and Viscous Fluxes
near Suction Surface from Inlet to Exit

-+--+- Dissipation without modification
-x--x- Viscous fluxes without modification
-Y--Y- Dissipation with gradient function
-x--x- Viscous fluxes with gradient function

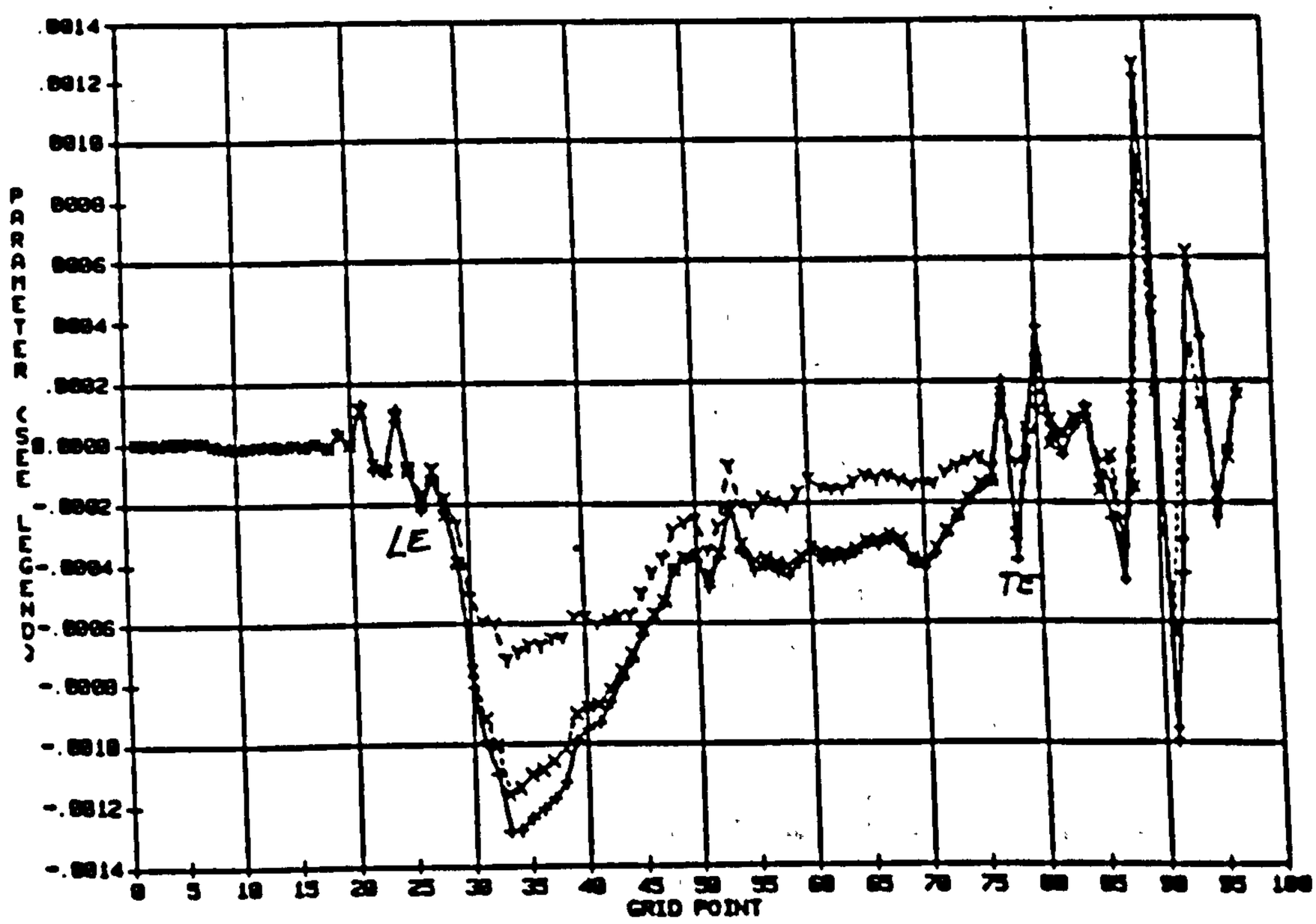

Figure-5.38 Dissipation near Suction Surface
from Inlet to Exit

-+--+- No modification
-x--x- Aspect ratio function
-Y--Y- Gradient function

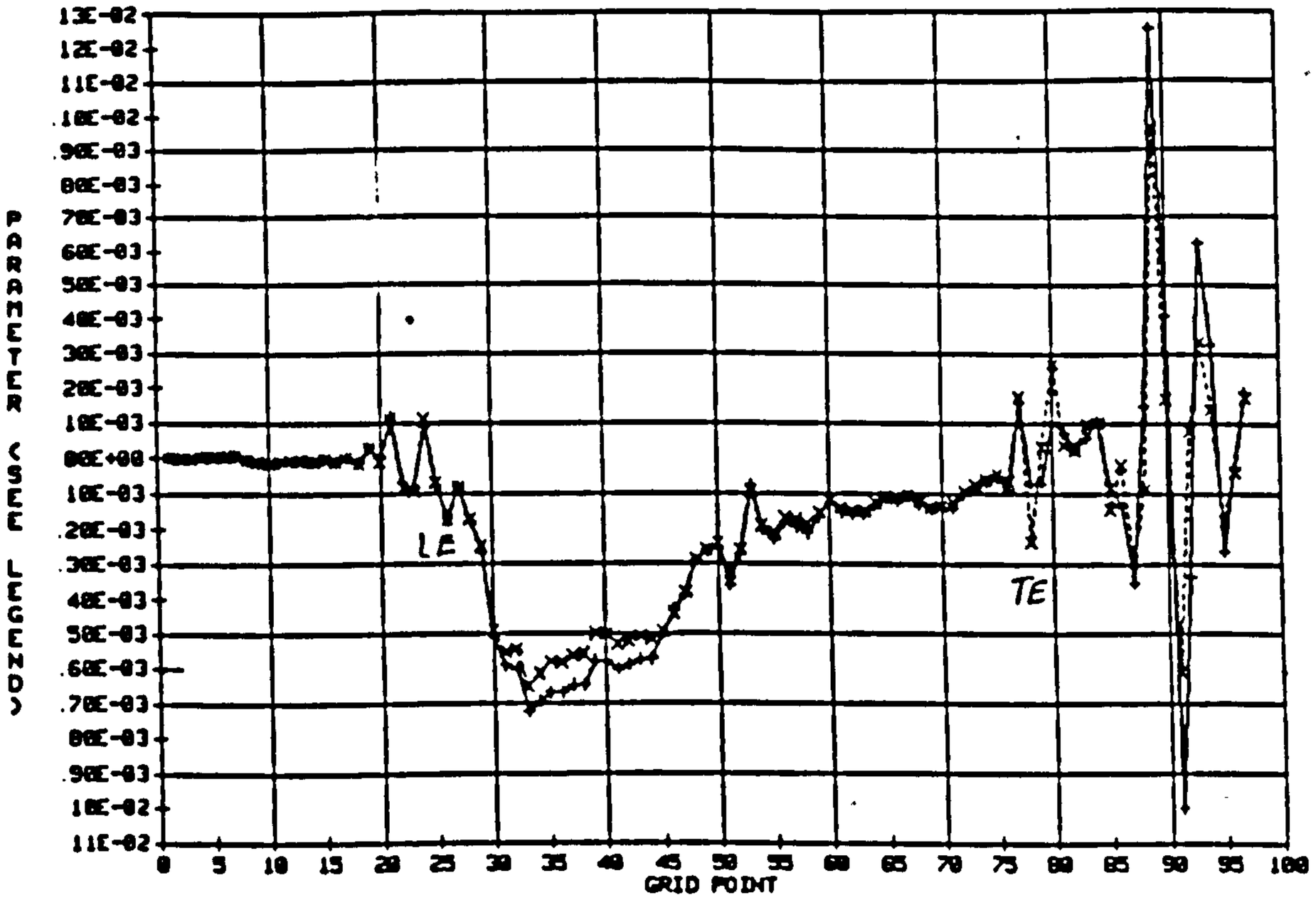

Figure-5.39 Dissipation near Suction Surface
from Inlet to Exit

-+--+- Gradient function
-x--x- Aspect ratio and gradient function

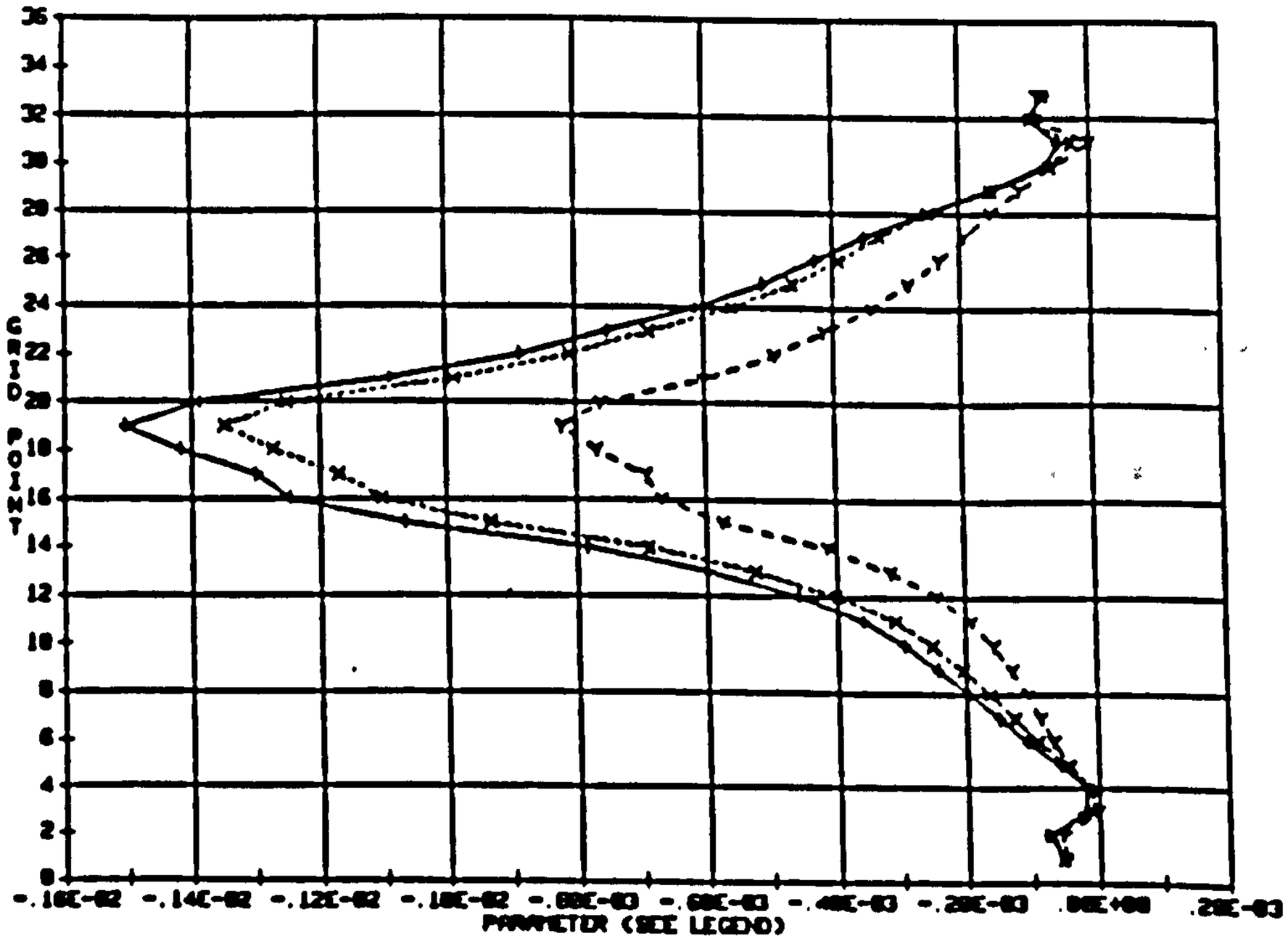

Figure-5.40 Dissipation near Suction Surface
along the Span

-+--+- No modification
-x--x- Aspect ratio function
-Y--Y- Gradient function

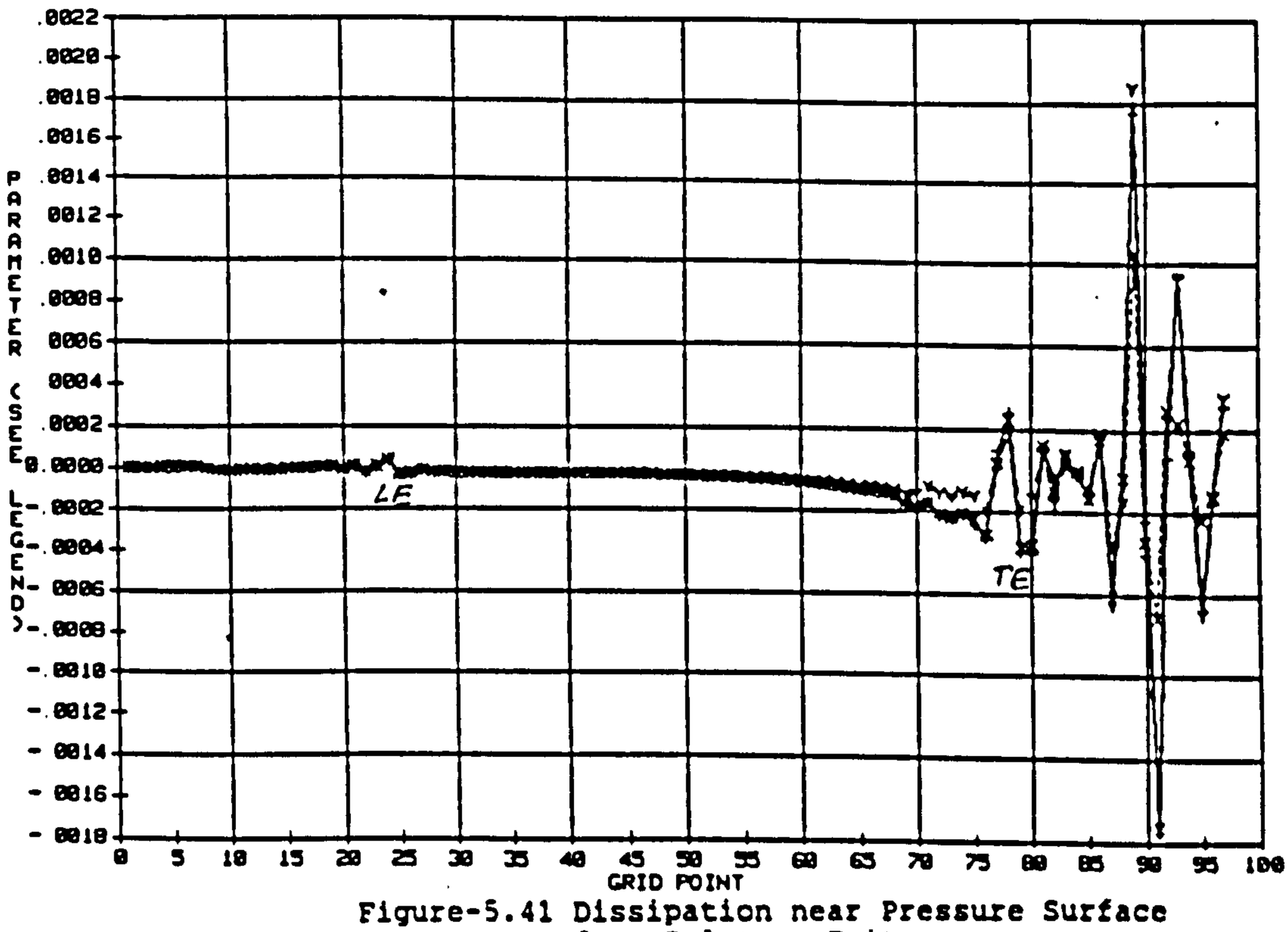

Figure-5.41 Dissipation near Pressure Surface from Inlet to Exit

-+--+- No modification
-x--x- Aspect ratio function
-Y--Y- Gradient function

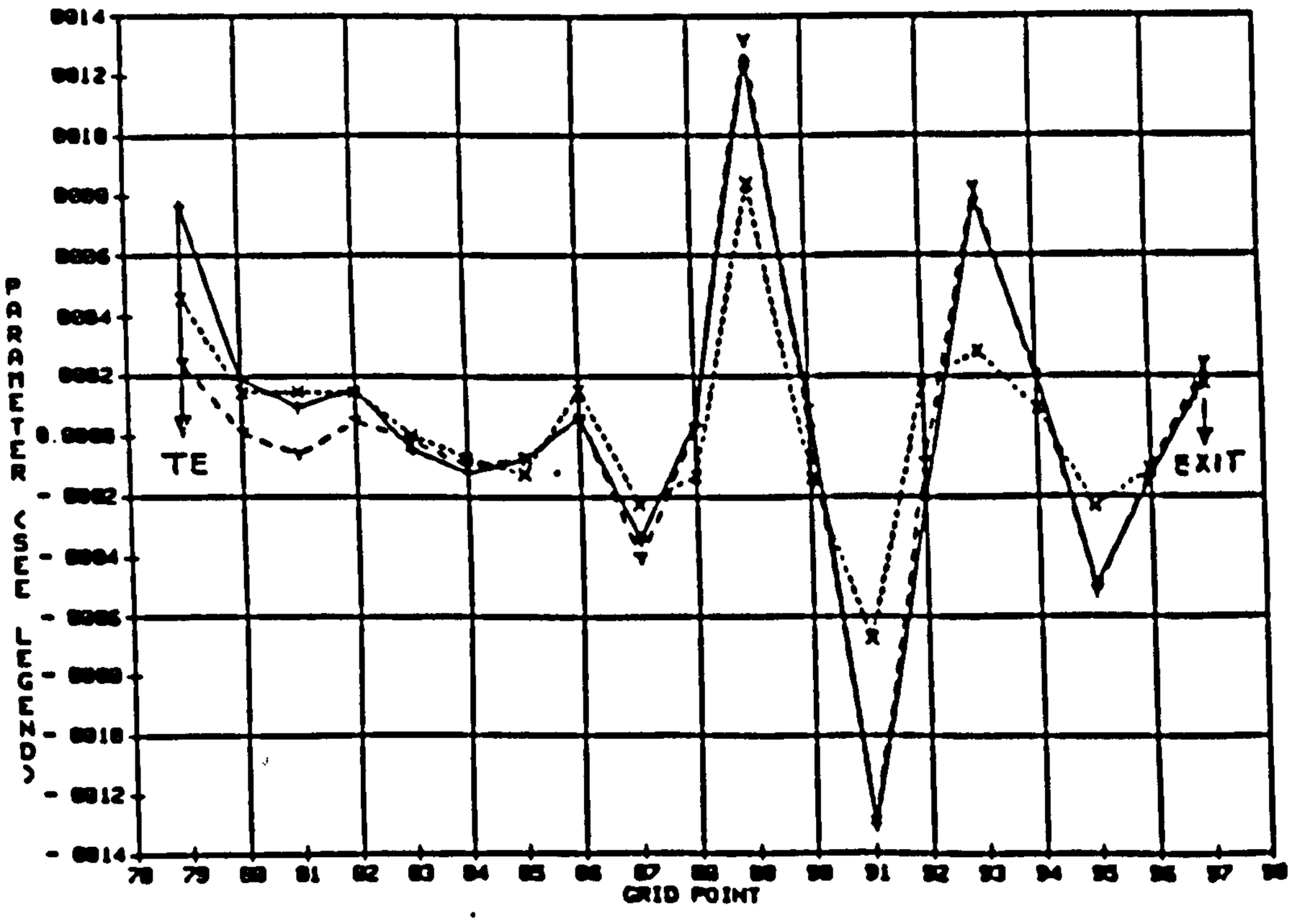

Figure-5.42 Dissipation in the Wake

-+--+- No modification
-x--x- Aspect ratio function
-Y--Y- Gradient function

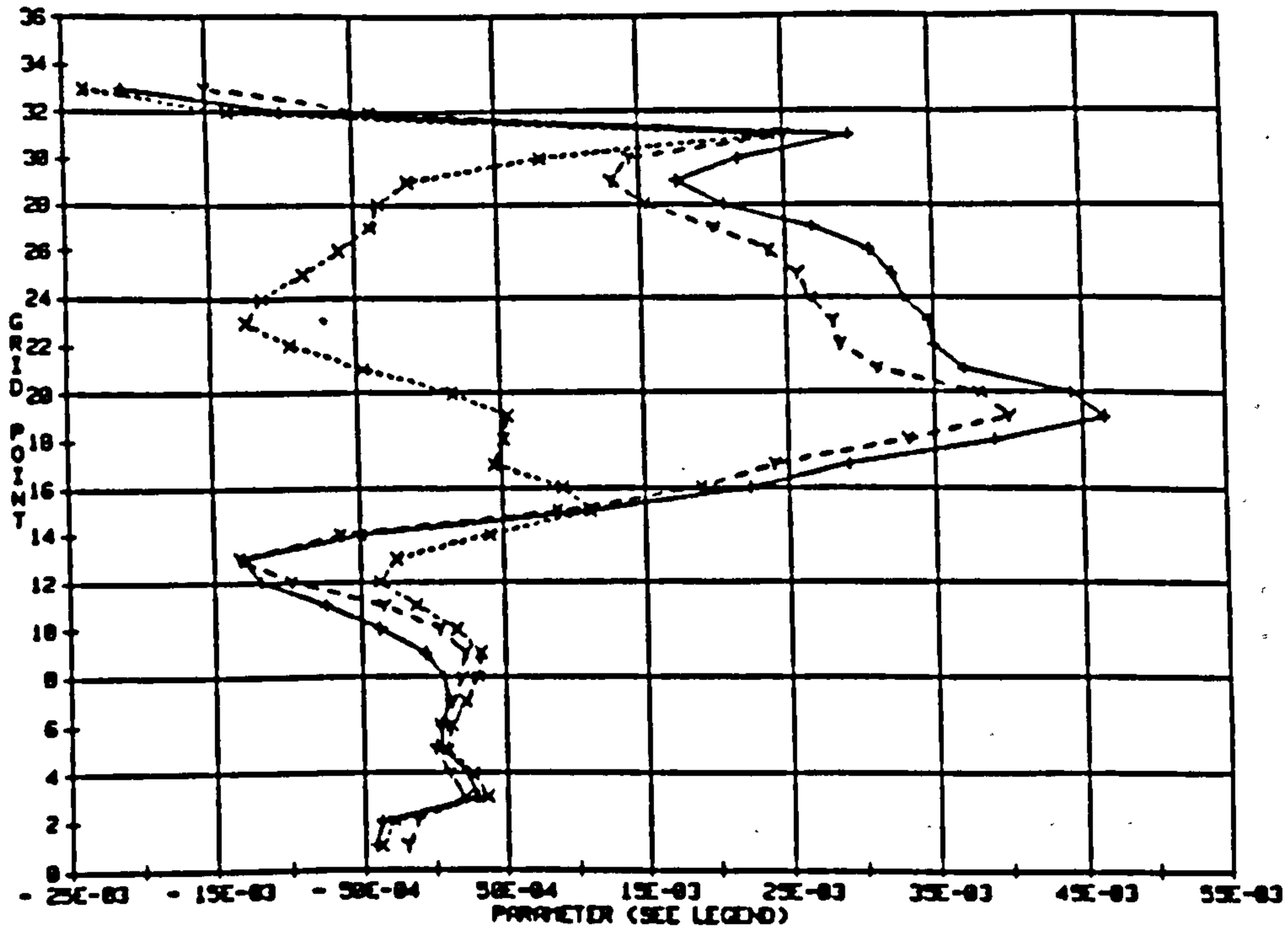

Figure-5.43 Dissipation near Exit in Wake
along the Span

-+--+- No modification
-x--x- Aspect ratio function
-Y--Y- Gradient function

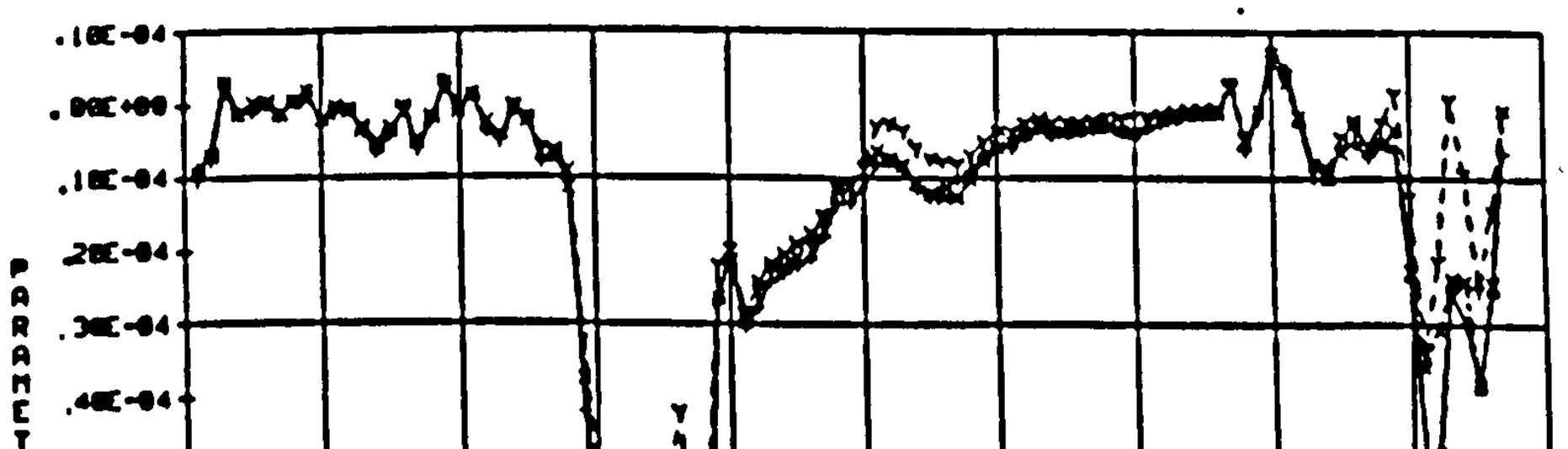

Figure-5.44 Dissipation in the Corner of
the Suction Surface and Hub

-+--+- No modification
-x--x- Aspect ratio function
-Y--Y- Gradient function

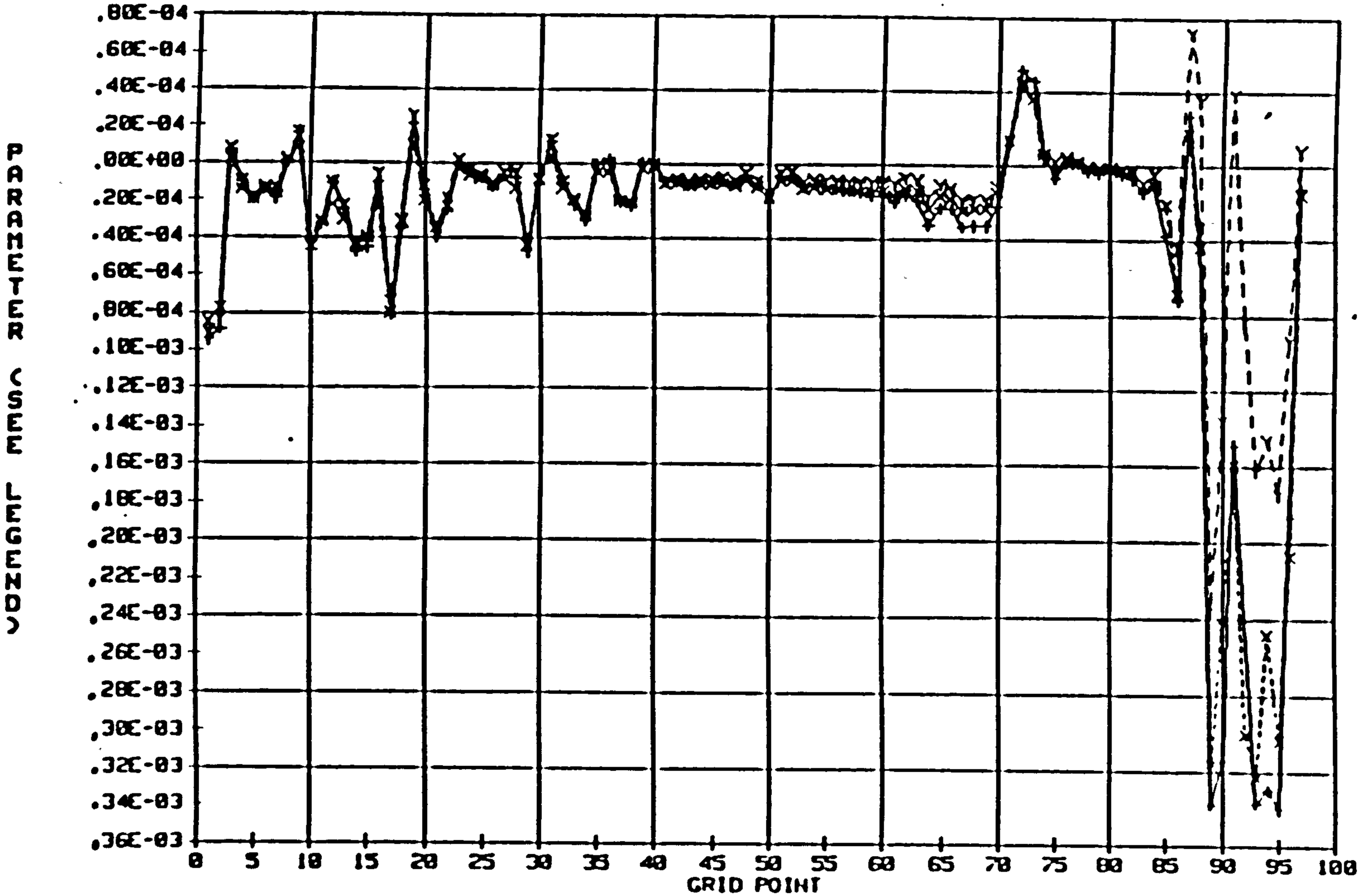

Figure-5.45 Dissipation near to the Hub away from Blade Surface from Inlet to Exit

-+--+- No modification
-x--x- Aspect ratio function
-Y--Y- Gradient function

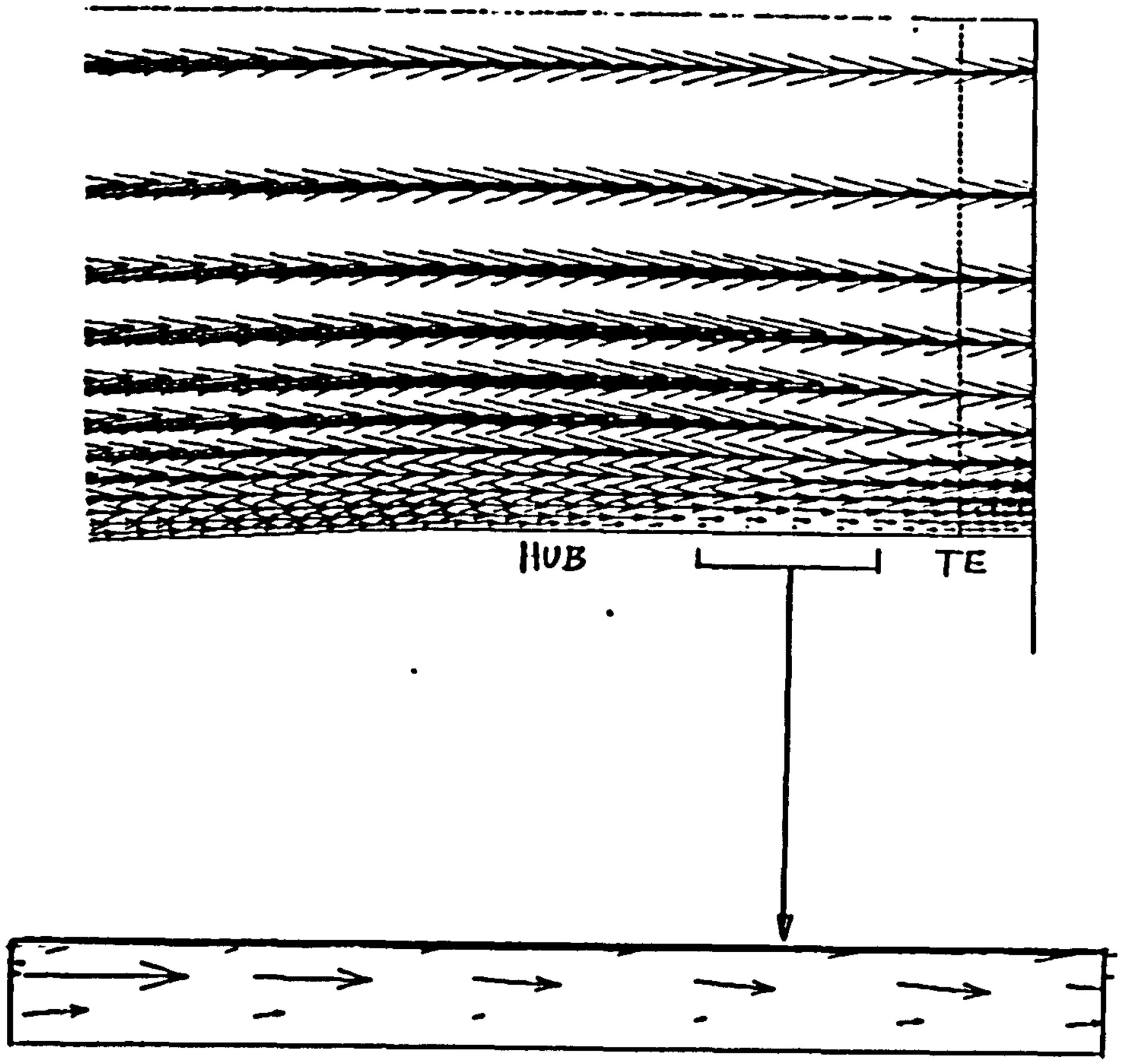

Figure-5.46a Velocity Vectors on the Meridional Plane at Mid Passage with Standard Dissipation

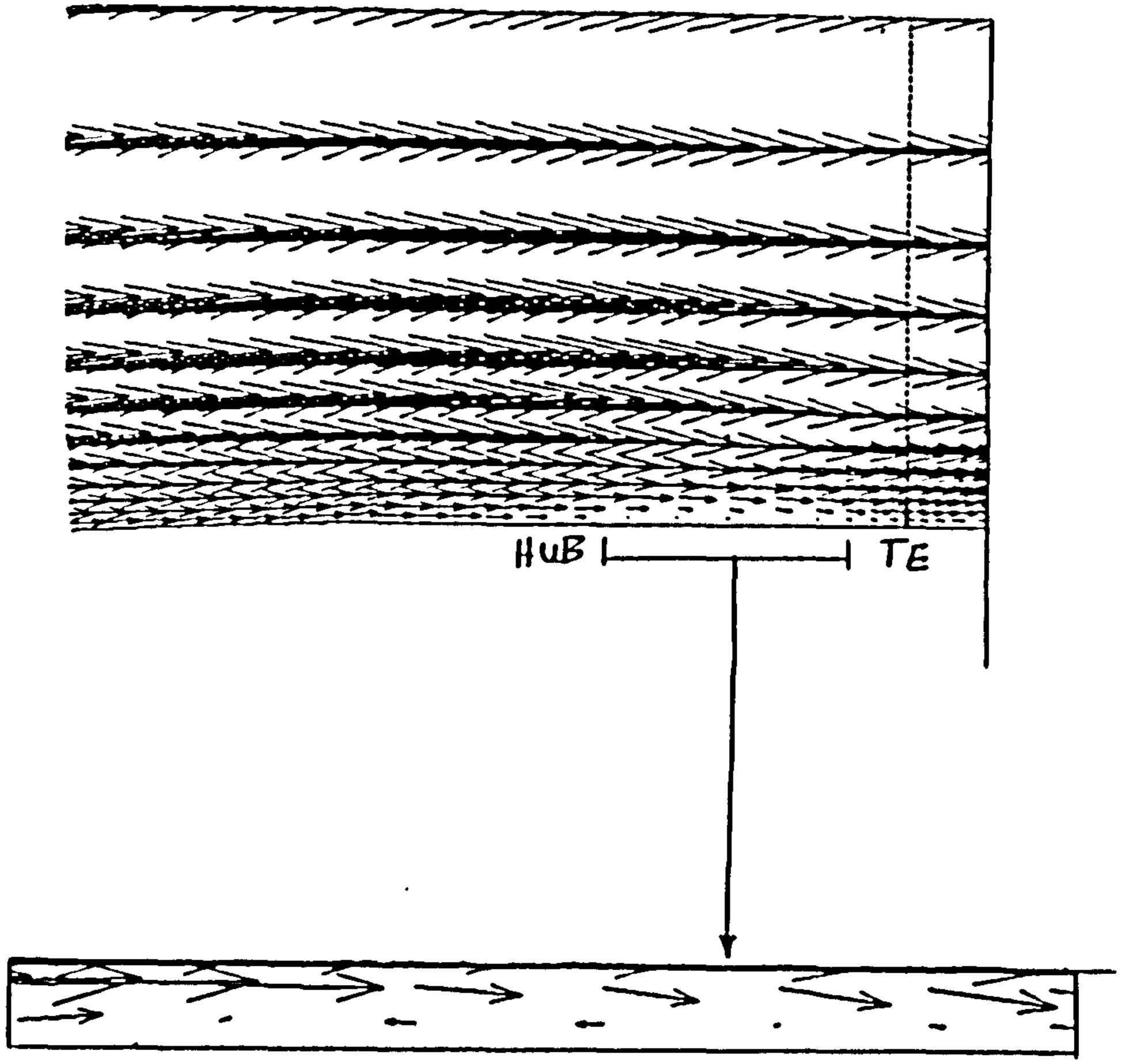

Figure-5.46b Velocity Vectors on the Meridional Plane at Mid Passage with Aspect Ratio and Gradient Functions

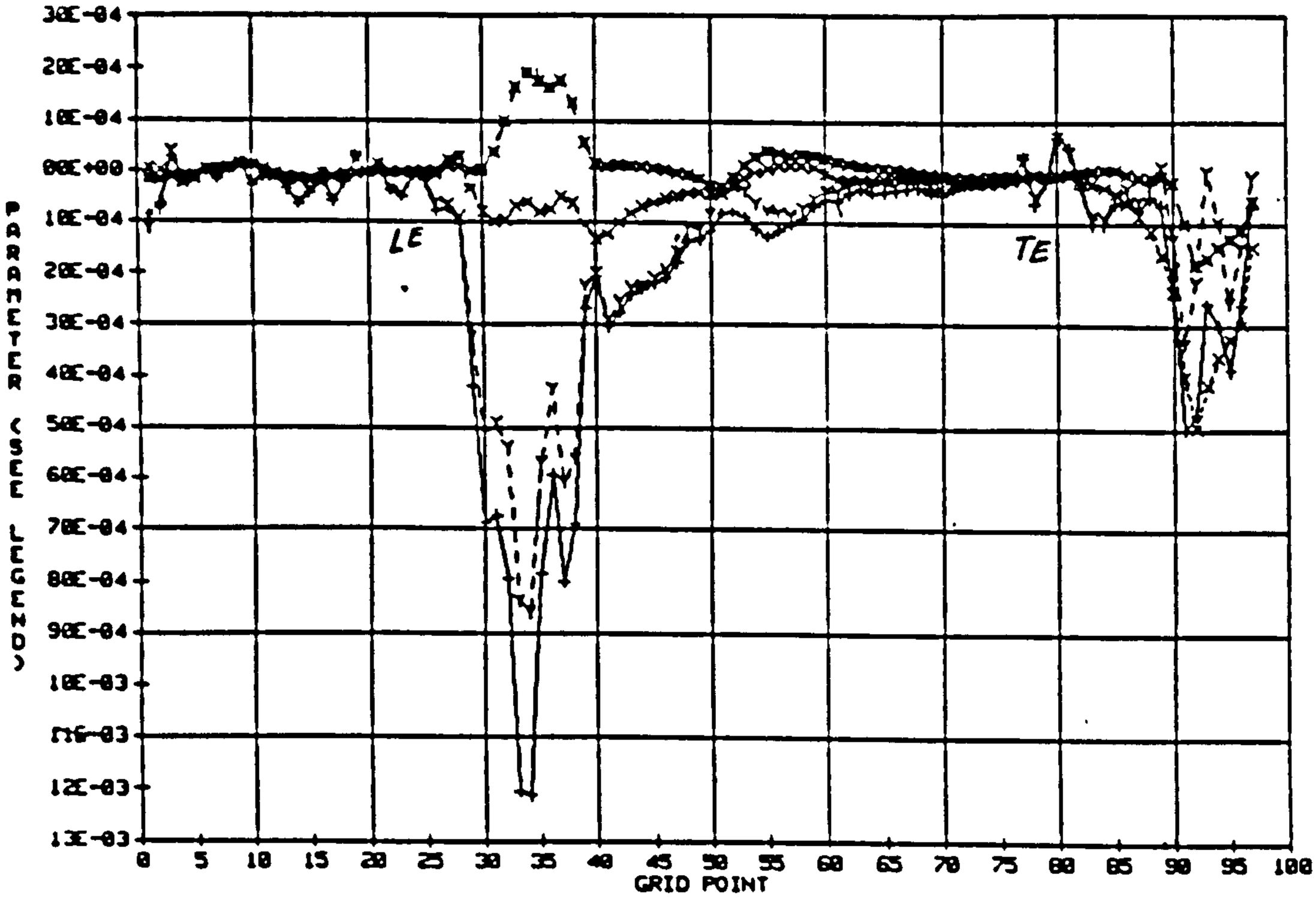

Figure-5.47 Dissipation and Viscous Fluxes at the Corner of the Hub and the Suction Surface from Inlet to Exit

-+--+- Dissipation without modification
-x--x- Viscous fluxes without modification
-Y--Y- Dissipation with gradient function
-*--*- Viscous fluxes with gradient function

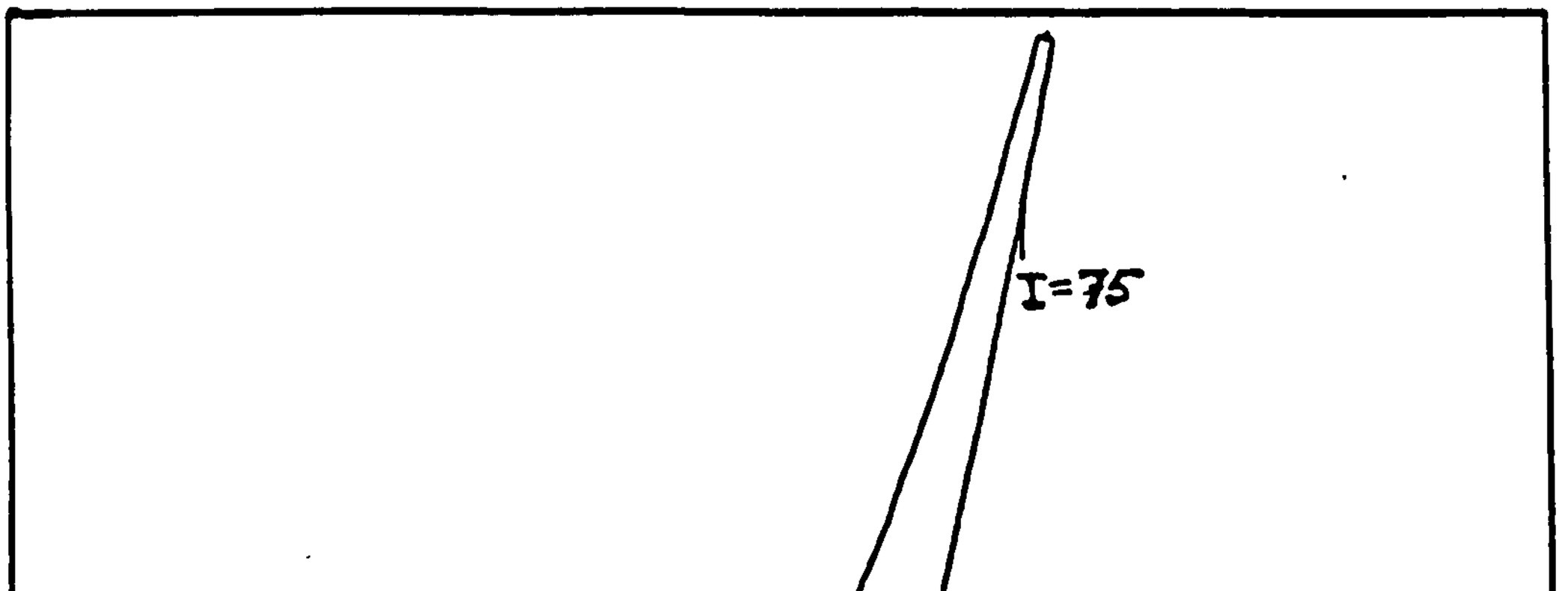

Figure-5.48 Axial Plane Locations

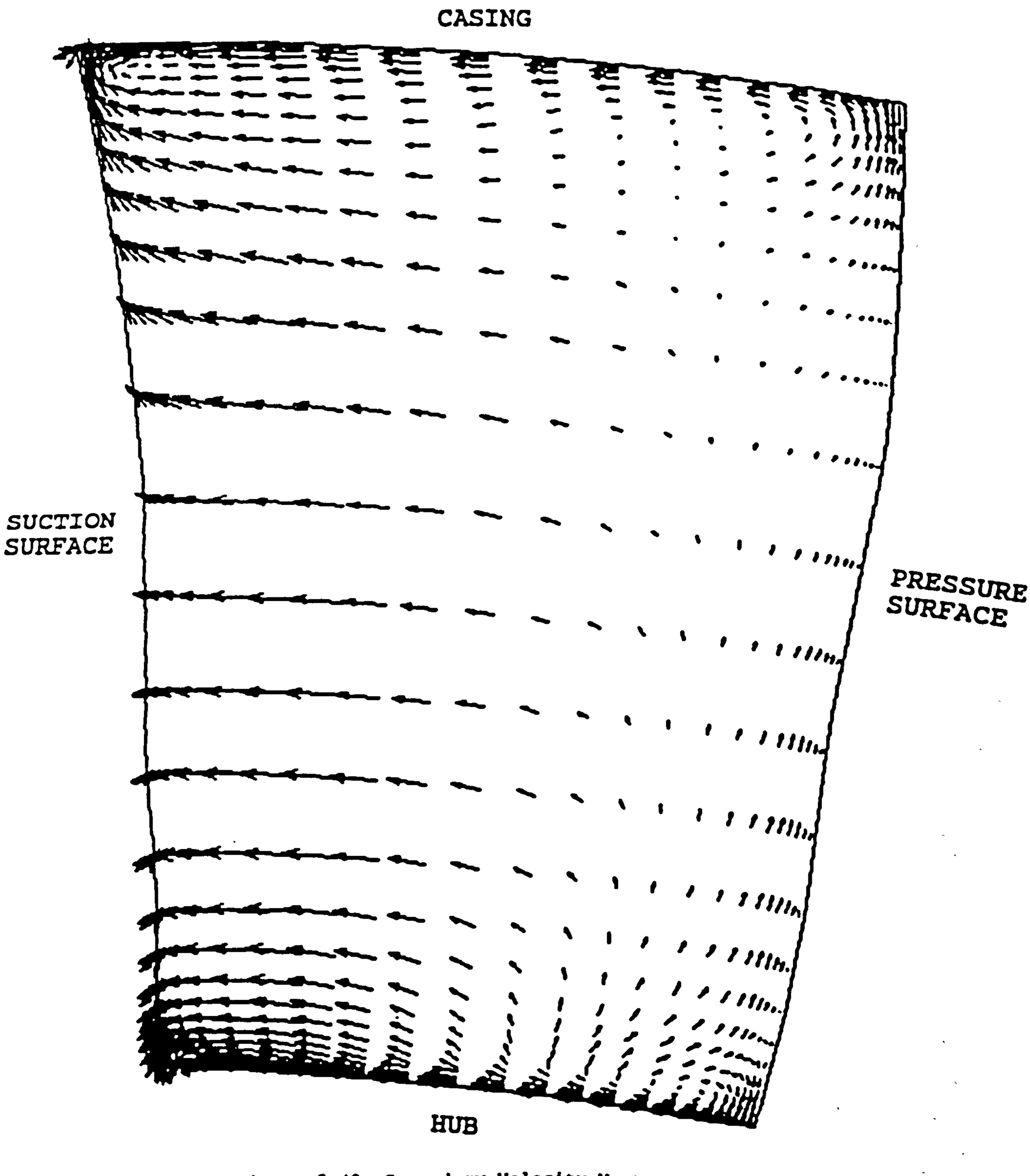

Figure-5.49a Secondary Velocity Vectors
at I=34 (see figure-5.48)
with Standard Dissipation

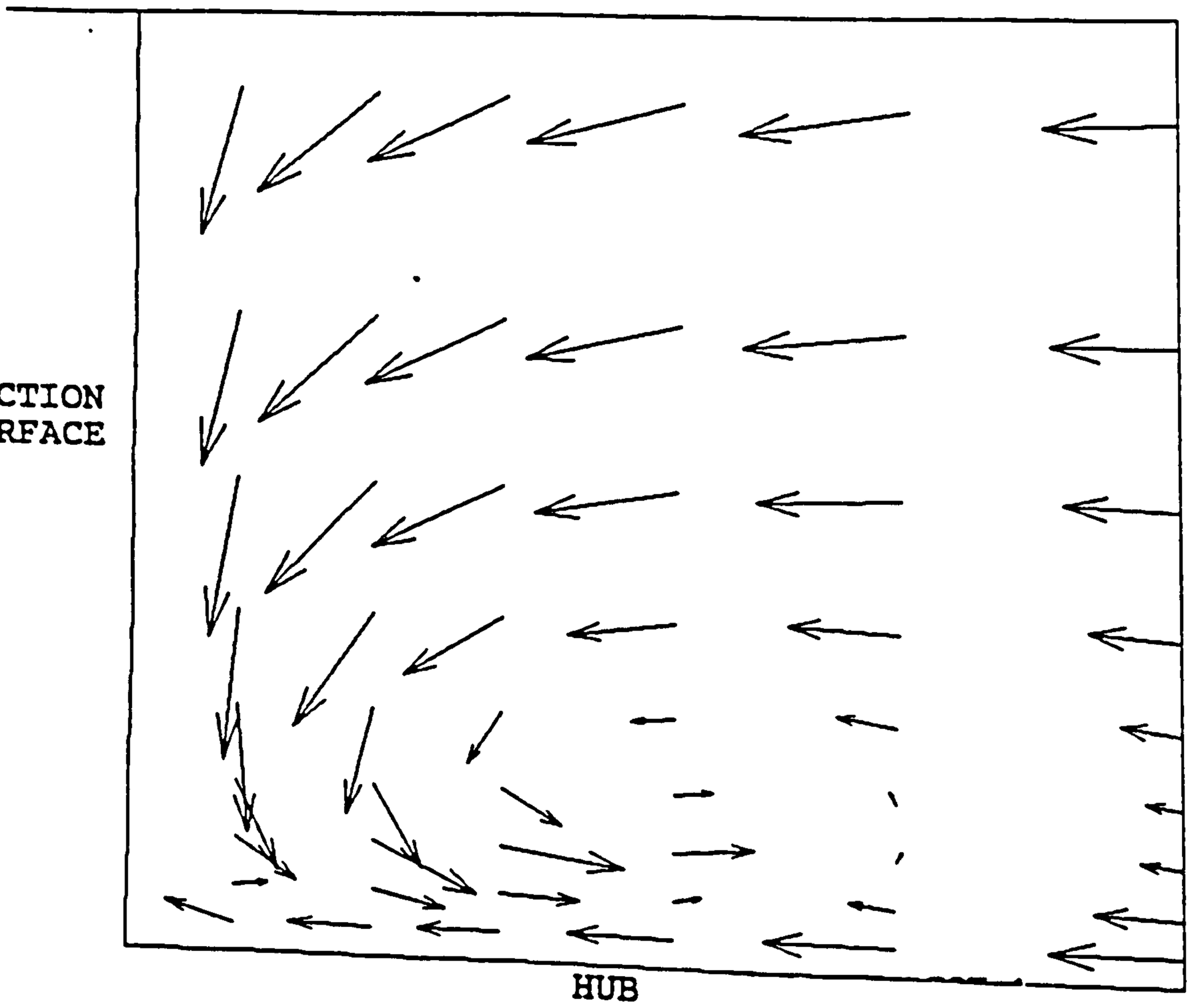

Figure-5.49b Horseshoe Vortex at Axial Plane
I=34 (see figure-5.48) in the
Corner of the Hub and the Suction Surface

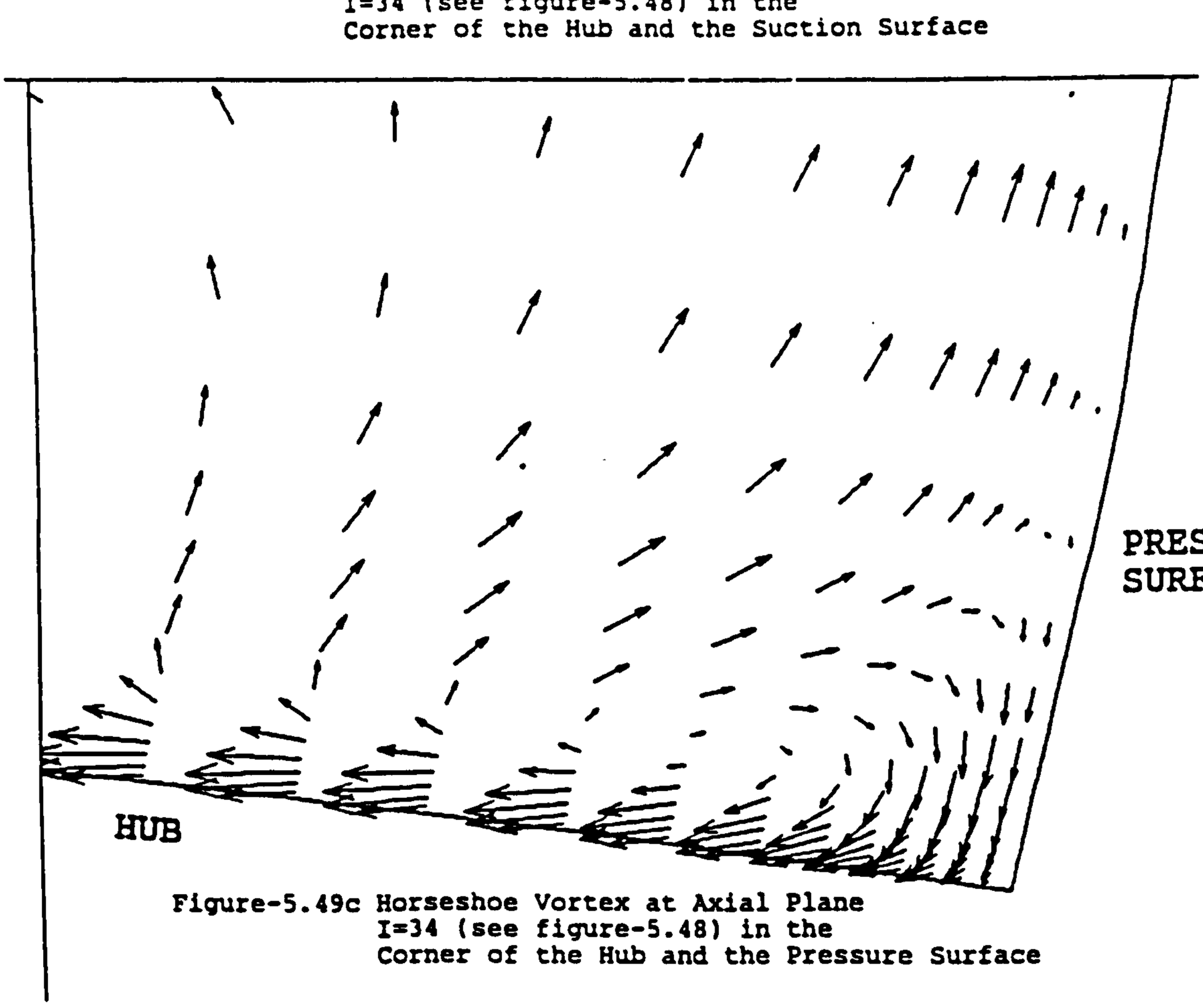

Figure-5.49c Horseshoe Vortex at Axial Plane
I=34 (see figure-5.48) in the
Corner of the Hub and the Pressure Surface

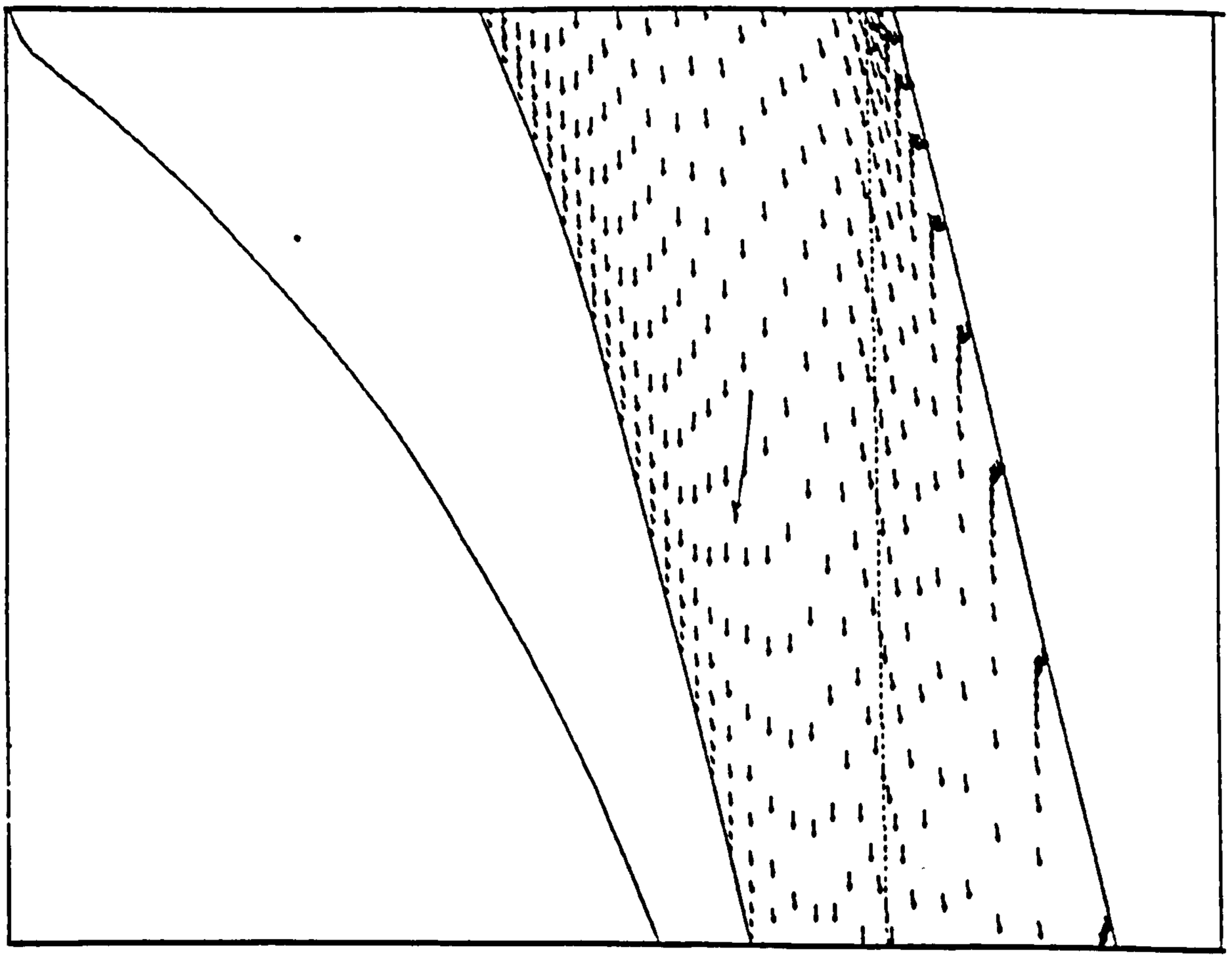

Figure-5.50 Velocity Vectors on the
Blade-to-Blade Plane near to the Hub

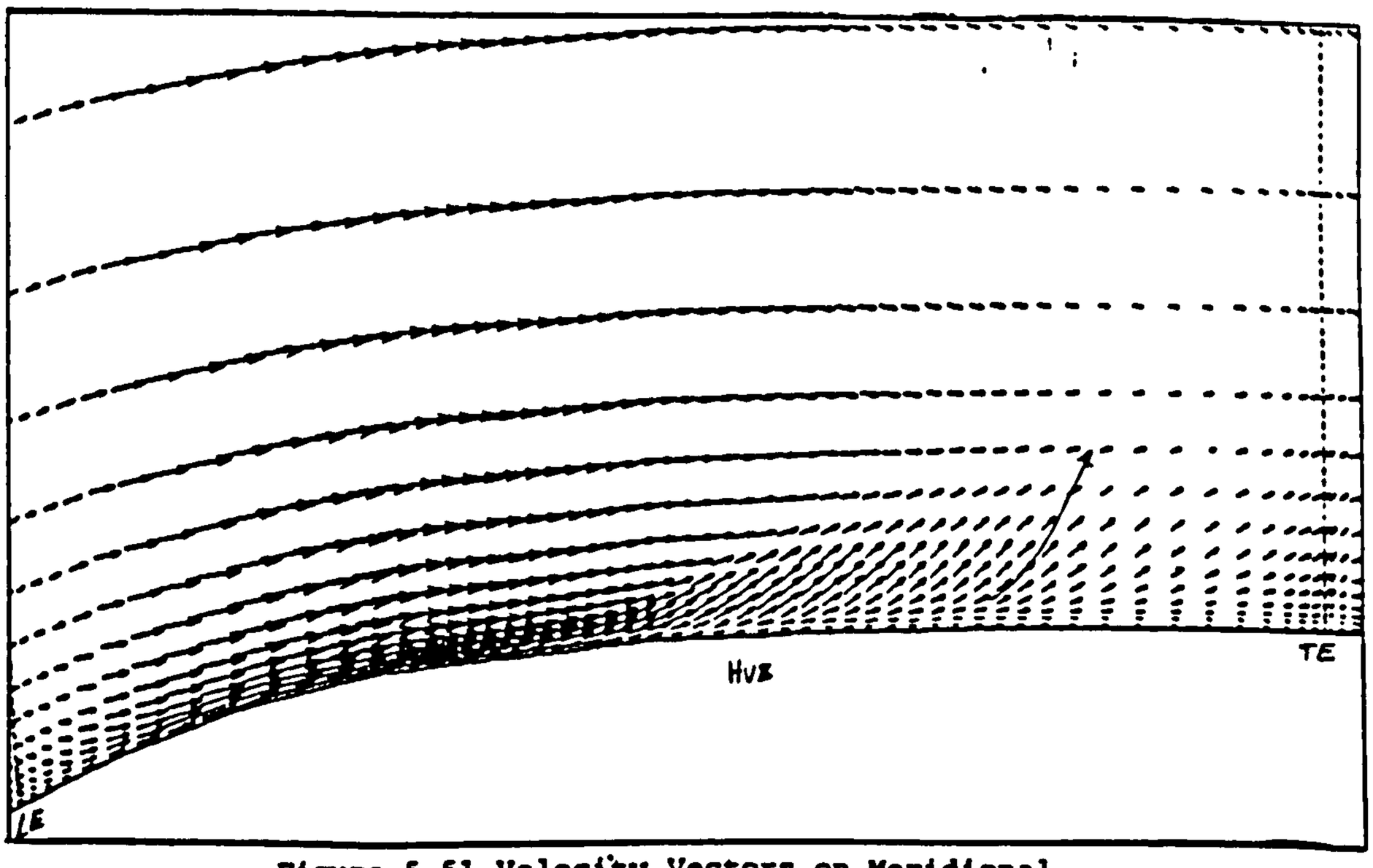

Figure-5.51 Velocity Vectors on Meridional
Plane near Suction Surface

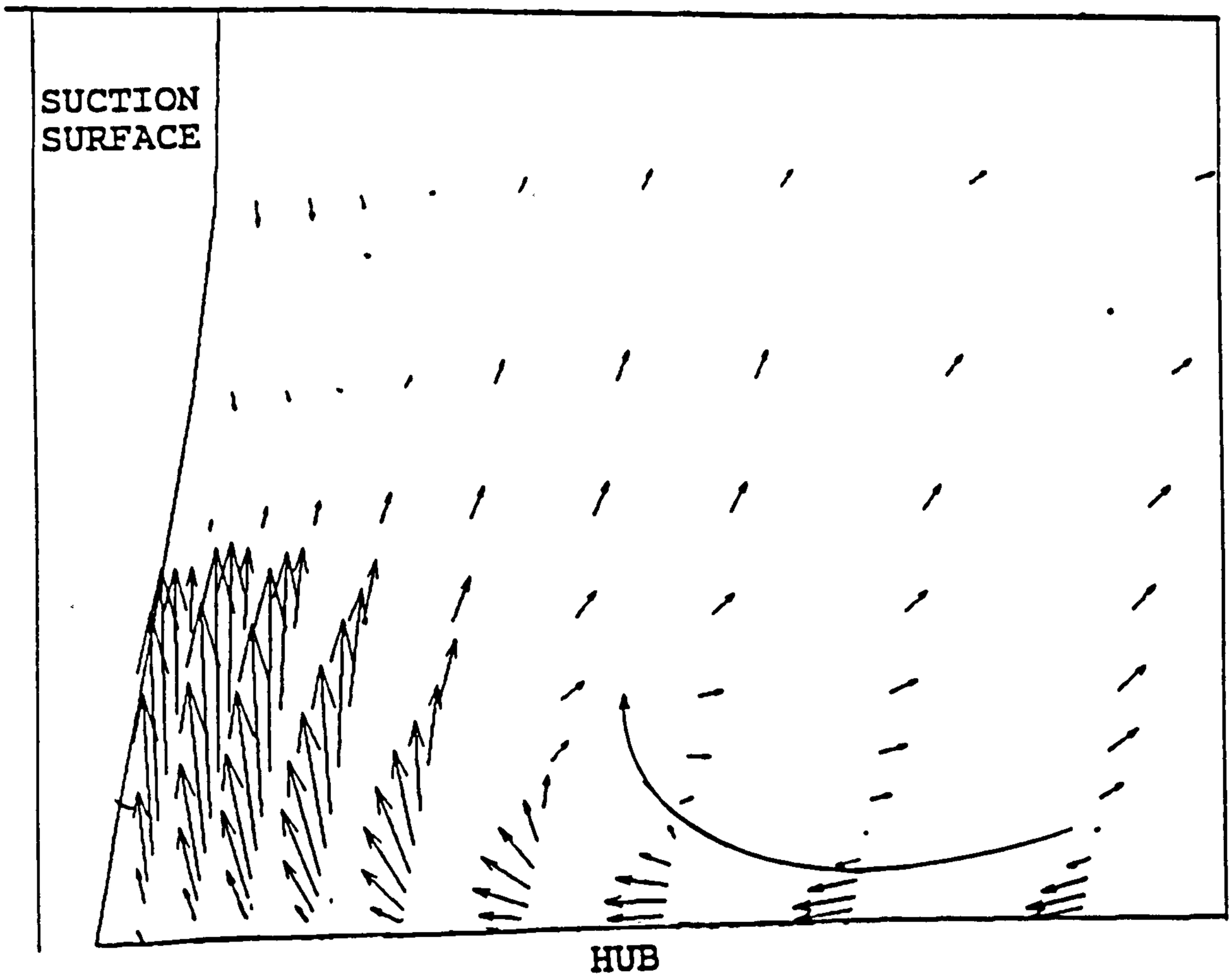

Figure-5.52 Passage Vortex at Axial Plane
I=62 (see figure-5.48)

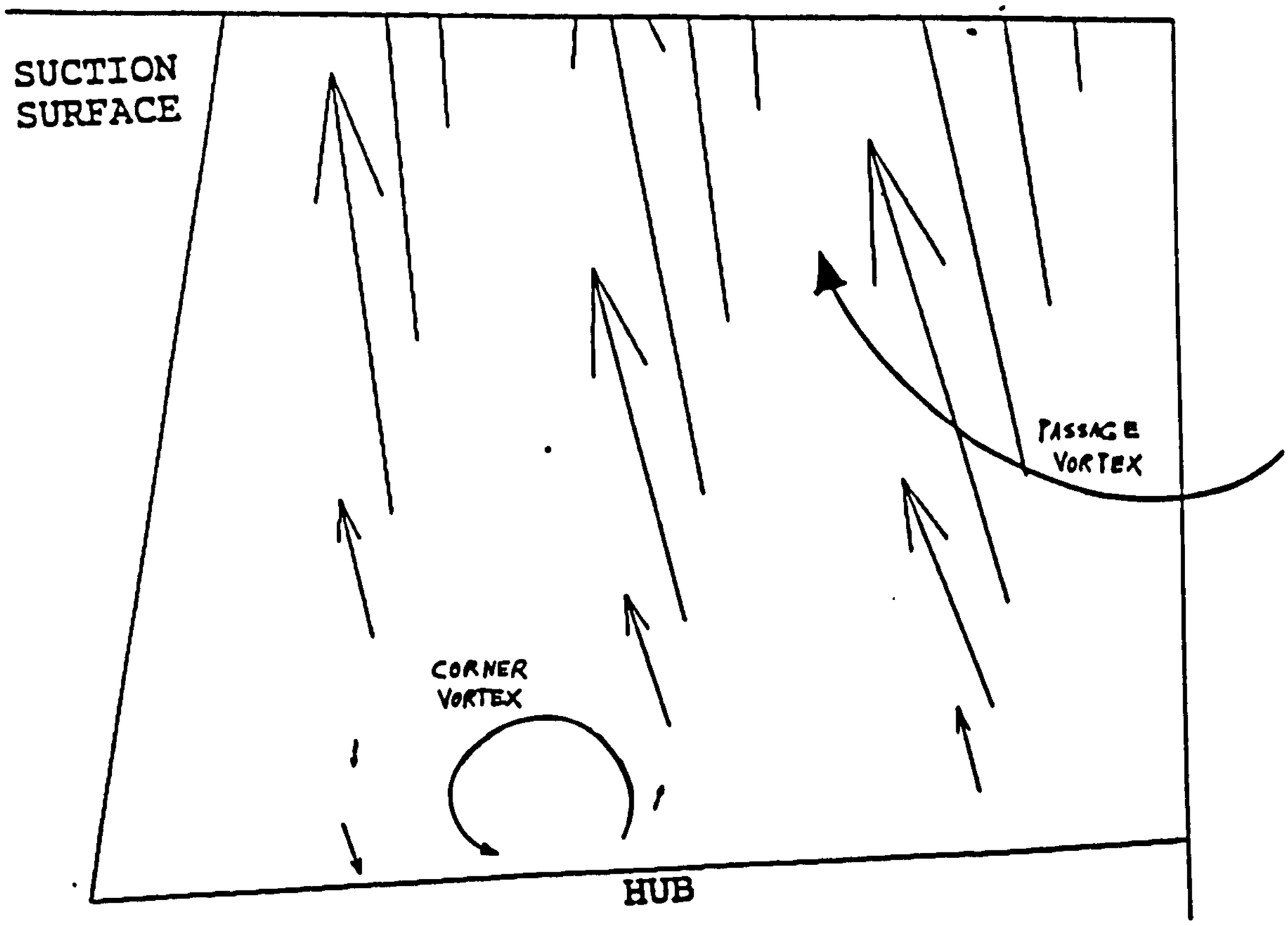

Figure-5.53 Passage and Corner Vortices
at Axial Plane I=64
(see figure-5.48)

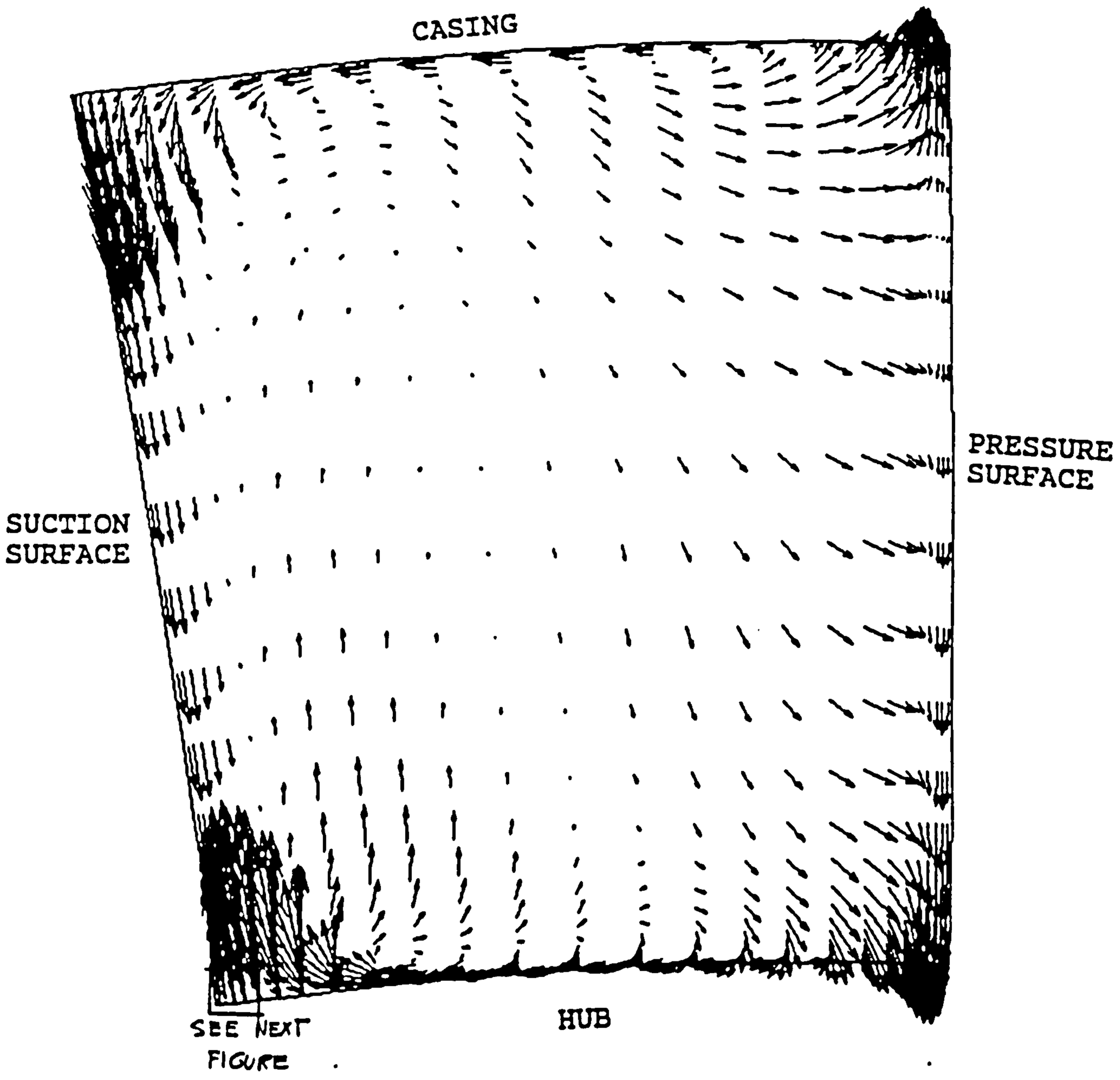

Figure-5.54a Secondary Velocity Vectors near to Trailing edge at I=75 (see figure-5.48) with standard Dissipation

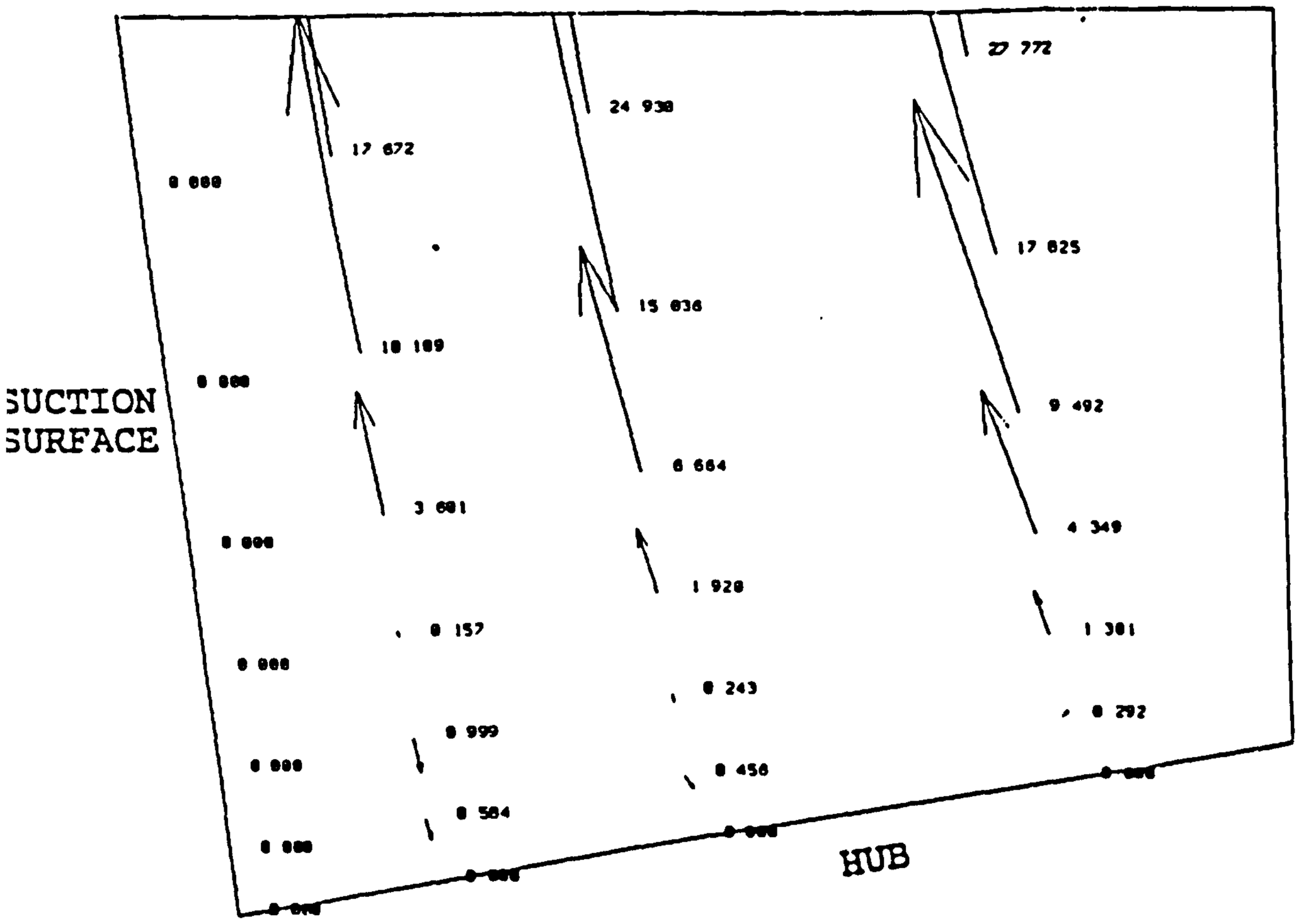

Figure-5.54b Secondary Velocity Vectors
(enlargement of figure-5.54a)

Figure-5.54c Secondary Velocity Vectors
near to Trailing edge at I=75
(see figure-5.48) with
Aspect Ratio and Gradient Function

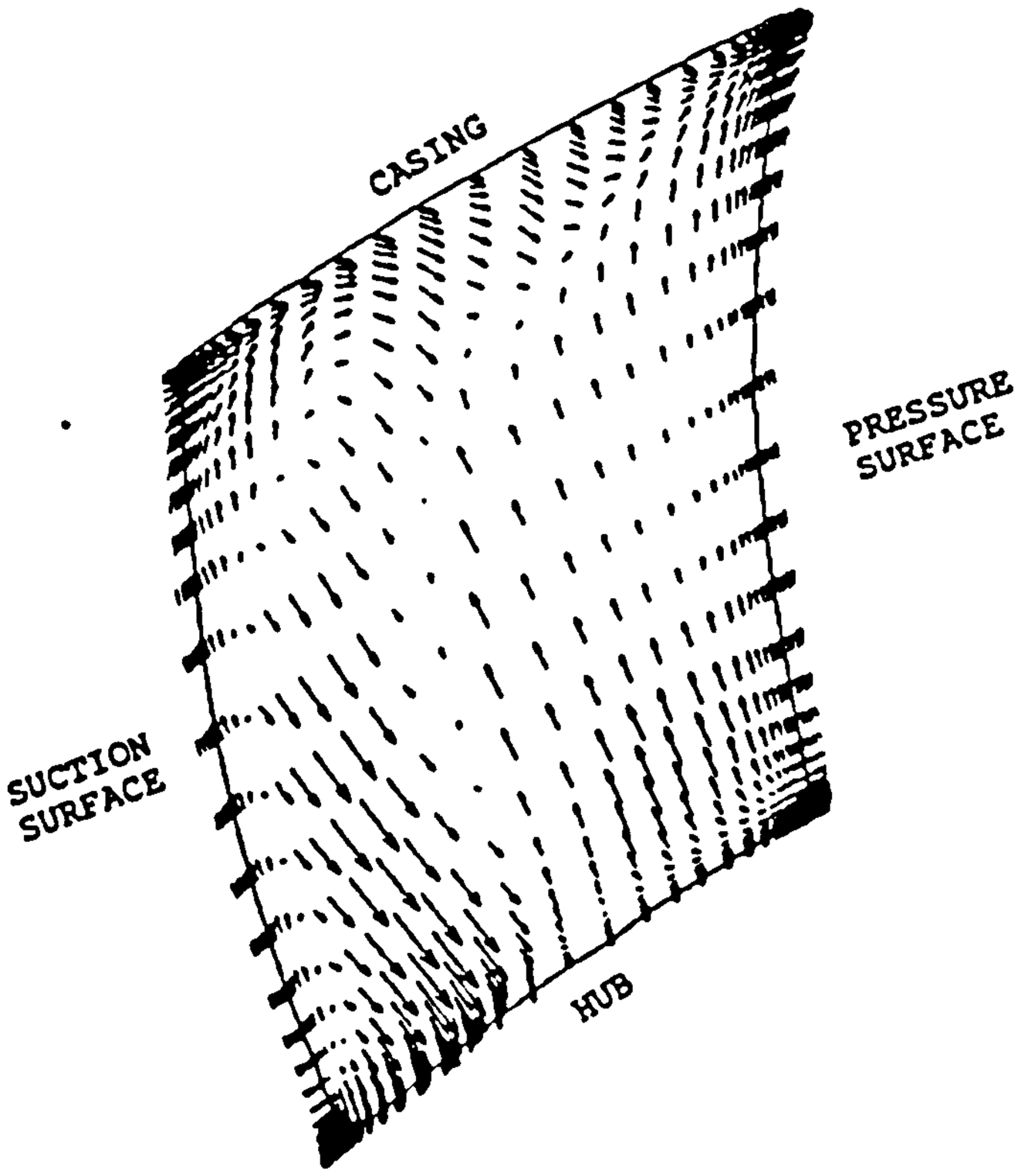

Figure-5.55a Secondary Flow on the Axial Plane near to the Exit without modification. Three Dimensional High Pressure Turbine

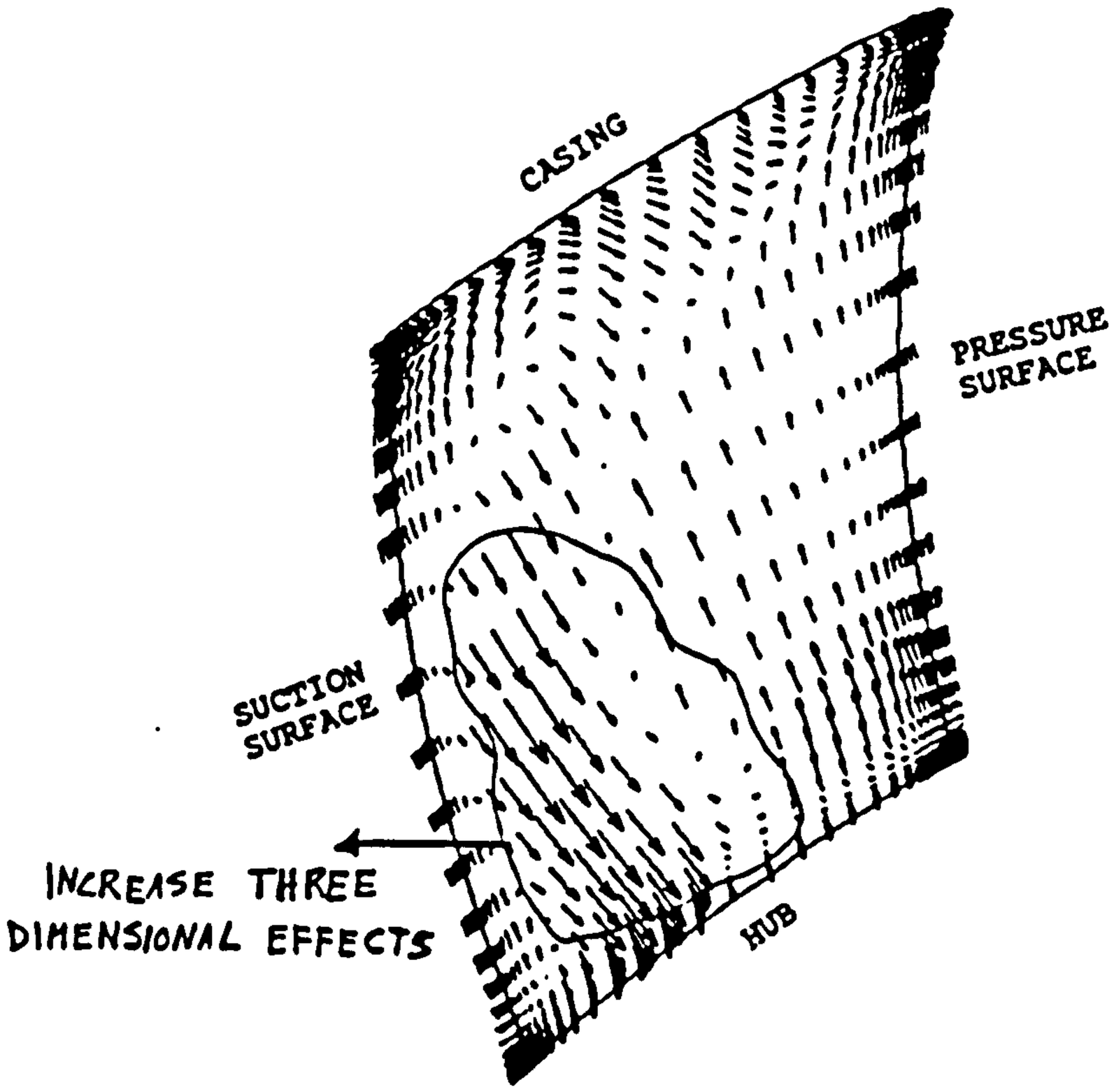

Figure-5.55b Secondary Flow on the Axial Plane near to the Exit with Aspect Ratio and Gradient Function modifications. Three Dimensional High Pressure Turbine

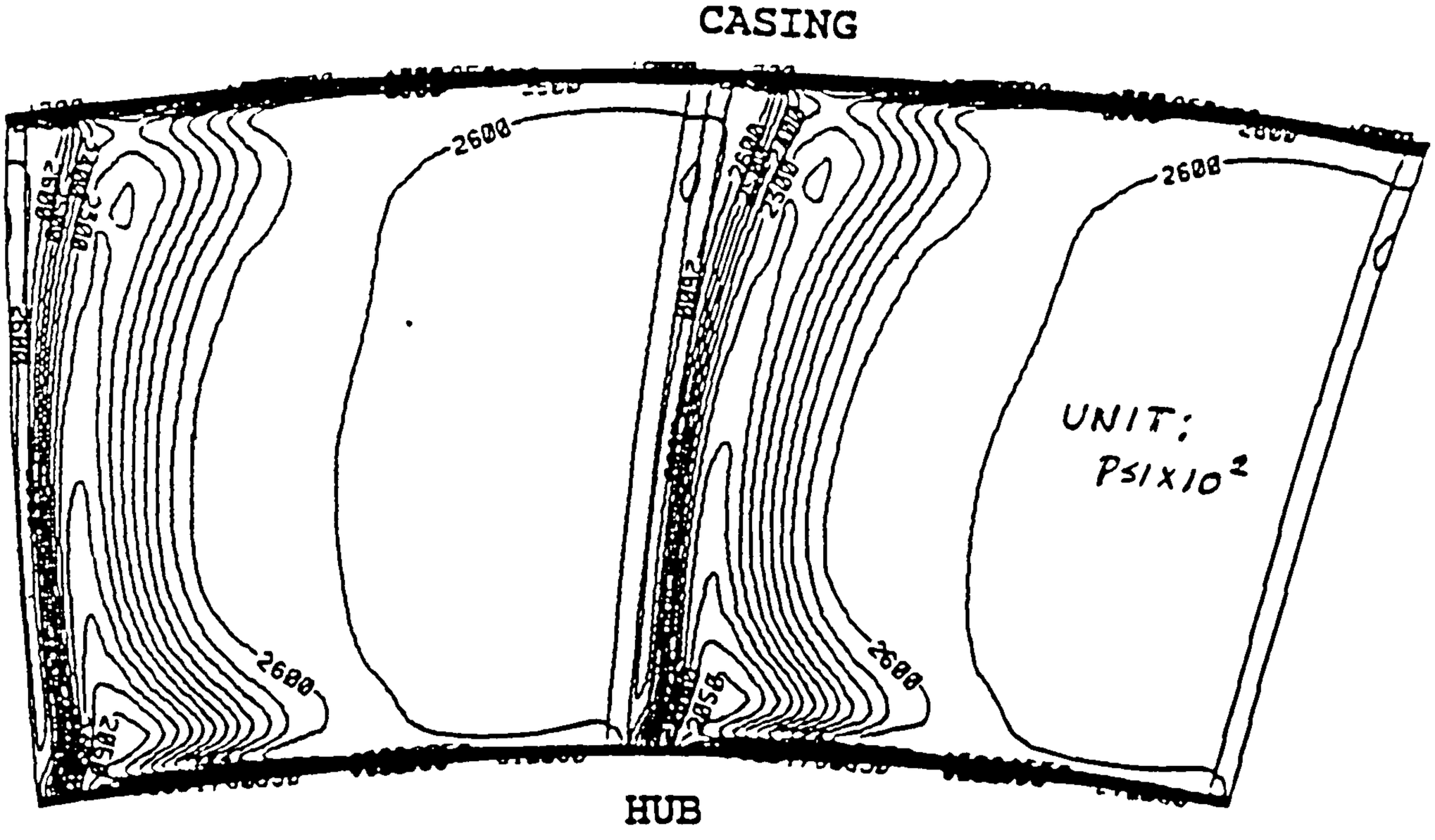

Figure-5.56a Computational Result of Wake
at Axial Position 7 mm downstream of
Trailing Edge (see figure-5.28)

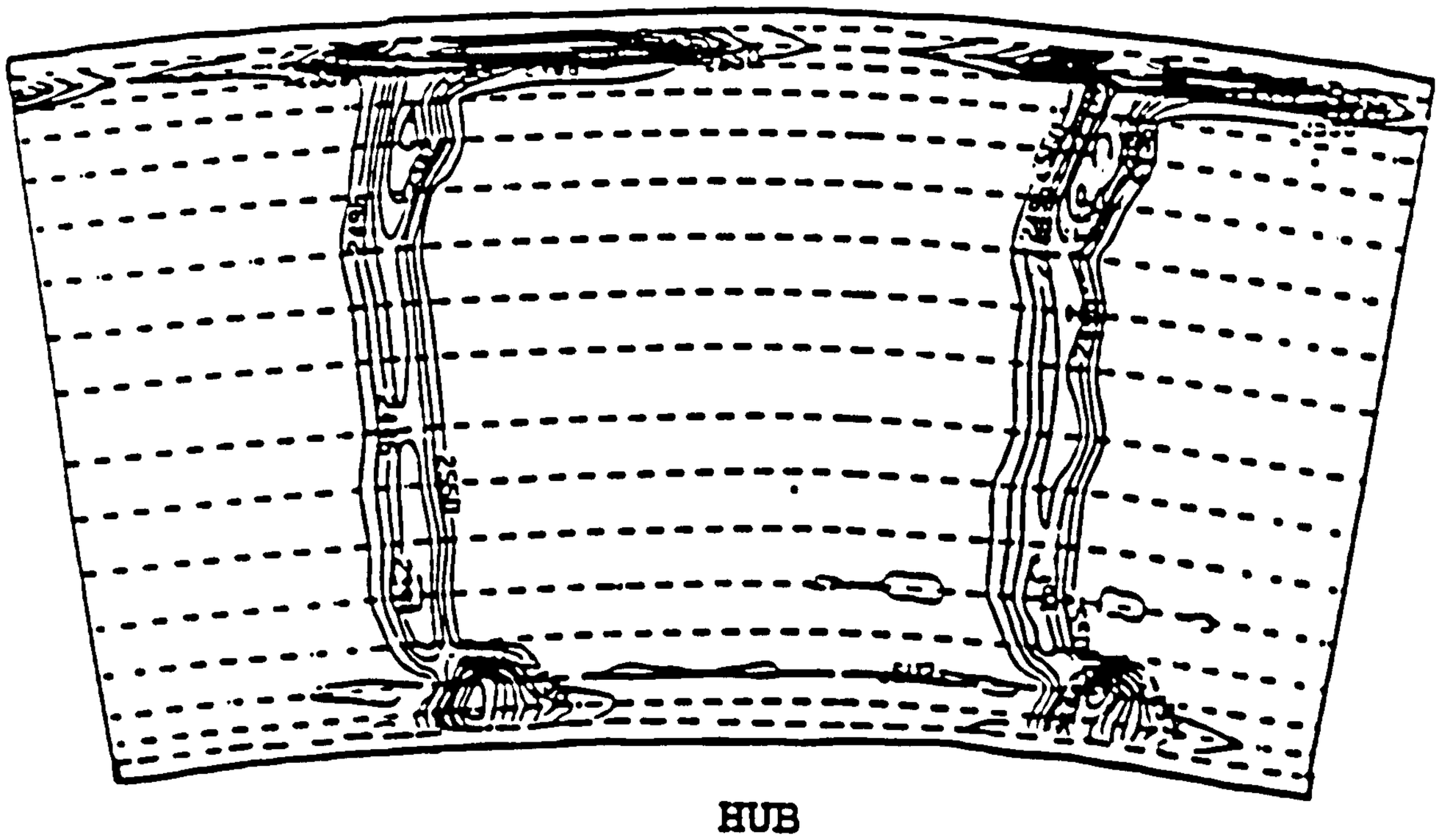

Figure-5.56b Experimental Result of Wake
at Axial Position 7 mm downstream of
Trailing Edge (see figure-5.28)

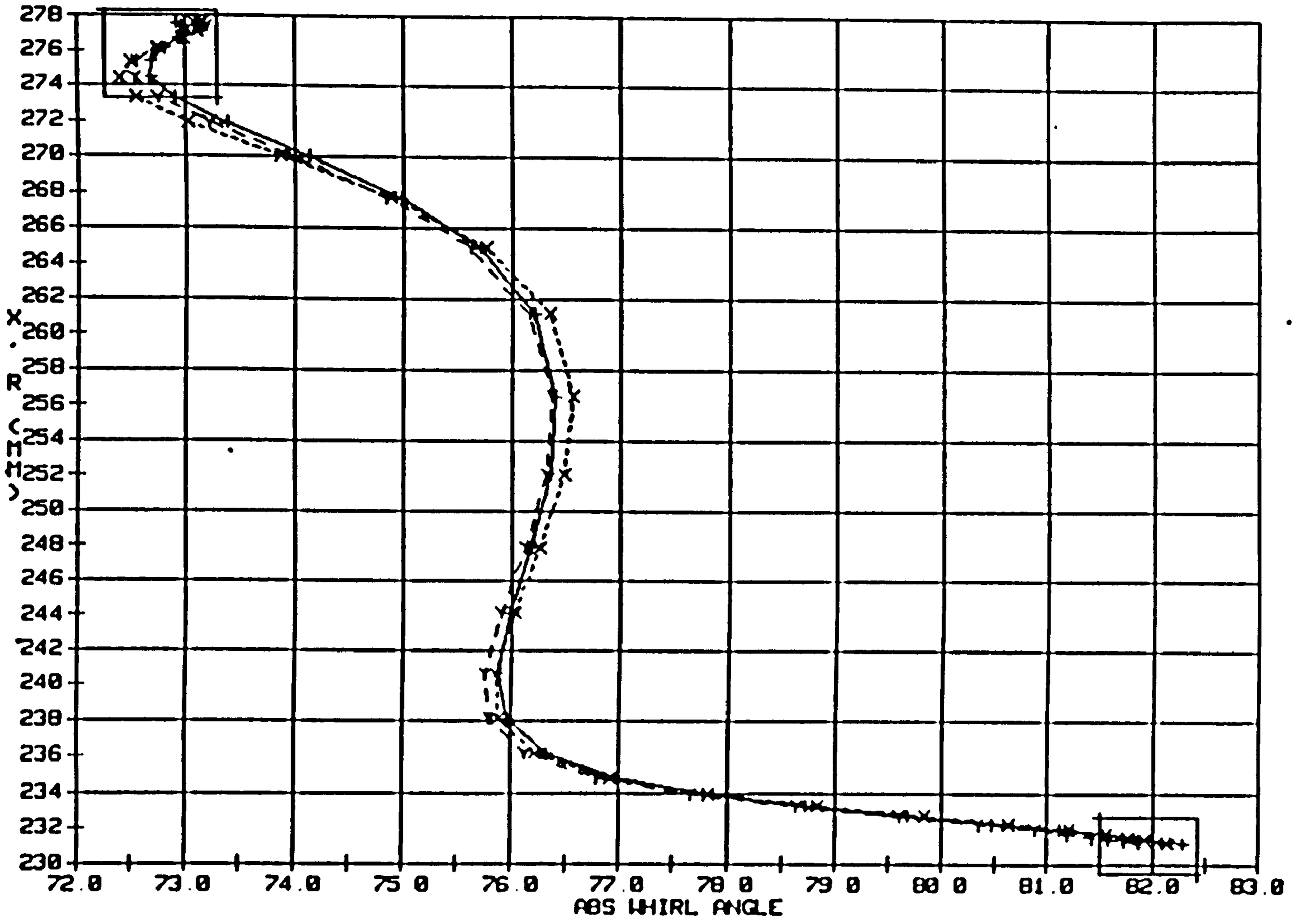

Figure-5.57 Whirl Angle at the Exit Plane in the Wake across the Span

-+--+- No modification
-x--x- Aspect ratio function
-Y--Y- Gradient function

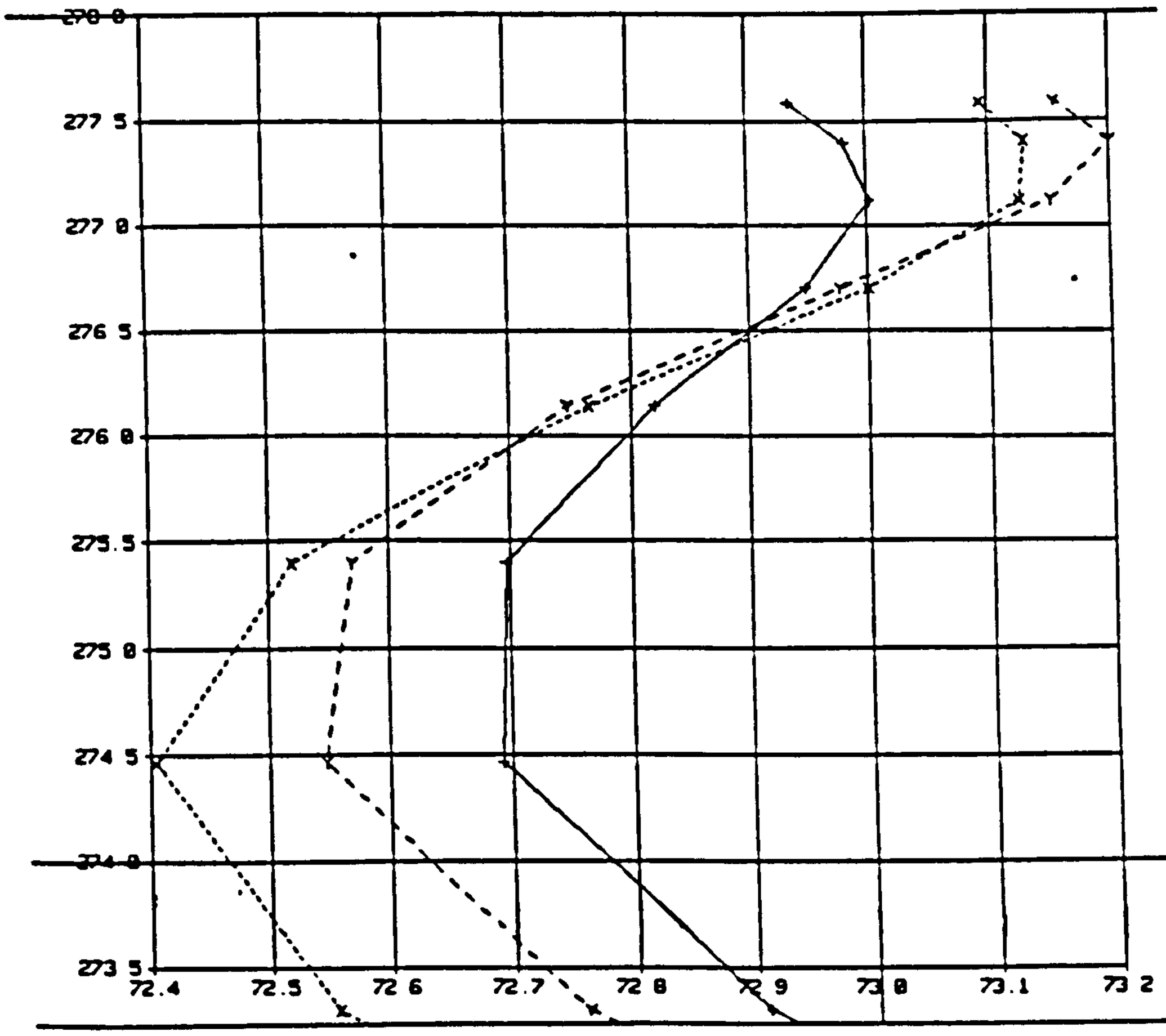

Region A near to the Casing
(see Figure-5.57)

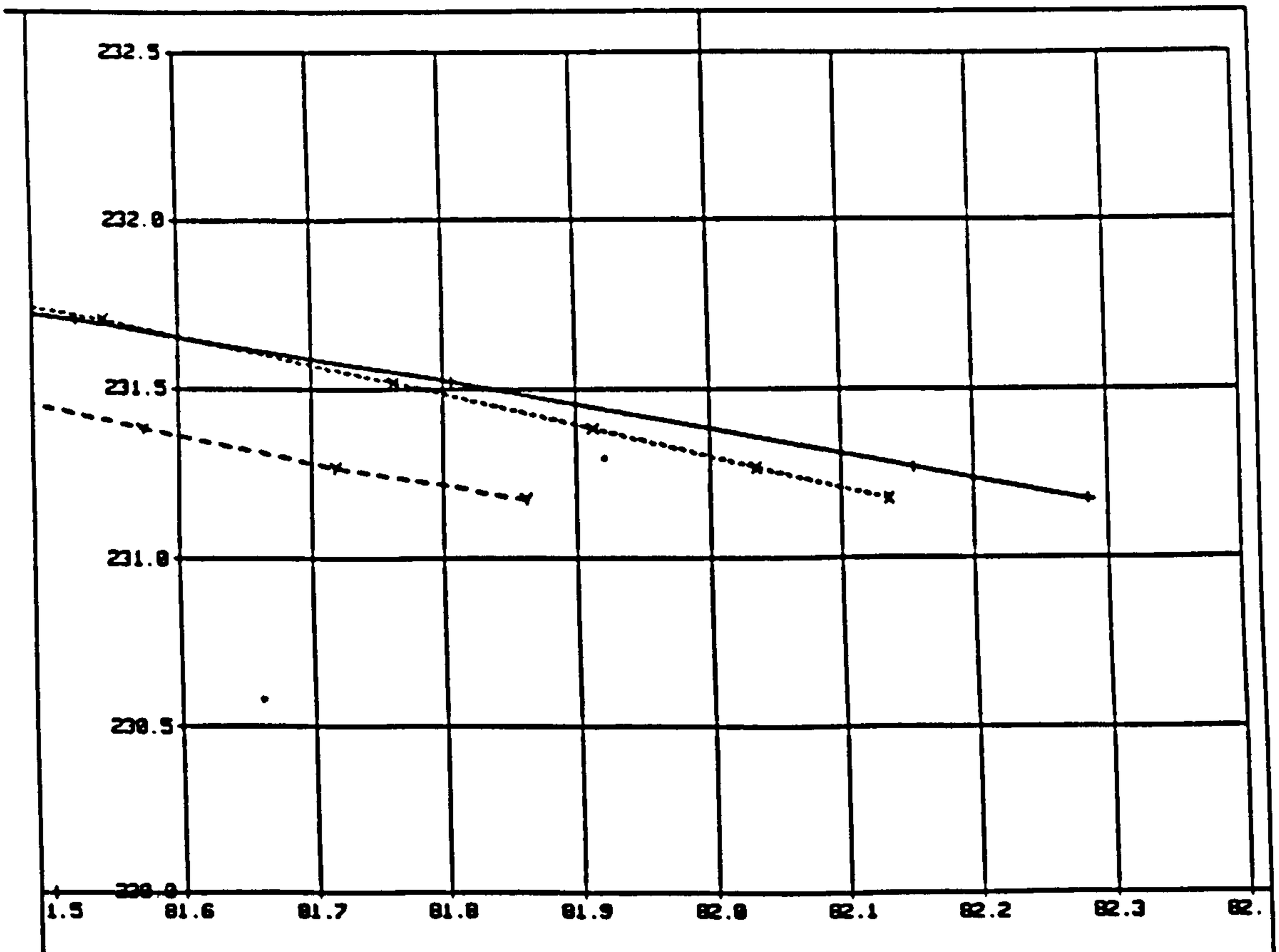

Region B near to the Hub
(see Figure-5.57)

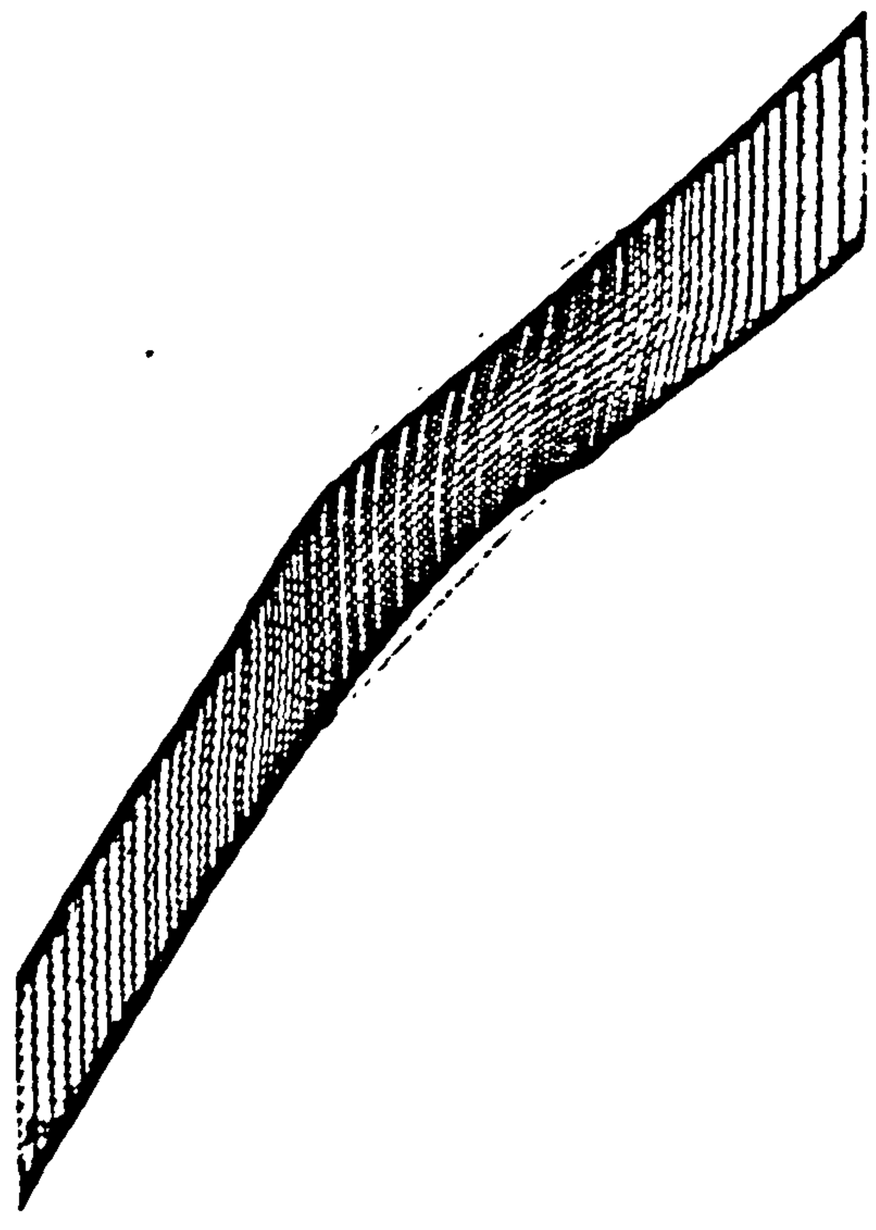

Figure-5.58a Fan Grid: Blade-to-Blade Plane

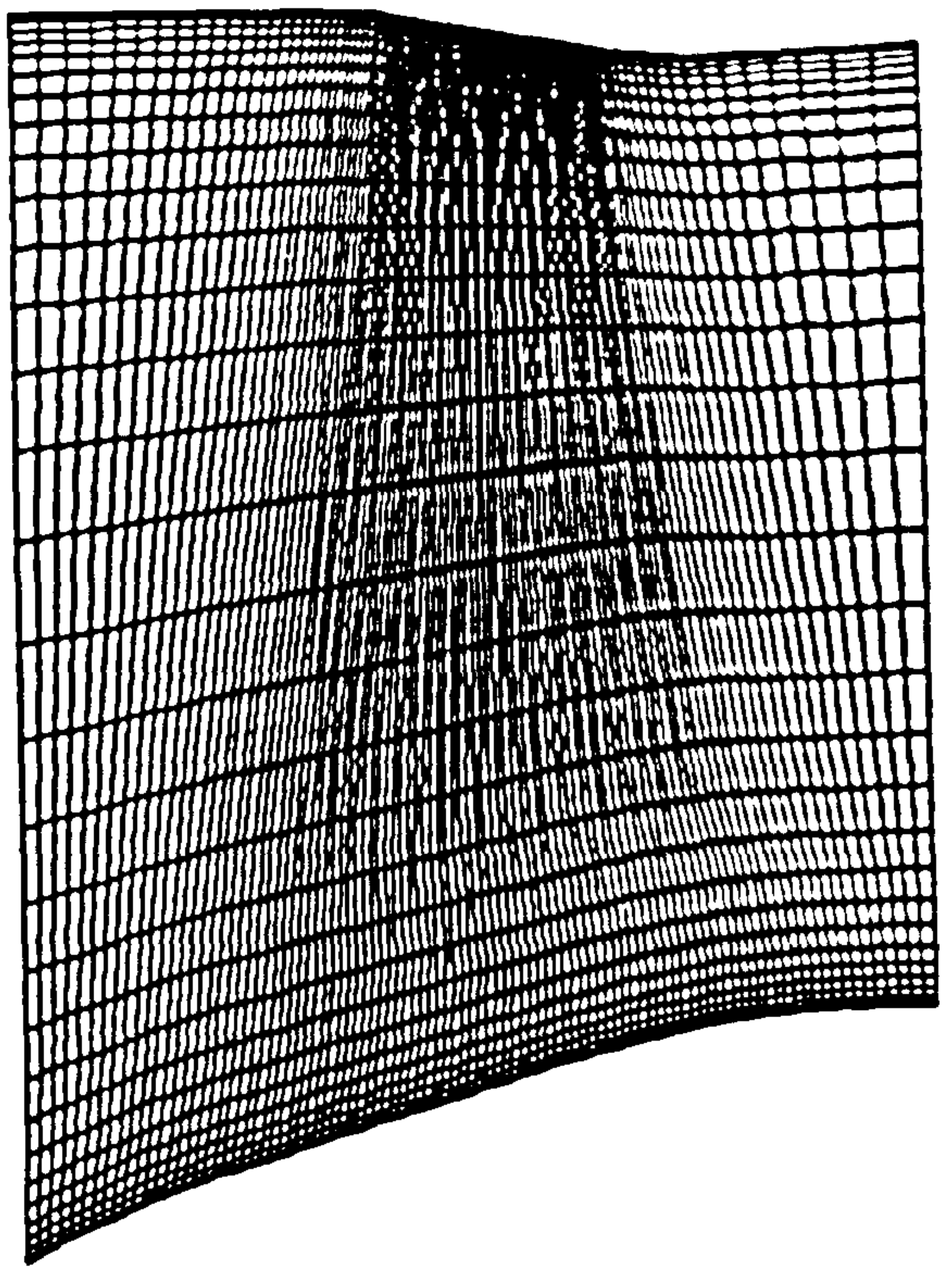

Figure-5.58b Fan Grid: Meridional Plane

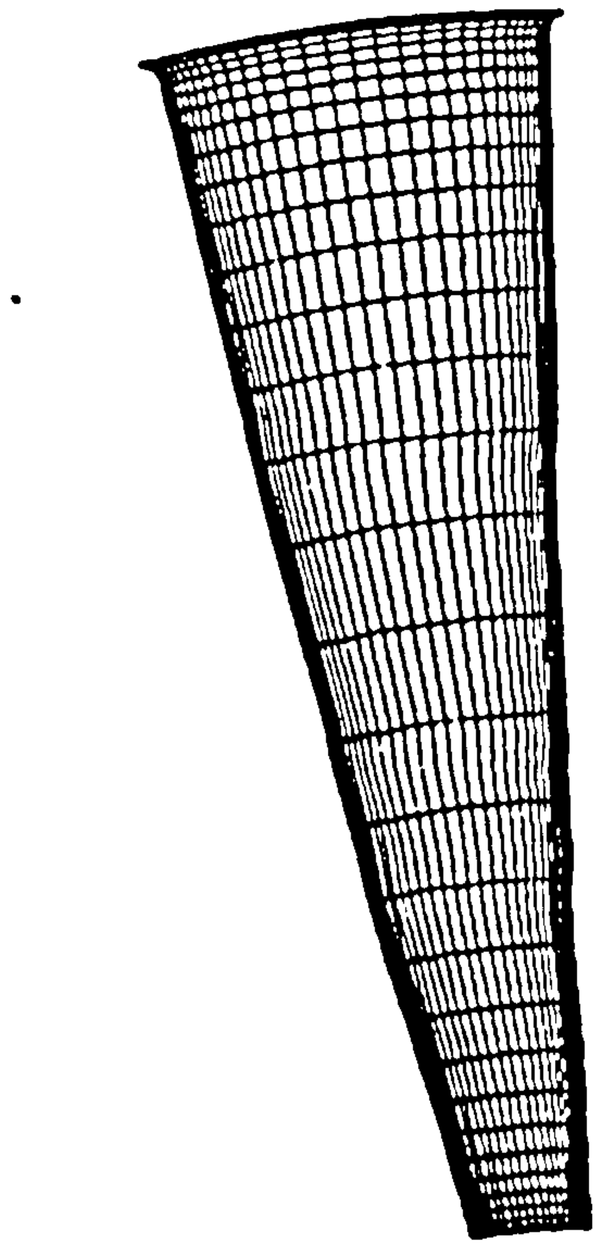

Figure-5.58c Fan Grid: Axial Plane in the Blade Passage

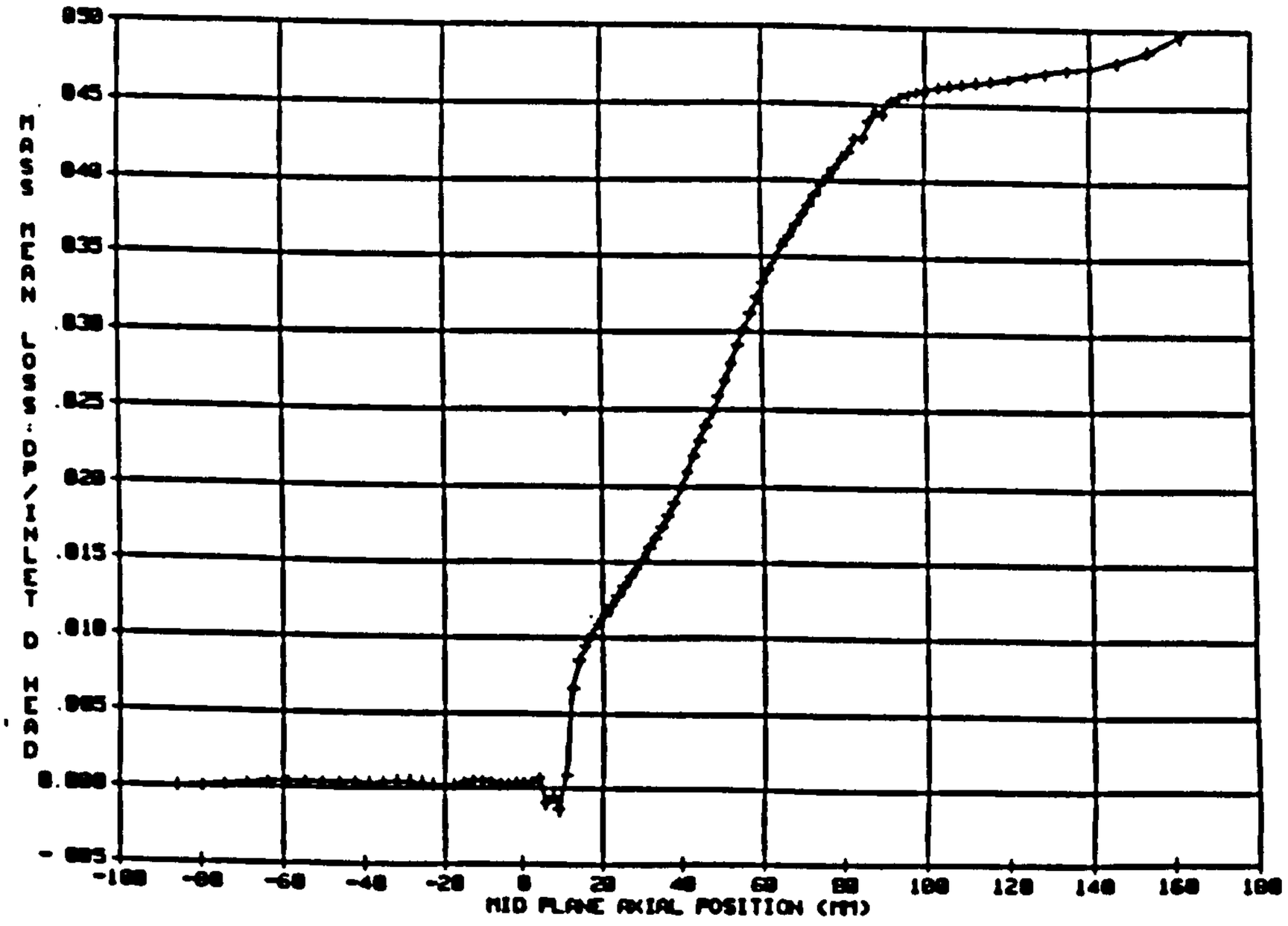

Figure-5:59 Total Pressure loss of the Fan Case

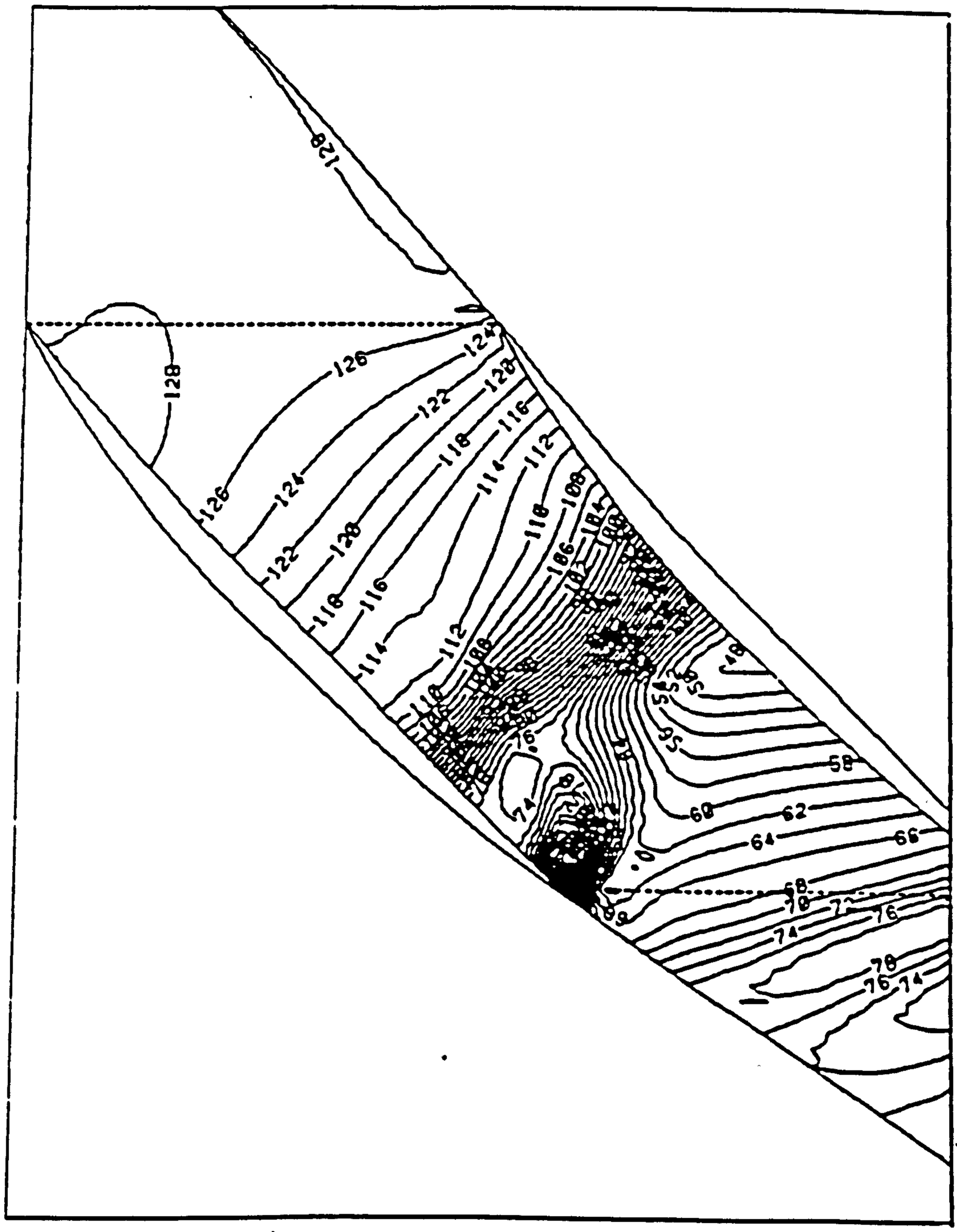

Figure-5.60 Static Pressure (In kPa) Contour of the Fan Case at Mid Span

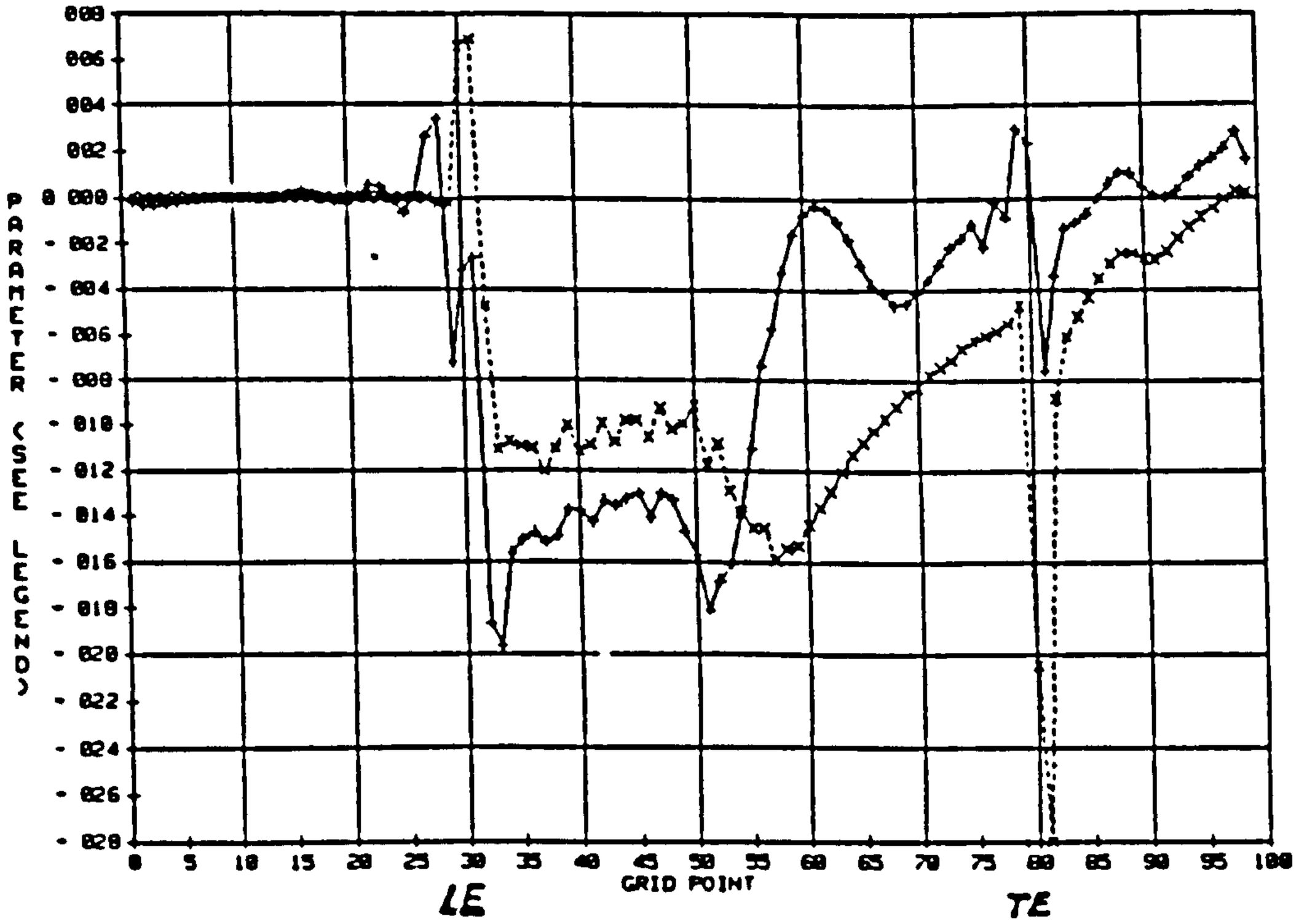

Figure-5.61 Dissipation and Viscous Fluxes
near to the Suction Surface
from Inlet to Exit

-+--+- Dissipation
-x--x- Viscous fluxes
LE=Leading Edge
TE=Trailing Edge

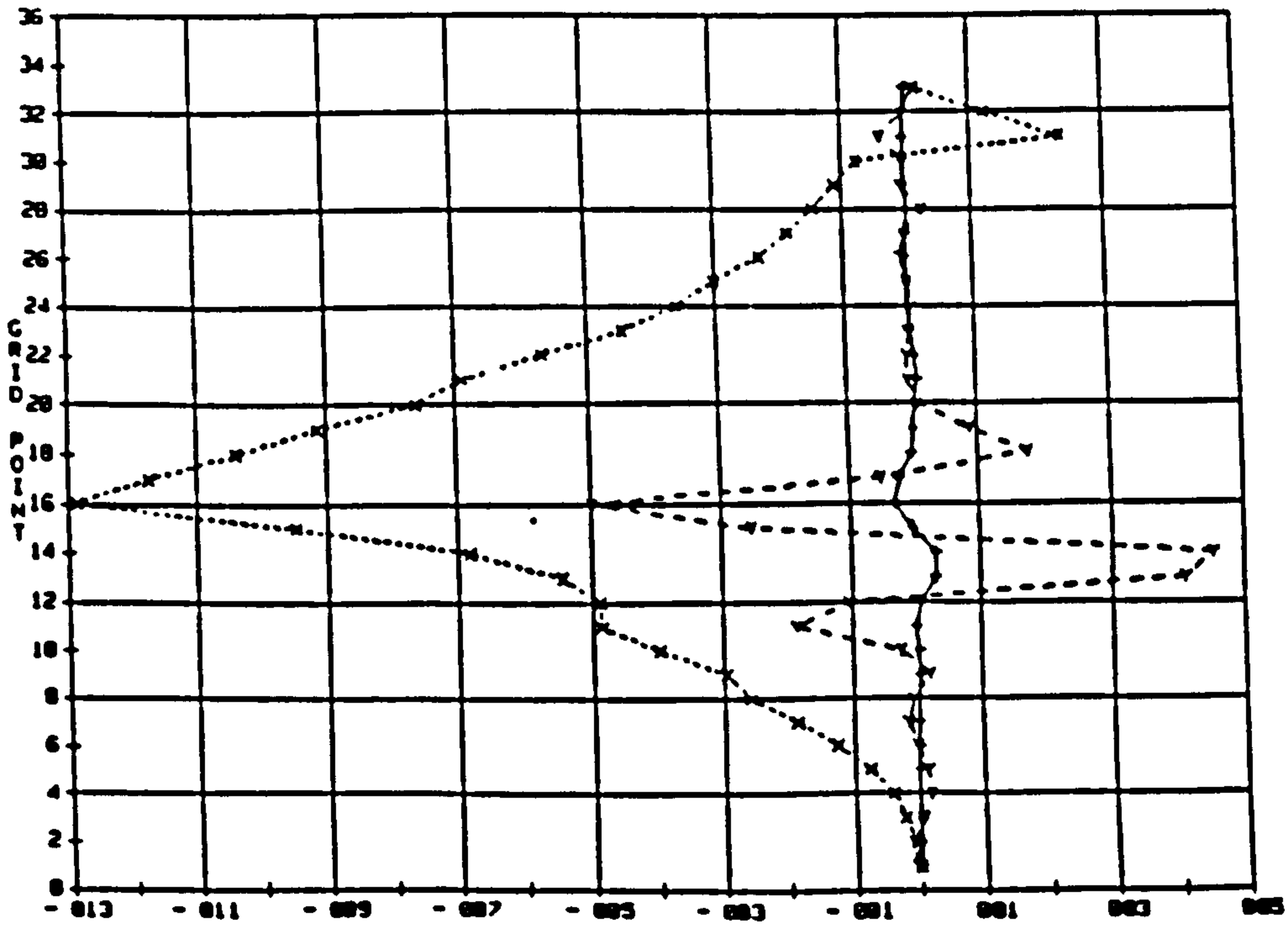

Figure-5.62 Dissipation Component
along the Span

-+--+- Flow Direction
-x--x- Blade to blade direction
-Y--Y- Radial direction

PAGE
NUMBERS
CUT OFF
IN
ORIGINAL

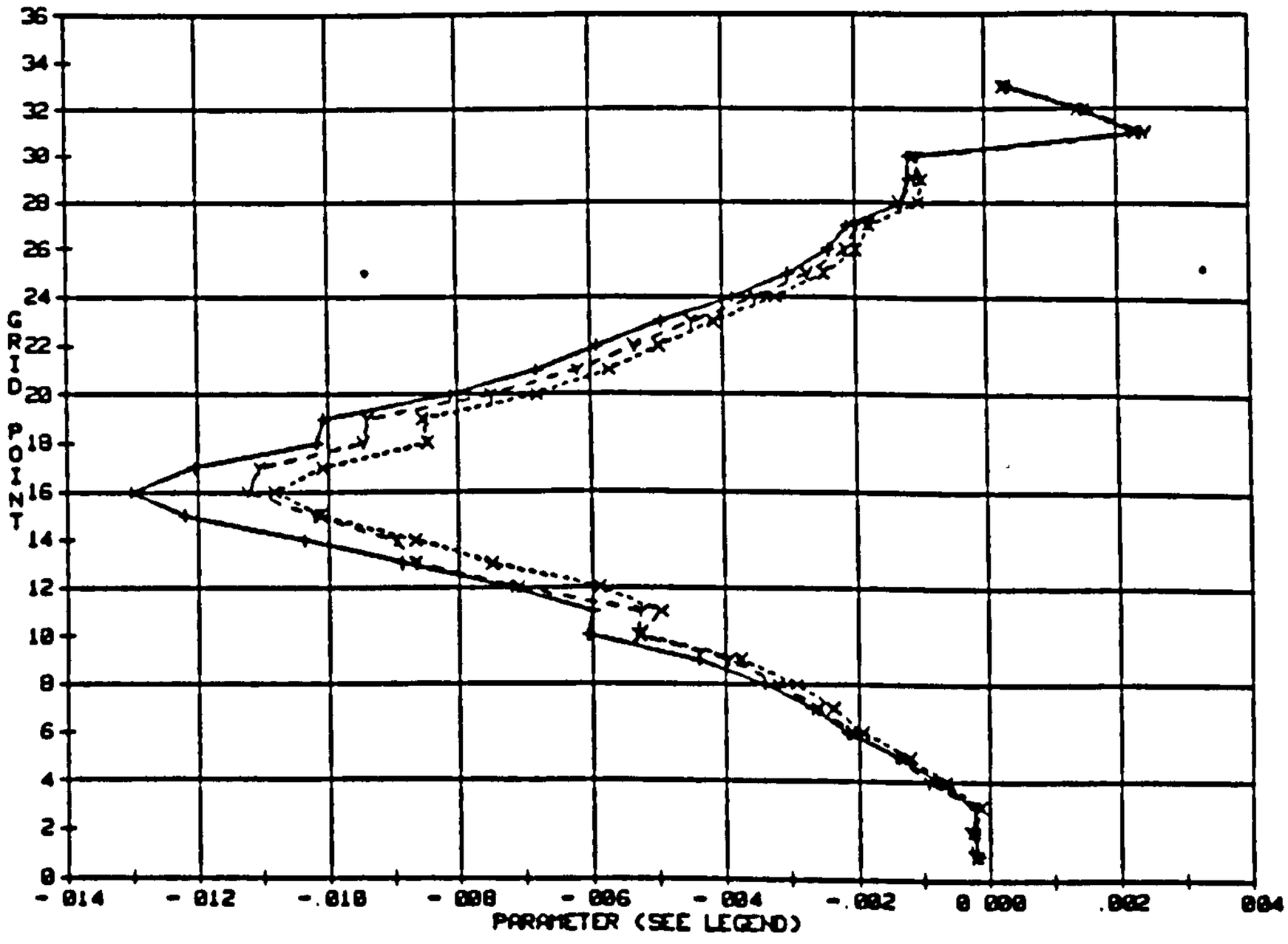

Figure-5.63 Dissipation near Suction Surface along the Span

-+--+- No modification
-x--x- Gradient function
-Y--Y- Aspect ratio and gradient functions

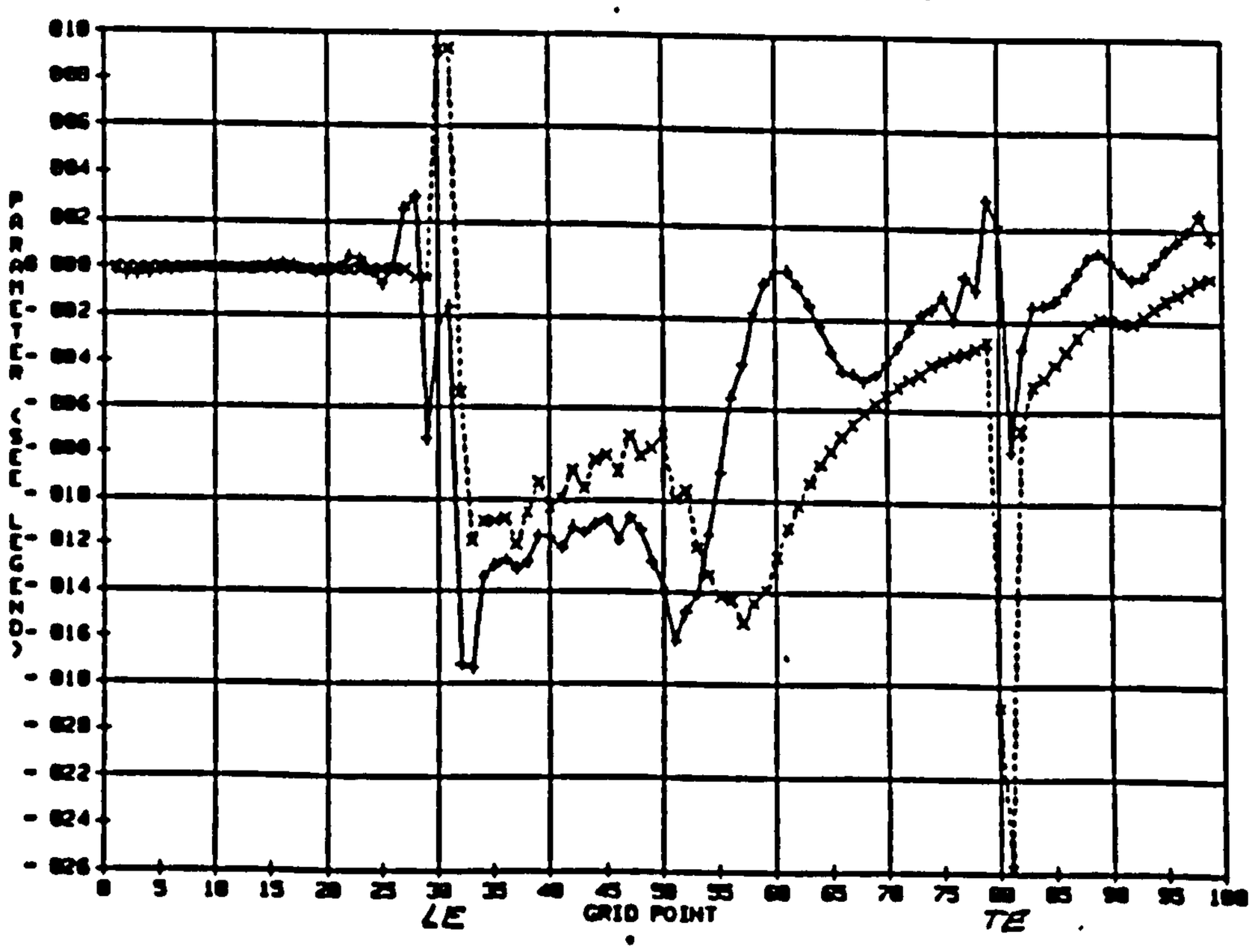

Figure-5.64 Dissipation and Viscous Fluxes with Gradient Function near to the Suction Surface from Inlet to Exit

-+--+- Dissipation
-x--x- Viscous fluxes

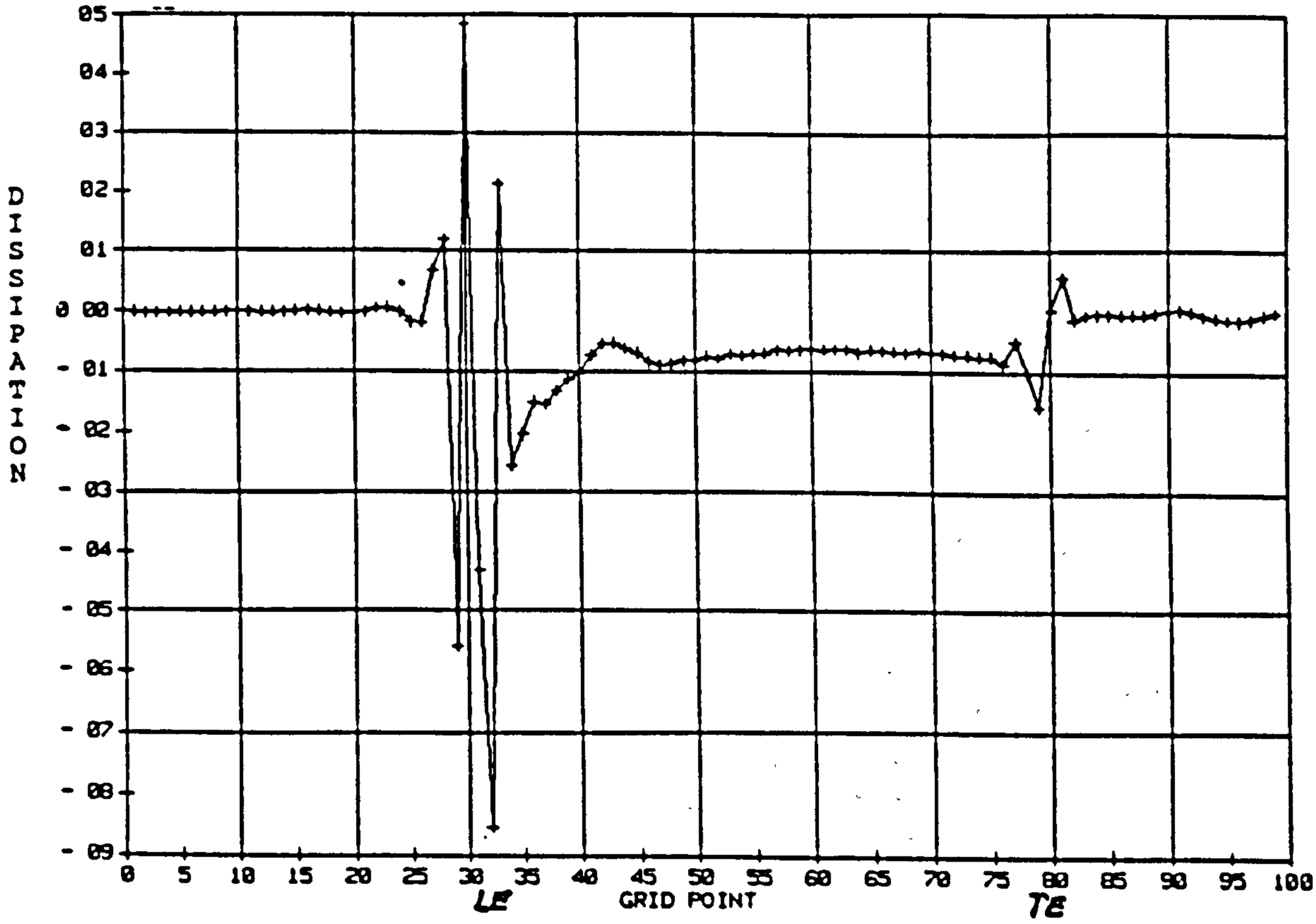

Figure-5.65 Standard Dissipation near to the Pressure Surface from Inlet to Exit

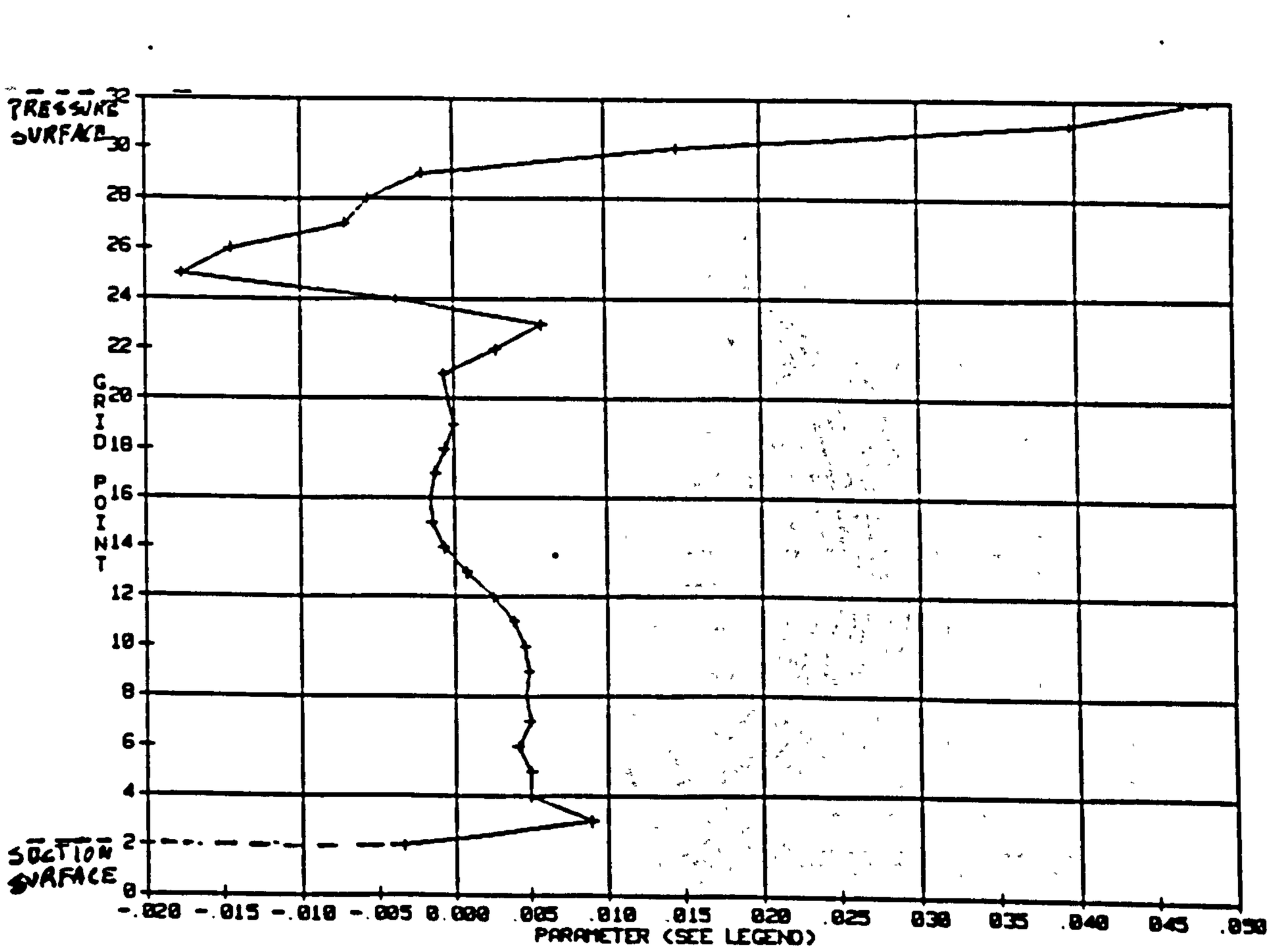

Figure-5.66 Standard Dissipation near to the Leading Edge from Suction Surface to Pressure Surface

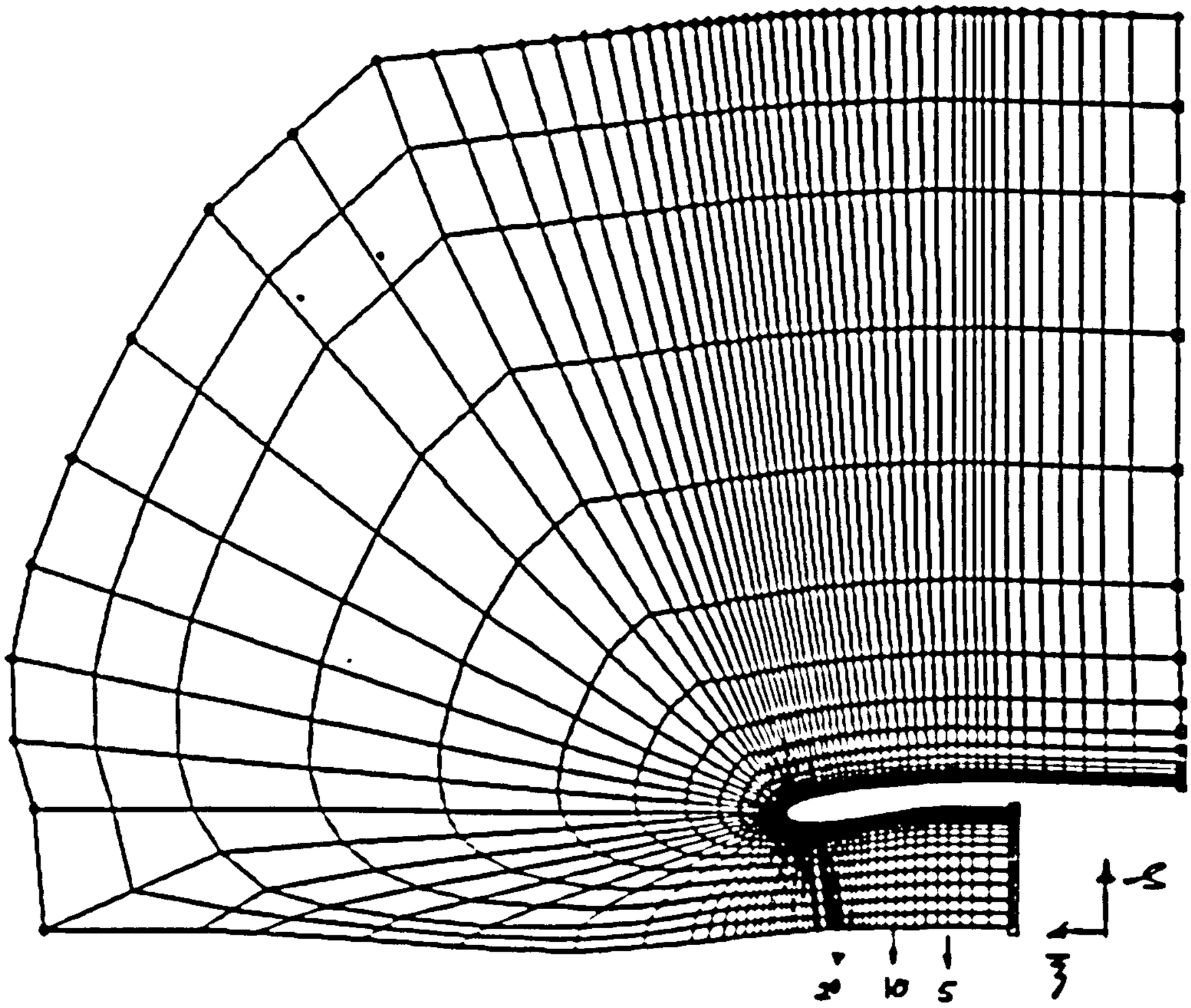

Figure-5.67a Intake Grid: Meridional Plane

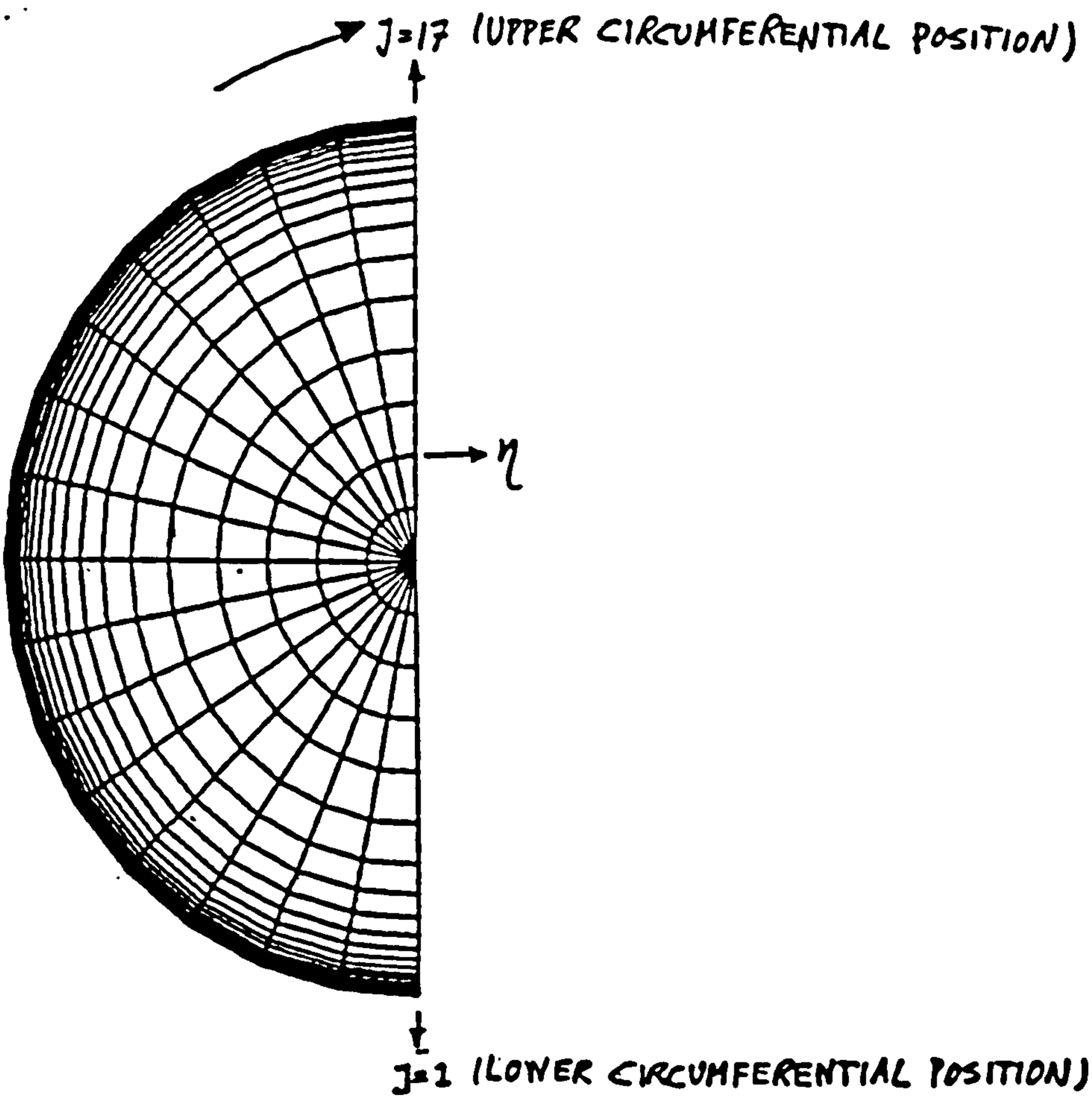

Figure-5.67b Intake Grid: Axial Plane

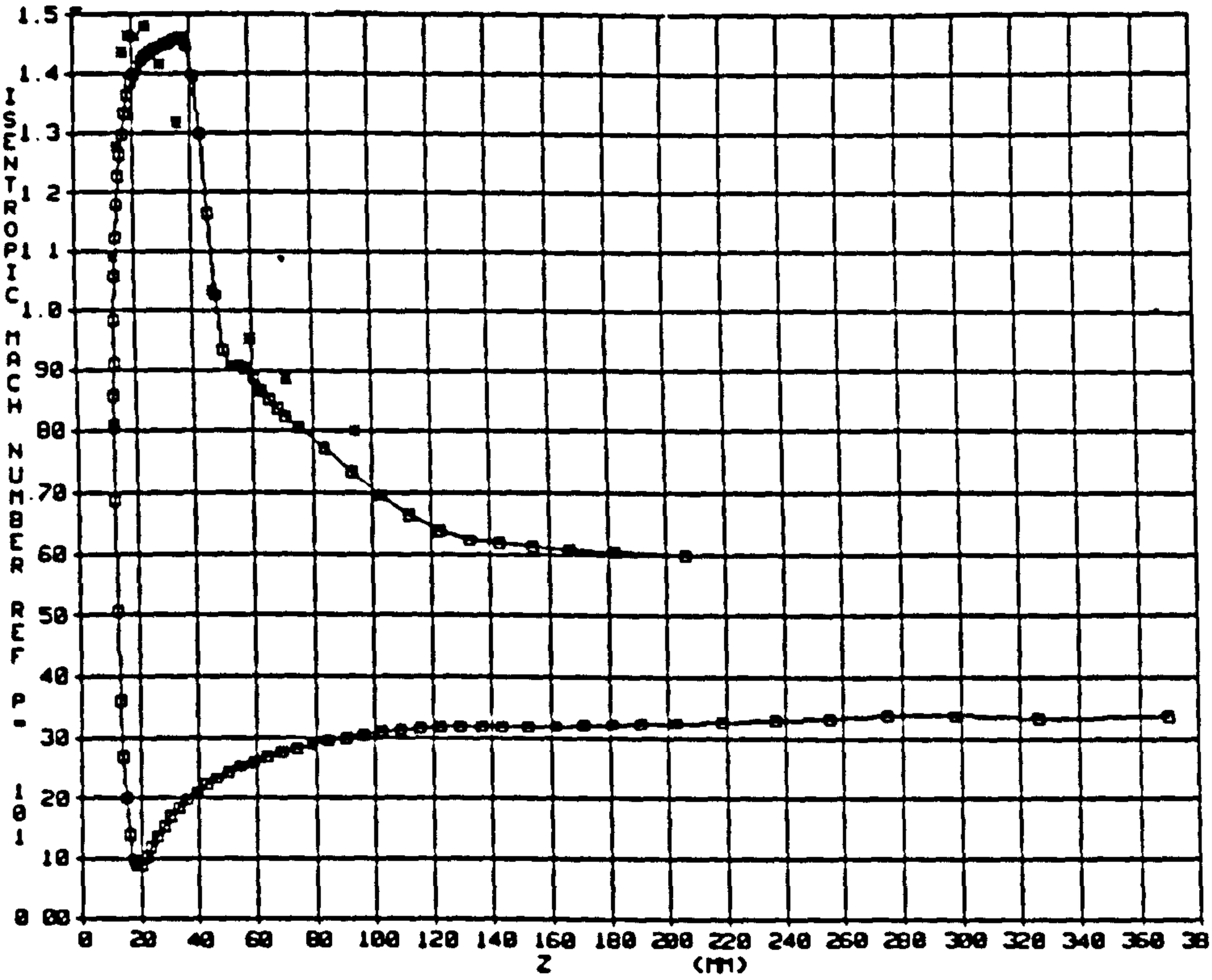

At j=1 (see Figure-5.67b)

At j=17 (see Figure-5.67b)

Figure-5.68 Isentropic Mach Number
* Experimental Data

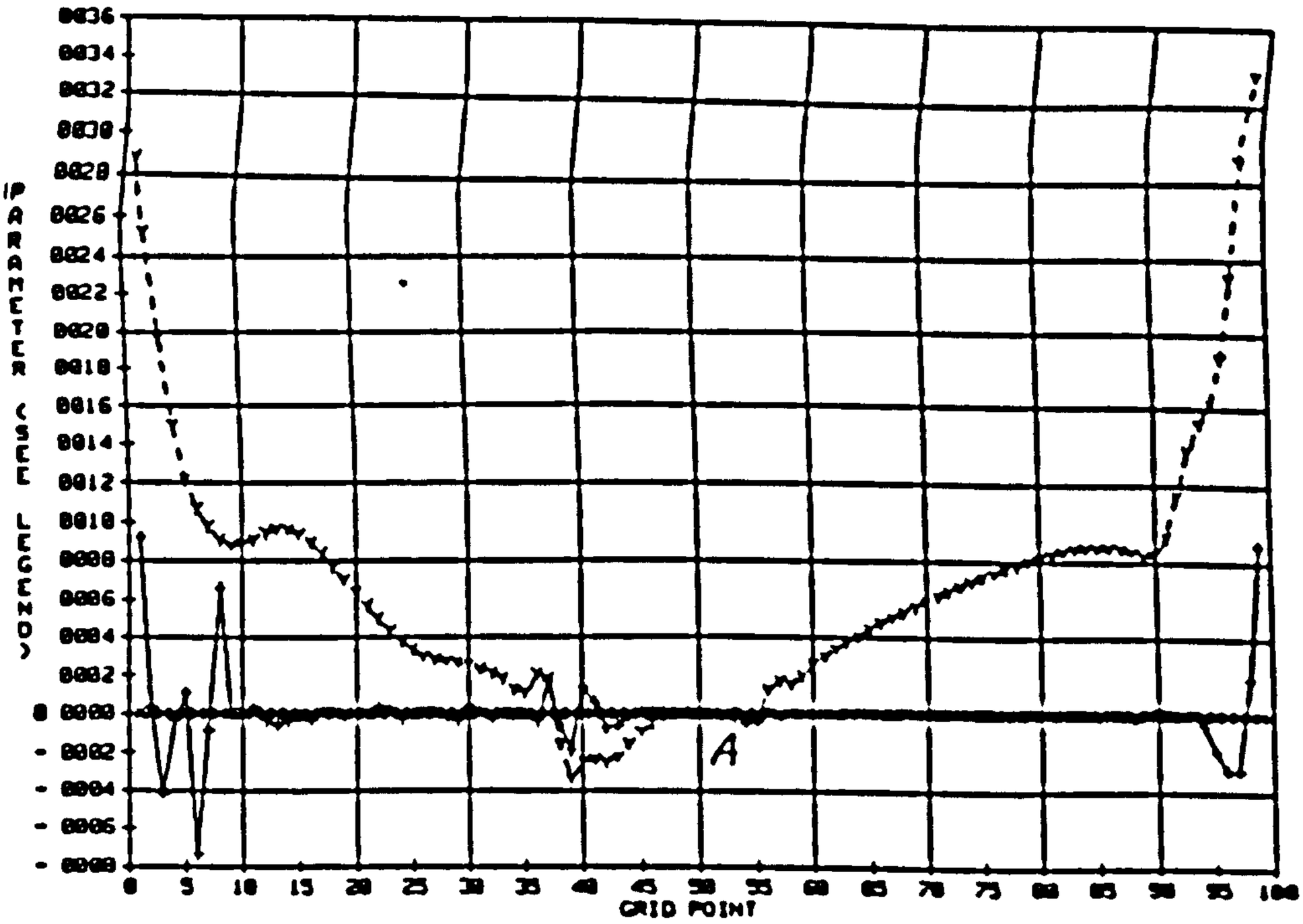

Figure-5.69 Decomposed Dissipation at the near wall region at Upper Circumferential Position (see Figure-5.67a & b)

-+--+- ξ - direction
-x--x- η - direction
-Y--Y- ζ - direction

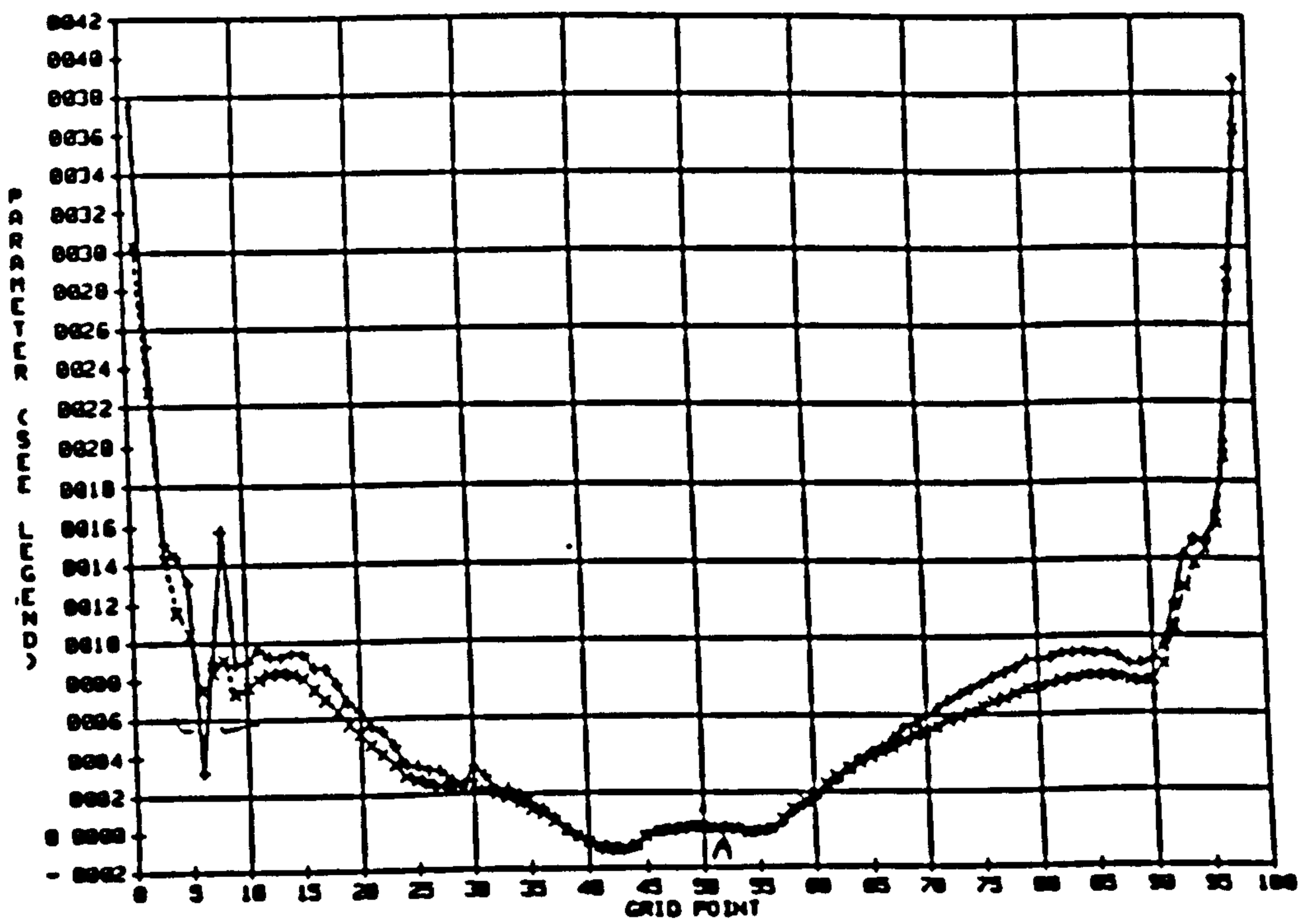

Figure-5.70a Dissipation at the near Wall Region at Upper Circumferential Position (see Figure-5.67a & b)

-+--+- No modification
-x--x- Aspect ratio and gradient function

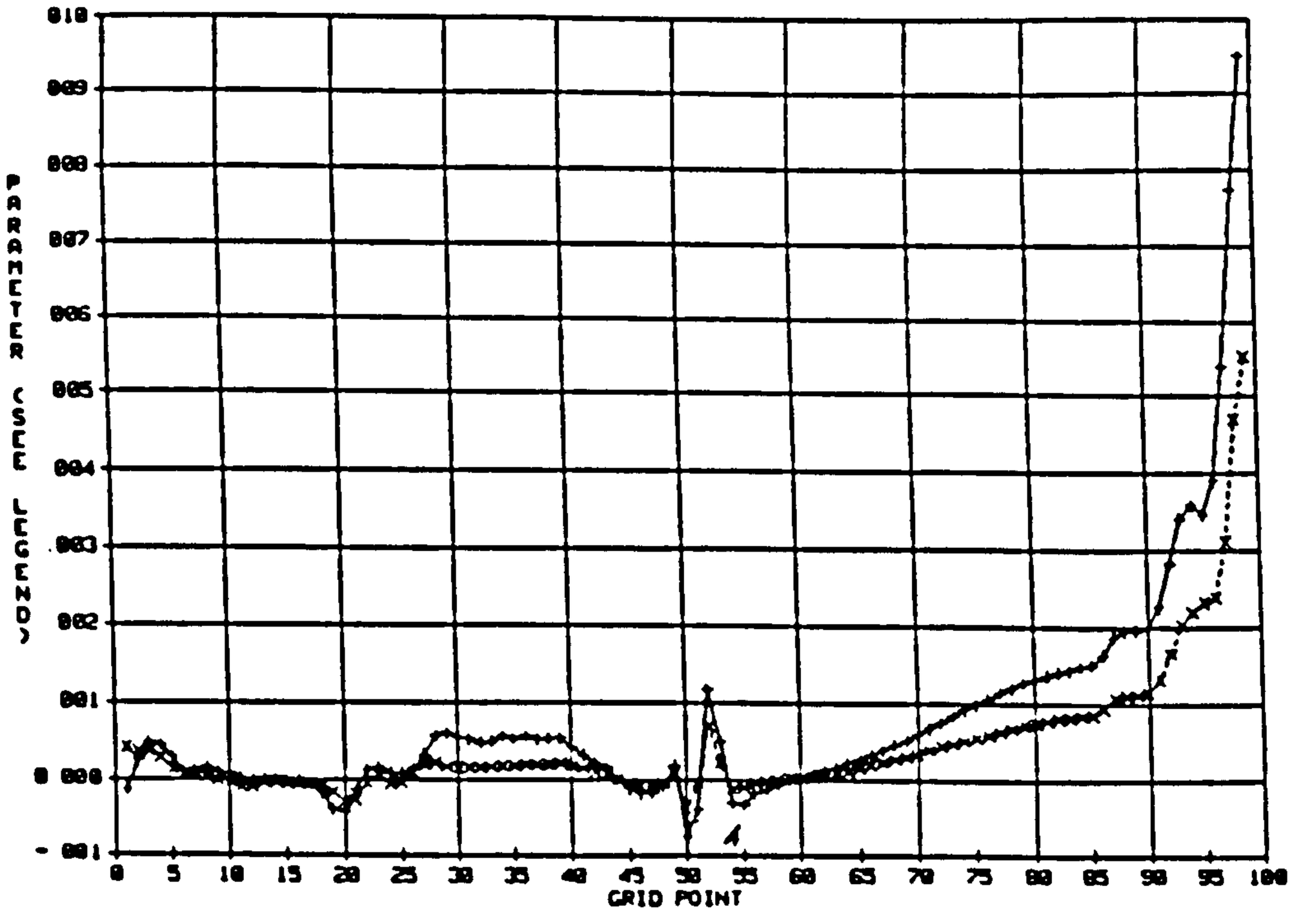

Figure-5.70b Dissipation at the near Wall Region
at Lower Circumferential Position
(see Figure-5.67a & b)

-+--+- No modification
-x--x- Aspect ratio and gradient function

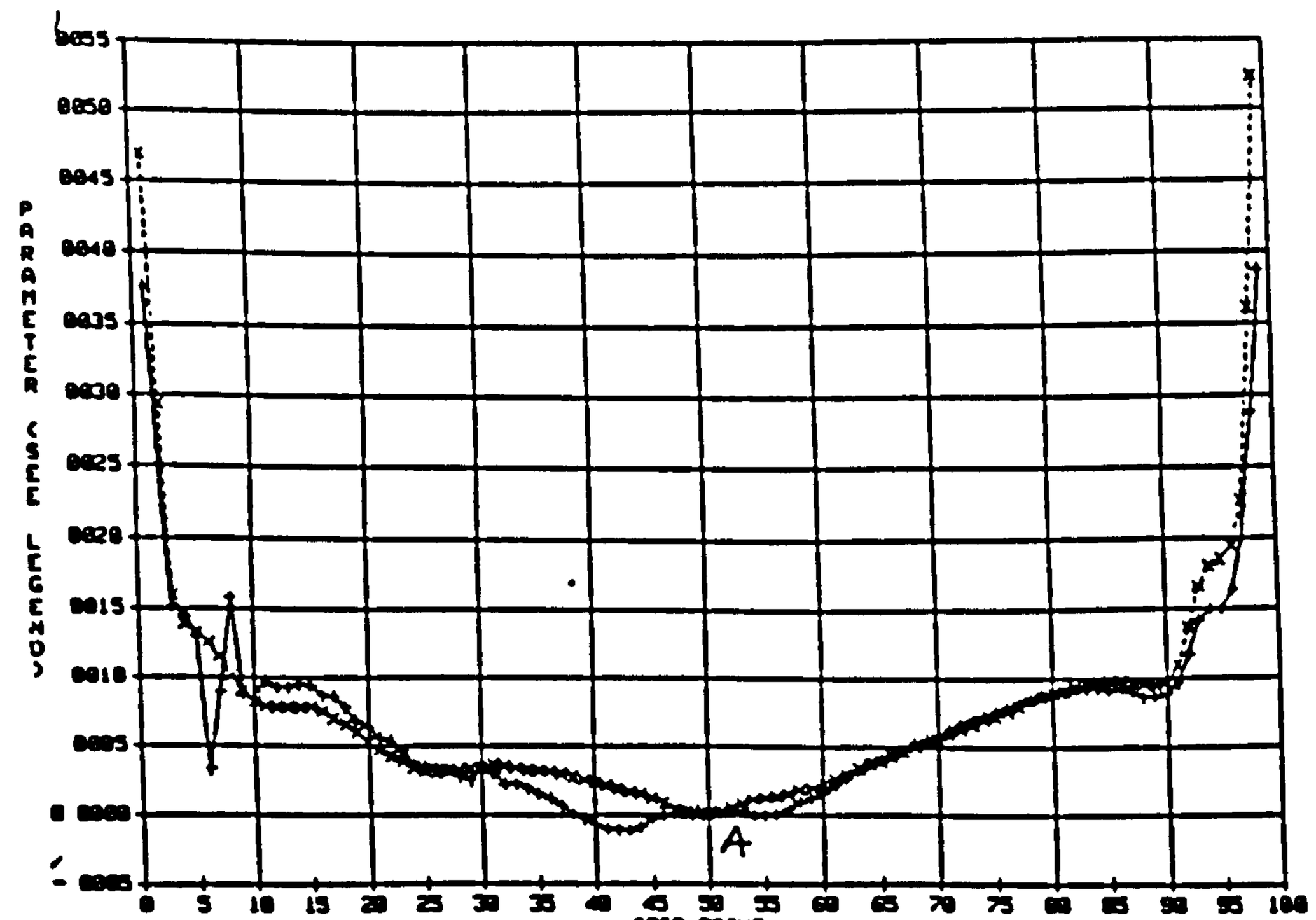

Figure-5.71a Near Wall Dissipation and Viscous Fluxes
with the Standard model at Upper .
Circumferential Position

-+--+- Dissipation
-x--x- Viscous fluxes

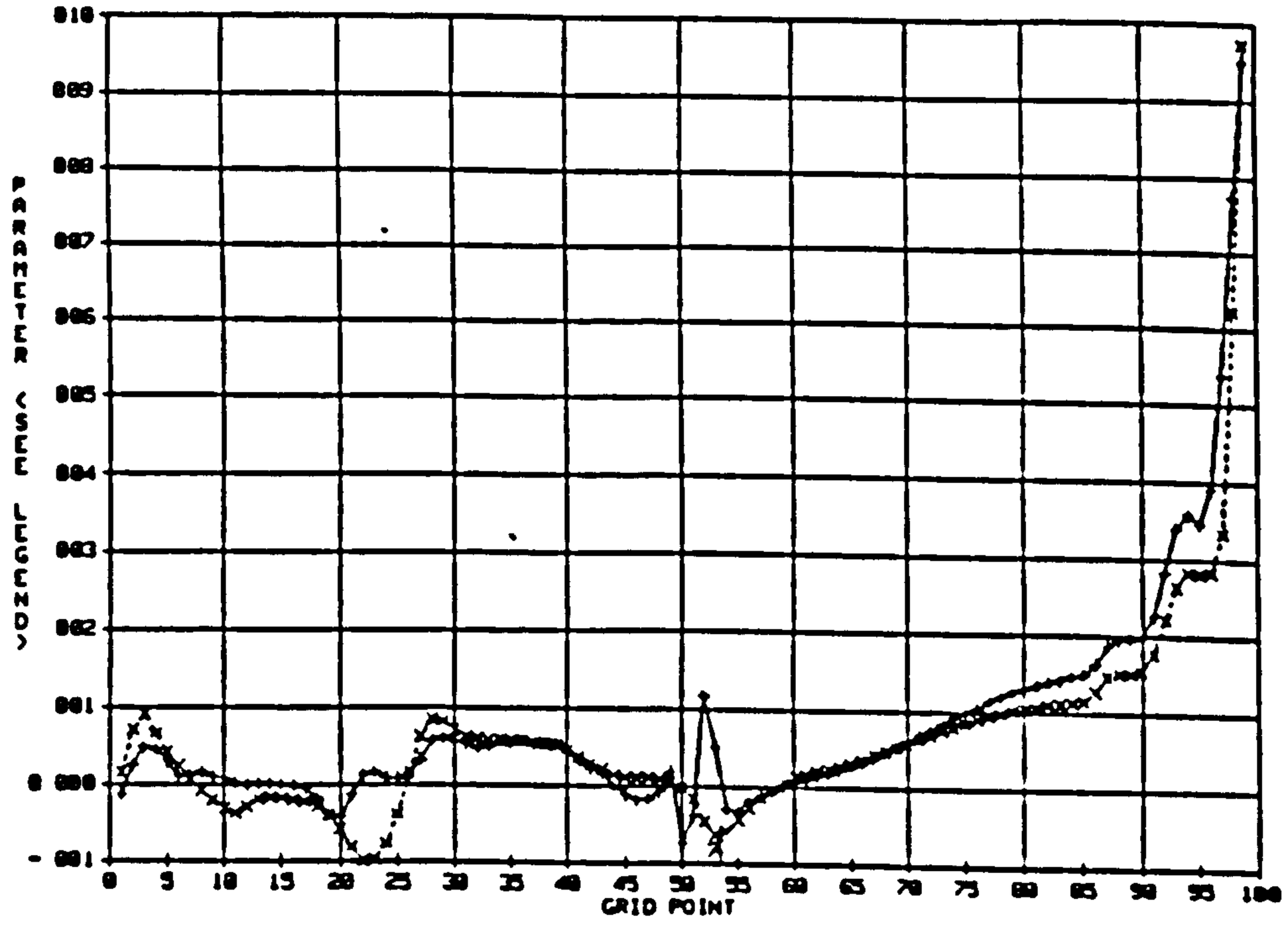

Figure-5.71b Near Wall Dissipation and Viscous Fluxes
with the Standard model at Lower
Circumferential Position

-+--+- Dissipation
-x--x- Viscous fluxes

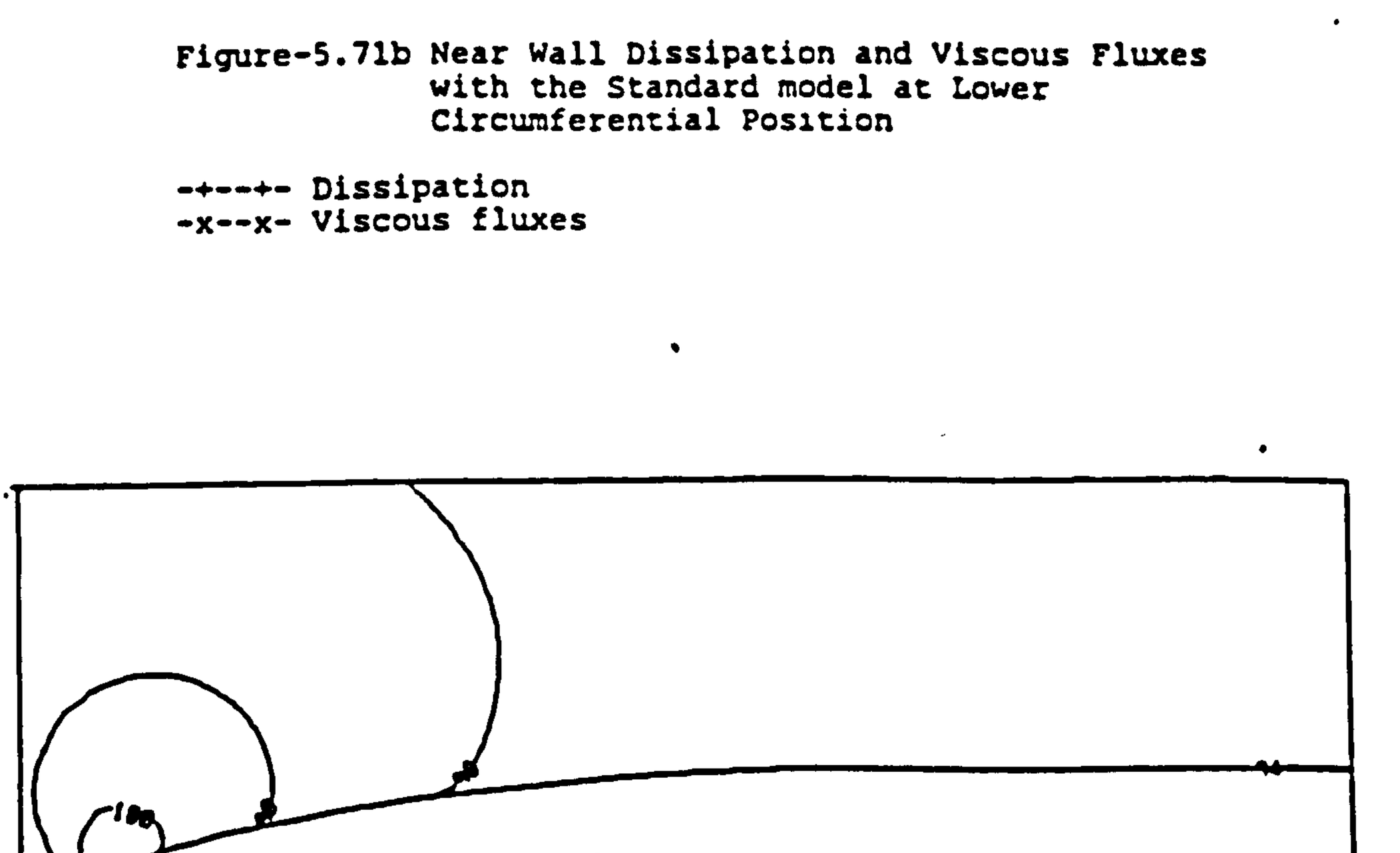

Figure-5.72 Static Pressure (in kPa) Contour
At Lower Circumferential Position

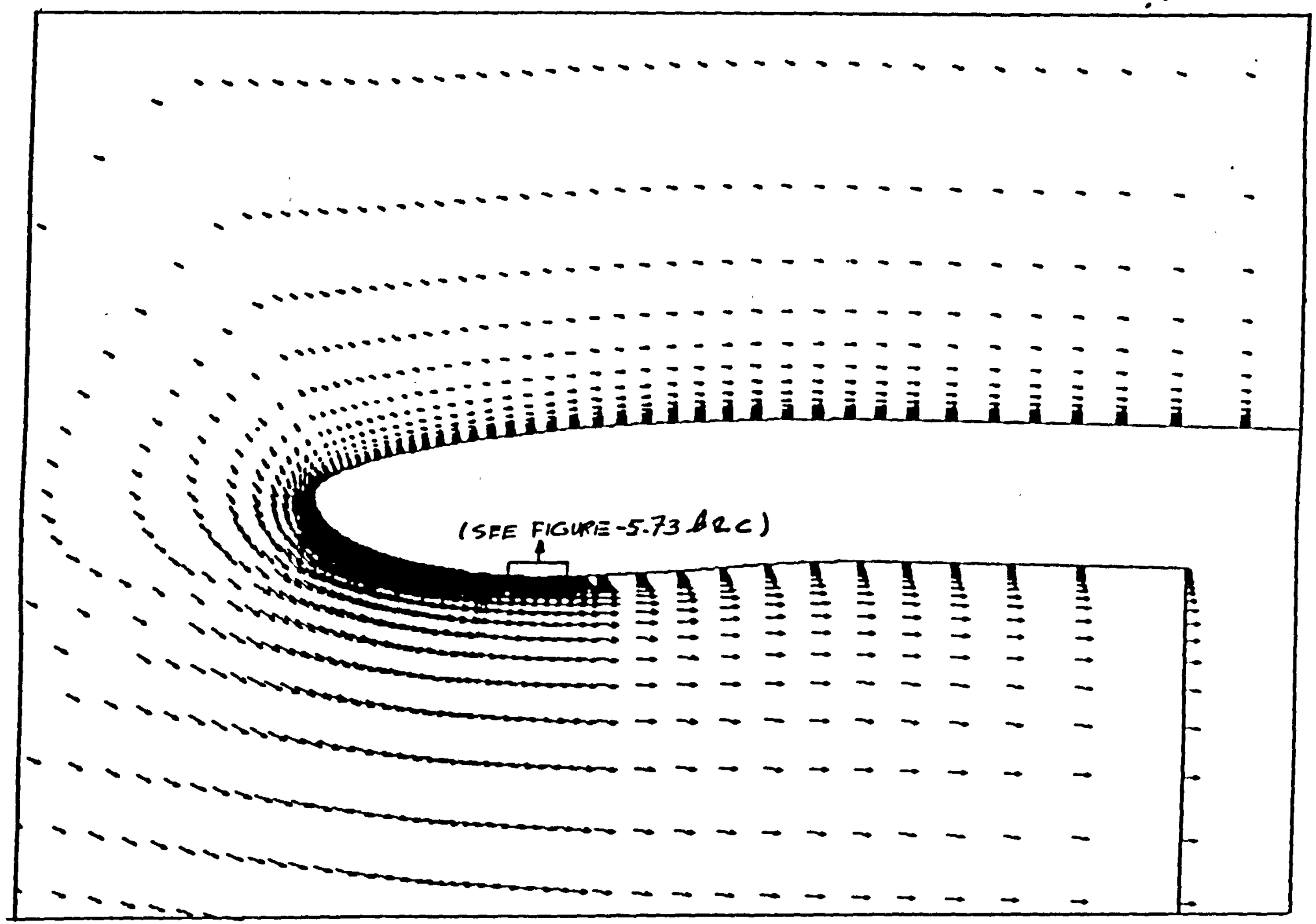

Figure-5.73a Velocity Vectors
At Lower Circumferential Position

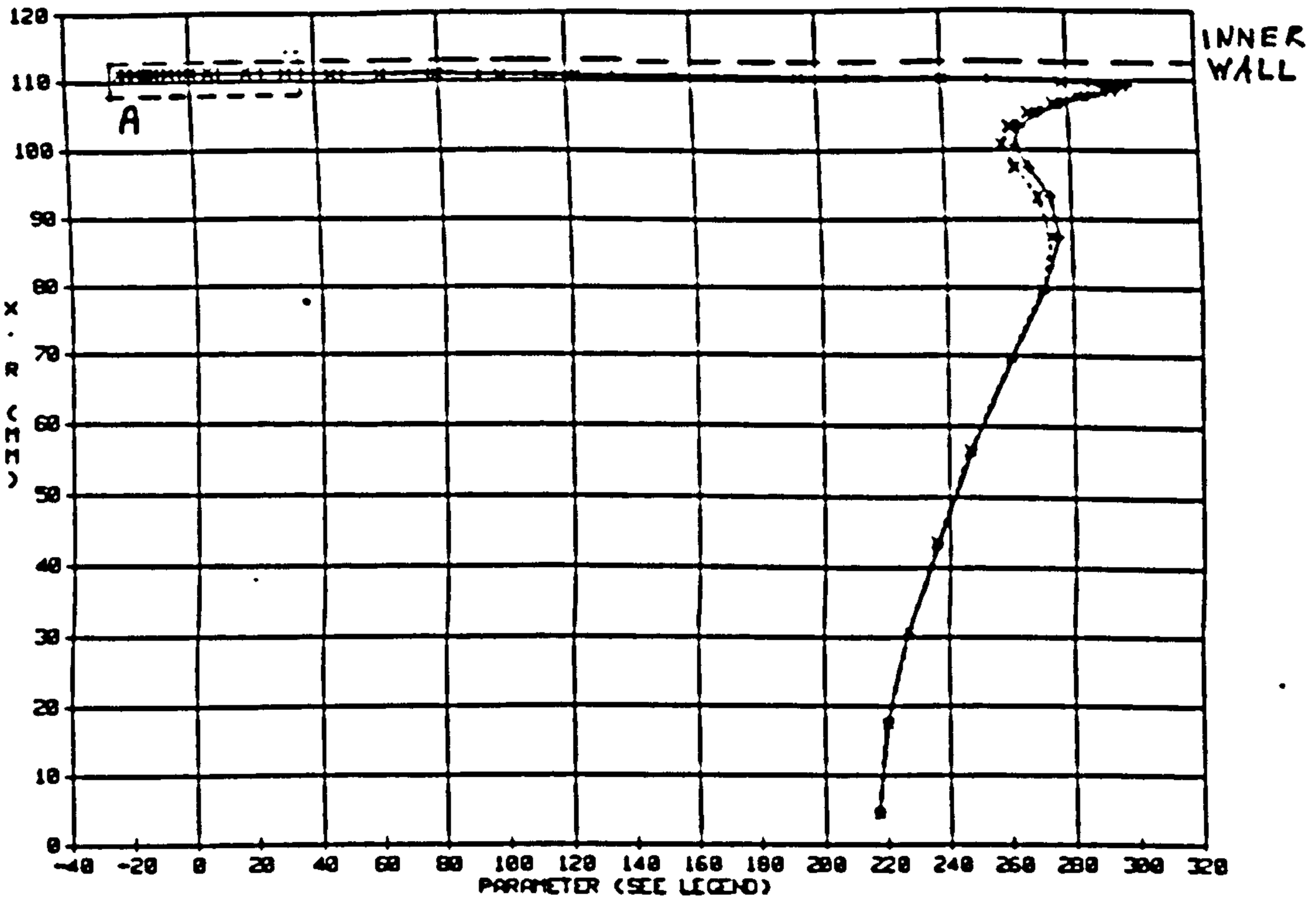

Figure-5.73b Velocity Profile Downstream of the Shock
(see Figure-5.73a)

-+--+- No modification
-x--x- Aspect ratio and gradient functions

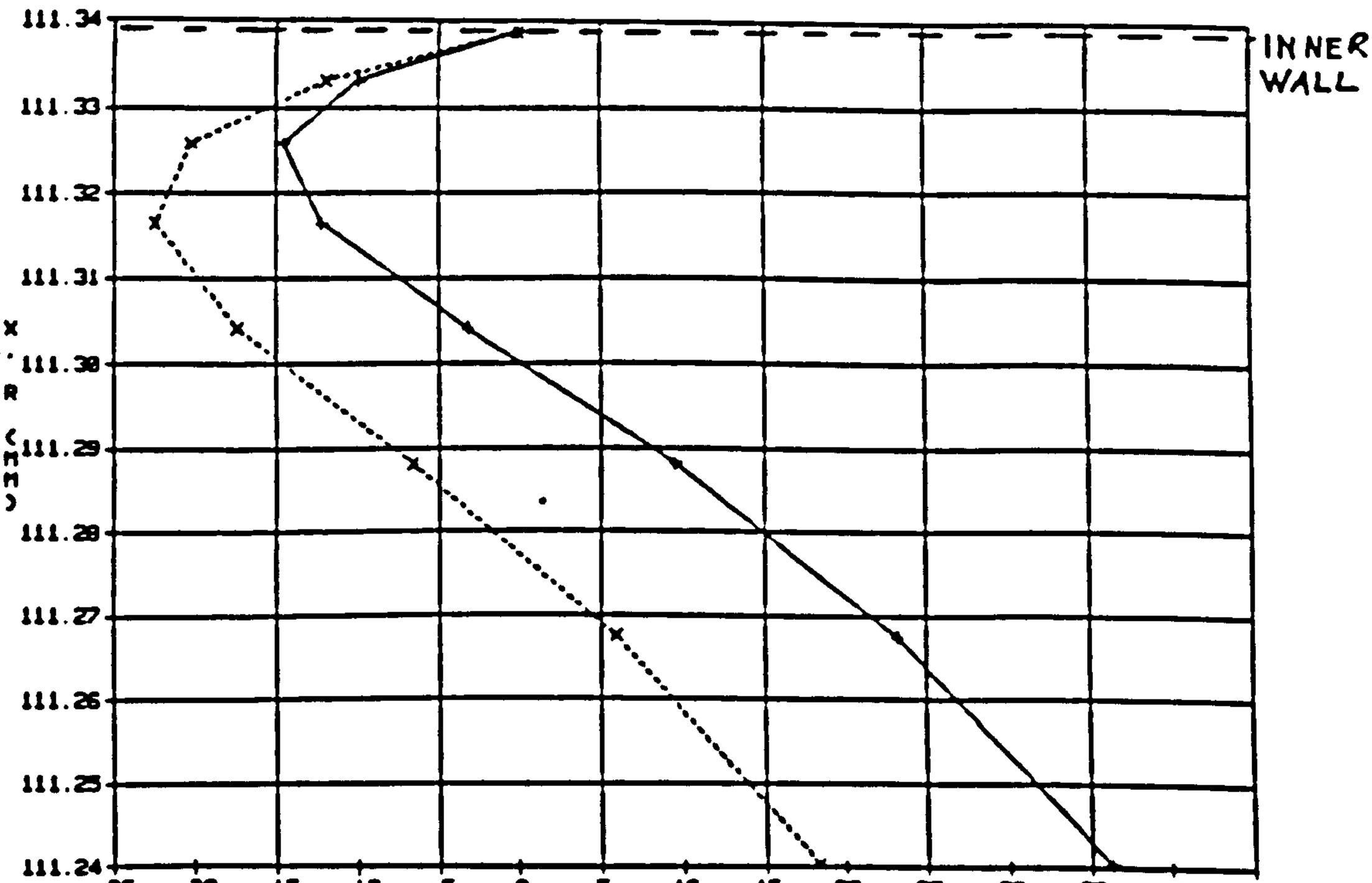

Figure-5.73 c Velocity Profile Downstream of the Shock
(Enlargement of Region A in Figure-5.73b)

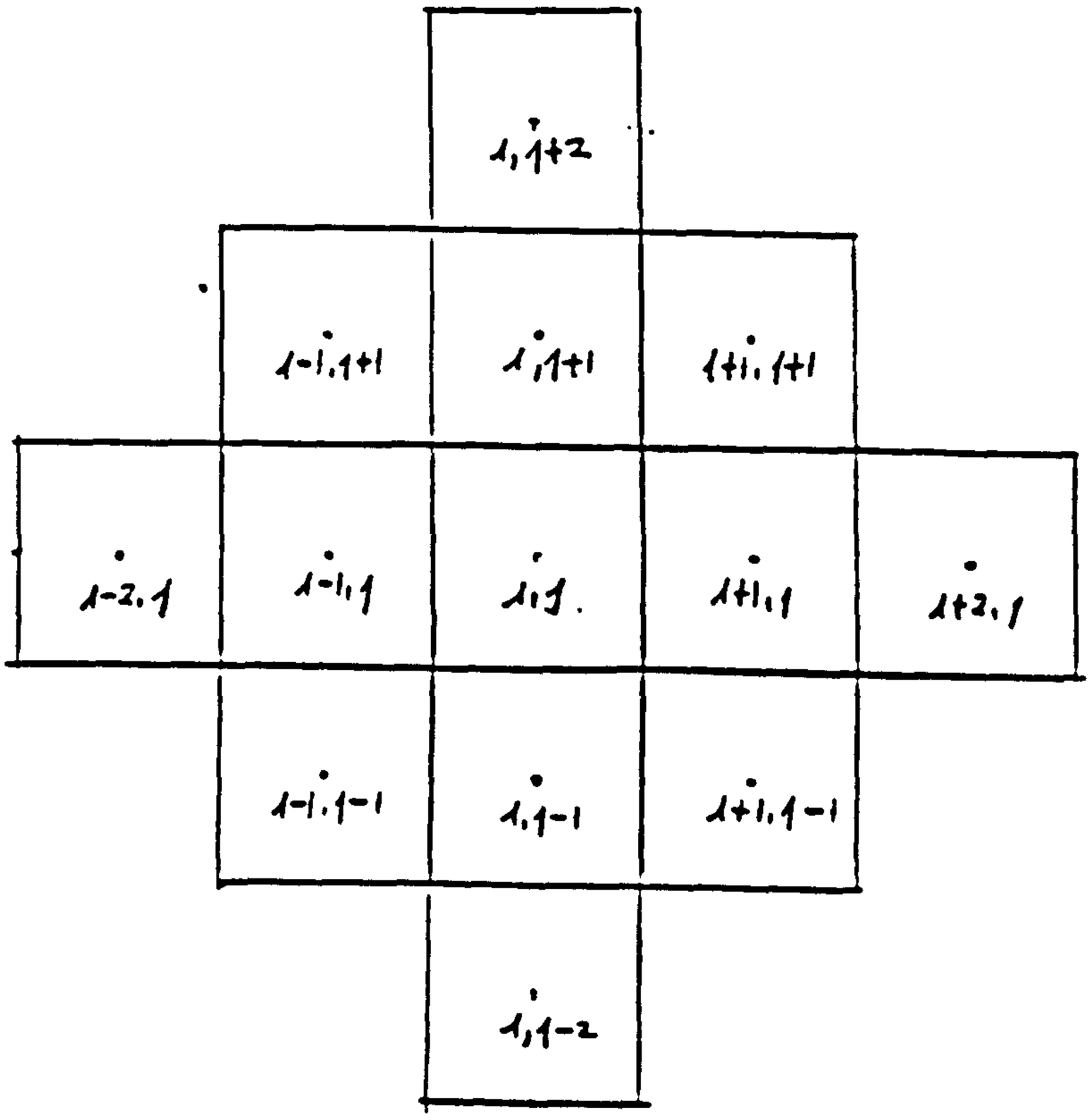

Figure-6.1 Cell Centred Stencil

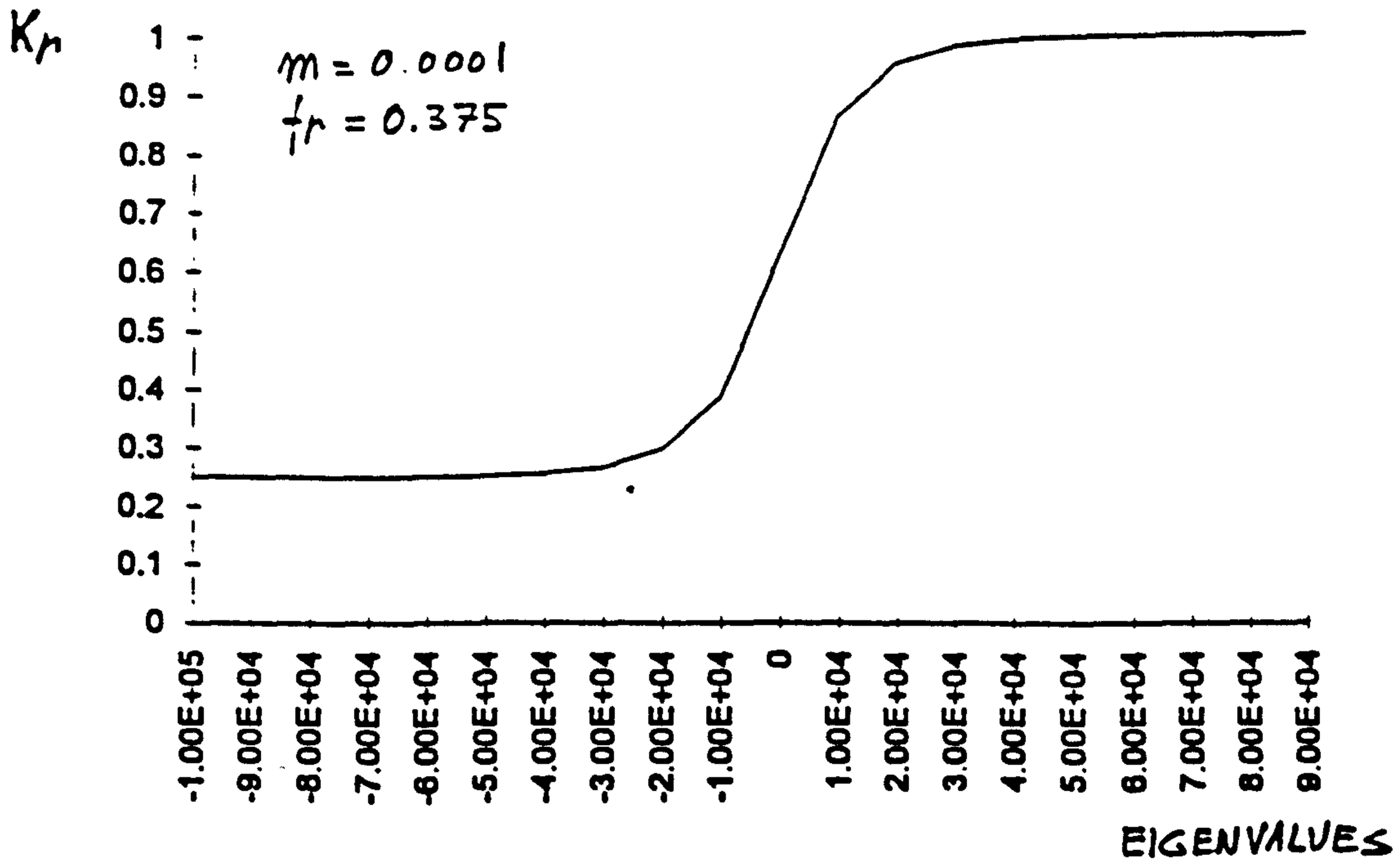

Figure-6.2 Reduction Function

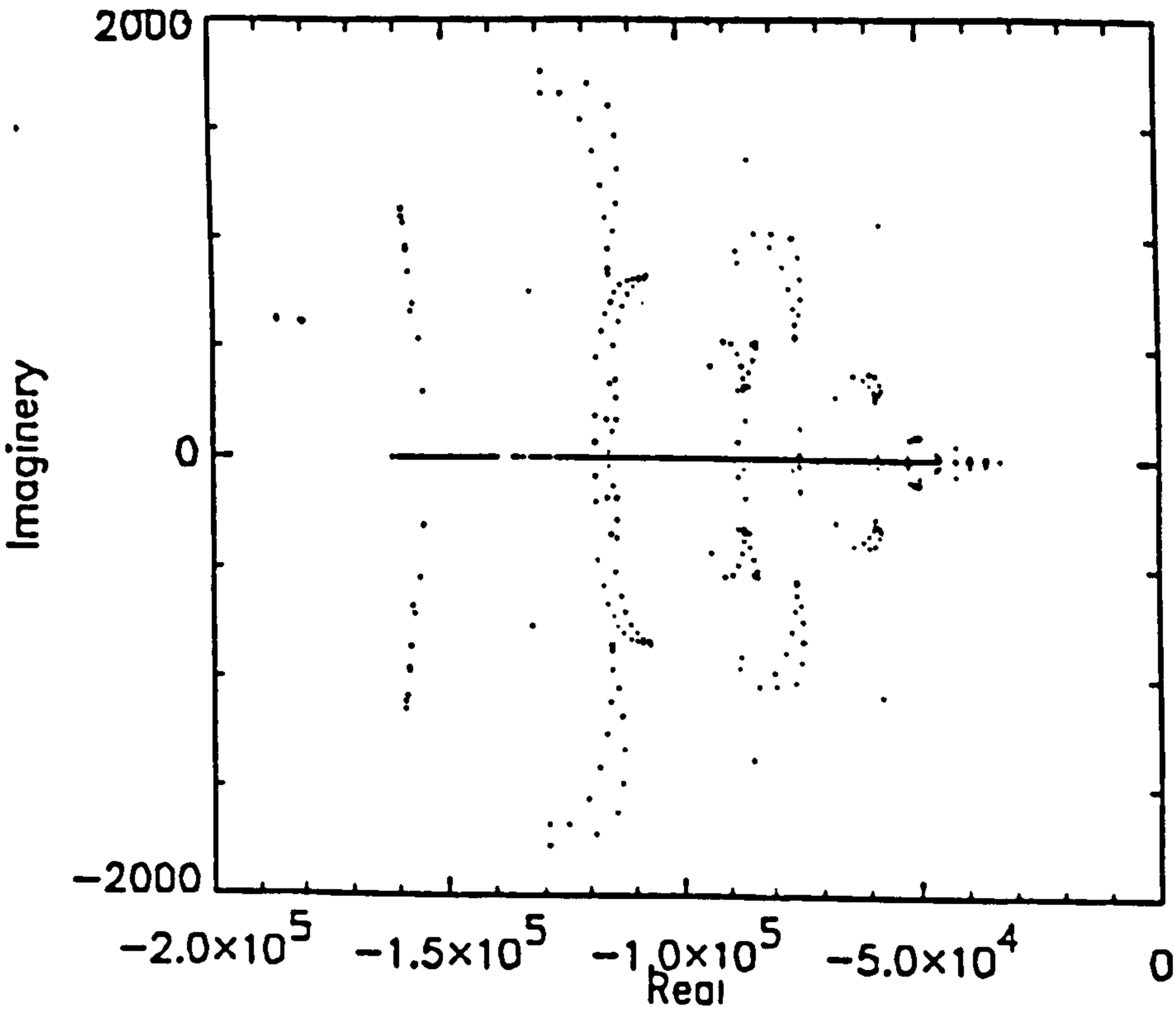

Figure-6.3 Eigenvalues of the Standard Dissipation model:
Inviscid Ni's Bump at Subsonic Condition

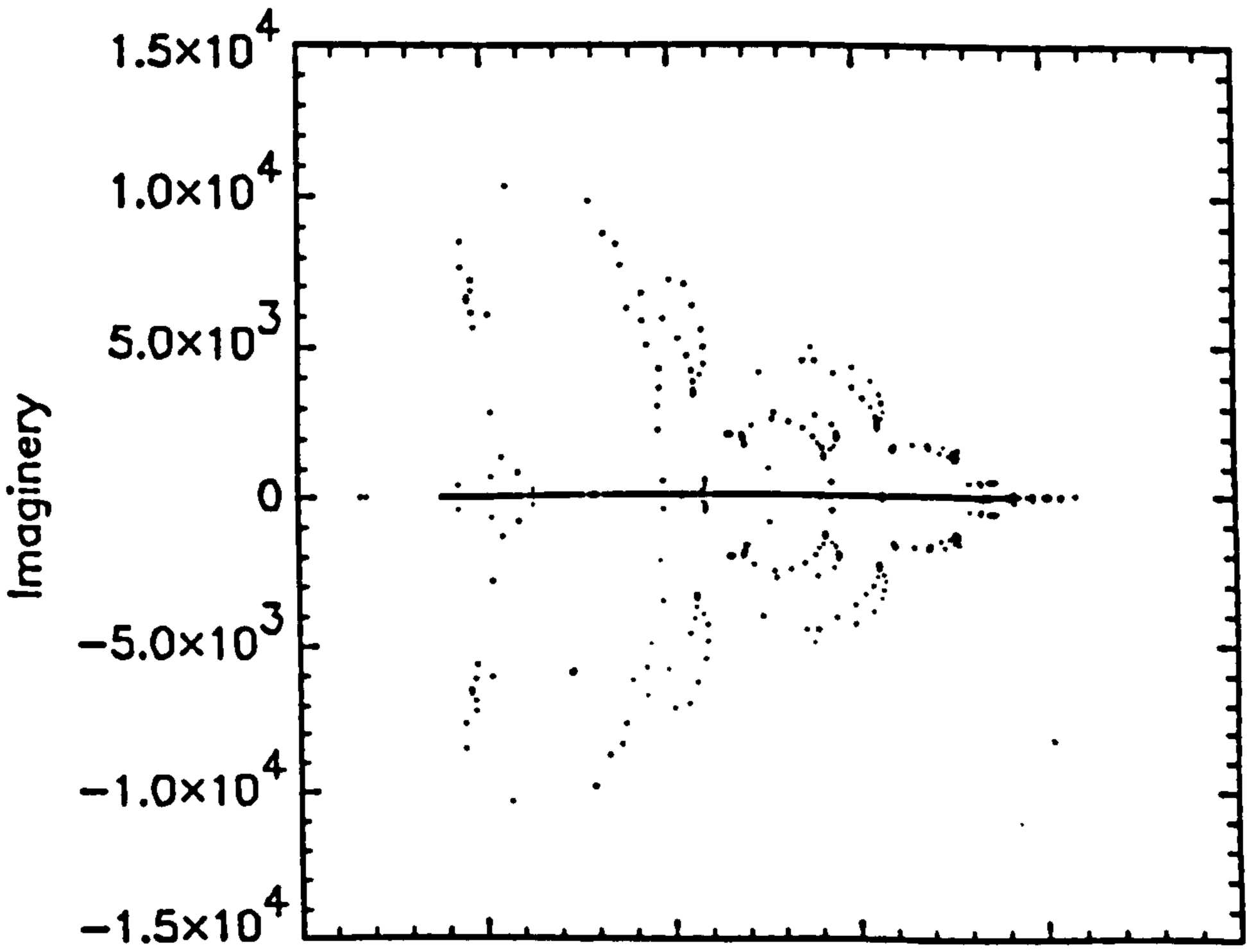

Figure-6.4 Eigenvalues of the Standard Dissipation model:
Inviscid Ni's Bump at Transonic Condition

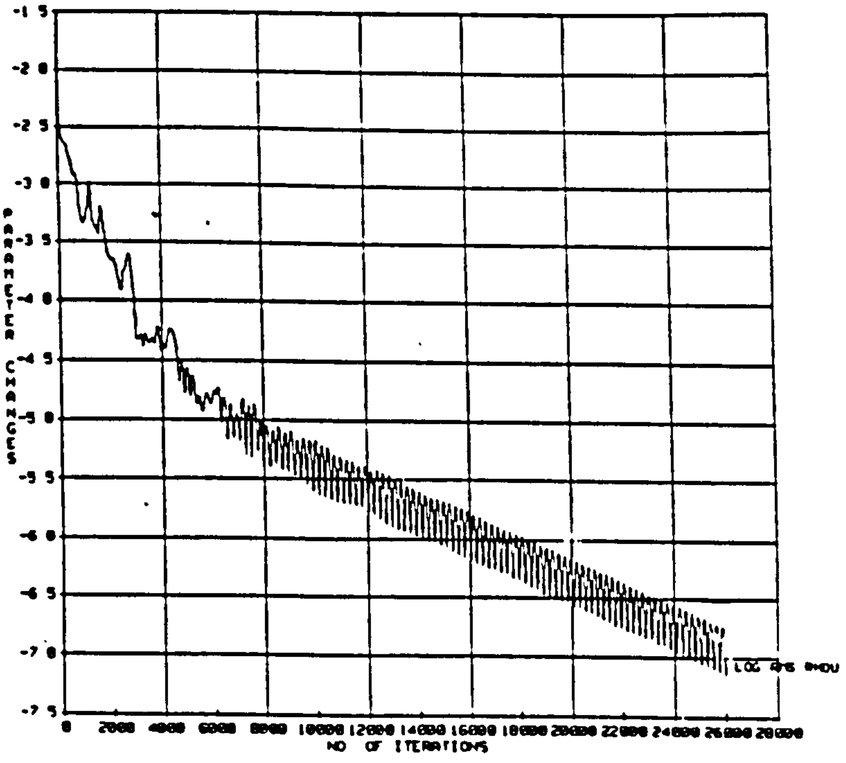

Figure-6.5 Logarithmic Root Mean Square of the ρu residual with Standard Dissipation Model. Inviscid Ni's Bump, Subsonic Case

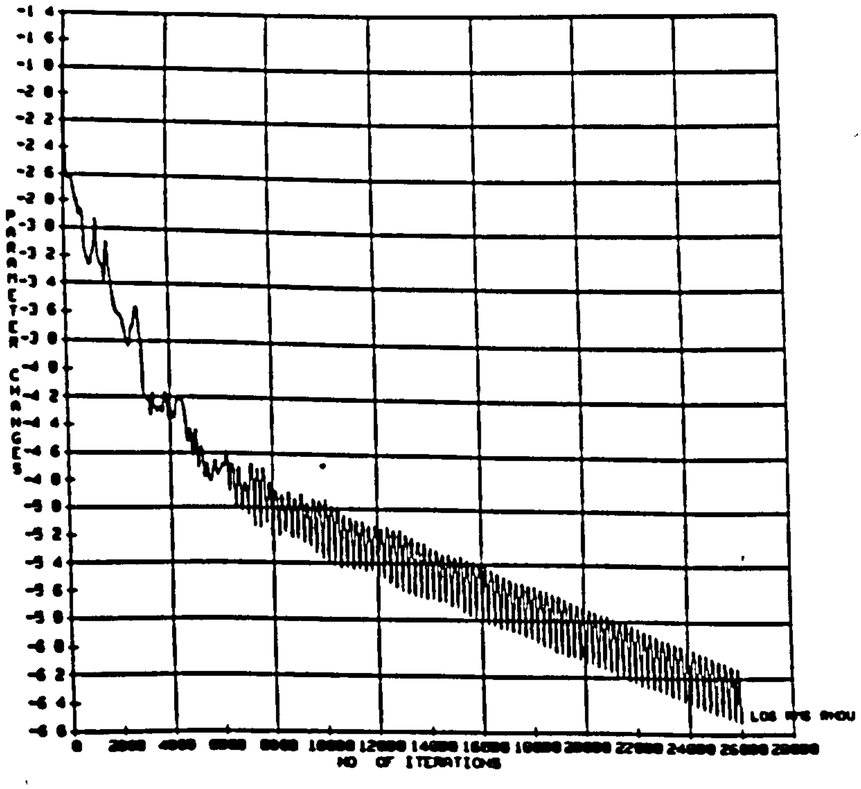

Figure-6.6 Logarithmic Root Mean Square of the ρu residual with Modified Dissipation Model. Inviscid Ni's Bump, Subsonic Case

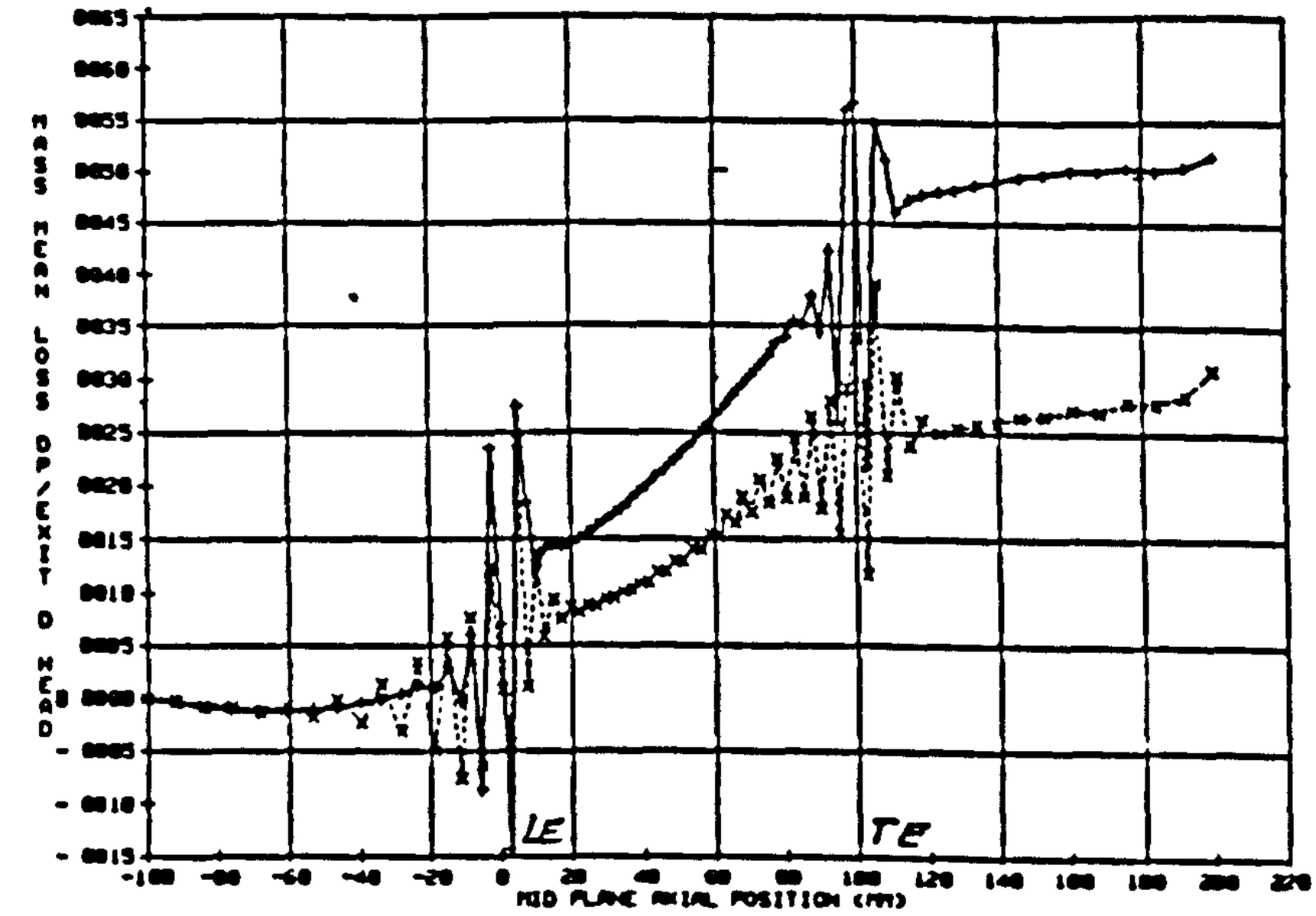

Figure-6.7 Total Pressure Loss for the Inviscid Ni's Bump Subsonic Case

-+--+- Standard dissipation model
-x--x- Modified dissipation model
LE = Leading Edge
TE = Trailing Edge

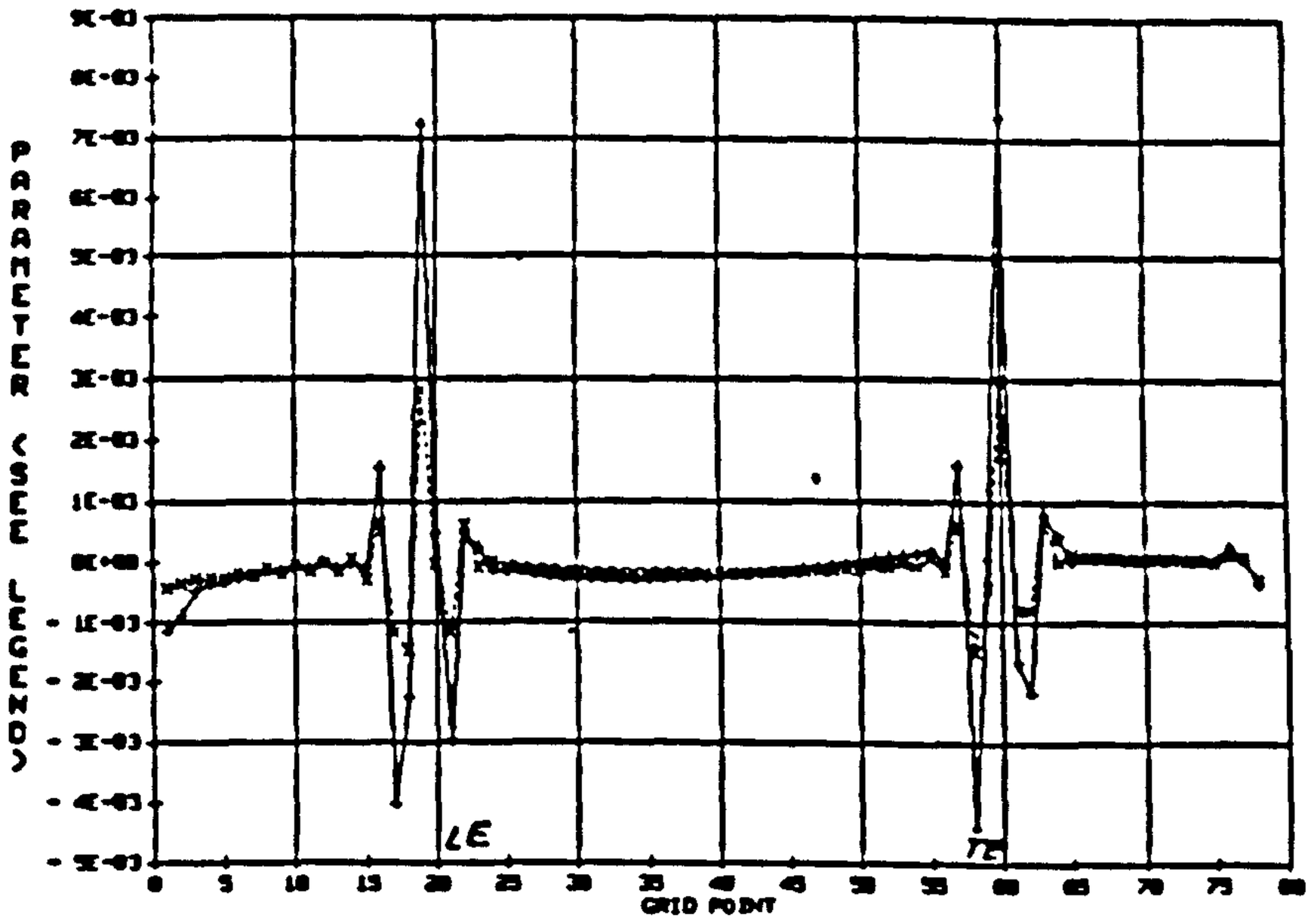

Figure-6.8 Dissipation of the ρu Component near Suction Surface from inlet to exit for Inviscid Subsonic Case

-+--+- Standard dissipation model
-x--x- Modified dissipation model

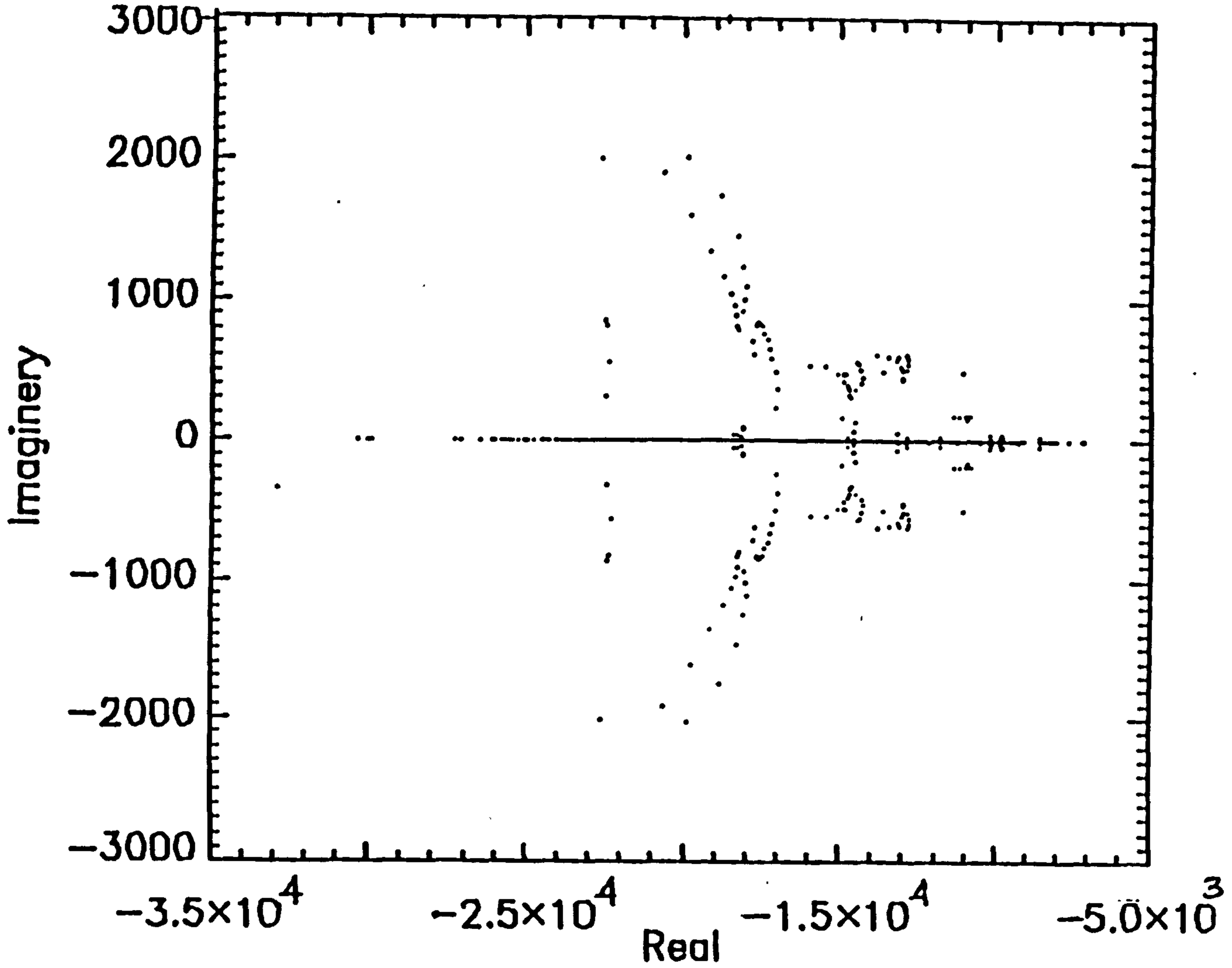

Figure-6.9 Eigenvalues of the Modified Dissipation model:
Inviscid Ni's Bump at Subsonic Condition

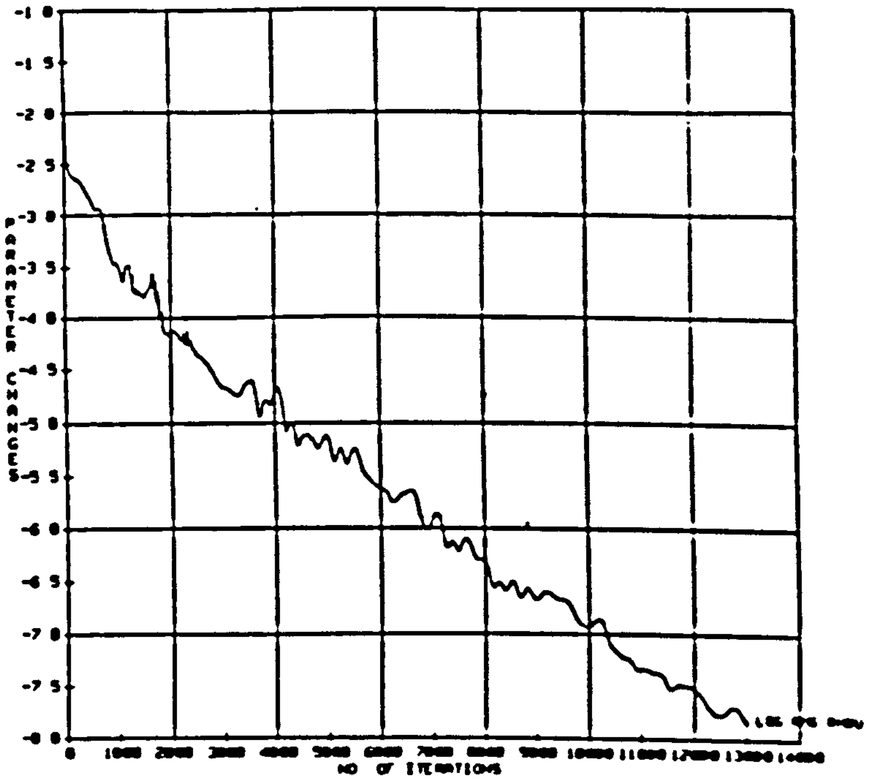

Figure-6.10 Logarithmic Root Mean Square of the ρu residual with Standard Dissipation Model. Inviscid Ni's Bump, Transonic Case

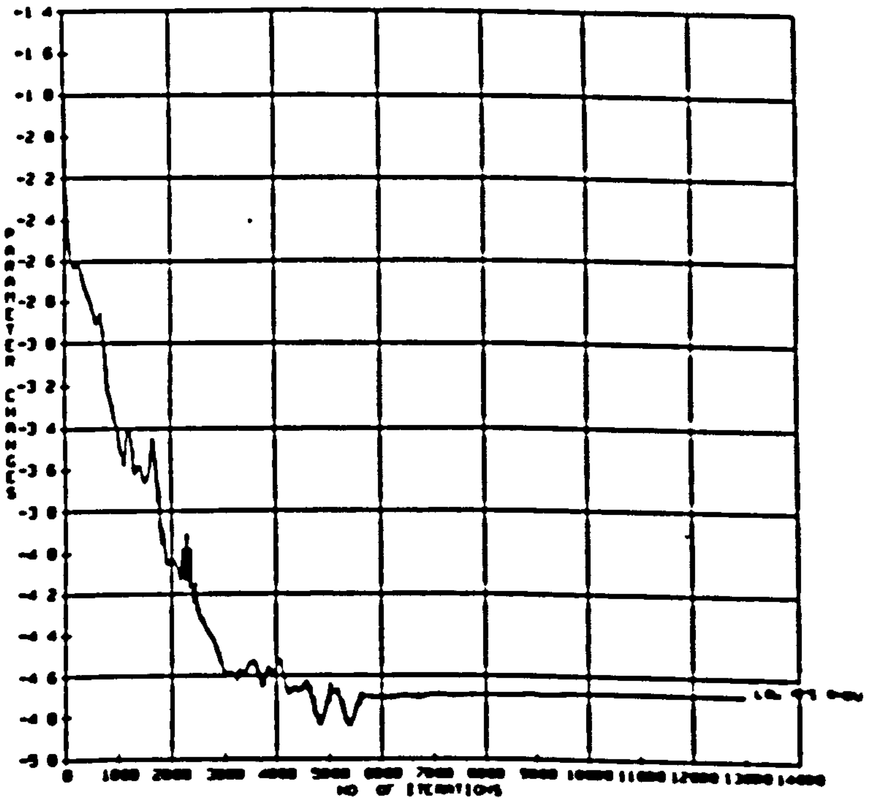

Figure-6.11 Logarithmic Root Mean Square of the ρu residual with Modified Dissipation Model. Inviscid Ni's Bump , Transonic Case

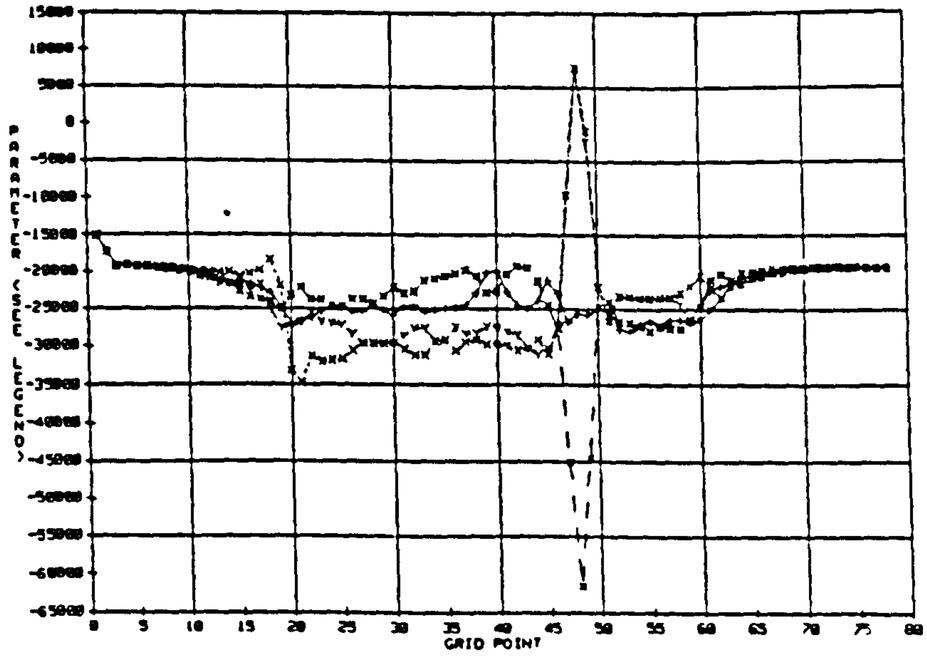

Figure-6.12 Line Plots of the Four Eigenvalues (-+--+-), (-x--x-), (-Y--Y-), and (-*--*-) near Blade Surface, from Inlet to Exit for the Inviscid Ni's Bump, Transonic Case.

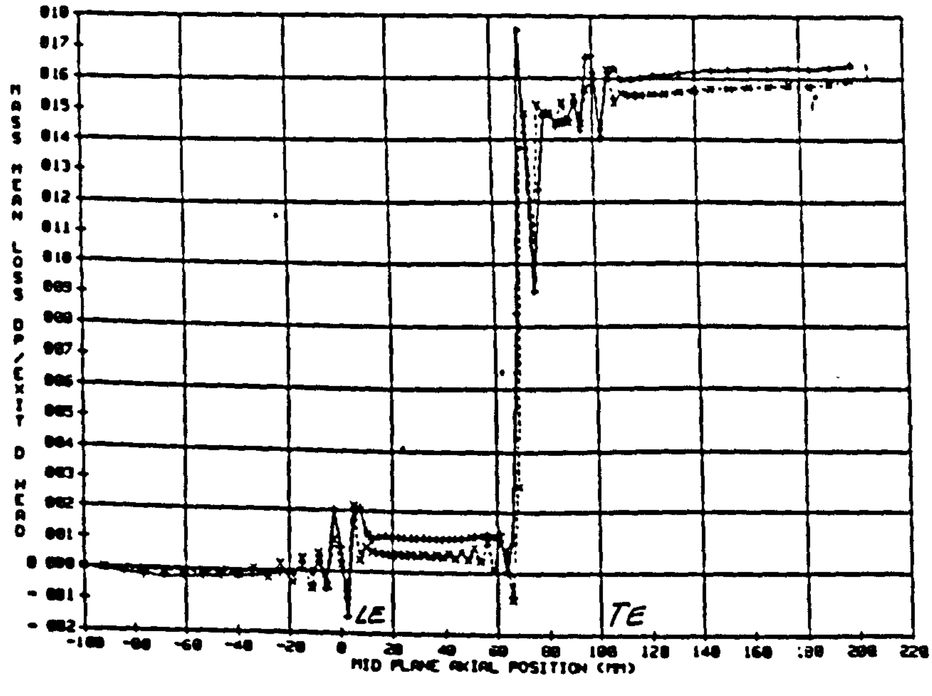

Figure-6.13 Total Pressure Loss for the Inviscid Ni's Bump Transonic Case

-+--+- Standard dissipation model
-x--x- Modified dissipation model
LE = Leading Edge
TE = Trailing Edge

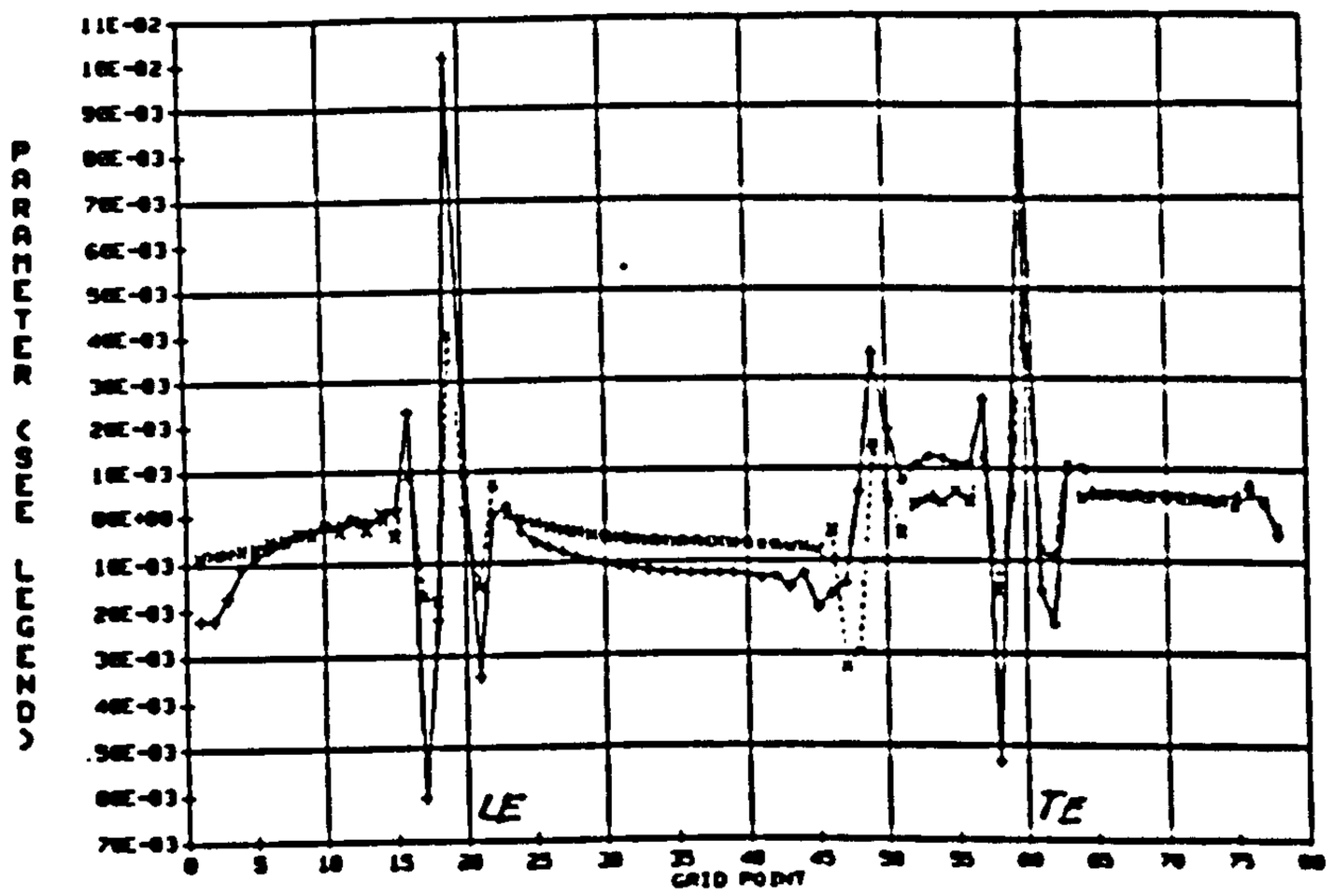

Figure-6.14 Dissipation of the ρu Component near Suction Surface from inlet to exit for Inviscid Transonic Case

-+--+- Standard dissipation model
-x--x- Modified dissipation model

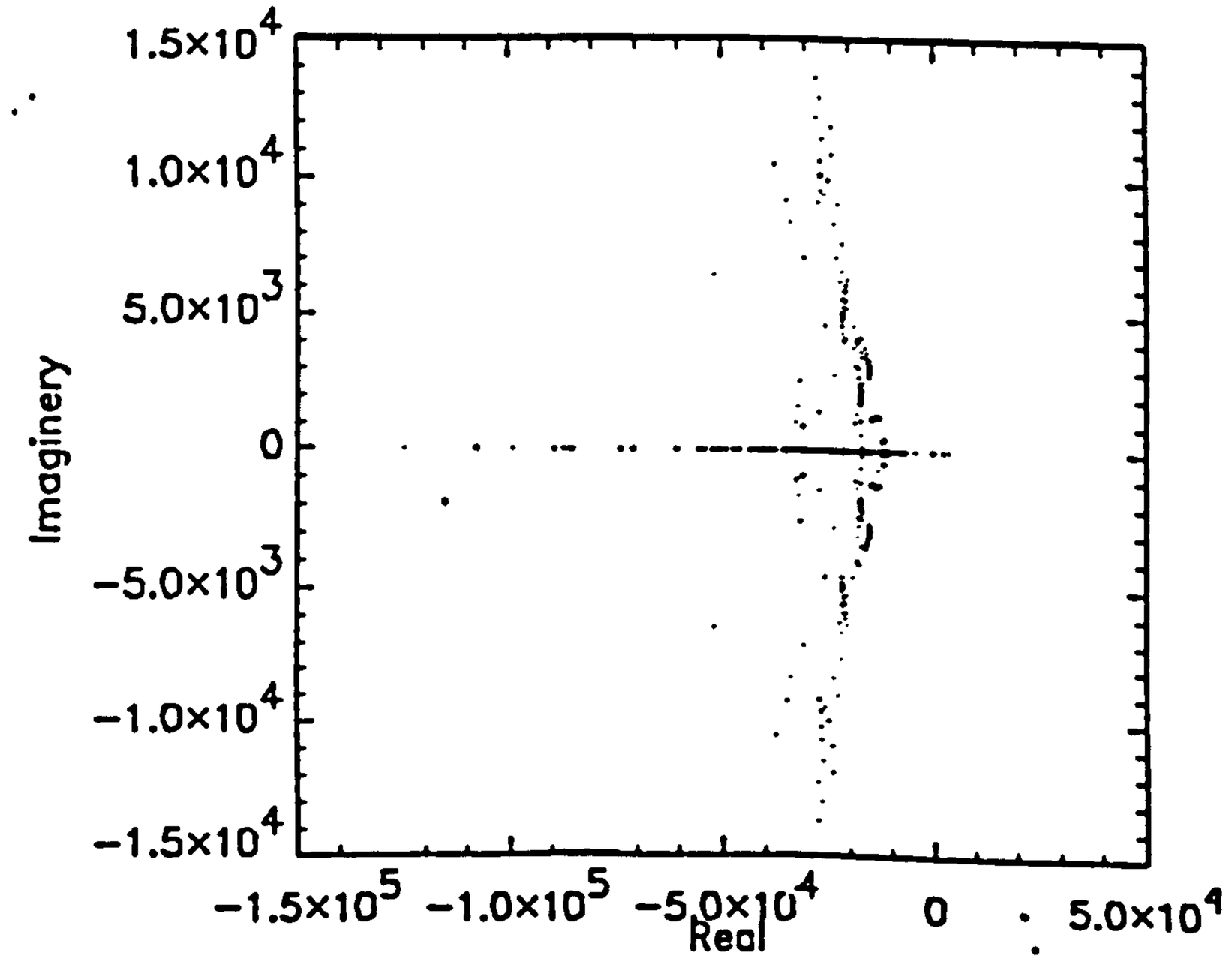

Figure-6.15 Eigenvalues of the Modified Dissipation model: Inviscid Ni's Bump at Transonic Condition

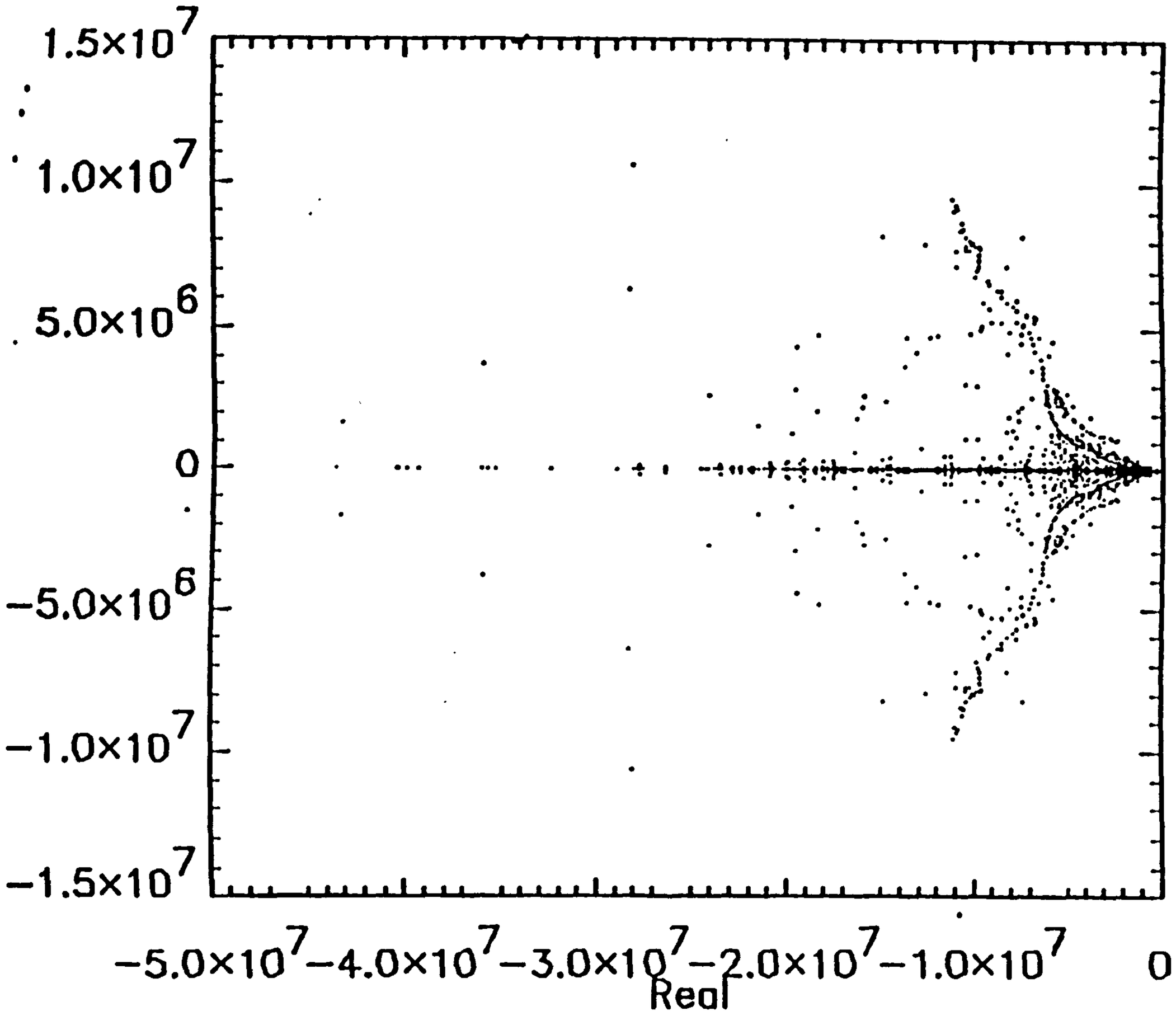

Figure-6.16 Eigenvalues of the Standard Dissipation model: Two Dimensional High Pressure Turbine Fully Viscous Case

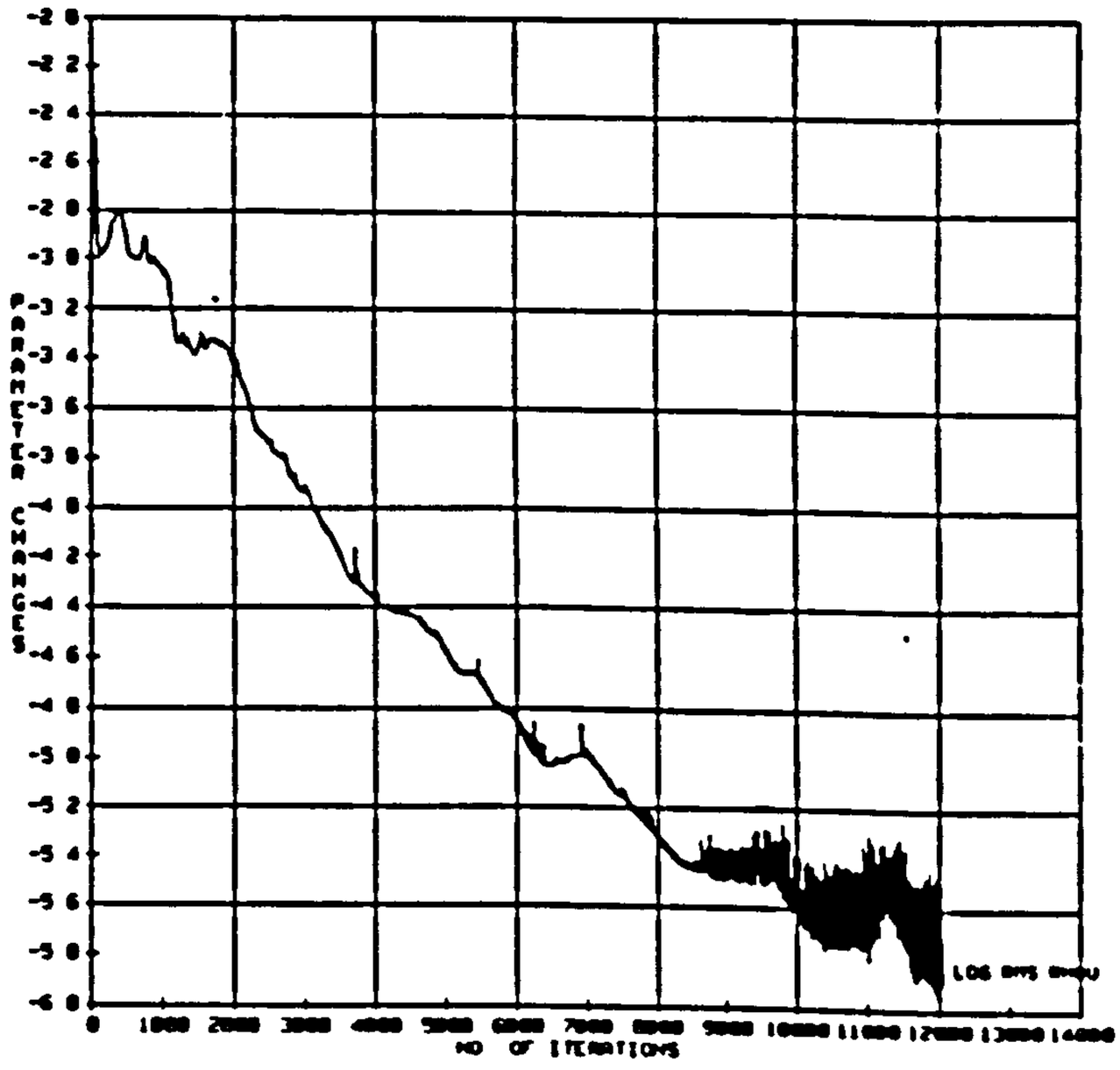

Figure-6.17 Logarithmic Root Mean Square of the ρu residual with Standard Dissipation Model. Two Dimensional High Pressure Turbine Fully Viscous Case

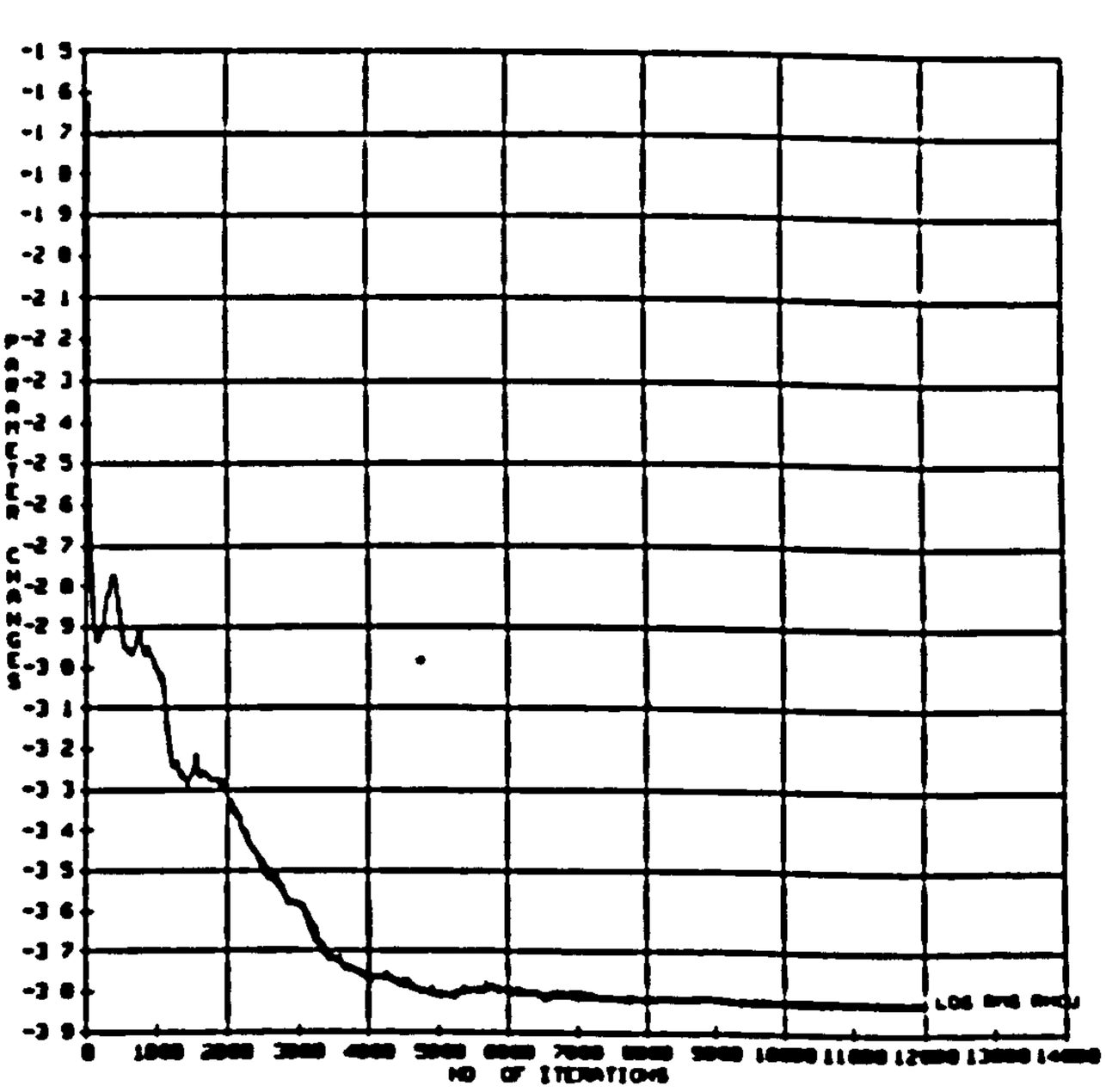

Figure-6.18 Logarithmic Root Mean Square of the ρu residual with Modified Dissipation Model. Two Dimensional High Pressure Turbine Viscous Case A

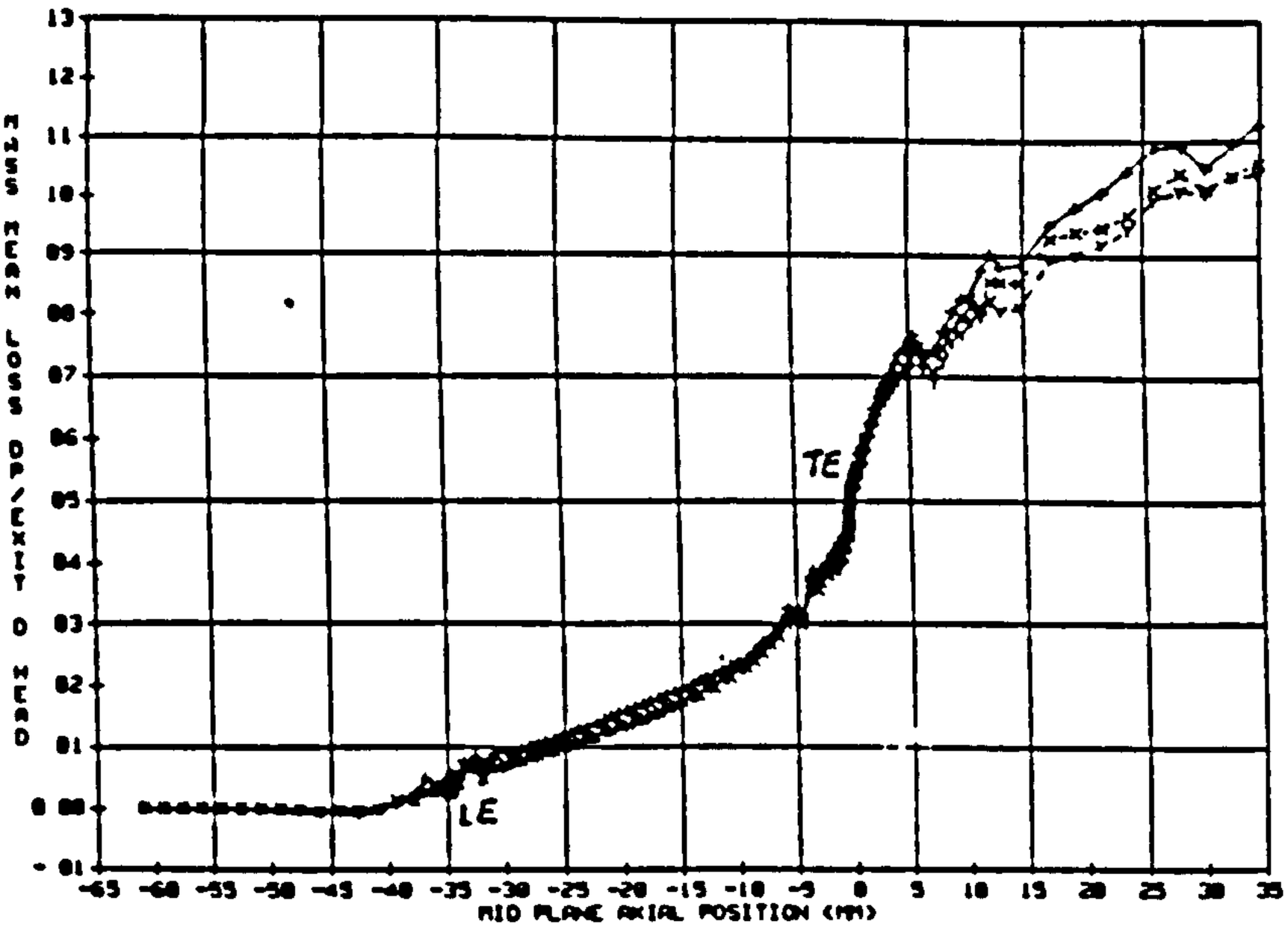

Figure-6.19 Total Pressure Loss for the Two Dimensional High Pressure Turbine Viscous Case

-+--+- Standard dissipation model
-x--x- Modified dissipation model, case A
-Y--Y- Modified dissipation model, case B
LE = Leading Edge
TE = Trailing Edge

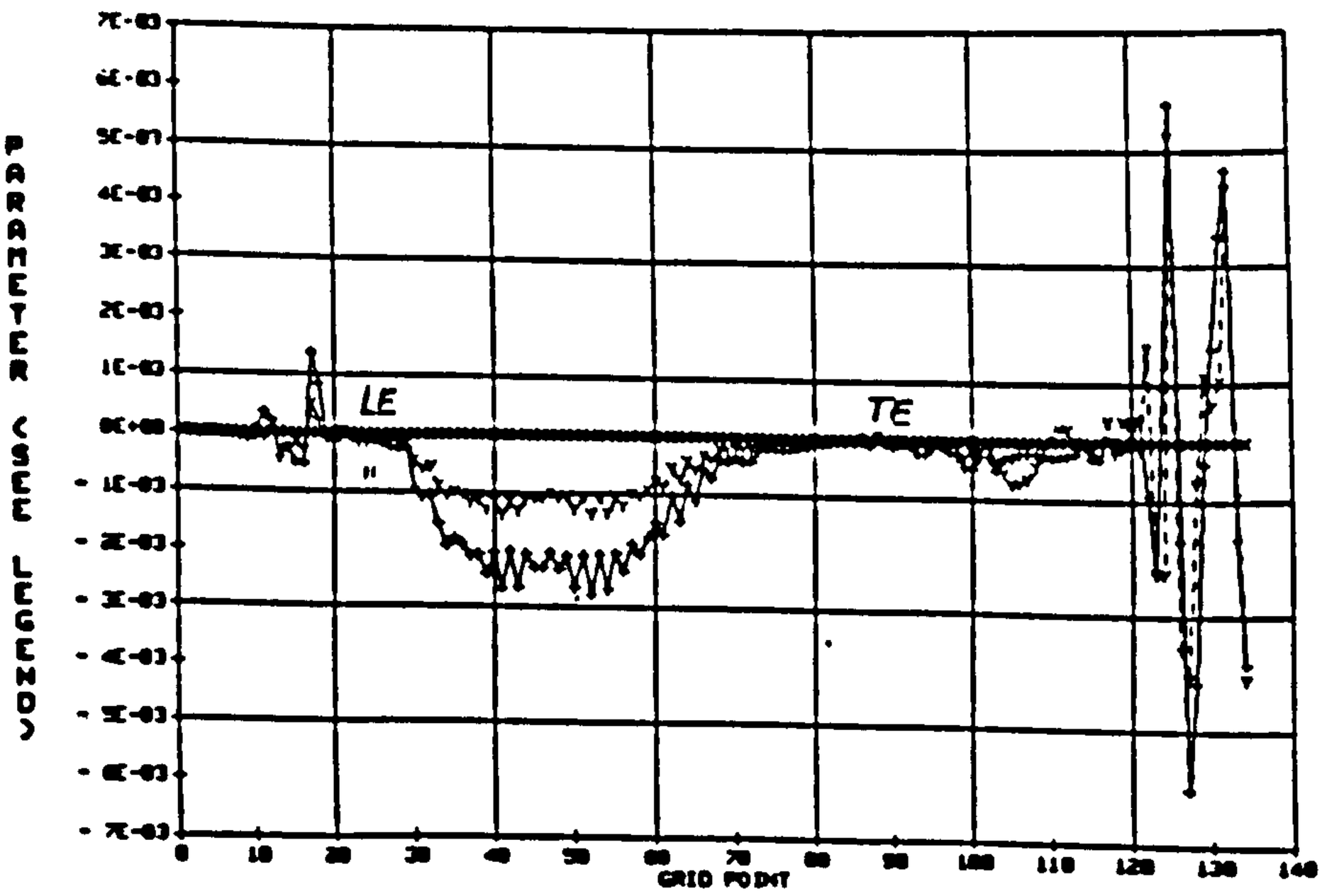

Figure-6.20 Dissipation of the ρu Component near Suction Surface from inlet to exit for the Viscous Case

-+--+- Standard dissipation model
-x--x- Modified dissipation model, case A
-Y--Y- Modified dissipation model, case B
LE = Leading Edge
TE = Trailing Edge

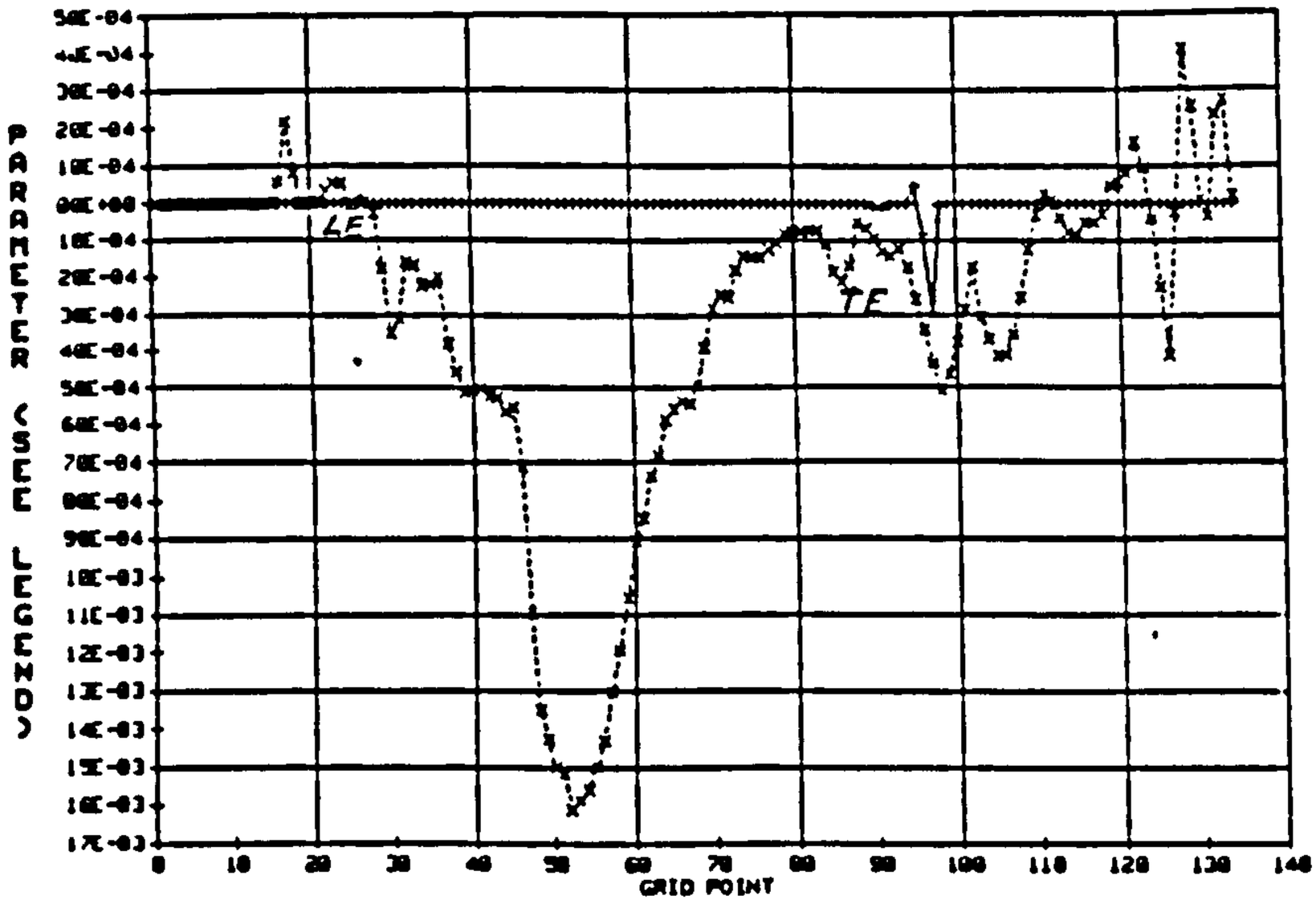

Figure-6.21 Dissipation and Viscous Fluxes of the Component near Suction Surface from Inlet to Exit for Viscous Case A

-+--+- Dissipation
-x--x- Viscous fluxes

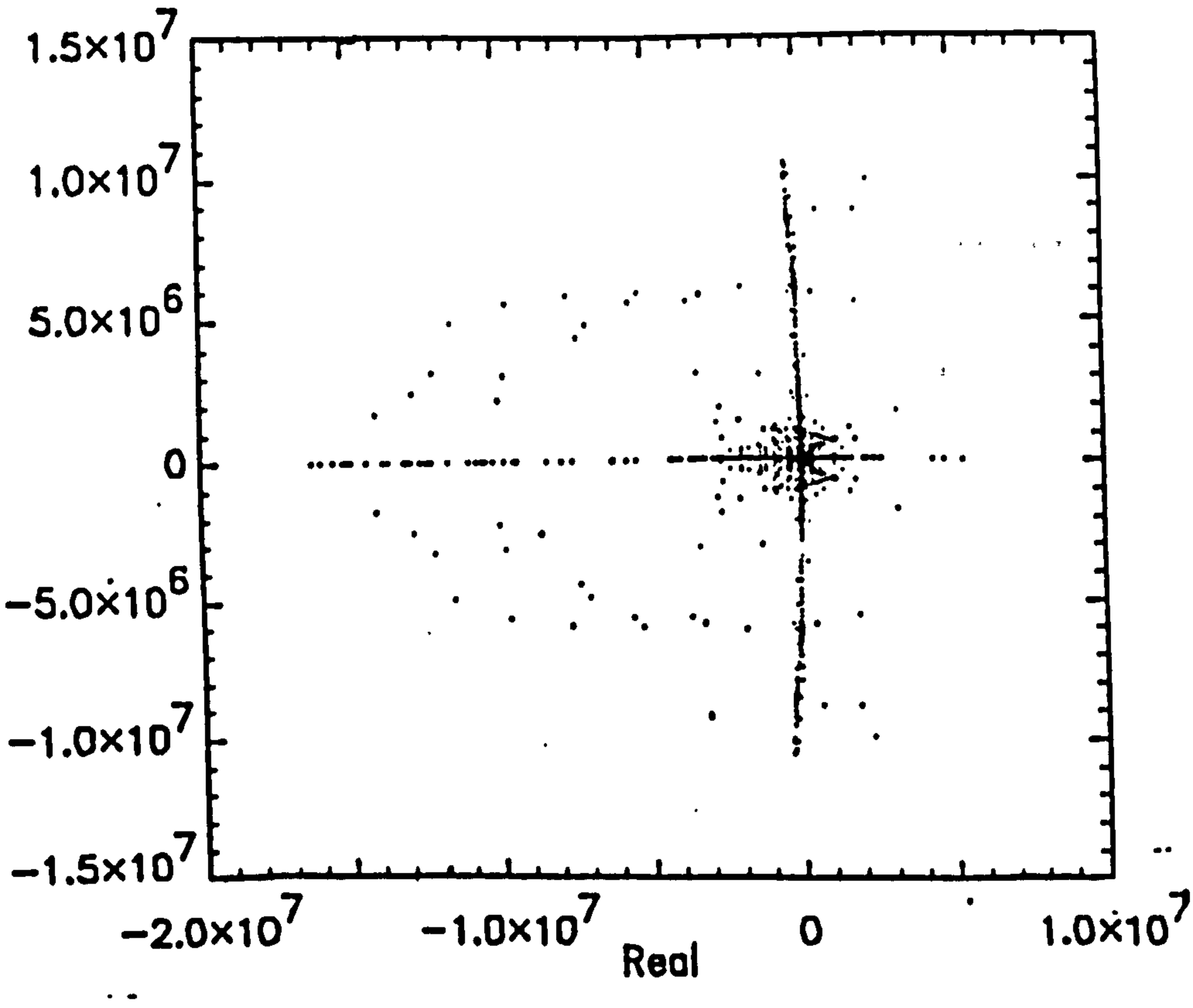

Figure-6.22 Eigenvalues of the Modified Dissipation model: Two Dimensional High Pressure Turbine Viscous Case A

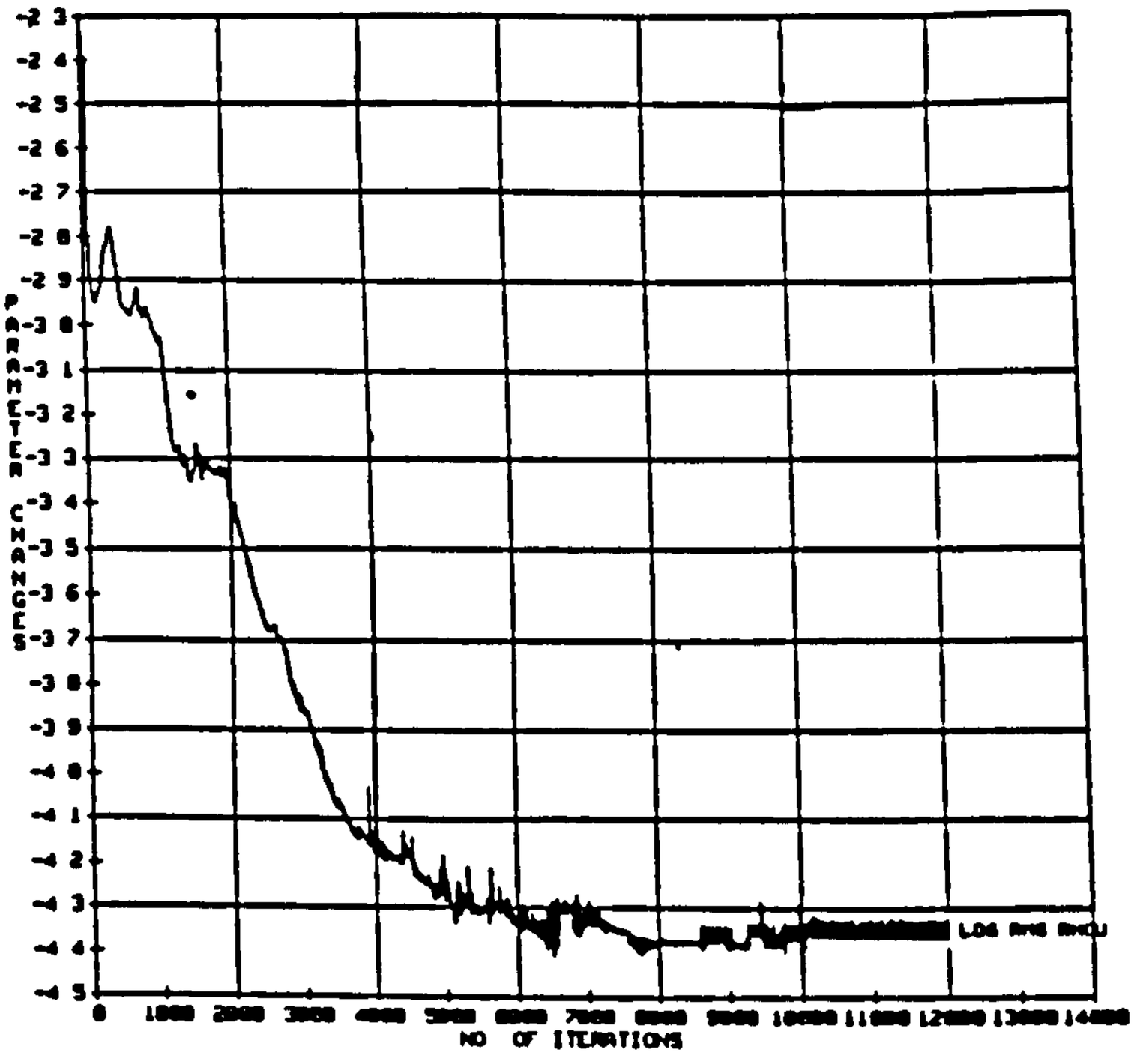

Figure-6.23 Logarithmic Root Mean Square of the ρu residual with Modified Dissipation Model. Two Dimensional High Pressure Turbine Viscous Case B

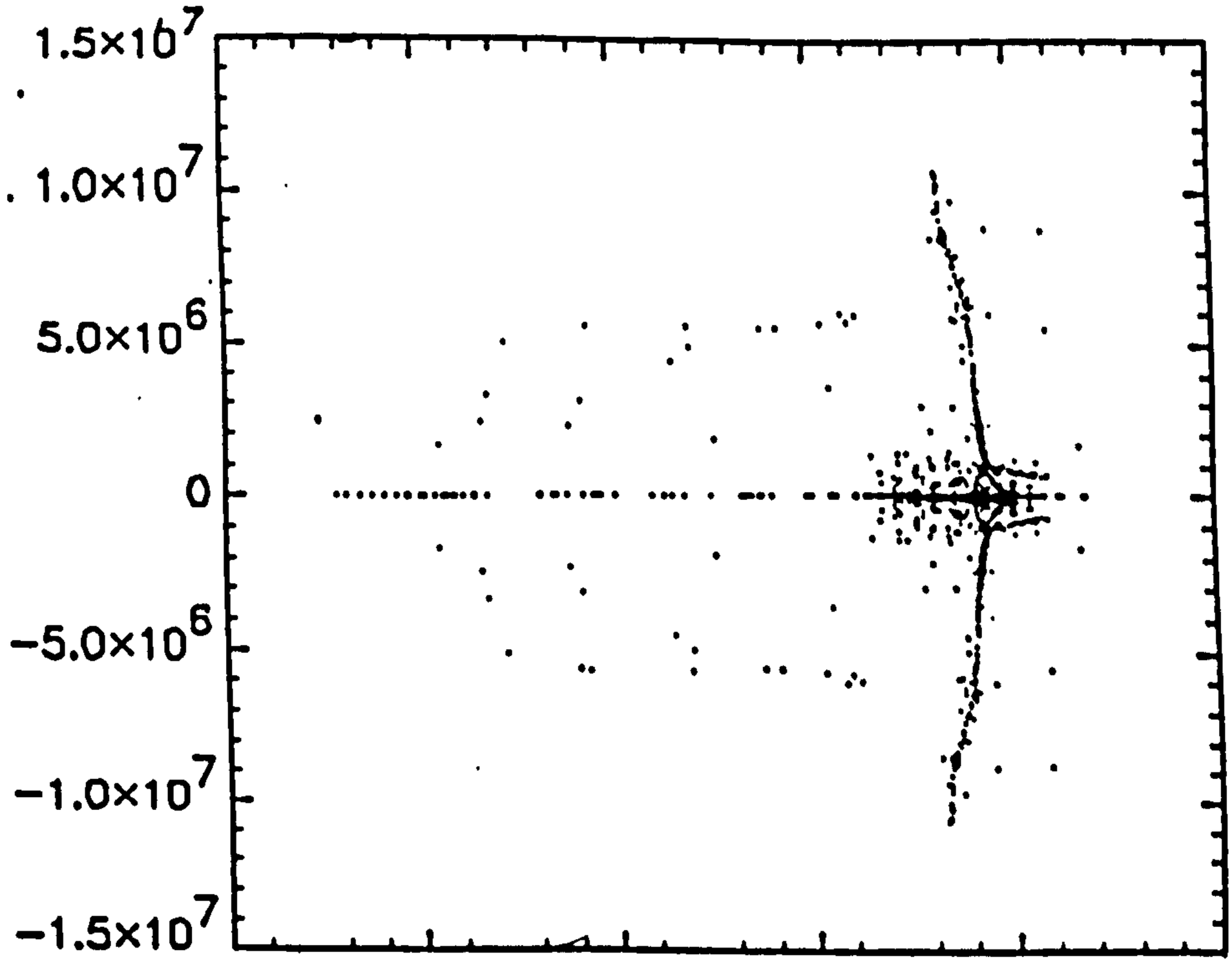

Figure-6.24 Eigenvalues of the Modified Dissipation model: Two Dimensional High Pressure Turbine Viscous Case B, iteration = 12000

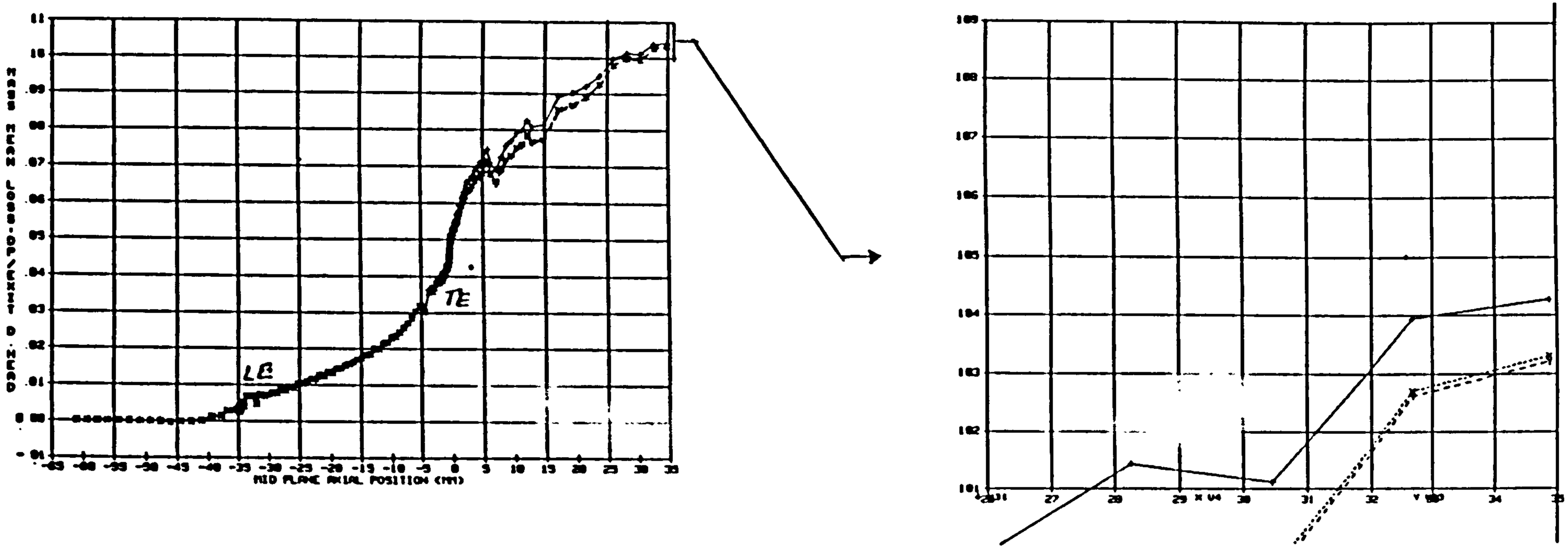

Figure-6.25 Total Pressure Loss: Modified Dissipation Model, Viscous Case B

-+--+- Iteration = 12000
-x--x- Iteration = 16000
-Y--Y- Iteration = 20000